Universitat de Girona

THE FLAVONOLIGNAN SILIBININ IN NON-SMALL CELL LUNG CANCER: MOLECULAR MECHANISMS AND THERAPEUTIC RELEVANCE

Sara Verdura Martínez

Universitat de Girona

DOCTORAL THESIS

THE FLAVONOLIGNAN SILIBININ IN NON-SMALL CELL LUNG CANCER:
MOLECULAR MECHANISMS AND THERAPEUTIC RELEVANCE

Sara Verdura Martínez

2023

DOCTORAL THESIS

THE FLAVONOLIGNAN SILIBININ IN NON-SMALL CELL LUNG CANCER:
MOLECULAR MECHANISMS AND THERAPEUTIC RELEVANCE

Sara Verdura Martínez

2023

Doctoral Programme in Molecular Biology, Biomedicine and Health

Supervised by:
Javier A. Menendez Menendez, Ph.D.
Joaquim Bosch Barrera, Ph.D., M.D.

Tutorized by:
Jose Manuel Fernández-Real Lemos Ph.D., M.D.

Submitted in total fulfillment of the requirements to obtain the PhD degree by the University of Girona

"La vida no es tracta de trobar-te a tu mateix,

sinó de crear-te a tu mateix "

Bernard Shaw

Als meus pares

A la meva família Pau Lua i Biel

ACKNOWLEDGMENTS

Són moltes les persones a les quals m'agradaria dirigir unes paraules d'agraïment, no només a aquelles que han fet possible la realització i culminació d'aquesta tesis, sinó també a totes aquelles persones que m'han acompanyat durant el transcurs de la meva vida, tant científica com personal, i que són tant importants per mi.

En primer lugar, y como no podía ser menos, a ti Javier. Te estaré siempre agradecida por la oportunidad que me has brindado de formar parte del equipo, y por apostar por mi carrera científica des del inicio. Por toda la formación y enseñanzas recibidas, soy muy afortunada por ello. Porqué nunca dejará de sorprenderme tu dedicación y resiliencia, tu capacidad de trabajo y de encontrar salida y explicación a los datos, tu infinito conocimiento y tu enorme visión y vocación científica. Aunque no ha sido un camino fácil de recorrer, finalmente este viaje termina y el esfuerzo se ve recompensado. Sin ti esto habría sido definitivamente imposible. Solamente puedo darte LAS GRÁCIAS.

A tu Bet, no tinc més que paraules d'agraïment. Perquè ets un pilar imprescindible del Lab i t'estaré eternament agraïda per tot, pel suport, pels bons moments compartits (i els no tant bons), per els teus inesgotables coneixements científics i tècnics, i per la teva capacitat de treball. T'admiro, us admiro com a equip. Sense la teva ajuda aquesta tesis tampoc hagués estat possible, així que gràcies, gràcies, gràcies.

A en Joaquim Bosch Barrera, pels pacients, projectes i dades aportades. Per la teva disposició i consells en els casos oncològics que m'han tocat de ben a prop. Moltes gràcies.

Als companys de l'IRTA, François i Cinta. Gràcies a vosaltres va començar el camí de la recerca. Em vau transmetre la passió per la ciència i em vau demostrar que amb dedicació i esforç tot és possible.

A mi Verita. Porqué, aunque mi paso por el PRBB fue un oscuro camino, en ese momento comprendí que todo ocurre por algo. Porqué eres una de la mejor persona que he conocido jamás. Soy muy afortunada por haberte conocido y haber podido

compartir (y seguir compartiendo) contigo tantas risas y buenos momentos. Gracias por seguir formando parte de mi vida.

Al resto de compañeros y amigos del PRBB, Yacine, Mònica, Chris… gracias a vosotros también.

Als antics companys del Lab de la Montse, tots vosaltres em vau ajudar a créixer: Ester, encara que per poc temps vaig aprendre i gaudir molt de formar equip amb tu. Octavio y Manu, por las risas y por todos los momentos vividos y experimentos compartidos, lo pasé genial trabajando con vosotros. Paula, l'alumna brillant, gràcies també pels moments compartits.

A mi querida Ana Aza. Porqué por esas hermosas casualidades de la vida coincidimos ese espacio tiempo, y aunque fugaz, no menos valioso. Por ser una de las personas con quien más me he reído en mi vida. Porqué espero poder seguir compartiendo risas y momentos entrañables contigo. Por todos esos buenos momentos, muchísimas gracias a ti también.

A tots els companys d'IDIBGI. En especial, als companys de Gencardio, David i Rebecca. Per tots els vostres moments "heaters", i per haver compartit tantes penes i alegries. Sou molt grans. També a l'Eric, encara que fa temps que vas marxar, segueixes present a IDIBGI.

A les noves incorporacions del Lab. A l'Àngela, per ser la nena "graciosa" del Lab. Perquè ets entranyable com poques persones, i la teva capacitat de relacionar-te amb la gent et farà arribar ben lluny. Espero veure't créixer, tant científica com personalment, i seguir compartint grans moment amb tu. A l'Eila, pel teu interès i disposició. Perquè encara que hem coincidit poc sempre és un plaer compartir una estona amb tu.

A tota la Familia Reixach, i en especial a l'Anna i a la Maria. M'heu fet sentir una més de la família. Gràcies per cuidar-nos tant a tots, sobretot als petits, sense el vostre suport incondicional això no hagués estat possible. Mil gràcies.

A la Iaia Pilar. Per la teva fortalesa i per ser un gran exemple, com a dona, mare i àvia. Encara que t'hagis oblidat de moltes coses, jo no m'oblido de tot el que has fet per nosaltres i per la família. Has lluitat i tirat del carro com bona "Mañica" que ets!

A mis titas Martínez, Montse y Xuli. Y a ti, Nio. Os debo parte de lo que soy. Gracias por regalarme tantos momentos mágicos y vivencias, desde la infancia hasta hoy.

A la Mama, perquè m'ho vas donar tot. Per desgràcia vas marxar massa d'hora, i sento que no hi siguis per poder compartir amb tu el final d'aquesta etapa. Però sé que allà on siguis estaràs orgullosa de mi. Et trobo a faltar. Al Papa, pels infinits viatges a la uni, per la teva inacabable disposició i per ser-hi sempre. Pel teu tarannà i sensibilitat. Ets un exemple a seguir. Ainooot! Per ser la meva companya de viatge d'infantesa, el meu referent des de petita i la millor de les germanes. Tots tres m'heu fet créixer i gràcies a vosaltres soc qui soc avui. Gràcies per creure sempre en mi i animar-me a tirar endavant. Ho sou tot i us ho dec tot.

Als tres amors de la meva vida, per tot el temps robat i que no us he dedicat. Al Pau, el millor company i pare. Pel teu inesgotable suport. Per cuidar-me i cuidar-nos com si cada dia fos l'últim. Per regalar-me el viatge de la vida al teu costat, i per aquesta família preciosa que hem format. Gràcies a tu arriba el final d'aquesta etapa que semblava inacabable. Als dos sols que il·luminen els meus dies, la Lua i en Biel. Lua, la meva nena, per iniciar-me en la fantàstica aventura de la maternitat. No puc estar més feliç i orgullosa d'haver-ho fet! Em fascina veure com creixes i et converteixes en una fantàstica personeta dia a dia. Biel, el petit de la casa. Per ser un nen feliç i contagiar-nos aquesta felicitat cada dia. El teu somriure ens omple de màgia, i espero que ho segueixi fent. Sou el meu món i la meva força.

A tots vosaltres, moltes gràcies.

LIST OF ORIGINAL PUBLICATIONS

The present thesis is presented as a compendium of six original research articles:

1. **Verdura S**, Encinar JA, Gratchev A, Llop-Hernández À, López J, Serrano-Hervás E, Teixidor E, López-Bonet E, Martin-Castillo B, Micol V, Bosch-Barrera J, Cuyàs E, Menendez JA. ***Silibinin is a suppressor of the metastasis-promoting transcription factor ID3***. Phytomedicine (Under review) **Impact factor: 7.9 (Q1/D1)**

2. **Verdura S**, Encinar JA, Teixidor E, Segura-Carretero A, Micol V, Cuyàs E, Bosch-Barrera J, Menendez JA. ***Silibinin Overcomes EMT-Driven Lung Cancer Resistance to New-Generation ALK Inhibitors***. Cancers (Basel). 2022;14(24):6101. doi: 10.3390/cancers14246101. **Impact factor: 5,2 (Q2)**

3. Bosch-Barrera J, **Verdura S**, Ruffinelli JC, Carcereny E, Sais E, Cuyàs E, Palmero R, Lopez-Bonet E, Hernández-Martínez A, Oliveras G, Buxó M, Izquierdo A, Morán T, Nadal E, Menendez JA. ***Silibinin Suppresses Tumor Cell-Intrinsic Resistance to Nintedanib and Enhances Its Clinical Activity in Lung Cancer***. Cancers (Basel). 2021;13(16):4168. doi: 10.3390/cancers13164168. **Impact factor: 6,575 (Q1)**

4. **Verdura S**, Encinar JA, Fernández-Arroyo S, Joven J, Cuyàs E, Bosch-Barrera J, Menendez JA. ***Silibinin Suppresses the Hyperlipidemic Effects of the ALK-Tyrosine Kinase Inhibitor Lorlatinib in Hepatic Cells***. Int J Mol Sci. 2022;23(17):9986. doi: 10.3390/ijms23179986. **Impact factor: 5,6 (Q1)**

5. Cuyàs E, **Verdura S**, Micol V, Joven J, Bosch-Barrera J, Encinar JA, Menendez JA. ***Revisiting silibinin as a novobiocin-like Hsp90 C-terminal inhibitor: Computational modeling and experimental validation***. Food Chem Toxicol. 2019;132:110645. doi: 10.1016/j.fct.2019.110645. **Impact factor: 4,679 (Q1)**

6. **Verdura S**, Cuyàs E, Llorach-Parés L, Pérez-Sánchez A, Micol V, Nonell-Canals A, Joven J, Valiente M, Sánchez-Martínez M, Bosch-Barrera J, Menendez JA. ***Silibinin is a direct inhibitor of STAT3***. Food Chem Toxicol. 2018;116(Pt B):161-172. doi: 10.1016/j.fct.2018.04.028. **Impact factor: 3,775 (Q1)**

Other scientific publications derived from this thesis (**Appendix I**):

Verdura S, Cuyàs E, Ruiz-Torres V, Micol V, Joven J, Bosch-Barrera J, Menendez JA. ***Lung Cancer Management with Silibinin: A Historical and Translational Perspective***. Pharmaceuticals (Basel). 2021;14(6):559. doi: 10.3390/ph14060559. **Impact factor: 5,215 (Q1)**

LIST OF ABBREVIATIONS

Abbreviation	Meaning
ABC	ATP-binding Cassette
ACTH	Adrenocorticotropic Hormone
ACVRL1	Activin A Receptor Like Type 1
AJCC	American Joint Committee on Cancer
AKT	Protein Kinase B
ALK	Anaplastic Lymphoma Kinase
ALK1	Activin-Like Kinase 1
ALK-TKI	Anaplastic Lymphoma Kinase Tyrosine Kinase Inhibitor
ATM	Ataxia Telangiectasia Mutated
ATP	Adenosine Triphosphate
AXL	AXL Receptor Tyrosine Kinase
BBB	Blood-Brain Barrier
Bcl-2	B-cell lymphoma 2
bHLH	Basic Helix-Loop-Helix
BIBF 1120	Nintedanib or angiokinase inhibitor
BMP	Bone Morphogenetic Protein
BMPR	Bone Morphogenic Protein Receptor
BMPR2	Bone Morphogenic Protein Receptor Type 2
BRAF	B-Raf Proto-Oncogene
CCND1	Cyclin D1
CDKis	Cyclin-dependent kinases inhibitors
CDKN2A	Cyclin-Dependent Kinase Inhibitor 2A
cKIT	Tyrosine-protein Kinase Kit
CNS	Central nervous system
COX2	Cyclooxygenase-2

CRISPR	Clustered Regularly Interspaced Short Palindromic Repeats
CREBBP	CREB binding protein
CSC	Cancer Stem Cells
$CSMD_3$	CUB And Sushi Multiple Domains 3
CT	Computed Tomography
CTCs	Circulating Tumor Cells
CT	Computed Tomography
CTCs	Circulating Tumor Cells
CTD	C-Terminal Domain
CYP_3A_4	Cytochrome P450 3A4
DBD	DNA-Binding Domain
DDR2	Discoidin Domain Receptor Tyrosine Kinase 2
DNA	Deoxyribonucleic acid
ECs	Endothelial cells
ECM	Extracellular Matrix
EGFR	Epidermal Growth Factor Receptor
EMT	Epithelial-to-Mesenchymal Transition
EML4	Echinoderm Microtubule-associated Protein-like 4
EPHA1	Ephrin Type-A Receptor 1
ERBB2	Erythroblastic leukemia viral oncogene homologue receptor 2
FDA	U.S. Food and Drug Administration
FGFR	Fibroblast Growth Factor Receptor
FLT-3	Fms-Like Tyrosine Kinase 3
GFP	Green Fluorescent Protein
GFPT2	Glutamine Fructose-6-Phosphate Aminotransferase 2
GR	Glucocorticoid Receptor
GST	Glutathione S-transferase
HDAC	Histone Deacetylase

HDL	High-Density Lipoprotein
HER2	Human Epidermal Growth Factor Receptor 2
HER3	Human Epidermal Growth Factor Receptor 3
HSP90	Heat-shock Protein 90
HR	Homologous recombination
ICIs	Immune Checkpoint Inhibitors
ID	Inhibitors of DNA-binding/differentiation
ID1	Inhibitor of DNA-binding/differentiation 1
ID3	Inhibitor of DNA-binding/differentiation 3
IGF-1	Insulin-like Growth Factor 1
IGF1R	Insulin-Like Growth Factor 1 Receptor
IL-1β	Interleukin-1 beta
IL-6	Interleukin-6
JAK1	Janus Kinase 1
JAK2	Janus Kinase 2
KIT	KIT Proto-Oncogene Receptor Tyrosine Kinase
KEAP1	Kelch-like ECH-associated 1
KRAS	Kirsten Rat Sarcoma Viral Oncogene
LC	Lung Cancer
LCC	Large Cell Carcinoma
LDL	Low-Density Lipoprotein
LRP1B	LDL Receptor Related Protein 1B
LUAD	Lung Adenocarcinoma
LUME-Lung 1	A clinical trial name
LUSC	Lung Squamous Cell Carcinoma
MAPK	Mitogen-Activated Protein Kinase
MET	Mesenchymal-to- Epithelial Transition
METPlatform	Medium-Throughput Drug-Screening Platform

MHC	Major histocompatibility complex
miRNA	MicroRNA
MMP-2	Matrix Metalloproteinase-2
MMPs	Matrix Metalloproteinases
MRI	Magnetic Resonance Imaging
MS	Mass Spectrometry
mTOR	Mammalian Target of Rapamycin
N-cadherin	Neural Cadherin
NER	Nucleotide excision repair
NF1	Neurofibromatosis type 1
NFE2L2	Nuclear factor erythroid 2-related factor 2 encoding gene
NF-κB	Nuclear Factor-kappa B
NOTCH1	Neurogenic locus notch homolog 1
NTRK1-3	Neurotrophic Tyrosine Receptor Kinase 1-3
NSCLC	Non-Small Cell Lung Cancer
ORR	Objective Response Rate
PD-1	Programmed Cell Death Protein 1
PDGFR	Platelet-Derived Growth Factor Receptor
PD-L1	Programmed Death-Ligand 1
PET	Positron Emission Tomography
PFS	Progression-free survival
P-gp	P-glycoprotein
PI3K	Phosphoinositide 3-Kinase
PIK3CA	Phosphatidylinositol-4,5-Bisphosphate 3-Kinase Catalytic Subunit Alpha
pK	Acid Dissociation Constant
PS	Performance Status
PTEN	Phosphatase and tensin homolog

qRT-PCR	Quantitative Reverse Transcription Polymerase Chain Reaction
R	Receptor
RA	Reactive Astrocytes
RB1	Retinoblasotoma 1
RET	Rearranged During Transfection
RNA	Ribonucleic Acid
ROS	Reactive Oxygen Species
ROS1	ROS Proto-Oncogene 1
RTKs	Receptor tyrosine kinases
SAR	Structural-Activity Relationship
SBE	SMAD Binding Element
SBRT	Stereotactic Body Radiation Therapy
SCLC	Small-Cell Lung Cancer
SH2	Src Homology 2
siRNA	Small Interfering RNA
SMAD	Small Mothers Against Decapentaplegic
SOX2	Sex-Determining Region Y-Box 2
SRC	Proto-Oncogene Tyrosine-Protein Kinase Src
SRS	Stereotactic Radiosurgery
$STAT_3$	Signal Transducer and Activator of Transcription 3
$STAT_3$is	$STAT_3$ Inhibitors
STK11	Serine/threonine kinase 11
TFs	Transcription Factors
TGF-β	Transforming Growth Factor-beta
TGFβR	Transforming Growth Factor-beta Receptor
TIMP-2	Tissue Inhibitor of Metalloproteinase-2
TKIs	Tyrosine Kinase Inhibitors

TMB	Tumor Mutational Burden
TME	Tumor Microenvironment
TNM	Tumor-Node-Metastasis
TP53	Tumoral protein 53
TR-FRET	Time-Resolved Fluorescence Energy Transfer
TWIST1	Twist Family BHLH Transcription Factor 1
UHPLC-ESI-QTOF-MS/	Ultra-High Pressure Liquid Chromatography Electrospray Ionization Quadrupole Time-of-Flight Mass Spectrometry
USA	United States of America
VEGF	Vascular Endothelial Growth Factor
VEGFR	Vascular Endothelial Growth Factor Receptor
WBRT	Whole-Brain Radiotherapy
WHO	World Health Organization
WNT	Wingless-Related Integration Site
Y705	Tyrosine 705
ZEB1	Zinc Finger E-Box Binding Homeobox 1

INDEX OF FIGURES

INDEX OF TABLES

INDEX OF CONTENTS

SUMMARY

Locally advanced and metastatic non-small cell lung cancer (NSCLC) is a therapeutically challenging disease. Despite several decades of improved clinical progress, there is an unmet need to investigate the emergence of therapeutic resistance across the spectrum of NSCLC molecular subtypes. In particular, management strategies to combat refractoriness to targeted therapies such as EGFR and ALK tyrosine kinase inhibitors (TKIs) represent an important challenge at hand. The incidence of NSCLC-associated brain metastases is expected to increase due to improved diagnostic accuracy, but more importantly due to the increasing number of systemic therapies that are successful extra-cranially but fail to provide therapeutic benefit in the brain. The study of brain metastases may reveal new targets and identify novel approaches to address the dismal prognosis and limited therapeutic options of NSCLC patients with brain metastases. Here, we report that the natural phytochemical silibinin –the bioactive flavonolignan of the silymarin extract obtained from the seeds of the milk thistle plant *Silybum marianum* (L.) – is a versatile therapeutic agent for the treatment of advanced stage NSCLC.

Commonly used as a hepatoprotective agent, silibinin is beginning to be considered as a chemopreventive and therapeutic biomolecule for cancer diseases. Based on molecular pharmacology and cancer biology, this study aimed to provide an in-depth, comprehensive exploration of the effects of silibinin in NSCLC therapeutic resistance and brain metastatic progression. This study hypothesized that the multi-target behavior of silibinin, a plausible consequence of the molecular promiscuity of natural phytochemicals, provides an opportunity to globally affect the multifactorial mechanisms underlying the biological aggressiveness of NSCLC, including therapeutic resistance and the ability to metastasize to the brain. We applied a modern phenotypic drug discovery approach to molecularly deconstruct and functionally monitor the *on-target* polypharmacology of silibinin that may underlie its therapeutic benefits against NSCLC therapeutic resistance and metastatic dissemination capacity.

Our study has four objectives: 1.) To elucidate the molecular mechanisms by which silibinin may reduce the brain tropism capacity of metastatic NSCLC cells in the primary tumor and/or in the brain microenvironment; 2.) to elucidate how silibinin

prevents the generation of NSCLC cell populations that are refractory to anti-brain metastatic ALK-TKIs and anti-angiogenic multi-TKIs; 3.) to elucidate whether the well-established hepatoprotective properties of silibinin can prevent the hyperlipidemic side effects of certain anti-brain metastasis ALK-TKIs; and 4.) to characterize the mechanism of action of silibinin against well-established tumor cell intrinsic (HSP90) and microenvironmental (STAT3) drivers of NSCLC brain metastasis.

First, we investigated the regulatory effects of silibinin on metastasis-initiating transcription factors such as the inhibitor of DNA-binding/differentiation 3 (ID3), which enhances metastasis-initiation and immune-escape properties at the primary tumor site as well as at the blood-brain barrier (BBB) extravasation sites. Silibinin suppressed ID3 expression in tumor cells and brain endothelial cells through transcriptional repression mediated by bone morphogenetic protein (BMP)-responsive elements and by directly inhibiting the kinase activity of the BMP receptors ACVRL1/ALK1 and BMPR2. Second, we evaluated the ability of silibinin to overcome a variety of molecular mechanisms underlying NSCLC resistance to targeted therapies. On the one hand, we determined the ability of silibinin to resensitize mesenchymal NSCLC cells to multi-generation ALK tyrosine kinase inhibitors (ALK-TKIs) by directly targeting the epithelial-to-mesenchymal (EMT)-promoting TGFβ/SMAD signaling axis. On the other hand, we observed how silibinin enhances the cytotoxic activity of the anti-angiogenic multi-TKI nintedanib against NSCLC cells by interfering with STAT3 hyperactivation and nintedanib sequestration in lysosomal "drug safe houses". Accordingly, a silibinin-containing nutraceutical was found to enhance the clinical activity of the nintedanib/docetaxel regimen in NSCLC patients. Third, we investigated whether the well-established hepatoprotective role of silibinin could prevent the undesirable hyperlipidemic effects of the brain metastasis-targeted, third-generation ALK-TKI lorlatinib. Silibinin was found to protect human hepatocytes from lorlatinib-induced dysregulated lipid metabolism and the consequent accumulation of triglycerides/cholesterol. Fourth, we investigated the ability of silibinin to directly interact with key molecular determinants of the colonization and growth of metastastic NSCLC cells in the brain microenvironment. On the one hand, silibinin was found to act as a novobiocin-like C-terminal inhibitor of the molecular chaperone HSP90, a cell-intrinsic driver of brain metastastic NSCLC cell aggressiveness. On the other hand,

silibinin was found to act as a dual-mode inhibitor of the transcriptional activity of $STAT_3$, a key target to drive the phenotype of reactive astrocytes that are required to enable colonization and adaptation of disseminated NSCLC cells to the brain microenvironment.

Our study has concluded that the molecular promiscuity of silibinin to target multi-factorial mechanisms underlying the biological aggressiveness of NSCLC tumors, including those that drive therapeutic resistance and the ability to metastasize and colonize the brain, can be exploited to develop novel prevention and treatment strategies for NSCLC. The polypharmacology of the phytochemical silibinin, a flavonolignan derived from the milk thistle plant, may be a valuable strategy in the nutraceutical treatment of NSCLC using clinically relevant formulations of silibinin. This study suggests that lessons learned from the natural chemistry of silibinin could be a guide for the development of next-generation silibinin derivatives with improved therapeutic activities against NSCLC.

RESUM

El càncer de pulmó no microcític (CPNM) localment avançat i metàstasic és una malaltia terapèuticament difícil. Malgrat diverses dècades de millores clíniques, existeix la necessitat d'investigar l'aparició de fenòmens de resistència al tractament farmacològic en l'espectre dels subtipus moleculars de CPNM. Un dels reptes és combatre la resistència a teràpies dirigides com els inhibidors de la tirosina quinasa (TKI) EGFR i ALK. Es preveu que la incidència de les metàstasis cerebrals associades al CPNM augmenti a causa de la millora de la precisió diagnòstica, però sobretot a causa del creixent nombre de teràpies sistèmiques que, sent efectives extracranialment, no aconsegueixen proporcionar beneficis terapèutics en el cervell. Un altre dels reptes pendents és identificar nous abordatges al pèssim pronòstic i les limitades opcions terapèutiques dels pacients amb CPNM amb metàstasis cerebrals. En aquest treball es descriu el fitoquímic natural silibinina –el flavonolignà bioactiu de l'extracte de silimarina obtingut de les llavors de la planta de card marià Silybum marianum (L.)– com un agent terapèutic versàtil per al tractament del CPNM en estadi avançat.

Utilitzada habitualment com un agent hepatoprotector, la silibinina és una biomolècula amb efectes quimiopreventius i terapèutics en el càncer. Aquest estudi, basat en la farmacologia molecular del càncer, ha tingut com a objectiu explorar exhaustivament els efectes de la silibinina en la resistència terapèutica del CPNM i la progressió metastàsica cerebral. La hipòtesi del nostre estudi és que el comportament multi-diana de la silibinina, una conseqüència esperable de la promiscuïtat molecular dels fitoquímics naturals, ofereix l'oportunitat de modular globalment els mecanismes multifactorials que subjauen a l'agressivitat biològica del CPNM, inclosa la resistència terapèutica i la capacitat de metastatizar al cervell. Mitjançant l'aplicació d'un enfocament de descobriment fenotípic de fàrmacs, hem de-construït molecularment i monitoritzat funcionalment la polifarmacología que subjau als seus beneficis terapèutics de la silibinina contra la resistència terapèutica i la capacitat de disseminació metastàsica del CPNM. L'estudi té quatre objectius: 1.) Establir els mecanismes moleculars pels quals la silibinina redueix la capacitat de tropisme cerebral de les cèl·lules metastàsiques del CPNM en el tumor primari i/o en el microambient cerebral; 2.) dilucidar com la silibinina preveu la generació de poblacions cel·lulars de

CPNM resistents a TKIs amb activitat anti-metastàtica cerebral i anti-angiogènica; 3.) avaluar si les propietats hepatoprotectors de la silibinina poden prevenir els efectes secundaris hiperlipidèmics d'uns certs ALK-TKI; i 4.) caracteritzar el mecanisme d'acció de la silibinina contra promotors moleculars intrínsecs (HSP90) i microambientals (STAT3) de la metàstasi cerebral del CPNM.

En primer lloc, vam investigar els efectes reguladors de la silibinina sobre factors de transcripció com l'inhibidor de la unió a l'ADN/diferenciació 3 (ID3), el qual potencia la iniciació de metàstasi i les propietats de fuita immunitària en el tumor primari, així com en els llocs d'extravasació de la barrera hematoencefàlica. La silibinina va suprimir l'expressió d'ID3 en cèl·lules tumorals i cèl·lules endotelials cerebrals a través d'un mecanisme de repressió transcripcional mediada per elements que responen a proteïnes morfogèniques òssies (BMPs) i mitjançant la inhibició directa de l'activitat quiinasa dels receptors BMP ACVRL1/ALK1 i BMPR2. En segon lloc, vam avaluar la capacitat de la silibinina per a suprimir mecanismes moleculars subjacents a la resistència del CPNM a teràpies dirigides. D'una banda, vam determinar la capacitat de la silibinina per a re-sensibilitzar cèl·lules mesenquimals de CPNM resistents a inhibidors de la tirosina quinasa ALK mitjançant la inhibició de l'eix de senyalització TGFβ/SMAD i la transició epiteli-mesènquima (EMT). D'altra banda, vam observar com la silibinina potència l'activitat citotòxica de nintedanib –un multi-TKI amb activitat antiangiogènica– en interferir amb la hiperactivació d'STAT3 i el segrest de nintedanib en "refugis de fàrmacs" lisosòmics. Un nutracèutic oral que conté silibinina va potenciar l'activitat clínica del règim nintedanib/docetaxel en pacients amb CPNM. En tercer lloc, vam investigar si la funció hepatoprotectora de la silibinina podria prevenir els efectes hiperlipidèmics indesitjables del lorlatinib, un ALK-TKI de tercera generació dirigit a les metàstasis cerebrals. La silibinina protegeix els hepatòcits humans de la desregulació del metabolisme lipídic induïda pel lorlatinib i la conseqüent acumulació de triglicèrids/colesterol. En quart lloc, vam investigar la capacitat de la silibinina per a interactuar directament amb determinants moleculars de la colonització i el creixement de cèl·lules metastàsiques del CPNM en el microambient cerebral. D'una banda, es va descobrir que la silibinina actua com un inhibidor del domini C-terminal de la xaperona molecular HSP90, un determinant intrínsec de l'agressivitat de les cèl·lules metastàsiques cerebrals. D'altra banda, es va descobrir que la silibinina actua com un

inhibidor dual de l'activitat transcripcional d'STAT3, un determinant de la funcionalitat dels astròcits reactius que permeten la colonització i adaptació de les cèl·lules metastàsiques disseminades en el microambient cerebral.

El nostre estudi ha conclòs que la promiscuïtat molecular de la silibinina contra els mecanismes multifactorials subjacents a l'agressivitat biològica dels tumors de CPNM, inclosos els responsables de resistència terapèutica i la capacitat de metastatizar i colonitzar el cervell, pot ser aprofitada per al desenvolupament de noves estratègies de prevenció i tractament del CPNM. La polifarmacología de la silibinina pot ser una estratègia valuosa en el tractament nutracèutic del CPNM. Les lliçons apreses de la química natural de la silibinina podrien servir de guia per al desenvolupament de derivats de silibinina de nova generació amb activitats terapèutiques millorades contra el CPNM.

RESUMEN

El cáncer de pulmón no microcítico (CPNM) localmente avanzado y metastásico es una enfermedad terapéuticamente difícil. A pesar de varias décadas de mejoras clínicas, existe la necesidad de investigar la aparición de fenómenos de resistencia al tratamiento farmacológico en el espectro de subtipos moleculares de CPNM. Uno de los retos es combatir la resistencia a terapias dirigidas como los inhibidores de la tirosina quinasa (TKI) EGFR y ALK. Se prevé que la incidencia de las metástasis cerebrales asociadas al CPNM aumente debido a la mejora de la precisión diagnóstica, pero sobre todo debido al creciente número de terapias sistémicas que, siendo efectivas extracranealmente, no consiguen proporcionar beneficios terapéuticos en el cerebro. Otro de los retos pendientes es identificar abordajes novedosos al pésimo pronóstico y las limitadas opciones terapéuticas de los pacientes con CPNM con metástasis cerebrales. En este trabajo se describe el fitoquímico natural silibinina –el flavonolignano bioactivo del extracto de silimarina obtenido de las semillas de la planta de cardo mariano *Silybum marianum* (L.)– como un agente terapéutico versátil para el tratamiento del CPNM en estadio avanzado.

Utilizada habitualmente como un agente hepatoprotector, la silibinina es una biomolécula con efectos quimiopreventivos y terapéuticos en el cáncer. Este estudio, basado en la farmacología molecular del cáncer, ha tenido como objetivo explorar exhaustivamente los efectos de la silibinina en la resistencia terapéutica del CPNM y la progresión metastásica cerebral. La hipótesis de nuestro estudio es que el comportamiento multi-diana de la silibinina, una consecuencia esperable de la promiscuidad molecular de los fitoquímicos naturales, ofrece la oportunidad de modular globalmente los mecanismos multifactoriales que subyacen a la agresividad biológica del CPNM, incluida la resistencia terapéutica y la capacidad de metastatizar al cerebro. Mediante la aplicación de un enfoque de descubrimiento fenotípico de fármacos, hemos de-construido molecularmente y monitorizado funcionalmente la polifarmacología que subyace a sus beneficios terapéuticos de la silibinina contra la resistencia terapéutica y la capacidad de diseminación metastásica del CPNM.

El estudio tiene cuatro objetivos: 1.) Establecer los mecanismos moleculares por los que la silibinina reduce la capacidad de tropismo cerebral de las células metastásicas de CPNM en el tumor primario y/o en el microambiente cerebral; 2.) dilucidar cómo la silibinina previene la generación de poblaciones celulares de CPNM resistentes a TKIs con actividad anti-metastática cerebral y anti-angiogénica; 3.) evaluar si las propiedades hepatoprotectoras de la silibinina pueden prevenir los efectos secundarios hiperlipidémicos de ciertos ALK-TKI; y 4.) caracterizar el mecanismo de acción de la silibinina contra promotores moleculares intrínsecos (HSP90) y microambientales (STAT3) de la metástasis cerebral del CPNM.

En primer lugar, investigamos los efectos reguladores de la silibinina sobre factores de transcripción como el inhibidor de la unión al ADN/diferenciación 3 (ID3), el cual potencia la iniciación de metástasis y las propiedades de escape inmunitario en el tumor primario, así como en los lugares de extravasación de la barrera hematoencefálica. La silibinina suprimió la expresión de ID3 en células tumorales y células endoteliales cerebrales a través de un mecanismo de represión transcripcional mediada por elementos que responden a proteínas morfogénicas óseas (BMPs) y mediante la inhibición directa de la actividad quinasa de los receptores BMP ACVRL1/ALK1 y BMPR2. En segundo lugar, evaluamos la capacidad de la silibinina para suprimir mecanismos moleculares subyacentes a la resistencia del CPNM a terapias dirigidas. Por un lado, determinamos la capacidad de la silibinina para re-sensibilizar células mesenquimales de CPNM resistentes a inhibidores de la tirosina quinasa ALK mediante la inhibición del eje de señalización TGFβ/SMAD y la transición epitelio-mesénquima (EMT). Por otra parte, hemos observado cómo la silibinina potencia la actividad citotóxica de nintedanib –un multi-TKI con actividad antiangiogénica– al interferir con la hiperactivación de STAT3 y el secuestro de nintedanib en "refugios de fármacos" lisosomales. Un nutracéutico oral que contiene silibinina potenció la actividad clínica del régimen nintedanib/docetaxel en pacientes con CPNM. En tercer lugar, investigamos si la función hepatoprotectora de la silibinina podría prevenir los efectos hiperlipidémicos indeseables del lorlatinib, un ALK-TKI de tercera generación dirigido a las metástasis cerebrales. La silibinina protege a los hepatocitos humanos de la desregulación del metabolismo lipídico inducida por el lorlatinib y la consiguiente acumulación de triglicéridos/colesterol. En cuarto lugar, investigamos la capacidad de

la silibinina para interactuar directamente con determinantes moleculares de la colonización y el crecimiento de células metastásicas de CPNM en el microambiente cerebral. Por un lado, se descubrió que la silibinina actúa como un inhibidor del dominio C-terminal de la chaperona molecular HSP90, un determinante intrínseco de la agresividad de las células metastásicas cerebrales. Por otra parte, se descubrió que la silibinina actúa como un inhibidor dual de la actividad transcripcional de $STAT_3$, un determinante de la funcionalidad de los astrocitos reactivos que permiten la colonización y adaptación de las células metastásicas diseminadas en el microambiente cerebral.

Nuestro estudio ha concluido que la promiscuidad molecular de la silibinina contra los mecanismos multifactoriales subyacentes a la agresividad biológica de los tumores CPNM, incluidos los responsables de resistencia terapéutica y la capacidad de metastatizar y colonizar el cerebro, puede ser aprovechada para el desarrollo de nuevas estrategias de prevención y tratamiento del CPNM. La polifarmacología de la silibinina puede ser una estrategia valiosa en el tratamiento nutracéutico del CPNM. Las lecciones aprendidas de la química natural de la silibinina podrían servir de guía para el desarrollo de derivados de silibinina de nueva generación con actividades terapéuticas mejoradas contra el CPNM.

I. INTRODUCTION

1. LUNG CANCER

According to the World Health Organization (WHO), lung cancer (LC) or lung carcinoma, arises as a result of progressive pathological changes and uncontrolled growth of epithelial cells in the lung parenchyma or within the bronchi, forming tumors that can interfere with the proper functioning of the lungs (Siddiqui et al., 2023). As LC tumors progress, they can acquire the ability to spread to different regions within the respiratory system and even beyond, invading distant organs and tissues throughout the entire body (Xie et al., 2022).

1.1. EPIDEMIOLOGY AND RISK FACTORS OF LUNG CANCER

With an estimated 2.2 million new cases (11.4%) and 1.8 million deaths (18%) in 2020, LC is one of the most commonly diagnosed cancers and the leading cause of cancer-related deaths worldwide (Siegel et al., 2023)(**Figure 1**), thereby representing a significant global health challenge (Sung et al., 2021).

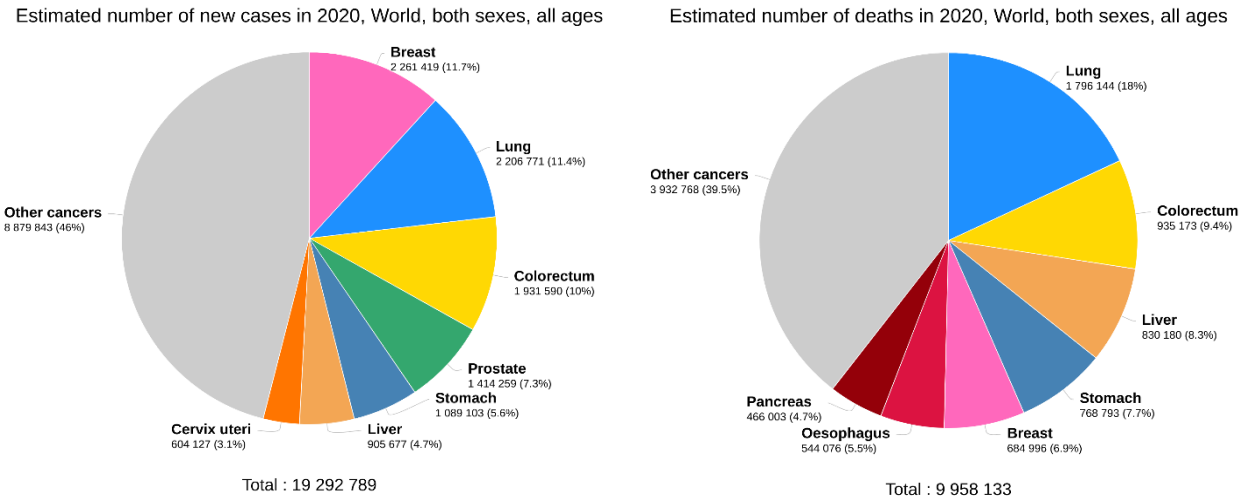

Figure 1. Estimated number of new cases (*left*) **and deaths** (*right*) **by cancer type worldwide in 2020.** Adapted from GLOBOCAN (https://gco.iarc.fr/)

The complex epidemiology of LC includes numerous factors that contribute to its occurrence, with smoking –both active and passive– being the primary risk factor (Alberg & Samet, 2003). While approximately 80-90% of LC cases are related to smoking, a significant 10-20% occur in non-smokers. The development of LC in non-

smokers is often due to a combination of genetic factors and exposure to environmental carcinogens such as asbestos, radon gas, and other forms of pollution. Lung diseases such as idiopathic pulmonary fibrosis or respiratory infections also increase the risk of LC independent of smoking (Charles S. Dela Cruz et al., 2011; Siddiqui et al., 2023).

The global burden of LC has increased significantly over the years. While it was a rare disease at the beginning of the 20th century, its later widespread occurrence is mainly due to increasing smoking rates (Alberg & Samet, 2003; Gouvinhas et al., 2018). The incidence and mortality of LC vary between regions and populations. In countries with higher incomes, rates are often lower (and declining) with better outcomes as a result of reduced tobacco consumption, strong tobacco control policies, improved air quality standards, advanced access to medical care, and healthy living (Leiter et al., 2023).

LC affects both men and women, but historically men have had and continue to have higher incidence rates **(Figure 2)**. However, the disparity is narrowing due to changing smoking patterns and increased tobacco use among women (Bade & Dela Cruz, 2020; Meza et al., 2015; Siddiqui et al., 2023). In addition, the incidence of LC is strongly associated with age, as approximately 40% of LCs are diagnosed at age 75 years or older (Coakley & Popat, 2020).

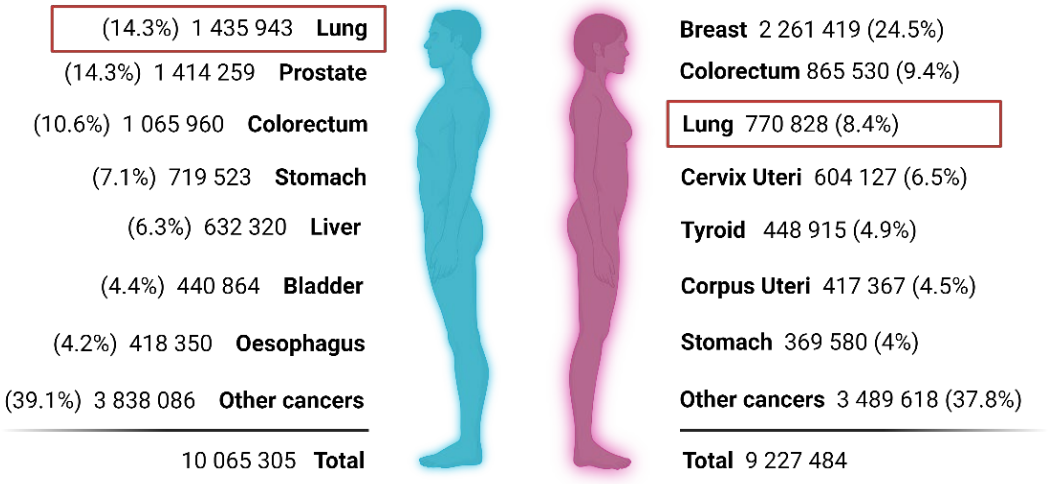

Figure 2. Global incidence of lung cancer by gender in 2020. Created with BioRender.com using GLOBOCAN data (https://gco.iarc.fr/)

Survival rates for LC depend on several factors including stage at diagnosis, age and general health, and how well the treatment plan works (T. Lu et al., 2019). Despite major advances in the diagnosis and treatment in recent decades, the 5-year relative survival rate remains very low (15% in Europe, 23% in the USA), making it one of the deadliest cancers (Leiter et al., 2023). Nevertheless, survival rates range from 65% for localized tumors (within the lung) to 9% for metastatic disease according to data from the American Society of Clinical Oncology (ASCO).

After colorectal, prostate and breast cancer, LC is the fourth most commonly diagnosed cancer in Spain. The 5-year survival rates from 2008 to 2013 were reported to be 12.7% for men and 17.6% for women. Notably, in 2017, LC emerged as the leading cause of cancer-related death in Spain for both sexes, accounting for 19.5% of cancer mortality (Remon et al., 2021).

Efforts to reduce the impact of LC include public health initiatives focused on smoking cessation, tobacco controlling policies, and increased awareness of environmental and occupational dangers (Leiter et al., 2023). Nevertheless, several obstacles remain in the fight against LC, such as late diagnosis of the disease, ineffective treatment options and the emergence of drug resistance, all of which exacerbate the unfavorable prognosis for those affected. Therefore, this multifaceted disease requires continued research and comprehensive strategies, not only in smoking cessation or addressing environmental risk factors but also in improving early detection, knowledge of disease-related mechanisms, and discovery and development of new therapies to reduce its impact on global health (Bade & Dela Cruz, 2020; Gouvinhas et al., 2018).

1.2. HISTOPATHOLOGICAL AND MOLECULAR FEATURES OF LUNG CANCER

1.2.1. Histopathology of Lung Cancer

LC is a heterogeneous disease characterized by a variety of clinicopathologic features. According to histopathological characterization, LC has been broadly classified into two major types, namely small cell lung cancer (SCLC) and non-small cell lung cancer (NSCLC) (**Figure 3**). SCLC, which accounts for 15-20% of LC cases, arises in the central airways and is thought to originate from neuroendocrine cells. In addition, SCLC is

characterized by rapid growth, a high propensity to metastasize, and poor survival rates, and is associated with heavy smoking (Gazdar et al., 2017; Thai et al., 2021). NSCLC accounts for the remaining 80–85% and is typically classified into three histologic subtypes: adenocarcinoma (LUAD), squamous cell carcinoma (LUSC), and large cell carcinoma (LCC) (Thai et al., 2021).

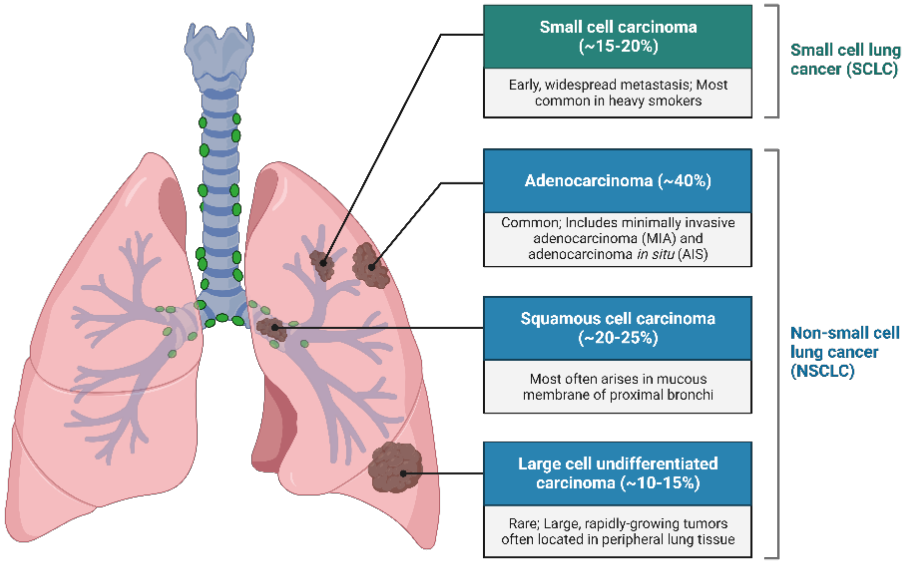

Figure 3: Histological classification of Lung Cancer. Created with BioRender.com

LUAD is the most common subtype (40% of LC) and occurs predominantly in patients who have never smoked. In contrast, LUSC (20% of LC) and LCC (10% of LC) are rarely unrelated to smoking history. While LUAD typically arises from glandular epithelium within the lung periphery, LUSC arise primarily in the central airways and segmental bronchi. LCC are poorly differentiated tumors and can arise anywhere in the lung, with a tendency to be located in the periphery (Thandra et al., 2021; Xie et al., 2022). Notably, the incidence of LUSC, previously the most common histologic type, has decreased significantly. This is partly due to lower smoking rates in high-income countries and changes in the composition of cigarettes (Alberg et al., 2013).

1.2.2. Lung cancer mutational landscape

Genomic studies have revealed a complex molecular profile of LC, with many oncogenes and tumor suppressor genes significantly altered across histologic subtypes

(Seidel et al., 2013). NSCLC is a highly mutated form of cancer, particularly LUAD and LUSC, which are among the top three malignancies with a significant burden of somatic genetic alterations **(Figure 4)**.

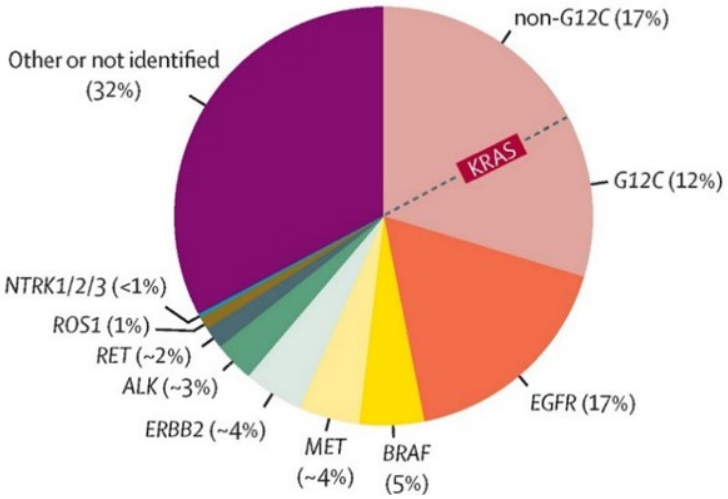

Figure 4. Mutational profile of NSCLC: frequencies of common oncogenic driver mutations. Adapted from Thai et al.,2021.

Although there are significant genomic differences between these two NSCLC subsets, certain similarities can be observed (Alexandrov et al., 2013). Notably, *TP53*, *LRP1B*, and *CSMD3* are tumor suppressor genes that are frequently mutated in all three major lung cancer subtypes. *TP53* undergoes inactivating mutations and is the most frequently mutated gene in LC with approximately 50% of LUAD and 80% of LUSC (Collisson et al., 2014; Hammerman et al., 2012). Other mutated tumor suppressor genes of interest include *STK11* in LUAD, *RB1* and *CREBBP* in SCLC, *NOTCH1* and *PTEN* in both SCLC and LUSC, and *NF1* and *KEAP1/NFE2L2* in both LUAD and LUSC (Alexandrov et al., 2013; George et al., 2015; Lockwood et al., 2012).

In LUAD cases, there are commonly identified driver oncogenes harboring activating mutations that are routinely evaluated in the clinic to take advantage of targeted therapies (Shi et al., 2016). These mutations activate tyrosine kinase receptors or downstream signaling molecules. *KRAS* is the most commonly mutated driver gene in Western populations (approximately 30%), with mutations mainly found in codons 12 and 13 (Karachaliou et al., 2013). *EGFR* is the second most frequently mutated driver gene in LUAD (10-15%). Common mutations in *EGFR* include deletions in exon 19 and point mutations in exon 21 (Kawada & Soejima, 2008; Mitsudomi & Yatabe, 2010). Less

common activating mutations in the *ERBB2*, *MET*, and *BRAF* genes are detected in approximately 4% of LUAD cases (Frampton et al., 2015; Tissot et al., 2016). Driver gene activation can also occur through gene rearrangements. For example, a fusion involving *ALK*, a gene not typically expressed in the lung, often occurs with *EML4* and is found in 3-8% of LUAD patients (X. Du et al., 2018). Other gene rearrangements include *ROS1*, *RET*, and *NTRK1-3*, albeit at lower frequencies (Takeuchi et al., 2012).

LUSC patients rarely have targetable activating genetic mutations in driver genes. Rather, they often have chromosomal copy number alterations in genes such as *SOX2*, *FGFR1*, *CCND1*, *CDKN2A*, and *EGFR*. While point mutations in *CDKN2A* and *PIK3CA* occur in about 15% of cases, alterations in the tyrosine kinase receptor genes *DDR2* and *FGFR3* are observed at lower rates (Hammerman et al., 2012; Seidel et al., 2013). LCC possesses complex genomic signatures, exhibiting a mix of LUAD, SCC, and SCLC characteristics (Seidel et al., 2013).

The identification of LC molecular subtypes based on specific oncogenic drivers has changed the natural history of the disease. For example, less than 20 years have elapsed from the identification of genetic alterations in *EGFR* and *ALK* kinases to the remarkable clinical improvement achieved in patients with *EGFR*-mutant or *ALK*-rearranged LC with various generations of EGFR and ALK tyrosine kinase inhibitor (TKIs) (Chan & Hughes, 2015; Halliday et al., 2019; Thomas et al., 2012).

1.3. DIAGNOSIS, STAGING, AND PROGNOSIS OF LUNG CANCER

Most cases of LC are diagnosed in advanced stages, leading to lower survival rates and higher symptom burden (Coakley & Popat, 2020; Mithoowani & Febbraro, 2022). While a small percentage of patients with LC are asymptomatic, most patients present with symptoms at the time of diagnosis. Some of the symptoms presented may be non-specific, such as fatigue, anorexia, or weight loss, while others are specifically related to the primary tumor or its spread, either within or beyond the thoracic region. Persistent cough, dyspnea, or coughing up blood are common manifestations of a primary tumor while chest pain, superior vena cava obstruction, or pleural effusion are more commonly associated with intrathoracic spread. Approximately 30% of individuals diagnosed with LC have evidence of metastases outside the thoracic region, most commonly in the bones, liver, brain, and lymph nodes. As a result, these patients

experience symptoms such as headache, bone pain, nausea, or vomiting (Collins et al., 2007).

Patients with respiratory symptoms undergo imaging tests, including chest x-rays or computed tomography (CT) scans. If a suspicious lung lesion is detected, a biopsy is performed by bronchoscopy, thoracocentesis, or surgery to obtain a tissue sample for further examination (Planchard et al., 2018; Siddiqui et al., 2023). The biopsy is then analyzed by pathologists to determine the particular histology and molecular profile of the sample (e.g., assessment of *EGFR*, *BRAF*, *ERBB2* and *MET* mutation status, *ALK/ROS1* rearrangements, and PD-L1 expression status), which is critical for treatment decisions (Planchard et al., 2018).

The extent of NSCLC spread is determined by staging, which includes additional imaging with PET or MRI, and is critical for treatment decisions and prognostication. The TNM system (**Table 1**), developed by the American Joint Committee on Cancer (AJCC), is the most commonly used staging system for NSCLC.

Table 1. **TNM staging in NSCLC.** Adapted from Rami-Porta et al., 2011

Tumor (T) Stage:
T0: No evidence of a primary tumor.
Tis (Carcinoma in situ): Abnormal cells are present but haven't invaded surrounding tissues.
T1: A small tumor that is generally 3 cm ol less and hasn't spread to the lymph nodes or adjacent structures.
T2: The tumor may be more than 3 cm but not more than 5 cm larger or may have spread to nearby structures.
T3: The tumor has more than 5 cm but not more than 7 cm or further extended into nearby structures like the chest wall, diaphragm, or other structures within the chest.
T4: The tumor has more than 7 cm or of any size and invaded nearby structures beyond the lungs, such as the heart, esophagus, or large blood vessels.
Node (N) Stage:
N0: No spread to nearby lymph nodes.
N1: Cancer has spread to nearby lymph nodes on the same side of the lung as the primary tumor.
N2: The cancer has spread to lymph nodes within the lung or in the area between the lungs (mediastinum).
N3: Cancer has spread to lymph nodes on the opposite side of the chest or to nodes further from the lungs.
Metastasis (M) Stage:
M0: No distant metastasis; cancer has not spread to other parts of the body.
M1: Cancer has spread to distant organs or tissues, which might include the bones, brain, liver, or other distant areas.

The TNM staging evaluates three primary factors: tumor size and location (T), lymph node involvement (N), and metastasis (M) (Boffa, 2018; Woodard et al., 2016). The combination of the T, N, and M categories results in an overall staging system (**Figure 5**):

Stage 0: Tis, No, Mo–Carcinoma *in situ*

Stage I: T1-2, No, Mo–Localized tumor, limited spread to lymph nodes.

Stage II: T1-2, N1-2, Mo–Tumor growth and spread to nearby lymph nodes

Stage III: T1-3, N2-3, Mo–Extensive spread to lymph nodes

Stage IV: Any T, Any N, M1–Advanced cancer with distant metastasis

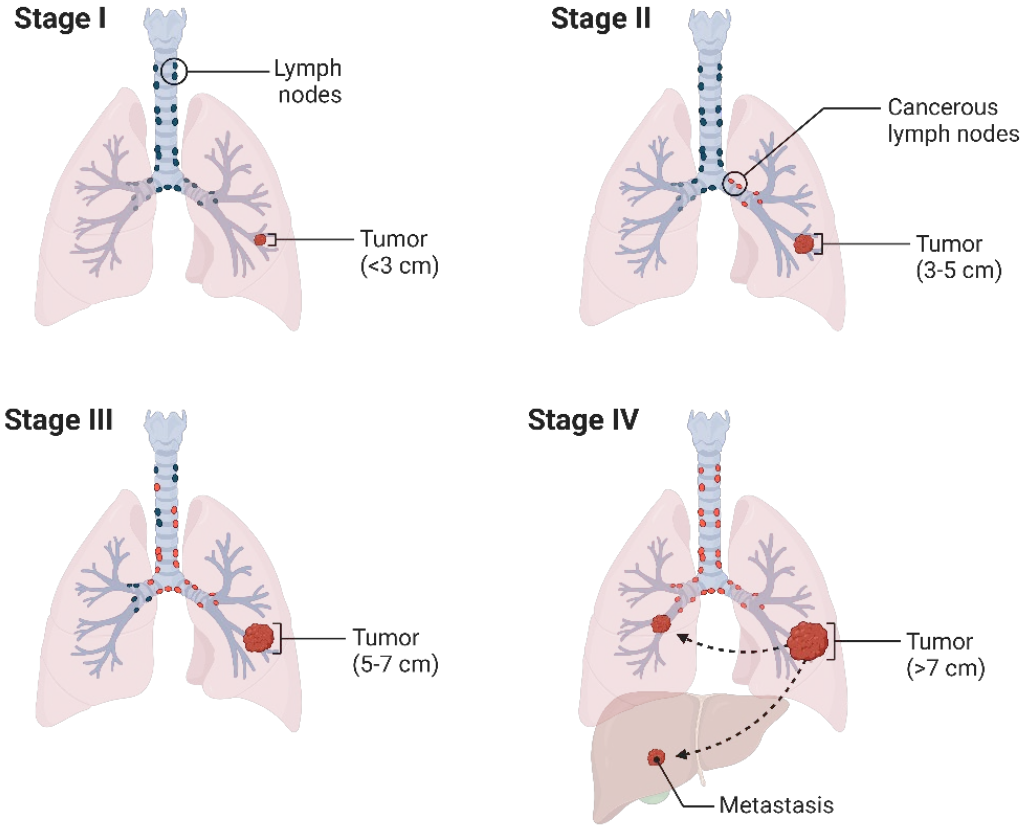

Figure 5: **NSCLC stages.** Created with BioRender.com

In the case of SCLC, the disease is classified as limited-stage if it is confined to the hemithorax or extensive-stage when it extends beyond the hemithorax (Coakley & Popat, 2020; Collins et al., 2007).

Early-stage NSCLC (stages 0 and I) is usually more favorable and can be treated with surgery, while more advanced stages (stages II to IV) have a worse prognosis and

may require a combination of treatments such as chemotherapy, radiation, targeted therapy, immunotherapy, or palliative care to manage symptoms (Woodard et al., 2016). The prognosis for LC varies widely based on factors such as the type of cancer, general health, age, treatment options, and individual response to treatment. It is important to note that prognosis is an estimate, and individual cases may vary. Early detection and treatment often result in better outcomes.

1.4. LUNG CANCER TREATMENT

Multiple treatment options are available to NSCLC patients depending on their histologic subtype, tumor stage, performance status (PS) and specific molecular characteristics. Available treatment options for LC include surgical resection, radiation, chemotherapy, targeted therapy and immunotherapy. It is important to note that while early stage patients are treated for cure, metastatic patients are treated to improve or maintain their quality of life and prolong overall survival (Mithoowani & Febbraro, 2022).

1.4.1. Surgical resection

Surgical removal of the affected lung, such as lobectomy, is considered the standard of care for patients with NSCLC diagnosed with early (stages I, II) and some locally advanced (stage III) disease (McDonald et al., 2017). Although surgery is primarily aimed at curing early-stage patients, recurrence occurs in 30-55% of cases. Therefore, platinum-based adjuvant chemotherapy after surgery is recommended for patients with nodal involvement (stage II and IIIA) and selected stage I disease to improve treatment outcomes. (Pignon et al., 2008). Adjuvant therapy has been shown to increase overall survival and disease-free survival rates by approximately 10% in advanced disease. Postoperative radiotherapy should be considered after incomplete resection or when N2 nodes are involved (Mithoowani & Febbraro, 2022).

1.4.2. Radiotherapy

Radiation therapy is a potential treatment option for early-stage NSCLC patients who cannot undergo surgery due to underlying health conditions (Mithoowani & Febbraro, 2022). Stereotactic body radiation therapy (SBRT), which delivers high-dose fractions

to a small target area, has demonstrated greater efficacy and fewer side effects than conventional fractionated radiotherapy (Vinod & Hau, 2020). For unresectable and locally advanced stage III NSCLC patients, the optimal treatment is a combination of radiotherapy and platinum-based chemotherapy (chemoradiotherapy), which results in a 5% increase in patient survival. However, this treatment also carries a higher risk of toxicity. Sequential chemoradiotherapy is considered for older or less fit patients (Eberhardt et al., 2015). In addition, radiotherapy plays an important role in the palliative care of patients with advanced disease by relieving pain and symptoms associated with bone or brain metastases (Reck et al., 2014).

1.4.3. Chemotherapy

Chemotherapy has traditionally been the standard of care for patients with LC, especially in advanced stages (some III and IV), when surgery is not feasible or when the cancer has spread (Baxevanos & Mountzios, 2018). Chemotherapy remains the first-line option for patients who cannot receive targeted therapies or immunotherapy (Mithoowani & Febbraro, 2022). There are four broad categories of chemotherapeutic agents: alkylating agents (platinum compounds such as cisplatin and carboplatin), microtubule-targeting agents (paclitaxel, docetaxel, and vinorelbine), antimetabolites (pemetrexed and gemcitabine), and topoisomerase inhibitors (etoposide) (Coakley & Popat, 2020).

For patients with a favorable performance status (PS), the recommended approach is to combine two cytotoxic drugs. This usually means combining a platinum-based drug such as cisplatin/carboplatin with pemetrexed, paclitaxel, docetaxel, vinorelbine, or gemcitabine, followed by maintenance therapy (Mithoowani & Febbraro, 2022). It is imperative to consider the histology of the tumor when selecting the appropriate drug, as pemetrexed has shown efficacy primarily in non-squamous NSCLC, while paclitaxel/gemcitabine has shown efficacy in squamous NSCLC (Genova et al., 2013). In specific cases where carboplatin and paclitaxel are administered, the addition of the anti-VEGF bevacizumab may be considered. For patients with poorer PS, a single-agent chemotherapy approach is preferred (Masters et al., 2015). For individuals with severely compromised PS, optimal supportive care is generally recommended, as the side effects associated with cytotoxic drugs can significantly

reduce quality of life. As noted above, chemotherapy may also be used as adjuvant therapy (administered after surgery to eradicate remaining cancer cells) or as neoadjuvant therapy (administered before surgery to reduce tumor size and facilitate removal).

1.4.4. Targeted therapies

As mentioned earlier, significant advances in genomics have allowed the identification of genetic alterations in numerous oncogenic genes, particularly in LUAD. These drivers are critical in regulating key functions of cancer cells, such as cell growth and survival. Therefore, targeting these oncogenic drivers provides an opportunity to effectively inhibit tumor growth (de Jong et al., 2023). Accordingly, molecular testing should be performed in all patients with metastatic non-squamous NSCLC who are never smokers or have a light smoking history to identify actionable oncogenic driver mutations (**Figure 6**).

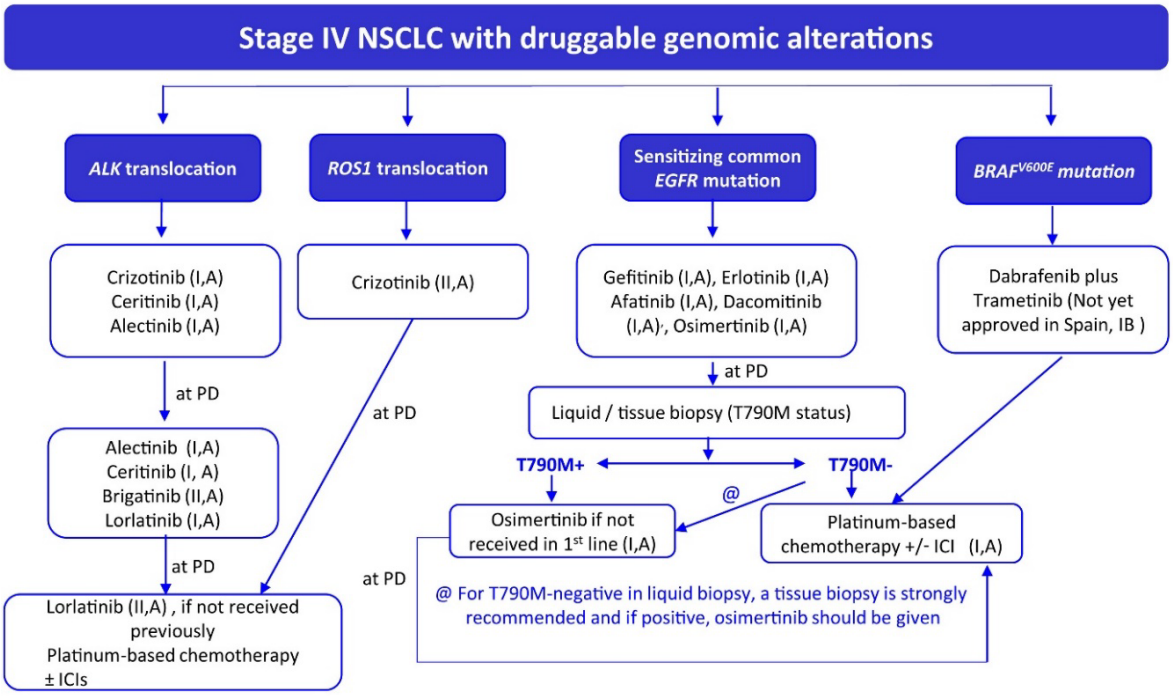

Figure 6. Current treatment guidelines for advanced NSCLC with oncogenic driver mutations in Spain. Adapted from Remon et al., 2021. PD, progression disease.

Although SCC has fewer actionable mutations, molecular testing is still recommended for never-smoking patients with metastatic SCC disease (Mithoowani & Febbraro,

2022). International guidelines recommend testing for *EGFR*, *ALK*, and *ROS1* at a minimum, with more recent guidelines expanding to include *BRAF*, *KRAS*, *MET*, *NTRK*, and *RET* (Ettinger et al., 2021; Lindeman et al., 2018). Treatment recommendations and eligibility criteria vary for patients with different types of NSCLC. For patients with actionable driver mutations, single-agent targeted therapy is preferred due to its better outcomes and reduced toxicity (Ettinger et al., 2022; Zhang et al., 2009).

TKIs such as gefitinib and erlotinib were the first targeted therapies developed for NSCLC, specifically against *EGFR*-activating mutations (**Figure 6**). Second-generation TKIs such as afatinib, which irreversibly binds to EGFR and HER2 receptors, have shown efficacy and are preferred for rare *EGFR* mutations. Osimertinib is a third-generation EGFR TKI designed to overcome resistance, particularly to the T790M mutation, and is currently used as a first-line treatment (Gower et al., 2014; Le & Gerber, 2019; Thai et al., 2021). Crizotinib is a multi-target TKI active against *ALK* or *ROS1* gene rearrangements. Resistance to crizotinib has led to the development of newer generations of ALK inhibitors that have shown improvement in progression-free survival (PFS) and central nervous system (CNS) activity compared to crizotinib. For first-line treatment, third-generation ALK TKIs such as alectinib, brigatinib, and lorlatinib are recommended (**Figure 6**) (Ettinger et al., 2022; Gower et al., 2014). Importantly, advanced ALK-positive NSCLC has a high incidence of brain metastases. Therefore, first-line treatment with prioritization of CNS activity is preferred. Lorlatinib has been specifically designed to cross the blood-brain barrier (BBB) and achieve high CNS concentrations. However, lorlatinib has been associated with undesirable adverse events including hypercholesterolemia, hypertriglyceridemia, edema, and peripheral neuropathy (Mithoowani & Febbraro, 2022).

High *MET* amplification or exon 14 skipping mutations can be targeted with TKIs such as capmatinib, cabozantinib, crizotinib or tepotinib (Herbst et al., 2018). For *ERBB2* (HER2) mutations, monotherapy options include ado-trastuzumab emtansine or fam-trastuzumab deruxtecan-nxki (Ettinger et al., 2021). Afatinib has also shown encouraging results in patients with specific insertions in exon 20 of ERBB2. *BRAF*-activating mutations can be effectively treated with a combination of dabrafenib and trametinib (Coakley & Popat, 2020). Several multi-kinase inhibitors have been investigated for the treatment of *RET* rearrangements, and selective RET inhibitors

such as LOXO-292 have shown promising results (Ettinger et al., 2022; Thai et al., 2021).

Activating mutations in *KRAS* have historically been considered difficult to target. Different approaches to target KRAS, including direct inhibition and targeting downstream signaling mediators such as RAF or MEK, have shown disappointing results. Sotorasib, a newly developed drug for NSCLC patients with the *KRAS* G12C mutation, has shown promise (Ettinger et al., 2022; Mithoowani & Febbraro, 2022).

Some anti-angiogenic therapies have been approved for use in first-line (such as the anti-VEGF antibody bevacizumab) and second-line (such as the anti-VEGFR/PDGFR/FGFR TKI nintedanib) treatment of advanced NSCLC in combination with chemotherapy in the absence of oncogenic mutations (Bosch et al., 2016; Lauro et al., 2014).

1.4.5. Immunotherapy

Immunotherapy is a type of cancer treatment that boosts the immune system's ability to recognize and eliminate cancer cells. Immune checkpoint inhibitors (ICIs) are drugs that target specific proteins present on both immune and cancer cells, disrupting the signals that cancer cells use to evade immune detection. Prominent checkpoint inhibitors target PD-1 (programmed cell death protein 1) receptors on immune cells and PD-L1 (programmed death ligand 1) receptors on cancer cells. Pembrolizumab and nivolumab inhibit PD-1, while atezolizumab and durvalumab inhibit PD-L1 (**Figure 7**) (Dong et al., 2019).

Immunotherapy has revolutionized the treatment of metastatic NSCLC without actionable oncogene mutations. It has demonstrated remarkable efficacy and has been approved as a first- and second-line treatment for patients with advanced NSCLC (**Figure 7**). It can be used as a monotherapy or in combination with chemotherapy or other targeted therapies, depending on the specific condition of the patient and characteristics of the tumor (Coakley & Popat, 2020b; Dong et al., 2019).

Assessment of PD-L1 expression on tumor cells prior to first-line therapy is a valuable predictive biomarker to guide treatment decisions for ICIs in NSCLC patients (Coakley & Popat, 2020). While a high PD-L1 expression is associated with a better response to PD-1/PD-L1 inhibitors, responses to ICIs can also occur in patients without

tumor PD-L1 expression (Dong et al., 2019; Herbst et al., 2018). Despite these complexities, evaluation of tumor PD-L1 expression is recommended for all tumor histologies in patients with newly diagnosed advanced NSCLC (Planchard et al., 2018)

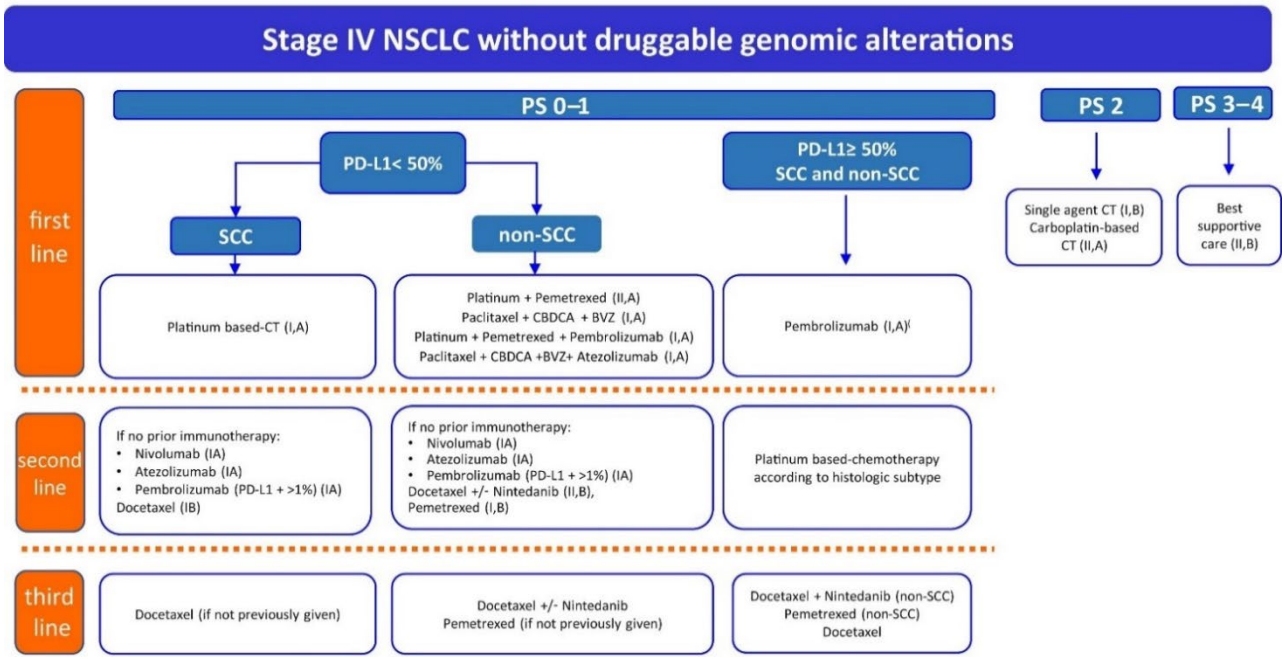

Figure 7. Current treatment guidelines for advanced NSCLC with non-oncogenic driver mutations in Spain. Adapted from Remon et al.,2021. BVZ, bevacizumab.

Pembrolizumab has been established as a first-line treatment for patients with advanced or metastatic NSCLC and high PD-L1 expression (≥ 50%), but not targetable molecular aberrations (Herbst et al., 2018). Combination chemo-immunotherapy strategies have become standard for PD-L1 negative or low positive (0-49%) tumors. Patients with contraindications to ICIs receive histology-specific chemotherapy (Coakley & Popat, 2020).

Tumor mutational burden (TMB) is also as a predictive factor for response to ICIs. Pembrolizumab has received FDA approval for patients with high TMB who have been previously treated, regardless of tumor type. However, the role of TMB in first-line treatment is still unknown and requires further research (Thai et al., 2021). It is noteworthy that ongoing research is exploring novel neoadjuvant and adjuvant methods, including ICIs and TKIs, which are developing strategies that may impact clinical practice in NSCLC (Thai et al., 2021).

1.4.6. Treatment of SCLC

In extensive-stage SCLC disease, platinum with etoposide has been the traditional first-line treatment, but ICIs have changed the treatment landscape. The addition of anti-PD-1 or anti-PD-L1 antibodies to platinum and etoposide regimens has been shown to increase overall survival compared to conventional chemotherapy. In the second-line setting, topotecan is the only FDA-approved agent available. Despite the need for improved outcomes, particularly in relapsed SCLC, the use of ICIs has made significant advances in treatment strategies (Thai et al., 2021).

1.5. MECHANISMS OF THERAPEUTIC RESISTANCE IN LUNG CANCER

Despite advances in the treatment of LC, the obstacle of treatment resistance remains a significant hurdle to achieve favorable clinical outcomes. The development of resistance leads to LC recurrence and metastasis of cancer, and ultimately shorten patients life. Therefore, understanding the molecular mechanisms behind treatment resistance is critical for the development of new strategies aimed at increasing the efficacy of existing treatments or developing more effective therapies to delay the onset of resistance (Ashrafi et al., 2022).

Resistance to treatment in LC can arise from several mechanisms, including both intrinsic and acquired resistance. **Intrinsic** or **primary resistance** refers to the inherent characteristics of cancer cells that make them unresponsive to initial therapeutic interventions. **Acquired** or **secondary resistance** refers to the development of resistance over time during therapy. While initial treatments may be effective, cancer cells can adapt and evolve, resulting in reduced responsiveness to the same treatment (Haider et al., 2020; Marine et al., 2020). Personalized treatment approaches, combination therapies, and ongoing research efforts are aimed at overcoming or preventing resistance to improve LC patient outcomes (Z. Wang et al., 2022).

1.5.1. General mechanisms of intrinsic and acquired resistance in lung cancer

Tumors exhibit diverse cellular and molecular mechanisms that contribute to intrinsic or acquired resistance (**Figure 8**), including alterations in drug targets, expression of

drug efflux pumps, detoxification mechanisms, increased ability to repair DNA damage, or altered proliferation among others (Cree & Charlton, 2017). Another critical facet of therapy resistance is based on alterations in **apoptotic signaling pathways** within cancer cells. Alterations in these pathways can render cancer cells resistant to cell death induced by chemotherapy or targeted agents (Thakur, 2019). Adaptations in cancer cell metabolism, including increased glycolysis and dependence on specific metabolic pathways, may contribute to therapy resistance by providing alternative energy sources. Thus, cancer cells can undergo **metabolic reprogramming** and switch to alternative metabolic pathways, which may provide cancer cells with a survival advantage and resistance to certain treatments (X. Chen et al., 2020; Min & Lee, 2021). In addition, the pharmacokinetics of therapeutic agents can influence their efficacy. For example, some agents, especially those with weak basic properties, can undergo **lysosomal sequestration** which reduces their availability and prevents them from reaching their intended target sites in the cancer cell, thereby contributing to treatment resistance (Halaby, 2019; Hraběta et al., 2020).

The complexity of therapeutic resistance extends beyond the tumor cells themselves, with several factor such as the tumor microenvironment (TME), intratumoral heterogeneity, and tumor-initiating cells contributing to resistance (Cree & Charlton, 2017) (**Figure 8**).

The dynamic interplay between tumor cells and stromal elements within the TME could influence the response of cancer cells to treatment. For example, low oxygen levels (hypoxia) in the TME may promote resistance to radiation and certain chemotherapeutic agents. In addition, interactions with the tumor stroma can create a protective niche that makes cancer cells less susceptible to treatment. Thus, adaptations in the TME can also contribute to acquired treatment resistance (Min & Lee, 2021; Rotow & Bivona, 2017; P. Sharma et al., 2017). Tumor cells can also **evade** the **immune system** through various mechanisms (**Figure 8**), such as downregulation of major histocompatibility complex (MHC) molecules or upregulation of immune checkpoint proteins such as PD-L1, resulting in resistance to immunotherapy (Boyero et al., 2020; P. Sharma et al., 2017). In addition, during treatment, tumor cells may evolve through these mechanisms to evade the immune system, leading to resistance to ICIs. Tumors with low TMB are also less likely to respond to ICIs (Boyero et al., 2020).

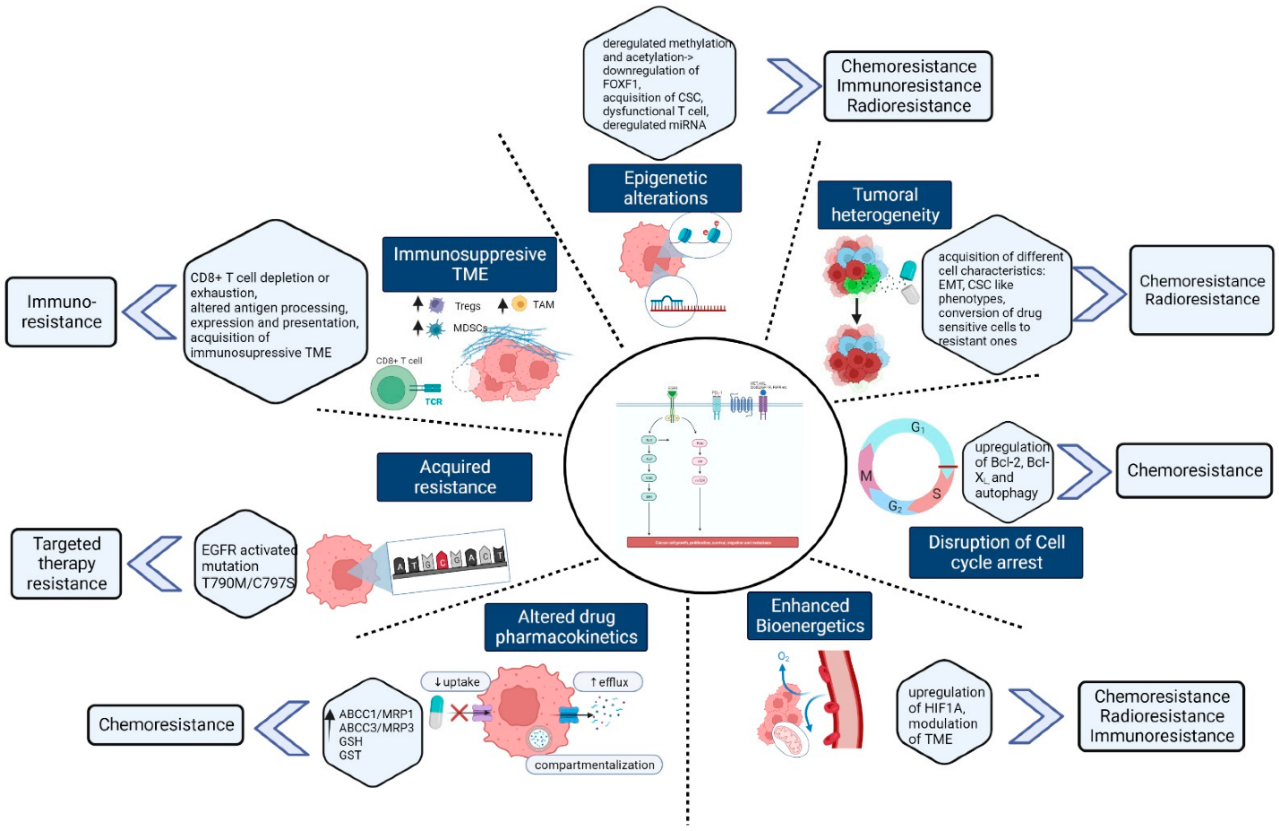

Figure 8. Mechanisms associated with therapeutic resistance in LC. Adapted from Ashrafi et al., 2022.

Lung tumors often exhibit **intratumoral heterogeneity** at the molecular and cellular levels, resulting in subpopulations of cancer cells with distinct characteristics. The presence of diverse cell populations within a tumor allows for the survival and evolution of subsets of cells with intrinsic resistance to specific treatments (Lim & Ma, 2019). As these subpopulations adapt over time, **clonal evolution** may lead to the emergence of resistant subclones in response to initial therapy (Iglesias et al., 2018; Lin & Shaw, 2016). **Cancer stem cells (CSC)** are a subset of tumor cells with self-renewal properties and resistance to conventional therapies. Their presence may also contribute to intratumoral heterogeneity, and consequently to treatment resistance and disease recurrence (X. Chen et al., 2020; Haider et al., 2020; Marine et al., 2020). Similarly, cells that undergo **epithelial-to-mesenchymal transition (EMT)** –a process by which cancer cells acquire mesenchymal properties that promote invasion and metastasis– become more resistant to apoptosis and acquire characteristics to reduce their response to chemotherapy and targeted therapy (Haider et al., 2020; Min & Lee,

2021). Notably, the signaling pathways activated during the EMT and CSC processes are very similar, as cells undergoing EMT exhibit similar characteristics to those found in CSCs, including increased drug efflux pumps and anti-apoptotic activity (B. Du & Shim, 2016).

1.5.2. Mechanisms of lung cancer chemoresistance

As mentioned above, chemotherapy remains the standard of care for advanced LC, but patients often develop resistance, leading to disease progression. Several factors contribute to chemoresistance, including alterations in drug influx and efflux, drug target alterations, epigenetic changes, and DNA damage repair. In addition to these factors, tumor TME, EMT, CSC-like phenotypes, and unregulated microRNA expression are important contributors to acquired chemoresistance (Ashrafi et al., 2022; Min & Lee, 2021). For example, the overexpression of ATP-binding cassette (ABC) transporters, such as P-glycoprotein, can lead to increased efflux of chemotherapeutic agents from cancer cells, reducing their intracellular concentration and efficacy (Robey et al., 2008; Volm et al., 1991). Upregulation of DNA repair pathways, particularly nucleotide excision repair (NER) and homologous recombination (HR), can also contribute to acquired resistance through efficient repair of DNA damage and reduction in the efficacy of some chemotherapies (Martin et al., 2008; Min & Lee, 2021).

Some glutathione S-transferase (GST) isoenzymes play a key role in the detoxification and inactivation of platinum drugs, contributing to chemotherapy resistance (Tew, 2016). Activation of signal transduction pathways, including EGFR, PI3K/Akt, MAPK, NF-κB, and STAT3, is also associated with chemoresistance (Liu et al., 2020; Stewart, 2007; Sun et al., 2019). Several studies suggest that targeting specific molecules, such as ATM or Bcl-2-like proteins, could restore sensitivity to chemotherapy (Hu et al., 2018; F. Zhang et al., 2017). Inhibition of Notch signaling and interference with lysosomal function also show promise in overcoming resistance. In addition, the WNT/b-catenin signaling pathway, TWIST1, and dysregulated miRNAs have been identified as potential targets for overcoming resistance to chemotherapy (Ashrafi et al., 2022).

1.5.3. Mechanisms of lung cancer resistance to targeted therapy

There are several mechanisms of intrinsic and acquired resistance to targeted therapies in NSCLC, especially to TKIs (Z. Wang et al., 2022). Certain genetic alterations such as *EGFR* mutations, particularly T790M and exon 20 insertions, can lead to primary resistance to EGFR TKIs in NSCLC (Tulpule & Bivona, 2020; Yasuda et al., 2013). *KRAS* mutations are also associated with resistance to EGFR-targeted therapies. Other mutations in genes such as *BRAF* or *PIK3* may contribute to primary resistance to EGFR TKIs (Z. Wang et al., 2022). Primary resistance can also occur due to intrinsic alterations, such as specific mutations in *ALK* or *ROS1* genes (Ashrafi et al., 2022). Acquired resistance to targeted therapies involves genetic alterations, both *on-target* and *off-target* resistance, as well as alternative pathological mechanisms such as histologic transformation, EMT or epigenetic alterations.

***On-target* resistance** includes secondary alterations in oncogenes, such as second site mutations, gatekeeper mutations, and covalent binding site mutations (Aldea et al., 2021). For example, patients with *EGFR*-mutant LC treated with EGFR TKIs often develop secondary mutations in the *EGFR* gene, such as T790M, leading to resistance. Third-generation EGFR TKIs, such as osimertinib, have been developed to target these resistance mutations (Lin & Shaw, 2016). Patients with *ALK*-rearranged lung cancer treated with ALK inhibitors may also develop resistance due to secondary mutations in the *ALK* gene, such as L1196M or G1202R (Choi et al., 2010; Dardaei et al., 2018). Strategies to overcome this resistance include the development of next-generation ALK inhibitors (Lin & Shaw, 2016). Similar to *ALK*, *ROS1*-rearranged lung tumors can acquire resistance mutations during treatment with ROS1 inhibitors. Therefore, novel agents must be explored to overcome resistance (Rotow & Bivona, 2017). In addition, oncogene amplification or loss is an alternative mechanism leading to therapeutic resistance. For example, the amplification of oncogenes such as *MET* or *HER2* leads to increased activation of these pathways and resistance to targeted therapies (Engelman et al., 2007; Gouji et al., 2014).

***Off-target* resistance** refers to alterations that occur in proteins other than the targeted oncoprotein. These *off-target* alterations activate signaling pathways

downstream or in parallel to the targeted oncoprotein, sustaining oncogenic signaling and promoting tumor cell survival and growth despite effective inhibition of the original oncogenic driver protein (Tulpule & Bivona, 2020). Several downstream signaling pathways, such as the MAPK pathway, PI3K-AKT pathway, JAK-STAT3 pathway, and SRC activation, can bypass the dependence on the upstream blocked oncoprotein and occur as a compensatory mechanism in response to EGFR inhibition (Z. Wang et al., 2022). In addition, the activation of parallel bypass signaling pathways involving proteins such as MET, AXL, EGFR, HER2, HER3, FGFR1, EPHA1, IGF1R, and KIT, most of which converge on the activation of **EMT**-like phenomena, contribute to *off-target* resistance to targeted therapies (Rotow & Bivona, 2017).

Histologic transformation, particularly from NSCLC to SCLC histology, is observed in some NSCLC patients with acquired EGFR or ALK TKI resistance (Cha et al., 2016; Sequist et al., 2011). **EMT** has also been observed in resistance to therapy with EGFR- and ALK-TKIs, with cellular changes favoring a more invasive mesenchymal phenotype (Aldea et al., 2021; H. R. Kim et al., 2013). The targeting of signaling pathways associated with EMT, such as inhibitors of SRC or inhibitors of IL-6 signaling, has shown promise in preclinical studies for the restoration of sensitivity to EGFR TKIs in (Wilson et al., 2014).

Epigenetic alterations, including increased histone deacetylation (HDAC) activity, are also associated with EGFR TKI resistance, and combination therapies, such as EGFR TKIs with HDAC inhibitors, are being explored to overcome resistance (Witta et al., 2006).

1.6. LUNG CANCER METASTASIS

1.6.1. The metastatic cascade

Organs within the body have well-defined boundaries that are delimited by surrounding basement membranes, structures composed of extracellular matrix (ECM) proteins, that restrict cellular migration. As a result, cells within a given tissue typically remain localized to that site. Nevertheless, cancer cells possess the unique ability to invade and spread from a primary site to other parts of the body through the process of metastasis (Hanahan & Weinberg, 2000). Metastasis represents a significant clinical challenge in cancer treatment because a large number of solid tumors have already

metastasized at the time of diagnosis, and while a primary tumor can be easily removed, once metastases are established throughout the body, they are virtually impossible to remove.

The metastatic cascade in LC is a complex and multi-step process involving the dissemination of malignant cells from the primary tumor in the lung to distant organs and tissues (H. H. Popper, 2016). Metastasis is a major contributing factor to the high mortality rate associated with LC. The metastatic cascade can be divided into distinct steps, including invasion, intravasation (both blood and lymphatic), transport, extravasation, and colonization, with each step involving specific molecular and cellular events (Lambert et al., 2017). The process begins with the **local invasion** of cancer cells from the primary tumor in the lung into surrounding tissues. This step requires degradation of the ECM by enzymes such as matrix metalloproteinases (MMPs), allowing cancer cells to invade nearby blood and lymphatic vessels. Cancer cells then undergo **intravasation**, a process of entering the bloodstream or lymphatic vessels, which facilitates their transport to distant parts of the body. Intravasation is the ability of cancer cells to penetrate the vessel walls and survive in the circulation. Intravasation involves the ability of cancer cells to penetrate vessel walls and survive in the circulation. Once in the bloodstream, cancer cells face challenges from the immune system, and only a small fraction of so-called circulating tumor cells (CTCs) ultimately survive. From this point, cancer cells must **extravasate** by leaving the bloodstream and infiltrating the parenchyma of a distant organ. Cancer cells that survive and develop in distant organs must adapt to the new microenvironment and may remain dormant before initiating growth as **micrometastases**. The dormancy and subsequent reactivation of cancer cells in these organs contributes to the variability in the timing of metastatic outgrowth. To support their growth, micrometastases induce **angiogenesis**, the formation of new blood vessels, providing the blood supply necessary to sustain tumor growth. As the tumor continues to grow, it forms **macrometastases**, which are clinically detectable masses. Metastatic growth is fueled by the recruitment of blood vessels and nutrients from the host tissue (Eslami-S et al., 2020; H. Popper, 2020). As noted above, LC is often detected at an advanced metastatic stage IV, with metastasis occurring through both lymphatic and blood vessels. It is common to observe vascular invasion in resected low-stage tumors, which can be the

cause of a higher rate of recurrence and a lower survival rate for patients. While lymphatic metastasis may take longer to establish distant metastases, blood vessel-mediated metastasis results to earlier dissemination (H. H. Popper, 2016).

Understanding the molecular and cellular mechanisms involved in each stage of the metastatic cascade is essential for the development of targeted therapies to prevent or treating metastatic LC. Ongoing research aims to identify molecular players, signaling pathways, and novel therapeutic targets that may improve outcomes and treatment options for patients with advanced metastatic LC (Ganesh & Massagué, 2021).

1.6.2. The EMT phenomenon

The process by which LC cells acquire the characteristics necessary for invasion is orchestrated by the aforementioned mechanism of EMT (Lambert et al., 2017; Nieto et al., 2016). EMT is a normal developmental program that involves the transformation of a tightly bound, adherent epithelial cell into a mesenchymal cell with highly migratory properties (Polyak & Weinberg, 2009). During early development, the embryo requires cell invasion and motility to orchestrate patterns for tissue formation. Furthermore, EMT also occurs during physiological processes such as tissue regeneration, organ fibrosis, and wound healing (Nieto et al., 2016; Roche, 2018). However, cancer cells can reactivate some cell behaviors that are active during early embryogenesis and exploit this process to initiate and progress through the metastatic cascade (**Figure 9**) (Craene & Berx, 2013).

Normal and metastatic EMT are molecularly similar: the loss of several important epithelial phenotypes, including tight cell-cell junctions, apical-basal polarity, and expression of epithelial biomarkers such as E-cadherin, upregulation of mesenchymal proteins such as N-cadherin and vimentin, and secretion of MMPs (Kalluri & Weinberg, 2009). However, EMT may be incomplete in cancer cells, which can exist in multiple transitional states and express a mixture epithelial and mesenchymal marker that contribute to cancer cell plasticity. These cells in partial EMT can move collectively and be more aggressive than cells with a complete EMT phenotype (Kalluri & Weinberg, 2009; Nieto et al., 2016). EMT is reversible by the mesenchymal-to-epithelial transition (MET), which occurs in circulating cancer cells that switch from

migratory to proliferative mode when they obtain a desirable metastatic niche for secondary tumor development (**Figure 9**) (Moustakas & de Herreros, 2017; Ocaña et al., 2012).

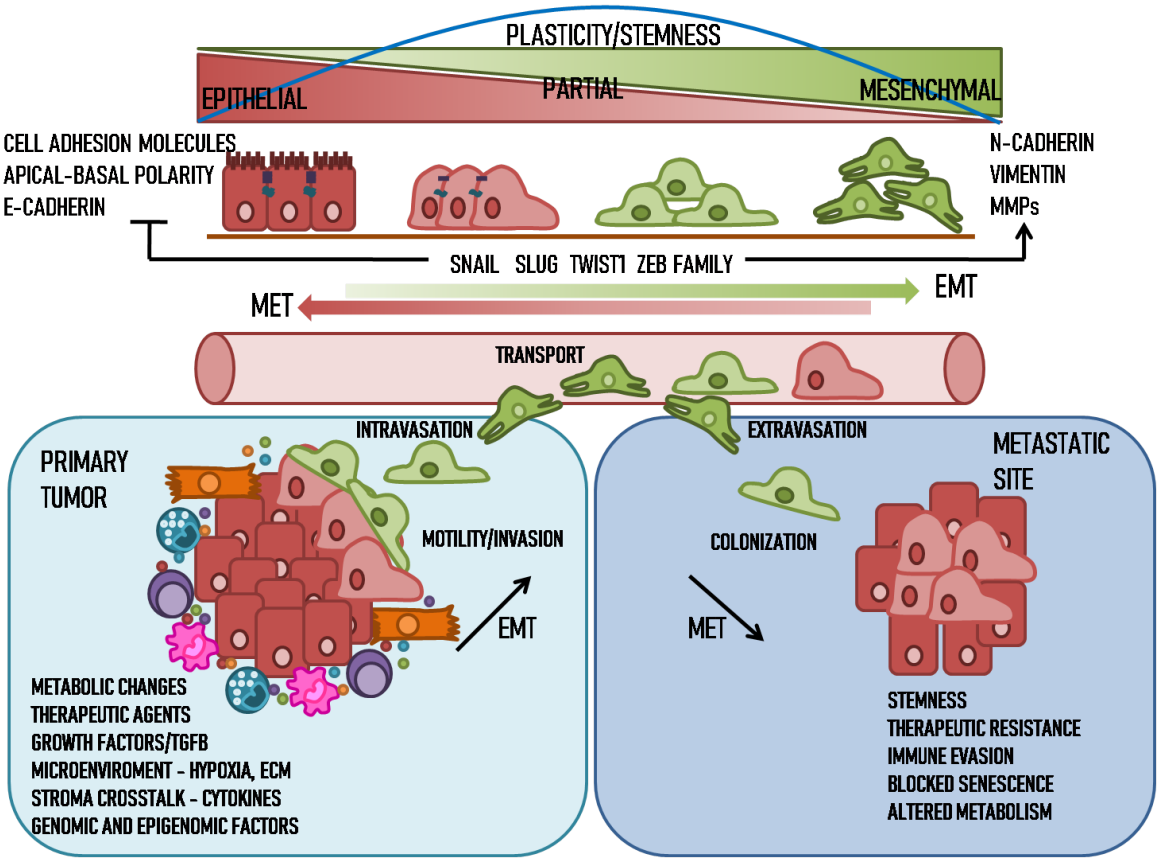

Figure 9. EMT and the process of the metastatic cascade

EMT inducers in cancer include hypoxia, cytokines, growth factors secreted by the TME, stroma crosstalk, metabolic changes, immune responses, and treatment with antitumor drugs (Roche, 2018). Signals from the tumor stroma, such as growth factors and TGF-β, induce EMT in neighboring tumor cells via their specific receptors and signal transducers, ultimately activating specific transcription factors such as SNAIL, SLUG, ZEB1 or TWIST (**Fig. 9**) (Dongre & Weinberg, 2019). The EMT-inducing gene expression switch is controlled by complex regulatory networks involving transcription factors, non-coding RNAs, chromatin remodeling and epigenetic modifications, alternative splicing, post-translational regulation, protein stability, and protein subcellular localization (Craene & Berx, 2013).

While the primary consequence of EMT is increased cellular mobility, it is particularly associated with tumor cell dissemination and metastasis. In this regard, carcinomas express EMT markers at the invasive front (Brabletz et al., 2001; Kahlert et al., 2011; Kunita et al., 2018) and in circulating tumor cells (Aktas et al., 2009), which represent the first steps of the metastatic cascade (invasion and intravasation). In addition, EMT plays a key role in the acquisition of malignant features during tumor progression, including immune evasion, altered metabolism, resistance to apoptosis, conferring stem cell properties (stemness) to tumoral cells, and therapy resistance (Hanahan & Weinberg, 2011; W. Lu & Kang, 2019). Thus, EMT not only enables tumor cells to acquire a migratory phenotype but also promotes their self-renewing capacity, which is essential for successful colonization. Not surprisingly, LC metastatic potential can be influenced by the subpopulation of CSCs in a primary tumor, which can be generated through EMT-like phenomena to acquire the capacity for self-renewal and drive tumorigenesis Chaffer & Weinberg, 2011).

1.6.3. The importance of the microenvironment

Many steps in the metastatic cascade require precise interactions between cancer cells and their microenvironment. Interestingly, certain cancers have a particular propensity to metastasize to certain tissues, which could be explained by the "seed and soil" theory: cancer cells are like "seeds" that require an optimal environment or "soil" to succeed (Akhtar et al., 2019; Ohyashiki, 2018). Therefore, an additional layer of complexity is added because both tumor cells and the TME play important roles in the process of metastasis. For example, the tumor receives signals from surrounding cells and the ECM, and these interactions can ultimately influence the metastatic ability of individual cancer cells (Quail & Joyce, 2013). This concept supports the establishment of the **pre-metastatic niche,** in which cancer cells in the primary tumor communicate with the microenvironment of distant organs through signaling molecules; this microenvironment consists of stromal cells, immune cells, and the ECM. These interactions are essential in preparing future metastatic sites, creating a supportive environment for colonization and growth (Psaila & Lyden, 2009).

1.7. TARGETING OF LUNG CANCER METASTASIS

The growing understanding of metastasis biology is creating opportunities to improve clinical outcomes by exploiting the vulnerabilities in both the metastasis-initiating cancer cells and the TME as potential targets for prevention and treatment of LC metastasis. Given the importance of the TME in the regulation of metastasis, promising effects have been observed in the development of therapies targeting the TME. These treatments include anti-angiogenic therapy, anti-inflammatory therapy, and immunotherapy (Ganesh & Massagué, 2021). In particular, antiangiogenic treatments that target the VEGF pathway, such as bevacizumab and nintedanib, have shown efficacy in clinical trials. However, only modest increases in overall survival have been observed. Anti-inflammatory treatments, such as aspirin and COX2 inhibitors, show mixed results, and ongoing trials with canakinumab, which targets IL-1β, aim to further investigate their potential. Immunotherapies, particularly ICIs, have revolutionized treatment of advanced LC disease with the approval of nivolumab and pembrolizumab. Although combinations of ICIs with chemotherapy or other targeted agents are expected to improve LC outcomes, the challenge of resistance to immunotherapies in the majority of LC patients remains, requiring further exploration into biomarkers and understanding of the mechanisms of immune evasion (Altorki et al., 2019).

1.7.1. EMT: a common mechanism for LC metastatic dissemination

The extensive involvement of EMT in the metastatic and malignant transformation processes has made it an increasingly interesting target for the development of new therapeutic approaches against metastasis initiation (Marcucci et al., 2016). Strategies targeting EMT can be challenging. However, they have the potential to inhibit cancer cells from invading and spreading, thereby preventing the formation of metastatic lesions. They may also reduce cancer stemness and increase the efficacy of conventional and targeted therapy.

Several signaling pathways, including Wnt, Notch, and bone morphogenic protein (BMP)/TGF-β, are involved in EMT during cancer metastasis. In particular, TGF-β is a versatile EMT-inducing cytokine that belongs to a larger family of structurally and functionally related proteins, including activins/inhibins and BMPs. This family of proteins plays a central role in the regulation of various cellular functions, including

proliferation, apoptosis, differentiation, EMT, and migration/invasion. Upon ligand binding to the TGF-β receptor, phosphorylation and activation of SMAD complexes occur, leading to the initiation of transcription of TGF-β target genes including EMT-transcription factors. In addition, the TGF-β signaling pathway exhibits multiple feedback mechanisms and engages diverse crosstalk with other signaling pathways, including receptor tyrosine kinases (RTKs) such as EGFR and c-Met. Upon activation, downstream RTKs recruit diverse proteins, resulting in the activation of multiple signaling cascades such as the RAS/MAPK, PI3K/AKT/mTOR, and JAK/STAT pathways. Not surprisingly, several direct inhibitors of TGF-β and indirect inhibitors of its cross-talking signaling pathways have been developed and tested both *in vitro* and *in vivo* (Jonckheere et al., 2022). Unfortunately, although EMT is becoming a target of primary interest for anti-LC therapy, with an ever-increasing number of compounds in clinical trials targeting either stimuli and signaling pathways or outcomes associated with EMT, their successful clinical application appears to be highly dependent on the mutational status of the cancer cells and the specific cellular context (Marcucci et al., 2016).

1.7.2. Brain-specific organotropism of metastatic LC: From mechanisms to therapeutic opportunities

LCs show selective metastasis to specific sites, including brain (29.9-41.9%), bone (28.5-38.8%), liver (13.2-26.3%), and adrenal gland (10.1-24.1%). Different types of LC also show specific preferences for metastasis, such as liver metastasis in SCLC and brain metastasis in both SCLC and LUAD. Several studies suggest a higher incidence of brain metastasis in LUAD with specific genetic mutations, including *EGFR* mutations or *EML4-ALK* rearrangements, whereas SCC typically invades the chest wall. Variations in metastatic tropism among different subtypes of LC may indicate different interactions between tumor cells and specific microenvironments (Pontis et al., 2023). In addition, the host immune system plays a critical role in either eliminating or allowing the survival and growth of disseminated cancer cells. In this sense, metastatic LC cells often evade the immune system through strategic adaptations, allowing their survival and growth in distant organs (H. H. Popper, 2016).

Around 20% of newly diagnosed patients with advanced NSCLC have brain metastases, and among patients with brain metastases, LC serves as the primary tumor in 40-50% of cases (Myall et al., 2021; Schroeder et al., 2020). Targeting molecular mechanisms that determine the tissue-specific metastatic organotropism could be a promising strategy to prevent metastases and potentially improve outcomes in a highly challenging metastatic site of NSCLC such as the brain (**Figure 10**) (Ganesh & Massagué, 2021).

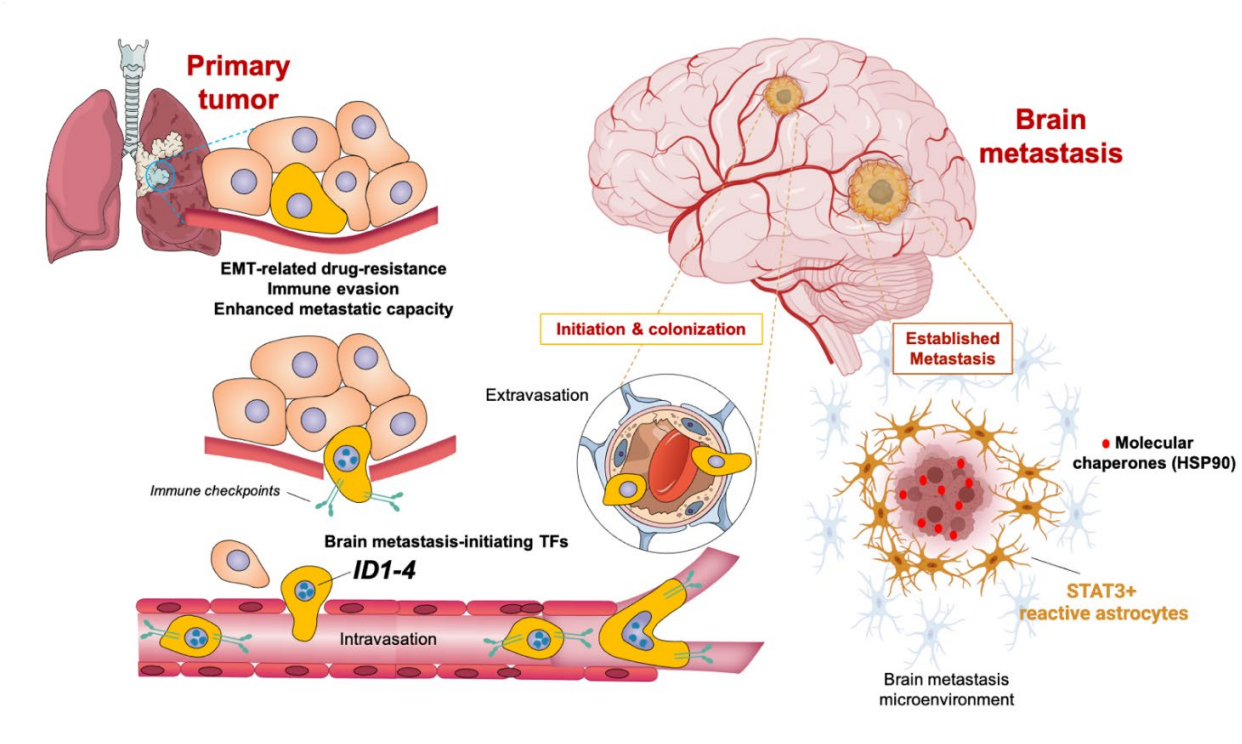

Figure 10. Targetable mechanisms in the process of NSCLC metastasis to the brain.

Created with Biorender

Metastasis-promoting transcription factors. Transcriptional regulation is an essential component of metastatic progression. Beyond the general dysregulation of oncogenic or tumor-suppressive transcription factors (TFs), master cell-fate and TME-modifying TFs are key regulators that influence multiple steps of the metastatic cascade, such as local invasion, dissemination, and eventual colonization of LC in distant organs, including the brain. A family of metastasis-promoting transcriptional regulators that fulfill such brain-tropic requirements in LC are the so-called inhibitor of differentiation/DNA binding (ID) proteins ID1, ID2, ID3, and ID4. ID1-4 TFs are dominant-negative inhibitors of basic helix-loop-helix (bHLH) TFs that not only promote proliferation, but more importantly, regulate cell fate and differentiation. ID

genes are frequently dysregulated in many cancers, including LC, which confer biological properties similar to those of normal stem cells. For example, activation of ID proteins facilitates metastatic spread by remodeling the TME, promoting tumor angiogenesis, and maintaining stem-like traits of endothelial cells (ECs) (Cells et al., 2012; Dingcheng Gao, 2008; Huang et al., 2019; Robert Benezra, 2001). This process may facilitate the migration of metastatic cells across the BBB and influence the reorganization of the cerebral microvasculature in reactive niches of brain tumors (Das & Felty, 2014; Jayanta K Das, 2022). In addition, expression of *ID* genes confers tumor-initiating capacity and resistance to chemotherapy and radiotherapy in specific subpopulations of CSC-like cells (Cells et al., 2012; Huang et al., 2019). In NSCLC, the combined expression of ID1 and ID3 has been shown to be negatively correlated with overall patient survival and positively correlated with several key EMT-related proteins. This suggests that *ID* genes may regulate the EMT process and promote vascular infiltration and distant organ metastasis in NSCLC (Gil-Bazo et al., 2014). However, to date, there are no effective treatments that can target the pro-metastatic expression and/or function of ID proteins.

Molecular chaperones. HSP90 is a molecular chaperone that is essential for maintaining the stability of many client proteins, including driver oncoproteins that are involved in tumorigenesis, in the post-translational assembly of oligomeric complexes. Several studies have shown that HSP90 overexpression correlates with poor prognosis and lymphatic metastasis in NSCLC patients (Jang-Ming Su et al., 2016). Importantly, a very recent study has identified HSP90 as a potential target for the prevention of brain metastasis formation and the treatment of pre-existing, established brain metastases (Zhu et al., 2022). Using the so-called METPlatform, which is based on organotypic cultures of patient-derived brain metastasis samples, the authors identified HSP90 inhibitors as new therapeutic agents with potent anti-brain metastasis activity. In addition, a molecular signature of four HSP90-related genes was found to identify patients with a more aggressive form of brain metastasis, suggesting that this poor prognostic signature may identify patients with greater sensitivity to HSP90 inhibitors (Zhu et al., 2022). Therefore, the use of HSP90 inhibitors appears to be a promising and alternative approach for the treatment of brain metastases in NSCLC patients,

especially those with a unique HSP90-overexpressing molecular profile or acquired resistance to other therapeutic agents. Many HSP90 inhibitors have been developed and have shown promising results in preclinical models of various tumor types, but never in brain metastases (Chatterjee et al., 2016). As these molecules have shown side effects and toxicities in clinical trials in cancer patients, a safe therapeutic window has to be found or their use in combination with other drugs has to be explored.

Phospho-STAT3-positive reactive astrocytes. Little is known about how metastatic cells adapt to the stressful microenvironment of the brain tissue. Addressing this gap could open avenues for a new generation of microenvironment-targeted therapeutic strategies that focus on the specific characteristics of the brain metastatic niche. Astrocytes have recently been identified as the primary host brain cells with which cancer cells interact with during brain metastasis and undergo profound morpho-functional changes, switching to a reactive phenotype that limits brain metastasis without infiltrating the lesion, but significantly influences the outcome of disseminated cancer cells. Understanding the role of RA in brain metastasis, with a focus on the signaling pathways and types of interactions critical for communication with cancer cells, can guide the development of innovative therapies (Wasilewski et al., 2017).

Although many signaling cascades have been implicated in astrocyte reactivity, the signal transducer and activator of transcription 3 (STAT3) is a central master driver and receiver of most of the complex molecular interactions of the specific brain metastasis-associated functional state of reactive astrocytes (RAs). Brain metastatic cells induce and maintain the co-option of a pro-metastatic program driven by STAT3 in a subpopulation of phospho-$STAT3^+$ RA surrounding metastatic lesions (Priego et al., 2018). In patients, active STAT3 in RA correlates with reduced survival from diagnosis of intracranial metastases. Phospho-$STAT3^+$ RA benefit brain metastatic cells by producing cytokines that compromise both innate and acquired immunity. Deletion of STAT3 in RA reduces the burden of brain metastases from various primary tumor sources including NSCLC, even at advanced stages of colonization, suggesting that STAT3-inhibiting drugs may be used as first-in-class targeted therapies for brain metastasis by targeting its tumor microenvironment (Priego et al., 2018). In addition, we have recently learned that the STAT3-positive reactive phenotype of brain

astrocytes significantly impairs cerebrovascular function and contributes to the neurological sequelae associated with brain metastases (Soto et al., 2020). Thus, selective targeting of STAT3-mediated astrocyte reactivity is not only expected to provide a therapeutic avenue for the clinical management of brain metastases in combination with metastatic cell-targeting drugs (McFarland & Benveniste, 2019; Priego et al., 2018), but also to ameliorate neurovascular dysfunction and improve neurological outcomes in patients with brain metastases (Soto et al., 2020). While a large number of STAT3 inhibitors are currently in clinical trials, most of them need to overcome low BBB permeability with low side effects and high specificity for STAT3-positive RA before they can be considered as drug candidates for targeting brain metastases in LC.

2. SILIBININ

2.1. MILK THISTLE AND THE FLAVONOLIGNAN SILIBININ

2.1.1. Silymarin and the silymarin flavonolignan silibinin

Silymarin is a crude extract from the fruits (often mistakenly called seeds) of the milk thistle *Silybum marianum* (L.) Gaertn., Asteraceae var. purple., a plant native to southern Europe, southern Russia, Asia Minor, and northern Africa. The term "milk thistle" comes from the legend that Mary and the baby Jesus took refuge in a shelter made of the thorny leaves of *Silybum marianum* while traveling to Egypt. During this time, Mary accidentally spilled some of her breast milk on the plant, creating the distinctive milky-white veins to appear on the leaves of the plant (Verdura et al., 2021).

Silymarin is obtained from milk thistle fruits which are pressed to remove most of the fats and further defatted with petroleum ether. The resulting cake is usually extracted with acetone or ethyl acetate, and the remaining fat is separated off after its dilution with water. Silymarin represents 1.5-3% of the fruit's dry weight and is an isomeric mixture of unique flavonolignan complexes or flavonolignans (**Figure 11**), a subclass of flavonoids found in various plant sources that are characterized by a combination of flavonoid and lignan (phenylpropanoid) components. As a crude extract of plant material, silymarin has a high degree of variability, but typically contains a 20-

30% fraction of flavonolignans, including silybin (also called silibinin) –as a quasi-equimolar mixture of silybin A and B diastereoisomers, which make up 50-60% of the extract and 20-40% of commonly used pharmaceutical preparations of silymarin– and other flavonolignans such as isosilybin A and B (~5%), silychristin A (~7%), and silydianin (~10%). In addition to flavonolignans, silymarin contains a non-flavonolignan fraction of taxifolin (2-5%), 2,3-dehydroflavonolignans (~3%), and some other polyphenolic compounds (**Figure 11**). The final composition of silymarin depends on many factors including plant origin, cultivation, and processing (Abenavoli et al., 2018; Bijak, 2017; Křen, 2021).

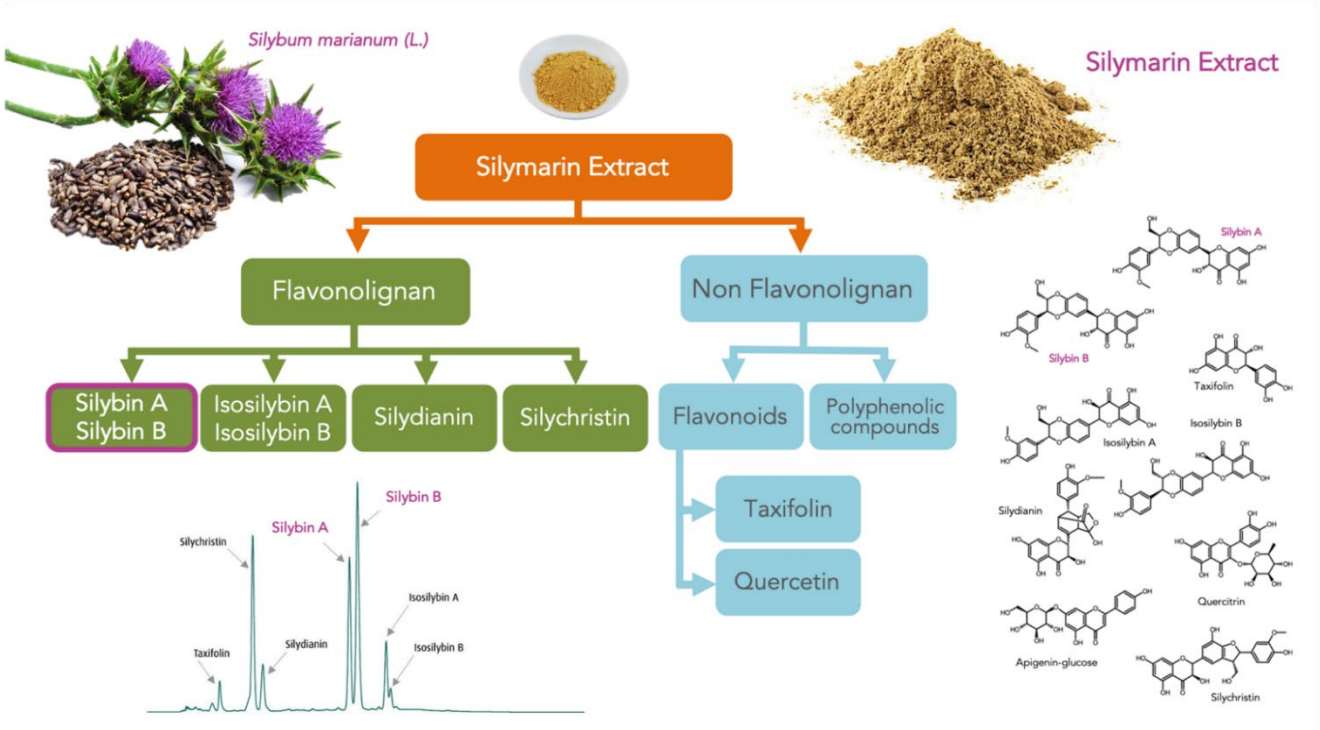

Figure 11. Components of the milk thistle-derived silymarin extract

Since the 1970s, the WHO has recognized milk thistle silymarin extract from as an official medicine for its health-promoting properties (Bijak, 2017). The polyphenolic flavonolignan silibinin is not only the main constituent of silymarin, but also the major bioactive component of the extract, which has been confirmed in numerous studies.

Silibinin consists of two main units, the first one based on a taxifolin and the second a phenylpropanoid unit, which are linked together in a structure by an oxeran ring.

2.1.2. Historical medical use of the silibinin-containing silymarin extract

The silibinin-containing silymarin extract has been used for over two thousand years to treat liver and bile-related disorders, with historical mentions in the Old Testament and documented medicinal use in ancient Greece, traditional Indian, and Chinese medicine. Ancient figures such as Theophrastus, Pedanios Dioscorides (**Figure 12**), and Plinius the Elder emphasized its therapeutic properties. During the Middle Ages, it gained prominence as an antidote to liver toxins and continued to be used by American Indians, 19th century physicians, and herbalists (Abenavoli et al., 2010; Bijak, 2017).

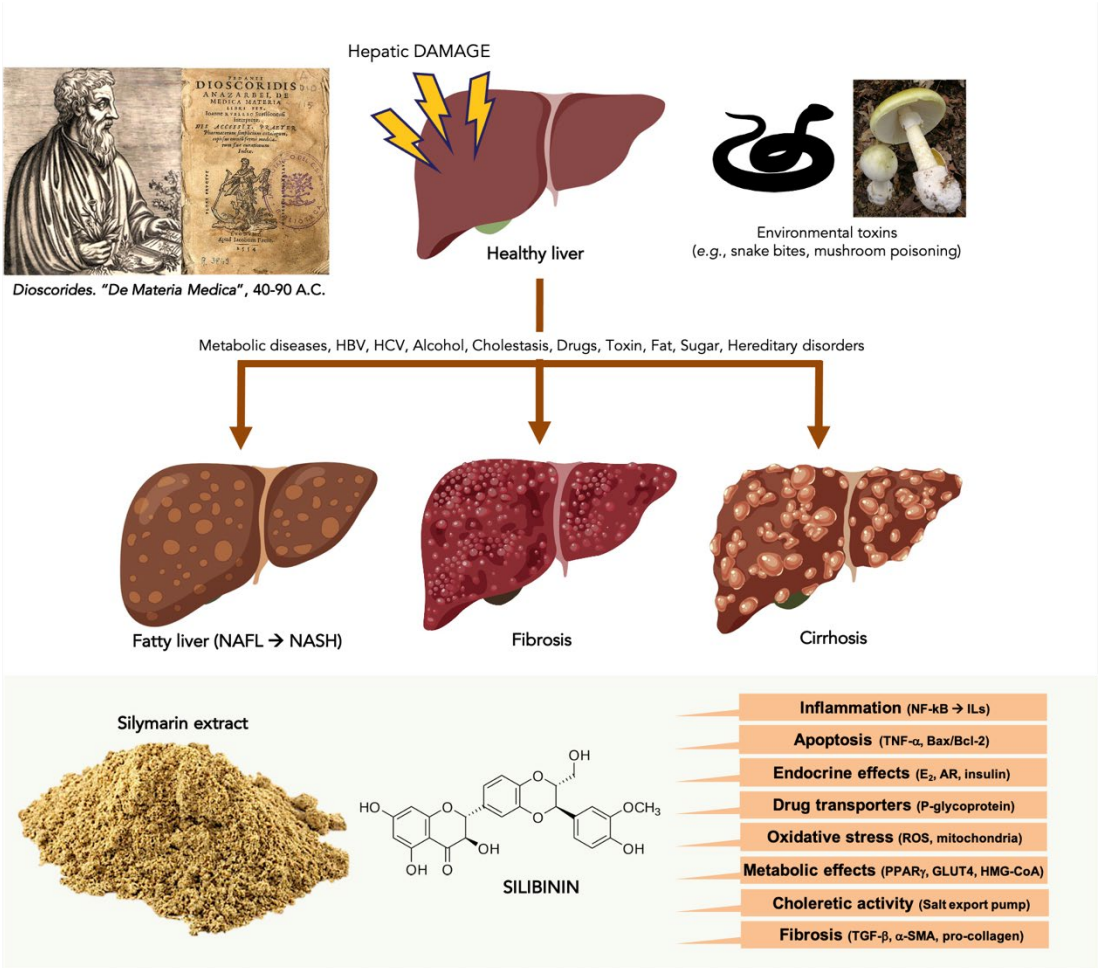

Figure 12. Liver-related therapeutic activity: central silymarin target since medieval times. Created with Biorender. Silibinin, originally known for its putative antidote effects against snake venom, has been extensively studied and is currently used clinically to treat amatoxin mushroom poisoning or lipotoxic injury in fatty liver disease (Verdura et al., 2021). Silibinin has been used as a medicinal agent since ancient times and has been extensively studied for its

potent hepatoprotective activity involving a wide variety of molecular mechanisms (Abenavoli et al., 2010, 2018; Bijak, 2017).

In the last 40–50 years, bioactive silymarin extracts have been extensively studied for the treatment of various liver diseases, including alcoholic liver disease, non-alcoholic liver disease, drug-induced liver injury, cirrhosis, viral hepatitis, and mushroom poisoning (**Figure 12**) (Abenavoli et al., 2010; Federico et al., 2017; Saller et al., 2007). Patients treated with silymarin have shown rapid improvements in liver function, and long-term use has significantly reduced mortality rates in patients with alcoholic liver cirrhosis (Anton Gillessen & Hartmut H-J Schmidt, 2020; Saller et al., 2001). Silymarin is now a widely sold dietary supplement for hepatitis and cirrhosis in the USA and Europe (Wellington et al., 2001).

2.2. ANTITUMORAL PROPERTIES OF SILIBININ

In recent years, there has been a growing body of scientific evidence suggesting that silibinin is a potential chemopreventive anticancer agent. The proposed anticancer properties of silibinin can be explained by an ever-growing list of preclinical studies demonstrating its ability to affect all of the characteristics or hallmarks commonly shared by human cancers (**Figure 13**) (Ramasamy & Agarwal, 2008). In groundbreaking studies, Dr. Agarwal and colleagues explored the potential of silibinin in the prevention and treatment of several human malignancies, including skin, prostate, and LC. Their research involved both short-term cell culture and long-term animal models. Using *in vivo* models, they observed the tissue distribution of systematically administered silibinin and found its potential to induce anti-cancer effects. The results strongly suggested that silibinin could effectively reach target organs and laid the groundwork for evaluating its cancer-preventive and interventional effects in experimental carcinogenesis models (Zhao & Agarwal, 1999).

Additional studies in various cancer types such as gastric, breast or prostate cancer have suggested that silibinin inhibits proliferation, induces apoptosis and causes cell cycle arrest of cancer cells through various mechanisms (**Figure 13**) (S. Kim et al., 2014; Y. X. Wang et al., 2014). Silibinin has been shown to enhance the cytotoxic effects of chemotherapy in various cancer models and to sensitize chemoresistant cells to

chemotherapeutic agents (Molavi et al., 2017). Preclinical studies have also demonstrated the ability of silibinin to target the migratory and invasive properties of cancer cells. Mechanistic analyses revealed that silibinin may target signaling molecules involved in the regulation of EMT, protease activation, adhesion, motility, invasiveness, and metastasis-supporting components of the TME. Although all of this robust preclinical evidence for silibinin's anti-tumor activity against various cancers can be explained, at least in part, by its ability to act as an inhibitor of $STAT_3$, the exact mechanism by which silibinin may indirectly or directly target $STAT_3$ remained unknown (Bosch-Barrera & Menendez, 2015).

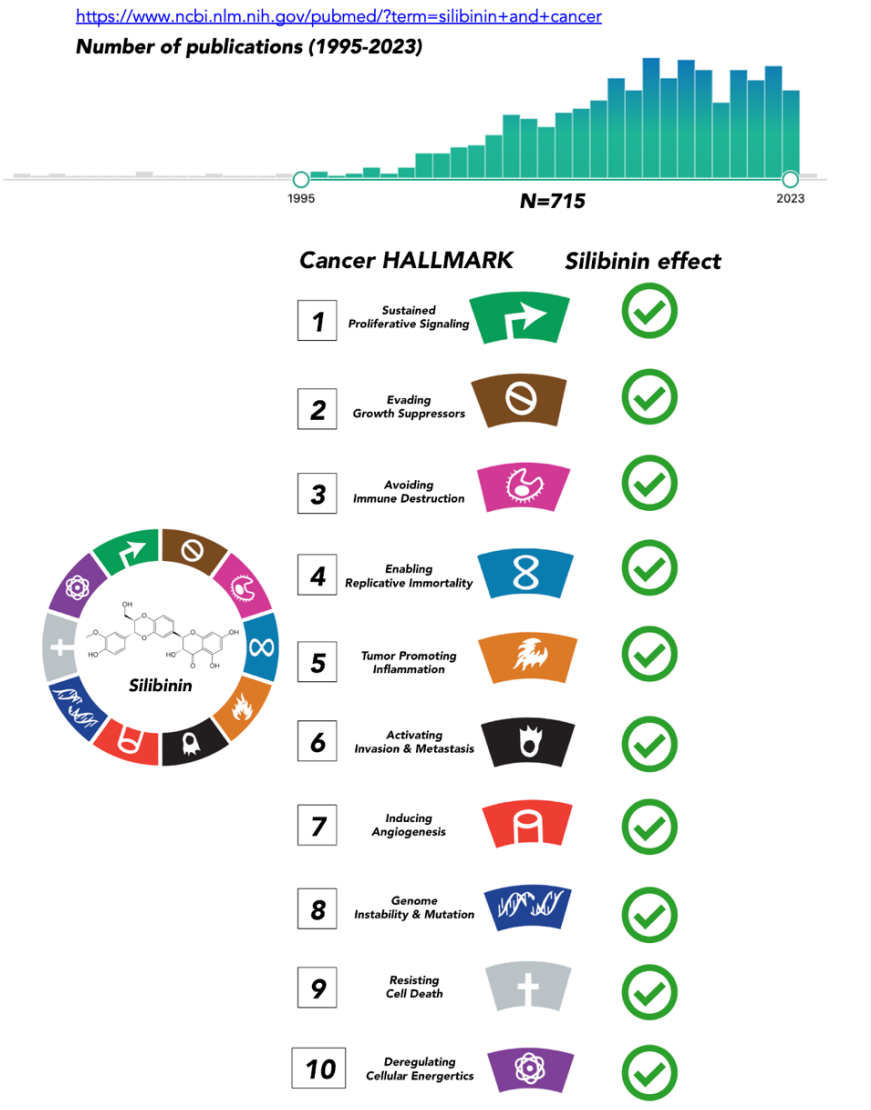

Figure 13. Cancer: A recent area of interest for silibinin

2.3. SILIBININ AND LUNG CANCER

Various studies have examined the potential inhibitory effects of silibinin on cultured LC cells and LC tumor xenografts (Mateen et al., 2010; G. Sharma et al., 2003). Using SCLC and NSCLC cell models, the Agarwal group reported that micromolar concentrations of silibinin caused significant growth inhibition, cell cycle arrest, and apoptotic cell death (G. Sharma et al., 2003). This led to further investigations to understand the efficacy and mechanisms of action of silibinin as a non-toxic therapeutic agent in a variety of LC models. The same group demonstrated that silibinin could inhibit NSCLC A549 xenograft tumor growth and enhance the efficacy of co-treatment with doxorubicin while significantly reducing chemotherapy-induced systemic toxicity (Singh et al., 2004). Because there was no reported 50% lethal dose in experimental animals and silibinin treatment has been considered exceptionally safe in both animals and humans, these findings provide strong support for the investigation of silibinin as a chemopreventive and anti-angiogenic agent to inhibit LC growth and metastatic progression in humans (Mateen, Raina, & Agarwal, 2013). Mechanistically, silibinin has been shown to target multiple LC-related cytokine-induced signaling pathways (including STAT3), ultimately reducing angiogenic factors (such as VEGF) (Chittezhath et al., 2008; Singh et al., 2004; Tyagi et al., 2009, 2012). In addition, silibinin shows synergy with certain chemotherapeutics agents in combating multidrug resistance (MDR) in SCLC cells, possibly through inhibition of ATP-binding cassette (ABC) transporters and downregulation of corresponding genes (Dinic et al., 2015; Dobiasová et al., 2020; Maitrejean et al., 1999; Sadava & Kane, 2013).

2.3.1. Silibinin and lung cancer resistance to targeted therapy

Several studies have investigated the potential of silibinin to enhance the efficacy of other therapeutic agents and counteract the development of drug resistance in preclinical models of LC, particularly those involving targeted therapies for NSCLC such as EGFR and ALK TKIs. Silibinin has shown promising results in overcoming drug resistance in NSCLC cells with acquired resistance to EGFR and ALK TKIs by restoring drug sensitivity *in vitro* and *in vivo*. Silibinin has shown potential to overcome primary and acquired resistance to first-generation EGFR TKIs such as gefitinib and erlotinib including resistance due to the *EGFR* T790M mutation and even in the absence of

secondary mutations (Cufí, Bonavia, Vazquez-Martin, Corominas-Faja, et al., 2013; Cufí, Bonavia, Vazquez-Martin, Oliveras-Ferraros, et al., 2013; Rho et al., 2010). Mechanistically, silibinin was found to drastically reduce the number of CSC-like cells, which are significantly higher in erlotinib-refractory cell populations (Corominas-Faja et al., 2013). Moreover, silibinin was able to overcome acquired resistance and restore sensitivity to the first-generation ALK TKI crizotinib in a pre-clinical model of *ALK*-translocated NSCLC with acquired refractoriness without additional mutations in the ALK kinase domain (Cuyàs et al., 2016). The impact of silibinin on chemosensitivity profiles in EGFR- and ALK-positive tumors resistant to standard TKIs remains an avenue for further investigation. This will provide insight into its potential therapeutic combination for patients with advanced LC.

2.3.2. Silibinin and lung cancer metastasis

Silibinin has been shown to have inhibitory effects on NSCLC metastatic features such as cell invasion and EMT (Xu et al., 2020). Silibinin has demonstrated a dose- and time-dependent inhibition of invasion and motility in highly metastatic NSCLC cell models. Inhibition of metalloproteinase-2 (MMP-2) and urokinase plasminogen activator and enhancement of tissue inhibitor of metalloproteinase (TIMP-2) expression may contribute to this effect (Chu et al., 2004). The interference of silibinin with NSCLC invasiveness involves inactivation of PI3K-AKT and MAPK signaling pathways, and more recent studies suggest that silibinin may inhibit MMPs by suppressing STAT3 activation (Byun et al., 2017; P. N. Chen et al., 2005).

In combination with EGFR blockade, silibinin has demonstrated preventive effects on NSCLC cell migration and tumor metastasis (Hou et al., 2018).Silibinin has shown efficacy in restoring drug sensitivity to NSCLC xenografts with EMT-driven resistance to EGFR-targeted inhibitors (Cufí, Bonavia, Vazquez-Martin, Oliveras-Ferraros, et al., 2013; Rho et al., 2010). Such inhibition of EMT by silibinin involved the targeting metastasis-initiating mechanisms such as the reversal of the miR-21/low miR-200c microRNA signature and the suppression of miR-21/miR-200c-related mesenchymal markers (Cufí et al., 2013). Combinatorial treatments with silibinin and epigenetic modifiers were shown to further modulate EMT events in NSCLC cell lines Mateen, Raina, Agarwal, et al., 2013). Notably, the responsiveness of mesenchymal

NSCLC cells to silibinin appears to be associated with a subnetwork of interconnected genes under STAT3 control rather than correlating with intrinsic EMT stages (Kaipa et al., 2020).

2.3.3. Silibinin and brain metastasis in lung cancer patients

Intestinal permeability studies of clinically relevant formulations of silibinin in Caco-2 cell monolayers revealed differential transport mechanisms and BBB permeabilities between different silibinin formulations, including silibinin-meglumine, a water-soluble form of silibinin complexed with the amino sugar meglumine; silibinin-phosphatidylcholine, the phytolipid delivery system Siliphos™; and Eurosil^{85}/Euromed, a milk thistle extract that is the active component of the nutraceutical Legasil with enhanced bioavailability (Pérez-Sánchez et al., 2019). The results of this study suggest that Eurosil^{85}/Euromed, but not the phytolipid delivery system, is a good candidate for BBB crossing. Accordingly, treatment with the silibinin-based nutraceutical Legasil® resulted in significant clinical and radiological improvement of brain metastases in two NSCLC patients with poor performance status who had progressed after whole brain radiotherapy and chemotherapy (Bosch-Barrera et al., 2016). The suppressive effects of the silibinin-based nutraceutical Legasil® on progressive BM included a significant reduction in peritumoral brain edema without affecting the outgrowth of the primary lung tumors in the same NSCLC patients. A clinical study in a larger cohort of 18 patients with NSCLC and brain metastases confirmed that responses to this silibinin-based therapy were remarkable in the brain, where several complete responses appeared to be achieved and a significantly better overall survival was observed in the cohort of patients treated with the silibinin-based nutraceutical Legasil® (Priego et al., 2018).

II. RATIONALE & HYPOTHESIS

The use of the milk thistle-derived flavonolignan silibinin in the treatment of cancer diseases has been discussed for the past several decades. Commonly used as a hepatoprotectant agent, silibinin is beginning to be considered as a chemopreventive and therapeutic biomolecule for NSCLC that may serve as a model example for other tumor types in the future (**Figure 14**).

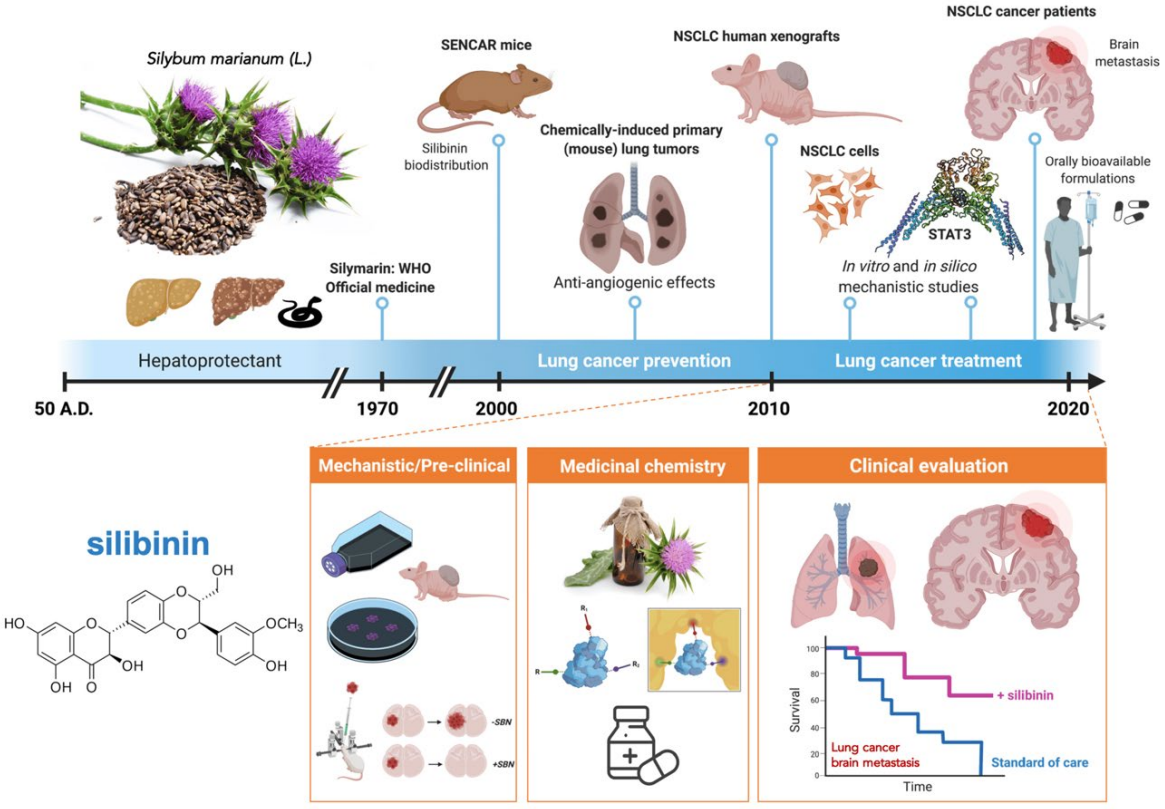

Figure 14. **Key achievements in the timeline of silibinin research in NSCLC.** Extracted from Verdura et al., 2021.

Although several authors have attempted to explain the putative link between silibinin and its multiple beneficial effects against the malignant process in LC diseases, we are accumulating evidence to support the notion that silibinin possesses a multi-targeted mechanism of action. Our project accepts the challenge to **determine whether the expected polypharmacology of silibinin may be better suited than target-selective drugs to globally regulate complex cancer processes with multiple underlying drivers, such as those involved in NSCLC therapeutic resistance and metastatic progression.**

Here, we hypothesized that:

The multi-target behavior of the flavonolignan silibinin, a plausible consequence of the molecular promiscuity of natural phytochemicals, provides an opportunity to globally affect the multifactorial mechanisms underlying the biological aggressiveness of non-small cell lung cancer (NSCLC), including therapeutic resistance and the ability to metastasize to the brain.

III. OBJECTIVES

Our project addresses the global challenge of **applying a modern phenotypic drug discovery approach to molecularly deconstruct and functionally monitor the *on-target* polypharmacology of silibinin that underlies its therapeutic benefits against NSCLC therapeutic resistance and metastatic dissemination capacity**.

Our specific objectives are:

1) To elucidate the molecular mechanisms by which silibinin may reduce the brain tropism capacity of metastatic NSCLC cells in the primary tumor and/or in the brain microenvironment.

2) To elucidate how silibinin prevents the generation of NSCLC cell populations that are refractory to anti-brain metastatic ALK-TKIs and anti-angiogenic multi-TKIs.

3) To elucidate whether the well-established hepatoprotective properties of silibinin can prevent the hyperlipidemic side effects of certain anti-brain metastasis ALK-TKIs.

4) To characterize the mechanism of action of silibinin against well-established tumor cell intrinsic (HSP90) and microenvironmental ($STAT_3$) drivers of NSCLC brain metastasis.

IV. METHODS & RESULTS

STUDY 1

Silibinin is a suppressor of the metastasis-promoting transcription factor ID3

Verdura S, Encinar JA, Gratchev A, Llop-Hernández À, López J, Serrano-Hervás E, Teixidor E, López-Bonet E, Martin-Castillo B, Micol V, Bosch-Barrera J, Cuyàs E, Menendez JA.

Phytomedicine (Under review)

Silibinin is a suppressor of the metastasis-promoting transcription factor ID3

Sara Verdura[a,b], José Antonio Encinar[c], Alexei Gratchev[d], Àngela Llop-Hernández[a,b], Júlia López[a,b], Eila Serrano-Hervás[a,b], Eduard Teixidor[e,f], Eugeni López-Bonet[b,g], Begoña Martin-Castillo[b,h], Vicente Micol[c], Joaquim Bosch-Barrera[e,f,j*], Elisabet Cuyàs[a,b*], Javier A. Menendez[a,b*]

[a] Program Against Cancer Therapeutic Resistance (ProCURE), Catalan Institute of Oncology, 17007 Girona, Spain
[b] Metabolism and Cancer Group, Girona Biomedical Research Institute (IDIBGI), 17190 Girona, Spain
[c] Institute of Research, Development and Innovation in Health Biotechnology of Elche (IDiBE), Universitas Miguel Hernández (UMH), 03202, Elche, Spain
[d] Laboratory for Tumor Stromal Cell Biology, Institute of Carcinogenesis, Nikolaj Nikolajevich (N.N.) Blokhin National Medical Research Center of Oncology, 115478 Moscow, Russia
[e] Precision Oncology Group (OncoGir-Pro), Girona Biomedical Research Institute (IDIBGI), 17190 Girona, Spain
[f] Medical Oncology, Catalan Institute of Oncology, 17007 Girona, Spain
[g] Department of Anatomical Pathology, Dr. Josep Trueta Hospital of Girona, 17007 Girona, Spain
[h] Unit of Clinical Research, Catalan Institute of Oncology, 17007 Girona, Spain
[i] CIBER Fisiopatología de la Obesidad y la Nutrición (CIBEROBN), Instituto de Salud Carlos III (ISCIII), 28029 Madrid, Spain.
[j] Department of Medical Sciences, Medical School, University of Girona, Girona, Spain

* J.A.M, E.C., and J. B-B. share senior authorship

JAVIER A. MENENDEZ, PhD
ELISABET CUYÀS, PhD
JOAQUIM BOSCH-BARRERA, MD PhD
Edifici M2, Parc Hospitalari Martí i Julià
E-17190, Salt (Girona), Spain
Program Against Cancer Therapeutic Resistance (ProCURE)
Catalan Institute of Oncology (ICO)
Girona Biomedical Research Institute
E-mail: jmenendez@idibgi.org ; ecuyas@idibgi.org ; jbosch@iconcologia.net
Phone: +34 872-987-087 Ext. 50
Fax: + 34 972-217-344

HIGHLIGHTS

- *ID3* transcription factor remains a gene that cannot be targeted for the prevention or treatment of cancer metastasis.
- Milk thistle flavonolignan silibinin blocks the inducible activation of ID3 in brain endothelial cells.
- Silibinin prevents the constitutive, acquired, and adaptive expression of ID3 in lung cancer cells.
- Silibinin blocks the transcription of the *ID3* gene through BMP-responsive elements and SMAD1/5-responsive enhancers.
- Silibinin directly inhibits the kinase activity of the BMP receptors ACVRL1/ALK1 and BMPR2.
- Silibinin suppresses ID3 overexpression *in vivo* at clinically relevant concentrations.

ABSTRACT

Background: ID3 (inhibitor of DNA binding/differentiation-3) is a transcription factor that enables metastasis by promoting stem cell-like properties in endothelial and tumor cells. The milk thistle flavonolignan silibinin is a phytochemical with anti-metastatic potential through mechanisms that are largely unknown. ***Hypothesis/purpose:*** We have mechanistically investigated the ability of the silibinin to inhibit the aberrant activation of ID3 in brain endothelium and non-small cell lung cancer (NSCLC) models. ***Methods:*** Bioinformatic analyses were performed to investigate the co-expression correlation between *ID3* and bone morphogenic protein (BMP)/BMP receptor (BMPR) genes in NSCLC patient datasets. ID3 expression was assessed by immunoblotting and qRT-PCR. Luciferase reporter assays were used to evaluate the gene sequences targeted by silibinin to regulate *ID3* transcription. *In silico* computational modeling and LanthaScreen TR-FRET kinase assays were used to characterize the BMPR inhibitory activity of silibinin. Tumor tissues from NSCLC xenograft models treated with oral silibinin were used to evaluate the *in vivo* anti-ID3 effects of silibinin. ***Results:*** Analysis of lung cancer patient datasets revealed a top-ranked positive association of *ID3* with the BMP9 endothelial receptor ACVRL1/ALK1 and the BMP ligand BMP6. Silibinin treatment blocked the BMP9-induced activation of the ALK1-phospho-SMAD1/5-ID3 axis in brain endothelial cells. Constitutive, acquired, and adaptive expression of ID3 in NSCLC cells were all significantly downregulated in response to silibinin. Silibinin blocked *ID3* gene transcription via BMP-responsive elements and SMAD1/5-responsive enhancers. Silibinin inhibited the kinase activities of BMPRs in the micromolar range, with the lower IC_{50} values occurring against ACVRL1/ALK1 and BMPR2. In an *in vivo* NSCLC xenograft model, tumoral overexpression of ID3 was completely suppressed by systematically achievable oral doses of silibinin. ***Conclusions:*** Silibinin is a novel suppressor of the transcription factor ID3 in both the endothelial and tumor cell compartments, which may be explored as a novel therapeutic approach to interfere with the metastatic dissemination capacity of NSCLC.

Key words: lung cancer; ID3; milk thistle; silibinin; bone morphogenic proteins; SMAD; BMP receptors

Abbreviations: bHLH, basic helix-loop-helix; BBB, blood-brain barrier (BBB); BMP, bone morphogenic protein; BMPR, bone morphogenic protein receptor; BRE, BMP-responsive element; CSC, Cancer Stem Cell; DMSO, Dimethyl sulfoxide; ECs, Endothelial cells; FBS, Fetal bovine serum; HRP, horseradish peroxidase; iPSCs, induced pluripotent stem cells; ID, Inhibitor of DNA binding/differentiation; LUAD, lung adenocarcinoma; MEC, Microvascular endothelial cell; NSCLC, non-small cell lung cancer; PBS, phosphate buffered saline; qRT-qPCR, quantitative real-time polymerase chain reaction; SDS-PAGE, sodium dodecyl sulfate polyacrylamide gel electrophoresis; SMAD, Mothers against decantaplegic homolog; TBST, Tris-buffered saline containing Tween; TR-FRET, Time-resolved fluorescence resonance energy transfer.

GRAPHICAL ABSTRACT

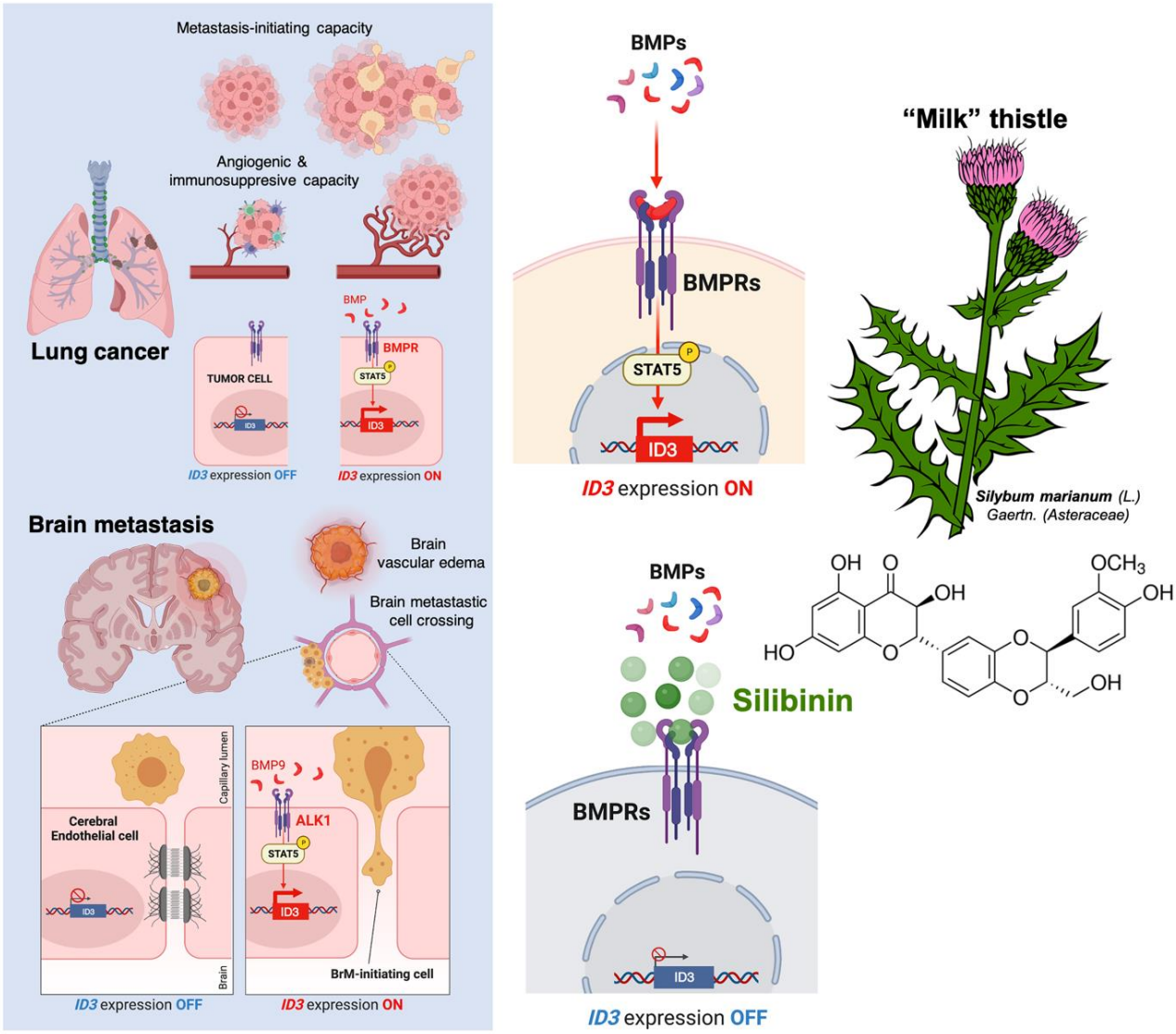

1. INTRODUCTION

The inhibitor of DNA-binding/differentiation (ID) proteins ID1-4 are transcriptional regulators that control cell differentiation by interfering with the DNA-binding activity of basic helix-loop-helix (bHLH) transcription factors (Lasorella et al., 2014; Perk and Iavarone, 2005; Roschger and Cabrele, 2017). ID proteins transcriptionally synchronize the determination of cell fate with the appropriate extracellular interactions in the niche microenvironment, thereby inhibiting differentiation and maintaining the self-renewal and multipotency capacity of stem/progenitor cells during development (Niola et al., 2012). ID protein expression is largely silent in most adult tissues, but can be reactivated in various disease processes such diabetes, Diamond-Blackfan anemia, Rett syndrome, and cancer (Ling et al., 2014; Wang and Baker, 2015). ID proteins are highly expressed in virtually all human tumors, where their presence in the cancer cell compartment and/or in the tumor vasculature is associated with an aggressive phenotype and a poor clinical outcome (Anido et al., 2010; Castañon et al., 2013; Lee et al., 2004; Lyden et al., 1999; Maw et al., 2008; Ponz-Sarvisé et al., 2011; Schindl et al., 2003; Schoppmann et al., 2003; Sharma et al., 2012;). *ID* gene expression confers tumor-initiating capacity and chemo-/radio-resistance to certain subpopulations of cancer stem cell (CSC)-like cells in the context of primary tumorigenesis and during the early stages of metastatic colonization (Gupta et al., 2007; Iavarone and Lasorella, 2006; Ke et al., 2018; Stankic et al., 2013). In addition, ID proteins can exert extrinsic actions to promote metastatic dissemination by remodeling the tumor microenvironment and promoting the activation and recruitment of endothelial cells (ECs) to support tumor angiogenesis at the primary and metastatic sites (Benezra, 2011; Gao et al., 2008). Activation of IDs further contributes to the stemness of ECs, a phenomenon that may facilitate not only the passage of brain metastatic cells across the blood-brain barrier (BBB), but also the reorganization of the cerebral microvasculature in reactive niches of primary and secondary brain tumors (Das and Felty, 2014,2015; Das et al., 2015,2022; Perez et al., 2022).

Disrupting the ID-driven cancer cell-intrinsic and extrinsic regulatory actions may provide additive or even synergistic anti-metastastic effects. However, it is well-known that transcription factors such as ID proteins are notoriously difficult to target with small molecule inhibitors (Nair et al., 2014; Wojnarowicz et al., 2021). First, with the exception of Burkitt's lymphoma (Richter et al., 2012), mutations or genomic rearrangements in the *ID* genes or their promoters are rarely found in most human malignancies. Second, although the feasibility and anti-tumor effects of systemic ID protein targeting have been supported by using siRNA/anti-

sense oligonucleotides delivery systems and cell permeable peptides that target ID proteins for degradation (Mern et al., 2010), the effectiveness of directly inactivating ID proteins might depend on the largely unknown biochemical nature of the ID proteins-containing transcriptional complexes. Third, although a valuable alternative is to target *ID* gene expression rather than ID function, one should acknowledge that cancer-associated reactivation of IDs is due to the convergence of numerous and diverse signaling cascades (e.g., MAPK kinase, Myc, Src, FLT3, VEGF, Wnt, Notch) on the *ID* gene promoters (Nair et al., 2014). Although a small molecule pan-ID antagonist (AGX51) has been shown to phenocopy the effects of *ID1* and *ID3* gene loss to regress therapy-resistant tumor growth and suppress metastatic colonization (Wojnarowicz et al., 2019; 2021), targeted pharmacologic inhibition of ID3 has been unavailable, even in preclinical cancer models. The bone morphogenic protein (BMP) signaling pathway, the major upstream regulator of ID expression in cell biology, may provide an alternate therapeutic path to target ID proteins including ID3. BMPs mediate cancer cell fate decisions, including proliferation, survival, and self-renewal cues, through transcriptional regulation of ID1/3 (Hayashi et al., 2016; Hollnagel et al., 1999; Kowanetz et al., 2004; Ying et al., 2003). Inhibition of BMP signaling decreases cell growth, induces cell death, and reduces stemness of cancer cells by down-regulating ID1/3 proteins. Several generations of small-molecule ATP-competitive inhibitors with varying affinity for the kinase domain of BMP type I and type II receptors (BMPR), such as dorsomorphin, LDN-193189, DMH-2, and JL-5, have been shown to act predominantly as ID1 (but not ID3) inhibitors (Langenfeld et al., 2013a,b).

The flavonolignan silibinin, the major bioactive component of silymarin extract from *Silybum marianum* (milk thistle) seeds, is a phytochemical with a well-established chemopreventive capacity to suppress tumor initiation and progression, but also with therapeutic potential to target metastatic progression (Bosch-Barrera and Menendez, 2015; Bosch-Barrera et al., 2017,2021; Deep and Agarwal, 2010; Mateen et al., 2013). Pre-clinical studies have repeatedly demonstrated the ability of silibinin to suppress signaling pathways involved in metastasis-related phenomena including adhesion, motility, invasiveness, and epithelial-to-mesenchymal transition (EMT) (Cufí et al., 2013a,b; Verdura et al., 2021,2022) by targeting not only not only cancer cells but also supporting components of the tumor microenvironment such as ECs (Deep and Agarwal, 2013; Deep et al., 2017; Mirzaaghaei et al., 2019). Therapeutic interventions with a silibinin-based nutraceutical (Legasil®) have demonstrated the groundbreaking activity of silibinin against established brain metastases (BM), but not against extracranial disease progression, in heavily pretreated non-small cell lung cancer (NSCLC) patients (Bosch-Barrera et al., 2017; Priego et al., 2018). As previously

demonstrated in models of ischemic stroke (Wang et al., 2012), the significant improvement in overall survival of silibinin-treated NSCLC patients (15.5 months versus 4 months in the control group) was accompanied by a marked reduction or prevention of tumor-associated vasogenic edema in BM lesions (Bosch-Barrera et al., 2017; Priego et al., 2018). Vasogenic edema result from the breakdown of the blood-brain barrier (BBB) (Solar et al., 2022), which composed of interacting cells such as ECs, pericytes, and astrocytes, strongly indicating that the anti-BM activity of silibinin may involve a reprogramming of BM-associated non-tumoral cell types (Priego and Valiente 2019; Wasilewski et al., 2017).

We here investigated the mechanistic ability of silibinin to target the expression of the metastasis-promoting *ID3* transcription factor in brain ECs and NSCLC cells. Combining experimental efforts with cultured ECs and NSCLC cell models, luciferase reporter assays with regulatory sequences of the *ID3* gene, *in silico* computational studies using docking and molecular dynamics simulations, and *in vitro* studies with purified BMPR kinases, we now present evidence that silibinin, acting at least in part as a BMP receptor antagonist, suppresses both the inducible expression of ID3 in the brain vasculature as well as the constitutive, acquired and adaptive expression of ID3 in therapy-resistant NSCLC cells.

2. MATERIALS and METHODS

2.1. ID3 gene correlations in lung cancer patients. Gene-level expression files were downloaded from the cBioportal for Cancer Genomics (https://www.cbioportal.org) for The Cancer Genome Atlas Lung Adenocarcinoma Collection (TCGA-LUAD) study, which includes RNAseq data from 510 samples. Patients/samples were categorized based on z-score ±1 threshold relative to all samples into high or low *ID3* mRNA expression groups. Person correlation analysis was performed in tumor samples between ID3 and several genes encoding proteins involved in the BMP signaling pathway. These genes include BMP ligands, activin/inhibins, GDFs, and BMP receptors.

2.2. Cell lines and culture conditions. Human NSCLC cell lines A549 (ATCC CCL-185), H460 (ATCC HTB-177), H1993 (ATCC CRL-5909), and H1975 (ATCC CRL-5908), and HEK293T (ATCC CRL-3216) were obtained from the ATCC (Manassas, VA, USA). The Human Cerebral Microvascular Endothelial Cell (MEC) Line hCMEC/D3 (#CLU512-A) was obtained from Cedarlane Laboratories Limited/Tebu-Bio (Burlington, NC, USA). H3122 (CVCL_5160) and H2228 (ATCC CRL-5935) cell lines, harboring the E13:A20 and E6a/b:A20 variants of the EML4-ALK fusion, respectively, were rendered resistant to crizotinib (H3122/CR and H2228/CR) by incremental and continuous exposure to crizotinib, as previously described (Kim et al., 2013; Verdura et al., 2022; Yamaguchi et al., 2014). Parental PC-9 (RRID:CVCL_B260) cells harboring an EGFR activating mutation (Δ746–750) were obtained from the IBL Cell Bank (Gunma, Japan) and rendered resistant to erlotinib (PC-9/ER) by incremental and continuous exposure to erlotinib, as described (Vazquez-Martin et al., 2013).

A549, PC-9, PC-9/ER, and HEK293T cells were routinely expanded in Dulbecco's modified Eagle's medium (DMEM, Gibco) supplemented with 10% heat-inactivated fetal bovine serum (FBS; Linus), 1% L-glutamine, 1% sodium pyruvate, 50 IU/mL penicillin, and

50 μg/mL streptomycin. H460, H1993, H1975, H3122, H3122/CR, H2228, H2228/CR were routinely expanded in RPMI 1640 (Gibco) supplemented with 10% heat-inactivated FBS, 1% L-glutamine, 50 IU/mL penicillin, and 50 μg/mL streptomycin. hCMEC/D3 cells were grown in EGM™-2 MV MEC Growth Medium-2 BulletKit™ containing EBM™-2 Basal Medium and EGM™-2 MV MEC Growth Medium SingleQuots™ supplements (#H3CC-3202) required for growth of MECs (Lonza) at the following concentrations: 0.025% (*v/v*) rhEGF, 0.025% (*v/v*) VEGF, 0.025% (*v/v*) IGF, 0.1% (*v/v*) rhFGF, 0.1% (*v/v*) gentamicin, 0.1% (*v/v*) ascorbic acid, 0.04% (*v/v*) hydrocortisone, and 2.5% (*v/v*) FBS as specified by Weksler et al. (2005). hCMEC/D3 cells were seeded onto tissue culture flasks were precoated with 1/100 collagen type I solution.

All cells were grown at 37 °C in a humidified atmosphere with 5% CO_2 and were in the logarithmic growth phase at the beginning of the experiments. Cell lines were authenticated by STR profiling, both performed by the manufacturer and confirmed in-house at the time of purchase according to ATCC guidelines. Cells were passaged by starting a low-passage cell stock every month until to 2–3 months after resuscitation. Cell lines were screened for mycoplasma contamination using a PCR-based method for *Mycoplasma* detection prior to experimentation and were intermittently tested thereafter.

2.3. Drugs, reagents, and antibodies. Silibinin (Cat. #S0417) was purchased from Sigma-Aldrich (Madrid, Spain). BMP4 (Cat. #120-05), BMP6 (Cat. #120-06), TGFβ1 (Cat. #AF-100-21C-B), and GDF2 (BMP9; Cat. #120-07-1MG) human recombinant proteins were purchased from PeproTech® EC, Ltd (London, UK). Rabbit monoclonal antibody against ID3 (Cat. #BCH-4/#3-3) and ID1 (Cat. #BCH-1/#195-14) were purchased from BioCheck, Inc. (San Francisco, CA, USA). Rabbit polyclonal antibodies against SMAD2/3 (Cat. #3102), phospho-SMAD2 (Ser465/467)/SMAD3 (Ser423/425) (Cat. #9510), SMAD1 (Cat. #D59D7), SMAD5 (Cat. #D4G2), and SMAD1/5 (Ser463/465) (Cat. #41D10) were purchased from Cell Signaling Technology (Danvers, MA, USA). Mouse monoclonal antibodies against GAPDH (Cat. #60004-1-Ig) and β-actin (Cat. #66009-1-Ig) were purchased from Proteintech (Rosemont, IL, USA). Dorsomorphin (Cat. #S7840) and K02288 (Cat. #S7359) were purchased from Selleckchem (Houston, TX, USA). The Dual-Glo Luciferase Assay System (Cat. #E2920) and the FuGENE® Transfection Reagent (Cat. #E2691) were purchased from Promega Corporation (Madison, WI, USA).

2.4. Luciferase assays. Functional identification and cloning of the *ID3* gene enhancers (ECR1 and ECR2) and *ID3* promoter regulatory sequences (BMP response element [BRE], CAGA boxes, bipartite BRE-CAGA enhancer elements) in ID3 reporter plasmids has been reported previously (Nurgazieva D et al., 2015; Shepherd et al., 2008). HEK293T cells were transfected with ID3 reporter plasmids using the FuGENE® Transfection Reagent according to the manufacturer's instructions. Briefly, cells were seeded 1 day prior to transfection at a density of 5×10^5 cells per well in 6-well plates. For all reporter gene assays, 4 μg of the luciferase reporter plasmid was co-transfected with 40 ng of the *Renilla* reporter plasmid. Twenty-four hours after transfection, the cells were harvested and re-plated in a white 96-well plate that had been pre-coated with 0.1% gelatin. The next day, the cells were stimulated with TGFβ, BMP4, BMP6 or BMP9 (all of them at 10 ng/mL) in the absence or presence of silibinin (100 μmol/L), dorsomorphin (5 μmol/L) or K02288 (1 μmol/L) in medium containing 2% FBS or left untreated, as indicated. All conditions were performed in duplicate. After 24 h of treatment, luciferase and *Renilla* activities were measured using the Dual-Glo Luciferase Assay System according to the manufacturer's instructions. Luminescence measurements were performed using a Cytation 5 plate reader (Biotek). The luciferase activity was first normalized to the Renilla activity and then referenced to the backbone of the corresponding empty plasmid.

2.5. Immunoblotting. Cells were seeded in 6-well plates at 200,000-250,000 cells/well and allowed to grow overnight in maintenance cell culture media containing 10% FBS. Following overnight serum starvation, cells were cultured in the absence or presence of varied concentrations of silibinin in the corresponding media containing 2% FBS (24-48 h). Cells were then washed with ice-cold phosphate buffered saline (PBS), and scraped immediately after adding 30–75 µL of 2% SDS, 1% glycerol, and 5 mmol/L Tris-HCl, pH 6.8. The protein lysates were collected in 1.5 mL microcentrifuge tubes and samples were sonicated for 1 min (under ice water bath conditions) with 2 s sonication at 2 s intervals to fully lyse cells and reduce viscosity. Protein content was determined by the Bradford protein assay (Bio-Rad, Hercules, CA). Sample buffer was added and extracts were boiled for 4 min at 100°C. Equal amounts of protein were electrophoresed on SDS-PAGE gels, transferred to nitrocellulose membranes and incubated with primary antibodies, followed by incubation with a horseradish peroxidase-conjugated secondary antibody and chemiluminescence detection. β-actin was employed as control for protein loading. Densitometric values of protein bands were quantified using densitometry (Image J software, which can be readily downloaded from the NIH website https://imagej.nih.gov/ij/download.html).

2.6. Quantitative Real-Time Polymerase Chain Reaction (qRT-PCR). Total RNA was extracted from cells using the RNA Plus Kit (Macherey-Nagel, Germany) to the manufacturer's instructions. Two micrograms of total RNA was reverse-transcribed to cDNA using the High-Capacity cDNA Reverse Transcription Kit (Applied Biosystems, Waltham, MA). The abundance of *ID3* (Hs00171409_m1) was evaluated in technical replicates relative to the housekeeping genes *ACTB* (Hs99999903_m1) and *GAPDH* (Hs99999905_m1) using an Applied Biosystems QuantStudio™ 7 PCR System with an automated baseline and threshold cycle detection. The transcript abundance was calculated using the comparative C_t method and presented as relative quantification (RQ) or fold-change, as specified.

2.7. Docking Calculations, Molecular Dynamics (MD) Simulations, and Binding Free Energy Analysis. Docking calculation, MD simulations, and molecular mechanics Poisson–Boltzmann surface area (MM/PBSA) calculations to in silico assess both the binding modes and the alchemical binding free energy of silibinin A and B against the 3D crystal structures 3MY0 (ACVRL1/ALK1), 3G2F (BMPR2), 3MDY (BMPR1B/ALK6), 4BGG (ACVR1/ALK2), 2QLU (ACVR2B/ActRIIB), and 3SOC (ACVR2A/ActRIIA) were performed using procedures described in previous works from our group (Cuyàs et al., 2019; Encinar and Menendez, 2020; Verdura et al., 2022). All of the figures were prepared using PyMol 2.0 software and all interactions were detected using the protein-ligand interaction profiler (PLIP) algorithm.

2.8. LanthaScreen kinase assays. To obtained 10-point titration results of the regulatory activity of silibinin on the ATP-dependent kinase activity of ACVRL1/ALK1, ACVR1/ALK2, BMPR1A/ALK3, BMPR2, BMPR1B/ALK6, ACVR2A/ActRIIA, ACVR2B/ActRIIB, LanthaScreen Eu kinase binding assays were outsourced to ThermoFisher Scientific using the SelectScreen™ Biochemical Kinase Profiling Service.

2.9. Statistical Analysis. All cell-based observations were confirmed by at least three independent experiments performed in triplicate for each cell line and for each condition. Data are presented as mean ± SD. Bar graphs, curves, and statistical analyses were generated using GraphPad Prism 10 (GraphPad Software, San Diego, CA). Two-group comparisons were performed using Student's t-test for paired and unpaired values. Comparisons of means of ≥3 groups were performed by ANOVA, and the existence of individual differences, in the case of significant F values in ANOVA, was tested by Tukey's multiple contrasts. p values < 0.05 and <0.005 were considered to be statistically significant (denoted as * and **, respectively). All statistical tests were two-tailed.

3. RESULTS

3.1. ID3 expression is associated with the BMP receptor ALK1/ACVRL1 and the BMP ligands BMP6/BMP2 in lung adenocarcinoma patients. Activation of *ID3* gene transcription is a highly complex output that is encoded in the various possible arrangements of specific BMP ligands and BMP receptor combinations that determine the signaling output of the BMP-SMAD signaling axis (Alsamarah et al., 2015; Antebu et al., 2017; Klumpe et al., 2022). Therefore, we evaluated the potential correlation between *ID3* expression levels and the expression of various BMP ligands and receptors in lung adenocarcinoma (LUAD), the most common histologic subtype of NSCLC. Using LUAD patient data available in the TCGA-LUAD database (n=510), we evaluated and ranked the magnitude and *p*-value of the correlation between *ID3* expression and BMP ligands, activins/inhibins, GDFs, and BMP receptors (**Fig. 1A**).

Among the BMP receptors, the expression of *ACVRL1/ALK1* had the highest positive and statistically significant association with *ID3* (r=0.35, p<0.0001; **Fig. 1A**, *left panels*). When patients were stratified based on median *ID3* expression, patients with high *ID3* expression had significantly higher expression levels of the gene encoding for the type I BMP receptor *ACVRL1/ALK1* (**Fig. 1B**, *top panels*). Endoglin (*ENG*), a co-receptor for the high-affinity ligand for ALK1 BMP9, was also significantly associated with the expression of *ID3* in LUAD patients (r=0.27, p < 0.0001). Among the ligands, *BMP6* expression showed the highest positive and statistically significant association with *ID3* (r=0.38, p<0.0001; **Fig. 1A**, *right panels*). When patients were stratified based on median *ID3* expression, patients with high *ID3* expression had significantly higher levels of *BMP6* (**Fig. 1B**, *bottom panels*). This suggests that high levels of the BMP ligand BMP6 may act as a potential driver of ID3 in LUAD. *BMP2* was also significantly associated with the expression of *ID3* in LUAD patients (r=0.35, p < 0.0001).

3.2. Silibinin inhibits the BMP9-ALK1-SMAD1/5-ID3 signaling pathway in endothelial cells. Given that the endothelial cell-restricted *ACVRL1/ALK1* receptor (Alsina-Sanchís et al., 2018) was significantly associated with *ID3* expression in LUAD patients, we first explored if the presence of silibinin may modify the ability of the ALK1 ligand BMP9 to activate the ALK1-SMAD1/5-ID3 signaling pathway in ECs. To address this question, we selected a clinically-relevant human brain microvascular model of ECs namely the hCMEC/D3 cells (Weksler et al., 2005), which acquire an *ID3*-driven stem cell-like signature in response to

microvascular injury and are widely used as a valuable model of human BBB permeability and brain metastatic cell crossing (Das and Felty, 2014, 2015; Das et al., 2015).

Immunoblotting confirmed that the addition of BMP9 strongly enhanced the SMAD1/5 phosphorylation and robustly upregulated the expression of ID3 protein in hCMEC/D3 ECs. Although TGFβ has been shown to induce lateral activation of SMAD1/5 via TβR1/ALK5 and ALK1 complexes in embryonic ECs (Hiepen et al., 2019; 2020), TGFβ treatment has no effect on either phospho-SMAD1/5 or ID3 status in hCMEC/D3 ECs (**Fig. 2A**). BMP9 can also phosphorylate SMAD2 through heterodimeric complexes of ALK1/ActR2 in HUVEC ECs (Hiepen et al., 2019; 2020), but we did not observe any activation of SMAD2 in response to either BMP9 or TGFβ in hCMEC/D3 ECs (**Fig. 2A**). Taken together, these results confirmed that hCMEC/D3 ECs are an ideal model to evaluate the ability of silibinin to inhibit the BMP9-ALK1-SMAD1/5-ID3 signaling pathway. Addition of silibinin significantly reduced BMP9-induced SMAD1/5 phosphorylation and completely blunted the downstream upregulation of ID3 protein in a time-dependent manner (**Fig. 2B**). Although with different temporal dynamics, silibinin was as efficient as the potent ALK1 inhibitor K02288 (Chen et al., 2021; Sanvitale et al., 2013) in preventing BMP9-stimulated activation of SMAD1/5 and ID3 protein expression. We then verified that the ability of silibinin to impede the BMP9 up-regulatory signaling on ID3 expression occurred at the transcriptional level by assessing the effect of silibinin and K02288 on BMP9-induced *ID3* gene expression in hCMEC/D3 ECs using quantitative real-time PCR (qRT-PCR). The drastic induction of *ID3* mRNA occurring upon stimulation with BMP9 was significantly prevented in the presence of silibinin, largely mimicking the inhibitory activity of the selective type I BMP receptor inhibitor K02288 (**Fig. 2B**).

3.3. Silibinin suppresses constitutive, acquired, and adaptive upregulation of ID3 expression in NSCLC cells. We then investigated the ability of silibinin to regulate ID3 protein expression in a broad panel of NSCLC cell lines with epithelial (E), mesenchymal (M) or mixed epithelial/mesenchymal (E/M) phenotypes (Schliekelman et al., 2015; Thomson et al., 2005; Verdura et al., 2022). Constitutive overexpression of the ID3 protein was detected exclusively in NSCLC models enriched with mesenchymal-like cell subpopulations, such as H460 and A549, the hybrid E/M cell line PC-9 and its erlotinib-resistant derivative PC-9/ER, which showed a further enrichment of EMT-related morphological and transcriptional features (Cufí et al., 2013a,b; Vazquez-Martin et al.., 2013), but not in the epithelial-like H3122 and H1993 cells (**Fig. 3A**, *top panel*). Notably, ID3 overexpression was an acquired trait in H2228/CR

cells, which are derived from ID3-low H2228 epithelial cells by stepwise selection with increasing concentrations of the ALK tyrosine kinase inhibitor (TKI) crizotinib over a period of 8 months and exhibit multiple EMT features driving cross-resistance to next-generation ALK TKIs (Kim et al., 2013; Verdura et al., 2022). In all ID3-positive NSCLC cell models tested, namely H460, A549, PC-9, PC-9/ER and H2228/CR, silibinin treatment significantly downregulated or completely suppressed ID3 protein overexpression in a dose- and time-dependent manner (**Fig. 3B**, *left panels*).

qRT-PCR analysis confirmed that the levels of *ID3* mRNA were significantly up-regulated in the mesenchymal-like NSCLC cell models that over-expressed the ID3 protein, indicating that specific changes in *ID3* mRNA expression closely correspond to changes in ID3 protein expression status in NSCLC cells (**Fig. 3A**, *bottom panel*). To determine whether silibinin could downregulate *ID3* expression at the mRNA level in NSCLC cells as it did in ECs, we used H2228/CR cells as a model of acquired ID3 overexpression (up to 7-fold higher *ID3* mRNA compared to parental H2228 cells). Treatment with silibinin reduced the *ID3* transcript levels by a factor of several fold in a dose- and time-dependent manner, even below the baseline levels observed in the parental H2228 cells (**Fig. 3B**, *right panels*).

Exposure of parental H2228 cells to multi-generation ALK TKIs, including crizotinib, brigatinib, and lorlatinib, promoted significant phospho-activation of SMAD1/5 (**Fig. 3C**). This was accompanied by upregulation of ID3 at both protein and mRNA levels. Silibinin and the pan-type BMPR inhibitor dorsomorphin, but not K02288 (with increased selectivity for ALK1 and ALK2 over other type I BMP receptors and reduced off-targets compared to dorsomorphin), prevented ALK TKIs-induced upregulation of ID3 protein and *ID3* transcripts, while reducing ALK TKIs-induced phospho-activation of SMAD1/5 (**Fig. 3C**).

3.4. Silibinin transcriptionally suppresses *ID3* gene expression via BMP-responsive elements. The above results suggest that silibinin could cause a decrease in *ID3* mRNA levels by inhibiting *ID3* gene transcription. To further confirm that silibinin can transcriptionally attenuate the BMP/SMAD1/5-mediated regulation of *ID3* gene expression, we used previously generated reporter plasmids with or without SMAD1/5-responsive enhancers or BMP-responsive elements in the regulatory sequences of the human *ID3* gene (Nurgazieva et al., 2015; Shepherd et al., 2008). Bioinformatics analysis of novel, potentially SMAD-dependent regulatory elements in the *ID3* gene has allowed the identification of enhancers located between -3177 and -2660 bp upstream of the transcription start site (i.e., a so-called evolutionary conserved region [ECR] 1) and ECR2 located between +4517 and 4662 bp downstream of the

ID3 gene that contains also BRE sites (Nurgazieva et al., 2015). The ECR1 overlaps with a previously described BMP-responsive element in the upstream enhancer of the ID3 gene (nucleotides -3138/-2923 base pairs) (Shepherd et al., 2008), while the ECR2 is a novel SMAD1/5-dependent regulatory element capable of enhancing promoter activity by acting synergistically with ECR1 (Nurgazieva et al., 2015). Reporter plasmids containing either ECR1, ECR2 or both ECR1/ECR2 regions cloned together with an approximately 1-kb fragment of the *ID3* gene promoter were transfected into HEK293 cells and luciferase activity was measured 24 h after transfection. When combined, ECR1 and ECR2 showed a more than additive effect, resulting in a highly significant upregulation of *ID3* promoter activity, particularly in response to BMPs (**Fig. 4A**). BMP6 was the most effective among the BMPs tested in stimulating *ID3* promoter activity in combination with ECRs, especially in the co-presence of ECR1 and ECR2. Silibinin closely mimicked the ability of dorsomorphin –a pan-BMP signaling inhibitor of all type I BMP receptors (ALK2, ALK3, and ALK6) that blocks BMP-mediated SMAD1/5/8 activation– in preventing BMP6- (and also BMP4-) induced activation of the regulatory sequences of the *ID3* gene. Silibinin partially phenocopied the potent ALK1 inhibitor K02288 to block the BMP9-driven hyperactivation of the ECR1/ECR2-dependent *ID3* promoter activity.

Given the exquisite ability of silibinin to prevent the transcriptional activation of the *ID3* gene promoted by BMP6, the BMP ligand with the highest positive correlation with ID3 in LUAD patients (**Fig. 1**), we decided to mechanistically investigate the DNA regulatory elements that control silibinin-mediated suppression of ID3 expression driven by BMP6 signal transduction. HEK293 cells transfected with a pGL2-hID3 reporter containing -4432 to +75 base pairs (bp) of the upstream region of the human *ID3* gene, which contains two clusters of SMAD binding sites (i.e., region A and region B), responded significantly to BMP6 (but not to TGFβ), confirming a similar regulation as previously observed with autocrine BMP4 signaling on the endogenous *ID3* gene in ovarian cancer cells (Shepherd et al., 2008; **Fig. 4B**). The BMP6-induced upregulation of the full-length *ID3* promoter regulatory region was significantly abolished by silibinin treatment. The existence of a BMP6 responsive region required for the ID3 regulatory effects of silibinin was confirmed by a large-scale deletion at the 5' end to -2728 bp. Deletion of the so-called region A including some putative SMAD elements resulted a similar BMP6 responsiveness that was completely abolished in the presence of silibinin. Indeed, the single BMP-responsive ID3 enhancer region (or regulatory region B), including a SMAD4-binding CAGA box and a conserved BMP-responsive element (BRE) site, was sufficient to confer a full BMP6 responsiveness that was exquisitely sensitive to the repressive regulatory

effects of silibinin (**Fig. 4B**). Using reporter constructs with point mutations within the -3138/-2923 region, we observed that while mutation of the CAGA box had no effect on the ability of BMP6 and silibinin to regulate reporter activity, the BMP6 and silibinin responsiveness of the *ID3* enhancer was completely abolished by mutation of the single BRE site that is adjacent to the second CAGA box of the region B (**Fig. 4B**).

3.5. Silibinin is a BMPR receptor inhibitor with significant inhibitory activities against ACVRL1/ALK1, BMPR2 and ALK6. We then investigated whether the above-described ability of silibinin to transcriptionally block the BMP/BMPR-ID3 signaling axis might reflect a direct inhibitory interaction of silibinin with one or various BMPRs. Given that most of the reported inhibitors of the type I BMP receptors work by displacing ATP from the catalytic pocket of the kinase domain, we first performed structural investigations to assess the compatibility of silibinin with the ATP pocket of BMPRs. As silibinin naturally occurs as a 1:1 diastereoisomer mixture of silybins A (*7'' R*, *8'' R*) and B (*7'' S*, *8'' S*) that configurationally differs in the lignan moiety (Křen et al., 2021; Sciacca et al., 2017), we performed classical molecular docking studies of silybin A and silybin B into the ATP/binding pocket of the seven types I and II BMP receptors (**Fig. 5A**). When silybin A was used, the resulting binding energies with the docking simulation were in the range of -9.3 to -10.2 kcal/mol, which probably reflects the high degree of structural similarity between the ATP-binding pocket in the BMP receptors. Slightly higher binding energies were observed for BMPR2 (-9.479 [A] versus -12.81 [B] kcal/mol), ALK6/BMPR1B (-9.667 [A] versus -12.32 [B] kcal/mol), and ALK1/ACVRL1 (-10.151 versus -11.35 [B] kcal/mol) when the silybin B diastereomer was used in the docking simulations. To better understand these predicted trends, we performed molecular dynamics (MD) simulations for each of the BMP receptor-silybin A/B complexes to account for protein flexibility at the target-binding site during the molecular recognition process, thus allowing to confirm the kinetic stability and to validate the binding poses obtained by docking. To rationalize structure-activity relationships and selectivity profiles of silybin A/B ligands, we first calculated the alchemical binding free energy of silibinin against BMP receptors from the entire MD simulation trajectory of 100 ns (or last 30 ns) using the binding free energy calculations under the molecular mechanics Poisson–Boltzmann surface area (MM/PBSA) approximation (**Fig. 5B**). Using >20 kcal/mol as a filtering criterion, only BMPR2 was catalogued as a putative target of silybin A. Four BMP receptors, namely BMPR2, ALK1, ALK2, and ALK6, were cataloged as putative targets of silybin B.

We then used the LanthaScreen Eu kinase binding assay to verify whether silibinin could function as an inhibitor of the ATP-dependent catalytic activity of BMPs. This assay is designed to detect any compound binding to the ATP site, including those binding to the ATP site and adjacent allosteric sites that may be exposed in inactive states of some kinases by monitoring the displacement of an Alexa Fluor 647-labeled "tracer" from the ATP-binding site of an epitope-tagged kinase (here, type II and type I BMP receptors) by a test compound (here, silibinin; **Fig. 5C**). Such a behavior results in a decreased time-resolved fluorescence resonance energy transfer (FRET) signal. The dose-response curves showed that although the emission ratio was decreased in a dose-dependent manner by graded concentrations of silibinin, the IC_{50} values of silibinin differed up to fivefold between the less sensitive and the more sensitive BMP receptor. Thus, while silibinin concentrations as high as 148 μmol/L were required to achieve a half-maximal degree of inhibition in the case of BMPR1A/ALK3, silibinin concentrations as low as 32 μmol/L were sufficient to achieve the IC_{50} value against ALK1/ACVRL1. BMPR2, which exclusively binds BMPs but not activin, and ALK6/BMPR1B, which preferentially binds BMP2 and BMP4, also exhibited IC_{50} values below 50 μmol/L, while IC_{50}s against ActRIIB/ACVR2B, ALK2/ACVR1, and ActRIIA/ACVR2A ranged from ~60 to 75 μmol/L silibinin. **Figure 5D** shows the best poses of silybin A and B coupled to the ATP-dependent catalytic cavities of BMPR2, ALK1, and ALK6 to assess the predicted amino acid residues involved in the different diastereoisomeric binding before (0 ns) and after (100 ns) the MD simulation.

3.6. Oral treatment with silibinin suppresses ID3 overexpression *in vivo*. Finally, to provide definitive validation of the translational potential of the ID3 inhibitory effects of silibinin in *in vitro* cell models, we evaluated the ability of an oral milk thistle extract formulation enriched (30% *w/w*) with a water-soluble form of silibinin complexed with the amino-sugar meglumine to downregulate ID3 overexpression in an *in vivo* xenograft model of PC-9/ER cells (Cufí et al., 2013a,b). After 35 days of oral treatment with vehicle control, erlotinib (100 mg/kg, 5 days a week), silibinin-meglumine (100 mg/kg, 5 days a week), or silibinin-meglumine plus erlotinib, tumors were collected and snap frozen for the isolation of protein. Remarkably, the extremely high levels of ID3 protein that were observed in PC-9/ER tumors, including those from the erlotinib-treated arm, were drastically down-regulated or completely suppressed in response to systemic treatment with either silibinin-meglumine as a single agent or the combination of erlotinib plus silibinin-meglumine (**Fig. 6**).

4. DISCUSSION

We report that the milk thistle-derived flavonolignan silibinin is a novel inhibitor of ID3, a transcription factor that is primarily expressed during development to inhibit differentiation, but is aberrantly re-expressed in vascular disease and biologically aggressive carcinomas (Ling et al., 2014; Perez and Felty, 2022). Our discovery that silibinin antagonizes activation of the metastasis-promoting ID3 transcription factor in both the endothelial and tumor cell compartments may be explored as a novel therapeutic approach to interfere with the metastatic dissemination capacity of NSCLC.

NSCLC is a paradigm of human malignancy in which the expression of ID proteins is a strong prognostic biomarker for poor clinical outcome in patients treated with chemoradiotherapy (Castañon et al., 2013; Ponz-Sarvisé et al., 2011). The expression levels of ID1 and ID3 are positively correlated, but the expression level of ID1 is significantly higher and more abundant than that of ID3 in NSCLC (Castañon et al., 2013). In view of the strong sequence similarity and presumed functional redundancy, it could be argued that such an imbalance reflects ID1 activation to functionally compensate for absence of ID3 (O'Brien et al., 2012; Teo et al., 2020). However, it could also reflect a different mechanistic regulation that is related to the different functions of ID1 and ID3 in the promotion of cancer phenotypes (Chaudhary et al., 2001; Perry et al., 2007;). ID3 may play a more important role than ID1 in the regulation of BMP-induced cell growth and survival in lung cancer cells (Langelfeld et al., 2013a). Both ID1 and ID3 downregulate all three cyclin-dependent kinase inhibitors CDKN1B (p27), CDKN1A (p21) and CDKN2B (p16) to accelerate cell proliferation rates. However, ID3 is a preferential regulator of p27 (Garrett-Engele et al., 2007; Chassot et al., 2007), suggesting that ID3 is a more potent therapeutic target than ID1. In spite of the presumed different roles of ID1 and ID3, little is known about the putative regulators of ID3 in lung cancer patients. In this regard, our current analyses in cohorts of LUAD cancer patients included in the TCGA datasets have established that the expression status of ID3 was significantly correlated with the expression of the BMP ligands BMP6 and BMP2, which are expected to be expressed in the tumor cell compartment of NSCLC and confer poor prognosis by stimulating stem-like phenotypes through the activation of IDs (Langenfeld et al., 2003, 2005, 2006; 2013a,b; Newman et al., 2018). Interestingly, the expression status of *ID3* was also significantly correlated with the expression status of the specialized type I BMP receptor ACVRL1/ALK1 and the co-receptor ENG, which expression pattern is largely restricted to the lung cancer endothelium and closely reflects the vascular nature of ALK1 (Bocci et al., 2019; Mahmoud et al., 2009; Oh et al., 2000). The well-known role of ALK1 as an orchestrator of blood vessels

development begins with the high affinity binding to its preferred ligands BMP9 and BMP10 in the vascular compartment (David et al., 2007), followed by the recruitment of the constitutively active BMPR2 and the auxiliary receptor ENG. The formation of this complex then triggers the phosphorylation of the ID3-activating transcription factors SMAD1/5/8. The expression of ID3 in lung cancer patients may therefore reflect, at least in part, the activation of biological processes that are under the control of ALK1 in the endothelial compartment to drive tumor angiogenesis and metastatic dissemination (Cunha and Pietras, 2011; Cunha et al., 2010, 2015). Interestingly, endothelial ALK1 expression has recently been implicated in the regulation of gene sets (e.g., "inflammatory response", "interferon-γ", and "IL6/JAK/STAT3") that control immune cell function and infiltration (Bocci et al., 2019). Thus, the expression of ACVRL1/ALK1 is not exclusively associated with the angiogenic process, but extends to other biological processes affecting non-malignant cellular entities in the tumor microenvironment, in particular the immune cells. Previous studies have shown an inverse correlation between ID1 expression and several immune response markers, including PD-L1; in fact, suppression of ID1 has been shown to promote PD-L1 expression on the surface of tumor cells (Baraibar et al., 2020). It may be tempting to suggest that ID1 and ID3 exert complementary but convergent immunoregulatory functions in NSCLC, with the former negatively regulating immune checkpoints in the tumor cell compartment and the latter involved in controlling the immune response downstream of the ALK1-positive endothelial compartment. Nevertheless, the ability of silibinin to function as an ALK1 blocker may warrant further investigation in combination with immunomodulatory drugs to elucidate the therapeutic value of interfering with the BMP9/ALK1/ID3 signaling axis in the endothelial compartment of NSCLC.

ID3 is a key contributor to vessel injury, including microvascular lesions in the lung and brain (Chu et al., 2022; Das and Felty, 2014, 2015; Das et al., 2015). In the lung, *ID3* is a redox-sensitive gene (Felty and Porther, 2008; Mueller et al., 2002) that contributes to the generation of mesenchymal-like, vascular lesion "initiating" ECs that share a molecular stem cell-like signature involving the activation of embryonic transcription factors (OCT4, NANOG, SOX2; Das et al., 2015; Yang et al., 2014) as seen in induced pluripotent stem cells (iPSCs; Hayashi et al., 2016) and tumor-initiating CSCs (Huang et al., 2019). Accordingly, ID3 has been proposed as a molecular risk factor that drives the generation of vascular stem cells under conditions of oxidative stress in the pathogenesis of benign and malignant vascular lesions (Perez and Felty, 2022). In the brain, ID3 overexpression in ECs exposed to oxidative stress conditions leads to increased neovascularization and abnormal vessel sprouting (Das and Felty, 2014). In this scenario, ID3 is a key transcriptional activator of brain angiopathy gene networks,

which are mainly involved in the repair of endothelial damage after vascular insults (Perez et al., 2023). Using hCMEC/D3 cells, a stable population of human cerebral microvascular ECs that stably maintains a normal BBB phenotype and is well suited for understanding the response of the brain endothelium to a variety of stimuli (Das and Felty, 2014, 2015; Das et al., 2015; Weksler et al., 2005), we confirmed the ability of silibinin to molecularly mimic the ALK1 inhibitor K02288 and completely block the inducible activation of the phospho-SMAD1/5-ID3 axis. Our current findings showing that silibinin may function as a novel therapeutic that targets the redox-sensitive transcriptional activation of ID3 to prevent microvascular lesions could be considered as a mechanism by which silibinin-based nutraceuticals clinically prevent the vasogenic edema resulting from BBB breakdown during the growth of established brain metastases (Bosch-Barrera et al., 2016; Priego et al., 2018). Moreover, given that ID3-overexpressing endothelial stem-like cells can direct metastatic cancer cells to cross the BBB (Jayanta et al., 2018), further studies should explore the possibility that anti-ID3 activity of silibinin in brain vascular endothelium may significantly modify both the ability to cross the BBB and the ultimate fate of brain-tropic metastatic cancer cells (i.e., overt BM formation, dormancy, or clearance) involving BBB remodeling.

We observed constitutive and acquired high levels of ID3 expression in NSCLC cell lines with either constitutive or acquired mesenchymal characteristics. Reactivation of fundamental embryonic processes such as EMT is associated with increased cancer cell plasticity, resistance to therapy, reprograming of the local immune response towards immunosuppressive microenvironments, and poor prognosis in several cancers including NSCLC (Byers et al., 2013; Chae et al., 2018; Mak et al., 2016; Thompson et al., 2020). ID3 overexpression in mesenchymal-like NSCLC cells, which may reflect a convergent downstream target of not only autocrine/paracrine BMP signals but also of commonly activated pro-proliferative and pro-oncogenic pathways in cancer cells. The transcriptional suppression of ID3 overexpression by silibinin was certainly notable in EMT-like NSCLCs with acquired resistance to ALK and EGFR TKIs (Cufí et al., 2013a,b; Kim et al., 2013; Vazquez-Martin et al., 2013; Verdura et al., 2022). A hyperactive BMP-BMPR-SMAD signaling leading to transcriptional activation of ID3 expression is critical for a successful reprogramming of differentiated cells into iPSCs (Hayashi et al., 2016). In addition, blockade of differentiation transcription factor by ID3 enables the self-renewal response to STAT3 activating signals such as the leukemia inhibitory factor (LIF), a pro-metastatic and immunomodulatory factor of the IL-6 cytokine superfamily (Yin et al., 2003). Given the well-established ability of silibinin to directly block STAT3 activity (Verdura et al., 2018) as an effective mechanism to suppress

brain metastasis and therapy-resistant EMT phenotypes (Priego et al., 2018; Verdura et al., 2021), it may be tempting to speculate that the unanticipated capacity of silibinin to inhibit ID3 overexpression could act in synergy with its anti-STAT3 activity to fine-tune the phenotypic plasticity and EMT switching of metastatic cancer cells. Immediate early genes such as *ID3* are rapidly and transiently expressed in response to stressful signals, particularly oxidative damage (Das and Felty, 2014; Mueller et al., 2002). ALK-TKIs such as crizotinib are known to produce excessive endogenous levels of oxidants as a major mechanism of cytotoxicity in various cell types, including cancer cells (Dai et al., 2017; Guo et al., 2021; Yan et al., 2019; Varma and Tiwari, 2021). Our finding that ID3 is transcriptionally activated in response to multi-generation ALK-TKIs (i.e., crizotinib, brigatinib, and erlotinib) may indicate that inducible activation of ID3 is an adaptive antioxidant-mitochondrial response that can be suppressed by silibinin to sensitize NSCLCs to ALK-TKIs.

Aberrant BMP signaling, which leads to the overexpression of *ID* genes observed in many human cancers, is initiated by one of ~ 20 different extracellular dimeric BMP ligands, typically acting in a paracrine or autocrine manner (Alsamarah et al., 2015; Antebu et al., 2017; Klumpe et al., 2022). BMP ligands signal by binding to three distinct type II receptors (BMPR2, ActR2A/ACVR2A, and ActR2B/ACVR2B), which differ in their ligand and oligomerization partner preferences, and at least four type I receptors commonly known as activin receptor-like kinases (ALK1/ACVRL1, ALK2/ACVR1, ALK3/BMPR1A, and ALK6/BMPR1B) (Nickel and Mueller, 2019). Subsequently, activated BMP type I receptors (ALK1/2/3/6) within the BMP receptor complex phosphorylate the BMP-responsive SMAD proteins 1 and 5 to facilitate nuclear translocation in complex with the co-SMAD SMAD4, thereby forming DNA sequence-specific transcription factor complexes at the regulatory sequences of BMP-responsive genes including *ID3*. Reporter assays were used to determine how silibinin affects the strong positive correlation between certain BMP ligands and ID3 expression in LUAD patients. Transcriptional reporters of the *ID3* regulatory sequences confirmed the ability of silibinin to block BMP-activated *ID3* gene transcription via BMP-responsive elements and SMAD1/5-responsive enhancers located upstream and downstream of intronic enhancers of the *ID3* gene (Nurgazieva et al., 2015; Shepherd et al., 2008). These data raise the possibility that silibinin may reduce endogenous *ID3* mRNA expression by blocking autocrine BMP signaling-induced DNA-protein interactions present at the enhancer elements of the *ID3* gene not only in NSCLC tumor cells themselves but also in the ID3-expressing neovascular endothelium of NSCLC tumors. Specifically, silibinin appears to target ID3 expression by preventing the SMAD complex binding to BRE enhancer elements. Using side-by-side comparisons of *in silico* computational

modeling studies with *in vitro* evaluation of kinase selectivity assays, we profiled the ability of silibinin to function as a putative BMP receptor kinase inhibitor to block the BMP/SMAD/ID3 axis upstream. Computational modeling of silibinin diastereoisomers (silybin A and silybin B) (Křen et al., 2021; Sciacca et al., 2017) at the catalytic ATP pocket of the BMPR kinase domains revealed that silibinin possesses a structural basis for the inhibition of specific BMP receptors as a small molecule. Our *in silico* approach suggested a putative role of silibinin stereochemistry in determining the inhibitory potential of silibinin against the kinase activity of BMP receptors, implicating silybin B as the major responsible for the observed BMP/SMAD1/5 signaling-targeted inhibitory effects of the diastereoisomeric silibinin mixture used in cell culture-based experiments. Silybin B, but not silybin A, was predicted to occupy the kinase hinge region of ALK1 in an ATP-mimetic fashion and directly hydrogen-bond to both His280 and the catalytic β3 lysine (Lys229), partially mimicking the inhibitory mechanisms of the ALK1 inhibitors LDN-193189 and K02288 (Kerr et al., 2015; Sanvitale et al., 2013). Silybin B, but not silybin A, was predicted to interact via hydrogen bonding with the kinase hinge region of BMPR2 and further hydrogen bonding with the Lys230-containing catalytic loop and the phosphate-binding loop (Chaikuad et al., 2019). Both silybin A and silybin B were predicted to occupy the ATP binding pocket of ALK6 involving direct interactions with the catalytic Lys231 (Rooney and Jones, 2012). To confirm the binding potency of silibinin to specific BMPRs, we used a LanthaScreen Eu-based time-resolved FRET-based kinase binding assay to compare the inhibitory potency of silibinin against seven different BMPRs. *In vitro* screening assays confirmed that silibinin can act as a promiscuous ATP-competitive antagonist of the serine/threonine kinase activity of BMP receptors type I (e.g., ALK1 and ALK6) and type II (e.g., BMPR2) in the tens of micromolar range. Except for ALK2, the predicted binding affinities were in very good agreement with the experimental ones obtained with the natural 1:1 silybin A:silybin B mixture. These computational findings may guide the development of silibinin and/or the next generation of silibinin derivatives as novel BMPR-targeting therapeutics to counter the ID3-driven metastatic phenotype in brain ECs and NSCLC cells.

Our study has several limitations that should be acknowledged. First, silibinin may affect ID3 expression not only by reducing *ID3* gene transcription (through the BMP/BMPR/SMAD pathway carefully dissected here), but also by promoting an imbalance between ID3 protein degradation and synthesis in some scenarios. Curcumin, the major phytochemical component of turmeric that synergistically interacts with silibinin to exert anticancer activity (Montgomery et al., 2016; Sayyed et al., 2022), can trigger the degradation of ID3 by promoting its proteasome-dependent proteolysis (Berse et al., 2004). Further studies

should explore whether silibinin can mimic curcumin to target an as yet unknown ID3 ubiquitin ligase and increase the rate of ubiquitin-dependent degradation of ID3. Second, silibinin may reduce ID3 protein synthesis without affecting ID3 protein degradation in NSCLC cells. Silibinin has been shown to block mammalian target of rapamycin (mTOR) signaling to inhibit translation initiation and global protein synthesis associated with reduced levels of eukaryotic initiation factor 4F complex (Garcia-Maceira et al., 2009; Jung et al., 2009; Lin et al., 2009). Whether the partial collapse of polysomes that can be observed in response to silibinin is accompanied by pronounced consequences on the specific translation of the *ID3* mRNA, as has been shown for cyclin D1 (Lin et al., 2009) or HIF-1α (Jung et al., 2009), deserves further investigation. Third, it remains to be determined whether silibinin-driven blockade of ID3 expression causally disrupts several metastatic features in the NSCLC phenotype, including cell spreading/motility, and/or EMT-related drug resistance phenomena.

Systemic administration of an orally active, water-soluble form of silibinin complexed with the amino-acid excipient meglumine (Cufí et al., 2013a,b) was able to completely suppress the extremely high levels of ID3 expression found in EGFR TKI-refractory xenografted tumor tissues *in vivo*. The corresponding human equivalent dose (HED) for the dose of silibinin used in our *in vivo* study, which was equivalent to 100 mg/kg mouse body weight, was 8.11 mg/kg. This corresponds to a dose of 486.49 mg of silibinin for a 60-kg individual, an HED that is likely within the dose range that can be achieved in target cancer tissues when using clinically available formulations of silibinin (Bosch-Barrera et al., 2016, Hoh et al., 2006; Kidd, 2009).

5. CONCLUSIONS

As evidence accumulates that ID3 plays a causative role in the spread of metastatic cancer cells to the brain (Das et al., 2022; Jayanta et al., 2018), in the development of adaptive drug resistance to TKI (Sachindra et al., 2017), and in T-cell exhaustion during CAR T-cell immunotherapy (Good et al., 2021), the discovery and development of novel ID3 suppressing agents are urgently needed. We here describe for the first time how the milk thistle flavonolignan silibinin, which has been marketed as a dietary supplement, operates as a novel drug-like inhibitor of *ID3*. Given the dual capacity of ID3 to drive metastasis by conferring molecular stem cell properties not only in microvascular ECs but also in biologically aggressive subsets of cancer cells, nutraceutical formulations of silibinin with improved bioavailability properties and demonstrated clinical activity could be explored as potential strategy to interfere with the ID3-driven metastastic traits in NSCLC.

Funding. The work in the Menendez laboratory is supported by the Ministerio de Ciencia e Innovación (MCIN, grants PID2019-10455GB-I00 and PID2022-141955OB-I00 to Javier A. Menendez, Plan Nacional de I+D+i, funded by the European Regional Development Fund, Spain) and the Emerging Research Group SGR 2021 01507 to Begoña Martin-Castillo from the Agència de Gestió d'Ajuts Universitaris i de Recerca (AGAUR, Generalitat de Catalunya). Elisabet Cuyàs holds a "Miguel Servet" research contract (CP20/00003) from the Instituto de Salud Carlos III (Spain) and is supported by the Grant PI22/00297 (Instituto de Salud Carlos III, Proyectos de I+D+I en Salud, Acción Estratégica en Salud 2021–2023, founded by the European Regional Development Fund, Spain). The work in the Jose A. Encinar laboratory is supported by the Spanish Ministry of Economy and Competitiveness (MINECO, Grant RTI2019-096724-B-C21) and the Generalitat Valenciana (PROMETEO/2021/059). Eila Serrano-Hervás holds an INVESTIGO research contract (2022 INV-1 00001, Next Generation Catalunya, Next Generation EU) from the Agència de Gestió d'Ajuts Universitaris i de Recerca (AGAUR, Generalitat de Catalunya). Eduard Teixidor holds a "Rio Hortega" research contract (CM22/00276, Proyectos de I+D+I en Salud, Acción Estratégica en Salud 2021–2023, founded by the European Regional Development Fund, Spain) from the Instituto de Salud Carlos III (Spain).

CRediT authorship contribution statement

Sara Verdura: Methodology, Investigation, Validation, Data Curation, Formal analysis, Visualization. **José Antonio Encinar:** Methodology, Investigation, Formal analysis, Visualization, Data Curation. **Alexei Gratchev:** Resources, Methodology, Investigation, Visualization. **Àngela Llop-Hernández:** Investigation, Formal analysis, Validation. **Júlia López:** Investigation, Formal analysis, Validation. **Eila Serrano-Hervás:** Investigation, Methodology, Formal analysis, Visualization. **Eduard Teixidor:** Methodology, Investigation, Validation. **Eugeni López-Bonet:** Methodology, Investigation, Visualization. **Begoña Martin-Castillo:** Project administration, Methodology, Investigation. **Vicente Micol:** Conceptualization, Resources, Methodology. **Joaquim Bosch-Barrera**: Conceptualization, Project administration, Supervision, Methodology, Writing–original draft. **Elisabet Cuyàs:** Project administration, Supervision, Resources, Methodology, Formal analysis, Visualization, Writing–original draft. **Javier A. Menendez:** Conceptualization, Project administration, Resources, Supervision, Methodology, Visualization, Writing–original draft, Writing– review & editing.

Declaration of Generative AI and AI-assisted technologies in the writing process. During the preparation of this paper, the authors did not use any AI tool/service or AI-assisted technologies in the writing process.

Conflict of interest. Joaquim Bosch-Barrera reports grants and personal fees from Pfizer, MSD Spain, BMS, AstraZeneca, Novartis, Boehringer-Ingelheim, Vifor, Sanofi, and LEO Pharma outside the submitted work. This study was supported in part by a research grant from Pfizer to Joaquim Bosch-Barrera and Javier A. Menendez. These funders had no role in the design of the study, in the collection, analyses, or interpretation of data, in the writing of the manuscript, or in the decision to publish the results.

Acknowledgments. We are very grateful to Mark W. Nachtigal for kindly providing us with all the pGL2-ID3 reporters, which were instrumental in the functional identification of the elements responsible for silibinin regulation of BMP-stimulated *ID3* gene transcription. We also thank Jin Kyung Rho (Department of Convergence Medicine, Asan Medical Center, University of Ulsan, College of Medicine, Seoul, South Korea) and Jae Cheol Lee (Department of Oncology, Asan Medical Center, University of Ulsan College of Medicine, Seoul, South Korea) for providing us the H2228–H2228/CR (crizotinib-resistant) cell line pair and Daniel B. Costa (Beth Israel Deaconess Medical Center, Harvard Medical Scholl, Boston, MA, USA) for providing the H3122–H3122/CR (crizotinib-resistant) cell line pair. We are grateful to the Servicio de Supercomputación of the University of Granada for allowing us to use the ALBAICIN computer cluster (**https://supercomputacion.ugr.es/arquitecturas/albaicin/**). We wish to especially thank Santiago Melchor for his kind help and collaboration. We are also grateful to the Cluster of Scientific Computing (**http://ccc.umh.es**) of the Universidad Miguel Hernández (UMH) for providing computing facilities.

REFERENCES

Alsamarah, A., LaCuran, A.E., Oelschlaeger, P., Hao, J., Luo, Y., 2015. Uncovering Molecular Bases Underlying Bone Morphogenetic Protein Receptor Inhibitor Selectivity. PLoS One. 10, e0132221.

Anido, J., Sáez-Borderías, A., Gonzàlez-Juncà, A., Rodón, L., Folch, G., Carmona, M.A., Prieto-Sánchez, R.M., Barba, I., Martínez-Sáez, E., Prudkin, L., Cuartas, I., Raventós, C., Martínez-Ricarte, F., Poca, M.A., García-Dorado, D., Lahn, M.M., Yingling, J.M., Rodón, J., Sahuquillo, J., Baselga, J., Seoane, J., 2010. TGF-β Receptor Inhibitors Target the CD44(high)/Id1(high) Glioma-Initiating Cell Population in Human Glioblastoma. Cancer Cell 18, 655–668.

Antebi, Y.E., Linton, J.M., Klumpe, H., Bintu, B., Gong, M., Su, C., McCardell, R., Elowitz, M.B., 2017. Combinatorial Signal Perception in the BMP Pathway. Cell 170, 1184–1196.

Alsina-Sanchís, E., García-Ibáñez, Y., Figueiredo, A.M., Riera-Domingo, C., Figueras, A., Matias-Guiu, X., Casanovas, O., Botella, L.M., Pujana, M.A., Riera-Mestre, A., Graupera, M., Viñals, F., 2018. ALK1 Loss Results in Vascular Hyperplasia in Mice and Humans Through PI3K Activation. Arterioscler. Thromb. Vasc. Biol. 38, 1216–1229.

Baraibar, I., Roman, M., Rodríguez-Remírez, M., López, I., Vilalta, A., Guruceaga, E., Ecay, M., Collantes, M., Lozano, T., Alignani, D., Puyalto, A., Oliver, A., Ortiz-Espinosa, S., Moreno, H., Torregrosa, M., Rolfo, C., Caglevic, C., García-Ros, D., Villalba-Esparza, M., De Andrea, C., Vicent, S., Pío, R., Lasarte, J.J., Calvo, A., Ajona, D., Gil-Bazo, I., 2020. Id1 and PD-1 Combined Blockade Impairs Tumor Growth and Survival of *KRAS*-mutant Lung Cancer by Stimulating PD-L1 Expression and Tumor Infiltrating $CD8^+$ T Cells. Cancers (Basel) 12, 3169.

Benezra, R., 2001. Role of Id proteins in embryonic and tumor angiogenesis. Trends Cardiovasc. Med. 11, 237–241.

Berse, M., Bounpheng, M., Huang, X., Christy, B., Pollmann, C., Dubiel, W., 2004. Ubiquitin-dependent degradation of Id1 and Id3 is mediated by the COP9 signalosome. J. Mol. Biol. 343, 361–370.

Bocci, M., Sjölund, J., Kurzejamska, E., Lindgren, D., Marzouka, N.A., Bartoschek, M., Höglund, M., Pietras, K., 2019. Activin receptor-like kinase 1 is associated with immune cell infiltration and regulates CLEC14A transcription in cancer. Angiogenesis 22, 117–131.

Bosch-Barrera, J., Menendez, J.A., 2015. Silibinin and STAT3: A natural way of targeting transcription factors for cancer therapy. Cancer Treat. Rev. 41, 540–546.

Bosch-Barrera, J., Queralt, B., Menendez, J.A., 2017. Targeting STAT3 with silibinin to improve cancer therapeutics. Cancer Treat. Rev. 58, 61–69.

Bosch-Barrera, J., Sais, E., Cañete, N., Marruecos, J., Cuyàs, E., Izquierdo, A., Porta, R., Haro, M., Brunet, J., Pedraza, S., Menendez, J.A., 2016. Response of brain metastasis from lung cancer patients to an oral nutraceutical product containing silibinin. Oncotarget 2016, 32006–32014.

Bosch-Barrera, J., Verdura, S., Ruffinelli, J.C., Carcereny, E., Sais, E., Cuyàs, E., Palmero, R., Lopez-Bonet, E., Hernández-Martínez, A., Oliveras, G., Buxó, M., Izquierdo, A., Morán, T., Nadal, E., Menendez, J.A., 2021. Silibinin Suppresses Tumor Cell-Intrinsic Resistance to Nintedanib and Enhances Its Clinical Activity in Lung Cancer. Cancers (Basel) 13, 4168.

Byers, L.A., Diao, L., Wang, J., Saintigny, P., Girard, L., Peyton, M., Shen, L., Fan, Y., Giri, U., Tumula, P.K., Nilsson, M.B., Gudikote, J., Tran, H., Cardnell, R.J., Bearss, D.J., Warner, S.L., Foulks, J.M., Kanner, S.B., Gandhi, V., Krett, N., Rosen, S.T., Kim, E.S., Herbst, R.S., Blumenschein, G.R., Lee, J.J., Lippman, S.M., Ang, K.K., Mills, G.B., Hong, W.K., Weinstein, J.N., Wistuba, I.I., Coombes, K.R., Minna, J.D., Heymach, J.V., 2013. An epithelial-mesenchymal transition gene signature predicts resistance to EGFR and PI3K inhibitors and identifies Axl as a therapeutic target for overcoming EGFR inhibitor resistance. Clin. Cancer Res. 19, 279–290.

Castañon, E., Bosch-Barrera, J., López, I., Collado, V., Moreno, M., López-Picazo, J.M., Arbea, L., Lozano, M.D., Calvo, A., Gil-Bazo, I., 2013. Id1 and Id3 co-expression correlates with clinical outcome in stage III-N2 non-small cell lung cancer patients treated with definitive chemoradiotherapy. J. Transl. Med. 11, 13.

Chae, Y.K., Chang, S., Ko, T., Anker, J., Agte, S., Iams, W., Choi, W.M., Lee, K., Cruz, M., 2018. Epithelial-mesenchymal transition (EMT) signature is inversely associated with T-cell infiltration in non-small cell lung cancer (NSCLC). Sci. Rep. 8, 2918.

Chaikuad, A., Thangaratnarajah, C., von Delft, F., Bullock, A.N., 2019. Structural consequences of BMPR2 kinase domain mutations causing pulmonary arterial hypertension. Sci. Rep. 9, 18351.

Chassot, A.A., Turchi, L., Virolle, T., Fitsialos, G., Batoz, M., Deckert, M., Dulic, V., Meneguzzi, G., Buscà, R., Ponzio, G., 2007. Id3 is a novel regulator of p27kip1 mRNA in early G1 phase and is required for cell-cycle progression. Oncogene 26, 5772–5783.

Chaudhary, J., Johnson, J., Kim, G., Skinner, M.K., 2001. Hormonal regulation and differential actions of the helix-loop-helix transcriptional inhibitors of differentiation (Id1, Id2, Id3, and Id4) in Sertoli cells. Endocrinology 142, 1727–1736.

Chen, H., Nio, K., Yamashita, T., Okada, H., Li, R., Suda, T., Li, Y., Doan, P.T.B., Seki. A., Nakagawa, H., Toyama, T., Terashima, T., Iida, N., Shimakami, T., Takatori, H., Kawaguchi, K., Sakai, Y., Yamashita, T., Mizukoshi, E., Honda, M., Kaneko, S., 2021. BMP9-ID1 signaling promotes EpCAM-positive cancer stem cell properties in hepatocellular carcinoma. Mol. Oncol. 15, 2203–2218.

Chu, Y.H., Lin, J.D., Nath, S., Schachtrup, C., 2022. Id proteins: emerging roles in CNS disease and targets for modifying neural stem cell behavior. Cell Tissue Res. 387, 433–449.

Cufí, S., Bonavia, R., Vazquez-Martin, A., Corominas-Faja, B., Oliveras-Ferraros, C., Cuyàs, E., Martin-Castillo, B., Barrajón-Catalán, E., Visa, J., Segura-Carretero, A., Bosch-Barrera, J., Joven, J., Micol, V., Menendez, J.A., 2013a. Silibinin meglumine, a water-soluble form of milk thistle silymarin, is an orally active anti-cancer agent that impedes the epithelial-to-mesenchymal transition (EMT) in EGFR-mutant non-small-cell lung carcinoma cells. Food Chem. Toxicol. 60, 360–368.

Cufí, S., Bonavia, R., Vazquez-Martin, A., Oliveras-Ferraros, C., Corominas-Faja, B., Cuyàs, E., Martin-Castillo, B., Barrajón-Catalán, E., Visa, J., Segura-Carretero, A., Joven, J., Bosch-Barrera, J., Micol, V., Menendez, J.A., 2013b. Silibinin suppresses EMT-driven erlotinib resistance by reversing the high miR-21/low miR-200c signature in vivo. Sci. Rep. 3, 2459.

Cunha, S.I., Bocci, M., Lövrot, J., Eleftheriou, N., Roswall, P., Cordero, E., Lindström, L., Bartoschek, M., Haller, B.K., Pearsall, R.S., Mulivor, A.W., Kumar, R., Larsson, C., Bergh, J., Pietras, K., 2015. Endothelial ALK1 Is a Therapeutic Target to Block Metastatic Dissemination of Breast Cancer. Cancer Res. 75, 2445–2456.

Cunha, S.I., Pardali, E., Thorikay, M., Anderberg, C., Hawinkels, L., Goumans, M.J., Seehra, J., Heldin, C.H., ten Dijke, P., Pietras, K., 2010. Genetic and pharmacological targeting of activin receptor-like kinase 1 impairs tumor growth and angiogenesis. J. Exp. Med. 207, 85–100.

Cunha, S.I., Pietras, K., 2011. ALK1 as an emerging target for antiangiogenic therapy of cancer. Blood 117, 6999–7006.

Cuyàs, E., Verdura, S., Micol, V., Joven, J., Bosch-Barrera, J., Encinar, J.A., Menendez, J.A., 2019. Revisiting silibinin as a novobiocin-like Hsp90 C-terminal inhibitor: Computational modeling and experimental validation. Food Chem. Toxicol. 132, 110645.

Dai, X., Guo, G., Zou, P., Cui, R., Chen, W., Chen, X., Yin, C., He, W., Vinothkumar, R., Yang, F., Zhang, X., Liang, G., 2017. (S)-crizotinib induces apoptosis in human non-small cell lung cancer cells by activating ROS independent of MTH1. J. Exp. Clin. Cancer Res. 36, 120.

Das, J.K., Deoraj, A., Roy, D., Felty, Q., 2022. Brain infiltration of breast cancer stem cells is facilitated by paracrine signaling by inhibitor of differentiation 3 to nuclear respiratory factor 1. J. Cancer Res. Clin. Oncol. 148, 2881–2891.

Das, J.K., Felty, Q., 2015. Microvascular lesions by estrogen-induced ID3: its implications in cerebral and cardiorenal vascular disease. J. Mol. Neurosci. 55, 618–631.

Das, J.K., Felty, Q., 2014. PCB153-induced overexpression of ID3 contributes to the development of microvascular lesions. PLoS One 9, e104159.

Das, J.K., Voelkel, N.F., Felty, Q., 2015. ID3 contributes to the acquisition of molecular stem cell-like signature in microvascular endothelial cells: its implication for understanding microvascular diseases. Microvasc. Res. 98, 126-138.

David, L., Mallet, C., Mazerbourg, S., Feige, J.J., Bailly, S., 2007. Identification of BMP9 and BMP10 as functional activators of the orphan activin receptor-like kinase 1 (ALK1) in endothelial cells. Blood 109, 1953–1961.

de Vinuesa, A.G., Bocci, M., Pietras, K., Ten Dijke, P., 2016. Targeting tumour vasculature by inhibiting activin receptor-like kinase (ALK)1 function. Biochem. Soc. Trans. 44, 1142–1149.

Deep, G., Agarwal, R., 2010. Antimetastatic efficacy of silibinin: molecular mechanisms and therapeutic potential against cancer. Cancer Metastasis Rev. 29, 447–463.

Deep, G., Agarwal, R., 2013. Targeting tumor microenvironment with silibinin: promise and potential for a translational cancer chemopreventive strategy. Curr. Cancer Drug Targets 13, 486–499.

Deep, G., Kumar, R., Nambiar, D.K., Jain, A.K., Ramteke, A.M., Serkova, N.J., Agarwal, C., Agarwal, R., 2017. Silibinin inhibits hypoxia-induced HIF-1α-mediated signaling, angiogenesis and lipogenesis in prostate cancer cells: In vitro evidence and in vivo functional imaging and metabolomics. Mol. Carcinog. 56, 833–848.

Encinar, J.A., Menendez, J.A., 2020. Potential Drugs Targeting Early Innate Immune Evasion of SARS-Coronavirus 2 via 2'-O-Methylation of Viral RNA. Viruses 12, 525.

Felty, Q., Porther, N., 2008. Estrogen-induced redox sensitive Id3 signaling controls the growth of vascular cells. Atherosclerosis 198, 12–21.

Gao, D., Nolan, D.J., Mellick, A.S., Bambino, K., McDonnell, K., Mittal, V., 2008. Endothelial progenitor cells control the angiogenic switch in mouse lung metastasis. Science 319, 195–198.

García-Maceira, P., Mateo, J., 2009. Silibinin inhibits hypoxia-inducible factor-1alpha and mTOR/p70S6K/4E-BP1 signalling pathway in human cervical and hepatoma cancer cells: implications for anticancer therapy. Oncogene 28, 313–324.

Garrett-Engele, C.M., Tasch, M.A., Hwang, H.C., Fero, M.L., Perlmutter, R.M., Clurman, B.E., Roberts, J.M., 2007. A mechanism misregulating p27 in tumors discovered in a functional genomic screen. PLoS Genet. 3, e219.

Good, C.R., Aznar, M.A., Kuramitsu, S., Samareh, P., Agarwal, S., Donahue, G., Ishiyama, K., Wellhausen, N., Rennels, A.K., Ma, Y., Tian, L., Guedan, S., Alexander, K.A., Zhang, Z., Rommel, P.C., Singh, N., Glastad, K.M., Richardson, M.W., Watanabe, K., Tanyi, J.L., O'Hara, M.H., Ruella, M., Lacey, S.F., Moon, E.K., Schuster, S.J., Albelda, S.M., Lanier, L.L., Young, R.M., Berger, S.L., June, C.H., 2021. An NK-like CAR T cell transition in CAR T cell dysfunction. Cell 184, 6081–6100.

Guo, L., Gong, H., Tang, T.L., Zhang, B.K., Zhang, L.Y., Yan, M., 2021. Crizotinib and Sunitinib Induce Hepatotoxicity and Mitochondrial Apoptosis in L02 Cells via ROS and Nrf2 Signaling Pathway. Front. Pharmacol. 12, 620934.

Gupta, G.P., Perk, J., Acharyya, S., de Candia, P., Mittal, V., Todorova-Manova, K., Gerald, W.L., Brogi, E., Benezra, R., Massagué, J., 2007. ID genes mediate tumor reinitiation during breast cancer lung metastasis. Proc. Natl. Acad. Sci. USA 104, 19506–19511.

Hayashi, Y., Hsiao, E.C., Sami, S., Lancero, M., Schlieve, C.R., Nguyen, T., Yano, K., Nagahashi, A., Ikeya, M., Matsumoto, Y., Nishimura, K., Fukuda, A., Hisatake, K., Tomoda, K., Asaka, I., Toguchida, J., Conklin, B.R., Yamanaka, S., 2016. BMP-SMAD-ID promotes reprogramming to pluripotency by inhibiting p16/INK4A-dependent senescence. Proc. Natl. Acad. Sci. USA 113, 13057–13062.

Hiepen, C., Jatzlau, J., Hildebrandt, S., Kampfrath, B., Goktas, M., Murgai, A., Cuellar Camacho, J.L., Haag, R., Ruppert, C., Sengle, G., Cavalcanti-Adam, E.A., Blank, K.G., Knaus,

P., 2019. BMPR2 acts as a gatekeeper to protect endothelial cells from increased TGFβ responses and altered cell mechanics. PLoS Biol. 17, e3000557.

Hiepen, C., Mendez, P.L., Knaus, P., 2020. It Takes Two to Tango: Endothelial TGFβ/BMP Signaling Crosstalk with Mechanobiology. Cells 9, 1965.

Hoh, C., Boocock, D., Marczylo, T., Singh, R., Berry, D.P., Dennison, A.R., Hemingway, D., Miller, A., West, K., Euden, S., Garcea, G., Farmer, P.B., Steward, W.P., Gescher, A.J., 2006. Pilot study of oral silibinin, a putative chemopreventive agent, in colorectal cancer patients: silibinin levels in plasma, colorectum, and liver and their pharmacodynamic consequences. Clin. Cancer Res. 12, 2944–2950.

Huang, L., Cai, J., Guo, H., Gu, J., Tong, Y., Qiu, B., Wang, C., Li, M., Xia, L., Zhang, J., Wu, H., Kong, X., Xia, Q., 2019. ID3 Promotes Stem Cell Features and Predicts Chemotherapeutic Response of Intrahepatic Cholangiocarcinoma. Hepatology 69, 1995–2012.

Iavarone, A., Lasorella, A., 2006. ID proteins as targets in cancer and tools in neurobiology. Trends Mol. Med. 12, 588–594.

Jayanta K. Das, Mayur Doke, Alok Deoraj, Quentin Felty, Deodutta Roy. Exosomal ID3 is pro-metastatic through guiding NRF1-induced breast cancer stem cells across the blood-brain-barrier [abstract]. In: Proceedings of the American Association for Cancer Research Annual Meeting 2018; 2018 Apr 14-18; Chicago, IL. Philadelphia (PA): AACR; Cancer Res 2018;78(13 Suppl):Abstract nr 1128.

Jung, H.J., Park, J.W., Lee, J.S., Lee, S.R., Jang, B.C., Suh, S.I., Suh, M.H., Baek, W.K., 2009. Silibinin inhibits expression of HIF-1alpha through suppression of protein translation in prostate cancer cells. Biochem. Biophys. Res. Commun. 390, 71–76.

Ke, J., Wu, R., Chen, Y., Abba, M.L., 2018. Inhibitor of DNA binding proteins: implications in human cancer progression and metastasis. Am. J. Transl. Res. 10, 3887–3910.

Kerr, G., Sheldon, H., Chaikuad, A., Alfano, I., von Delft, F., Bullock, A.N., Harris, A.L., 2015. A small molecule targeting ALK1 prevents Notch cooperativity and inhibits functional angiogenesis. Angiogenesis 18, 209–217.

Kidd, P.M., 2009. Bioavailability and activity of phytosome complexes from botanical polyphenols: the silymarin, curcumin, green tea, and grape seed extracts. Altern. Med. Rev. 14, 226–246.

Kim, H.R., Kim, W.S., Choi, Y.J., Choi, C.M., Rho, J.K., Lee, J.C., 2013. Epithelial-mesenchymal transition leads to crizotinib resistance in H2228 lung cancer cells with EML4-ALK translocation. Mol. Oncol. 7, 1093–1102.

Klumpe, H.E., Langley, M.A., Linton, J.M., Su, C.J., Antebi, Y.E., Elowitz, M.B., 2022. The context-dependent, combinatorial logic of BMP signaling. Cell Syst. 13, 388–407.

Kowanetz, M., Valcourt, U., Bergström, R., Heldin, C.H., Moustakas, A., 2004. Id2 and Id3 define the potency of cell proliferation and differentiation responses to transforming growth factor beta and bone morphogenetic protein. Mol. Cell. Biol. 24, 4241–4254.

Křen V., 2021. Chirality Matters: Biological Activity of Optically Pure Silybin and Its Congeners. Int. J. Mol. Sci. 22:7885.

Langenfeld, E., Deen, M., Zachariah, E., Langenfeld, J., 2013a. Small molecule antagonist of the bone morphogenetic protein type I receptors suppresses growth and expression of Id1 and Id3 in lung cancer cells expressing Oct4 or nestin. Mol. Cancer. 12, 129.

Langenfeld, E., Hong, C.C., Lanke, G., Langenfeld, J., 2013b. Bone morphogenetic protein type I receptor antagonists decrease growth and induce cell death of lung cancer cell lines. PLoS One 8, e61256.

Langenfeld, E.M., Bojnowski, J., Perone, J., Langenfeld, J., 2005. Expression of bone morphogenetic proteins in human lung carcinomas. Ann. Thorac. Surg. 80, 1028–1032.

Langenfeld, E.M., Calvano, S.E., Abou-Nukta, F., Lowry, S.F., Amenta, P., Langenfeld, J., 2003. The mature bone morphogenetic protein-2 is aberrantly expressed in non-small cell lung carcinomas and stimulates tumor growth of A549 cells. Carcinogenesis 24, 1445–1454.

Langenfeld, E.M., Kong, Y., Langenfeld, J., 2006. Bone morphogenetic protein 2 stimulation of tumor growth involves the activation of Smad-1/5. Oncogene 25, 685–692.

Lasorella, A., Benezra, R., Iavarone, A., 2014. The ID proteins: master regulators of cancer stem cells and tumour aggressiveness. Nat. Rev. Cancer 14, 77–91.

Lee, K.T., Lee, Y.W., Lee, J.K., Choi, S.H., Rhee, J.C., Paik, S.S., Kong, G., 2004. Overexpression of Id-1 is significantly associated with tumour angiogenesis in human pancreas cancers. Br. J. Cancer 90, 1198–1203.

Lewis, T.C., Prywes, R., 2013. Serum regulation of Id1 expression by a BMP pathway and BMP responsive element. Biochim. Biophys. Acta 1829, 1147–1159.

Lin, C.J., Sukarieh, R., Pelletier, J., 2009. Silibinin inhibits translation initiation: implications for anticancer therapy. Mol. Cancer Ther. 8, 1606–1612.

Ling, F., Kang, B., Sun, X.H., 2014. Id proteins: small molecules, mighty regulators. Curr. Top. Dev. Biol. 110, 189–216.

Lyden, D., Young, A.Z., Zagzag, D., Yan, W., Gerald, W., O'Reilly, R., Bader, B.L., Hynes, R.O., Zhuang, Y., Manova, K., Benezra, R., 1999. Id1 and Id3 are required for neurogenesis, angiogenesis and vascularization of tumour xenografts. Nature 401, 670–677.

Mahmoud, M., Borthwick, G.M., Hislop, A.A., Arthur, H.M., 2009. Endoglin and activin receptor-like-kinase 1 are co-expressed in the distal vessels of the lung: implications for two familial vascular dysplasias, HHT and PAH. Lab. Invest. 89, 15–25.

Mak, M.P., Tong, P., Diao, L., Cardnell, R.J., Gibbons, D.L., William, W.N., Skoulidis, F., Parra, E.R., Rodriguez-Canales, J., Wistuba, I.I., Heymach, J.V., Weinstein, J.N., Coombes, K.R., Wang, J., Byers, L.A., 2016. A Patient-Derived, Pan-Cancer EMT Signature Identifies

Global Molecular Alterations and Immune Target Enrichment Following Epithelial-to-Mesenchymal Transition. Clin. Cancer Res. 22, 609–620.

Mateen, S., Raina, K., Agarwal, R., 2013. Chemopreventive and anti-cancer efficacy of silibinin against growth and progression of lung cancer. Nutr. Cancer 65 Suppl 1, 3–11.

Maw, M.K., Fujimoto, J., Tamaya, T., 2008. Expression of the inhibitor of DNA-binding (ID)-1 protein as an angiogenic mediator in tumour advancement of uterine cervical cancers. Br. J. Cancer 99, 1557-1563.

Mern, D.S., Hasskarl, J., Burwinkel, B., 2010. Inhibition of Id proteins by a peptide aptamer induces cell-cycle arrest and apoptosis in ovarian cancer cells. Br. J. Cancer 103, 1237–1244.

Mirzaaghaei, S., Foroughmand, A.M., Saki, G., Shafiei, M., 2019. Combination of Epigallocatechin-3-gallate and Silibinin: A Novel Approach for Targeting Both Tumor and Endothelial Cells. ACS Omega 4, 8421–8430.

Montgomery, A., Adeyeni, T., San, K., Heuertz, R.M., Ezekiel, U.R., 2016. Curcumin Sensitizes Silymarin to Exert Synergistic Anticancer Activity in Colon Cancer Cells. J. Cancer. 7, 1250–1257.

Mueller, C., Baudler, S., Welzel, H., Böhm, M., Nickenig, G., 2002. Identification of a novel redox-sensitive gene, Id3, which mediates angiotensin II-induced cell growth. Circulation 105, 2423–2428.

Nair, R., Teo, W.S., Mittal, V., Swarbrick, A., 2014. ID proteins regulate diverse aspects of cancer progression and provide novel therapeutic opportunities. Mol. Ther. 22, 1407–1415.

Newman, J.H., Augeri, D.J., NeMoyer, R., Malhotra, J., Langenfeld, E., Chesson, C.B., Dobias, N.S., Lee, M.J., Tarabichi, S., Jhawar, S.R., Bommareddy, P.K., Marshall, S., Sadimin, E.T., Kerrigan, J.E., Goedken, M., Minerowicz, C., Jabbour, S.K., Li, S., Carayannopolous, M.O., Zloza, A., Langenfeld, J., 2018. Novel bone morphogenetic protein receptor inhibitor JL5 suppresses tumor cell survival signaling and induces regression of human lung cancer. Oncogene 37, 3672–3685.

Nickel, J., Mueller, T.D., 2019. Specification of BMP Signaling. Cells 8, 1579.

Niola, F., Zhao, X., Singh, D., Castano, A., Sullivan, R., Lauria, M., Nam, H.S., Zhuang, Y., Benezra, R., Di Bernardo, D., Iavarone, A., Lasorella, A., 2012. Id proteins synchronize stemness and anchorage to the niche of neural stem cells. Nat. Cell. Biol. 14, 477–487.

Nurgazieva, D., Mickley, A., Moganti, K., Ming, W., Ovsyi, I., Popova, A., Sachindra, Awad, K., Wang, N., Bieback, K., Goerdt, S., Kzhyshkowska, J., Gratchev, A., 2015. TGF-β1, but not bone morphogenetic proteins, activates Smad1/5 pathway in primary human macrophages and induces expression of proatherogenic genes. J. Immunol. 194, 709–718.

O'Brien, C.A., Kreso, A., Ryan, P., Hermans, K.G., Gibson, L., Wang, Y., Tsatsanis, A., Gallinger, S., Dick, J.E., 2012. ID1 and ID3 regulate the self-renewal capacity of human colon cancer-initiating cells through p21. Cancer Cell 21, 777–792.

Oh, S.P., Seki, T., Goss, K.A., Imamura, T., Yi, Y., Donahoe, P.K., Li, L., Miyazono, K., ten Dijke, P., Kim, S., Li, E., 2000. Activin receptor-like kinase 1 modulates transforming growth factor-beta 1 signaling in the regulation of angiogenesis. Proc. Natl. Acad. Sci. USA 97, 2626–2631.

Perez, C.M., Felty, Q., 2022. Molecular basis of the association between transcription regulators nuclear respiratory factor 1 and inhibitor of DNA binding protein 3 and the development of microvascular lesions. Microvasc. Res. 141, 104337.

Perez, C.M., Gong, Z., Yoo, C., Roy, D., Deoraj, A., Felty, Q., 2023. Inhibitor of DNA Binding Protein 3 (ID3) and Nuclear Respiratory Factor 1 (NRF1) Mediated Transcriptional Gene Signatures are Associated with the Severity of Cerebral Amyloid Angiopathy. Mol. Neurobiol. 2023 Sep 5. doi: 10.1007/s12035-023-03541-2

Perk, J., Iavarone, A., Benezra, R., 2005. Id family of helix-loop-helix proteins in cancer. Nat. Rev. Cancer 5, 603–614.

Perry, S.S., Zhao, Y., Nie, L., Cochrane, S.W., Huang, Z., Sun, X.H., 2007. Id1, but not Id3, directs long-term repopulating hematopoietic stem-cell maintenance. Blood 110, 2351–2360.

Ponz-Sarvisé, M., Nguewa, P.A., Pajares, M.J., Agorreta, J., Lozano, M.D., Redrado, M., Pio, R., Behrens, C., Wistuba, I.I., García-Franco, C.E., García-Foncillas, J., Montuenga, L.M., Calvo, A., Gil-Bazo, I., 2011. Inhibitor of differentiation-1 as a novel prognostic factor in NSCLC patients with adenocarcinoma histology and its potential contribution to therapy resistance. Clin. Cancer Res. 17, 4155–4166.

Priego, N., Valiente, M., 2019. The Potential of Astrocytes as Immune Modulators in Brain Tumors. Front. Immunol. 10, 1314.

Priego, N., Zhu, L., Monteiro, C., Mulders, M., Wasilewski, D., Bindeman, W., Doglio, L., Martínez, L., Martínez-Saez, E., Ramón y Cajal, S., Megías, D., Hernández-Encinas, E., Blanco-Aparicio, C., Martínez, L., Zarzuela, E., Muñoz, J., Fustero-Torre, C., Piñeiro-Yáñez, E., Hernández-Laín, A., Bertero, L., Poli, V., Sanchez-Martinez, M., Menendez, J.A., Soffietti, R., Bosch-Barrera, J., Valiente, M., 2018. STAT3 labels a subpopulation of reactive astrocytes required for brain metastasis. Nat. Med. 24, 1024–1035.

Richter, J., Schlesner, M., Hoffmann, S., Kreuz, M., Leich, E., Burkhardt, B., Rosolowski, M., Ammerpohl, O., Wagener, R., Bernhart, S.H., Lenze, D., Szczepanowski, M., Paulsen, M., Lipinski, S., Russell, R.B., Adam-Klages, S., Apic, G., Claviez, A., Hasenclever, D., Hovestadt, V., Hornig, N., Korbel, J.O., Kube, D., Langenberger, D., Lawerenz, C., Lisfeld, J., Meyer, K., Picelli, S., Pischimarov, J., Radlwimmer, B., Rausch, T., Rohde, M., Schilhabel, M., Scholtysik, R., Spang, R., Trautmann, H., Zenz, T., Borkhardt, A., Drexler, H.G., Möller, P., MacLeod, R.A., Pott, C., Schreiber, S., Trümper, L., Loeffler, M., Stadler, P.F., Lichter, P., Eils, R., Küppers, R., Hummel, M., Klapper, W., Rosenstiel, P., Rosenwald, A., Brors, B., Siebert, R.; ICGC MMML-Seq Project., 2012. Recurrent mutation of the ID3 gene in Burkitt lymphoma identified by integrated genome, exome and transcriptome sequencing. Nat. Genet. 44, 1316–1320.

Rooney, L., Jones, C., 2021. Recent Advances in ALK2 Inhibitors. ACS Omega 6, 20729–20734.

Roschger, C., Cabrele, C., 2017. The Id-protein family in developmental and cancer-associated pathways. Cell. Commun. Signal. 15, 7.

Sachindra, Larribère, L., Novak, D., Wu, H., Hüser, L., Granados, K., Orouji, E., Utikal, J., 2017. New role of ID3 in melanoma adaptive drug-resistance. Oncotarget 8, 110166–110175.

Sanchez-Duffhues, G., Williams, E., Goumans, M.J., Heldin, C.H., Ten Dijke, P., 2020. Bone morphogenetic protein receptors: Structure, function and targeting by selective small m olecule kinase inhibitors. Bone 138, 115472.

Sanvitale, C.E., Kerr, G., Chaikuad, A., Ramel, M.C., Mohedas, A.H., Reichert, S., Wang, Y., Triffitt, J.T., Cuny, G.D., Yu, P.B., Hill, C.S., Bullock, A.N., 2013. A new class of small molecule inhibitor of BMP signaling. PLoS One 8, e62721.

Sayyed, A., Heuertz, R., Ezekiel, U.R., 2022. Curcumin, but not its degradation products, in combination with silibinin is primarily responsible for the inhibition of colon cancer cell proliferation. MicroPubl. Biol. 2022, 10.17912/micropub.biology.000617.

Schindl, M., Schoppmann, S.F., Ströbel, T., Heinzl, H., Leisser, C., Horvat, R., Birner, P., 2003. Level of Id-1 protein expression correlates with poor differentiation, enhanced malignant potential, and more aggressive clinical behavior of epithelial ovarian tumors. Clin. Cancer Res. 9, 779–785.

Schliekelman, M.J., Taguchi, A., Zhu, J., Dai, X., Rodriguez, J., Celiktas, M., Zhang, Q., Chin, A., Wong, C.H., Wang, H., McFerrin, L., Selamat, S.A., Yang, C., Kroh, E.M., Garg, K.S., Behrens, C., Gazdar, A.F., Laird-Offringa, I.A., Tewari, M., Wistuba, I.I., Thiery, J.P., Hanash, S.M., 2015. Molecular portraits of epithelial, mesenchymal, and hybrid States in lung adenocarcinoma and their relevance to survival. Cancer Res. 75, 1789–1800.

Schoppmann, S.F., Schindl, M., Bayer, G., Aumayr, K., Dienes, J., Horvat, R., Rudas, M., Gnant, M., Jakesz, R., Birner, P., 2003. Overexpression of Id-1 is associated with poor clinical outcome in node negative breast cancer. Int. J. Cancer 104, 677–682.

Sciacca, M.F.M., Romanucci, V., Zarrelli, A., Monaco, I., Lolicato, F., Spinella, N., Galati, C., Grasso, G., D'Urso, L., Romeo, M., Diomede, L., Salmona, M., Bongiorno, C., Di Fabio, G., La Rosa, C., Milardi, D., 2017. Inhibition of Aβ Amyloid Growth and Toxicity by Silybins: The Crucial Role of Stereochemistry. ACS Chem. Neurosci. 8, 1767–1778.

Sharma, P., Patel, D., Chaudhary, J., 2012. Id1 and Id3 expression is associated with increasing grade of prostate cancer: Id3 preferentially regulates CDKN1B. Cancer Med. 1, 187–197.

Shepherd, T.G., Thériault, B.L., Nachtigal, M.W., 2008. Autocrine BMP4 signalling regulates ID3 proto-oncogene expression in human ovarian cancer cells. Gene 414, 95–105.

Solar, P., Hendrych, M., Barak, M., Valekova, H., Hermanova, M., Jancalek, R., 2022. Blood-Brain Barrier Alterations and Edema Formation in Different Brain Mass Lesions. Front. Cell. Neurosci. 16, 922181.

Stankic, M., Pavlovic, S., Chin, Y., Brogi, E., Padua, D., Norton, L., Massagué, J., Benezra, R., 2013. TGF-β-Id1 signaling opposes Twist1 and promotes metastatic colonization via a mesenchymal-to-epithelial transition. Cell Rep. 5, 1228–1242.

Teo, W.S., Holliday, H., Karthikeyan, N., Cazet, A.S., Roden, D.L., Harvey, K., Konrad, C.V., Murali, R., Varghese, B.A., Thankamony, A.P., Chan, C.L., McFarland, A., Junankar, S., Ye, S., Yang, J., Nikolic, I., Shah, J.S., Baker, L.A., Millar, E.K.A., Naylor, M.J., Ormandy, C.J., Lakhani, S.R., Kaplan, W., Mellick, A.S., O'Toole, S.A., Swarbrick, A., Nair, R., 2020. Id Proteins Promote a Cancer Stem Cell Phenotype in Mouse Models of Triple Negative Breast Cancer via Negative Regulation of Robo1. Front. Cell. Dev. Biol. 8, 552.

Thompson, J.C., Hwang, W.T., Davis, C., Deshpande, C., Jeffries, S., Rajpurohit, Y., Krishna, V., Smirnov, D., Verona, R., Lorenzi, M.V., Langer, C.J., Albelda, S.M., 2020. Gene signatures of tumor inflammation and epithelial-to-mesenchymal transition (EMT) predict responses to immune checkpoint blockade in lung cancer with high accuracy. Lung Cancer 139, 1–8.

Thomson, S., Buck, E., Petti, F., Griffin, G., Brown, E., Ramnarine, N., Iwata, K.K., Gibson, N., Haley, J.D., 2005. Epithelial to mesenchymal transition is a determinant of sensitivity of non-small-cell lung carcinoma cell lines and xenografts to epidermal growth factor receptor inhibition. Cancer Res. 65, 9455–9462.

Varma, D.A., Tiwari, M., 2021. Crizotinib-induced anti-cancer activity in human cervical carcinoma cells via ROS-dependent mitochondrial depolarization and induction of apoptotic pathway. J. Obstet. Gynaecol. Res. 47, 3923–3930.

Vazquez-Martin, A., Cufí, S., Oliveras-Ferraros, C., Torres-Garcia, V.Z., Corominas-Faja, B., Cuyàs, E., Bonavia, R., Visa, J., Martin-Castillo, B., Barrajón-Catalán, E., Micol, V., Bosch-Barrera, J., Menendez, J.A., 2013. IGF-1R/epithelial-to-mesenchymal transition (EMT) crosstalk suppresses the erlotinib-sensitizing effect of EGFR exon 19 deletion mutations. Sci. Rep. 3, 2560.

Verdura, S., Cuyàs, E., Llorach-Parés, L., Pérez-Sánchez, A., Micol, V., Nonell-Canals, A., Joven, J., Valiente, M., Sánchez-Martínez, M., Bosch-Barrera, J., Menendez, J.A., 2018. Silibinin is a direct inhibitor of STAT3. Food Chem. Toxicol. 116, 161–172.

Verdura, S., Cuyàs, E., Ruiz-Torres, V., Micol, V., Joven, J., Bosch-Barrera, J., Menendez, J.A., 2021. Lung Cancer Management with Silibinin: A Historical and Translational Perspective. Pharmaceuticals (Basel) 14, 559.

Verdura, S., Encinar, J.A., Teixidor, E., Segura-Carretero, A., Micol, V., Cuyàs, E., Bosch-Barrera, J., Menendez, J.A., 2022. Silibinin Overcomes EMT-Driven Lung Cancer Resistance to New-Generation ALK Inhibitors. Cancers (Basel) 14, 6101.

Wang, C., Wang, Z., Zhang, X., Zhang, X., Dong, L., Xing, Y., Li, Y., Liu, Z., Chen, L., Qiao, H., Wang, L., Zhu, C., 2012. Protection by silibinin against experimental ischemic stroke: up-regulated pAkt, pmTOR, HIF-1α and Bcl-2, down-regulated Bax, NF-κB expression. Neurosci. Lett. 529, 45–50.

Wang, L.H., Baker, N.E., 2015. E Proteins and ID Proteins: Helix-Loop-Helix Partners in Development and Disease. Dev. Cell. 35, 269–280.

Wasilewski, D., Priego, N., Fustero-Torre, C., Valiente, M., 2017. Reactive Astrocytes in Brain Metastasis. Front. Oncol. 7, 298.

Weksler, B.B., Subileau, E.A., Perrière, N., Charneau, P., Holloway, K., Leveque, M., Tricoire-Leignel, H., Nicotra, A., Bourdoulous, S., Turowski, P., Male, D.K., Roux, F., Greenwood, J., Romero, I.A., Couraud, P.O., 2005. Blood-brain barrier-specific properties of a human adult brain endothelial cell line. FASEB J. 19, 1872–1874.

Wojnarowicz, P.M., Escolano, M.G., Huang, Y.H., Desai, B., Chin, Y., Shah, R., Xu, S., Yadav, S., Yaklichkin, S., Ouerfelli, O., Soni, R.K., Philip, J., Montrose, D.C., Healey, J.H., Rajasekhar, V.K., Garland, W.A., Ratiu, J., Zhuang, Y., Norton, L., Rosen, N., Hendrickson, R.C., Zhou, X.K., Iavarone, A., Massague, J., Dannenberg, A.J., Lasorella, A., Benezra, R., 2021. Anti-tumor effects of an ID antagonist with no observed acquired resistance. NPJ Breast Cancer 7, 58.

Wojnarowicz, P.M., Lima, E Silva, R., Ohnaka, M., Lee, S.B., Chin, Y., Kulukian, A., Chang, S.H., Desai, B., Garcia Escolano, M., Shah, R., Garcia-Cao, M., Xu, S., Kadam, R., Goldgur, Y., Miller, M.A., Ouerfelli, O., Yang, G., Arakawa, T., Albanese, S.K., Garland, W.A., Stoller, G., Chaudhary, J., Norton, L., Soni, R.K., Philip, J., Hendrickson, R.C., Iavarone, A., Dannenberg, A.J., Chodera, J.D., Pavletich, N., Lasorella, A., Campochiaro, P.A., Benezra, R., 2019. A Small-Molecule Pan-Id Antagonist Inhibits Pathologic Ocular Neovascularization. Cell Rep. 29, 62–75.

Yamaguchi, N., Lucena-Araujo, A.R., Nakayama, S., de Figueiredo-Pontes, L.L., Gonzalez, D.A., Yasuda, H., Kobayashi, S., Costa, D.B., 2014. Dual ALK and EGFR inhibition targets a mechanism of acquired resistance to the tyrosine kinase inhibitor crizotinib in ALK rearranged lung cancer. Lung Cancer 83, 37–43.

Yan, H., Du, J., Chen, X., Yang, B., He, Q., Yang, X., Luo, P., 2019. ROS-dependent DNA damage contributes to crizotinib-induced hepatotoxicity via the apoptotic pathway. Toxicol. Appl. Pharmacol. 383, 114768.

Yang, J., Li, X., Morrell, N.W., 2014. Id proteins in the vasculature: from molecular biology to cardiopulmonary medicine. Cardiovasc. Res. 104, 388–398.

FIGURE LEGENDS

Figure 1. Correlation of ID3 with the expression levels of BMP ligands and BMP receptors in patients with lung adenocarcinoma (LUAD). A. Pearson correlation coefficients and *p*-values between *ID3* mRNA expression levels and several BMP receptor (*left panels*) and BMP ligand (*right panels*) genes in patients with LUAD (*n=510*). **B.** cBioPortal "oncoprint" representation of co-alterations in ID3 and BMP receptor genes (*left panels*) and BMP ligands (*right panels*). Numbers indicate the frequency of *ID3* mRNA expression changes (low/high). *Inset schematic: ID3* expression is positively correlated with the mRNA expression levels of specific members of the BMP/BMPR signaling pathway (i.e., ALK1/ENG receptors and BMP6/BMP2 ligands) in patients with LUAD.

Figure 2. Silibinin inhibits the BMP9-ALK1-SMAD1/5-ID signaling axis in cerebral endothelial cells. A. *Left panel.* BMP9 binds only ALK1, whereas TGFβ activates both ALK1 and ALK5 type I receptors expressed in ECs. In addition, endoglin acts as a co-receptor that modulates signaling through ALK1. SMAD 1 and 5 are preferentially phosphorylated and activated by ALK1, whereas SMAD 2 and 3 act as downstream effectors of ALK5. Subsequently, the SMADs are translocated to the nucleus, where they regulate the expression of specific genes (e.g., ID3/ID1 through phospho-SMAD1/5) (Cunha and Pietras, 2011). *Middle panels.* Representative brightfield microscopy images of hCMEC/D3 cells showing changes in cell morphology after BMP9 (10 ng/mL) and TGFβ (10 ng/mL) treatments for 3 days. Scale bar= 100 μm. *Right panels.* Expression levels of P-SMAD2/3, SMAD2/3, P-SMAD1/5, SMAD1, SMAD5, ID3, and ID1 proteins were detected by immunoblotting in lysates of hCMEC/D3 cells stimulated with TGFβ (10 ng/mL) or BMP9 (10 ng/mL) for 6 and 24 hours using specific antibodies. The figures show representative immunoblots from multiple ($n \geq 3$) independent experiments. Intensity of ID3 protein bands was measured using the ImageJ software and the fold-change relative to untreated cells was calculated using GAPDH as a loading control. *ID3* transcript abundance was calculated using the $\Delta\Delta C_t$ method and presented as relative expression; ** $p < 0.005$, statistically significant differences relative to untreated cells. **B.** *Left panel.* Expression levels of P-SMAD1/5, SMAD1, SMAD5, ID3, and ID1 proteins were detected by immunoblotting in lysates from hCMEC/D3 cells stimulated with BMP9 (10 ng/mL) in the absence or presence of either silibinin or K02288. Figures show representative immunoblots of multiple ($n \geq 3$) independent experiments. *Right panels.* The intensity of the P-SMAD1/5 and ID3 protein bands was measured using the ImageJ software and the fold-change relative to untreated cells was calculated using GAPDH as a loading control. *ID3* transcript abundance was calculated using the $\Delta\Delta C_t$ method and presented as relative expression; *$p < 0.05$, ** $p < 0.005$, statistically significant differences.

Figure 3. Silibinin prevents constitutive, acquired, and inducible ID3 expression in NSCLC cells. A. *Top panel.* Basal expression levels of the ID3 protein were detected by immunoblotting in lysates from NSCLC cell lines using a specific anti-ID3 antibody. Shown is a representative immunoblot from multiple ($n \geq 3$) independent experiments. *Bottom panels.* The intensity of the ID3 protein bands was measured using the ImageJ software and the fold-change relative to untreated cells was calculated using GAPDH as a loading control. *ID3* transcript abundance was calculated using the $\Delta\Delta C_t$ method and presented as relative expression. **B.** *Left panels.* Expression levels of ID3 were detected by immunoblotting in NSCLC cell models grown in the absence/presence of graded concentrations of silibinin for 24 or 48 h. The intensity of the ID3 protein bands was measured using the ImageJ software. The fold change of each protein relative to untreated samples was calculated using GAPDH as a loading control. The figure shows representative immunoblots from multiple ($n \geq 3$)

independent experiments. *Right panels. ID3* transcript abundance of was calculated using the $\Delta\Delta C_t$ method and presented as either relative or fold-change expression (compared to untreated H2228 parental cells) expression. *$p < 0.05$, ** $p < 0.005$, statistically significant differences. n.s. not significant. **C.** *Top panel.* Expression levels of P-SMAD1/5 and ID3 proteins were detected by immunoblotting in lysates from H2228 NSCLC cells exposed to the ALK-TKIs crizotinib, brigatinib, and lorlatinib (1 μmol/L each) for 24 h in the absence or presence of either silibinin (100 μmol/L) or K02288 (1 μmol/L). Shown are representative immunoblots from multiple ($n \geq 3$) independent experiments. *Bottom panels.* The intensity of the P-SMAD1/5 and ID3 protein bands was measured using the ImageJ software and the fold-change relative to untreated cells was calculated using GAPDH as a loading control. *ID3* transcript abundance was calculated using the $\Delta\Delta C_t$ method and presented as relative expression; *$p < 0.05$, ** $p < 0.005$, statistically significant differences. n.s. not significant.

Figure 4. Identification of the *ID3* gene regulatory regions targeted by silibinin. A. *Top.* Structure of the *ID3* genomic locus showing the enhancers located within the ECR1 and ECR2 regulatory regions and schematic structure of the luciferase plasmid constructs. *Bottom.* Luciferase reporter gene assays of TGFβ-, BMP4-, BMP6-, and BMP9-induced *ID3* promoter and enhancer activities in transfected HEK239T cells cultured in the absence or presence of silibinin (100 μmol/L), dorsomorphin (1 μmol/L) or K02288 (1 μmol/L). Each bar represents the mean ± S.D. and the data are representative of three independent experiments performed in triplicate. *$p < 0.05$, ** $p < 0.005$, statistically significant differences. n.s. not significant. **B.** *Top.* BMP-responsive elements of the upstream ECR1 enhancer region of *ID3* and schematic structure of the luciferase plasmid constructs. *Bottom.* Luciferase reporter gene assays of BMP6-induced *ID3* (ECR1) enhancer activity in transfected HEK239T cells cultured in the absence or presence of silibinin (100 μmol/L) or dorsomorphin (1 μmol/L). Each bar represents the mean ± S.E. and the data are representative of three independent experiments performed in triplicate. *$p < 0.05$, ** $p < 0.005$, statistically significant differences. DSM, dorsomorphin; SBN, silibinin; RLU, relative light units. n.s. not significant.

Figure 5. *In silico* prediction and *in vitro* verification of silibinin as a direct inhibitor of BMPRs. A. Molecular docking simulations and binding energies (ΔG, in kcal/mol) of the silibinin diastereoisomers silybin A (SBN-A) and silybin B (SBN-B) to the ATP-catalytic site of BMPRs. **B.** Molecular mechanics Poisson-Boltzmann surface area (MM/PBSA) binding energy analyses calculated from the entire trajectory of the 100 ns (or last 30 ns) molecular dynamics (MD) simulations of SBN-A and SBN-B coupled to the catalytic site of BMPRs. **C.** *Left.* Schematic of the LanthaScreen Eu Kinase Binding Assay. Binding of an Alexa Fluor™ conjugate or "tracer" to a kinase is detected by the addition of an Eu-labeled anti-tag antibody. Binding of the tracer and antibody to a BMPR kinase results in a high level of FRET, whereas displacement of the tracer with a putative BMPR kinase inhibitor results in a loss of FRET. The tracers are based on ATP-competitive kinase inhibitors, making them suitable for the detection of any compound that binds to the BMPR ATP site (type I BMPR kinase inhibitors) and/or to an allosteric site that alters the conformation of the ATP site (type II BMPR kinase inhibitors). *Right.* Bar graphs showing the IC_{50} values of silibinin for the ATP-dependent activity of BMPRs calculated from dose-response curves of LanthaScreen Eu kinase binding assays measuring the decreases in emission ratios induced by graded concentrations of silibinin (see "Materials and methods" section). Results are presented as the means (*columns*) ± S.D (*bars*) of three independent experiments performed in duplicate. **D.** The best positions of SBN-A and SBN-B coupled to the catalytic site of ACVRL1/ALK1, BMPR2, and ALK6 before (0 ns) and after (100 ns) the MD simulations are shown. The protein is plotted as a function of the hydrophobicity of its surface amino acids, and the Na^+ and Cl^- ions have been removed to

facilitate visualization. Each inset shows the detailed interactions of the participating amino acids involved and the type of interaction (hydrogen bonds, hydrophilic interactions, salt bridges, Π-stacking, etc.).

Figure 6. *In vivo* anti-ID3 activity of a water-soluble form of silibinin. *Top schematic.* Systemic administration by daily oral gavage of a non-toxic, orally active, milk thistle extract rich in silibinin-meglumine, a water-soluble form of silibinin complexed with the excipient amino-sugar meglumine, reduces tumor volumes of erlotinib-refractory PC-9/ER xenografts by approximately 50%, while a complete abrogation of tumor growth was observed with the co-treatment of erlotinib and silibinin-meglumine (Cufí et al., 2013a,b). *Bottom.* Representative immunoblots for ID3 in tumor tissues obtained from PC-9/ER xenograft-bearing mice treated with vehicle control, erlotinib (100 mg/kg, 5 days a week), silibinin-meglumine (100 mg/kg, 5 days a week), or silibinin-meglumine plus erlotinib. Also shown are β-actin loading controls.

Graphical Abstract

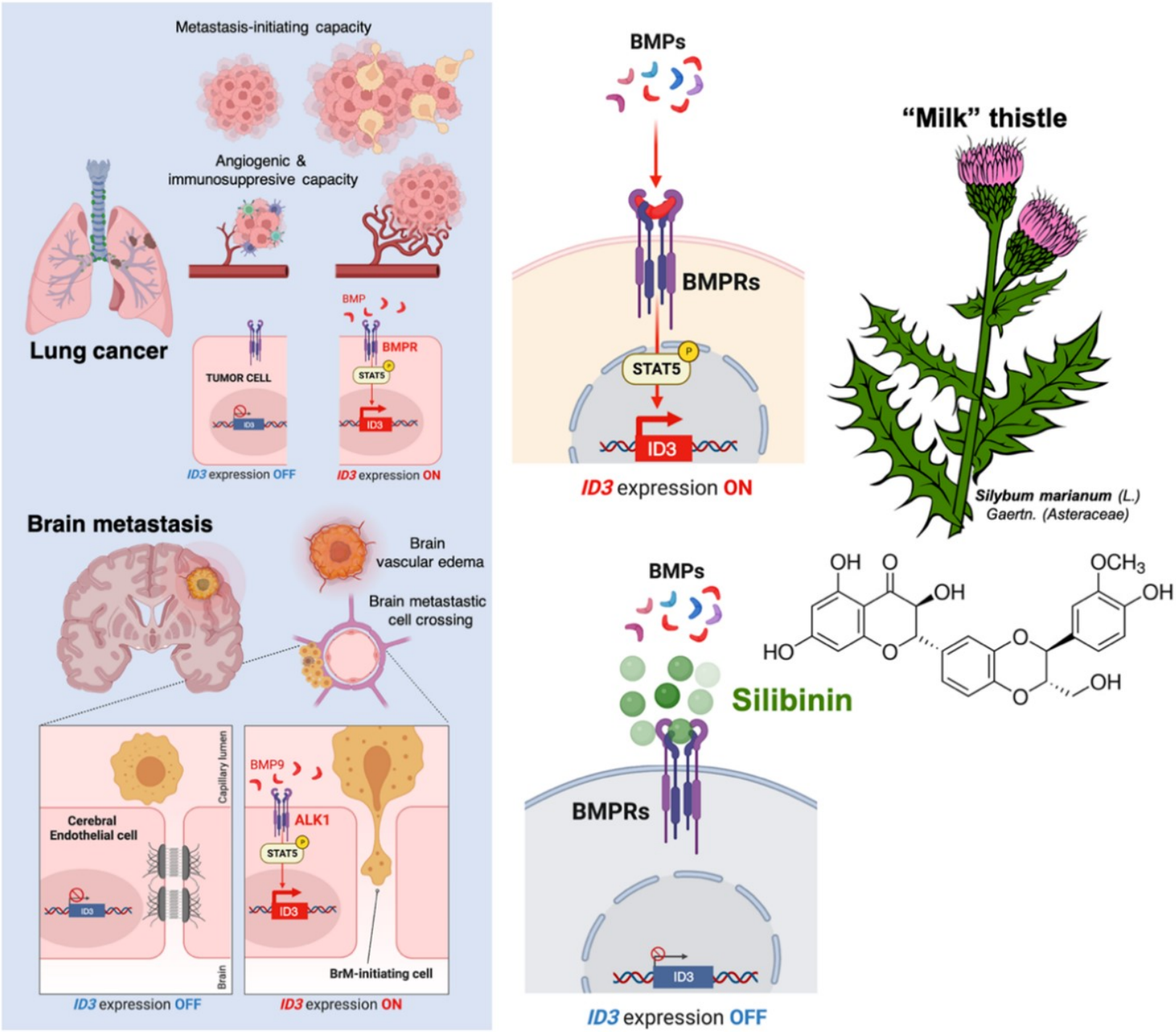

Figure 1

Click here to access/download;Figure;Figure 1.tif

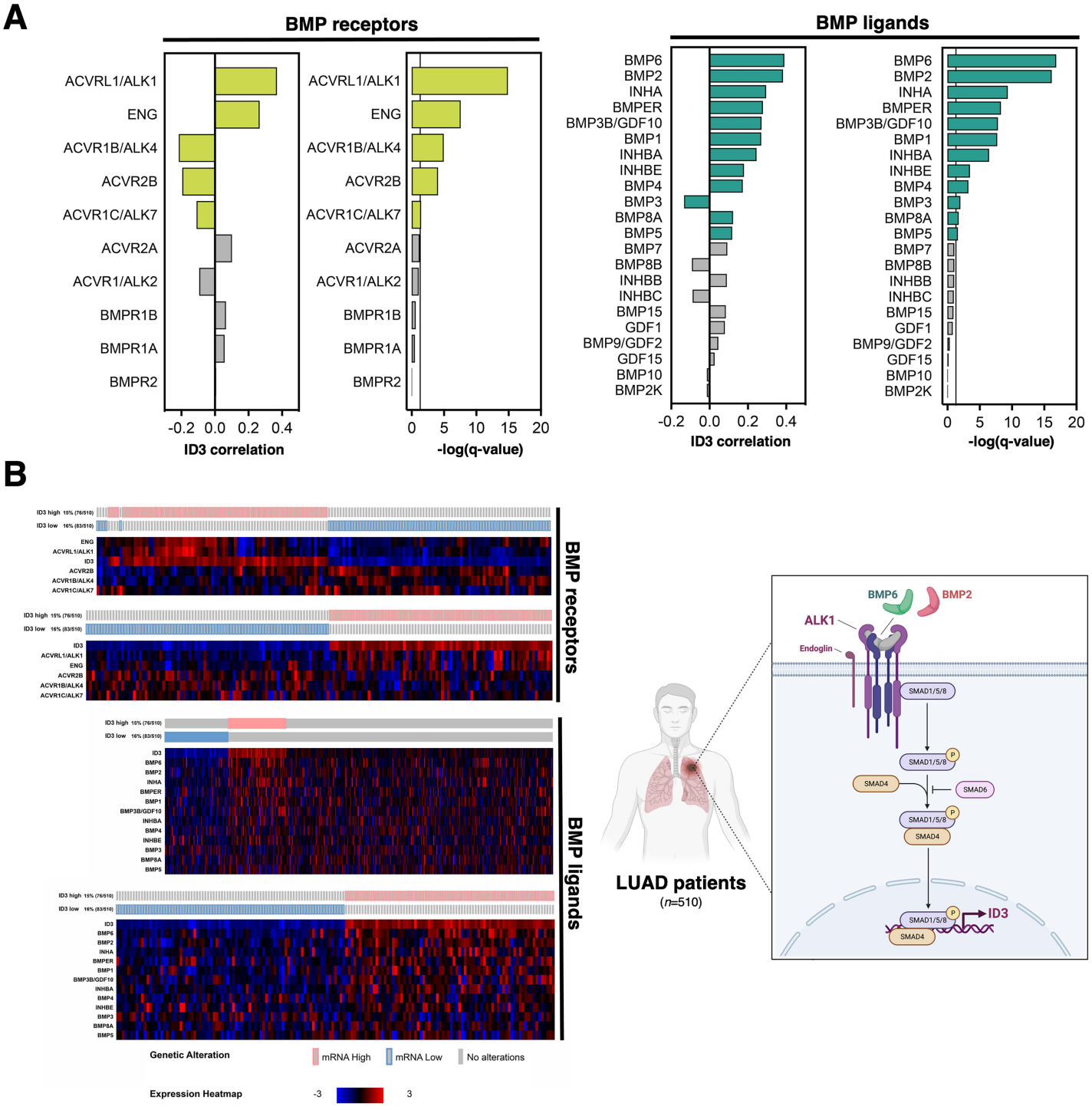

Figure 2

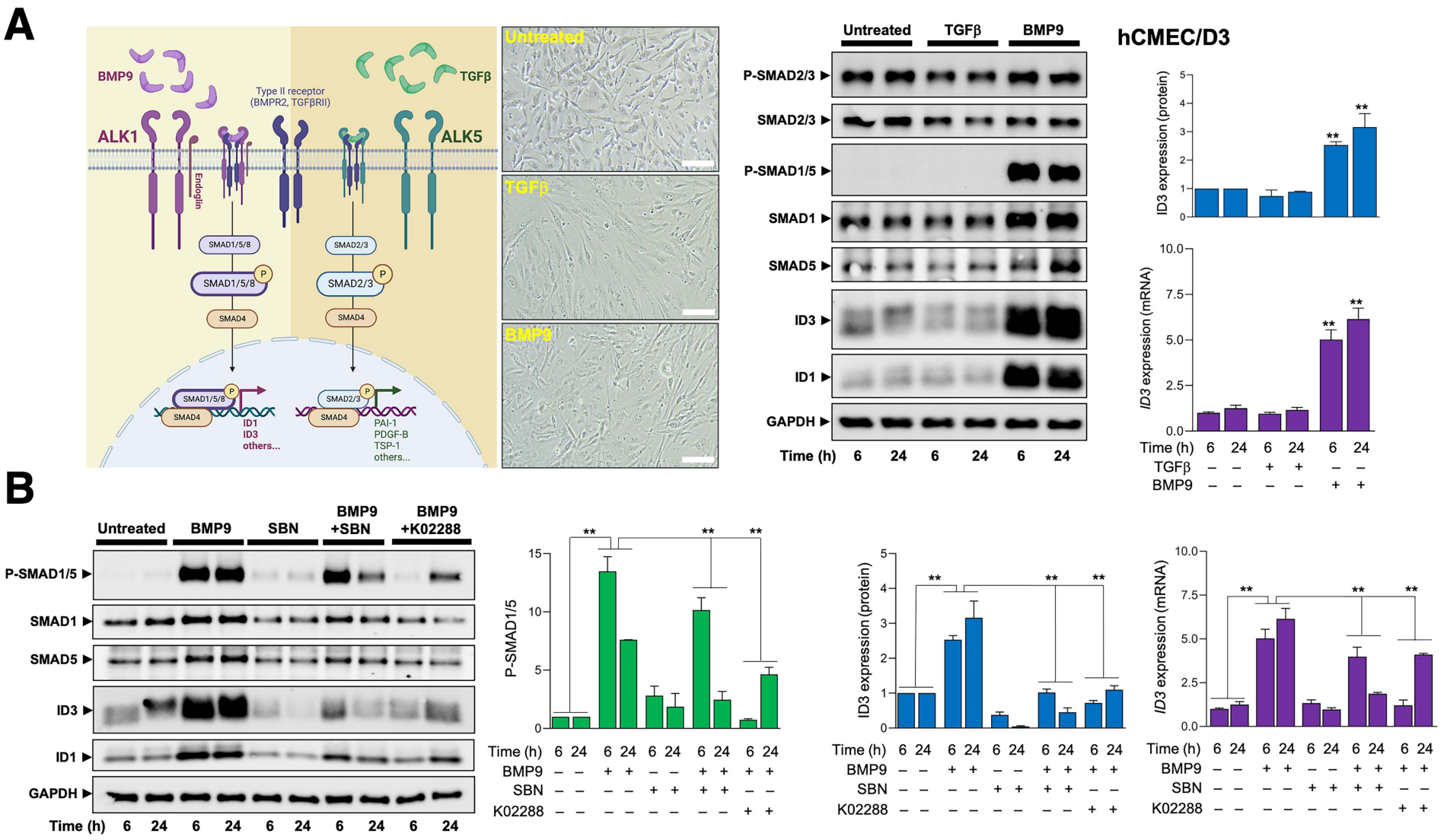

Figure 3

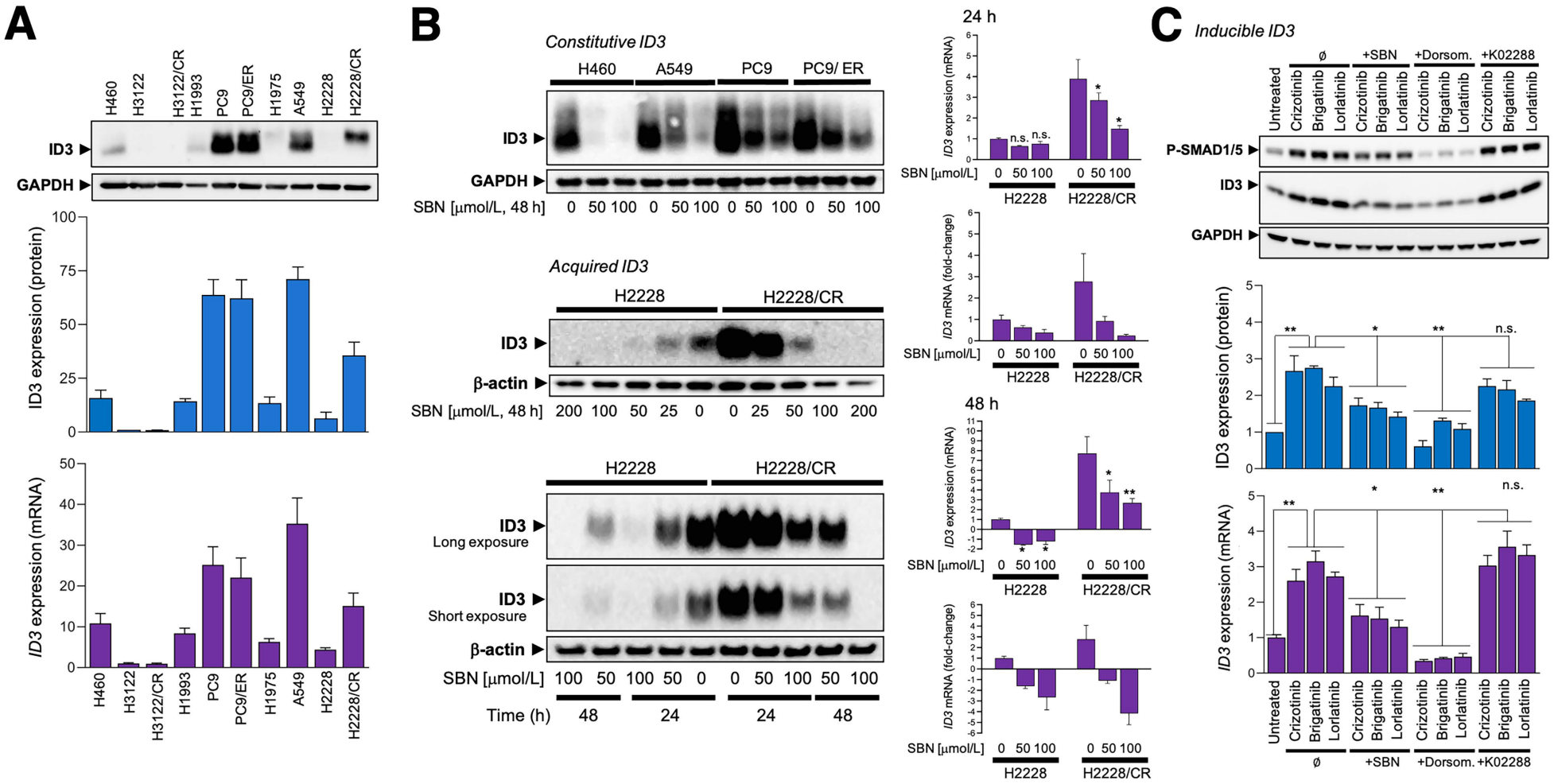

Figure 4

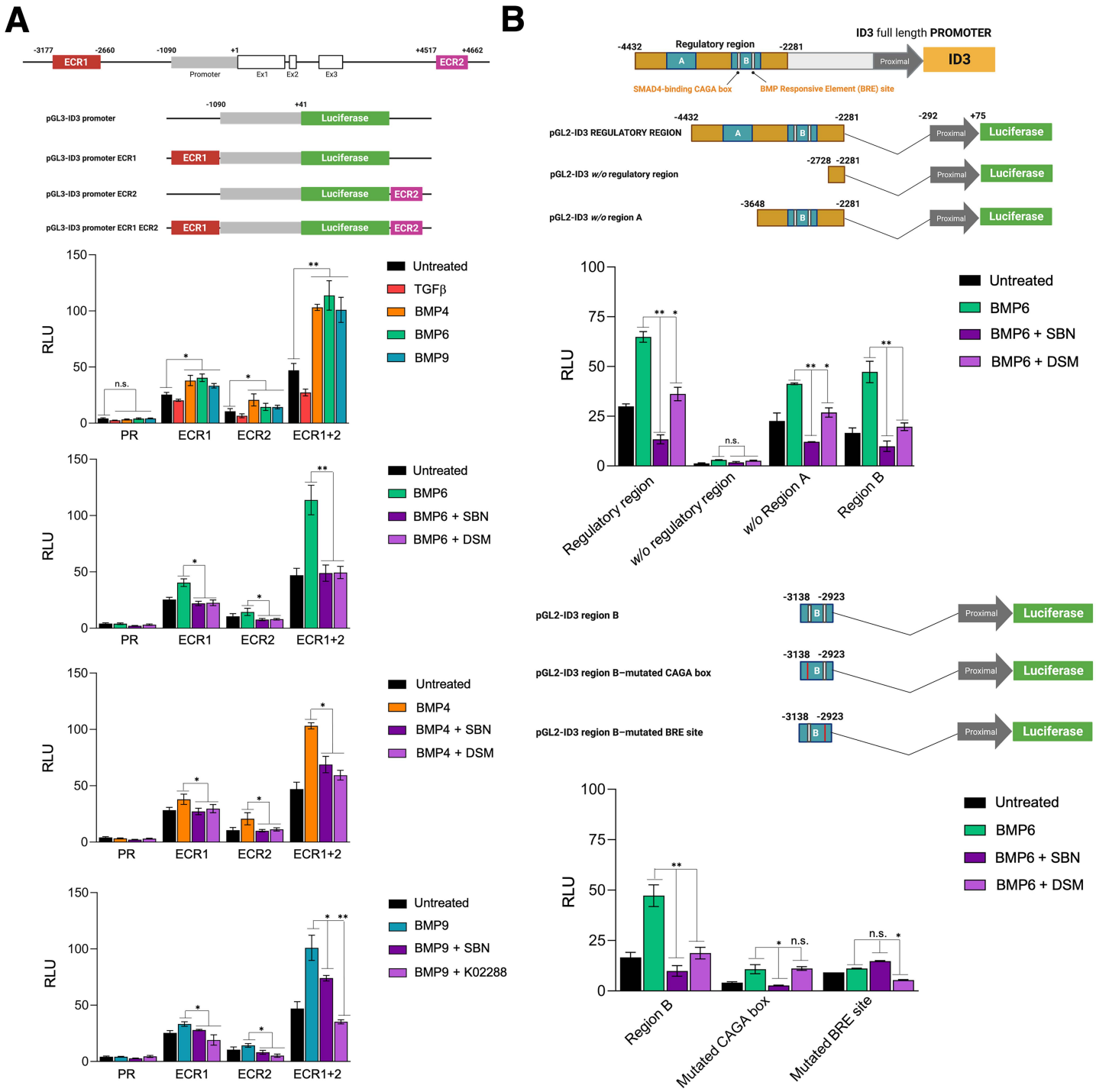

Figure 5

Click here to access/download;Figure;Figure 5.tif

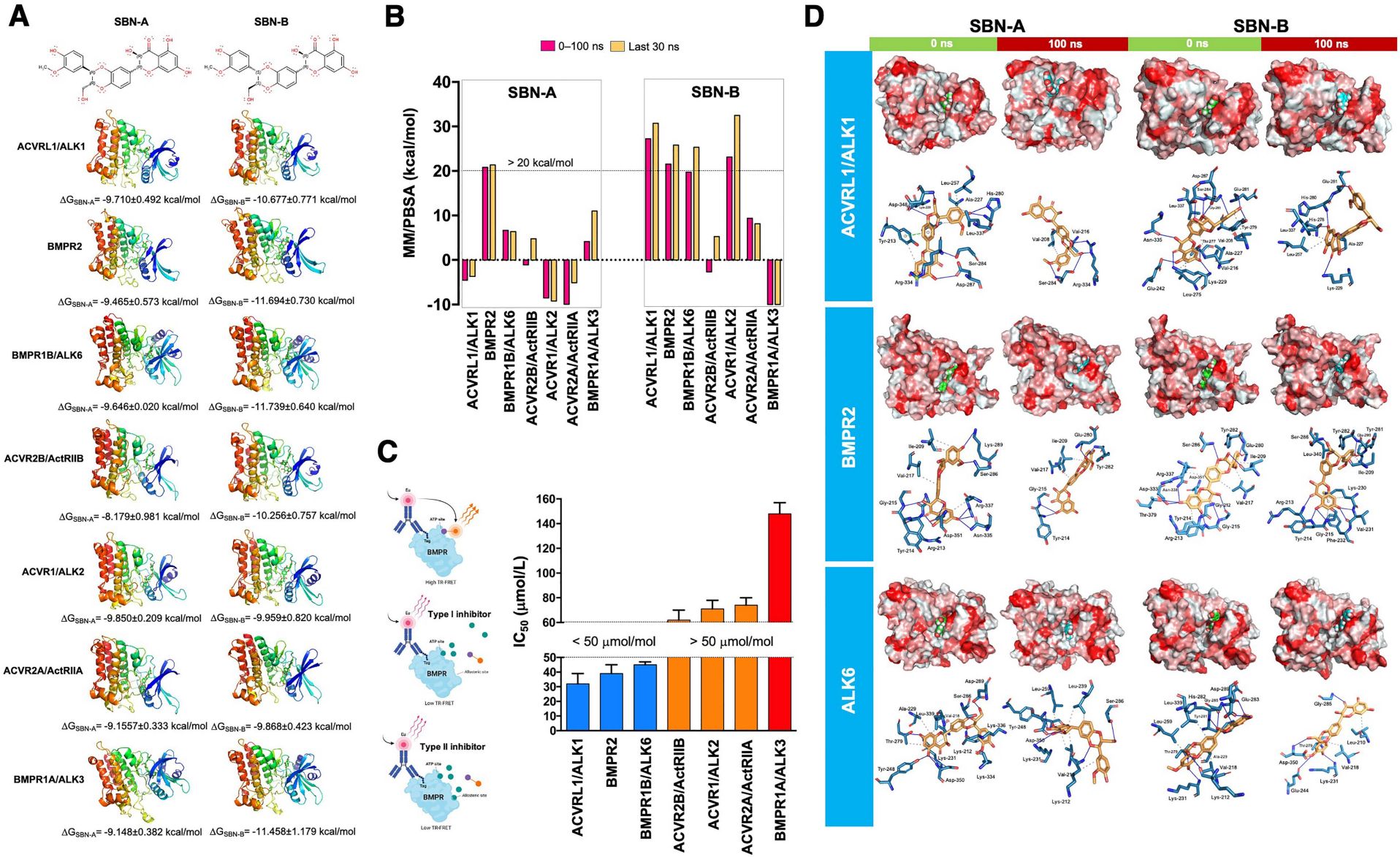

Figure 6

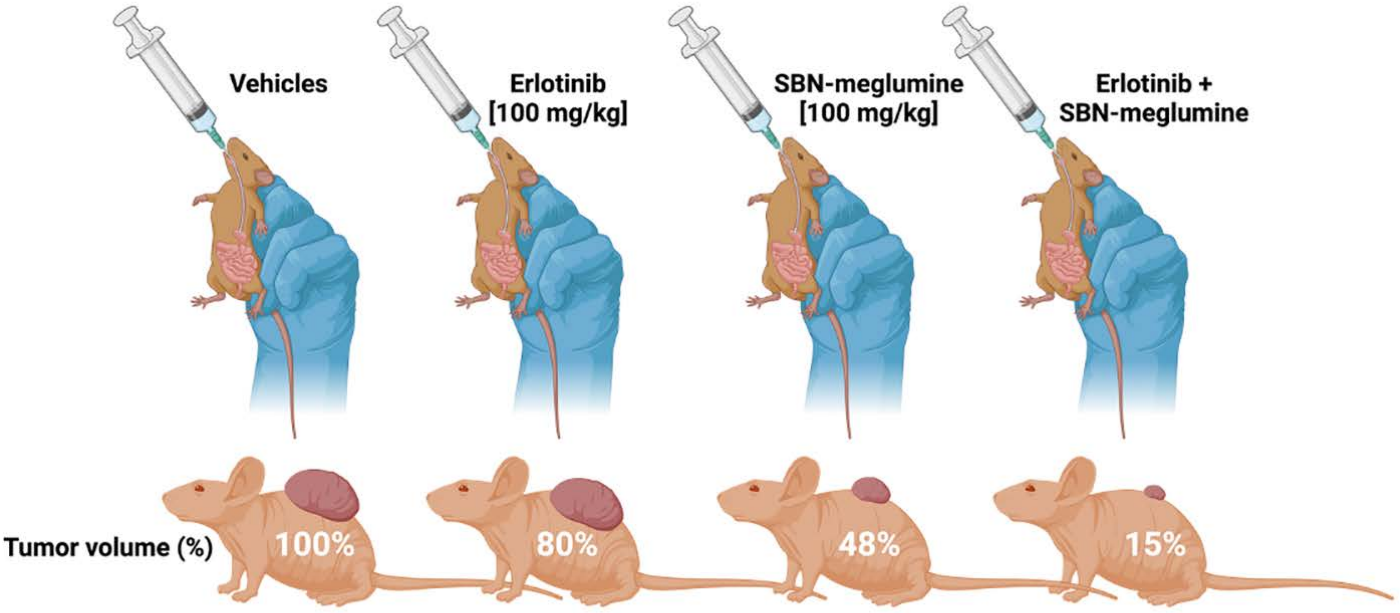

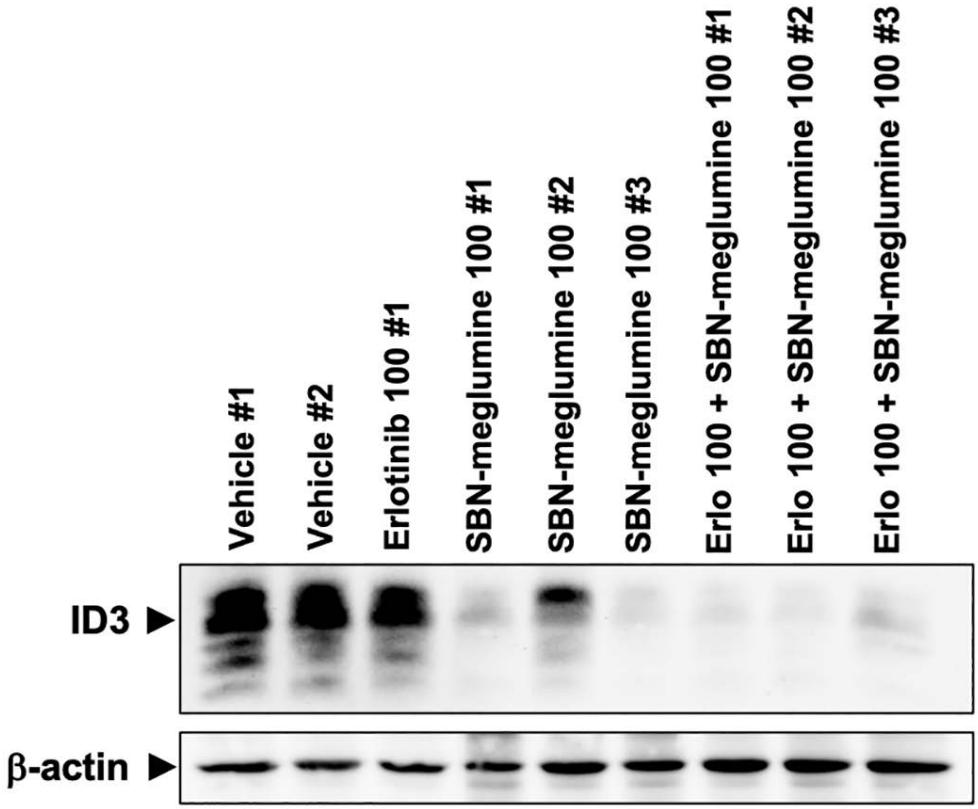

STUDY 2

Silibinin Overcomes EMT-Driven Lung Cancer Resistance to New-Generation ALK Inhibitors

Verdura S, Encinar JA, Teixidor E, Segura-Carretero A,

Micol V, Cuyàs E, Bosch-Barrera J, Menendez JA.

Cancers (Basel). 2022 Dec 11;14(24):6101

doi: 10.3390/cancers14246101

cancers

MDPI

Article

Silibinin Overcomes EMT-Driven Lung Cancer Resistance to New-Generation ALK Inhibitors

Sara Verdura [1,2], Jose Antonio Encinar [3], Eduard Teixidor [2,4], Antonio Segura-Carretero [5], Vicente Micol [3,6], Elisabet Cuyàs [1,2,*], Joaquim Bosch-Barrera [2,4,7] and Javier A. Menendez [1,2,*]

1 Metabolism and Cancer Group, Program Against Cancer Therapeutic Resistance (ProCURE), Catalan Institute of Oncology, 17005 Girona, Spain
2 Girona Biomedical Research Institute, Salt, 17190 Girona, Spain
3 Institute of Research, Development and Innovation in Biotechnology of Elche (IDiBE) and Molecular and Cell Biology Institute (IBMC), Miguel Hernández University (UMH), 03202 Elche, Spain
4 Medical Oncology, Catalan Institute of Oncology, 17007 Girona, Spain
5 Department of Analytical Chemistry, University of Granada, 18071 Granada, Spain
6 CIBEROBN (Physiopathology of Obesity and Nutrition CB12/03/30038) Carlos III Health Institute, 28029 Madrid, Spain
7 Department of Medical Sciences, Medical School University of Girona, 17071 Girona, Spain
* Correspondence: ecuyas@idibgi.org (E.C.); jmenendez@idibgi.org or jmenendez@iconcologia.net (J.A.M.)

Simple Summary: Epithelial-to-mesenchymal transition (EMT) is a cellular plasticity program that can confer invasiveness, dissemination, and therapy resistance to cancer cells. Although inhibitors of this cellular process are expected to work as good "partners" for chemotherapy, immunotherapy or targeted therapy drugs, direct targeting of the EMT phenomenon is, in most cases, pharmacologically challenging. The objective of this work was twofold: On the one hand, to determine if the mere process of EMT is sufficient to foster the resistance of lung cancer cells to various generations of ALK tyrosine kinase inhibitors (TKIs); on the other hand, to test the capacity of the natural compound silibinin to re-sensitize lung cancer cells that gained a mesenchymal phenotype to the anti-tumor activity of ALK–TKIs. Our findings show that not all ALK-aberrant lung cancer cells exhibit the same propensity to undergo an EMT process, thereby determining whether they are able to acquire multi-resistance to various ALK–TKIs. We have also discovered the ability of silibinin to decrease the hypersecretion of the EMT-driver TGFβ, to directly block, to some extent, the activity of purified TGFβ receptors, and to attenuate the activation status of the SMAD pathway in response to ALK–TKIs. Since there exist bioavailable formulations of silibinin with proven clinical activity in oncology patients, our results suggest a new therapeutic strategy that would merit exploration to prevent or reverse resistance to ALK–TKIs induced by the EMT phenomenon.

Abstract: Epithelial-to-mesenchymal transition (EMT) may drive the escape of ALK-rearranged non-small-cell lung cancer (NSCLC) tumors from ALK-tyrosine kinase inhibitors (TKIs). We investigated whether first-generation ALK–TKI therapy-induced EMT promotes cross-resistance to new-generation ALK–TKIs and whether this could be circumvented by the flavonolignan silibinin, an EMT inhibitor. ALK-rearranged NSCLC cells acquiring a bona fide EMT phenotype upon chronic exposure to the first-generation ALK–TKI crizotinib exhibited increased resistance to second-generation brigatinib and were fully refractory to third-generation lorlatinib. Such cross-resistance to new-generation ALK–TKIs, which was partially recapitulated upon chronic TGFβ stimulation, was less pronounced in ALK-rearranged NSCLC cells solely acquiring a partial/hybrid E/M transition state. Silibinin overcame EMT-induced resistance to brigatinib and lorlatinib and restored their efficacy involving the transforming growth factor-beta (TGFβ)/SMAD signaling pathway. Silibinin deactivated TGFβ-regulated SMAD2/3 phosphorylation and suppressed the transcriptional activation of genes under the control of SMAD binding elements. Computational modeling studies and kinase binding assays predicted a targeted inhibitory binding of silibinin to the ATP-binding pocket of TGFβ type-1 receptor 1 (TGFBR1) and TGFBR2 but solely at the two-digit micromolar range. A secretome profiling confirmed the ability of silibinin to normalize the augmented release of

Citation: Verdura, S.; Encinar, J.A.; Teixidor, E.; Segura-Carretero, A.; Micol, V.; Cuyàs, E.; Bosch-Barrera, J.; Menendez, J.A. Silibinin Overcomes EMT-Driven Lung Cancer Resistance to New-Generation ALK Inhibitors. *Cancers* **2022**, *14*, 6101. https://doi.org/10.3390/cancers14246101

Academic Editors: Elisabetta Aldieri and Weiguang Wang

Received: 6 November 2022
Accepted: 9 December 2022
Published: 11 December 2022

TGFβ into the extracellular fluid of ALK–TKIs-resistant NSCLC cells and reduce constitutive and inducible SMAD2/3 phosphorylation occurring in the presence of ALK–TKIs. In summary, the ab initio plasticity along the EMT spectrum may explain the propensity of ALK-rearranged NSCLC cells to acquire resistance to new-generation ALK–TKIs, a phenomenon that could be abrogated by the silibinin-driven attenuation of the TGFβ/SMAD signaling axis in mesenchymal ALK-rearranged NSCLC cells.

Keywords: ALK; crizotinib; brigatinib; lorlatinib; silibinin; EMT; TGFβ; lung cancer

1. Introduction

The identification of molecular subtypes of non-small-cell lung cancer (NSCLC) based on specific oncogenic drivers has changed the natural history of the disease. Less than 15 years have elapsed from the first identification of the anaplastic lymphoma kinase (ALK) fusion oncogene in a patient with NSCLC [1,2] to the remarkable improvement in clinical outcomes achieved by patients with ALK-rearranged NSCLC with the first-generation ALK tyrosine kinase inhibitor (ALK–TKI) crizotinib [3–5]. Despite this advance, however, most patients inevitably relapse due to acquired resistance, which commonly occurs via ALK-dependent on-target mechanisms mediated by the appearance of secondary mutations in the *ALK* gene [6–8]. This can be observed in 25–33% of patients progressing to crizotinib [9–13], and increases to ~50% in response to second-generation ALK–TKIs such as ceritinib (LDK378), alectinib (CH5424802), and brigatinib (AP26113) [14–16]. The development of more selective and potent third-generation ALK–TKIs with improved central nervous system activity, such as lorlatinib (PF-06463922), has enabled better management of patients with resistant ALK mutant forms that are common causes of resistance against first- and second-generation ALK–TKIs [17–22]. Unfortunately, there is ever-growing evidence that several ALK-independent off-target mechanisms of acquired resistance to ALK–TKIs can occur with no involvement of ALK [23,24].

ALK-rearranged NSCLC tumors can lose their reliance on ALK, and instead become dependent on the alternative activation of signaling axes, for example, alterations in EGFR, KRAS/MAPK, cKIT, MET, HER2/HER3, AXL and IGF-1/IGF-1R pathways, among others [12,25,26]. Epithelial-to-mesenchymal (EMT)—a cellular process during which epithelial cells acquire mesenchymal phenotypes and behavior following the downregulation of epithelial features—is now recognized as a common downstream node in which ALK-dependent and -independent mechanisms converge to drive intrinsic and acquired resistance to ALK–TKIs [27–33]. Indeed, not only do ALK-rearranged tumors frequently exhibit EMT traits compared with other NSCLC genotypes, but also EMT-like processes are actively involved in mediating resistance against ALK–TKIs independently of ALK mutation status [34,35]. Furthermore, ALK-resistance mutations and an EMT component can simultaneously co-exist in two different tumor cell subpopulations in patients with ALK-rearranged NSCLC who are resistant to crizotinib [10,36]. Whether the shift from epithelial to mesenchymal phenotypes should be viewed as an ALK mutation-independent, cancer cell-autonomous phenomenon that drives cross-resistance to new-generation ALK–TKIs is still under debate [10,36]. Nonetheless, the circumvention of EMT-associated resistance to ALK–TKIs to restore the sensitivity of mesenchymal-type tumor cells to ALK–TKIs, remains an unmet need of targeted drug therapy in ALK-rearranged NSCLC.

Here, we studied whether the EMT phenomenon that drives acquired resistance to first-generation ALK–TKI therapy suffices to promote cross-resistance to new-generation ALK–TKIs and whether the known anti-EMT [37–40]/anti-TGFβ [41–44] signaling activity of the flavonolignan silibinin could be exploited to re-sensitize drug-refractory mesenchymal NSCLC cells to ALK–TKIs, and explored the mechanisms involved. We confirm that the mesenchymal phenotype generated upon a bona fide late, full EMT phenomenon induces robust cross-resistance to multiple-generation ALK–TKIs. We also describe how the

capacity of silibinin to attenuate a hyperactive TGFβ/SMAD signaling axis can overcome EMT-driven resistance to multiple-generation ALK–TKIs in ALK-rearranged NSCLC cells.

2. Materials and Methods

2.1. Materials

Crizotinib was kindly provided by Pfizer. Brigatinib (AP26113; Cat. #S8229) and lorlatinib (PF-6463922; Cat. #S7536) were purchased from Selleckchem (Houston, TX, USA). Silibinin (Cat. #S0417) was purchased from Sigma-Aldrich (Madrid, Spain). All reagents were dissolved in sterile dimethylsulfoxide (DMSO) to prepare 10 mmol/L stock solutions, which were stored in aliquots at −20 °C until use. Working concentrations were diluted in culture medium prior to each experiment.

Antibodies against E-cadherin (#3195), SMAD2/3 (#3102) and phospho-SMAD2 (Ser465/467)/SMAD3 (Ser423/425) (#9510) were purchased from Cell Signaling Technology (Danvers, MA, USA). Antibodies against GADPH (#60004-1-Ig) and β-actin (#66009-1-Ig) were purchased from Proteintech Group, Inc (Rosemont, IL, USA). Antibodies against vimentin (#V6630) and SNAIL (#MA5-14801) were purchased from Sigma-Aldrich and ThermoFisher Scientific Inc. (Waltham, MA, USA), respectively.

The Applied Biosystems™ TaqMan™ Array Human TGFβ Pathway 96-well Plate (Cat. #4414097) was purchased from Applied Biosystems (Foster City, CA, USA). RayBio® C-Series Human TGFβ Array C2 (Cat. #AAH-TGFB-2-2) was purchased from RayBiotech, Inc. (Norcross, GA, USA).

2.2. Cell Lines

The establishment of crizotinib resistance in H2228 cells (H2228/CR) and H3122 cells (H3122/CR) by incremental and continuous exposure to crizotinib has been described [27,45]. In order to assess the stability of acquired resistance in H2228/CR and H3122/CR cell lines, sensitivity to crizotinib was assessed after freezing and thawing as well as following drug withdrawal as previously described [46]. To generate transdifferentiated H2228 and H3122 cells (H2228/TD and H3122/TD, respectively), cells were repeatedly treated with TGFβ1 at 10 ng/mL every 3 days for 60 days. The cells were then aliquoted into vials and frozen. Newly thawed TD cells were used for up to 30 days, during which time they were exposed to TGFβ1 at 5 ng/mL once weekly. For EMT marker studies, H2228/TD and H3122/TD cells were cultured in low-serum for 24 h before treatment for an additional 24 h with 10 ng/mL TGFβ1. The SBE Reporter–HEK293 cell line (Cat. #60653; BPS Bioscience, San Diego, CA, USA) was employed for monitoring the impact of silibinin on the activity of the TGFβ/SMAD signaling pathway.

2.3. Quantitative Real-Time Polymerase Chain Reaction (qRT-PCR)

Total RNA extracted from cells was evaluated in technical triplicates for the abundance of *CDH1* (Hs01023894_m1), *CDH2* (Hs00983056_m1), *VIM* (Hs00185584_m1), *SNAI1* (Hs00195591_m1), *SNAI2/SLUG* (Hs00950344_m1), and *ZEB1* (Hs00232783_m1) relative to the housekeeping genes 18*s* (Hs99999901_s1) and *PPIA* (Hs99999904_m1) using an Applied Biosystems QuantStudio™ Flex PCR System with an automated baseline and threshold cycle detection. The transcript abundance was calculated using the delta Ct method and presented as relative quantification (RQ) or log2 fold-change, as specified.

2.4. Immunoblotting Analyses

HEK293 cells were seeded in 6-well plates at 250,000 cells/well and allowed to grow overnight in DMEM culture media containing 10% FBS. The media were then replaced with DMEM containing 0.1% FBS with or without TGFβ1 and/or silibinin. The cells were incubated for a further 24 h, washed with ice-cold PBS, and then immediately scraped off the plate after adding 30–75 µL of 2% SDS, 1% glycerol, and 5 mmol/L Tris-HCl, pH 6.8. Protein lysates were collected in 1.5 mL microcentrifuge tubes and the samples were sonicated for 1 min (in an ice bath) with 2 s of sonication at 2-s intervals to fully lyse

the cells and reduce viscosity. Protein content was determined by the Bradford protein assay (Bio-Rad, Hercules, CA, USA). Sample buffer was added and extracts were boiled for 4 min at 100 °C. Equal amounts of protein were electrophoresed on 15% SDS-PAGE gels, transferred to nitrocellulose membranes and incubated with primary antibodies as specified, followed by incubation with a horseradish peroxidase-conjugated secondary antibody and chemiluminescence detection. GADPH and β-actin were employed as protein loading controls.

2.5. Cell Viability Assay

The cell viability effects of ALK–TKIs and silibinin were determined using the colorimetric MTT (3-4,5-dimethylthiazol-2-yl-2,5-diphenyl-tetrazolium bromide) reduction assay. Dose-response curves to graded concentrations of drugs were plotted as a percentage of the control cell absorbance, which was obtained from control cells containing the vehicle processed simultaneously. For each treatment, cell viability was evaluated using the following equation: (OD_{570} of the treated sample/OD_{570} of the untreated sample) × 100. Sensitivity to agents was expressed in terms of the concentrations required for a 50% (IC_{50}) reduction in cell viability. Since the percentage of control absorbance was considered to be the surviving fraction of cells, the IC_{50} values were defined as the concentration of drug that produced a 50% reduction in control absorbance (by interpolation).

2.6. Colony Formation Assays

Anchorage-dependent clonogenic growth assays were performed by initially seeding NSCLC cells into 12-well plates at low densities (500–1000 cells/well) and culturing in the presence or absence of graded concentrations of ALK–TKIs and/or silibinin for 7 days (without refeeding) in a humidified atmosphere with 5% CO_2, at 37 °C. The colonies were stained with crystal violet (0.5% *w*/*v*) in 80% methanol and 37% formaldehyde.

2.7. SMAD-Binding Element Reporter Assays

SBE Reporter–HEK293 cells were seeded at 40,000 cells per well into white clear-bottom 96-well microplates in 100 µL of assay medium and incubated at 37 °C and 5% CO_2 overnight. The next day, the medium was removed and 3-fold serial dilutions of either SB5235443 or silibinin were prepared in the assay medium without antibiotics; 50 µL of diluted SB5235443 or silibinin was added to the wells, and 50 µL of assay medium with the same concentration of DMSO without compound was added to control wells. Additionally, 55 µL of assay medium with DMSO was added to cell-free control wells (for determining background luminescence). The cells were incubated at 37 °C and 5% CO_2 for 4–5 h. Subsequently, 5 µL of diluted human TGFβ1 in the assay medium was added to wells (final (TGFβ1) = 20 ng/mL); 5 µL of the assay medium was added to the unstimulated control wells. The cells were treated overnight, lysed and the luciferase activity was measured using the ONE-Step luciferase assay system (BPS Bioscience): 55 µL of One-Step Luciferase reagent was added per well and the plates rocked at room temperature for ~30 min. Luminescence was measured using a BioTek Synergy™ 2 luminometer (BioTek Instruments, Winooski, VT, USA).

2.8. Human TGFβ Array

Total RNA was extracted from H2228 and H2228/CR cells cultured in the absence or presence of silibinin (48 h) using the Qiagen RNeasy Kit and QIAshredder columns (Qiagen, Hilden, Germany). The Applied Biosystems™ TaqMan™ Array Human TGFβ Pathway 96-well plate, which contained 92 assays for TGFβ-associated genes and 4 assays for candidate endogenous control genes, was processed and analyzed as per the manufacturer's instructions using an Applied Biosystems QuantStudio™ 7 Flex PCR System. The data were interpreted using web-based PCR array analysis tools, applying a false discovery rate lower than 1% (FDR1%) and a fold-change cut-off of $\geq$2 ($p < 0.05$).

2.9. TGFβ-Related Secretome

Assays with antibody arrays for TGFβ-related proteins were carried out as per the manufacturer's instructions. Briefly, array membranes were blocked with 5% BSA/TBS (0.01 mol/L Tris-HCl pH 7.6/0.15 mol/L NaCl) for 1 h. The membranes were then incubated with ~1 mL of conditioned media prepared from the different cell lines after normalization for equal amounts of protein. After extensive washing with TBS/0.1% *v*/*v* Tween 20 (3 times, 5 min each) and TBS (2 times, 5 min each) to remove unbound material, the membranes were incubated with a cocktail of biotin-labeled antibodies against different individual TGFβ-related proteins. The membranes were then washed and incubated with horseradish peroxidase (HRP)-conjugated streptavidin (2.5 pg/mL) for 1 h at room temperature. Unbound HRP-streptavidin was washed out with TBS/0.1% *v*/*v* Tween 20 and TBS. Chemiluminescent readings were taken using a ChemiDoc MP imaging system (Bio-Rad Laboratories, Inc., Hercules, CA, USA) and densitometric values were quantified using ImageJ software.

2.10. Docking Calculations, Molecular Dynamics Simulations, and Binding Free Energy Analysis

Docking calculations, MD simulations, and MM/PBSA calculations to determine the alchemical binding free energy of silibinin A and B against the 3D crystal structures 5E8S (human TGFβR1/ALK5) and 5E8Y (human TGFβR2 in complex with staurosporine) [47] were performed using procedures described in previous works from our group [48–53]. To perform the docking studies with AutoDockVina (v1.1.2, San Diego, CA, USA), crystal structures were transformed to the PDBQT format, including the atomic charges and atom-type definitions. These preparations were performed using the AutoDock/Vina plugin with scripts from the AutoDock Tools package [54]. YASARA dynamics v19.9.17 (Vienna, Austria) was employed for all MD simulations with the AMBER14 force field. All simulation steps were run using a pre-installed macro (md_run.mcr) within the YASARA suite. Data were collected every 100 ps during 100 ns. The MM/PBSA calculations of solvation binding energy were calculated using the YASARA macro md_analyzebindenergy.mcr, with more negative values indicating instability. MM/PBSA was implemented with the YASARA macro md_analyzebindenergy.mcr to calculate the binding free energy with solvation of the ligand, complex, and free protein, as described in [48–53]. All of the figures were prepared using PyMol 2.0 software and all interactions were detected using the protein–ligand interaction profiler (PLIP) algorithm [55].

2.11. LanthaScreen Eu Kinase Binding Assays

To obtain 10-point titration results of the inhibitory activity of silibinin towards the ATP-dependent kinase activity of TGFβR1/ALK5 and TGFβ2R, LanthaScreen Eu kinase binding assays were outsourced to ThermoFisher Scientific using the SelectScreen™ Biochemical Kinase Profiling Service.

2.12. Statistical Analysis

All observations were confirmed by at least three independent experiments performed in triplicate for each cell line and for each condition. The data are presented as mean ± SD. Two-group comparisons were performed using Student's *t*-test for paired and unpaired values. Comparisons of means of ≥3 groups were performed by ANOVA, and the existence of individual differences, in case of significant F values with ANOVA, was tested by Scheffé's multiple contrasts; *p*-values <0.05 and <0.005 were considered to be statistically significant (denoted as * and **, respectively). All statistical tests were two-sided.

3. Results

3.1. Acquisition of a Mesenchymal-Like Phenotype Promotes Cross-Resistance to First-, Second-, and Third-Generation ALK–TKIs in ALK-Rearranged NSCLC Cells

To explore whether acquired resistance to first-generation crizotinib might be accompanied by cross-resistance to second- and third-generation ALK–TKIs in an EMT-dependent

manner, we characterized two crizotinib-resistant sublines (H2228/CR and H3122/CR) derived from the crizotinib-sensitive H2228 and H3122 NSCLC cell lines harboring the ALK variants 3a/b and 1, respectively [56]. H2228/CR and H3122/CR cells were derived by incremental and continuous exposure of parental lines to increasing concentrations of crizotinib over several months [27,45,57]. H2228/CR and H3122/CR cells lack amplification or resistance mutations in the ALK kinase domain, thus offering two idoneous models to explore the involvement of EMT as an ALK-independent, off-target resistance mechanism to new-generation ALK–TKIs (Figure 1).

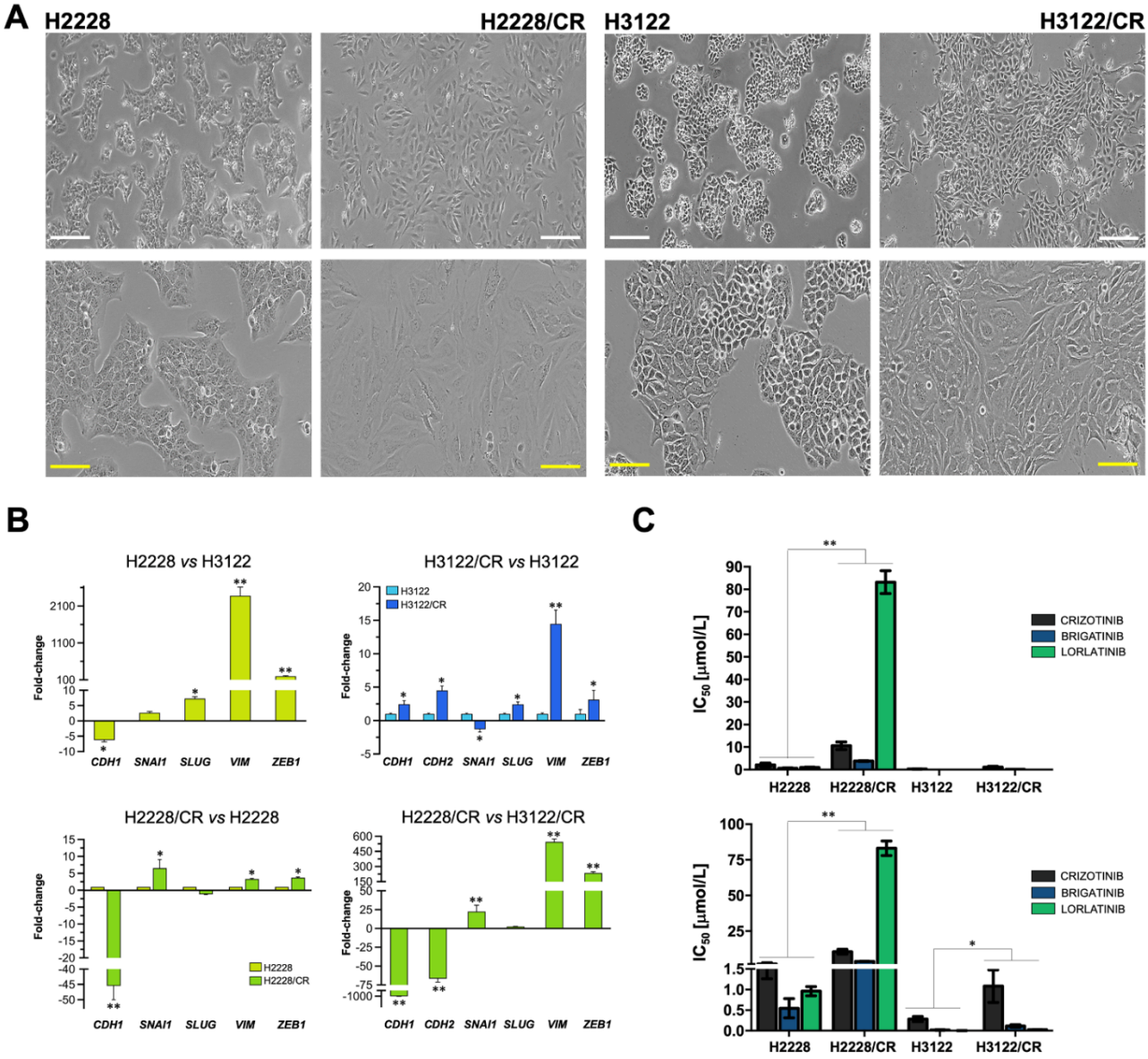

Figure 1. EMT-related traits in ALK-rearranged NSCLC cells with acquired cross-resistance to multiple-generation ALK–TKIs. (**A**) Representative phase contrast microphotographs of H2228/H2228CR and H3122/H3122CR ALK-rearranged NSCLC cell line pairs. CR: crizotinib resistance; Scale bar, 100 μm. (**B**) The transcript abundance of *CDH1*, *CDH2*, *SNAI1*, *SLUG*, *VIM*, and *ZEB1* was calculated using the ΔC_t method and presented as fold-change in H2228/H2228CR and H3122/H3122CR cells; * $p < 0.05$ and ** $p < 0.005$, statistically significant differences. (**C**) Bar graphs showing the MTT-based IC_{50} values of crizotinib, brigatinib, and lorlatinib for H2228/H2228CR and H3122/H3122CR cells. The results are presented as the means (*columns*) ± S.D (*bars*) ($n = 5$, in triplicate). * $p < 0.05$ and ** $p < 0.005$, statistically significant differences.

Examination of morphological and molecular features of H2228/CR and H3122/CR cells revealed that the characteristic "cobblestone" morphology of parental H2228 epithelial cells was absent in H2228/CR cells, which instead assumed an elongated morphology with evident disruption of tight cell-cell contacts and a notably lower refringent aspect (Figure 1A). By contrast, H3122/CR cells failed to fully phenocopy the mesenchymal-like morphology of H2228/CR cells as they acquired a more marked spindle-shaped morphology and retained numerous cell-cell contacts and a refringent aspect (Figure 1A). Quantitative real-time PCR (qRT-PCR) analyses revealed that H2228 cells exhibited more EMT-like traits than H3122 cells in terms of mesenchymal markers such as vimentin (VIM) (Figure 1B). Crizotinib resistance in H2228/CR cells was accompanied by the acquirement of a bona fide EMT program involving a marked transcriptional down-regulation of the epithelial marker E-cadherin (CDH1) and activation of EMT-driven transcription factors and EMT-related markers (SNAI1, VIM) (Figure 1B). Crizotinib resistance in H3122/CR cells was also accompanied by a notable gain in mesenchymal gene expression including the mesenchymal N-cadherin (CDH2) and VIM, but CDH1 expression was retained (Figure 1B).

MTT-based viability assays revealed notably higher half-maximal inhibitory concentration (IC_{50}) values to crizotinib in H2228 cells than in H3122 cells, confirming that NSCLC cells with the variant 3a/b have an inferior response to ALK–TKIs and more aggressive behavior that those with variant 1 (Table S1; Figure 1C) [58–61]. H2228/CR cells, which were ~5-fold more resistant to crizotinib than parental H2228 cells, showed substantial cross-resistance to the second-generation ALK–TKI brigatinib (~8-fold increase in IC_{50}) and were largely unresponsive to the cytotoxic effects of the third-generation ALK–TKI lorlatinib. Indeed, a >80-fold higher concentration of lorlatinib was necessary to obtain an IC_{50} in H2228/CR cells compared with parental H2228 parental cells (Table S1; Figure 1C). Although H3122/CR cells exhibited a similar cross-resistance to crizotinib, brigatinib, and lorlatinib (between ~4- and 6-fold), the IC_{50} values of ALK–TKIs against H3122/CR cells were substantially lower than those for H2228/CR cells (>3000-fold for lorlatinib; Table S1; Figure 1C).

Overall, these findings strongly suggest that when a bona fide, full mesenchymal phenotype develops upon chronic exposure of intrinsically aggressive variant 3a/b-harboring ALK-rearranged NSCLC cells to a first-generation ALK–TKI (crizotinib), those cells are no longer responsive to second and third-generation ALK–TKIs. This cross-resistance phenotype is less pronounced when intrinsically sensitive variant 1-harboring ALK-rearranged NSCLC cells acquire a partial E/M transition state.

3.2. Silibinin Re-Sensitizes Mesenchymal NSCLC Cells to ALK–TKIs

We next examined the ability of the flavonolignan silibinin to re-sensitize mesenchymal cells to ALK–TKIs. H3122/CR cells showed a notably improved sensitivity to crizotinib (~3-fold), brigatinib (~6-fold), and lorlatinib (~4-fold) when MTT-based IC_{50} values were re-calculated in the presence of an optimal concentration of silibinin (100 μmol/L) (Table S1; Figure 2A). Although silibinin co-exposure also decreased the IC_{50} values of ALK–TKIs against H3122/CR cells, such sensitizing activity could be attributed to silibinin toxicity as single agent (Table S1; Figure 2B).

To further examine the sensitizing effects of silibinin on EMT-driven cross-resistance to ALK–TKIs, we performed long-term colony formation assays using doses of ALK–TKIs optimized to maximally discriminate between cell growth in monotherapy and combination therapy with silibinin (75 μmol/L). The combination of ALK–TKIs and silibinin was markedly more effective than ALK–TKIs or silibinin used in monotherapy in attenuating the colony formation potential of mesenchymal-like H2228/CR cells (Figure 2C, left panels). Co-treatment with silibinin re-sensitized non-mesenchymal H3122/CR cells to crizotinib; however, less evident changes were observed when combining silibinin with sub-optimal concentrations of brigatinib and lorlatinib, which remained highly active against H3122/CR cells even at nanomolar concentrations (Figure 2C, right panels).

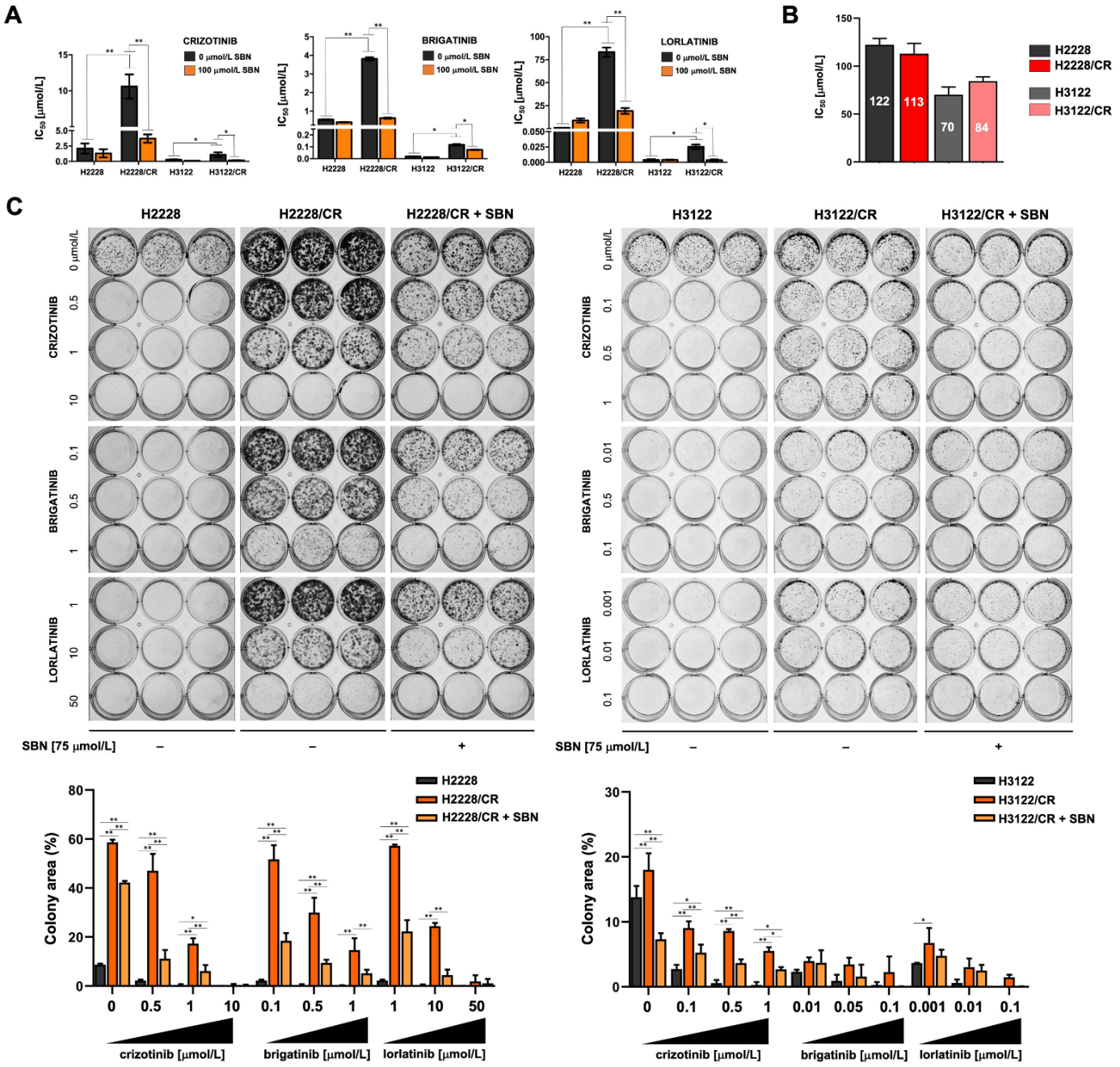

Figure 2. Sensitizing effects of silibinin against EMT-related acquisition of cross-resistance to multiple-generation ALK–TKIs. (**A**) Bar graphs showing the MTT-based IC_{50} values of crizotinib, brigatinib, and lorlatinib for H2228/H2228CR and H3122/H3122CR cells calculated in the absence or presence of 100 µmol/L of silibinin. (**B**) Bar graphs showing the MTT-based IC_{50} values of silibinin in H2228/H2228CR and H3122/H3122CR cells. The results in A and B are presented as the means (*columns*) ± S.D (*bars*) ($n = 5$, in triplicate). * $p < 0.05$ and ** $p < 0.005$, statistically significant differences; n.s. not significant. (**C**) Top: Representative images of clonogenic survival analyses (7 days) of H2228/H2228CR (left) and H3122/H3122CR cells (right) in response to graded concentrations of ALK–TKIs in the absence or presence of 75 µmol/L silibinin. Bottom: Colony area (%) was calculated using the ImageJ plugin "ColonyArea". The results are presented as the means (*columns*) ± S.D (*bars*) ($n = 3$, in triplicate). * $p < 0.05$ and ** $p < 0.005$, statistically significant differences; n.s. not significant.

Because exacerbated TGFβ1 signaling has been shown to drive the EMT-like phenotype in H2228/CR cells [27], we evaluated the ability of silibinin to modulate ALK–TKI

activity in a transdifferentiated (TD) cell model established by chronic exposure of H2228 cells to TGFβ1 (Figure S1A). qRT-PCR analyses confirmed that long-term treatment of H2228 cells with TGFβ (10 ng/mL) was sufficient by itself to induce EMT, as characterized by the acquisition of mesenchymal-like morphological traits equivalent to those found in H2228/CR cells, including the up-regulation of the EMT markers SNAI1, SLUG, VIM, and ZEB1 and the marked downregulation of CDH1 expression (Figure S1B). Additionally, H2228/TD cells exhibited a cross-resistant phenotype to multiple-generation ALK–TKIs, which was particularly striking for the third-generation lorlatinib (>9-fold increase in the IC_{50} value of H2228/TD cells compared with parental H2228 cells; Figure S1C). H3122/TD failed to acquire a bona fide activation of the EMT transcriptional program after TGFβ1 stimulation, with the exception of a notable up-regulation of VIM (Figure S1B). Chronic TGFβ stimulation failed to promote acquired resistance to crizotinib but significantly augmented the IC_{50} values of brigatinib and lorlatinib (~5-fold increase in the case of the third-generation ALK–TKI lorlatinib; Figure S1C). Silibinin treatment significantly reduced the IC_{50} values of ALK–TKIs against H2228/TD and H3122/TD cells (Figure S1C).

Altogether, these findings strongly suggest that silibinin re-sensitizes mesenchymal NSCLC cells to ALK–TKIs, at least in part, by targeting the EMT-driving TGFβ signaling.

3.3. Silibinin Suppresses the TGFβ/SMAD Signaling Pathway

Given our findings thus far, we evaluated whether the acquisition of the mesenchymal phenotype in ALK–TKI-refractory H2228/CR cells involved changes in TGFβ/SMAD signaling [62–64]. Immunoblotting analysis confirmed an increase in total SMAD3 expression in H2228/CR cells concomitant with the constitutive hyperactivation of regulatory SMADs (SMAD2 and SMAD3; Figure 3A), which was largely phenocopied by chronic TGFβ1 stimulation in H2228/TD cells (Figure S1B). Activation of SMAD signaling in H2228/CR cells was accompanied by the conspicuous loss of E-cadherin expression, a slight increase in the abundance of vimentin, and a marked accumulation of the EMT-inducible transcription factor SNAIL (Figure 3A). By contrast, no significant changes were observed in the phosphorylation status of regulatory SMADs in H3122/CR cells, which fully retained the expression of E-cadherin along with a significant up-regulation of vimentin but no induction of SNAIL expression (Figure 3A). Chronic stimulation with TGFβ1 in H3122/TD cells, however, notably promoted both vimentin and SNAIL expression (Figure S1B).

We next tested whether TGFβ/SMAD signaling could be targeted by silibinin using the TGFβ/SMAD Signaling Pathway SBE Reporter-HEK293 cell line, a stable transfected HEK293 cell line expressing the Renilla luciferase gene under the transcriptional control of synthetic SMAD binding elements (SBE) (Figure 3B). When SBE activity was measured in SBE-HEK293 cells stimulated with TGFβ1 in the absence or presence of graded concentrations of silibinin for 24 h, we observed a dose-dependent inhibition of TGFβ1-induced SBE activity with an IC_{50} value of ~25 μmol/L (Figure 3B). To confirm that silibinin can shut down the activation of SMADs as intracellular signaling mediators transducing TGFβ1 extracellular signals to the nucleus, SBE Reporter-HEK293 cells were treated with TGFβ1 in the absence or presence of either silibinin or SB431542, a potent inhibitor of intracellular TGFβ signaling. The results showed a time-dependent increase in the levels of phospho-SMAD2/3 upon TGFβ1 treatment, whereas silibinin co-treatment largely mimicked SB431542 in preventing TGFβ1-induced SMAD2/3 phosphorylation (Figure 3B).

We next evaluated how silibinin treatment might impact the transcriptional expression of TGFβ/SMAD-responsive genes in ALK–TKI-responsive H2228 and ALK TKI-refractory H2228/CR cells using the Applied Biosystems™ TaqMan™ Array Human TGFβ Pathway panel (Figure 3C). Of the 92 assays for ligands, receptors, and mediators of the TGFβ/BMP superfamily, the analyses revealed 7 genes exclusively down-regulated in parental H2228 cells (GDF5, SOX4, ACVRL1, INHBA, BMP2, TSC22D1, TGFB1 | 1), 9 genes commonly down-regulated in H2228 and H2228/CR cells (SMAD1, BMP4, TGFB3, NOG, COL1A1, ID1, TNFSF10, BMPR1A, RUNX1), and 11 genes exclusively regulated in H2228/CR cells

(THBS1, TGFBR2, TGFB2, TGFB1, BMP6, BMP1, COL1A2, SMAD3, ATF4, FST, SMURF1) (Figure 3C).

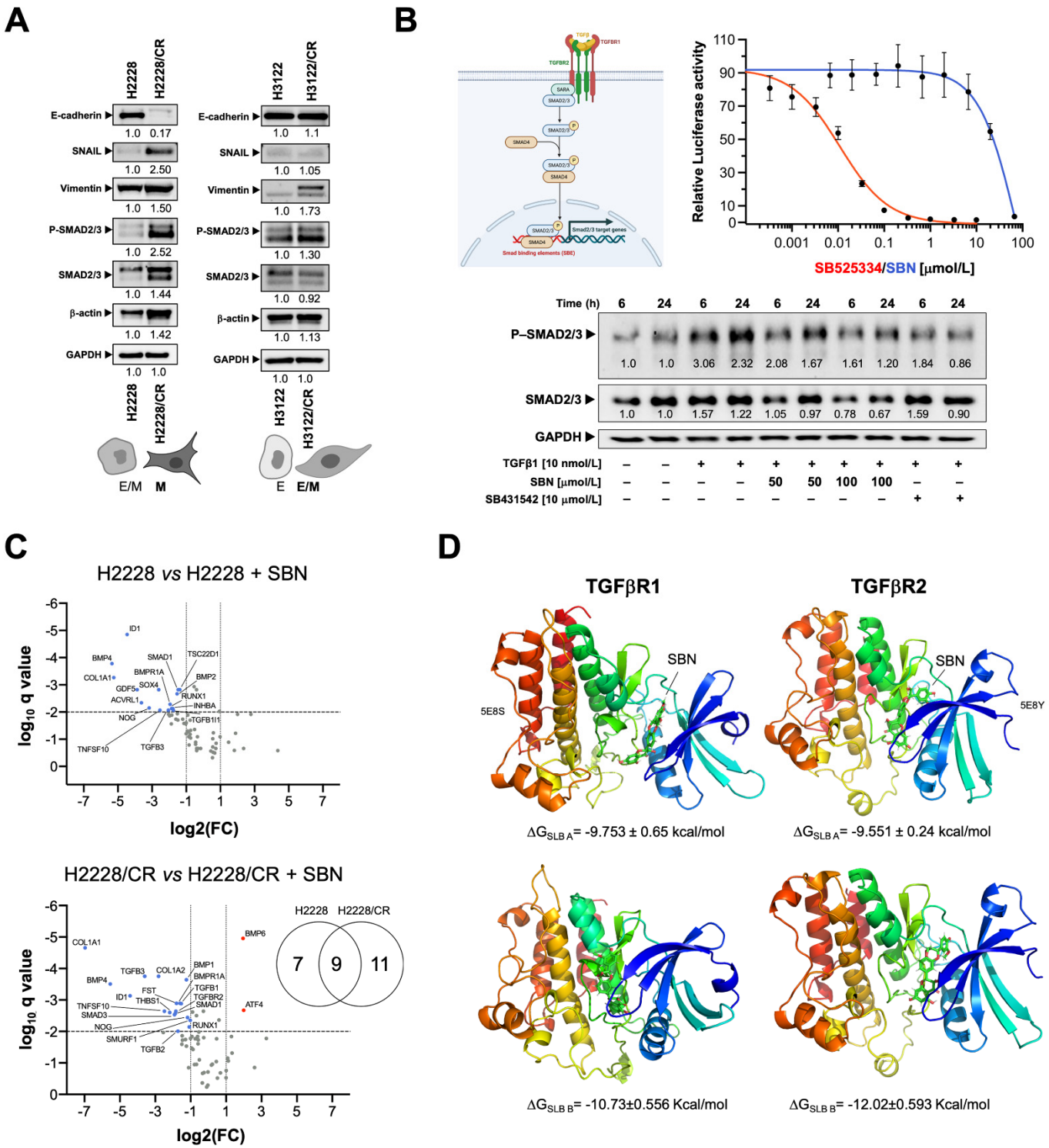

Figure 3. Targeted effects of silibinin against the TGFβ/TGFβR/SMAD signaling pathway. (**A**) Expression levels of E-cadherin, SNAIL, vimentin, phospho-SMAD2/3, total SMAD2/3 were detected by immunoblotting in H2228/H2228CR and H3122/H3122CR cells using specific antibodies. The intensity of the bands was measured using the ImageJ software. Fold-change of each protein relative to parental cells was calculated using GAPDH as a loading control. The figure shows representative immunoblots of multiple ($n \geq 5$) independent experiments. E: Epithelial; M: Mesenchymal. (**B**) Top: Relative luciferase activity using SBE Reporter–HEK293 cells pre-incubated during 4–5 h with graded

concentrations of SB525334 and silibinin before stimulation with TGFβ1. Bottom: Expression levels of phospho-SMAD2/3 and total SMAD2/3 were detected by immunoblotting in HEK293 cells stimulated with TGFβ1 (0, 6, and 24 h) in the absence/presence of either silibinin or SB431542 using specific antibodies. The intensity of the bands was measured using the ImageJ software. Fold-change of each protein relative to untreated samples was calculated using GAPDH as a loading control. The figure shows representative immunoblots of multiple ($n \geq 3$) independent experiments. (**C**) Volcano plots of the results from analyses of the Applied Biosystems™ TaqMan™ Array Human TGFβ Pathway in H2228/H2228CR cells cultured in the absence/presence of silibinin (100 μmol/L) for 48 h. Each dot represents a transcript with its corresponding mean Log2 fold-change (FC) (x axis) and Benjamini–Hochberg corrected p-value (−log10, y axis). Colored dots illustrate differential lipid species, using a cutoff of $p < 0.05$ and log2FC > 1 or < 1. (**D**) The figure depicts the backbone of the overall crystal structure of TGFβR1 (5E8S) and TGFβR2 (5E8Y) with rainbow colors showing the best docked poses of silibinin A and silibinin B at the catalytic site. The uncropped western blot figures were presented in Figure S2.

3.4. Silibinin Is Predicted to Directly Inhibit the Kinase Activity of TGFβR1/2

As the complex EMT-promoting function of TGFβ depends on the activation of the highly conserved single transmembrane serine/threonine kinases type 1 (TGFβR1 or ALK5) and type 2 (TGFβR2) receptors, we explored the possibility that silibinin might directly inhibit TGFβR1/2 kinase activity.

To initially test a putative interaction or binding of silibinin with TGFβ receptors, we computationally docked silibinin into the ATP/ligand binding pocket of TGFβR1/ALK5 and TGFβR2 (Figure 3D). As silibinin is almost a 1:1 mixture of the diastereomers A and B, we performed classical molecular docking studies of silibinin A and B against the 3D crystal structures 5E8S (human TGFβR1/ALK5) and 5E8Y (human TGFβR2 in complex with staurosporine) [46]. The resulting binding energies with the docking simulations of TGFβR1/ALK5 (−9.753 [A] and −10.73 [B] kcal/mol) and TGFβR2 (−9.551 [A] and −12.02 [B] kcal/mol) were marginally superior for the diastereomer B against TGFβR2. To better understand the predicted tendencies, we performed molecular dynamics (MD) simulations for each of the TGFβR1/2-silibinin A/B complexes (Figure 4).

The MD approach considers the protein flexibility at the target-binding site during the molecular recognition process, thereby allowing confirmation of the kinetic stability and validation of the binding poses obtained by docking. The TGFβR1/2 protein backbone root mean square deviation (RMSD) plots of the silibinin heavy atoms, measured after superimposing TGFβR1/2 onto its (apo) reference structure during MD simulations, were prepared in parallel. This approach is summarized in Figure 4A and detects the following: the best poses of silibinin A and silibinin B coupled to the catalytic cavities of TGFβR1/2 before (0 ns) and after (100 ns) the MD simulation, the time evolution of RMSD relative to the initial structure of TGFβR1/2 in the absence and presence of silibinin A/B, the binding free energy calculations under the molecular mechanics Poisson–Boltzmann surface area (MM/PBSA) approximation from the entire MD simulation trajectory of 100 ns (or last 30 ns), and the identification of amino acid residues participating in the silibinin A/B-TGFβR1/2 binding pocket. Close inspection of the different conformations revealed that silibinin A was not predicted to interact with TGFβR1 His-283 (or its equivalent in TGFβR2 His-328) or TGFβR1 Asp-281 (or its equivalent in TGFβR2 Ala-326), which are two key residues in the hinge region of TGFβRs critically involved in the binding of selective TGFβR1 and pan-TGFβR1/2 inhibitors [46]. Silibinin A was predicted to stably interact throughout the entire MD simulation with TGFβR1 Lys-232, the third key residue in the hinge region, as well as with TGFβR1 Ile-211 and Val-219, two residues establishing non-polar contacts with pan-TGFβR1/2 and selective TGFβR1 inhibitors. By contrast, silibinin B was predicted to interact with the key residues TGFβR2 His-328/Ala-326 as well as with Val-250, Val-258, and Leu-386, three residues establishing non-polar contacts with pan-TGFβR1/2 inhibitors. Moreover, silibinin B was predicted to stably interact with

Lys-277, a crucial residue located at the ATP-binding site whose mutation destroys the kinase and signaling activities of TGFβR2 [65].

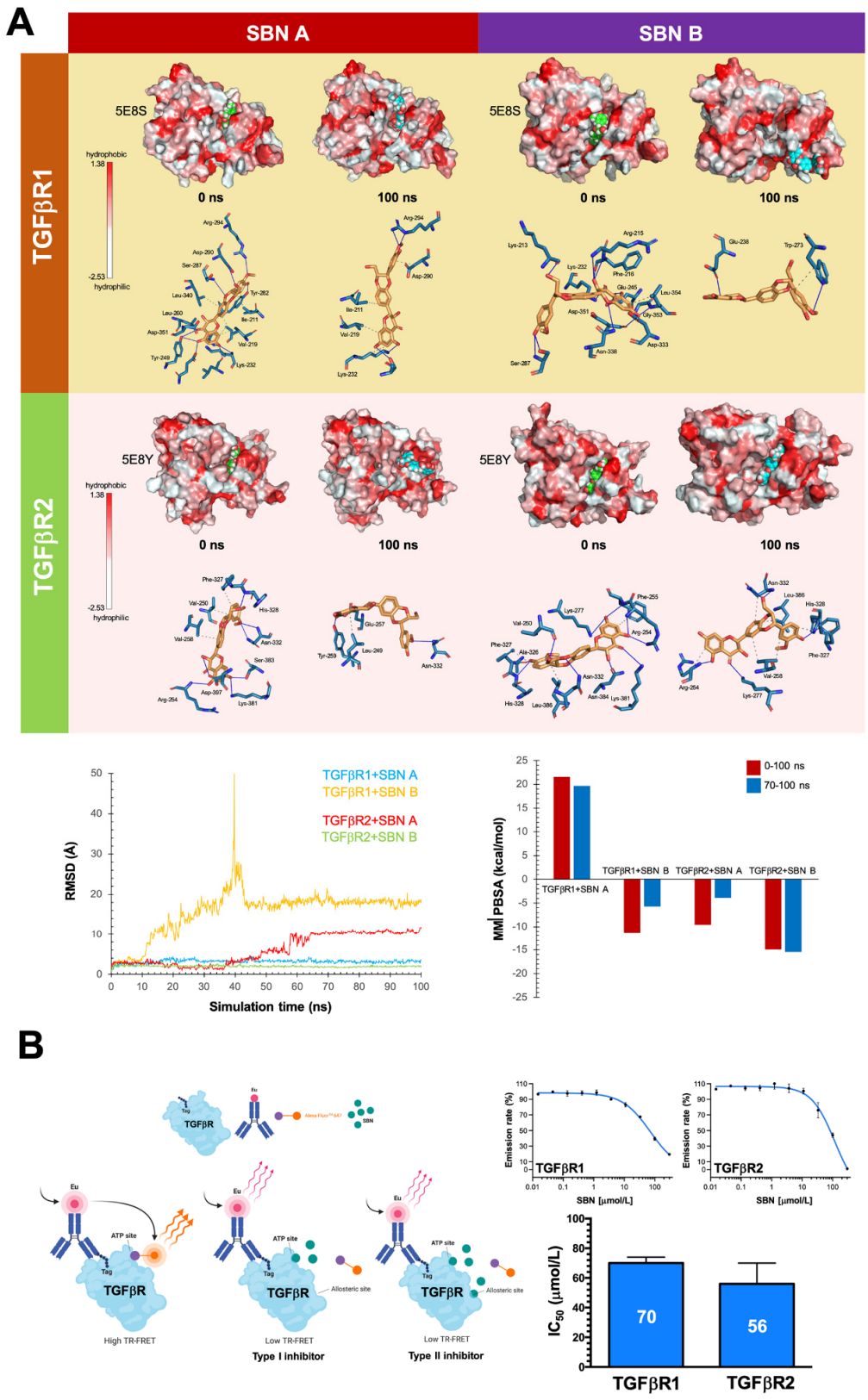

Figure 4. In silico prediction and in vitro verification of silibinin as a weak, direct inhibitor of TGFβRs 1 and 2. (**A**) Top: The best poses of silibinin A and silibinin B coupled to the catalytic site of TGFβR1 (5E8S) and TGFβR2 (5E8Y) before (0 ns) and after (100 ns) the molecular dynamics (MD) simulations

are shown. The protein is represented as a function of the hydrophobicity of its surface amino acids, and the Na^+ and Cl^- ions have been eliminated to facilitate visualization. Each inset shows the detailed interactions of the participating amino acids involved and the type of interaction (hydrogen bonds, hydrophilic interactions, salt bridges, Π-stacking, etc). Bottom: The root means square deviation (RMSD, Å) of the heavy atoms of silibinin A and silibinin B over the simulation time, measured after superposing the protein onto its reference structure, and the molecular mechanics Poisson–Boltzmann surface area (MM/PBSA) binding energy analyses calculated from the entire trajectory of the 100 ns (or last 30 ns) MD simulation, are shown. (**B**) Top: Dose-response curves of LanthaScreen Eu TGFβR1 and TGFβR2 kinase binding assays showing dose-dependent decreases in emission ratios induced by graded concentrations of silibinin. Bottom: Bar graphs showing the IC_{50} values of silibinin for the ATP-dependent activity of TGFβR1 and TGFβR2. The results are presented as the means (*columns*) ± S.D (*bars*). All experiments were carried out two times in duplicate to assess reproducibility.

We used LanthaScreen Eu kinase binding assays to test whether silibinin could function as a TGFβR1/2 kinase inhibitor. This assay monitors the displacement of a labeled "tracer" (Alexa Fluor™ conjugate) from a protein (in our case TGFβRs) by a putative inhibitor, which is detected as a loss of fluorescence resonance energy transfer (FRET) (Figure 4B, left panel). Dose-response curves showed that the emission ratio was dose-dependently decreased by silibinin with IC_{50} values against TGFβR1/ALK5 and TGFβR2 of 70 and 56 μmol/L, respectively (Figure 4B, right panel).

The computational modeling and in vitro enzymatic analyses altogether indicate that silibinin could bind the ATP-binding sites to operate as a direct inhibitor of the TGFβR1/2 kinase activities but solely at the two-digit micromolar range.

3.5. Silibinin Normalizes TGFβ Oversecretion and SMAD2/3 Hyperactivation in ALK–TKI-Resistant NSCLC Cells

We explored whether silibinin treatment might impact both the secretome for proteins linked to the TGFβ signaling pathway and the activation of SMAD2/3 in ALK–TKI-resistant NSCLC cells. We took advantage of the RayBio® C-Series Human TGFβ Array C2 (RayBiotech, Inc., Norcross, GA, USA), which simultaneously detects twenty-five TGFβ signaling-related proteins (Figure 5). As expected, we noticed that TGFβ1 was notably elevated in the culture supernatant of H2228/CR cells compared with H2228 parental cells [27]. Although less markedly, higher levels of TGFβ1 were detected in the in the culture supernatant of H3122/CR cells compared with H3122 parental cells. Silibinin treatment reverted the oversecretion of TGFβ1 in H2228/CR and H3122/CR cells back to the baseline levels found in H2228 and H3122 parental cells (Figure 5). The secretion levels of the divergent member of the TGFβ superfamily GDF15 were found to be drastically decreased in culture supernatants from H2228/CR cells. Moreover, whereas silibinin treatment further augmented baseline GDF15 secretion in H2228 parental cells, it partially recovered the extremely low levels of GDF15 in H2228/CR cells.

Immunoblotting procedures confirmed that silibinin treatment partially but significantly alleviated the constitutive hyperactivation of SMAD2/3 in H2228/CR cells irrespective of the presence of ALK–TKIs (Figure 5). Moreover, ALK–TKIs were found to promote a marked phosphorylation of SMAD2/3 in H3122 and H3122/CR cells (e.g., brigatinib), an activating effect that was largely prevented in the presence of silibinin (Figure 5).

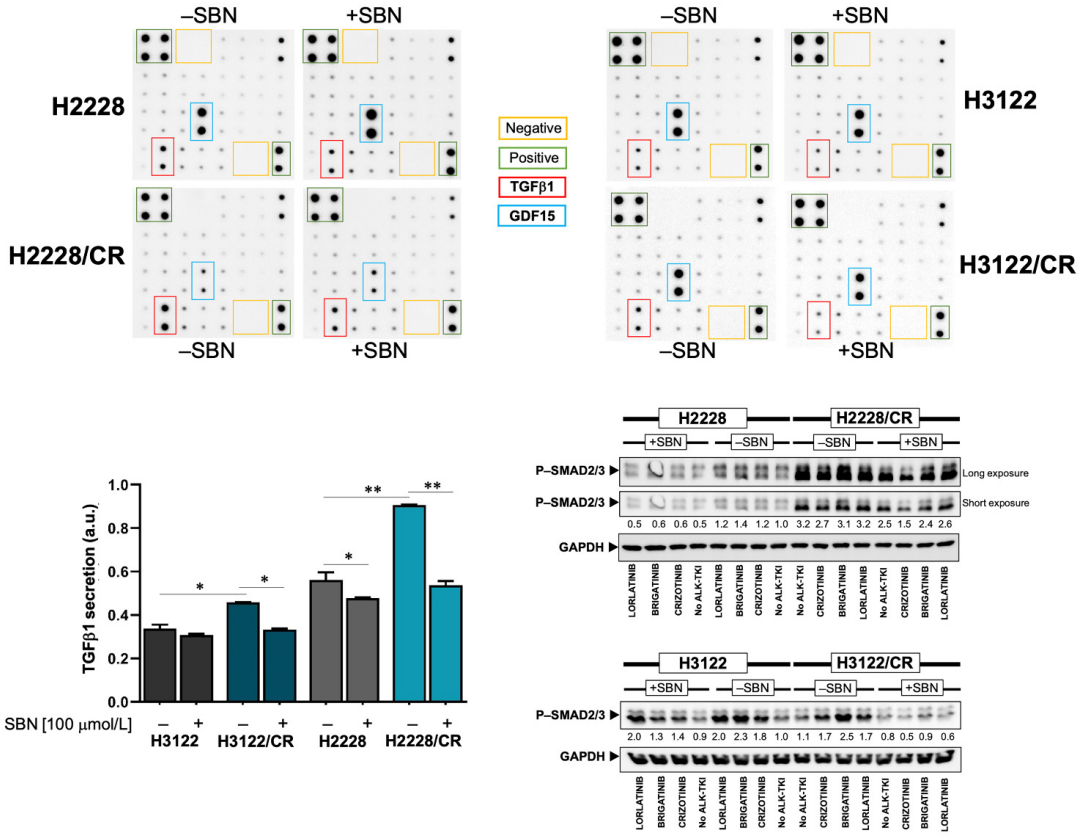

Figure 5. Effects of silibinin on the TGFβ/SMAD signaling axis in ALK–TKIs-resistant NSCLC cells. Top: Low-serum (0.2% FBS), 24-hour-conditioned media from H2228/H2228CR and H3122/H3122CR cells cultured in the absence or presence of silibinin (100 μmol/L) were assayed for the content of 25 TGFβ-related secreted proteins, as described in the Materials and Methods section. Shown are representative results (n = 3) revealing conspicuous changes in TGFβ1 and GDF15. Bottom left: The intensity of TGFβ1 dots was measured using the ImageJ software. Relative changes in TGFβ1 secretion were calculated following subtraction of membrane background signal and normalization to positive control readings. Bottom right: Expression levels of phospho-SMAD2/3 were detected by immunoblotting in H2228/H2228CR and H3122/H3122CR cells treated with crizotinib, brigatinib or lorlatinib (1 μmol/L, 24 h) in the absence/presence of silibinin (100 μmol/L) using a specific antibody. The intensity of the bands was measured using the ImageJ software. The fold-change of each protein relative to untreated samples was calculated using GAPDH as a loading control. The figure shows representative immunoblots of multiple (n = 3) independent experiments. The uncropped western blot figures were presented in Figure S2. * $p < 0.05$ and ** $p < 0.005$.

4. Discussion

The mesenchymal phenotype induced by EMT appears to be an independent resistance mechanism to the first-generation ALK–TKI crizotinib in patients with ALK-rearranged NSCLC [10,36]. If this also occurs in relation to second- and third-generation ALK–TKIs with activity against crizotinib-resistant ALK mutations, the EMT phenomenon could significantly compromise the possible use of next-generation ALK–TKIs as first-line treatment in ALK-rearranged NSCLC. We show that the acquisition of a mesenchymal phenotype by ALK-rearranged NSCLC cells following chronic exposure to crizotinib or to TGFβ stimulation increases resistance to the second-generation ALK–TKI brigatinib and promotes full refractoriness to the third-generation ALK–TKI lorlatinib. Our findings also identify the flavonolignan silibinin as a potential candidate for treating EMT-driven cross-resistance to new-generation ALK–TKIs.

There is evidence from cell line-based experimental models and from in vivo profiling of post-treatment biopsy specimens from ALK–TKI-resistant tumors strongly supporting

EMT as a central off-target mechanism of acquired resistance to ALK–TKIs without the involvement of *ALK* mutations [10,27,36]. Indeed, sustained ALK activity driven by different ALK rearrangements induces an EMT signature in NSCLC but with a noteworthy degree of heterogeneity [35]. ALK-rearranged NSCLC cells exhibiting an EMT-like signature are intrinsically less sensitive to ALK–TKIs than equivalent cells with an epithelial-like signature [66]. Moreover, the acquisition of resistance to ALK–TKIs associates with an EMT phenotype that can be secondary to activation of TGFβ signaling induced by hypoxia or by yet-to-be-defined mechanisms [27,67–69]. Lastly, although ALK-resistant mutations and mesenchymal tumor cells can coexist in a single crizotinib-resistant lesion, the ALK-resistant mutation is largely restricted to epithelial-type tumor cells, whereas tumor cells with the mesenchymal phenotype can exhibit cross-resistance to crizotinib and new-generation ALK–TKIs, including alectinib, ceritinib, and lorlatinib [36]. We provide evidence that ALK-rearranged NSCLC cells gaining a bona fide mesenchymal phenotype caused by a late, full EMT upon chronic exposure to crizotinib, but not those acquiring only a partial/hybrid E/M transition state, exhibit cross-resistance to multiple-generation ALK–TKIs (Figure 6). Our data strongly support a molecular scenario wherein the plasticity along the EMT spectrum determines the propensity of ALK-rearranged NSCLC cells to exhibit cross-resistance to multiple-generation ALK–TKIs. Accordingly, the more epithelial an ALK-rearranged NSCLC cell population is, the lower the capacity to acquire a mesenchymal phenotype refractory to new-generation ALK–TKIs, and vice versa. As cellular heterogeneity along this spectrum is a paramount feature in most tumors including ALK-rearranged NSCLC, forthcoming studies should evaluate whether the utilization of the so-called EMT scores, which have been developed based on pan-cancer signatures of EMT identified from preclinical and/or clinical data [70–74], in a primary/metastatic tumor can be used to predict resistance to ALK–TKIs.

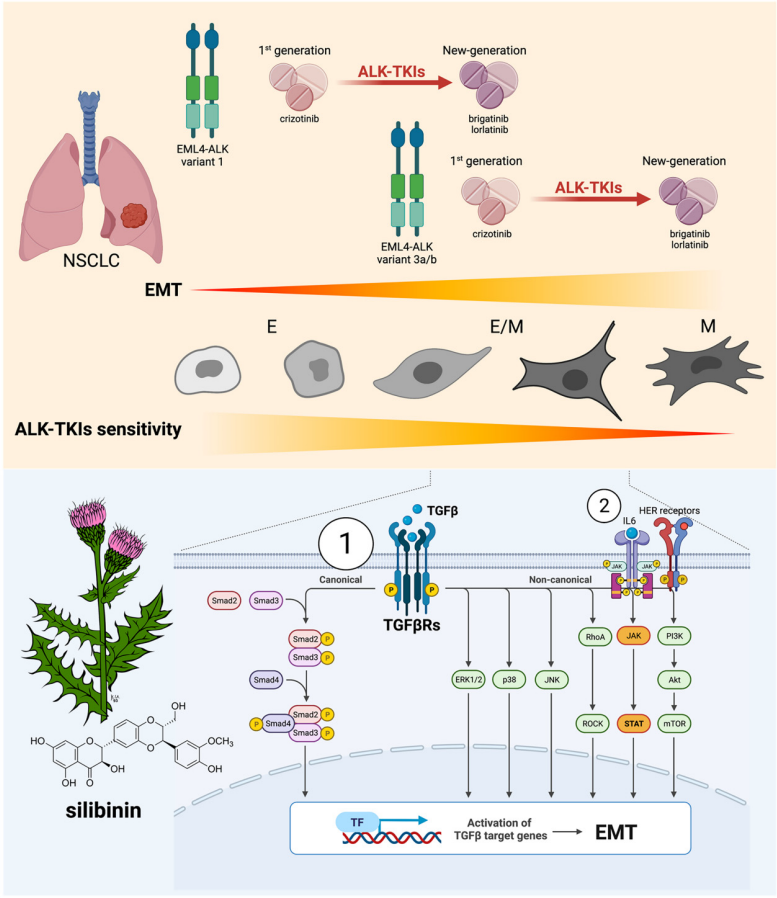

Figure 6. EMT-ness and resistance to multiple-generation ALK–TKIs: a therapeutic opportunity for silibinin. Top: The plasticity along the EMT spectrum might determine the propensity of ALK-rearranged

NSCLC cells to exhibit cross-resistance to multiple-generation ALK–TKIs. The more epithelial an ALK-rearranged NSCLC cell population is (e.g., EML4-ALK variant 1), the lower the capacity to acquire a mesenchymal phenotype refractory to new-generation ALK–TKIs, and vice versa, the more mesenchymal an ALK-rearranged NSCLC cell population is (e.g., EML4-ALK variant 3a/b), the higher the capacity to acquire a mesenchymal phenotype refractory to new-generation ALK–TKIs. ALK-rearranged NSCLC cells gaining a bona fide mesenchymal phenotype caused by a late, full EMT upon chronic exposure to crizotinib, but not those acquiring only a partial/hybrid E/M transition state, exhibit an augmented resistance to the 2nd generation ALK–TKI brigatinib and complete refractoriness to the 3rd generation ALK–TKI lorlatinib. Bottom: The flavonolignan silibinin can overcome EMT-driven cross-resistance to new-generation ALK–TKIs by attenuating the hyperactivation of the TGFβ/SMAD signaling axis (**1**). Nonetheless, silibinin can exert additional ALK–TKIs sensitizing effects via direct inhibition of STAT3 [75] and EGFR [76] (**2**), thereby preventing a functional landscape of resistance to ALK inhibition in NSCLC involving the activation of the IL6/JAK1/STAT3 [77] and HER [78] signaling pathways. Created with Biorender.com.

A pioneering study on the functional landscape of resistance to ALK inhibition in lung cancer proposed several possible agents (including inhibitors of EGFR, HER2/HER3, or PKC) that might be combined with ALK inhibitors to overcome or delay a range of resistance mechanisms in ALK-rearranged NSCLC cells (H3122) with marked sensitivity to ALK–TKIs [78]. Nevertheless, novel therapeutic strategies capable of circumventing EMT underpinning short-lived responses to various cytotoxic and targeted drugs including multiple-generation ALK–TKIs remain an unmet clinical need in ALK-rearranged NSCLC [79–84]. The flavonolignan silibinin, the bioactive principle of the silymarin extract isolated from the dried fruits of the milk thistle (*Silybum marianum*) [85–88], has been shown to exert anti-tumor activities, at least in part, by targeting EMT-related molecular traits in cancer cells. Its ability to concurrently prevent the loss of epithelial markers (E-cadherin) and activate proteins associated with the mesenchymal phenotype (vimentin, N-cadherin, CD44) was previously ascribed to its regulatory effects on major EMT transcriptional regulators, including the transcription factors SNAIL, SLUG, and ZEB and the microRNA miR-21/miR-200c [37–40,57,89–92]. Additionally, silibinin was shown to inhibit fibrotic responses in several tissues via suppression of TGFβ1/SMAD2/3 signaling [42,44,93]. We confirm here the ability of silibinin to control TGFβ/SMAD signaling, as demonstrated by the deactivation of SMAD2, the prevention of SBE-controlled transcriptional responses, and the transcriptional down-regulation of TGFβ-associated genes. TGFβ signaling is initiated by ligand binding to TGFβR2 (TβRII, TGFBR2), a transmembrane receptor with intracellular serine/threonine kinase activity [62–64]. Ligand binding leads to dimerization and autophosphorylation of TGFβR2, which then binds and stimulates the serine/threonine kinase activity of TGFβR1/ALK5. In turn, TGFBR1/ALK5 phosphorylates the cytoplasmic signaling proteins SMAD2 and SMAD3, which associate with SMAD4 to translocate into the nucleus as a multiprotein complex that stimulates the transcription of TGFβ-responsive genes. Our study might add a missing piece to the mechanistic puzzle of the anti-EMT activity of silibinin by revealing that it binds the ATP-binding domain of TGFβR kinases, inhibiting their ATP kinase activity and blocking downstream signaling cascades. In silico, silibinin is predicted to interact with the catalytic site of TGFβR1/ALK5 and TGFβR2, showing shared but mostly distinct contacts to pan- and selective TGFβR inhibitors [46]. These findings confirm not only that flavonolignans such as silibinin should be viewed as specific ligands of biological targets according to the "lock-and-key" concept, but also that the two silibinin diastereomers A and B might behave differently in terms of their biological activity as optically pure components against TGFβRs [94,95].

Beyond underscoring a possible role for stereochemistry in determining the inhibitory potency of silibinin against TGFβRs, we failed to observe a good correlation between the timeline representation of MM/PBSA binding energies of the silibinin diastereomers and the experimental inhibitory activities of the diastereomeric mixture of silibinin A/B using

the LanthaScreen™ Eu Kinase Binding Assay, which is established on the binding and displacement of an ATP-competitive kinase inhibitor scaffold to the TGFβR1 and 2 kinases. As the tracers are based on ATP-competitive kinase inhibitors, they are suitable for detection of any compound that binds the ATP site, including those that bind to both the ATP site and a second "allosteric" site. Our in silico versus experimental data highlight the importance of the use of the respective optically pure components of the silibinin diastereomeric pair to molecularly understand (and therapeutically develop) the anti-TGFβR inhibitory activity of silibinin. Whether the discrepancy between in silico predictions and the observed dose-response curves of silibinin against TGFβR1 and 2 at micromolar concentrations in vitro involves the presence of various inhibitor sites at the kinases or other enzyme-inhibitor parameters (e.g., enzyme concentration >> K_d value of silibinin) deserves careful consideration in the further development of silibinin as an anti-TGFβR/SMAD signaling therapeutic [96]. More importantly, one should acknowledge that the ability of silibinin to function as a direct inhibitor of the TGFβR1/2 kinase activities took place at the two-digit micromolar range, which makes a direct and unique mechanistic involvement of the TGFβR1/2 kinase activities in the ALK–TKIs sensitizing activity of silibinin to some extent improbable. A secretome profiling confirmed the ability of silibinin to normalize the augmented release of TGFβ into the extracellular fluid of ALK–TKIs-resistant NSCLC cells while significantly reducing constitutive and inducible SMAD2/3 phosphorylation in the presence of ALK–TKIs. The ability of silibinin to normalize the enhanced expression and augmented secretion of the EMT-driving factor TGFβ1 into the extracellular milieu might rather explain, at least in part, its ability to attenuate the TGFβ/SMAD signaling axis in ALK–TKIs-resistant NSCLC cells. Nonetheless, as ALK–TKI resistance based on EMT-like phenomena has cross-sensitivity to inhibitors of the Hsp90 chaperone such as ganetespib, 17-AGG, 17-DMAG, and NVP-AUY922 [22,27,69,97–99], we cannot exclude the possibility that the reported capacity of silibinin as a novobiocin-like Hsp90 inhibitor could promote the degradation of client proteins, including not only mutant ALK but also TGFβRs in mesenchymal ALK-rearranged cells with acquired resistance to ALK–TKIs [100,101]. Our previous experience with water-soluble, bioavailable formulations of silibinin demonstrated a complete abrogation of tumor growth in xenograft models of EMT-driven resistance to EGFR TKIs [39,40]. Forthcoming studies should take up the challenge of confirming if clinically relevant formulations of silibinin (e.g., silibinin complexed with the amino-sugar meglumine; silibinin-phosphatidylcholine, the phytolipid delivery system Siliphos; and Eurosil^{85}/Euromed, a milk thistle extract that is the active component of the nutraceutical Legasil with enhanced bioavailability [102]) could similarly abrogate the ALK–TKIs-refractory tumor growth in vivo.

5. Conclusions

The ab initio plasticity along the EMT spectrum should be viewed as a key determinant of the propensity of ALK-rearranged NSCLC cells to acquire resistance to new-generation ALK–TKIs. EMT-driven NSCLC cross-resistance can be abrogated by silibinin, which directly inhibits TGFβR kinase activity and blocks the SMAD signaling cascade in mesenchymal ALK-rearranged NSCLC cells. As EMT is an increasingly recognized driver of innate and acquired resistance to various cytotoxic and targeted drugs, clinically-relevant bioavailable formulations of silibinin with proven anti-cancer activity [103–105] could be explored as cost-effective and feasible approaches for patients with NSCLC resistant to ALK–TKIs.

Supplementary Materials: The following supporting information can be downloaded at: https://www.mdpi.com/article/10.3390/cancers14246101/s1, Figure S1: EMT caused by chronic TGFβ stimulation drives cross-resistance to multiple-generation ALK–TKIs; Figure S2: Uncropped western blot figures. Table S1: Comparison of ALK–TKIs IC_{50} values (in μmol/L) in ALK-rearranged NSCLC cells cultured in the absence/presence of SBN.

Author Contributions: Conceptualization, S.V., E.C., J.B.-B. and J.A.M.; methodology, S.V., J.A.E., A.S.-C., E.C. and J.A.M.; formal analysis, S.V., J.A.E., E.T., A.S.-C., V.M., E.C., J.B.-B. and J.A.M.; investigation, E S.V., J.A.E., E.T., A.S.-C., V.M., E.C., J.B.-B. and J.A.M.; validation, S.V., J.A.E., E.T., A.S.-C., V.M., E.C., J.B.-B. and J.A.M.; data curation, S.V., J.A.E., E.C. and J.A.M.; resources, J.A.E., A.S.-C., E.C. and J.A.M.; writing—original draft preparation, J.A.E., E.C. and J.A.M.; writing—review and editing, J.A.M.; visualization, S.V., J.A.E., E.C. and J.A.M.; supervision, E.C. and J.A.M.; project administration, E.C.; funding acquisition, E.C., J.B.-B. and J.A.M. All authors have read and agreed to the published version of the manuscript.

Funding: Work in the Menendez laboratory is supported by the Spanish Ministry of Science and Innovation (Grant PID2019-10455GB-I00, Plan Nacional de l+D+I, founded by the European Regional Development Fund, Spain) and by an unrestricted research grant from the Fundació Oncolliga Girona (Lliga catalana d'ajuda al malalt de càncer, Girona). Work in the Jose A. Encinar laboratory is supported by the Spanish Ministry of Economy and Competitiveness (MINECO, Grant RTI2019-096724-B-C21) and the Generalitat Valenciana (PROMETEO/2021/059). Joaquim Bosch-Barrera is the recipient of Research Grants from Grupo Español de Cáncer de Pulmón (GECP), La Marató de TV3 foundation (201906), and the Health Research and Innovation Strategic Plan (SLT006/17/114; PERIS 2016-2020; Pla stratègic de recerca i innovació en salut; Departament de Salut, Generalitat de Catalunya). Elisabet Cuyàs holds a "Miguel Servet" research contract (CP20/00003) from the Instituto de Salud Carlos III (Spain) and is supported by the Spanish Ministry of Science and Innovation (Grant PI22/00297, Proyectos de I+D+I en Salud, Acción Estratégica en Salud 2021-2023, founded by the European Regional Development Fund, Spain). The authors would like to heartily thank König for their generous donation to fund our cancer research on silibinin in Girona.

Institutional Review Board Statement: Not applicable.

Informed Consent Statement: Not applicable.

Data Availability Statement: All data generated or analyzed during this study are included in this published article (and its supplementary information file).

Acknowledgments: We are greatly indebted to Jin Kyung Rho (Department of Convergence Medicine, Asan Medical Center, University of Ulsan, College of Medicine, Seoul, South Korea) and Jae Cheol Lee (Department of Oncology, Asan Medical Center, University of Ulsan College of Medicine, Seoul, South Korea) for providing us the H2218/H2218 crizotinib-resistant pair of cell lines and to Daniel B. Costa (Beth Israel Deaconess Medical Center, Harvard Medical Scholl, Boston, MA, USA) for providing the H3122/H3122 crizotinib-resistant pair of cell lines, which have been instrumental in the realization of this work. We are grateful to the Servicio de Supercomputación of the Granada University for letting us to take advantage of the ALBAICIN computer cluster (https://supercomputacion.ugr.es/arquitecturas/albaicin/, accessed on 1 June 2022). We wish to especially thank Santiago Melchor for his kind assistance and cooperation. We are also grateful to the Cluster of Scientific Computing (http://ccc.umh.es, accessed on 1 June 2022) of the Miguel Hernández University (UMH) for providing computer facilities. The authors would like to thank Kenneth McCreath for detailed editing of this manuscript.

Conflicts of Interest: J.B.-B. reports grants and personal fees from Pfizer, MSD Spain, BMS, AstraZeneca, Novartis, Boehringer-Ingelheim, Vifor, Sanofi, and LEO Pharma outside the submitted work. This study was supported in part by a research grant from Pfizer to J.B.-B and J.A.M. These funders had no role in the design of the study, in the collection, analyses, or interpretation of data, in the writing of the manuscript, or in the decision to publish the results.

References

1. Soda, M.; Choi, Y.L.; Enomoto, M.; Takada, S.; Yamashita, Y.; Ishikawa, S.; Fujiwara, S.; Watanabe, H.; Kurashina, K.; Hatanaka, H.; et al. Identification of the transforming EML4-ALK fusion gene in non-small-cell lung cancer. *Nature* **2007**, *448*, 561–566. [CrossRef] [PubMed]
2. Rikova, K.; Guo, A.; Zeng, Q.; Possemato, A.; Yu, J.; Haack, H.; Nardone, J.; Lee, K.; Reeves, C.; Li, Y.; et al. Global survey of phosphotyrosine signaling identifies oncogenic kinases in lung cancer. *Cell* **2007**, *131*, 1190–1203. [CrossRef] [PubMed]
3. Shaw, A.T.; Yeap, B.Y.; Solomon, B.J.; Riely, G.J.; Gainor, J.; Engelman, J.A.; Shapiro, G.I.; Costa, D.B.; Ou, S.H.; Butaney, M.; et al. Effect of crizotinib on overall survival in patients with advanced non-small-cell lung cancer harbouring ALK gene rearrangement: A retrospective analysis. *Lancet Oncol.* **2011**, *12*, 1004–1012. [CrossRef] [PubMed]

4. Shaw, A.T.; Kim, D.W.; Nakagawa, K.; Seto, T.; Crinó, L.; Ahn, M.J.; De Pas, T.; Besse, B.; Solomon, B.J.; Blackhall, F.; et al. Crizotinib versus chemotherapy in advanced ALK-positive lung cancer. *N. Engl. J. Med.* **2013**, *368*, 2385–2394. [CrossRef]
5. Malik, S.M.; Maher, V.E.; Bijwaard, K.E.; Becker, R.L.; Zhang, L.; Tang, S.W.; Song, P.; Liu, Q.; Marathe, A.; Gehrke, B.; et al. U.S. Food and Drug Administration approval: Crizotinib for treatment of advanced or metastatic non-small cell lung cancer that is anaplastic lymphoma kinase positive. *Clin. Cancer Res* **2014**, *20*, 2029–2034. [CrossRef] [PubMed]
6. Solomon, B.J.; Mok, T.; Kim, D.W.; Wu, Y.L.; Nakagawa, K.; Mekhail, T.; Felip, E.; Cappuzzo, F.; Paolini, J.; Usari, T.; et al. First-line crizotinib versus chemotherapy in ALK-positive lung cancer. *N. Engl. J. Med.* **2014**, *371*, 2167–2177. [CrossRef] [PubMed]
7. Iacono, D.; Chiari, R.; Metro, G.; Bennati, C.; Bellezza, G.; Cenci, M.; Ricciuti, B.; Sidoni, A.; Baglivo, S.; Minotti, V.; et al. Future options for ALK-positive non-small cell lung cancer. *Lung Cancer* **2015**, *87*, 211–219. [CrossRef]
8. van der Wekken, A.J.; Pelgrim, R.; Hart, N.; Werner, N.; Mastik, M.F.; Hendriks, L.; van der Heijden, E.H.F.M.; Looijen-Salamon, M.; de Langen, A.J.; Staal-van den Brekel, J.; et al. Dichotomous ALK-IHC Is a Better Predictor for ALK Inhibition Outcome than Traditional ALK-FISH in Advanced Non-Small Cell Lung Cancer. *Clin. Cancer Res.* **2017**, *23*, 4251–4258. [CrossRef]
9. Camidge, D.R.; Doebele, R.C. Treating ALK-positive lung cancer—Early successes and future challenges. *Nat. Rev. Clin. Oncol.* **2012**, *9*, 268–277. [CrossRef]
10. Gainor, J.F.; Dardaei, L.; Yoda, S.; Friboulet, L.; Leshchiner, I.; Katayama, R.; Dagogo-Jack, I.; Gadgeel, S.; Schultz, K.; Singh, M.; et al. Molecular Mechanisms of Resistance to First- and Second-Generation ALK Inhibitors in ALK-Rearranged Lung Cancer. *Cancer Discov.* **2016**, *6*, 1118–1133. [CrossRef]
11. Doebele, R.C.; Pilling, A.B.; Aisner, D.L.; Kutateladze, T.G.; Le, A.T.; Weickhardt, A.J.; Kondo, K.L.; Linderman, D.J.; Heasley, L.E.; Franklin, W.A.; et al. Mechanisms of resistance to crizotinib in patients with ALK gene rearranged non-small cell lung cancer. *Clin. Cancer Res.* **2012**, *18*, 1472–1482. [CrossRef] [PubMed]
12. Katayama, R.; Shaw, A.T.; Khan, T.M.; Mino-Kenudson, M.; Solomon, B.J.; Halmos, B.; Jessop, N.A.; Wain, J.C.; Yeo, A.T.; Benes, C.; et al. Mechanisms of acquired crizotinib resistance in ALK-rearranged lung Cancers. *Sci. Transl. Med.* **2012**, *4*, 120ra17. [CrossRef] [PubMed]
13. Choi, Y.L.; Soda, M.; Yamashita, Y.; Ueno, T.; Takashima, J.; Nakajima, T.; Yatabe, Y.; Takeuchi, K.; Hamada, T.; Haruta, H.; et al. EML4-ALK mutations in lung cancer that confer resistance to ALK inhibitors. *N. Engl. J. Med.* **2010**, *363*, 1734–1739. [CrossRef] [PubMed]
14. Peters, S.; Camidge, D.R.; Shaw, A.T.; Gadgeel, S.; Ahn, J.S.; Kim, D.W.; Ou, S.I.; Pérol, M.; Dziadziuszko, R.; Rosell, R.; et al. Alectinib versus Crizotinib in Untreated ALK-Positive Non-Small-Cell Lung Cancer. *N. Engl. J. Med.* **2017**, *377*, 829–838. [CrossRef]
15. Shaw, A.T.; Kim, D.W.; Mehra, R.; Tan, D.S.; Felip, E.; Chow, L.Q.; Camidge, D.R.; Vansteenkiste, J.; Sharma, S.; De Pas, T.; et al. Ceritinib in ALK-rearranged non-small-cell lung cancer. *N. Engl. J. Med.* **2014**, *370*, 1189–1197. [CrossRef]
16. Gettinger, S.N.; Bazhenova, L.A.; Langer, C.J.; Salgia, R.; Gold, K.A.; Rosell, R.; Shaw, A.T.; Weiss, G.J.; Tugnait, M.; Narasimhan, N.I.; et al. Activity and safety of brigatinib in ALK-rearranged non-small-cell lung cancer and other malignancies: A single-arm, open-label, phase 1/2 trial. *Lancet Oncol.* **2016**, *17*, 1683–1696. [CrossRef]
17. Zou, H.Y.; Friboulet, L.; Kodack, D.P.; Engstrom, L.D.; Li, Q.; West, M.; Tang, R.W.; Wang, H.; Tsaparikos, K.; Wang, J.; et al. PF-06463922, an ALK/ROS1 Inhibitor, Overcomes Resistance to First and Second Generation ALK Inhibitors in Preclinical Models. *Cancer Cell* **2015**, *28*, 70–81. [CrossRef]
18. Shaw, A.T.; Felip, E.; Bauer, T.M.; Besse, B.; Navarro, A.; Postel-Vinay, S.; Gainor, J.F.; Johnson, M.; Dietrich, J.; James, L.P.; et al. Lorlatinib in non-small-cell lung cancer with ALK or ROS1 rearrangement: An international, multicentre, open-label, single-arm first-in-man phase 1 trial. *Lancet Oncol.* **2017**, *18*, 1590–1599. [CrossRef]
19. Solomon, B.; Shaw, A.; Ou, S.; Besse, B.; Felip, E.; Bauer, T.; Soo, R.; Bearz, A.; Lin, C.; Clancy, J.; et al. Phase 2 study of lorlatinib in patients with advanced ALK$^+$/ROS1$^+$ non-small-cell lung cancer (abstract OA05.06). *J. Thorac. Oncol.* **2017**, *12* (Suppl. 2), S1756. [CrossRef]
20. Wu, J.; Savooji, J.; Liu, D. Second- and third-generation ALK inhibitors for non-small cell lung cancer. *J. Hematol. Oncol.* **2016**, *9*, 19. [CrossRef]
21. Akamine, T.; Toyokawa, G.; Tagawa, T.; Seto, T. Spotlight on lorlatinib and its potential in the treatment of NSCLC: The evidence to date. *OncoTargets Ther.* **2018**, *11*, 5093–5101. [CrossRef] [PubMed]
22. Pan, Y.; Deng, C.; Qiu, Z.; Cao, C.; Wu, F. The Resistance Mechanisms and Treatment Strategies for ALK-Rearranged Non-Small Cell Lung Cancer. *Front. Oncol.* **2021**, *11*, 713530. [CrossRef] [PubMed]
23. Redaelli, S.; Ceccon, M.; Zappa, M.; Sharma, G.G.; Mastini, C.; Mauri, M.; Nigoghossian, M.; Massimino, L.; Cordani, N.; Farina, F.; et al. Lorlatinib Treatment Elicits Multiple On- and Off-Target Mechanisms of Resistance in ALK-Driven Cancer. *Cancer Res.* **2018**, *78*, 6866–6880. [CrossRef] [PubMed]
24. Yoda, S.; Lin, J.J.; Lawrence, M.S.; Burke, B.J.; Friboulet, L.; Langenbucher, A.; Dardaei, L.; Prutisto-Chang, K.; Dagogo-Jack, I.; Timofeevski, S.; et al. Sequential ALK Inhibitors Can Select for Lorlatinib-Resistant Compound *ALK.* Mutations in ALK-Positive Lung Cancer. *Cancer Discov.* **2018**, *8*, 714–729. [CrossRef] [PubMed]
25. Toyokawa, G.; Seto, T. Updated Evidence on the Mechanisms of Resistance to ALK Inhibitors and Strategies to Overcome Such Resistance: Clinical and Preclinical Data. *Oncol. Res. Treat.* **2015**, *38*, 291–298. [CrossRef]
26. Dagogo-Jack, I.; Shaw, A.T. Crizotinib resistance: Implications for therapeutic strategies. *Ann. Oncol.* **2016**, *27* (Suppl. 3), iii42–iii50. [CrossRef]

27. Kim, H.R.; Kim, W.S.; Choi, Y.J.; Choi, C.M.; Rho, J.K.; Lee, J.C. Epithelial-mesenchymal transition leads to crizotinib resistance in H2228 lung cancer cells with EML4-ALK translocation. *Mol. Oncol.* **2013**, *7*, 1093–1102. [CrossRef]
28. Gower, A.; Hsu, W.H.; Hsu, S.T.; Wang, Y.; Giaccone, G. EMT is associated with, but does not drive resistance to ALK inhibitors among EML4-ALK non-small cell lung cancer. *Mol. Oncol.* **2016**, *10*, 601–609. [CrossRef]
29. Kogita, A.; Togashi, Y.; Hayashi, H.; Sogabe, S.; Terashima, M.; De Velasco, M.A.; Sakai, K.; Fujita, Y.; Tomida, S.; Takeyama, Y.; et al. Hypoxia induces resistance to ALK inhibitors in the H3122 non-small cell lung cancer cell line with an ALK rearrangement via epithelial-mesenchymal transition. *Int. J. Oncol.* **2014**, *45*, 1430–1436. [CrossRef]
30. Nakamichi, S.; Seike, M.; Miyanaga, A.; Chiba, M.; Zou, F.; Takahashi, A.; Ishikawa, A.; Kunugi, S.; Noro, R.; Kubota, K.; et al. Overcoming drug-tolerant cancer cell subpopulations showing AXL activation and epithelial-mesenchymal transition is critical in conquering ALK-positive lung cancer. *Oncotarget* **2018**, *9*, 27242–27255. [CrossRef]
31. Debruyne, D.N.; Bhatnagar, N.; Sharma, B.; Luther, W.; Moore, N.F.; Cheung, N.K.; Gray, N.S.; George, R.E. ALK inhibitor resistance in ALK(F1174L)-driven neuroblastoma is associated with AXL activation and induction of EMT. *Oncogene* **2016**, *35*, 3681–3691. [CrossRef] [PubMed]
32. Recondo, G.; Mezquita, L.; Facchinetti, F.; Planchard, D.; Gazzah, A.; Bigot, L.; Rizvi, A.Z.; Frias, R.L.; Thiery, J.P.; Scoazec, J.Y.; et al. Diverse Resistance Mechanisms to the Third-Generation ALK Inhibitor Lorlatinib in ALK-Rearranged Lung Cancer. *Clin. Cancer Res.* **2020**, *26*, 242–255. [CrossRef]
33. Urbanska, E.M.; Sørensen, J.B.; Melchior, L.C.; Costa, J.C.; Santoni-Rugiu, E. Changing ALK-TKI-Resistance Mechanisms in Rebiopsies of *ALK*-Rearranged NSCLC: *ALK*- and *BRAF*-Mutations Followed by Epithelial-Mesenchymal Transition. *Int. J. Mol. Sci.* **2020**, *21*, 2847. [CrossRef] [PubMed]
34. Kim, H.; Jang, S.J.; Chung, D.H.; Yoo, S.B.; Sun, P.; Jin, Y.; Nam, K.H.; Paik, J.H.; Chung, J.H. A comprehensive comparative analysis of the histomorphological features of ALK-rearranged lung adenocarcinoma based on driver oncogene mutations: Frequent expression of epithelial-mesenchymal transition markers than other genotype. *PLoS ONE* **2013**, *8*, e76999. [CrossRef]
35. Guo, F.; Liu, X.; Qing, Q.; Sang, Y.; Feng, C.; Li, X.; Jiang, L.; Su, P.; Wang, Y. EML4-ALK induces epithelial-mesenchymal transition consistent with cancer stem cell properties in H1299 non-small cell lung cancer cells. *Biochem. Biophys. Res. Commun.* **2015**, *459*, 398–404. [CrossRef] [PubMed]
36. Fukuda, K.; Takeuchi, S.; Arai, S.; Katayama, R.; Nanjo, S.; Tanimoto, A.; Nishiyama, A.; Nakagawa, T.; Taniguchi, H.; Suzuki, T.; et al. Epithelial-to-Mesenchymal Transition Is a Mechanism of ALK Inhibitor Resistance in Lung Cancer Independent of *ALK* Mutation Status. *Cancer Res.* **2019**, *79*, 1658–1670. [CrossRef] [PubMed]
37. Singh, R.P.; Raina, K.; Sharma, G.; Agarwal, R. Silibinin inhibits established prostate tumor growth, progression, invasion, and metastasis and suppresses tumor angiogenesis and epithelial-mesenchymal transition in transgenic adenocarcinoma of the mouse prostate model mice. *Clin. Cancer Res.* **2008**, *14*, 7773–7780. [CrossRef] [PubMed]
38. Wu, K.; Zeng, J.; Li, L.; Fan, J.; Zhang, D.; Xue, Y.; Zhu, G.; Yang, L.; Wang, X.; He, D. Silibinin reverses epithelial-to-mesenchymal transition in metastatic prostate cancer cells by targeting transcription factors. *Oncol. Rep.* **2010**, *23*, 1545–1552.
39. Cufí, S.; Bonavia, R.; Vazquez-Martin, A.; Oliveras-Ferraros, C.; Corominas-Faja, B.; Cuyàs, E.; Martin-Castillo, B.; Barrajón-Catalán, E.; Visa, J.; Segura-Carretero, A.; et al. Silibinin suppresses EMT-driven erlotinib resistance by reversing the high miR-21/low miR-200c signature in vivo. *Sci. Rep.* **2013**, *3*, 2459. [CrossRef]
40. Cufí, S.; Bonavia, R.; Vazquez-Martin, A.; Corominas-Faja, B.; Oliveras-Ferraros, C.; Cuyàs, E.; Martin-Castillo, B.; Barrajón-Catalán, E.; Visa, J.; Segura-Carretero, A.; et al. Silibinin meglumine, a water-soluble form of milk thistle silymarin, is an orally active anti-cancer agent that impedes the epithelial-to-mesenchymal transition (EMT) in EGFR-mutant non-small-cell lung carcinoma cells. *Food Chem. Toxicol* **2013**, *60*, 360–368. [CrossRef]
41. Cho, J.W.; Il, K.J.; Lee, K.S. Downregulation of type I collagen expression in silibinin-treated human skin fibroblasts by blocking the activation of Smad2/3-dependent signaling pathways: Potential therapeutic use in the chemoprevention of keloids. *Int. J. Mol. Med.* **2013**, *31*, 1148–1152. [CrossRef] [PubMed]
42. Chen, Y.H.; Liang, C.M.; Chen, C.L.; Chen, J.T.; Chang, Y.H.; Lu, D.W.; Chien, K.H.; Tai, M.C. Silibinin inhibits myofibroblast transdifferentiation in human tenon fibroblasts and reduces fibrosis in a rabbit trabeculectomy model. *Acta Ophthalmol.* **2013**, *91*, e506–e515. [CrossRef] [PubMed]
43. Ko, J.W.; Shin, N.R.; Park, S.H.; Lee, I.C.; Ryu, J.M.; Kim, H.J.; Cho, Y.K.; Kim, J.C.; Shin, I.S. Silibinin inhibits the fibrotic responses induced by cigarette smoke via suppression of TGF-β1/Smad 2/3 signaling. *Food Chem. Toxicol* **2017**, *106*, 424–429. [CrossRef]
44. Liu, R.; Wang, Q.; Ding, Z.; Zhang, X.; Li, Y.; Zang, Y.; Zhang, G. Silibinin Augments the Antifibrotic Effect of Valsartan Through Inactivation of TGF-β1 Signaling in Kidney. *Drug Des. Dev. Ther.* **2020**, *14*, 603–611. [CrossRef] [PubMed]
45. Yamaguchi, N.; Lucena-Araujo, A.R.; Nakayama, S.; de Figueiredo-Pontes, L.L.; Gonzalez, D.A.; Yasuda, H.; Kobayashi, S.; Costa, D.B. Dual ALK and EGFR inhibition targets a mechanism of acquired resistance to the tyrosine kinase inhibitor crizotinib in ALK rearranged lung cancer. *Lung Cancer* **2014**, *83*, 37–43. [CrossRef] [PubMed]
46. McDermott, M.; Eustace, A.J.; Busschots, S.; Breen, L.; Crown, J.; Clynes, M.; O'Donovan, N.; Stordal, B. In vitro Development of Chemotherapy and Targeted Therapy Drug-Resistant Cancer Cell Lines: A Practical Guide with Case Studies. *Front. Oncol.* **2014**, *4*, 40. [CrossRef] [PubMed]
47. Tebben, A.J.; Ruzanov, M.; Gao, M.; Xie, D.; Kiefer, S.E.; Yan, C.; Newitt, J.A.; Zhang, L.; Kim, K.; Lu, H.; et al. Crystal structures of apo and inhibitor-bound TGFβR2 kinase domain: Insights into TGFβR isoform selectivity. *Acta Crystallogr. D Struct. Biol.* **2016**, *72*, 658–674. [CrossRef]

48. Corominas-Faja, B.; Cuyàs, E.; Lozano-Sánchez, J.; Cufí, S.; Verdura, S.; Fernández-Arroyo, S.; Borrás-Linares, I.; Martin-Castillo, B.; Martin, Á.G.; Lupu, R.; et al. Extra-virgin olive oil contains a metabolo-epigenetic inhibitor of cancer stem cells. *Carcinogenesis* **2018**, *39*, 601–613. [CrossRef]
49. Verdura, S.; Cuyàs, E.; Lozano-Sánchez, J.; Bastidas-Velez, C.; Llorach-Parés, L.; Fernández-Arroyo, S.; Hernández-Aguilera, A.; Joven, J.; Nonell-Canals, A.; Bosch-Barrera, J.; et al. An olive oil phenolic is a new chemotype of mutant isocitrate dehydrogenase 1 (IDH1) inhibitors. *Carcinogenesis* **2019**, *40*, 27–40. [CrossRef]
50. Cuyàs, E.; Castillo, D.; Llorach-Parés, L.; Lozano-Sánchez, J.; Verdura, S.; Nonell-Canals, A.; Brunet, J.; Bosch-Barrera, J.; Joven, J.; Valdés, R.; et al. Computational de-orphanization of the olive oil biophenol oleacein: Discovery of new metabolic and epigenetic targets. *Food Chem. Toxicol* **2019**, *131*, 110529. [CrossRef]
51. Encinar, J.A.; Menendez, J.A. Potential Drugs Targeting Early Innate Immune Evasion of SARS-Coronavirus 2 via 2'-O-Methylation of Viral RNA. *Viruses* **2020**, *12*, 525. [CrossRef] [PubMed]
52. Tramonti, A.; Cuyàs, E.; Encinar, J.A.; Pietzke, M.; Paone, A.; Verdura, S.; Arbusà, A.; Martin-Castillo, B.; Giardina, G.; Joven, J.; et al. Metformin Is a Pyridoxal-5'-phosphate (PLP)-Competitive Inhibitor of SHMT2. *Cancers* **2021**, *13*, 4009. [CrossRef] [PubMed]
53. Verdura, S.; Cuyàs, E.; Cortada, E.; Brunet, J.; Lopez-Bonet, E.; Martin-Castillo, B.; Bosch-Barrera, J.; Encinar, J.A.; Menendez, J.A. Resveratrol targets PD-L1 glycosylation and dimerization to enhance antitumor T-cell immunity. *Aging* **2020**, *12*, 8–34. [CrossRef] [PubMed]
54. Seeliger, D.; de Groot, B.L. Ligand docking and binding site analysis with PyMOL and Autodock/Vina. *J. Comput. Aided Mol. Des.* **2010**, *24*, 417–422. [CrossRef] [PubMed]
55. Salentin, S.; Schreiber, S.; Haupt, V.J.; Adasme, M.F.; Schroeder, M. PLIP: Fully automated protein-ligand interaction profiler. *Nucleic. Acids Res.* **2015**, *43*, W443–W447. [CrossRef]
56. Koivunen, J.P.; Mermel, C.; Zejnullahu, K.; Murphy, C.; Lifshits, E.; Holmes, A.J.; Choi, H.G.; Kim, J.; Chiang, D.; Thomas, R.; et al. EML4-ALK fusion gene and efficacy of an ALK kinase inhibitor in lung cancer. *Clin. Cancer Res.* **2008**, *14*, 4275–4283. [CrossRef]
57. Cuyàs, E.; Pérez-Sánchez, A.; Micol, V.; Menendez, J.A.; Bosch-Barrera, J. STAT3-targeted treatment with silibinin overcomes the acquired resistance to crizotinib in ALK-rearranged lung cancer. *Cell Cycle* **2016**, *15*, 3413–3418. [CrossRef]
58. Heuckmann, J.M.; Balke-Want, H.; Malchers, F.; Peifer, M.; Sos, M.L.; Koker, M.; Meder, L.; Lovly, C.M.; Heukamp, L.C.; Pao, W.; et al. Differential protein stability and ALK inhibitor sensitivity of EML4-ALK fusion variants. *Clin. Cancer Res.* **2012**, *18*, 4682–4690. [CrossRef]
59. Yoshida, T.; Oya, Y.; Tanaka, K.; Shimizu, J.; Horio, Y.; Kuroda, H.; Sakao, Y.; Hida, T.; Yatabe, Y. Differential Crizotinib Response Duration Among ALK Fusion Variants in ALK-Positive Non-Small-Cell Lung Cancer. *J. Clin. Oncol.* **2016**, *34*, 3383–3389. [CrossRef]
60. Woo, C.G.; Seo, S.; Kim, S.W.; Jang, S.J.; Park, K.S.; Song, J.Y.; Lee, B.; Richards, M.W.; Bayliss, R.; Lee, D.H.; et al. Differential protein stability and clinical responses of EML4-ALK fusion variants to various ALK inhibitors in advanced ALK-rearranged non-small cell lung cancer. *Ann. Oncol.* **2017**, *28*, 791–797. [CrossRef]
61. Li, M.; Hou, X.; Chen, J.; Zhang, B.; Wang, N.; Han, H.; Chen, L. ALK fusion variant 3a/b, concomitant mutations, and high PD-L1 expression were associated with unfavorable clinical response to second-generation ALK TKIs in patients with advanced ALK-rearranged non-small cell lung cancer (GASTO 1061). *Lung Cancer* **2022**, *165*, 54–62. [CrossRef] [PubMed]
62. Massagué, J.; Gomis, R.R. The logic of TGFbeta signaling. *FEBS Lett.* **2006**, *580*, 2811–2820. [CrossRef] [PubMed]
63. Massagué, J. TGFβ signalling in context. *Nat. Rev. Mol. Cell. Biol* **2012**, *13*, 616–630. [CrossRef] [PubMed]
64. Seoane, J.; Gomis, R.R. TGF-β Family Signaling in Tumor Suppression and Cancer Progression. *Cold Spring Harb. Perspect. Biol.* **2017**, *9*, a022277. [CrossRef]
65. Wrana, J.L.; Attisano, L.; Wieser, R.; Ventura, F.; Massagué, J. Mechanism of activation of the TGF-beta receptor. *Nature* **1994**, *370*, 341–347. [CrossRef]
66. Voena, C.; Varesio, L.M.; Zhang, L.; Menotti, M.; Poggio, T.; Panizza, E.; Wang, Q.; Minero, V.G.; Fagoonee, S.; Compagno, M.; et al. Oncogenic ALK regulates EMT in non-small cell lung carcinoma through repression of the epithelial splicing regulatory protein 1. *Oncotarget* **2016**, *7*, 33316–33330. [CrossRef]
67. Huang, S.; Hölzel, M.; Knijnenburg, T.; Schlicker, A.; Roepman, P.; McDermott, U.; Garnett, M.; Grernrum, W.; Sun, C.; Prahallad, A.; et al. MED12 controls the response to multiple cancer drugs through regulation of TGF-β receptor signaling. *Cell* **2012**, *151*, 937–950. [CrossRef]
68. Sang, J.; Acquaviva, J.; Friedland, J.C.; Smith, D.L.; Sequeira, M.; Zhang, C.; Jiang, Q.; Xue, L.; Lovly, C.M.; Jimenez, J.P.; et al. Targeted inhibition of the molecular chaperone Hsp90 overcomes ALK inhibitor resistance in non-small cell lung cancer. *Cancer Discov.* **2013**, *3*, 430–443. [CrossRef]
69. Shen, J.; Meng, Y.; Wang, K.; Gao, M.; Du, J.; Wang, J.; Li, Z.; Zuo, D.; Wu, Y. EML4-ALK G1202R mutation induces EMT and confers resistance to ceritinib in NSCLC cells via activation of STAT3/Slug signaling. *Cell. Signal* **2022**, *92*, 110264. [CrossRef]
70. Byers, L.A.; Diao, L.; Wang, J.; Saintigny, P.; Girard, L.; Peyton, M.; Shen, L.; Fan, Y.; Giri, U.; Tumula, P.K.; et al. An epithelial-mesenchymal transition gene signature predicts resistance to EGFR and PI3K inhibitors and identifies Axl as a therapeutic target for overcoming EGFR inhibitor resistance. *Clin. Cancer Res.* **2013**, *19*, 279–290. [CrossRef]
71. Tan, T.Z.; Miow, Q.H.; Miki, Y.; Noda, T.; Mori, S.; Huang, R.Y.; Thiery, J.P. Epithelial-mesenchymal transition spectrum quantification and its efficacy in deciphering survival and drug responses of cancer patients. *EMBO Mol. Med.* **2014**, *6*, 1279–1293. [CrossRef] [PubMed]

72. George, J.T.; Jolly, M.K.; Xu, S.; Somarelli, J.A.; Levine, H. Survival Outcomes in Cancer Patients Predicted by a Partial EMT Gene Expression Scoring Metric. *Cancer Res.* **2017**, *77*, 6415–6428. [CrossRef] [PubMed]
73. Chakraborty, P.; George, J.T.; Tripathi, S.; Levine, H.; Jolly, M.K. Comparative Study of Transcriptomics-Based Scoring Metrics for the Epithelial-Hybrid-Mesenchymal Spectrum. *Front. Bioeng. Biotechnol.* **2020**, *8*, 220. [CrossRef] [PubMed]
74. Bocci, F.; Mandal, S.; Tejaswi, T.; Jolly, M.K. Investigating epithelial-mesenchymal heterogeneity of tumors and circulating tumor cells with transcriptomic analysis and biophysical modeling. *Comput. Syst. Oncol.* **2021**, *1*, e1015. [CrossRef]
75. Verdura, S.; Cuyàs, E.; Llorach-Parés, L.; Pérez-Sánchez, A.; Micol, V.; Nonell-Canals, A.; Joven, J.; Valiente, M.; Sánchez-Martínez, M.; Bosch-Barrera, J.; et al. Silibinin is a direct inhibitor of STAT3. *Food Chem. Toxicol.* **2018**, *116 Pt B*, 161–172. [CrossRef]
76. Rho, J.K.; Choi, Y.J.; Jeon, B.S.; Choi, S.J.; Cheon, G.J.; Woo, S.K.; Kim, H.R.; Kim, C.H.; Choi, C.M.; Lee, J.C. Combined treatment with silibinin and epidermal growth factor receptor tyrosine kinase inhibitors overcomes drug resistance caused by T790M mutation. *Mol. Cancer Ther.* **2010**, *9*, 3233–3243. [CrossRef]
77. Shien, K.; Papadimitrakopoulou, V.A.; Ruder, D.; Behrens, C.; Shen, L.; Kalhor, N.; Song, J.; Lee, J.J.; Wang, J.; Tang, X.; et al. JAK1/STAT3 Activation through a Proinflammatory Cytokine Pathway Leads to Resistance to Molecularly Targeted Therapy in Non-Small Cell Lung Cancer. *Mol. Cancer Ther.* **2017**, *16*, 2234–2245. [CrossRef]
78. Wilson, F.H.; Johannessen, C.M.; Piccioni, F.; Tamayo, P.; Kim, J.W.; Van Allen, E.M.; Corsello, S.M.; Capelletti, M.; Calles, A.; Butaney, M.; et al. A functional landscape of resistance to ALK inhibition in lung cancer. *Cancer Cell* **2015**, *27*, 397–408. [CrossRef]
79. Yang, J.; Antin, P.; Berx, G.; Blanpain, C.; Brabletz, T.; Bronner, M.; Campbell, K.; Cano, A.; Casanova, J.; Christofori, G.; et al. EMT International Association (TEMTIA). Guidelines and definitions for research on epithelial-mesenchymal transition. *Nat. Rev. Mol. Cell Biol.* **2020**, *21*, 341–352. [CrossRef]
80. Shibue, T.; Weinberg, R.A. EMT, CSCs, and drug resistance: The mechanistic link and clinical implications. *Nat. Rev. Clin. Oncol.* **2017**, *14*, 611–629. [CrossRef]
81. Dongre, A.; Weinberg, R.A. New insights into the mechanisms of epithelial-mesenchymal transition and implications for cancer. *Nat. Rev. Mol. Cell Biol.* **2019**, *20*, 69–84. [CrossRef] [PubMed]
82. Wilson, M.M.; Weinberg, R.A.; Lees, J.A.; Guen, V.J. Emerging Mechanisms by which EMT Programs Control Stemness. *Trends Cancer* **2020**, *6*, 775–780. [CrossRef] [PubMed]
83. Davis, F.M.; Stewart, T.A.; Thompson, E.W.; Monteith, G.R. Targeting EMT in cancer: Opportunities for pharmacological intervention. *Trends Pharmacol. Sci.* **2014**, *35*, 479–488. [CrossRef] [PubMed]
84. Marcucci, F.; Stassi, G.; De Maria, R. Epithelial-mesenchymal transition: A new target in anticancer drug discovery. *Nat. Rev. Drug Discov.* **2016**, *15*, 311–325. [CrossRef]
85. Post-White, J.; Ladas, E.J.; Kelly, K.M. Advances in the use of milk thistle (Silybum marianum). *Integr. Cancer Ther.* **2007**, *6*, 104–109. [CrossRef] [PubMed]
86. Gazák, R.; Walterová, D.; Kren, V. Silybin and silymarin–new and emerging applications in medicine. *Curr. Med. Chem.* **2007**, *14*, 315–338. [CrossRef]
87. Agarwal, R.; Agarwal, C.; Ichikawa, H.; Singh, R.P.; Aggarwal, B.B. Anticancer potential of silymarin: From bench to bed side. *Anticancer Res.* **2006**, *26*, 4457–4498.
88. Singh, R.P.; Agarwal, R. Prostate cancer chemoprevention by silibinin: Bench to bedside. *Mol. Carcinog.* **2006**, *45*, 436–442. [CrossRef]
89. Verdura, S.; Cuyàs, E.; Ruiz-Torres, V.; Micol, V.; Joven, J.; Bosch-Barrera, J.; Menendez, J.A. Lung Cancer Management with Silibinin: A Historical and Translational Perspective. *Pharmaceuticals* **2021**, *14*, 559. [CrossRef]
90. Bosch-Barrera, J.; Menendez, J.A. Silibinin and STAT3: A natural way of targeting transcription factors for cancer therapy. *Cancer Treat. Rev.* **2015**, *41*, 540–546. [CrossRef]
91. Bosch-Barrera, J.; Queralt, B.; Menendez, J.A. Targeting STAT3 with silibinin to improve cancer therapeutics. *Cancer Treat. Rev.* **2017**, *58*, 61–69. [CrossRef] [PubMed]
92. Deep, G.; Gangar, S.C.; Agarwal, C.; Agarwal, R. Role of E-cadherin in antimigratory and antiinvasive efficacy of silibinin in prostate cancer cells. *Cancer Prev. Res.* **2011**, *4*, 1222–1232. [CrossRef] [PubMed]
93. Ma, Z.; Zang, W.; Wang, H.; Wei, X. Silibinin enhances anti-renal fibrosis effect of MK-521 via downregulation of TGF-β signaling pathway. *Hum. Cell.* **2020**, *33*, 330–336. [CrossRef]
94. Křen, V. Chirality Matters: Biological Activity of Optically Pure Silybin and Its Congeners. *Int. J. Mol. Sci.* **2021**, *22*, 7885. [CrossRef] [PubMed]
95. Sciacca, M.F.M.; Romanucci, V.; Zarrelli, A.; Monaco, I.; Lolicato, F.; Spinella, N.; Galati, C.; Grasso, G.; D'Urso, L.; Romeo, M.; et al. Inhibition of Aβ Amyloid Growth and Toxicity by Silybins: The Crucial Role of Stereochemistry. *ACS Chem. Neurosci.* **2017**, *8*, 1767–1778. [CrossRef] [PubMed]
96. Shoichet, B.K. Interpreting steep dose-response curves in early inhibitor discovery. *J. Med. Chem.* **2006**, *49*, 7274–7277. [CrossRef] [PubMed]
97. Dhawan, A.; Nichol, D.; Kinose, F.; Abazeed, M.E.; Marusyk, A.; Haura, E.B.; Scott, J.G. Collateral sensitivity networks reveal evolutionary instability and novel treatment strategies in ALK mutated non-small cell lung cancer. *Sci. Rep.* **2017**, *7*, 1232. [CrossRef] [PubMed]

98. Geng, K.; Liu, H.; Song, Z.; Zhang, C.; Zhang, M.; Yang, H.; Cao, J.; Geng, M.; Shen, A.; Zhang, A. Design, synthesis and pharmacological evaluation of ALK and Hsp90 dual inhibitors bearing resorcinol and 2,4-diaminopyrimidine motifs. *Eur. J. Med. Chem.* **2018**, *152*, 76–86. [CrossRef] [PubMed]
99. Rong, B.; Yang, S. Molecular mechanism and targeted therapy of Hsp90 involved in lung cancer: New discoveries and developments (Review). *Int. J. Oncol.* **2018**, *52*, 321–336. [CrossRef]
100. Riebold, M.; Kozany, C.; Freiburger, L.; Sattler, M.; Buchfelder, M.; Hausch, F.; Stalla, G.K.; Paez-Pereda, M. A C-terminal HSP90 inhibitor restores glucocorticoid sensitivity and relieves a mouse allograft model of Cushing disease. *Nat. Med.* **2015**, *21*, 276–280. [CrossRef]
101. Cuyàs, E.; Verdura, S.; Micol, V.; Joven, J.; Bosch-Barrera, J.; Encinar, J.A.; Menendez, J.A. Revisiting silibinin as a novobiocin-like Hsp90 C-terminal inhibitor: Computational modeling and experimental validation. *Food. Chem. Toxicol.* **2019**, *132*, 110645. [CrossRef] [PubMed]
102. Pérez-Sánchez, A.; Cuyàs, E.; Ruiz-Torres, V.; Agulló-Chazarra, L.; Verdura, S.; González-Álvarez, I.; Bermejo, M.; Joven, J.; Micol, V.; Bosch-Barrera, J.; et al. Intestinal Permeability Study of Clinically Relevant Formulations of Silibinin in Caco-2 Cell Monolayers. *Int. J. Mol. Sci.* **2019**, *20*, 1606. [CrossRef] [PubMed]
103. Bosch-Barrera, J.; Sais, E.; Cañete, N.; Marruecos, J.; Cuyàs, E.; Izquierdo, A.; Porta, R.; Haro, M.; Brunet, J.; Pedraza, S.; et al. Response of brain metastasis from lung cancer patients to an oral nutraceutical product containing silibinin. *Oncotarget* **2016**, *7*, 32006–32014. [CrossRef] [PubMed]
104. Priego, N.; Zhu, L.; Monteiro, C.; Mulders, M.; Wasilewski, D.; Bindeman, W.; Doglio, L.; Martínez, L.; Martínez-Saez, E.; Ramón y Cajal, S.; et al. STAT3 labels a subpopulation of reactive astrocytes required for brain metastasis. *Nat. Med.* **2018**, *24*, 1024–1035. [CrossRef] [PubMed]
105. Bosch-Barrera, J.; Verdura, S.; Ruffinelli, J.C.; Carcereny, E.; Sais, E.; Cuyàs, E.; Palmero, R.; Lopez-Bonet, E.; Hernández-Martínez, A.; Oliveras, G.; et al. Silibinin Suppresses Tumor Cell-Intrinsic Resistance to Nintedanib and Enhances Its Clinical Activity in Lung Cancer. *Cancers* **2021**, *13*, 4168. [CrossRef]

STUDY 3

Silibinin Suppresses Tumor Cell-Intrinsic Resistance to Nintedanib and Enhances Its Clinical Activity in Lung Cancer

Bosch-Barrera J, Verdura S, Ruffinelli JC, Carcereny E, Sais E, Cuyàs E, Palmero R, Lopez-Bonet E, Hernández-Martínez A, Oliveras G, Buxó M, Izquierdo A, Morán T, Nadal E, Menendez JA.

Cancers (Basel). 2021 Aug 19;13(16):4168

doi: 10.3390/cancers13164168

cancers

MDPI

Article

Silibinin Suppresses Tumor Cell-Intrinsic Resistance to Nintedanib and Enhances Its Clinical Activity in Lung Cancer

Joaquim Bosch-Barrera [1,2,3,*,†], Sara Verdura [3,†], José Carlos Ruffinelli [4], Enric Carcereny [5,6], Elia Sais [1], Elisabet Cuyàs [3], Ramon Palmero [4], Eugeni Lopez-Bonet [7], Alejandro Hernández-Martínez [1], Gloria Oliveras [7], Maria Buxó [3], Angel Izquierdo [1,2,8], Teresa Morán [5,6], Ernest Nadal [4] and Javier A. Menendez [3,9,*]

1 Medical Oncology, Catalan Institute of Oncology, Dr. Josep Trueta Hospital of Girona, 17007 Girona, Spain; esais@iconcologia.net (E.S.); ahmartinez@iconcologia.net (A.H.-M.); aizquierdo@iconcologia.net (A.I.)
2 Department of Medical Sciences, Medical School, University of Girona, 17003 Girona, Spain
3 Girona Biomedical Research Institute (IDIBGI), 17190 (Salt) Girona, Spain; sverdura@idibgi.org (S.V.); ecuyas@idibgi.org (E.C.); mbuxo@idibgi.org (M.B.)
4 Medical Oncology Department, Catalan Institute of Oncology, Hospital Duran i Reynals, 08908 L'Hospitalet de Llobregat, Spain; jruffinelli@iconcologia.net (J.C.R.); rpalmero@iconcologia.net (R.P.); enadal@iconcologia.net (E.N.)
5 Medical Oncology Department, Catalan Institute of Oncology, Hospital Germans Trias i Pujol, 08916 Badalona, Spain; ecarcereny@iconcologia.net (E.C.); tmoran@iconcologia.net (T.M.)
6 B-ARGO Group (Badalona Applied Research Group in Oncology), Germans Trias i Pujol Research Institute (IGTP), 08916 Badalona, Spain
7 Department of Anatomical Pathology, Dr. Josep Trueta Hospital of Girona, 17007 Girona, Spain; elopezbonet.girona.ics@gencat.cat (E.L.-B.); goliveras@iconcologia.net (G.O.)
8 Hereditary Cancer Program, Epidemiology Unit and Girona Cancer Registry, Oncology Coordination Plan, Catalan Institute of Oncology-Girona Biomedical Research Institute (IDIBGI), 17007 Girona, Spain
9 Program against Cancer Therapeutic Resistance (ProCURE), Metabolism & Cancer Group, Catalan Institute of Oncology, 17190 (Salt) Girona, Spain
* Correspondence: jbosch@iconcologia.net (J.B.-B.); jmenendez@iconcologia.net or jmenendez@idibgi.org (J.A.M.)
† Joaquim Bosch-Barrera and Sara Verdura contributed equally to this work.

Simple Summary: Nintedanib is an anti-angiogenic agent that has received approval in the European Union for the treatment of non-small cell lung cancer (NSCLC) after first-line chemotherapy. Here, we explore the possibility that the flavonolignan silibinin—the major bioactive component from the seeds of the milk thistle herb (*Silybum marianum*)—can provide clinical benefit in patients with advanced NSCLC treated with nintedanib. In vitro studies revealed that silibinin targets biological functions important for the therapeutic efficacy of nintedanib; specifically, activation of the transcription factor STAT3 and sequestration into lysosomal "safe houses". Supplementation with the silibinin-based nutraceutical Legasil® to patients with NSCLC receiving nintedanib/docetaxel was associated with increased clinical responses and a significantly longer time to treatment failure. Our findings provide a biological and clinical rationale for combining silibinin with nintedanib in a patient population for whom few effective second-line chemotherapy regimens are available.

Abstract: The anti-angiogenic agent nintedanib has been shown to prolong overall and progression-free survival in patients with advanced non-small-cell lung cancer (NSCLC) who progress after first-line platinum-based chemotherapy and second-line immunotherapy. Here, we explored the molecular basis and the clinical benefit of incorporating the STAT3 inhibitor silibinin—a flavonolignan extracted from milk thistle—into nintedanib-based schedules in advanced NSCLC. First, we assessed the nature of the tumoricidal interaction between nintedanib and silibinin and the underlying relevance of STAT3 activation in a panel of human NSCLC cell lines. NSCLC cells with poorer cytotoxic responses to nintedanib exhibited a persistent, nintedanib-unresponsive activated STAT3 state, and deactivation by co-treatment with silibinin promoted synergistic cytotoxicity. Second, we tested whether silibinin could impact the lysosomal sequestration of nintedanib, a lung cancer cell-intrinsic mechanism of nintedanib resistance. Silibinin partially, but significantly, reduced the massive lysosomal entrapment of nintedanib occurring in nintedanib-refractory NSCLC cells, augmenting the ability of nintedanib to reach its intracellular targets. Third, we conducted a retrospective, observational multicenter

check for updates

Citation: Bosch-Barrera, J.; Verdura, S.; Ruffinelli, J.C.; Carcereny, E.; Sais, E.; Cuyàs, E.; Palmero, R.; Lopez-Bonet, E.; Hernández-Martínez, A.; Oliveras, G.; et al. Silibinin Suppresses Tumor Cell-Intrinsic Resistance to Nintedanib and Enhances Its Clinical Activity in Lung Cancer. *Cancers* **2021**, *13*, 4168. https://doi.org/10.3390/cancers13164168

Academic Editors: Akiteru Goto and Philippe Icard

Received: 13 July 2021
Accepted: 13 August 2021
Published: 19 August 2021

Publisher's Note: MDPI stays neutral with regard to jurisdictional claims in published maps and institutional affiliations.

study to determine the efficacy of incorporating an oral nutraceutical product containing silibinin in patients with NSCLC receiving a nintedanib/docetaxel combination in second- and further-line settings (n = 59). Overall response rate, defined as the combined rates of complete and partial responses, was significantly higher in the study cohort receiving silibinin supplementation (55%) than in the control cohort (22%, p = 0.011). Silibinin therapy was associated with a significantly longer time to treatment failure in multivariate analysis (hazard ratio 0.43, p = 0.013), despite the lack of overall survival benefit (hazard ratio 0.63, p = 0.190). Molecular mechanisms dictating the cancer cell-intrinsic responsiveness to nintedanib, such as STAT3 activation and lysosomal trapping, are amenable to pharmacological intervention with silibinin. A prospective, powered clinical trial is warranted to confirm the clinical relevance of these findings in patients with advanced NSCLC.

Keywords: nintedanib; non-small cell lung cancer; silibinin; STAT3; lysosome; lysosomal trapping

1. Introduction

Nintedanib (formally known as BIBF 1120) is an orally administered, broad-spectrum angiokinase inhibitor of growth factor receptors, including VEGFR1–3, PDGFRα/β and FGFR 1–4, as well as of FLT-3 and SRC non-receptor tyrosine kinases [1]. This multikinase inhibitor profile suggested that nintedanib could provide therapeutic benefit where other anti-angiogenic agents had failed. The pivotal phase III LUME-Lung 1 trial demonstrated that nintedanib plus docetaxel significantly improved progression-free survival compared with docetaxel alone in patients with advanced NSCLC treated with one line of platinum-based therapy [2]. Overall survival was also significantly extended in nintedanib/docetaxel-treated patients with adenocarcinoma histology, and a better disease control rate was observed in the patients in the nintedanib-containing arm despite a similar overall response rate in both arms. Based on these findings, nintedanib, in combination with docetaxel, was approved by the European Medicines Agency in November 2014 for the treatment of advanced NSCLC with adenocarcinoma tumor histology after first-line chemotherapy. Recent studies have supported the efficacy of nintedanib/docetaxel in patients with adenocarcinoma NSCLC after progression on prior chemotherapy followed by immune checkpoint inhibitor (ICI) therapy in real-world settings [3,4]. Despite the encouraging clinical data, however, the introduction of immunotherapy as second- and third-line treatment and the lack of new efficacy data on the nintedanib/docetaxel combination in daily clinical practice have largely discouraged lung oncologists from using this combination in off-trial settings.

In animal models of lung cancer in which, after initial nintedanib-induced regression, tumor growth resumes in the absence of active tumor revascularization, nintedanib treatment promotes either vascular normalization with hypoxia correction [5–7] or vascular pruning with elevated hypoxia [8–14]. Patients receiving neoadjuvant nintedanib show both normalization and increases in hypoxia, with the pattern of hypoxia correction correlating with tumor responses [15]. In this scenario, the question of whether the multikinase inhibition profile of nintedanib can directly affect tumor cell proliferation and survival becomes highly pertinent, as it might offer a tumor cell autonomous route to circumvent nintedanib via microenvironmental adaptive responses in a clinical setting. Intriguingly, the therapeutic activity of nintedanib extends beyond the targeting of angiogenic cell compartments [1] to involve not only fibroblasts in idiopathic lung fibrosis [16–20], but also cancer cells themselves. Indeed, single-agent nintedanib can directly inhibit cell proliferation and the survival of tumor cells in vitro—an effect that has been observed across a wide range of tumor types bearing a variety of cancer-driving genetic alterations [21–24].

The anti-proliferative/apoptotic activity of nintedanib on tumor cells seems to occur, at least in part, through the negative regulation of the signal transducer and activator of transcription 3 (STAT3) [24,25]. Nintedanib can operate as an agonist of the Src homology (SH2) domain-containing protein tyrosine phosphatase 1 (SHP-1), thus enhancing its capac-

ity to dephosphorylate STAT3 at its activating tyrosine 705 (Tyr 705) residue [24,25]. Because over-activation of Janus associated kinase (JAK) or growth factor receptor-associated tyrosine kinase (SRC) contributes to the hyper-phosphorylation of STAT3, nintedanib might also inhibit STAT3 activity downstream of its actions on PDGFRβ, FGFR and SRC [26–31]. Importantly, ectopic overexpression and constitutive hyperactivation of STAT3 suffices to suppress the growth-inhibitory and apoptotic effects of nintedanib on cancer cells, revealing that the activation status of STAT3 [32–36] might be crucial in determining its non-angiogenic cancer cell-targeted activity.

Common strategies for inhibiting STAT3 signaling include indirect inhibition of upstream receptors (JAKs, IL-6R) or direct blockade of STAT3 dimerization by obstructing the STAT3 domain, impeding STAT3-DNA binding and inhibiting STAT3 transcription. Unfortunately, the majority of direct STAT3 inhibitors (STAT3i) have yet to enter clinical evaluation and, despite decades of research, very few FDA-approved STAT3i have emerged [37–42]. Using computational and experimental approaches, we recently delineated the ability of the flavonolignan silibinin—the major bioactive component in the silymarin extract obtained from the seeds of the milk thistle herb (*Silybum marianum*) [43–46] to inhibit STAT3 activity. Silibinin operates as a direct STAT3i by blocking the STAT3 SH2 domain, which is crucial for both STAT3 phosphoactivation and nuclear translocation, while also targeting the STAT3 DNA-binding domain, which is crucial to drive STAT3 transcriptional activity irrespective of its activation/dimerization status [47]. Such multifaceted activity of silibinin against STAT3, when used orally as part of the bioavailable Eurosil-85®/Euromed nutraceutical formulation contained in the nutraceutical product Legasil® [48], has proven therapeutically effective in patients with advanced NSCLC and was particularly notable in the central nervous system, where it provided greater than 4-fold survival benefit in patients with established brain metastases [49,50]. This groundbreaking clinical activity of silibinin was accompanied by low toxicity and reversible secondary effects and was compatible with the standard-of-care in oncology patients [51,52].

Here, we explore the molecular basis and the clinical benefit of incorporating silibinin into the nintedanib/docetaxel schedule in NSCLC. First, we assess the nature of the tumoricidal interaction between nintedanib and silibinin and the underlying impact on STAT3 activity in a panel of human NSCLC cell lines [53–58]. Second, we explore the impact of silibinin on additional molecular mechanisms that might confer cancer cell-intrinsic resistance to nintedanib such as sequestration inside the lysosomal "drug safehouse" [59,60]. Third, we conduct a retrospective, observational multicenter study to assess the efficacy of Legasil® in patients with NSCLC receiving the nintedanib/docetaxel combination in second- and further-line settings.

2. Results

2.1. Inverse Correlation between Nintedanib and Silibinin Sensitivity in Human NSCLC Cell Lines

We first characterized the cytotoxic effects of nintedanib and silibinin as single agents against a panel of molecularly diverse NSCLC cell lines (n = 7) (Table 1). Cells were seeded in microtiter plates and then cultured without or with increasing concentrations of nintedanib or silibinin for 72 h. Metabolic status, as a measure of viability, was assessed by the conversion of the tetrazolium salt, MTT, to its formazan product. We observed a dose-dependent reduction in cell viability in response to both nintedanib and silibinin, but with evident differences in sensitivity between cell lines. To examine this more closely, we generated concentration-effect curves by plotting the fraction of unaffected (surviving) cells against nintedanib/silibinin concentrations and calculated IC_{50} values: for nintedanib, IC_{50} values ranged from 2.83 ± 0.45 μmol/L in PC-9 cells harboring an EGFR activating mutation (Δ746–750) to 9.31 ± 0.40 μmol/L in FGFR1-overexpressing H1975 cells harboring the EGFR T790M resistance mutation (Figure 1A); IC_{50} values for silibinin ranged from 52.58 ± 1.65 μmol/L in KRAS (Q61H)-mutant H460 cells to 122.13 ± 6.66 μmol/L in H2228 cells bearing the EML4-ALK E6a/b:A20 variant 3 (Figure 1A). We also observed a tendency for a negative correlation between the apparent degree of sensitivity of NSCLC cell lines

to the drugs, with those more sensitive to nintedanib being less sensitive to silibinin, and vice versa. In terms of IC_{50} values, on average, cell lines more responsive to nintedanib were ~2-fold more resistant to silibinin, whereas cell lines more responsive to silibinin were ~3-fold more resistant to nintedanib.

Table 1. NSCLC cell lines characteristics.

Cell Line	Mutational Features
A549	EGFR WT; KRAS mutant (G12S)
H460	EGFR WT; KRAS mutant (Q61H)
H1993	EGFR WT; MET amplification
H3122	EGFR WT; EML4-ALK variant 1
H2228	EGFR WT; EML4-ALK variant 3
H1975	EGFR mutant (L858R/T790M); KRAS WT
PC9	EGFR mutant (DelE746-A750)

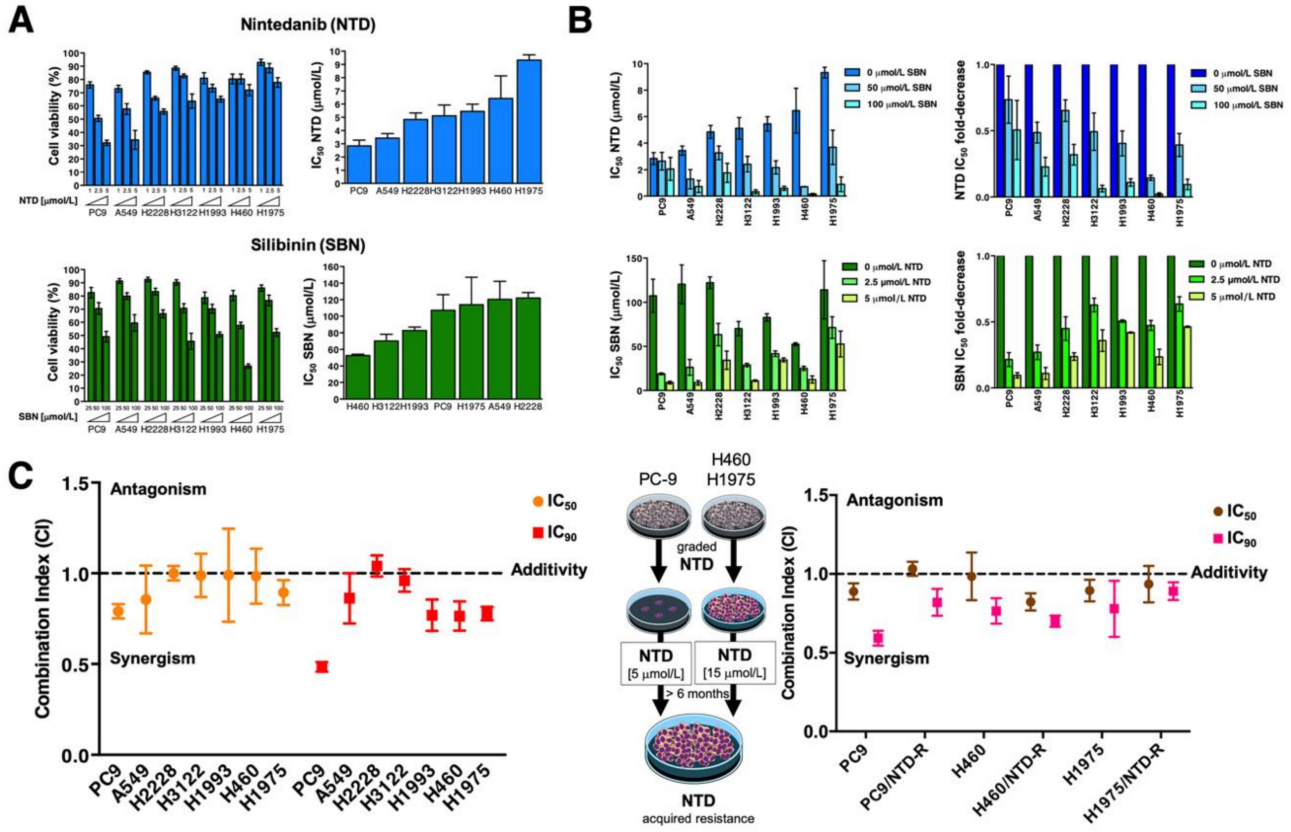

Figure 1. Analysis of the cytotoxic interaction between nintedanib and silibinin in NSCLC cells. (**A**) *Left panels.* The metabolic status of PC9, A549, H2228, H3122, H1993, H460, and H1975 NSCLC cell lines treated with increasing concentrations of nintedanib (NTD; 1.25, 2.5, and 5 μmol/L) and silibinin (SBN; 25, 50, and 100 μmol/L) was measured using MTT uptake assays, and cell viability was expressed as % uptake relative to untreated control cells (=100% cell viability). *Right panels.* Bar graphs of the IC_{50} values for each cell line calculated from the MTT assays as described in "Materials and methods". The results are presented as the means (*columns*) ± S.D. (*bars*) (n = 3, in triplicate). (**B**) *Left panels.* Bar graphs showing the MTT-based IC_{50} values of NTD (*top*) and SBN (*bottom*) for each cell line calculated in the absence or presence of graded concentrations of SBN and NTD, respectively. *Right panels.* Bar graphs showing the fold-change in NTD (*top*) and SBN (*bottom*) IC_{50} values obtained in the absence or presence of graded concentrations of SBN and NTD, respectively. (**C**) Computed combination index (CI) values for the combination of NTD and SBN at 50% and 90% effect levels. CI values less than, equal to or greater than 1 indicates synergy, additivity or antagonism, respectively. The horizontal line at CI = 1 is the line of additivity. The results in A, B, and C panels are presented as the means (*columns*) ± S.D. (*bars*) (n = 3, in triplicate).

2.2. Synergistic Interactions between Nintedanib and Silibinin in Human NSCLC Cells

To investigate whether silibinin co-exposure might improve the cytotoxic activity of nintedanib, we treated the same NSCLC cell lines with nintedanib in the absence or presence of fixed concentrations of silibinin (50 and 100 μmol/L). Likewise, NSCLC cell lines were exposed to silibinin in the absence or presence of fixed concentrations of nintedanib (2.5 and 5 μmol/L) to evaluate the sensitizing effects of nintedanib towards silibinin. To measure changes in sensitivity, sensitization factors were determined by dividing the IC_{50} values of nintedanib or silibinin as single agents by those in the presence of silibinin or nintedanib, respectively (Figure 1B). Results showed that silibinin enhanced the cytotoxic activity of nintedanib in a dose-dependent manner, which was particularly notable in the cell lines exhibiting intrinsically higher IC_{50} values for nintedanib (H460 and H1975, hereafter "nintedanib-resistant"). Indeed, treatment with 100 μmol/L silibinin increased the cytotoxic activity of nintedanib by >50-fold. In the converse experiment, nintedanib increased the cytotoxic activity of silibinin in a dose-dependent manner and this was particularly evident in those cell lines exhibiting intrinsically higher IC_{50} values for silibinin (PC-9 and A549, hereafter "silibinin-resistant"), with 5 μmol/L nintedanib increasing the cytotoxic activity of silibinin ~10-fold (Figure 1B).

As single agents, silibinin and nintedanib suppressed NSCLC cell viability at the concentrations employed as sensitization agents. Because the observed sensitization effect might be due to their own toxicity, potential synergistic interactions could not be accurately discriminated from additive or antagonistic effects based on these data alone. Although there is controversy over which method is best for detecting true in vitro synergy of drug combinations, we elected to analyze the impact of the nintedanib plus silibinin combination at different concentration levels, so that a constant molar ratio of nintedanib to silibinin was maintained. When the dose ratio of the drugs was fixed at 1:20 (nintedanib:silibinin), the extent of the cytotoxic interaction was again cell line dependent. The true nature of the interaction was then assessed using the Compusyn program (https://www.combosyn.com/; accessed on 1 June 2020) to calculate the CI parameter, which indicates whether the doses of the 2 agents required to produce a given degree of cell toxicity are greater than the doses that would be required if the effects of nintedanib and silibinin were strictly additive (Figure 1C, *left*). Combinations of nintedanib and silibinin generated CI values of 0.79 to 1.00 for IC_{50} and 0.49 to 1.04 for IC_{90}, indicating additive effects in most cases. Of note, however, was the finding of synergistic interactions in those cell lines exhibiting intrinsically higher IC_{50} values for nintedanib (H1975 and H460) or to silibinin (PC-9 and A549). Such synergistic interactions were more evident at high levels of cell killing (IC_{90}) (Figure 1C, *left*). Moreover, the nature of the interaction between nintedanib and silibinin remained largely unaltered in NSCLC cells chronically adapted to nintedanib by incremental and continuous exposure to the drug for >6 months (Figure 1C, *right*).

2.3. Synergistic Interactions between Silibinin and Nintedanib in NSCLC Cells with Acquired Resistance to EGFR- and ALK-Tyrosine Kinase Inhibitors

We questioned whether the generalized progression of EGFR-mutant and ALK-translocated NSCLC after an initial response to EGFR and ALK tyrosine kinase inhibitors (TKIs) in a clinical setting would alter the nature of the interaction between nintedanib and silibinin. To do this we used three cell lines: PC-9/ER cells, a pre-clinical model of acquired resistance to the EGFR TKI erlotinib established by growing PC-9 cells in the continuous presence of high doses of erlotinib, but lacking additional inactivating mutations in the EGFR kinase domain [55,56]; H2228/CR cells, a crizotinib-resistant variant obtained through long-term exposure to increasing concentrations of crizotinib that activates the epithelial-to-mesenchymal transition (EMT) program [54]; and H3122/CR cells, a crizotinib-resistant variant capable of growing in the presence of 1 μmol/L crizotinib due to activation of "bypass" alternative kinases (EGFR), but lacking amplification or mutations in the kinase domain of ALK [53]. In terms of IC_{50} values, responsiveness to nintedanib was slightly decreased in PC-9/ER cells, whereas a significant collateral resistance to nintedanib

was observed in cell lines with acquired resistance to crizotinib (Figure S1A). In H3122/CR cells the IC_{50} value of nintedanib increased more than 2-fold. Conversely, we failed to detect a difference in sensitivity to silibinin in any of the EGFR-TKI and ALK-TKI resistant derivatives (Figure S1A).

Co-treatment with silibinin enhanced the cytotoxic activity of nintedanib in a dose-dependent manner, which was particularly evident in EGFR-TKI and ALK-TKI resistant cells (Figure S1B,C). Analysis of the cell viability data of the nintedanib plus silibinin combination from automated determination of CIs demonstrated that the synergistic interaction in erlotinib-responsive PC-9 cells remained unaltered in PC-9/ER cells (Figure S1D). Moreover, the nature of the interaction between nintedanib and silibinin switched from additive in crizotinib-responsive H2228 and H3122 parental cells to synergistic in the isogenic H2228/CR and H3122/CR derivatives with acquired resistance to crizotinib (Figure S1D).

2.4. Synergistic Interactions between Nintedanib and Docetaxel in NSCLC Cells

When we characterized the baseline cytotoxic effects of docetaxel as a single agent in the same panel of molecularly diverse NSCLC cell lines, we noted that sensitivity was lower in cell lines with primary resistance to erlotinib. H1993 cells bearing a MET amplification, which is recognized as one of the molecular mechanisms of EGFR-mutant NSCLC resistance to EGFR-TKIs, were >5-fold more resistant to docetaxel than were A549, H2228, and H3122 cells, which were exquisitely responsive (Figure S2A). Notably, EGFR-mutant PC-9/ER cells exhibited a prominent cross-resistance to docetaxel (Figure S2B).

When docetaxel was combined with nintedanib at a 1:1 ratio, an additive interaction was observed in most cell lines. When the relative amount of nintedanib in the combination was increased to achieve a 1:5 docetaxel:nintedanib ratio, most of the combinations were synergistic (Figure 2A). Such nintedanib-driven augmentation of the synergistic effects of the docetaxel:nintedanib combination was also evident in EGFR-TKI and ALK-TKI resistant derivatives (Figure S2C, *left*). When docetaxel was combined with silibinin, a strong synergism was observed in silibinin-resistant A549 cells at all tested ratios (1:10, 1:20, 1:100) of combined drugs. In nintedanib-resistant H1993 cells, the most efficacious combinations occurred at higher combination ratios (Figure 2B). In EGFR-TKI and ALK-TKI resistant derivatives, a higher number of synergistic interactions occurred at lower combination ratios of docetaxel and silibinin (Figure S2C, *right*).

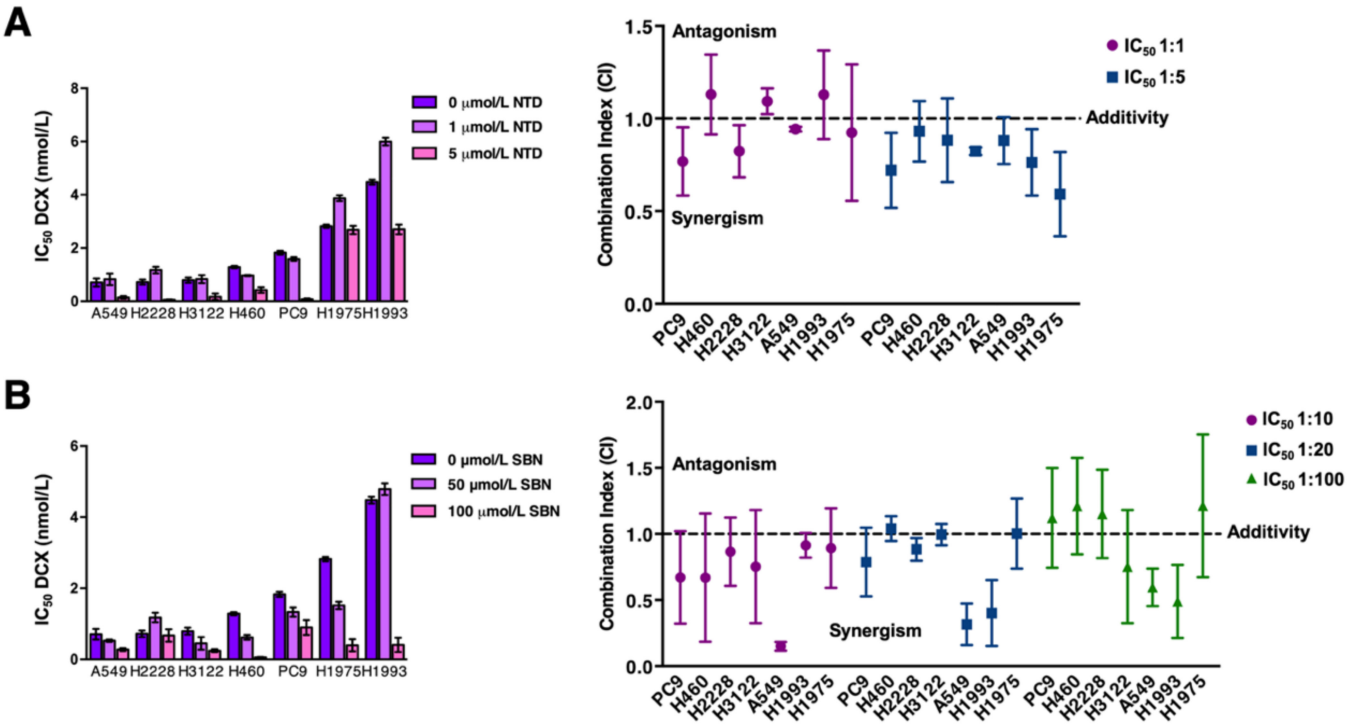

Figure 2. Analysis of the cytotoxic interaction between docetaxel, nintedanib, and silibinin in NSCLC cells. *Left panels.* Bar graph showing the MTT-based IC_{50} values of docetaxel (DCX) for each cell line calculated in the absence or presence of graded concentrations of NTD (**A**) and SBN (**B**). *Right panels*. Computed combination index (CI) values for the combination of DCX *plus* NTD (**A**) and DCX *plus* SBN (**B**) at 50% effect levels using different fixed ratio combinations of the drugs. CI values less than, equal to or greater than 1 indicates synergy, additivity or antagonism, respectively. The horizontal line at CI = 1 is the line of additivity. The results in A, B, C and D panels are presented as the means (*columns*) ± S.D. (*bars*) (n = 3, in triplicate).

2.5. Silibinin Suppresses Nintedanib-Unresponsive STAT3 Hyperactivation in NSCLC Cells

Ectopic overexpression and constitutive activation of STAT3 can prevent the tumoricidal effects of nintedanib on cancer cells [23,24]. Similarly, cells engineered to overexpress a constitutively active form of STAT3 remain largely unresponsive to the effects of silibinin [50]. We therefore speculated that, similar to other pathway-targeted cancer drugs [61], cell lines in which the nintedanib-driven blockade of the FGFR/SRC/STAT3 axis fails to fully suppress STAT3 activity could activate the JAK/STAT3 axis as a compensatory mechanism, which might be responsive to silibinin (Figure 3). To test this hypothesis, we first explored the correlation between the activation status of STAT3 and intrinsic responsiveness to nintedanib in our panel of NSCLC cell lines. Nintedanib-responsive PC-9 and A549 cells exhibited low constitutive levels of phospho-active $STAT3^{Tyr705}$ that were fully suppressed in the presence of nintedanib (Figure S3A). Conversely, nintedanib-resistant H460 and H1975 cells exhibited a noteworthy constitutive hyperactivation of STAT3 that was fully unresponsive or further augmented in response to nintedanib (Figure S3A).

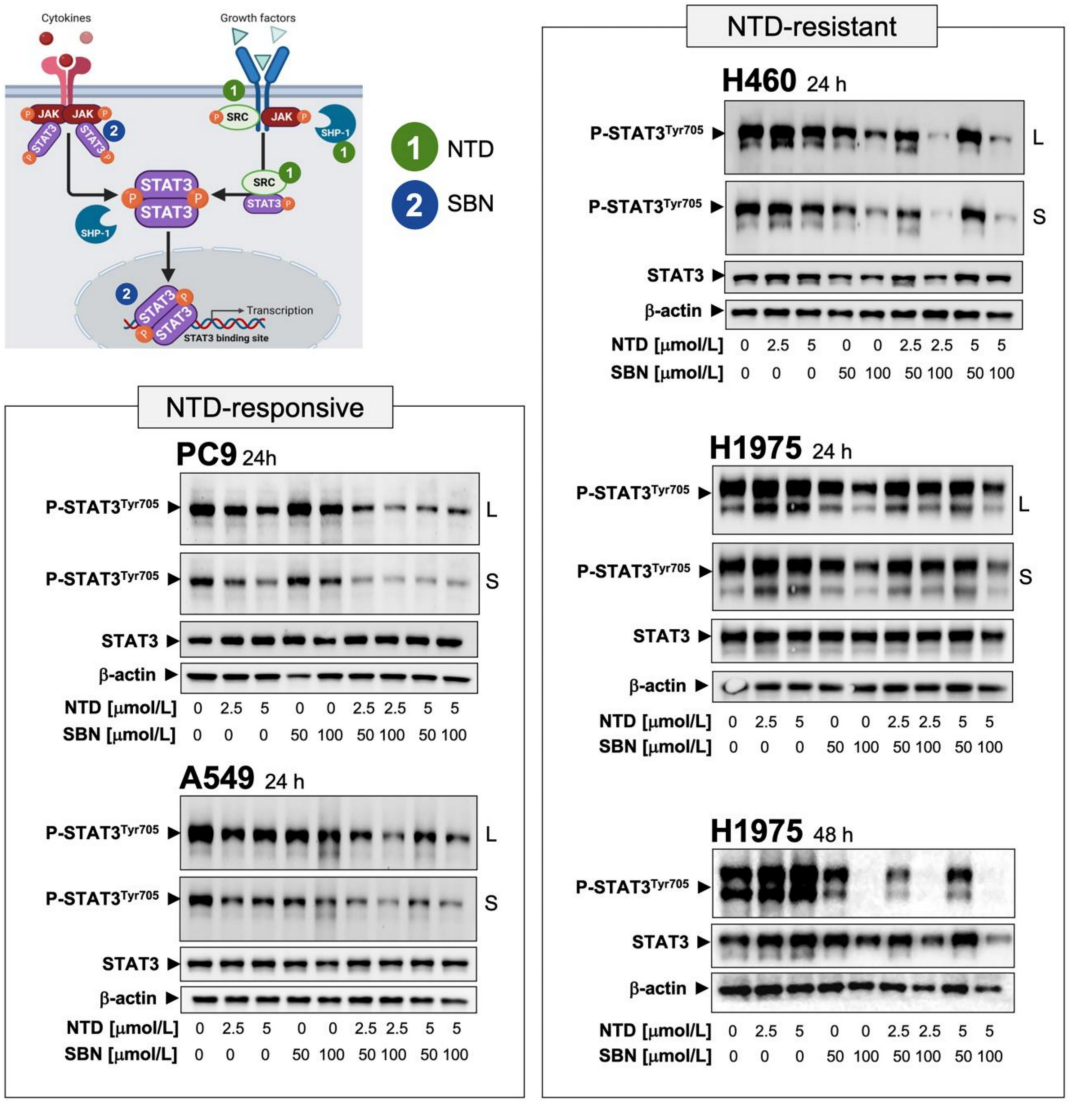

Figure 3. STAT3-targeted effects of the interaction between nintedanib and silibinin in NSCLC cells. Unstimulated STAT3 is activated by recruitment to phospho-tyrosine motifs existing within complexes of cytokine receptors (e.g., IL-6 receptor), growth factor receptors (e.g., EGFR, PDGFR, FGFR), or non-receptor tyrosine kinases (e.g., SRC) through its SH2 domain. STAT3 is then phosphorylated on the Tyr705 residue by activated tyrosine kinases (e.g., JAK, SRC) in receptor complexes. Phosphorylated STAT3 forms homodimers (and heterodimers with other STAT isoforms) and translocates to the nucleus, where STAT3 dimers bind to specific promoter elements of target genes to regulate gene expression via the STAT3 DNA-binding domain (DBD). Enhancing the activity of the SH2 domain-containing protein tyrosine phosphatase 1 (SHP-1) by the SHP-1 agonistic activity of nintedanib (NTD) can directly dephosphorylate STAT3 or its upstream JAKs to decrease the phospho-active STAT3 proteins (1). NTD might also inhibit STAT3 activity downstream of its direct actions on growth factor receptors such as PDGFRβ and FGFR or non-receptor tyrosine kinases such as SRC (1). Silibinin (SBN) can directly bind to the (JAK and SRC-activated) SH2 domain of STAT3 to prevent Y705 phosphorylation-related STAT3 activation and dimerization (2). SBN can also establish direct interactions with DNA in its targeting to the STAT3 DBD (2), thereby preventing the binding of STAT3 to its consensus DNA sequence. Dual blockade of the STAT3 activating events by combining NTD and SBN might efficiently prevent NSCLC cells from escaping from STAT3 inhibition in response to NTD/SBN as single agents, thereby providing a basis for a molecular rationale for the incorporation of SBN into nintedanib-based schedules in NSCLC. NTD-responsive PC-9 and A549 cells, and NTD-resistant H460 and H1975 cells were serum-starved overnight and then left untreated or treated with NTD in the absence or presence of SBN for 24 or 48 h. Levels of phospho-STAT3^{Tyr705} and STAT3 were detected by immunoblotting using specific antibodies (S: short exposure; L: long exposure). Figure Shows representative immunoblots of multiple ($n \geq 5$) independent experiments. The uncropped blots and molecular weight markers are shown in Supplementary Materials.

Once we established that STAT3 hyperactivation might be a key signaling alteration that contributes to primary/de novo nintedanib resistance in NSCLC cells, we explored whether the above-described capacity of silibinin to significantly rescue the sensitivity of NSCLC cells to nintedanib occurred upon silibinin-induced STAT3 inhibition. Immunoblot analyses in whole cell lysates confirmed that co-treatment with nintedanib and silibinin suppressed the residual STAT3 activity remaining after single-agent therapy in nintedanib-responsive PC-9 and A549 cells (Figure 3). Moreover, silibinin co-treatment for 24 h markedly suppressed nintedanib-unresponsive STAT3 hyperactivation in nintedanib-resistant H460 cells (Figure 3). The ability of silibinin to fully suppress nintedanib-unresponsive hyperactivation of STAT3 in nintedanib-resistant H1975 cells required a longer exposure (48 h; Figure 3).

To confirm that silibinin targeted the canonical role of STAT3 as a nuclear transcription factor, we examined the intracellular distribution of STAT3 and phospho-STAT3^{Tyr705} by immunoblot analysis of nuclear and cytosolic fractions of nintedanib-treated cells cultured in the absence or presence of silibinin (Figure S3B). Phospho-STAT3^{Tyr705} generated in nintedanib-sensitive PC-9 cells in response to IL-6 stimulation was found almost exclusively in the nucleus, a stimulatory effect that was fully prevented in the presence of silibinin (Figure S3B, *top*). In nintedanib-resistant H460 cells, constitutive immunoreactivity for phospho-active STAT3 was found almost exclusively in nuclear extracts and increased further in the presence of nintedanib. Silibinin treatment notably decreased constitutive activation of STAT3 and fully suppressed the nuclear hyperactivation of STAT3 occurring in the presence of nintedanib (Figure S3B, *bottom*). Consistent with the inhibition of STAT3 activation, silibinin markedly attenuated nuclear translocation of STAT3 in nintedanib-treated H460 cells. Immunofluorescent analysis confirmed the ability of silibinin to prevent cytoplasm-to-nuclear translocation and nuclear accumulation of phospho-active STAT3, regardless of the presence or absence of nintedanib (Figures S3C and S4).

2.6. Silibinin Prevents Lysosome Sequestration of Nintedanib in NSCLC Cells

Reversible sequestration and inactivation of nintedanib in acidic vesicles, a process known as lysosomal trapping [62–66], has been proposed as an intrinsic mechanism of resistance to nintedanib in FGFR-driven lung cancer cells [59,60]. This property prompted us to question whether silibinin might be capable of reversing lysosomal nintedanib sequestration.

We took advantage of the previous observation that nintedanib has autofluorescent properties [59], and we monitored its localization in NSCLC cells by light microscopy. Live-cell imaging revealed that upon nintedanib treatment, the drug accumulated in discrete structures in the cytoplasm of tumor cells. Co-staining of cells with LysoTracker® Red—a fluorescent dye used for labeling acidic lysosomes in live cells—revealed a notable overlap with nintedanib staining, confirming the selective accumulation of nintedanib in lysosomes (Figure 4, *top panels*). We observed that nintedanib-resistant cell lines displayed a markedly greater accumulation of nintedanib than nintedanib-sensitive cells. Using flow cytometry, we established that the fluorescence signal produced by nintedanib was notably higher in nintedanib-resistant H460 and H1975 cells than in nintedanib-sensitive PC-9 and A549 cells (up to 30-fold; Figure 4, *bottom panels*).

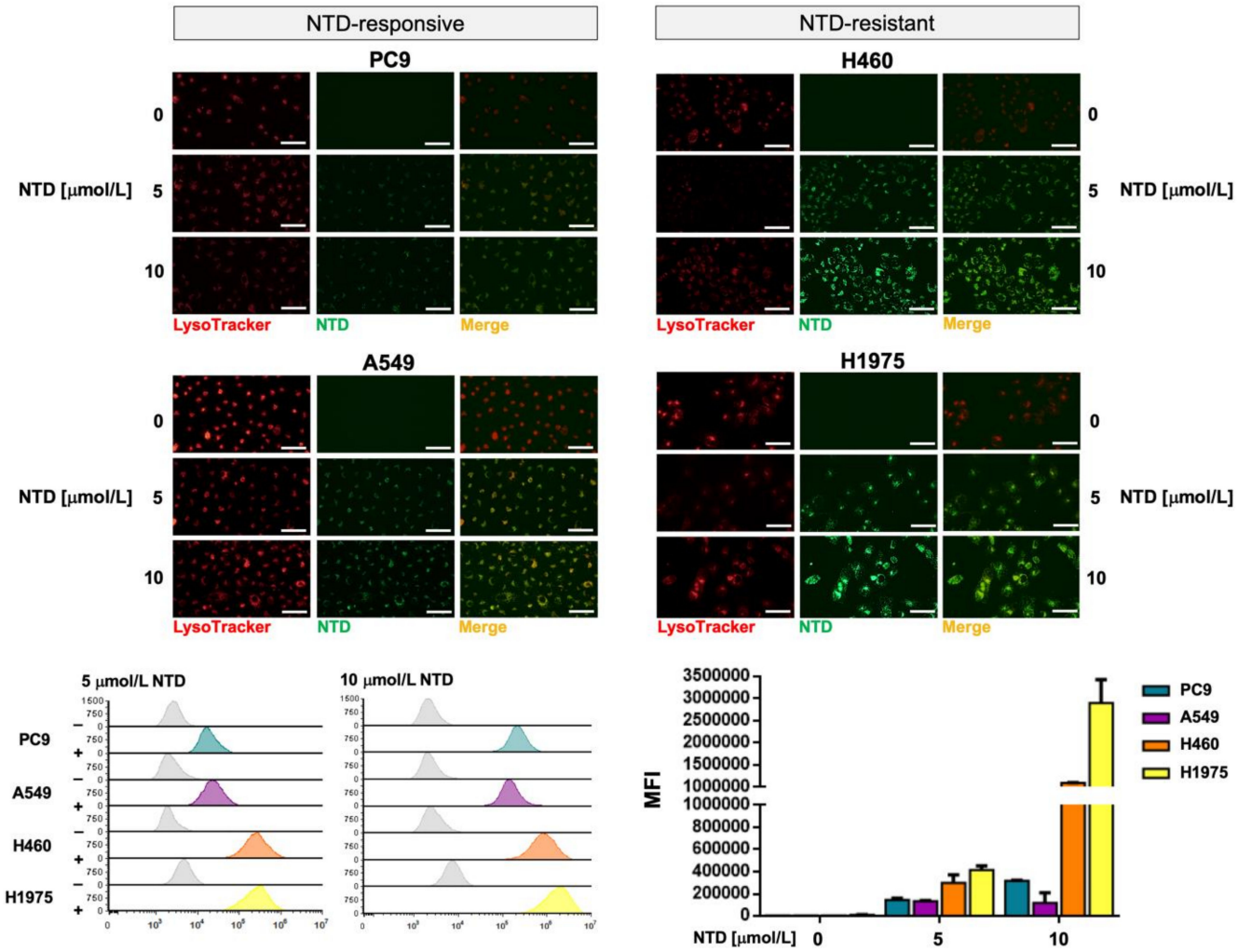

Figure 4. Lysosomal sequestration of nintedanib in NSCLC cell lines. *Top.* Subcellular distribution of 5 and 10 μmol/L nintedanib in PC-9, A549, H460 and H1975 cells after 3 h drug exposure was analyzed by live cell fluorescence microscopy in the FITC channel. LysoTracker® Red served as a marker for the lysosomal compartment. Nintedanib/LysoTracker® spatial overlap is also shown. The scale bar indicates 50 μm. *Bottom.* Dose-dependent green fluorescence activity of nintedanib (NTD) in NTD-responsive PC-9 and A549 cells and in NTD-resistant H460 and H1975 cells was analyzed by flow cytometry. Each experimental value represents the mean NTD-associated fluorescence (*columns*) ± S.D. (*bars*) of 3 independent experiments. (MFI: Median Fluorescence Intensity).

Live cell fluorescence microscopy and flow cytometry analyses revealed that silibinin treatment promoted a significantly reduced lysosomal sequestration of nintedanib (up to 5- to 6-fold reduction) in nintedanib-resistant H460 and H1975 cells (Figure 5). No significant effects of silibinin were observed in nintedanib-sensitive PC-9 and A549 cells (Figure S5).

Exploiting the ability of the lipophilic weak base ammonium chloride (NH_4Cl) to neutralize the acidic endosome-lysosome system as well as the well-known capacity of the specific inhibitor of vacuolar-type H^+-ATPases bafilomycin A to directly inhibit lysosomal acidification, we explored to what extent the lysosomal alkalization sufficed to abrogate the lysosomal accumulation of nintedanib in nintedanib-resistant NSCLC cells. Silibinin treatment more closely resembled the ability of NH_4Cl to partially abrogate the green fluorescence of nintedanib than that of bafilomycin A, which fully abolished the lysosomal accumulation of nintedanib (Figure S6). The proton capturing ability of the weak-base chloroquine to de-acidify the lysosome recapitulated the partial reversion of nintedanib lysosomal sequestration promoted by silibinin and NH_4Cl (data not shown).

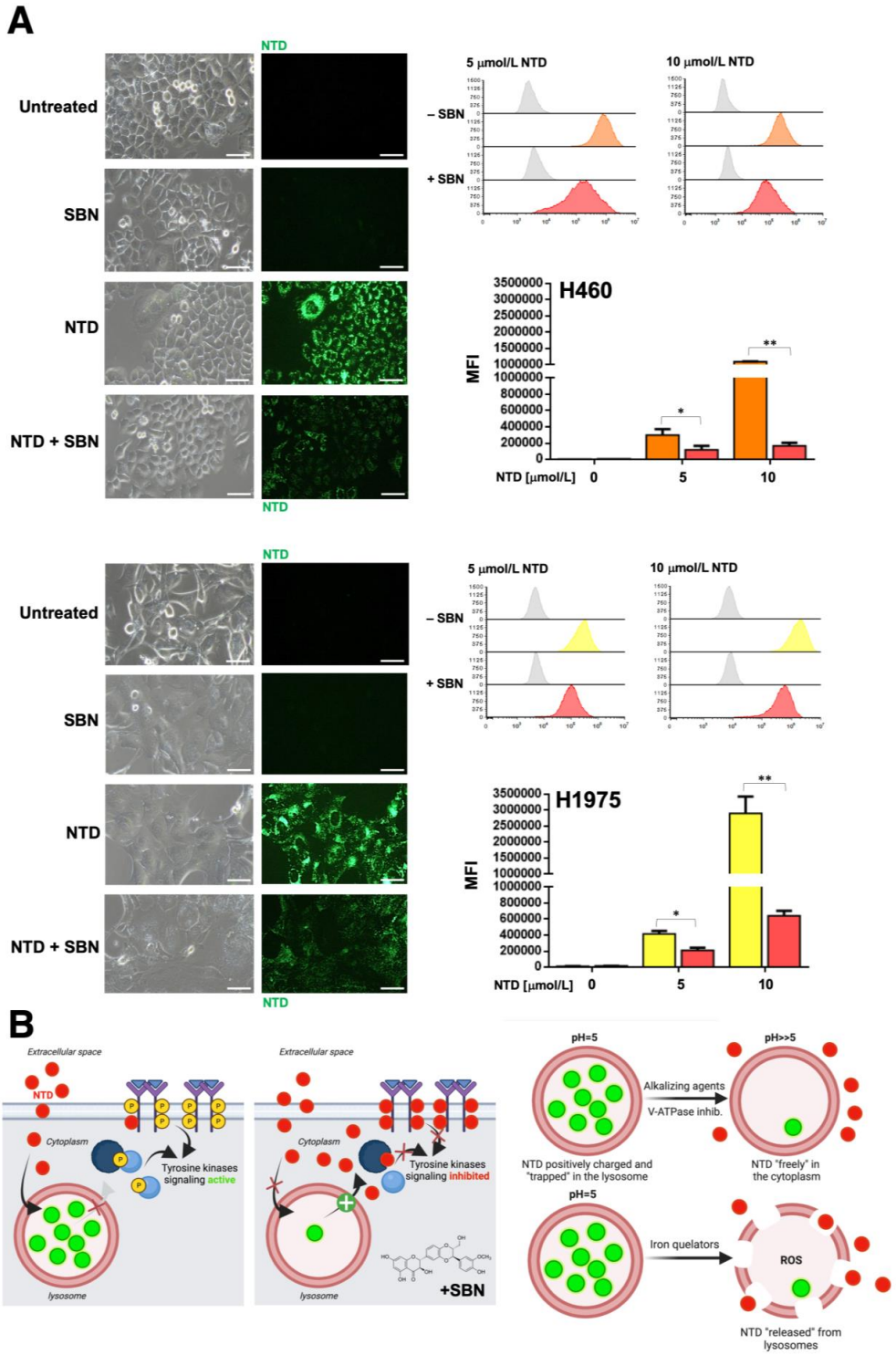

Figure 5. Effects of silibinin on the lysosomal sequestration of nintedanib in nintedanib-resistant NSCLC tumor cells. (**A**) The impact of 100 µmol/L silibinin (SBN; 1 h pre-treatment) on the intracellular accumulation of 5 and 10 µmol/L nintedanib (NTD) was analyzed by live cell fluorescence microscopy (*left panels*) and flow cytometry (*right panels*) after 3 h drug exposure. Each experimental value represents the mean NTD-associated fluorescence (*columns*) ± S.D. (*bars*) of 3 independent experiments. The scale bar indicates 50 µm. Comparisons of means were performed by ANOVA. p values < 0.01 and < 0.001 were considered to be statistically significant (denoted as * and **, respectively; n.s. not significant). (**B**) Sequestration of NTD into lysosomes provides a mechanism of NTD resistance in NSCLC cells. Overcoming NTD trapping by alkalizing lysosomes (e.g., by using NH_4Cl, chloroquine, bafilomycin A) or disrupting lysosomes containing sequestered NTD (e.g., by iron chelators) can potentiate the effects of NTD treatment. (MFI: Median Fluorescence Intensity).

2.7. Clonogenic Assays and Real-Time Monitoring of Cell Proliferation Confirms the Synergistic Interaction between Silibinin and Nintedanib in NSCLC Cells

To assess the long-term effects of nintedanib and/or stress signals on cell survival, we tested the capacity of NSCLC cells to proliferate efficiently to form colonies. Clonogenic survival analyses revealed that nintedanib-resistant H460 cells failed to generate colonies long-term when cultured with the nintedanib plus silibinin combination. Co-treatment with silibinin fully suppressed colony formation in nintedanib-resistant H460 cells (Figure 6). Silibinin-resistant PC-9 cells failed to generate colonies long-term when cultured with the silibinin plus nintedanib combination (Figure 6).

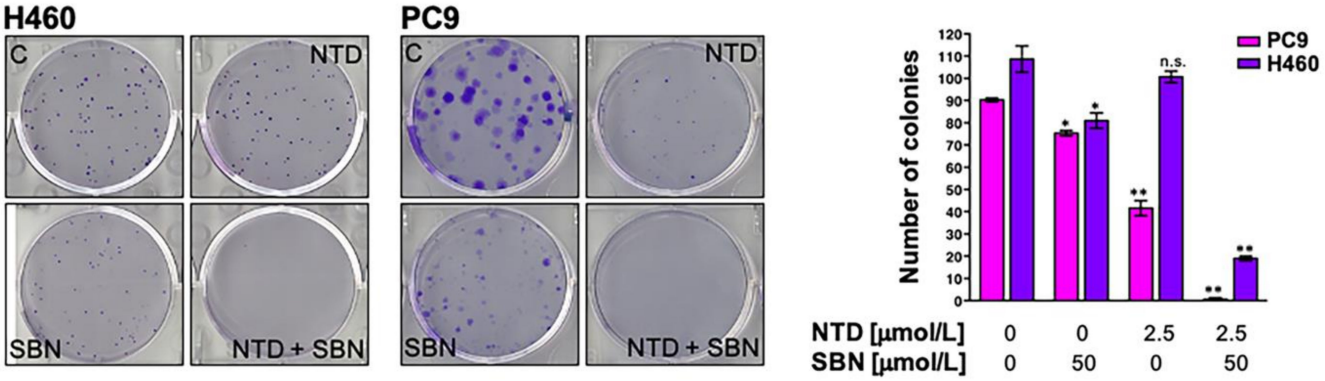

Figure 6. Analysis of clonogenic survival in response to nintedanib plus silibinin. *Left.* Representative images from 6-well plates of colonies of H460 and PC-9 cells treated with nintedanib and/or silibinin. ImageJ (NIH) was used to quantify the number of 7-day-old colonies stained with crystal violet. *Right. Columns* and *error bars* represent mean values and S.D., respectively. Comparisons of means were performed by ANOVA. p values < 0.01 and < 0.001 were considered to be statistically significant (denoted as * and **, respectively; n.s. not significant).

A limitation of the MTT reduction-based assay is that because it is an end-point assay, it provides only a snapshot of a dynamic process. We therefore employed the impedance-based RTCA platform (xCELLigence), which is a label-free environment for cancer cells that can accurately inform about the characteristics of the response to treatment without the use of toxic/end-point assays, leading to the termination of the experiment. Using this platform, we captured real-time kinetic data on cell growth after treatment with the nintedanib/docetaxel combination in the absence or presence of silibinin (Figure S7, *top panels*). Cell proliferation rates and doubling times for PC-9, A549 and H460 cells cultured with or without nintedanib, docetaxel, silibinin and their respective combinations, were calculated as the slope of the growth curve of best fit from cell index recordings within a given time frame (i.e., between the 24 and 80 h interval). We found that co-treatment with silibinin augmented the ability of nintedanib to reduce the cell proliferation of PC-9, A549, and H460 cells. Accordingly, highly significant, supra-additive increases in cell doubling times were observed in those cells simultaneously exposed to nintedanib and silibinin (Figure S7, *bottom panels*).

2.8. The Nutraceutical Use of Silibinin Enhances the Clinical Response to Nintedanib/Docetaxel in Advanced Lung Adenocarcinoma

To assess the clinical impact of adding silibinin to the nintedanib/docetaxel combination in daily clinical practice, we carried out a retrospective, observational multicenter study assessing the efficacy of silibinin (5 capsules/day of Legasil®, equating to a 630 mg/day dose silibinin regimen [49,50]) in patients with advanced lung adenocarcinoma receiving the nintedanib/docetaxel combination in second- and further-line settings (Figure 7A).

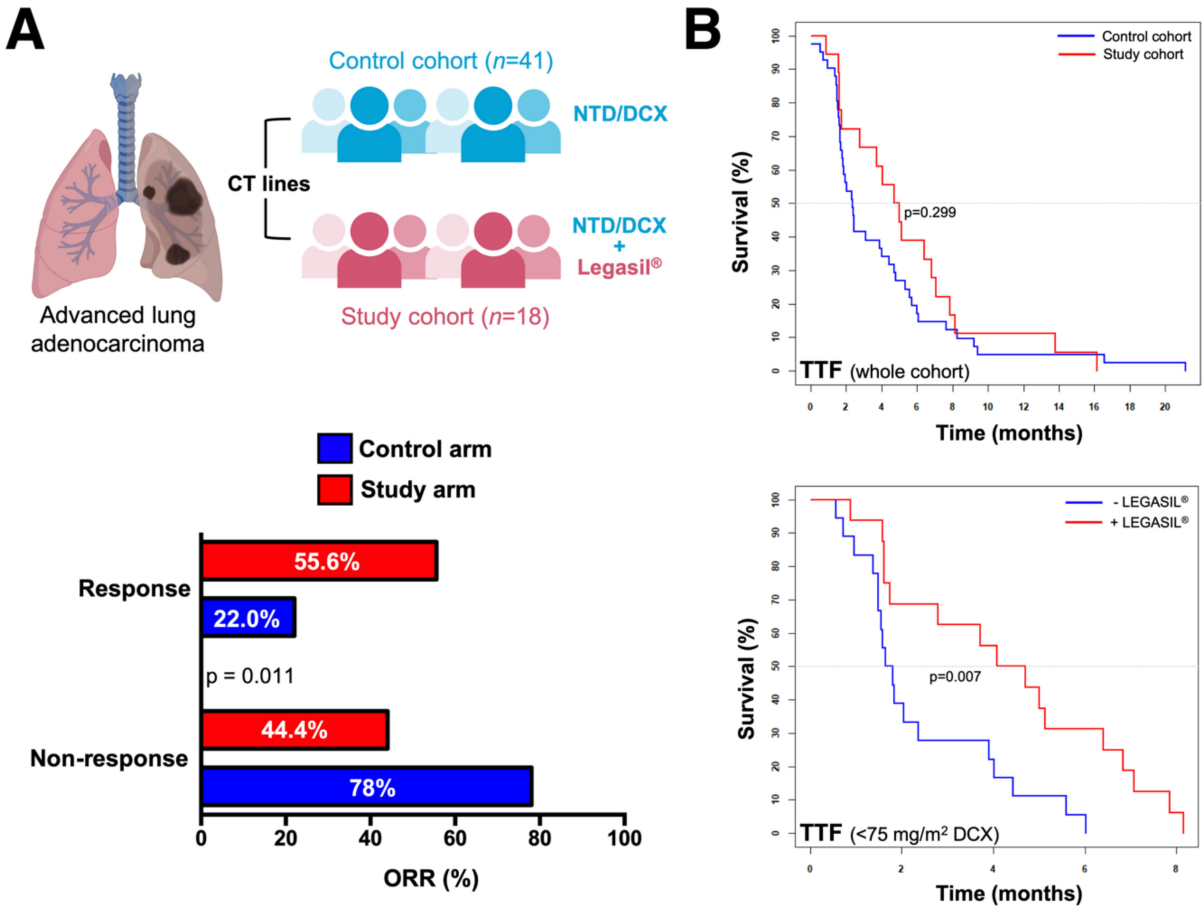

Figure 7. Impact of the silibinin-containing nutraceutical Legasil® on the clinical efficacy of the nintedanib/docetaxel combination in advanced lung adenocarcinoma. (**A**) *Top.* We conducted a retrospective, observational multicenter study to assess the efficacy of incorporating the oral nutraceutical product Legasil® containing silibinin in patients with advanced lung adenocarcinoma receiving nintedanib/docetaxel combination in second- and further-line settings (n = 59). *Bottom.* Overall response rate (ORR, in %)—defined as the combined rates of complete and partial responses—in the control and study arms. (**B**) Kaplan–Meier TFF curves of patients stratified by control/study arms (*top*) and (−) Legasil®/(+) Legasil® co-treatment (*bottom*).

Fifty-nine patients who started treatment between June 2014 and November 2017 were included in the study. Patients and tumor characteristics are summarized in Table 2. Forty-one (69.5%) patients received nintedanib plus docetaxel (control cohort) and 18 (30.5%) received the nintedanib/docetaxel combination and supplementation with Legasil® (study cohort). In the whole cohort, the median follow-up was 20.2 months (interquartile range: 17.8–34.6). Most patients (78%) received nintedanib as second-line treatment and only 42% of patients received the recommended dose of docetaxel of 75 mg/m^2. A significantly higher number of patients required a further dose reduction of docetaxel in the study cohort than in the control cohort (88.9% vs. 43.9%, p = 0.001).

Table 2. Baseline demographics of the cohorts and tumor characteristics.

	Study Cohort (*n* = 18)	**Control Cohort (*n* = 41)**	***p*-Value**
Sex			0.187
Male	12 (67%)	34 (83%)	
Female	6 (33%)	7 (17%)	
Age			0.490
Mean ± SD (range)	61.2 ± 10.3 (43–79)	59.5 ± 7.3 (45–71)	
Line of treatment			1.000
2nd line	14 (78%)	32 (78%)	
≥3rd line	4 (22%)	9 (22%)	
TTF 1st line (months)			0.439
Median (p25,p75)	4.7 (4.1, 6.5)	4.4 (1.9, 7.6)	
Response to 1st line			0.188
Response (PR)	5 (27.8%)	13 (31.7%)	
Stable disease	9 (50.0%)	11 (26.8%)	
Progression disease	4 (22.2%)	17 (41.5%)	
Initial docetaxel dose			0.001
75 mg/m^2	2 (11%)	23 (56%)	
<75 mg/m^2	16 (88.9%)	18 (44%)	
ECOG PS			0.144
0	5 (27.8%)	3 (7.3%)	
1	13 (72.2%)	36 (87.8%)	
2	0 (0%)	2 (4.9%)	
EGFR status			0.546
EGFR-mutant	0 (0%)	3 (7.3%)	
EGFR-wild-type	18 (100%)	38 (92.7%)	
KRAS status			0.099
KRAS-mutant	4 (22.2%)	12 (29.3%)	
KRAS-wild-type	4 (22.2%)	18 (43.9%)	
KRAS-not evaluable	10 (55.6%)	11 (26.8%)	
PD-L1 status			0.222
0%	3 (16.7%)	11 (26.8%)	
1–49%	1 (5.5%)	5 (12.2%)	
≥50%	3 (16.7%)	1 (2.4%)	
Not evaluable	11 (61.1%)	24 (58.6%)	

TTF: Time-to-treatment failure; PR: Partial response; ECOG PS: Eastern Cooperative Oncology Group Performance status; PD-L1: Programmed death-ligand 1.

The ORR was significantly higher in the study cohort than in the control cohort (55.6% vs. 22%; $p = 0.011$; Figure 7A). In the control cohort, no statistically significant differences were observed in the ORR according to *KRAS* status (wild-type: 22.2%, mutated: 25.0%, not evaluable: 18.2%, $p = 1.000$) or *EGFR* mutation (wild-type: 18.4%, mutated: 66.7%, $p = 0.116$). In the study cohort, no statistically significant differences were observed in the ORR according to *KRAS* status (wild-type: 50%, mutated: 25%, not evaluable: 70.0%, $p = 0.320$). All the patients included in the experimental cohort were EGFR wild-type, thus precluding the statistical analysis.

The median TTF was 2.8 months (95% confidence interval [CI]: 1.1–4.5) in the whole cohort, with no statistically significant differences between patients receiving second- or third-line treatment ($p = 0.979$). Median TTF was significantly higher in responders to nintedanib/docetaxel (6.0 months, 95%CI: 4.8–7.2) than in non-responders (1.8 months, 95%CI: 1.6–2.1) ($p = 0.001$; Figure S4). Compared with those receiving a reduced of dose docetaxel, patients receiving standard docetaxel dosing had higher median TTF (4.7 months 95%CI: 0.9–8.5 vs. 2.0 months 95%CI: 0.6–3.4, $p = 0.006$; Figure S4).

No significant differences were observed in the median TTF between the study and control cohorts in univariate analysis (4.7 months 95%CI: 2.8–6.6 vs. 2.4 months 95%CI: 1.8–2.9, $p = 0.299$; Figure 7B). In the subgroup of patients receiving a reduced dose of

docetaxel (n = 34), the supplementation with Legasil® was associated with a significant increase in median TTF (4.1 months 95%CI: 2.1–6.0 vs. 1.6 months 95%CI: 1.2–2.1, p = 0.007; Figure 7B). In the subgroup of patients receiving standard docetaxel dosing (n = 25), median TTF was 3.1 months (95%CI: 0.4–5.9) in the control cohort and 13.8–16.1 months in the two patients in the study cohort (no statistical analysis was performed because of the extremely small sample size). In multivariate analysis, both the supplementation with Legasil® (hazard ratio [HR] 0.43, p = 0.013) and docetaxel dose reduction (HR 3.3, p < 0.001) were significantly associated with longer and shorter TTF, respectively (Table 3).

Table 3. Univariate and multivariate Cox proportional analysis for TTF.

	Univariate Analysis			Multivariate Analysis		
	HR	**(95%CI)**	***p*-Value**	**HR**	**(95%CI)**	***p*-Value**
Age (years)						
≤65	1	(referent)		1	(referent)	
>65	0.60	(0.33–1.10)	0.096	0.74	(0.39–1.37)	0.335
Sex						
Female	1	(referent)		1	(referent)	
Male	1.06	(0.57–1.98)	0.847	0.72	(0.47–1.70)	0.890
Docetaxel						
75 mg/m^2	1	(referent)		1	(referent)	
<75 mg/m^2	2.23	(1.18–4.22)	0.013 *	3.30	(1.69–6.45)	<0.001 *
Legasil®						
No	1	(referent)		1	(referent)	
Yes	0.74	(0.42–1.31)	0.302	0.43	(0.22–0.84)	0.013 *

HR: hazard ratio; CI: confidence interval; * statistically significant (p < 0.05).

In the whole cohort, median OS since the beginning of first-line chemotherapy (OS1L) was 12.5 months (95%CI: 10.6–14.4) and median OS since the beginning of nintedanib/docetaxel combination (OS2L) was 6.8 months (95%CI: 4.6–8.9). There were no differences in median OS1L and OS2L between the study and control cohorts (13.2 months 95%CI: 3.5–22.8 vs. 12.4 months 95%CI: 10.4–14.4, p = 0.595; and 6.6 95%CI: 4–9.6 vs. 6.8 months 95%CI: 3.6–9.8, p = 0.877, respectively; Figure S8). No differences in median OS2L were observed between nintedanib/docetaxel-treated patients treated in second- or further-lines (p = 0.454). In the control cohort, OS2L was significantly higher in patients with *KRAS*-mutant than with *KRAS*-wild-type (10.1 months 95%CI: 0–22.9 vs. 7.3 months 95%CI: 2.7–11.9, respectively; p = 0.034; Figure S8), when patients with unknown *KRAS* mutational status were excluded from the analysis. Although a contrary trend was observed in the study cohort (3.0 months 95%CI: 0.3–6.0 in *KRAS*-mutant vs. 7.0 months 95%CI: 0.0–15.2 in *KRAS*-wild-type; p = 0.100), this trend in OS2L did not reach statistical significance (p = 0.100; Figure S8).

A significant increase of OS1L was observed in responders to first-line treatment compared with non-responders (14.1 months 95%CI: 4.3–23.8 vs. 11.4 months 95%CI: 9.6–13.3, p = 0.037). Patients achieving partial response to nintedanib/docetaxel showed also a higher median OS2L (10.9 months 95%CI: 6.8–15.1 vs. 5.4 months 95%CI: 4.7–6.1, p = 0.043). Patients with shorter TTF to first-line treatment (<9 months vs. > = 9 months) had shorter OS1L (11.2 months 95%CI: 9.7–12.7 vs. 29.6 months 95%CI: 21.1–38.2, p < 0.001) and OS2L (5.4 months 95%CI: 4.6–6.3 vs. 12.4 months 95%CI: 8.8–15.9, p = 0.013). In multivariate analysis, the sole variable that remained significant for OS2L was the reduced dosage of docetaxel in the first cycle (HR 2.282 p = 0.014) (Table 4).

Table 4. Univariate and multivariate Cox proportional analysis for OS2L.

	Univariate Analysis			Multivariate Analysis		
	HR	**(95% CI)**	***p*-Value**	**HR**	**(95% CI)**	***p*-Value**
Age (years)						
≤65	1	(referent)		1	(referent)	
>65	1.05	(0.56–1.95)	0.886	1.07	(0.58–2.00)	0.823
Sex						
Female	1	(referent)		1	(referent)	
Male	1.26	(0.65–2.45)	0.503	1.19	(0.60–2.32)	0.621
Docetaxel						
75 mg/m^2	1	(referent)		1	(referent)	
<75 mg/m^2	1.80	(1.02–3.15)	0.041 *	2.22	(1.18–4.17)	0.014 *
Legasil®						
No	1	(referent)		1	(referent)	
Yes	0.95	(0.52–1.75)	0.878	0.63	(0.32–1.25)	0.190

HR: hazard ratio; CI: confidence interval; * statistically significant ($p < 0.05$).

3. Discussion

In the pivotal LUME-Lung 1 study [4], nintedanib in combination with docetaxel was found to improve the control of previously treated NSCLC disease and prolong overall and progression-free survival in patients with adenocarcinoma [4]. However, the lack of a clear improvement in the response rate, which is usually <10% in patients treated with docetaxel alone, has largely discouraged oncologists from using the nintedanib/docetaxel combination in an off-trial setting. Our present study provides a biological and clinical rationale for the addition of the flavonolignan silibinin to increase the efficacy of the nintedanib/docetaxel combination in patients with advanced NSCLC, for whom few effective second-line chemotherapy regimens are available.

Nintedanib is known to inhibit cell proliferation and induce apoptotic cell death in the three cell types contributing to angiogenesis: endothelial cells, pericytes, and smooth muscle cells [1]. Accordingly, the clinical benefit derived from nintedanib in patients with lung adenocarcinoma and fast-progressing tumors, and with primary or acquired resistance to chemotherapy, would suggest a bona fide anti-angiogenic functioning of the drug. However, resistance to nintedanib is common and patients ultimately relapse. In an attempt to elucidate the causes of recurrence, many studies have focused on tumor microenvironmental responses to the metabolic conditions induced by nintedanib, but we still lack strategies to target these mechanisms of resistance and clinically improve the efficacy of nintedanib. Importantly, we are now learning that the whole tumor system can develop resistance mechanisms in response to anti-angiogenic agents beyond those triggered by their anti-vascular effects [67–69]. To fully understand the resistance mechanisms to nintedanib, its anti-tumor effects must be elucidated both in the tumor vasculature and in the tumor cells themselves. In this regard, a potential direct impact of anti-angiogenic agents with multi-receptor TKI activity, such as nintedanib on tumor cell intracellular pathways, cannot be overlooked, as such downstream signaling pathways might be key to elicit the evasion adaptation of resistant cancer cells. By investigating how nintedanib acts on molecularly diverse NSCLC cells in terms of cytotoxicity, we found that those NSCLC cells with poorer responses to nintedanib exhibited increased activation levels of phospho-STAT3^{Tyr705} which were unresponsive to nintedanib. The suppression of nintedanib-refractory STAT3 hyperactivation by concurrent treatment with the STAT3i silibinin promoted synergistic anti-cancer effects. These findings might suggest that the refractoriness of NSCLC cells to nintedanib might rely, at least in part, on redundant or compensatory STAT3 signaling in tumor cells themselves. In FGFR-overexpressing cancer cells, tyrosine phosphorylation of STAT3 is also dependent on the concomitant FGFR-dependent activity of SRC and JAK2 kinase [70]. Since PDGFRβ has been reported to also induce the JAK2/STAT3 pathway by activating SRC, nintedanib might inhibit JAK2

by directly inhibiting PDGFRβ and SRC. Therefore, a multi-blockade of STAT3 activating events in response to nintedanib and silibinin appears to efficiently prevent NSCLC cells from escaping STAT3 inhibition. Nevertheless, our present findings suggest that direct inhibition of STAT3 activity with silibinin might represent a promising clinical strategy to circumvent NSCLC cancer cell-intrinsic nintedanib resistance.

Nintedanib is among the growing list of cancer drugs that can be sequestered in the lysosome [59,60], which reduces its therapeutic concentration in the cytosol. Nintedanib sequestration into the so-called lysosomal drug "safe-houses"—which results in an organelle-specific and pH-dependent nintedanib fluorescence—has been identified as an intrinsic mechanism of nintedanib resistance in FGFR-driven lung cancer cells [59]. Accordingly, treatment of NSCLC cells with chemicals capable of countering the lysosomal acidification such as chloroquine, which directly scavenges protons in the lysosomal lumen, and bafilomycin A1, which actively counteracts proton influx by H^+-ATPase inhibition, which suppress the lysosomal sequestration of nintedanib and restore sensitivity to nintedanib [59]. We confirmed that massive lysosomal sequestration occurs in nintedanib-refractory NSCLC cells. Silibinin partially, but significantly, reduced the lysosomal entrapment of nintedanib in nintedanib-refractory NSCLC cells. The ability of silibinin to reverse lysosomal nintedanib sequestration in a similar way to the shift promoted by pharmacological agents which decrease acidifications by disrupting the ΔpH (i.e., NH_4Cl and chloroquine) but not to those collapsing the whole $\Delta\mu H^+$ (bafilomycin A), likely reflects similarities and differences between their modes of action. Beyond lysosomotropic agents neutralizing the acidic endosome-lysosome system, possible strategies that might reverse lysosomal drug sequestration include alkalinizing agents, acid-labile conjugates, photodestruction and iron chelators, among others [59,60,71,72]. Although an alkalizing effect of silibinin has been reported in cancer cells [73], the molecular mechanism explaining the behavior of silibinin as a bona fide lysosome alkalizing small molecule is unclear. Silibinin is known to act as an iron chelator, even at acidic pH [74–76], and has been proposed as a chelation therapy for chronic iron overload [77,78]. Whether silibinin operates as a novel, metal-binding P-glycoprotein substrate like-drug that can be transported into lysosomes to trigger lysosomal membrane destabilization [60,79,80] and return nintedanib to the cytosol (Figure 5B), remains to be explored. Given that STAT3 enhances the lysosomal system [81] and directly associates with vacuolar H^+-ATPase to regulate cytosolic and lysosomal pH [82], it is tempting to suggest that the STAT3 inhibitory activity of silibinin compromises lysosomal acidification, to exert synergetic growth inhibitory effects with nintedanib. However, it should be noted that the ability of lysosomal-associated STAT3 to maintain the alkaline cytosol and acidic lysosomal lumen occurs regardless of the activating SH2 binding site phosphorylation and DNA-binding activity of STAT3 [82]. Nevertheless, the significant prevention of subcellular lysosomal trapping, which is expected to increase cytosolic drug concentrations and, thus, the multikinase inhibition-based cytotoxic potential of nintedanib, represents an unforeseen mechanism through which silibinin could increase nintedanib availability at the target site and, consequently, circumvent lung cancer cell-intrinsic nintedanib resistance.

Most of the direct STAT3 targeted agents evaluated to date have been disappointing in the clinical arena due to suboptimal potency, unfavorable pharmacokinetic properties and other concerns over the relative lack of potency and selectivity [83]. While natural pharmacological inhibitors of STAT3 such as curcumin and butein have attracted attention because of their favorable toxicity profiles, their capacity to inhibit STAT3 phosphorylation, dimerization, acetylation and DNA-binding ability has been considered indirect and non-specific [84]. Although the definition of an ideal STAT3 inhibitor for clinical use remains to be established, we took advantage of silibinin, which we have previously assessed in silico and experimentally validated with regards to its capacity to impair STAT3 activation [47–50]. Gain-of-function mutations computationally predicted to reduce the ability of silibinin to bind STAT3 with high affinity fully prevented its ability to inhibit STAT3 functionality, demonstrating the STAT3-dependency and largely eliminating the possibility

that additional potential targets of silibinin might play a role in the biological actions [50]. Encouraged by these results, the lack of toxicity of silibinin and its oral bioavailability when provided as a commercially available nutraceutical (Legasil®), we evaluated its performance in a clinical study of 18 patients with lung cancer and brain metastases, which revealed its highly significant therapeutic activity, low toxicity, reversible secondary effects and compatibility with the standard-of-care [50]. The retrospective, observational multicenter study reported here assessed the efficacy of incorporating a nutraceutical supplementation of silibinin (5 capsules/day of Legasil®—630 mg/day dose) in patients with NSCLC receiving nintedanib/docetaxel combination in second- and further-line settings. The study cohort receiving silibinin benefited from an ORR (combined rates of complete and partial responses) greater than twice that observed in the control cohort. The patients supplemented with silibinin also benefited from a 2-fold decreased risk of treatment failure in multivariate analysis. Silibinin supplementation failed to provide significant benefit in terms of overall survival, which, in addition, was numerically lower than that originally reported in the LUME-Lung 1 study. A reason for this might be selection bias arising from the selection of a higher proportion of patients with poorer prognosis in the control and study groups, possibly resulting in non-random non-response. In this regard, our findings linking the sensitizing effects of silibinin to the lysosomotropic behavior of nintedanib might be clinically relevant. Thus, although the combination approach with silibinin might circumvent intrinsic nintedanib resistance through the lysosomal system, it might also distinctly alter the pharmacokinetic properties of nintedanib via (STAT3-dependent or -independent) modification of intracellular trafficking, autophagic activity, lysosomal load, lysosome biogenesis and/or lysosome-mediated cell death. Our laboratory is currently investigating how key characteristics of the lysosomal compartment in NSCLC cells, such as lysosome number, size and/or stability might impact on nintedanib responsiveness.

Since the publication of the LUME-Lung 1 trial [2], few data have been reported for the use of the nintedanib/docetaxel combination in NSCLC. The nintedanib Named Patient Use program suggested an encouraging efficacy of nintedanib/docetaxel combination following first-line platinum-based chemotherapy and subsequent immunotherapy in a real-world setting (n = 11) [3]. The prospective, noninterventional VARGADO study, which described data from a cohort of 22 patients who received nintedanib/docetaxel after progression on ICI therapy, highlighted the potential clinical benefit of rational treatment sequencing with nintedanib after progression on ICIs [4]. The prospective, multicenter, non-interventional LUMNE-BioNIS study, which has recently presented data from 67 patients with prior immunotherapy given in first- and later- lines, has shown that when used according to the approved label in routine practice, the nintedanib/docetaxel combination showed clinically relevant effectiveness [85]. Although we recognize that a major limitation of our current clinical study is its retrospective nature and the absence of randomization to each treatment intervention, it represents, to our best knowledge, one of the largest clinical series of patients with NSCLC treated with nintedanib/docetaxel without prior immunotherapy in everyday clinical practice reported thus far.

4. Materials and Methods

4.1. Cell Lines

The human NSCLC cell lines A549 (ATCC CCL-185), H460 (ATCC HTB-177), H1993 (ATCC CRL-5909) and H1975 (ATCC CRL-5908) were obtained from the ATCC (Manassas, VA, USA). H3122 (CVCL_5160) and H2228 (ATCC CRL-5935) cell lines, which harbor the E13:A20 and E6a/b:A20 variants of the EML4-ALK fusion, respectively, were made resistant to crizotinib (H3122/CR and H2228/CR) by incremental and continuous exposure to crizotinib, as described in [53,54]. PC-9 (RRID:CVCL_B260) cells, which harbor an EGFR activating mutation (Δ746–750), were made resistant to erlotinib (PC-9/ER) by incremental and continuous exposure to erlotinib, as described in [55,56]. PC-9, H460, and H1975 were made resistant to nintedanib (PC-9/NTD-R, H460/NTD-R, and H1975/NTD-R) by prolonged culture in graded concentrations of nintedanib. Parental PC-9 cells were

obtained from the IBL cell bank (Gunma, Japan). All cells were routinely propagated in Dulbecco's modified Eagle's medium (DMEM) supplemented with 10% heat-inactivated fetal bovine serum (FBS; BioWhittaker Inc., Walkersville, MD, USA), 1% L-glutamine, 1% sodium pyruvate, 50 U/mL penicillin, and 50 µg/mL streptomycin. All cells were grown at 37 °C in a humidified atmosphere with 5% CO_2 and were in the logarithmic growth phase at the initiation of the experiments. Cell lines were authenticated by STR profiling, both performed by the manufacturer and confirmed in-house at time of purchase following ATCC guidelines. Cells were passaged by starting a low-passage cell stock every month, up to 2–3 months after resuscitation. Cell lines were regularly screened for mycoplasma contamination using the MycoAlert Mycoplasma Detection Kit (Lonza, Verviers, Belgium).

4.2. Reagents

Nintedanib (BIBF 1120) and docetaxel were obtained from Selleck Chemicals LLC (Houston, TX, USA). Silibinin was purchased from Sigma-Aldrich (St. Louis, MO, USA). All reagents were dissolved in sterile dimethylsulfoxide (DMSO) to prepare 10 mmol/L stock solutions, which were stored in aliquots at −20 °C until use. Working concentrations were diluted in culture medium prior each experiment. Antibodies against total STAT3 (124H6, Cat. No 9139), phospho-STAT3 Tyr705 (D3A7, Cat. No 9145S), and phospho-STAT3 Ser727 (Cat. No 9134) were purchased from Cell Signaling Technology (Beverly, MA, USA). Antibodies against β-actin (Clone #2D4H5, Cat. No 66009-1-Ig,) and human recombinant human IL-6 (Cat. HZ-1019-10) were purchased from Proteintech Group, Inc., Rosemont, IL, USA). Lysotracker® Red DND-99 (Cat. No L7528) was purchased from Thermo Fisher Scientific (Waltham, MA, USA). Ammonium chloride was purchased from Sigma-Aldrich (Cat. No A9434). Bafilomycin A1 was obtained from Calbiochem (Cat. No 196000).

4.3. MTT-Based Cell Viability Assays

For cell viability assays, NSCLC cells were seeded at 5×10^3 cells/well in 100 µL of growth medium in 96-well plates. After overnight culture, cells were treated for 72 h with the indicated concentrations of each compound, combinations thereof or DMSO (v/v) (control wells). Compounds were not renewed during the entire period of cell exposure. For MTT assays, experimental media was replaced with fresh culture media (100 µL) and MTT (5 mg/mL in PBS) was added to each well at a 1/10 volume. After incubation for 3 h at 37 °C, the supernatants were carefully aspirated, 100 µL of DMSO was added to each well, plates were agitated to dissolve the crystal product and the optical density was measured at 570 nm using a multi-well plate reader. Cell viability in the presence of agents was reported as a percentage of the control cell optical density, which was obtained from control wells treated with the appropriate concentration of vehicle (DMSO) and processed simultaneously. For each treatment, cell viability was evaluated using the following equation: (OD_{570} of treated sample/OD_{570} of untreated sample) × 100.

Sensitivity of NSCLC cell lines to agents was expressed in terms of the concentration of drug required to decrease cell viability by 50% cell viability (IC_{50}). Since the percentage of control absorbance was considered to be the surviving fraction of cells, the IC_{50} values were defined as the concentration of agents that produced 50% reduction in control absorbance and were estimated using non-linear regression analyses of dose-response curves.

4.4. Combination Index

The median effect analysis originally proposed by Chou and Talalay [57,58] was employed to determine the nature (synergism, additivity and antagonism) of drugs and drug interactions. Cells were treated with serial dilutions of each drug alone or with drug combinations at fixed ratios based on their corresponding IC_{50} values. The computed parameter, termed the combination index (CI), allows the quantitative determination of drug interactions at increasing levels of cell killing by classifying the tumoricidal activity as additive (CI value 1.0), synergistic (CI < 1.0), or antagonistic (CI > 1.0).

4.5. Immunoblotting

Cells were seeded in 6-well plates at 250,000 cells/well and allowed to grow overnight in maintenance cell culture media containing 10% FBS. The media were then replaced with DMEM containing 0.1% FBS with or without nintedanib and/or silibinin. Cells were incubated for a further 24 h, washed with ice-cold phosphate buffered saline (PBS), and scraped immediately after adding 30–75 µL of 2% SDS, 1% glycerol, and 5 mmol/L Tris-HCl, pH 6.8. The protein lysates were collected in 1.5 mL microcentrifuge tubes and samples were sonicated for 1 min (under ice water bath conditions) with 2 s sonication at 2 s intervals to fully lyse cells and reduce viscosity. Protein content was determined by the Bradford protein assay (Bio-Rad, Hercules, CA, USA). Sample buffer was added and extracts were boiled for 4 min at 100 °C. Equal amounts of protein were electrophoresed on 12% SDS-PAGE gels, transferred to nitrocellulose membranes and incubated with antibodies against STAT3 and phospho-STAT3 Tyr705, followed by incubation with a horseradish peroxidase-conjugated secondary antibody and chemiluminescence detection. β-actin (66009-1-Ig, Clone #2D4H5; Proteintech Group, Inc., Rosemont, IL, USA) was employed as control for protein loading.

4.6. Subcellular Fractionation

For immunoblotting of STAT3 and phospho-STAT3 Tyr705 in nuclear and cytosolic extracts, nuclei were purified using the Active Motif nuclear extract kit (Cat. No 40010 & 40410) according to the manufacturer's protocol.

4.7. Immunofluorescence Microscopy

Cells seeded on gelatin-coated glass cover slips in a 24-well plate were fixed with 4% paraformaldehyde for 15 min, washed three times with ice-cold PBS, permeabilized by adding ice-cold 100% methanol and incubated with the respective antibodies against STAT3 (1:200 dilution) and phospho-STAT3 Tyr705 (1:1000 dilution). Antibody binding was localized with either a goat anti-rabbit IgG (H+L) secondary antibody, Alexa Fluor® 594 conjugate or a goat anti-mouse IgG (H+L) secondary antibody, Alexa Fluor® 488 conjugate (both from Invitrogen). Nuclei were counterstained with Hoechst 33342. Images were obtained with a Nikon Eclipse 50i fluorescence microscope including NIS-Elements imaging software.

4.8. Nintedanib Fluorescence

4.8.1. Live Cell Fluorescence Microscopy

4×10^4 cells were seeded in 12-well plates. After 24 h, cells were treated with graded concentrations of nintedanib and intracellular drug accumulation was imaged after 3 h on a live cell microscope (Nikon Eclipse Ts2) using a 20× objective equipped with a MicroScopia Digital XM Full HD Camera. To investigate the impact of lysosomal pH on the intralysosomal accumulation of nintedanib, cells were pretreated with 100 µmol/L silibinin, 10 mmol/L NH_4Cl, 50 nmol/L bafilomycin A or 100 nmol/L LysoTracker® Red prior to exposure to nintedanib. Images were merged using ImageJ software.

4.8.2. Flow Cytometry

Nintedanib fluorescence was detected using 488 nm laser excitation wavelength (FITC channel) on a BD Accuri C6 Flow Cytometer. Data were analyzed using FCS Express 7 software (De Novo™ Software, Pasadena, CA, USA) and were depicted as mean fluorescence intensities (arbitrary units) of three independent experiments.

4.9. Real-Time Cell Growth Rate

Proliferation was measured using the xCELLigence Real Time Cell Analysis (RTCA) DP instrument (ACEA Biosciences, San Diego, CA, USA). NCSCL cells were plated at 5000 cells/well in 100 µL of fresh medium in an E-plate 16. Initial attachment and growth were continuously monitored for approximately 24 h at 37 °C and 5% CO_2 for stabilization.

Then, 100 µL of medium was removed from each well and replaced with fresh medium with or without drugs to achieve the appropriate final concentration. The plate remained in the RTCA Station for 96 h and impedance was monitored every 5 min for approximately 24 h at 37 °C and every 15 min for the next 72 h. Growth curves were plotted using the RTCA Software Package 1.2 (xCELLigence RTCA, Roche, Basel, Switzerland) and normalized to the time point of initial treatment; time-dependent cell index (CI), doubling time and slope graphs were generated as per the manufacturer's instructions. Three biological replicates were evaluated in each experiment, which permits normalization to any time point, and results can be directly viewed in the software window. We conducted the normalization at one time point before the treatment.

4.10. Colony Formation Assays

Anchorage-dependent clonogenic growth assays were performed by initially seeding NSCLC cells into six-well plates at very low densities (~100 cells/well) and culturing in the presence or absence of graded concentrations of nintedanib and/or silibinin for 10 days (without refeeding) in a humidified atmosphere with 5% CO_2, at 37 °C. Colonies were stained with crystal violet (0.5% *w*/*v*) in 80% methanol and 37% formaldehyde and the number of colonies with >50 cells/each were counted using ImageJ software.

4.11. Patients

We retrospectively reviewed all patients (n = 59) with NSCLC treated with the nintedanib/docetaxel combination in our institution (Catalan Institute of Oncology, Barcelona, Spain), which comprises three university cancer centers in Catalonia (Spain). All patients had adenocarcinoma histology and had received at least one previous systemic treatment. Patients treated between December 2014 and December 2015 were treated within the expanded compassionate program provided by Boheringer Ingelheim. Patients treated since January 2016 received treatments according to the approved indication by the Catalan Department of Health; that is, patients with advanced NSCLC adenocarcinoma histology whose tumors progressed within 9 months from the beginning of first-line treatment.

4.11.1. Silibinin Regimen

Eighteen individuals received silibinin supplementation with Legasil® (Mylan—Meda Pharma, Barcelona, Spain) at the Catalan Institute of Oncology, Hospital Universitari Dr. Josep Trueta of Girona (Spain). Each capsule of Legasil® contains 210 mg Eurosil^{85} (60% of silibinin isoforms), which, according to the product patent data, has an increased release rate (80%) and improved absorbability. A titration was started with 2 capsules of Legasil® (1-0-1) each day for the first three days of the plan and an additional capsule was then added until a 5 capsules dosage (2-2-1) was achieved or toxicity was observed. At the posology of five capsules per day of Legasil®, we provided 1050 mg of Eurosil^{85}, which equated to a 630 mg-dose-a day silibinin regimen. Diarrhea was the sole drug-related adverse reaction that could lead to Legasil® dose reduction. Once diarrhea resolved, treatment with Legasil® was reinitiated at a lower dose.

4.11.2. Outcomes Definitions

Tumor response was assessed using the Response Evaluation Criteria in Solid Tumors (RECIST), version 1.1. Efficacy analysis included all evaluable patients and the exploratory assessments analyzed were the following: overall response rate (ORR), defined as the combined rates of complete and partial responses; disease control rate (DCR), defined as the combined rates of complete response, partial response, and stable disease; time-to-treatment failure (TTF), defined as the time from date of first nintedanib/docetaxel treatment until first evidence of disease progression; overall survival (OS) since the beginning of first-line chemotherapy (OS1L), calculated from the first day of administration of first-line chemotherapy until the patient's death or last date of follow-up; and overall survival since the beginning of nintedanib/docetaxel combination (OS2L), calculated from

the first day of administration of the nintedanib/docetaxel combination until the patient's death or last date of follow-up.

4.12. Statistical Analysis

4.12.1. Cell-Based Assays

All observations were confirmed by at least three independent experiments performed in triplicate for each cell line and for each condition. Data are presented as mean ± SD. Two-group comparisons were performed using Student's *t*-test for paired and unpaired values. Comparisons of means of ≥ 3 groups were performed by ANOVA, and the existence of individual differences, in case of significant F values at ANOVA, was tested by Scheffé's multiple contrasts. p values < 0.01 and < 0.001 were considered to be statistically significant (denoted as * and **, respectively). All statistical tests were two-sided.

4.12.2. Patients

Descriptive statistical analyses were conducted as appropriate. Kaplan-Meier survival curves were constructed and log-rank tests were used to compare survival between groups. Univariate and multivariate Cox regression analyses were conducted to compare the survival date. All tests were two-sided and $p \leq 0.05$ was set as statistically significant. Statistical analyses were carried out using SPSS (release 2017, v25.0; IBM Corp., Armonk, NY, USA) and STATA (release 2013; StataCorp LP, College Station, TX, USA).

5. Conclusions

The dual activity of nintedanib as a TKI that targets not only angiogenesis in the tumor stroma, but also genetic alterations occurring in tumor cells such as those involving FGFRs and PDGFRs, has been suggested as an advantage over more selective anti-angiogenics. However, because numerous TKs share a common ability to induce downstream signaling effectors, nintedanib-treated NSCLC cells can engage feedback activation mechanisms such as STAT3, which are capable of promoting cell survival and limiting overall drug response in tumor cells themselves. Nintedanib is also among those TKIs that experience lysosomal drug sequestration as a tumor-cell intrinsic mechanism of multi-drug resistance that prevents them from reaching their targets. Here, we explored the molecular basis and the clinical benefit of incorporating silibinin—a flavonolignan extracted from milk thistle—into nintedanib-based schedules in advanced NSCLC. Molecular mechanisms dictating the cancer cell-intrinsic responsiveness to nintedanib such as STAT3 activation and lysosomal trapping were both amenable to pharmacological intervention with silibinin. The present in vitro data and clinical results should serve to accelerate the evaluation of the nutraceutical Legasil® that contains a clinically relevant formulation of silibinin as an adjunct cancer treatment to the nintedanib/docetaxel combination. A prospective, powered clinical trial is warranted to confirm the clinical relevance of these findings in patients with advanced NSCLC.

Supplementary Materials: The following are available online at https://www.mdpi.com/article/10.3390/cancers13164168/s1, Figure S1: Analysis of the cytotoxic interaction between nintedanib and silibinin in NSCLC cells with acquired resistance to erlotinib and crizotinib; Figure S2: Analysis of the cytotoxic interaction between docetaxel, nintedanib, and silibinin in NSCLC cells with acquired resistance to erlotinib and crizotinib; Figure S3: Effects of silibinin on the intracellular distribution of STAT3 and phospho-STAT3^{Tyr705}; Figure S4: Effects of nintedanib and silibinin on the intracellular distribution of STAT3 and phospho-STAT3^{Tyr705}; Figure S5: Effects of silibinin on the lysosomal sequestration of nintedanib in nintedanib-sensitive NSCLC tumor cells; Figure S6: Comparative analysis of the effects of silibinin and alkalizing agents on the lysosomal sequestration of nintedanib in nintedanib-resistant NSCLC tumor cells; Figure S7: Real-time monitoring of cell proliferation in response to nintedanib, silibinin, and/or docetaxel; Figure S8: Impact of the silibinin-containing nutraceutical Legasil® on the clinical efficacy of the nintedanib/docetaxel combination in advanced lung carcinoma.

Author Contributions: Conceptualization, J.B.-B. and J.A.M.; methodology, J.B.-B., S.V., M.B. and J.A.M.; formal analysis, J.B.-B., S.V., M.B. and J.A.M.; investigation, J.B.-B., S.V., J.C.R., E.C. (Enric Carcereny), E.S., E.C. (Elisabet Cuyàs), R.P., E.L.-B., G.O., A.H.-M., A.I., T.M., E.N.; validation, J.B.-B., S.V., J.C.R., Enric Carcenery, E.S., Elisabet Cuyàs., R.P., E.L.-B., A.H.-M., A.I., T.M., E.N. and J.A.M.; data curation, J.B.-B., S.V., M.B. and J.A.M.; writing—original draft preparation, J.B.-B., S.V., M.B., E.N. and J.A.M.; writing—review and editing, J.A.M.; visualization, J.B.-B. and J.A.M.; supervision, J.B.-B. and J.A.M.; funding acquisition, J.B.-B. and J.A.M. All authors have read and agreed to the published version of the manuscript.

Funding: Work in the Menendez laboratory is supported by the Spanish Ministry of Science and Innovation (Grants SAF2016-80639-P and PID2019-104055GB-I00, Plan Nacional de I+D+I, founded by the European Regional Development Fund, Spain) and by an unrestricted research grant from the Fundació Oncolliga Girona (Lliga catalana d'ajuda al malalt de càncer, Girona). Joaquim Bosch-Barrera is the recipient of Research Grants from Grupo Español de Cáncer de Pulmón (GECP), La Marató de TV3 foundation (201906), and the Health Research and Innovation Strategic Plan (SLT006/17/114; PERIS 2016-2020; Pla stratègic de recerca i innovació en salut; Departament de Salut, Generalitat de Catalunya). Elisabet Cuyàs holds a research contract "Miguel Servet" (CP20/00003) from the Instituto de Salud Carlos III, Spanish Ministry of Science and Innovation (Spain). The authors would like to heartily thank König (www.konig.cat, access date 30 May 2021) for their generous donation to fund our cancer research on silibinin in Girona.

Institutional Review Board Statement: The experimental protocol was approved by the Ethics Committee of the Hospital Universitari Dr. Josep Trueta (CEA.HUJT:17/06). We certify that all applicable institutional regulations concerning the ethical use of information from human patients were followed during this research.

Informed Consent Statement: All individuals gave written informed consent.

Data Availability Statement: The data that support the findings of this study are available from the corresponding authors, upon reasonable request.

Acknowledgments: We are greatly indebted to Daniel B. Costa (Beth Israel Deaconess Medical Center, Harvard Medical School) for providing the H3122 and H3122/CR cells, and to Jae Cheol Lee (Department of Thoracic and Cardiovascular Surgery, Asian Medical Center, College of Medicine, University of Ulsan, Seoul, Republic of Korea) for providing the H2228 and H2228/CR cells used in this work. The authors would like to thank Kenneth McCreath for editorial support.

Conflicts of Interest: J.B.-B. reports grants and personal fees from Roche-Genentech, grants from Pfizer and Pierre Fabre, and personal fees from MSD, BMS, AstraZeneca, Boehringer-Ingelheim, and Novartis, outside the submitted work. Enric Carcenery. reports speaker, advisory role from Roche, BMS, MSD, Pfizer, AstraZeneca, Boehringer-Ingelheim, Takeda, and Novartis, outside the submitted work. Enric Carcenery. reports also travel expenses from Roche, Pfizer, and Takeda. T.M. reports personal fees (lectures, travel grants) from Roche-Genentech, BMS, AstraZeneca, Boehringer-Ingelheim, and research grants from Kyowa Kirin, outside the submitted work. This study was supported in part by a research grant from Boehringer-Ingelheim to J.B.-B. The authors declare that the research was conducted in the absence of any commercial or financial relationships that could be construed as a potential conflict of interest.

References

1. Hilberg, F.; Roth, G.J.; Krssak, M.; Kautschitsch, S.; Sommergruber, W.; Tontsch-Grunt, U.; Garin-Chesa, P.; Bader, G.; Zoephel, A.; Quant, J.; et al. BIBF 1120: Triple Angiokinase Inhibitor with Sustained Receptor Blockade and Good Antitumor Efficacy. *Cancer Res.* **2008**, *68*, 4774–4782. [CrossRef]
2. Reck, M.; Kaiser, R.; Mellemgaard, A.; Douillard, J.-Y.; Orlov, S.; Krzakowski, M.; von Pawel, J.; Gottfried, M.; Bondarenko, I.; Liao, M.; et al. Docetaxel plus nintedanib versus docetaxel plus placebo in patients with previously treated non-small-cell lung cancer (LUME-Lung 1): A phase 3, double-blind, randomised controlled trial. *Lancet Oncol.* **2014**, *15*, 143–155. [CrossRef]
3. Corral, J.; Majem, M.; Rodríguez-Abreu, D.; Carcereny, E.; Cortes, Á.A.; Llorente, M.; Picazo, J.M.L.; Garcia, Y.G.; Domine, M.; Criado, M.P.L. Efficacy of nintedanib and docetaxel in patients with advanced lung adenocarcinoma treated with first-line chemotherapy and second-line immunotherapy in the nintedanib NPU program. *Clin. Transl. Oncol.* **2019**, *21*, 1270–1279. [CrossRef]

4. Grohé, C.; Gleiber, W.; Haas, S.; Losem, C.; Mueller-Huesmann, H.; Schulze, M.; Franke, C.; Basara, N.; Atz, J.; Kaiser, R. Nintedanib plus docetaxel after progression on immune checkpoint inhibitor therapy: Insights from VARGADO, a prospective study in patients with lung adenocarcinoma. *Future Oncol.* **2019**, *15*, 2699–2706. [CrossRef] [PubMed]
5. Navarro, P.; Bueno, M.J.; Zagorac, I.; Mondejar, T.; Sanchez, J.; Mourón, S.; Munoz, J.; López, G.G.; Jimenez-Renard, V.; Mulero, F.; et al. Targeting Tumor Mitochondrial Metabolism Overcomes Resistance to Antiangiogenics. *Cell Rep.* **2016**, *15*, 2705–2718. [CrossRef]
6. Quintela-Fandino, M. Normoxic or hypoxic adaptation in response to antiangiogenic therapy: Clinical implications. *Mol. Cell. Oncol.* **2016**, *3*, e1217368. [CrossRef]
7. Bueno, M.J.; Mouron, S.; Quintela-Fandino, M. Personalising and targeting antiangiogenic resistance: A complex and multifactorial approach. *Br. J. Cancer* **2017**, *116*, 1119–1125. [CrossRef] [PubMed]
8. Sonveaux, P.; Vegran, F.; Schroeder, T.; Wergin, M.C.; Verrax, J.; Rabbani, Z.N.; De Saedeleer, C.J.; Kennedy, K.M.; Diepart, C.; Jordan, B.F.; et al. Targeting lactate-fueled respiration selectively kills hypoxic tumor cells in mice. *J. Clin. Investig.* **2008**, *118*, 3930–3942. [CrossRef] [PubMed]
9. Porporato, P.E.; Dhup, S.; Dadhich, R.K.; Copetti, T.; Sonveaux, P. Anticancer Targets in the Glycolytic Metabolism of Tumors: A Comprehensive Review. *Front. Pharmacol.* **2011**, *2*, 49. [CrossRef] [PubMed]
10. Pisarsky, L.; Bill, R.; Fagiani, E.; Dimeloe, S.; Goosen, R.W.; Hagmann, J.; Hess, C.; Christofori, G. Targeting Metabolic Symbiosis to Overcome Resistance to Anti-angiogenic Therapy. *Cell Rep.* **2016**, *15*, 1161–1174. [CrossRef]
11. Jiménez-Valerio, G.; Martínez-Lozano, M.; Bassani, N.; Vidal, A.; Ochoa-De-Olza, M.; Suárez, C.; García-Del-Muro, X.; Carles, J.; Viñals, F.; Graupera, M.; et al. Resistance to Antiangiogenic Therapies by Metabolic Symbiosis in Renal Cell Carcinoma PDX Models and Patients. *Cell Rep.* **2016**, *15*, 1134–1143. [CrossRef] [PubMed]
12. Allen, E.; Miéville, P.; Warren, C.M.; Saghafinia, S.; Li, L.; Peng, M.-W.; Hanahan, D. Metabolic Symbiosis Enables Adaptive Resistance to Anti-angiogenic Therapy that Is Dependent on mTOR Signaling. *Cell Rep.* **2016**, *15*, 1144–1160. [CrossRef] [PubMed]
13. Jiménez-Valerio, G.; Casanovas, O. Angiogenesis and Metabolism: Entwined for Therapy Resistance. *Trends Cancer* **2017**, *3*, 10–18. [CrossRef]
14. Jiménez-Valerio, G.; Casanovas, O. Antiangiogenic resistance via metabolic symbiosis. *Mol. Cell. Oncol.* **2016**, *3*, e1211979. [CrossRef]
15. Quintela-Fandino, M.; Lluch, A.; Manso, L.; Calvo, I.; Cortes, J.; García-Saenz, J.A.; Gil-Gil, M.; Martinez-Jánez, N.; Gonzalez-Martin, A.; Adrover, E.; et al. (18)F-fluoromisonidazole PET and Activity of Neoadjuvant Nintedanib in Early HER2-Negative Breast Cancer: A Window-of-Opportunity Randomized Trial. *Clin. Cancer Res.* **2017**, *23*, 1432–1441. [CrossRef] [PubMed]
16. Richeldi, L.; Costabel, U.; Selman, M.; Kim, D.S.; Hansell, D.M.; Nicholson, A.G.; Brown, K.K.; Flaherty, K.R.; Noble, P.W.; Raghu, G.; et al. Efficacy of a Tyrosine Kinase Inhibitor in Idiopathic Pulmonary Fibrosis. *N. Engl. J. Med.* **2011**, *365*, 1079–1087. [CrossRef]
17. Hostettler, K.E.; Zhong, J.; Papakonstantinou, E.; Karakiulakis, G.; Tamm, M.; Seidel, P.; Sun, Q.; Mandal, J.; Lardinois, D.; Lambers, C.; et al. Anti-fibrotic effects of nintedanib in lung fibroblasts derived from patients with idiopathic pulmonary fibrosis. *Respir. Res.* **2014**, *15*, 1–9. [CrossRef]
18. Atanelishvili, I.; Akter, T.; Noguchi, A.; Vuyiv, O.; Wollin, L.; Silver, R.M.; Bogatkevich, G.S. Antifibrotic efficacy of nintedanib in a cellular model of systemic sclerosis-associated interstitial lung disease. *Clin. Exp. Rheumatol.* **2019**, *37* (Suppl. S119), 115–124.
19. Li, X.; Liu, X.; Deng, R.; Gao, S.; Yu, H.; Huang, K.; Jiang, Q.; Liu, R.; Li, X.; Zhang, L.; et al. Nintedanib Inhibits Wnt3a-Induced Myofibroblast Activation by Suppressing the Src/β-Catenin Pathway. *Front. Pharmacol.* **2020**, *11*, 310. [CrossRef]
20. Glass, D.S.; Grossfeld, D.; Renna, H.A.; Agarwala, P.; Spiegler, P.; Kasselman, L.J.; Glass, A.D.; DeLeon, J.; Reiss, A.B. Idiopathic pulmonary fibrosis: Molecular mechanisms and potential treatment approaches. *Respir. Investig.* **2020**, *58*, 320–335. [CrossRef]
21. Awasthi, N.; Hinz, S.; Brekken, R.A.; Schwarz, M.A.; Schwarz, R.E. Nintedanib, a triple angiokinase inhibitor, enhances cytotoxic therapy response in pancreatic cancer. *Cancer Lett.* **2015**, *358*, 59–66. [CrossRef]
22. Hibi, M.; Kaneda, H.; Tanizaki, J.; Sakai, K.; Togashi, Y.; Terashima, M.; De Velasco, M.; Fujita, Y.; Banno, E.; Nakamura, Y.; et al. FGFR gene alterations in lung squamous cell carcinoma are potential targets for the multikinase inhibitor nintedanib. *Cancer Sci.* **2016**, *107*, 1667–1676. [CrossRef]
23. Hilberg, F.; Tontsch-Grunt, U.; Baum, A.; Le, A.T.; Doebele, R.C.; Lieb, S.; Gianni, D.; Voss, T.; Garin-Chesa, P.; Haslinger, C.; et al. Triple Angiokinase Inhibitor Nintedanib Directly Inhibits Tumor Cell Growth and Induces Tumor Shrinkage via Blocking Oncogenic Receptor Tyrosine Kinases. *J. Pharmacol. Exp. Ther.* **2018**, *364*, 494–503. [CrossRef] [PubMed]
24. Tai, W.-T.; Shiau, C.-W.; Li, Y.-S.; Chang, C.-W.; Huang, J.-W.; Hsueh, T.-T.; Yu, H.-C.; Chen, K.-F. Nintedanib (BIBF-1120) inhibits hepatocellular carcinoma growth independent of angiokinase activity. *J. Hepatol.* **2014**, *61*, 89–97. [CrossRef] [PubMed]
25. Vignais, M.L.; Sadowski, H.B.; Watling, D.; Rogers, N.; Gilman, M. Platelet-derived growth factor induces phosphorylation of multiple JAK family kinases and STAT proteins. *Mol. Cell. Biol.* **1996**, *16*, 1759–1769. [CrossRef] [PubMed]
26. Vignais, M.L.; Gilman, M. Distinct Mechanisms of Activation of Stat1 and Stat3 by Platelet-Derived Growth Factor Receptor in a Cell-Free System. *Mol. Cell. Biol.* **1999**, *19*, 3727–3735. [CrossRef] [PubMed]
27. Yan, J.-F.; Huang, W.-J.; Zhao, J.-F.; Fu, H.-Y.; Zhang, G.-Y.; Huang, X.-J.; Lv, B.-D. The platelet-derived growth factor receptor/STAT3 signaling pathway regulates the phenotypic transition of corpus cavernosum smooth muscle in rats. *PLoS ONE* **2017**, *12*, e0172191. [CrossRef]

28. Bohrer, L.R.; Chuntova, P.; Bade, L.K.; Beadnell, T.C.; Leon, R.P.; Brady, N.; Ryu, Y.; Goldberg, J.E.; Schmechel, S.C.; Koopmeiners, J.S.; et al. Activation of the FGFR—STAT3 Pathway in Breast Cancer Cells Induces a Hyaluronan-Rich Microenvironment That Licenses Tumor Formation. *Cancer Res.* **2014**, *74*, 374–386. [CrossRef]
29. Li, P.; Huang, T.; Zou, Q.; Liu, D.; Wang, Y.; Tan, X.; Wei, Y.; Qiu, H. FGFR2 Promotes Expression of PD-L1 in Colorectal Cancer via the JAK/STAT3 Signaling Pathway. *J. Immunol.* **2019**, *202*, 3065–3075. [CrossRef]
30. Garcia, R.; Bowman, T.L.; Niu, G.; Yu, H.; Minton, S.; A Muro-Cacho, C.; E Cox, C.; Falcone, R.; Fairclough, R.; Parsons, S.; et al. Constitutive activation of Stat3 by the Src and JAK tyrosine kinases participates in growth regulation of human breast carcinoma cells. *Oncogene* **2001**, *20*, 2499–2513. [CrossRef]
31. Byers, L.A.; Sen, B.; Saigal, B.; Diao, L.; Wang, J.; Nanjundan, M.; Cascone, T.; Mills, G.B.; Heymach, J.V.; Johnson, F.M. Reciprocal Regulation of c-Src and STAT3 in Non-Small Cell Lung Cancer. *Clin. Cancer Res.* **2009**, *15*, 6852–6861. [CrossRef] [PubMed]
32. Demaria, M.; Giorgi, C.; Lebiedzińska-Arciszewska, M.; Esposito, G.; D'Angeli, L.; Bartoli, A.; Gough, D.; Turkson, J.; Levy, D.; Watson, C.J.; et al. A STAT3-mediated metabolic switch is involved in tumour transformation and STAT3 addiction. *Aging* **2010**, *2*, 823–842. [CrossRef] [PubMed]
33. Camporeale, A.; Demaria, M.; Monteleone, E.; Giorgi, C.; Wieckowski, M.R.; Pinton, P.; Poli, V. STAT3 Activities and Energy Metabolism: Dangerous Liaisons. *Cancers* **2014**, *6*, 1579–1596. [CrossRef]
34. Demaria, M.; Camporeale, A.; Poli, V. STAT3 and metabolism: How many ways to use a single molecule? *Int. J. Cancer* **2014**, *135*, 1997–2003. [CrossRef]
35. Poli, V.; Camporeale, A. STAT3-Mediated Metabolic Reprograming in Cellular Transformation and Implications for Drug Resistance. *Front. Oncol.* **2015**, *5*, 121. [CrossRef] [PubMed]
36. Lee, M.; Hirpara, J.L.; Eu, J.-Q.; Sethi, G.; Wang, L.; Goh, B.-C.; Wong, A.L. Targeting STAT3 and oxidative phosphorylation in oncogene-addicted tumors. *Redox Biol.* **2019**, *25*, 101073. [CrossRef]
37. Furtek, S.L.; Backos, D.; Matheson, C.J.; Reigan, P. Strategies and Approaches of Targeting STAT3 for Cancer Treatment. *ACS Chem. Biol.* **2016**, *11*, 308–318. [CrossRef]
38. Siveen, K.S.; Sikka, S.; Surana, R.; Dai, X.; Zhang, J.; Kumar, A.P.; Tan, B.K.; Sethi, G.; Bishayee, A. Targeting the STAT3 signaling pathway in cancer: Role of synthetic and natural inhibitors. *Biochim. Biophys. Acta (BBA) Bioenerg.* **2014**, *1845*, 136–154. [CrossRef]
39. Zhao, M.; Jiang, B.; Gao, F.-H. Small molecule inhibitors of STAT3 for cancer therapy. *Curr. Med. Chem.* **2011**, *18*, 4012–4018. [CrossRef]
40. Masciocchi, D.; Gelain, A.; Villa, S.; Meneghetti, F.; Barlocco, D. Signal transducer and activator of transcription 3 (STAT3): A promising target for anticancer therapy. *Futur. Med. Chem.* **2011**, *3*, 567–597. [CrossRef]
41. Shih, P.-C. Revisiting the development of small molecular inhibitors that directly target the signal transducer and activator of transcription 3 (STAT3) domains. *Life Sci.* **2020**, *242*, 117241. [CrossRef] [PubMed]
42. Gelain, A.; Mori, M.; Meneghetti, F.; Villa, S. Signal Transducer and Activator of Transcription Protein 3 (STAT3): An Update on its Direct Inhibitors as Promising Anticancer Agents. *Curr. Med. Chem.* **2019**, *26*, 5165–5206. [CrossRef] [PubMed]
43. Kim, N.-C.; Graf, T.N.; Sparacino, C.M.; Wani, M.C.; Wall, M.E. Complete isolation and characterization of silybins and isosilybins from milk thistle (*Silybum marianum*). *Org. Biomol. Chem.* **2003**, *1*, 1684–1689. [CrossRef]
44. Gazák, R.; Walterova, D.; Kren, V. Silybin and Silymarin—New and Emerging Applications in Medicine. *Curr. Med. Chem.* **2007**, *14*, 315–338. [CrossRef]
45. Bijak, M. Silybin, a Major Bioactive Component of Milk Thistle (*Silybum marianum* L. Gaernt.)—Chemistry, Bioavailability, and Metabolism. *Molecules* **2017**, *22*, 1942. [CrossRef]
46. Abenavoli, L.; Izzo, A.A.; Milić, N.; Cicala, C.; Santini, A.; Capasso, R. Milk thistle (*Silybum marianum*): A concise overview on its chemistry, pharmacological, and nutraceutical uses in liver diseases. *Phytother. Res.* **2018**, *32*, 2202–2213. [CrossRef]
47. Verdura, S.; Cuyàs, E.; Llorach-Pares, L.; Pérez-Sánchez, A.; Micol, V.; Nonell-Canals, A.; Joven, J.; Valiente, M.; Sanchez-Martinez, M.; Bosch-Barrera, J.; et al. Silibinin is a direct inhibitor of STAT3. *Food Chem. Toxicol.* **2018**, *116*, 161–172. [CrossRef] [PubMed]
48. Pérez-Sánchez, A.; Cuyàs, E.; Ruiz-Torres, V.; Agulló-Chazarra, L.; Verdura, S.; González-Álvarez, I.; Bermejo, M.; Joven, J.; Micol, V.; Bosch-Barrera, J.; et al. Intestinal Permeability Study of Clinically Relevant Formulations of Silibinin in Caco-2 Cell Monolayers. *Int. J. Mol. Sci.* **2019**, *20*, 1606. [CrossRef]
49. Bosch-Barrera, J.; Sais, E.; Cañete, N.; Marruecos, J.; Cuyàs, E.; Izquierdo, A.; Porta, R.; Haro, M.; Brunet, J.; Pedraza, S.; et al. Response of brain metastasis from lung cancer patients to an oral nutraceutical product containing silibinin. *Oncotarget* **2016**, *7*, 32006–32014. [CrossRef]
50. Priego, N.; Zhu, L.; Monteiro, C.; Mulders, M.; Wasilewski, D.; Bindeman, W.; Doglio, L.; Martínez, L.; Martínez-Saez, E.; Ramón YCajal, S.; et al. STAT3 labels a subpopulation of reactive astrocytes required for brain metastasis. *Nat. Med.* **2018**, *24*, 1024–1035. [CrossRef]
51. Bosch-Barrera, J.; Menendez, J. Silibinin and STAT3: A natural way of targeting transcription factors for cancer therapy. *Cancer Treat. Rev.* **2015**, *41*, 540–546. [CrossRef]
52. Bosch-Barrera, J.; Queralt, B.; Menendez, J. Targeting STAT3 with silibinin to improve cancer therapeutics. *Cancer Treat. Rev.* **2017**, *58*, 61–69. [CrossRef]
53. Yamaguchi, N.; Lucena-Araujo, A.R.; Nakayama, S.; Pontes, L.L.D.F.; Gonzalez, D.A.; Yasuda, H.; Kobayashi, S.; Costa, D.B. Dual ALK and EGFR inhibition targets a mechanism of acquired resistance to the tyrosine kinase inhibitor crizotinib in ALK rearranged lung cancer. *Lung Cancer* **2014**, *83*, 37–43. [CrossRef] [PubMed]

54. Kim, H.R.; Kim, W.S.; Choi, Y.J.; Choi, C.M.; Rho, J.K.; Lee, J.C. Epithelial-mesenchymal transition leads to crizotinib resistance in H2228 lung cancer cells with EML4-ALK translocation. *Mol. Oncol.* **2013**, *7*, 1093–1102. [CrossRef] [PubMed]
55. Vazquez-Martin, A.; Cufí, S.; Oliveras-Ferraros, C.; Torres-Garcia, V.Z.; Corominas-Faja, B.; Cuyàs, E.; Bonavia, R.; Visa, J.; Martín-Castillo, B.; Barrajón-Catalán, E.; et al. IGF-1R/epithelial-to-mesenchymal transition (EMT) crosstalk suppresses the erlotinib-sensitizing effect of EGFR exon 19 deletion mutations. *Sci. Rep.* **2013**, *3*, srep02560. [CrossRef] [PubMed]
56. Corominas-Faja, B.; Oliveras-Ferraros, C.; Cuyàs, E.; Segura-Carretero, A.; Joven, J.; Martin-Castillo, B.; Barrajón-Catalán, E.; Micol, V.; Bosch-Barrera, J.; Menendez, J.A. Stem cell-like ALDH(bright) cellular states in EGFR-mutant non-small cell lung cancer: A novel mechanism of acquired resistance to erlotinib targetable with the natural polyphenol silibinin. *Cell Cycle* **2013**, *12*, 3390–3404. [CrossRef]
57. Chou, T.C. Drug Combination Studies and Their Synergy Quantification Using the Chou-Talalay Method. *Cancer Res.* **2010**, *70*, 440–446. [CrossRef]
58. Chou, T.-C. Theoretical Basis, Experimental Design, and Computerized Simulation of Synergism and Antagonism in Drug Combination Studies. *Pharmacol. Rev.* **2006**, *58*, 621–681. [CrossRef]
59. Englinger, B.; Kallus, S.; Senkiv, J.; Heilos, D.; Gabler, L.; Van Schoonhoven, S.; Terenzi, A.; Moser, P.; Pirker, C.; Timelthaler, G.; et al. Intrinsic fluorescence of the clinically approved multikinase inhibitor nintedanib reveals lysosomal sequestration as resistance mechanism in FGFR-driven lung cancer. *J. Exp. Clin. Cancer Res.* **2017**, *36*, 122. [CrossRef]
60. Geisslinger, F.; Müller, M.; Vollmar, A.M.; Bartel, K. Targeting Lysosomes in Cancer as Promising Strategy to Overcome Chemoresistance—A Mini Review. *Front. Oncol.* **2020**, *10*, 1156. [CrossRef] [PubMed]
61. Lee, H.-J.; Zhuang, G.; Cao, Y.; Du, P.; Kim, H.-J.; Settleman, J. Drug Resistance via Feedback Activation of Stat3 in Oncogene-Addicted Cancer Cells. *Cancer Cell* **2014**, *26*, 207–221. [CrossRef] [PubMed]
62. Giuliano, S.; Cormerais, Y.; Dufies, M.; Grépin, R.; Colosetti, P.; Belaid, A.; Parola, J.; Martin, A.; Lacas-Gervais, S.; Mazure, N.M.; et al. Resistance to sunitinib in renal clear cell carcinoma results from sequestration in lysosomes and inhibition of the autophagic flux. *Autophagy* **2015**, *11*, 1891–1904. [CrossRef] [PubMed]
63. Llanos, S.; Megias, D.; Blanco-Aparicio, C.; Hernández-Encinas, E.; Rovira, M.; Pietrocola, F.; Serrano, M. Lysosomal trapping of palbociclib and its functional implications. *Oncogene* **2019**, *38*, 3886–3902. [CrossRef]
64. Fassl, A.; Brain, C.; Abu-Remaileh, M.; Stukan, I.; Butter, D.; Stepien, P.; Feit, A.S.; Bergholz, J.; Michowski, W.; Otto, T.; et al. Increased lysosomal biomass is responsible for the resistance of triple-negative breast cancers to CDK4/6 inhibition. *Sci. Adv.* **2020**, *6*, eabb2210. [CrossRef] [PubMed]
65. Halaby, R. Influence of lysosomal sequestration on multidrug resistance in cancer cells. *Cancer Drug Resist.* **2019**, *2*, 31–42. [CrossRef]
66. Hraběta, J.; Belhajová, M.; Šubrtová, H.; Rodrigo, M.A.M.; Heger, Z.; Eckschlager, T. Drug Sequestration in Lysosomes as One of the Mechanisms of Chemoresistance of Cancer Cells and the Possibilities of Its Inhibition. *Int. J. Mol. Sci.* **2020**, *21*, 4392. [CrossRef]
67. Simon, T.; Coquerel, B.; Petit, A.; Kassim, Y.; Demange, E.; Le Cerf, D.; Perrot, V.; Vannier, J.-P. Direct Effect of Bevacizumab on Glioblastoma Cell Lines In Vitro. *NeuroMolecular Med.* **2014**, *16*, 752–771. [CrossRef]
68. Simon, T.; Gagliano, T.; Giamas, G. Direct Effects of Anti-Angiogenic Therapies on Tumor Cells: VEGF Signaling. *Trends Mol. Med.* **2017**, *23*, 282–292. [CrossRef]
69. Tomida, C.; Yamagishi, N.; Nagano, H.; Uchida, T.; Ohno, A.; Hirasaka, K.; Nikawa, T.; Teshima-Kondo, S. VEGF pathway-targeting drugs induce evasive adaptation by activation of neuropilin-1/cMet in colon cancer cells. *Int. J. Oncol.* **2018**, *52*, 1350–1362. [CrossRef]
70. Dudka, A.A.; Sweet, S.M.M.; Heath, J.K. Signal Transducers and Activators of Transcription-3 Binding to the Fibroblast Growth Factor Receptor Is Activated by Receptor Amplification. *Cancer Res.* **2010**, *70*, 3391–3401. [CrossRef]
71. Zhitomirsky, B.; Assaraf, Y.G. Lysosomes as mediators of drug resistance in cancer. *Drug Resist. Updates* **2016**, *24*, 23–33. [CrossRef]
72. Zhitomirsky, B.; Assaraf, Y.G. Lysosomal accumulation of anticancer drugs triggers lysosomal exocytosis. *Oncotarget* **2017**, *8*, 45117–45132. [CrossRef] [PubMed]
73. Yousefi, M.; Ghaffari, S.H.; Zekri, A.; Hassani, S.; Alimoghaddam, K.; Ghavamzadeh, A. Silibinin induces apoptosis and inhibits proliferation of estrogen receptor (ER)-negative breast carcinoma cells through suppression of nuclear factor kappa B activation. *Arch. Iran. Med.* **2014**, *17*, 366–371.
74. Borsari, M.; Gabbi, C.; Ghelfi, F.; Grandi, R.; Saladini, M.; Severi, S.; Borella, F. Silybin, a new iron-chelating agent. *J. Inorg. Biochem.* **2001**, *85*, 123–129. [CrossRef]
75. Kovacevic, Z.; Kalinowski, D.S.; Lovejoy, D.B.; Yu, Y.; Rahmanto, Y.S.; Sharpe, P.C.; Bernhardt, P.V.; Richardson, D.R. The medicinal chemistry of novel iron chelators for the treatment of cancer. *Curr. Top. Med. Chem.* **2011**, *11*, 483–499. [CrossRef] [PubMed]
76. Gharagozloo, M.; Khoshdel, Z.; Amirghofran, Z. The effect of an iron (III) chelator, silybin, on the proliferation and cell cycle of Jurkat cells: A comparison with desferrioxamine. *Eur. J. Pharmacol.* **2008**, *589*, 1–7. [CrossRef] [PubMed]
77. Hutchinson, C.; Bomford, A.; A Geissler, C. The iron-chelating potential of silybin in patients with hereditary haemochromatosis. *Eur. J. Clin. Nutr.* **2010**, *64*, 1239–1241. [CrossRef] [PubMed]
78. Moayedi Esfahani, B.A.; Reisi, N.; Mirmoghtadaei, M. Evaluating the safety and efficacy of silymarin in β-thalassemia patients: A review. *Hemoglobin* **2015**, *39*, 75–80. [CrossRef] [PubMed]

79. Ravikumar Reddy, D.; Khurana, A.; Bale, S.; Ravirala, R.; Samba Siva Reddy, V.; Mohankumar, M.; Godugu, C. Natural flavonoids silymarin and quercetin improve the brain distribution of co-administered P-gp substrate drugs. *SpringerPlus* **2016**, *5*, 1618. [CrossRef]
80. Abdallah, H.; Al-Abd, A.; El-Dine, R.S.; El-Halawany, A.M. P-glycoprotein inhibitors of natural origin as potential tumor chemo-sensitizers: A review. *J. Adv. Res.* **2015**, *6*, 45–62. [CrossRef] [PubMed]
81. Lloyd-Lewis, B.; Krueger, C.C.; Sargeant, T.; D'Angelo, M.; Deery, M.J.; Feret, R.; Howard, J.A.; Lilley, K.S.; Watson, C.J. Stat3-mediated alterations in lysosomal membrane protein composition. *J. Biol. Chem.* **2018**, *293*, 4244–4261. [CrossRef] [PubMed]
82. Liu, B.; Palmfeldt, J.; Lin, L.; Colaco, A.; Clemmensen, K.K.B.; Huang, J.; Xu, F.; Liu, X.; Maeda, K.; Luo, Y.; et al. STAT3 associates with vacuolar H+-ATPase and regulates cytosolic and lysosomal pH. *Cell Res.* **2018**, *28*, 996–1012. [CrossRef] [PubMed]
83. Wong, A.L.; Hirpara, J.L.; Pervaiz, S.; Eu, J.-Q.; Sethi, G.; Goh, B.-C. Do STAT3 inhibitors have potential in the future for cancer therapy? *Expert Opin. Investig. Drugs* **2017**, *26*, 883–887. [CrossRef]
84. Chai, E.Z.P.; Shanmugam, M.K.; Arfuso, F.; Dharmarajan, A.; Wang, C.; Kumar, A.P.; Samy, R.P.; Lim, L.; Wang, L.; Goh, B.C.; et al. Targeting transcription factor STAT3 for cancer prevention and therapy. *Pharmacol. Ther.* **2016**, *162*, 86–97. [CrossRef] [PubMed]
85. Reck, M.; Syrigos, L.; Miliasukas, S.; Zöchbauer-Müller, S.; Buchner, H.; Kitzing, T.; Kerr, K.M. 80P- Nintedanib (N) + docetaxel (D) after immunotherapy in adenocarcinoma non-small cell lung cancer (NSCLC): First results from the non-interventional LUME-BioNIS study. *Ann. Oncol.* **2019**, *30*, xi28–xi29. [CrossRef]

STUDY 4

Silibinin Suppresses the Hyperlipidemic Effects of the ALK-Tyrosine Kinase Inhibitor Lorlatinib in Hepatic Cells

Verdura S, Encinar JA, Fernández-Arroyo S, Joven J, Cuyàs E, Bosch-Barrera J, Menendez JA.

Int J Mol Sci. 2022 Sep 1;23(17):9986

doi: 10.3390/ijms23179986

International Journal of
Molecular Sciences

MDPI

Article

Silibinin Suppresses the Hyperlipidemic Effects of the ALK-Tyrosine Kinase Inhibitor Lorlatinib in Hepatic Cells

Sara Verdura [1,2], José Antonio Encinar [3], Salvador Fernández-Arroyo [4,5], Jorge Joven [4,5], Elisabet Cuyàs [1,2,*], Joaquim Bosch-Barrera [2,6,7] and Javier A. Menendez [1,2,*]

1 Metabolism and Cancer Group, Program Against Cancer Therapeutic Resistance (ProCURE), Catalan Institute of Oncology, 17007 Girona, Spain
2 Girona Biomedical Research Institute (IDIBGI), Salt, 17190 Girona, Spain
3 Institute of Research, Development and Innovation in Biotechnology of Elche (IDiBE) and Molecular and Cell Biology Institute (IBMC), Miguel Hernández University (UMH), 03207 Elche, Spain
4 Department of Medicine and Surgery, Universitat Rovira i Virgili, 43204 Reus, Spain
5 Unitat de Recerca Biomèdica (URB-CRB), Hospital Universitari de Sant Joan, Institut d'Investigació Sanitaria Pere Virgili, Universitat Rovira i Virgili, 43204 Reus, Spain
6 Medical Oncology, Catalan Institute of Oncology, 17007 Girona, Spain
7 Department of Medical Sciences, Medical School, University of Girona, 17071 Girona, Spain
* Correspondence: ecuyas@idibgi.org (E.C.); jmenendez@idibgi.org (J.A.M.)

Abstract: The third-generation anaplastic lymphoma tyrosine kinase inhibitor (ALK-TKI) lorlatinib has a unique side effect profile that includes hypercholesteremia and hypertriglyceridemia in >80% of lung cancer patients. Here, we tested the hypothesis that lorlatinib might directly promote the accumulation of cholesterol and/or triglycerides in human hepatic cells. We investigated the capacity of the hepatoprotectant silibinin to modify the lipid-modifying activity of lorlatinib. To predict clinically relevant drug–drug interactions if silibinin were used to clinically manage lorlatinib-induced hyperlipidemic effects in hepatic cells, we also explored the capacity of silibinin to interact with and block CYP3A4 activity using in silico computational descriptions and in vitro biochemical assays. A semi-targeted ultrahigh pressure liquid chromatography accurate mass quadrupole time-of-flight mass spectrometry with electrospray ionization (UHPLC-ESI-QTOF-MS/MS)-based lipidomic approach revealed that short-term treatment of hepatic cells with lorlatinib promotes the accumulation of numerous molecular species of cholesteryl esters and triglycerides. Silibinin treatment significantly protected the steady-state lipidome of hepatocytes against the hyperlipidemic actions of lorlatinib. Lipid staining confirmed the ability of lorlatinib to promote neutral lipid overload in hepatocytes upon long-term exposure, which was prevented by co-treatment with silibinin. Computational analyses and cell-free biochemical assays predicted a weak to moderate inhibitory activity of clinically relevant concentrations of silibinin against CYP3A4 when compared with recommended (rosuvastatin) and non-recommended (simvastatin) statins for lorlatinib-associated dyslipidemia. The elevated plasma cholesterol and triglyceride levels in lorlatinib-treated lung cancer patients might involve primary alterations in the hepatic accumulation of lipid intermediates. Silibinin could be clinically explored to reduce the undesirable hyperlipidemic activity of lorlatinib in lung cancer patients.

Keywords: lorlatinib; hypertriglyceridemia; hypercholesteremia; silibinin; lipidomics; CYP3A4; statins

Citation: Verdura, S.; Encinar, J.A.; Fernández-Arroyo, S.; Joven, J.; Cuyàs, E.; Bosch-Barrera, J.; Menendez, J.A. Silibinin Suppresses the Hyperlipidemic Effects of the ALK-Tyrosine Kinase Inhibitor Lorlatinib in Hepatic Cells. *Int. J. Mol. Sci.* **2022**, *23*, 9986. https://doi.org/10.3390/ijms23179986

Academic Editor: Cristobal Miranda

Received: 5 August 2022
Accepted: 30 August 2022
Published: 1 September 2022

1. Introduction

The small macrocyclic compound lorlatinib (product name PF-06463922) is a third-generation anaplastic lymphoma kinase (ALK) tyrosine kinase inhibitor (TKI) originally developed to inhibit ALK mutant forms causing resistance to first- and second-generation ALK-TKIs (e.g., crizotinib, ceritinib, alectinib or brigatinib) in patients with advanced non-small-cell lung cancer (NSCLC) [1–6]. Consistent with its broad ALK mutational coverage and optimized central nervous system penetration through the blood–brain barrier,

lorlatinib has shown substantial systemic and intracranial activity both in treatment-naïve patients and in patients with relapse after first- and second-generation ALK TKIs [7–12]. It has been approved for the treatment of patients with ALK-positive metastatic NSCLC whose disease has progressed after alectinib or ceritinib as the first ALK-TKI, or after crizotinib and at least one other ALK-TKI [13].

Lorlatinib has a unique treatment-related adverse event profile compared with other ALK-TKIs that is characterized by the frequent incidence of hypercholesteremia and hypertriglyceridemia, which have been found to occur in 61% and 82% of lorlatinib-treated patients included in a pooled safety analysis (n = 295) [14,15]. Results from the global phase 2 study B7461001 (NCT01970865) revealed that grade 3 or 4 elevations in total cholesterol and triglycerides both occurred at a frequency of 16% [2]. Hyperlipidemia—comprising the cluster terms hypercholesterolemia and hypertriglyceridemia—is the most commonly reported adverse reaction to lorlatinib, which usually arises within the first few weeks of treatment (median time to onset, 15 days). Lorlatinib-induced hyperlipidemia is a common reason for temporary (but not permanent) discontinuation and dose-reduction of lorlatinib in the clinical setting, which necessitates the rapid initiation of lipid-lowering medications. Accordingly, the majority (>80%) of patients receive at least one lipid-lowering agent within 3 weeks of the first lorlatinib dose (median time to onset, 20 days), and ~25% of patients who received a lipid-lowering agent for hypercholesterolemia or hypertriglyceridemia require the addition of a second agent. While statins are the most commonly prescribed lipid-lowering agents to clinically manage lorlatinib-related hyperlipidemia, the choice and dosing of statins should be guided by the differential metabolism of the CYP450 pathway [16]. As lorlatinib is metabolized primarily by CYP3A4, the so-called 3A4 statin substrates atorvastatin, lovastatin, and simvastatin should not be co-administered as lipid-lowering agents in lorlatinib-treated patients. The non-3A4 statin substrates rosuvastatin, pravastatin, and pitavastatin are not significantly metabolized by CYP3A4 enzymes, and so the potential for adverse statin-lorlatinib interactions is notably reduced. Rosuvastatin is currently the only lipid-lowering agent recommended for lorlatinib-associated hyperlipidemia based on its low involvement with CYP450 enzymes that are able to interact with lorlatinib [17].

Given the improvements in prognosis and survival of patients with ALK translocations, a better understanding of the primary causes underlying lorlatinib-triggered hypercholesterolemia/hypertriglyceridemia might inform new therapeutic strategies to prevent or manage the undesirable lipid-modifying activity of lorlatinib in patients with ALK-positive NSCLC. Here, we tested the hypothesis that lorlatinib might directly promote hypercholesteremic and hypertriglyceridemic effects in human hepatocytes. First, using non-targeted lipidomics comprising ultrahigh pressure liquid chromatography accurate-mass quadrupole time-of-flight mass spectrometry with electrospray ionization (UHPLC-ESI-QTOF-MS/MS) [18], and imaging of neutral lipids, we explored the ability of lorlatinib to alter the lipidome of hepatoma tissue-derived Huh-7 and HepG2 cells [19–24], which were employed as substitutes for primary hepatocytes. Second, we investigated whether silibinin—-a flavonolignan that functions as a hepatoprotectant in patients with acute and chronic liver injury [25–30]—-might prevent the lipid-modifying activity of lorlatinib in hepatocytes. To predict potentially relevant drug–drug interactions if silibinin were used to clinically manage lorlatinib-associated hyperlipidemia, we finally explored the capacity of silibinin to interact with and block CYP3A4 activity in comparison with currently employed statins. We now provide first-in-class evidence that the hyperlipidemic effects of lorlatinib might involve, at least in part, the induction of an increased content of cholesterol and triglycerides in hepatic cells, which can be prevented or reversed by silibinin.

2. Results

2.1. Hepatic Cells Treated with Lorlatinib Accumulate Cholesteryl Esters and Triglycerides

We first carried out MTT-based viability tests to evaluate the sensitivity of human hepatoma-derived Huh-7 cells, which closely mimic primary hepatocytes for drug

metabolism and toxicity studies, to lorlatinib. As shown in Figure 1A, the IC_{50} of lorlatinib for Huh-7 cells (22 ± 5 µmol/L) was similar to that for ALK-negative A549 NSCLC cells (19 ± 5 µmol/L), but was tens or even hundreds of thousands higher than that obtained for H2228 and H3122 NSCLC cell lines (0.9 ± 0.2 and 0.003 ± 0.0002 µmol/L, respectively) harboring ALK rearrangements (variants 3a/b and 1, respectively) [31,32].

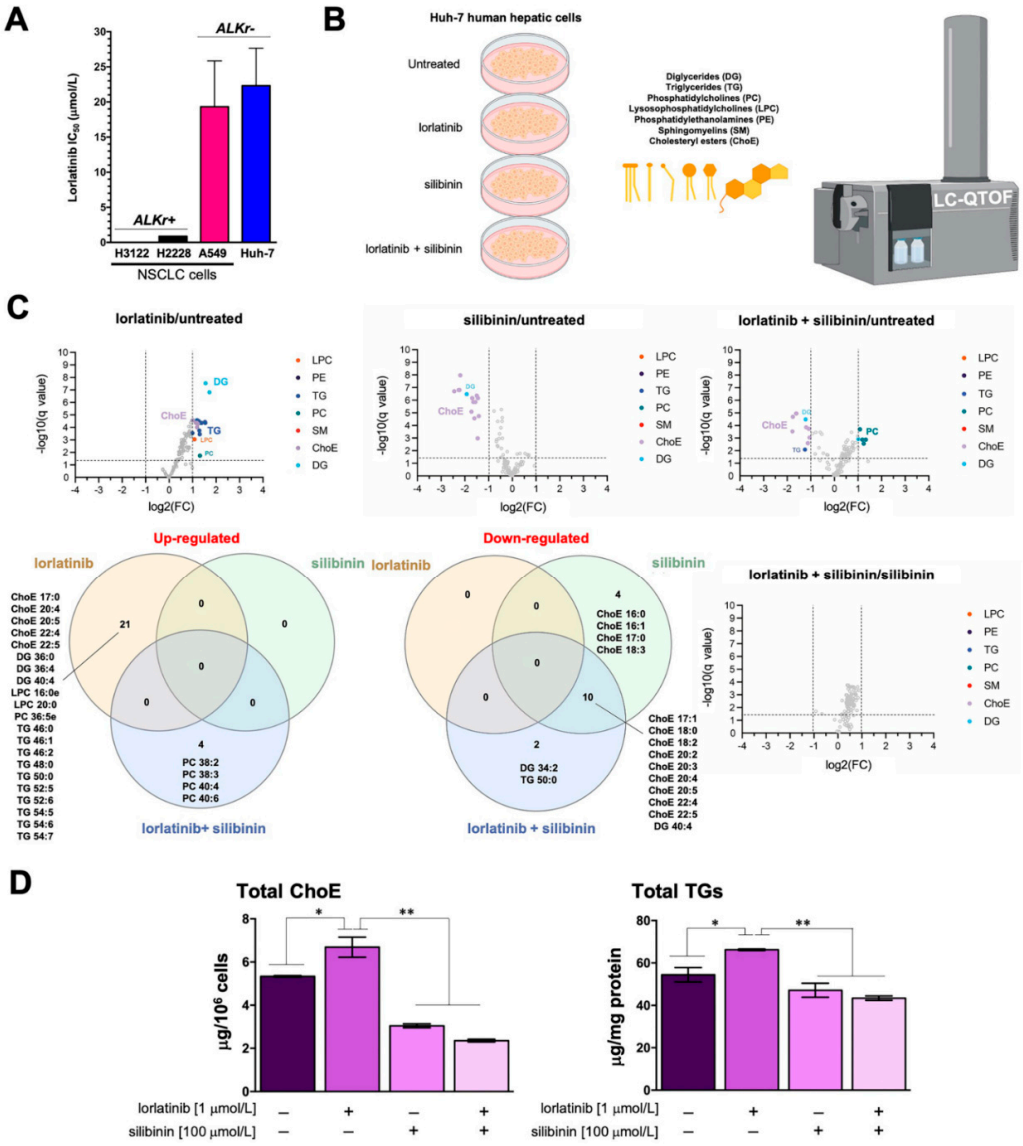

Figure 1. Silibinin prevents lorlatinib-driven lipidome alterations in human hepatic cells: (**A**) bar graphs of the IC_{50} values for each cell line calculated from the MTT assays as described in "Materials and Methods"; the results are presented as the means (*columns*) ± S.D. (*bars*) ($n \geq 3$ in technical replicates); (**B**) to test the hypothesis that lorlatinib could directly promote the accumulation of triglycerides and/or cholesterol in human hepatocytes, we carried out an untargeted UHPLC-ESI-QTOF-MS/MS-based lipidomic analysis of > 100 molecular lipid species in Huh-7 cells cultured in the absence/presence of lorlatinib and/or silibinin; (**C**) Volcano plots and Venn diagrams of the results from lipidomic analyses (**B**) in human Huh-7 cells treated with lorlatinib (1 µmol/L), silibinin (100 µmol/L) or their combination for 48 h. Each dot represents a lipid species with its corresponding mean Log2 fold-change (FC) (*x* axis) and Benjamini–Hochberg corrected *p*-value (-log10, *y* axis). Colored dots illustrate differential lipid species, using a cutoff of $p < 0.05$ and log2FC > 1 or <1. (**D**). ELISA-based quantification of cholesteryl esters (*left*) and triglycerides (*right*) in Huh-7 cells treated with lorlatinib (1 µmol/L), silibinin (100 µmol/L) or their combination for 48 h. *p*-values < 0.01 (*) and <0.001 (**).

We then questioned whether lorlatinib used at concentrations efficacious against ALK-rearranged lung cancer cells but non-toxic to ALK-negative cells could promote substantial lipidome changes in Huh-7 cells (Figure 1B; Table 1). Accordingly, Huh-7 cells were treated with 1 µmol/L lorlatinib for 48 h, and the lipidome was characterized in a semi-targeted approach using a UHPLC-ESI-QTOF-MS/MS method, in which we matched mass spectra with commercial standards (SPLAH mix), databases such as METLIN-PCDL and Lipid MAPS (accessed on 1 July 2022), as well as corroboration of tentative lipid species upon obtaining their MS/MS spectrum. Representative chromatograms of lipidomic analyses in Huh-7 cells can be found in Figure S1.

Table 1. Lipid species (*n* = 124) identified using a UHPLC-ESI-QTOF-MS/MS method (e:ester).

DG (*n* = 9)	TG (*n* = 25)	PC (*n* = 40)	LPC (*n* = 9)	PE (*n* = 4)	SM (*n* = 24)	ChoE (*n* = 13)
DG 34:1	TG 46:0	PC 30:0	LPC 15:0	PE 32:0	SM 32:0	ChoE 16:0
DG 34:2	TG 46:1	PC 31:0	LPC 16:0	PE 36:4	SM 32:1	ChoE 16:1
DG 34:3	TG 46:2	PC 32:0	LPC 16:0e	PE 36:5e	SM 32:2	ChoE 17:0
DG 36:0	TG 48:0	PC 32:1	LPC 18:0	PE 38:5e	SM 33:1	ChoE 17:1
DG 36:1	TG 48:1	PC 32:1e	LPC 18:0e		SM 34:1	ChoE 18:0
DG 36:2	TG 48:2	PC 32:2	LPC 18:1		SM 34:2	ChoE 18:2
DG 36:3	TG 48:3	PC 33:0	LPC 18:2		SM 35:0	ChoE 18:3
DG 36:4	TG 50:0	PC 33:1	LPC 20:0		SM 35:1	ChoE 20:2
DG 40:4	TG 50:1	PC 33:2	LPC 20:3		SM 36:0	ChoE 20:3
	TG 50:2	PC 34:0			SM 36:1	ChoE 20:4
	TG 50:3	PC 34:1			SM 36:2	ChoE 20:5
	TG 50:4	PC 34:1e			SM 38:1	ChoE 22:4
	TG 51:2	PC 34:2			SM 38:2	ChoE 22:5
	TG 52:1	PC 34:2e			SM 39:1	
	TG 52:2	PC 34:3			SM 40:0	
	TG 52:3	PC 34:4			SM 40:1	
	TG 52:4	PC 35:1			SM 40:2	
	TG 52:5	PC 35:2			SM 41:1	
	TG 52:6	PC 35:4			SM 41:2	
	TG 54:2	PC 36:0			SM 42:1	
	TG 54:3	PC 36:1			SM 42:2	
	TG 54:4	PC 36:2			SM 42:3	
	TG 54:5	PC 36:2e			SM 43:1	
	TG 54:6	PC 36:3			SM 43:2	
	TG 54:7	PC 36:4				
		PC 36:5				
		PC 36:5e				
		PC 38:2				
		PC 38:3				
		PC 38:4				
		PC 38:5				
		PC 38:5e				
		PC 38:6				
		PC 38:6e				
		PC 40:4				
		PC 40:4e				
		PC 40:5				
		PC 40:6				
		PC 42:4e				
		PC 42:5e				

We identified and quantified more than 100 lipid species belonging to six different families: diglycerides (DG), triglycerides (TG), phosphatidylcholines (PC), lysosophosphatidylcholines (LPC), phosphatidylethanolamines (PE), sphingomyelins (SM), and cholesterol esters (ChoE). Lorlatinib treatment was found to significantly increase several species of ChoE, numerous molecular species of long-chain TG, and several DG, LPC, and PC species (Figure 1C; Figure S2; Tables S1–S7).

2.2. Silibinin Fully Protects the Steady-State Lipidome of Hepatic Cells against the Hyperlipidemic Effects of Lorlatinib

Volcano plots and Venn diagrams of differentially accumulated lipid species revealed that, when used as a single agent, silibinin (100 μmol/L, 48 h) treatment significantly lowered the baseline abundance of many ChoE species in Huh-7 cells. Similarly, silibinin co-treatment completely blunted the significant lorlatinib-induced rise in numerous ChoE and TG/DG species in Huh-7 cells. Indeed, cells co-treated with silibinin and lorlatinib showed notable decreases in the abundance of various ChoE species, and this was accompanied by the compensatory generation of PC species (Figure 1C; Figure S2). Of note, no significant changes in any lipid species were observed when comparing silibinin-treated hepatocytes with those co-treated with silibinin and lorlatinib (Figure 1C; Figure S2).

Colorimetric enzymatic assays confirmed the ability of silibinin to inhibit the accumulation of cholesterol esters and triglycerides in lorlatinib-treated Huh-7 cells (Figure 1D).

2.3. Silibinin Prevents the Lorlatinib-Induced Chronic Accumulation of Neutral Lipids in Hepatic Cell

To evaluate the potential clinical relevance of silibinin's ability to acutely suppress lorlatinib-induced hyperlipidemia in hepatic cells, we designed a protocol of repeated daily exposure to lorlatinib and/or silibinin using a silibinin concentration (10 μmol/L) that can be practically achieved in a clinical setting. We first employed a conventional index of fatty liver disease—-the intracellular accumulation of neutral lipids (steatosis)—-to confirm the ability of lorlatinib to trigger hypertriglyceridemia and hypercholesteremia. The results of Oil red O- and LipidTOX™-based staining of neutral lipids (cholesteryl esters and triglycerides) in lorlatinib-treated Huh-7 cells cultured with or without silibinin are shown in Figure 2A. As expected, in the lorlatinib only-treated arm, hepatic cells accumulated large amounts of lipid droplet-like neutral lipids, whereas this pattern was largely lost in the presence of clinically relevant concentrations of silibinin, which notably decreased the quantity and size of the lipid droplets formed by exposure to lorlatinib.

To confirm these findings, we employed an independent in vitro model of fatty liver disease involving non-tumorigenic HepG2 cells, which are routinely employed as an inducible fatty liver cell model to screen for therapeutic drugs to eliminate lipid accumulation. The results of Oil red O staining of lorlatinib-treated HepG2 cells cultured with or without silibinin are shown in Figure 2B. Lorlatinib-treated HepG2 cells contained a greater number of larger lipid droplets than untreated cells. By contrast, there were markedly fewer and smaller neutral lipid depots in the presence of silibinin even at the highest tested concentration of lorlatinib.

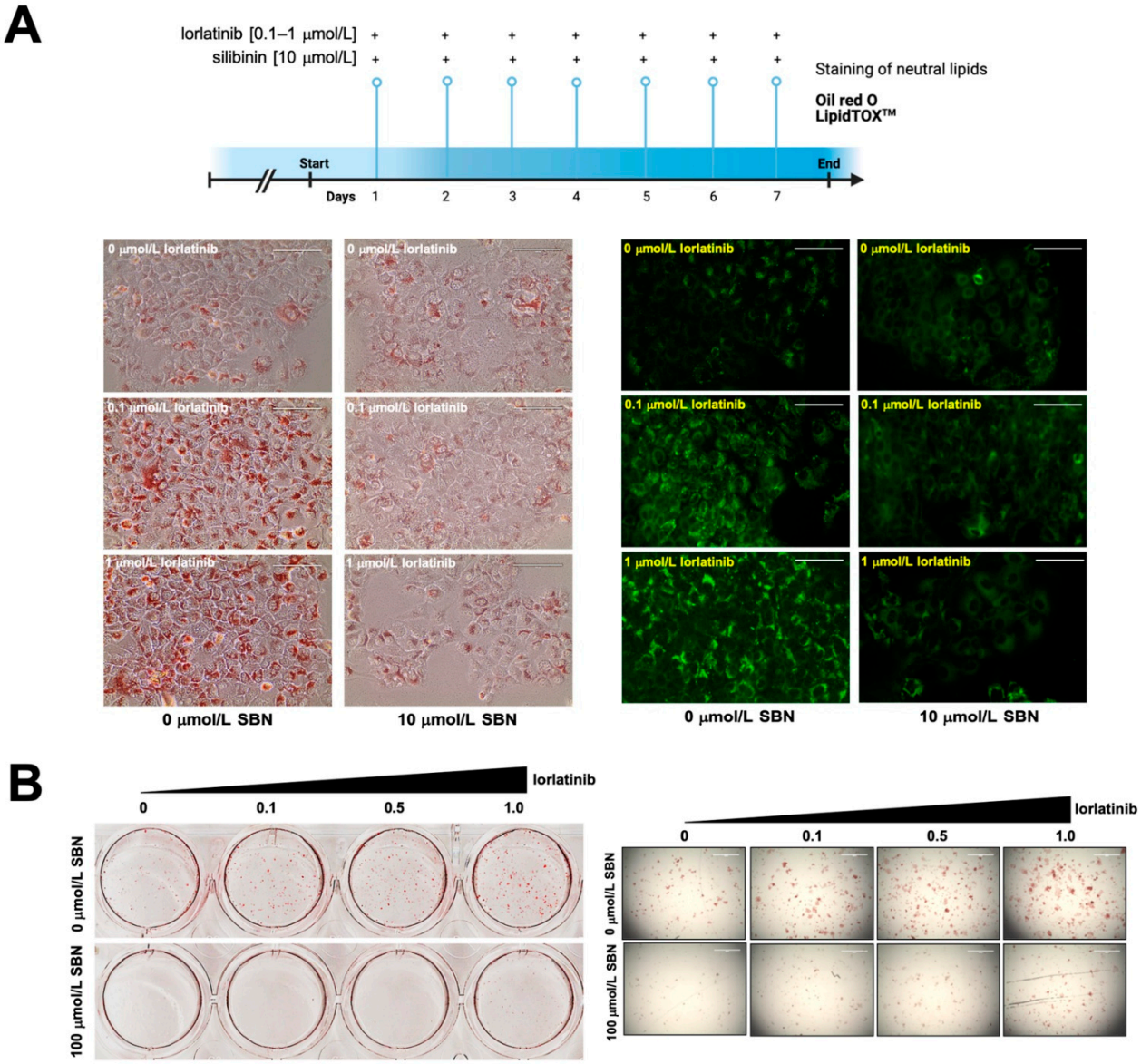

Figure 2. Silibinin inhibits the chronic accumulation of neutral lipids in lorlatinib-treated hepatic cells (**A**) Conventional indices of fatty acid liver disease —-lipid droplet content in hepatic cells—- were assessed using Oil Red O- and LipidTOX green-based staining of neutral lipids in Huh-7 (**A**) and HepG2 (**B**) cells chronically (**A**) or acutely (**B**) exposed to lorlatinib in the absence or presence of silibinin. (Chronic exposure: 7 days at 10 µmol/L silibinin; acute exposure: 48 h at 100 µmol/L silibinin). Scale bar = 100 µm.

2.4. Silibinin Does Not Overlap the Binding Mode of Lorlatinib to Cytochrome P450 3A4 (CYP3A4) In Silico

To predict clinically relevant drug–drug interactions if silibinin were used to clinically manage lorlatinib-induced hyperlipidemic effects in hepatic cells, we explored the capacity of silibinin to interact with and block the lorlatinib-metabolizing CYP3A4 isoenzyme using in silico computational descriptions and in vitro biochemical assays. First, to shed some light on the capacity of silibinin to interact with CYP3A4, we performed a computational study comparing the predicted molecular interactions between silibinin and CYP3A4 with those of lorlatinib and ritonavir, which is the most potent CYP3A4A inhibitor in clinical use. As silibinin is almost a 1:1 mixture of the diastereomers A and B, we performed classical molecular dockings of silibinin A and B against the 3D crystal structure of human CYP3A4 bound to an inhibitor (PDB:7KVS) [33] (Figure 3).

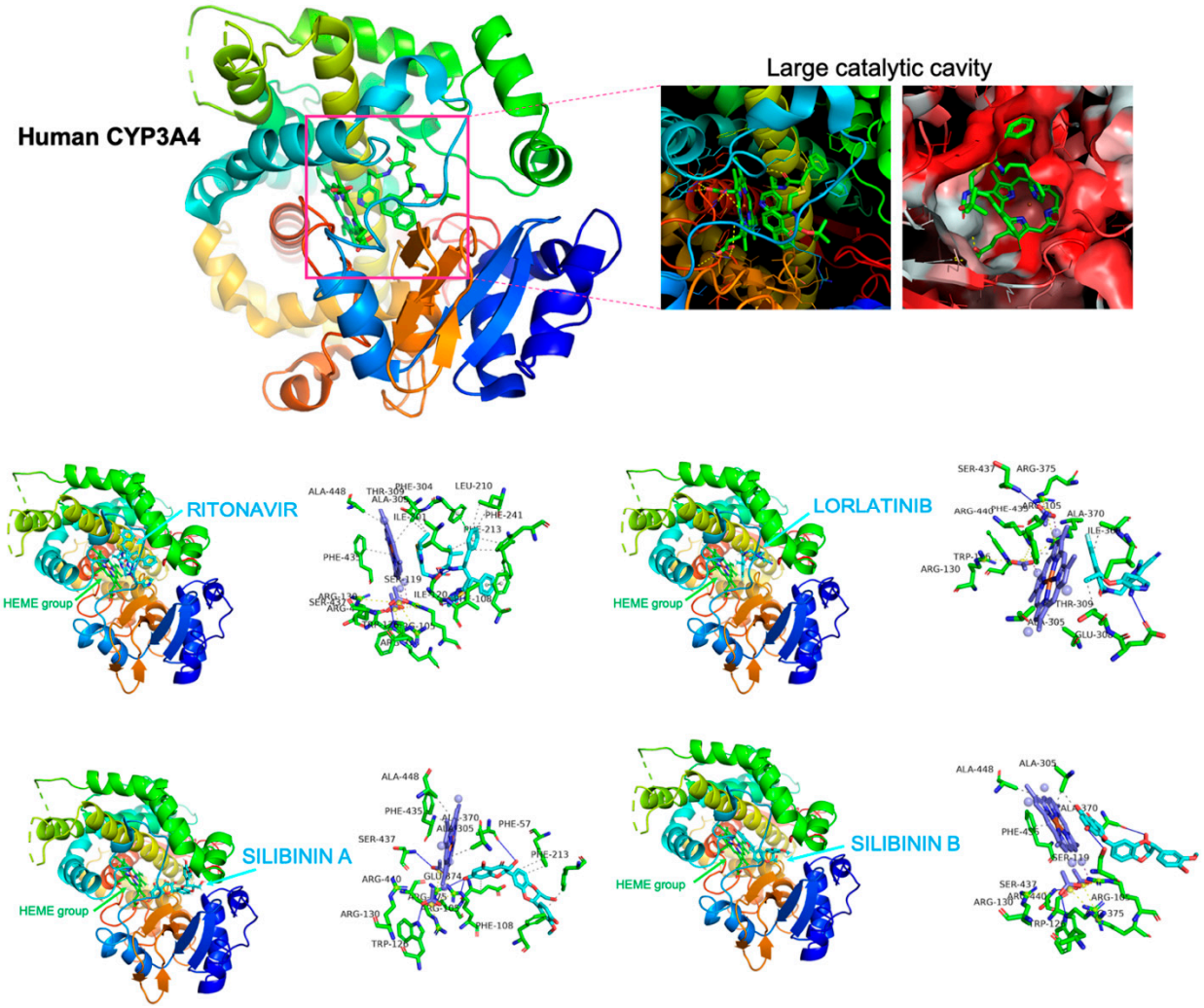

Figure 3. Silibinin does not share the binding mode of lorlatinib to CYP3A4. Figure depicts the backbone of the overall crystal structure of CYP3A4 (7KVS) with rainbow colors showing the best docked poses of silibinin A, silibinin B, ritonavir, and lorlatinib at the catalytic site. Each inset shows the detailed interactions of silibinin docked to CYP3A4, indicating the participating amino acids involved in the interaction and the type of interaction (hydrogen bonds, hydrophilic interactions, salt bridges, II-stacking, etc).

To characterize the potential binding of silibinin A and B to the large catalytic cavity of CYP3A4, which allows CYP3A4 to bind a broad range of substrates as compared with other CYP isoenzymes, a total of 75 flexible docking runs were set around the putative binding sites of lorlatinib and ritonavir using AutoDock Vina implemented by YASARA. The resulting binding energies with the docking simulations of silibinin A (−10.323 kcal/mol) and B (−9.561 kcal/mol) were similar to those obtained with lorlatinib (−9.876 kcal/mol) and ritonavir (−9.962 kcal/mol). However, closer inspection of the different conformations revealed that the predicted interaction of silibinin A and B with the active site cavity of CYP3A4 shared only 39–46% of the 12 amino acid residues involved in the lorlatinib binding mode, and 45–59% of the 22 participating amino acids involved in the ritonavir binding mode (Table 2).

Table 2. Details of the interaction between silibinin A/B, ritonavir and lorlatinib to CYP3A4.

ΔG (kcal/mol)	K_d [nM]	Drug	Residues Involved in the Interaction (7KVS.pdb)
−10.323	27.1	silibinin A	TYR 53, PHE 57, ASP 76, ARG 105, ARG 106, PHE 108, GLY 109, PHE 213, PHE 215, PHE 220, ILE 223, THR 224, PRO 227, ILE 230, VAL 240, ALA 370, MET 371, ARG 372, LEU 373, GLU 374, ARG 375, **HEME 601**
−9.962	49.9	ritonavir	PHE 57, ARG 105, ARG 106, PHE 108, MET 114, SER 119, ILE 120, LEU 210, LEU 211, PHE 213, PHE 241, ILE 300, ILE 301, PHE 304, ALA 305, THR 309, ILE 369, ALA 370, MET 371, ARG 372, LEU 373, GLU 374, **HEME 601**
−9.876	57.6	lorlatinib	PHE 57, ARG 105, SER 119, LEU 211, PHE 304, GLU 308, THR 309, SER 312, ILE 369, ALA 370, MET 371, LEU 373, LEU 482, **HEME 601**
−9.651	84.3	silibinin B	PHE 57, ARG 105, ARG 106, PRO 107, PHE 108, SER 119, ILE 301, ALA 305, THR 309, ALA 370, MET 371, ARG 372, LEU 373, GLU 374, **HEME 601**

Unlike lorlatinib and ritonavir, neither silibinin A nor silibinin B were predicted to interact with PHE304, which is critically important for CYP3A4 substrate specificity and catalytic capacity [34–36]. Moreover, neither silibinin A nor silibinin B were predicted to interact with a majority of the hydrophobic pocket near the I-helix (the so-called Phe-1 site) including PHE108, LEU210, LEU211, PHE241, ILE301, and PHE304 [37,38] (Figure 3). Silibinin is, therefore, predicted to interact with the catalytic site of CYP3A4 through a unique binding mode lacking the involvement of the gatekeeper residues regulating the access of CYP3A4 substrates to the heme group, suggesting a highly improbable interaction between silibinin and lorlatinib at the CYP3A4 active site.

2.5. Silibinin Is a Weak Inhibitor of the Lorlatinib-Metabolizing Cytochrome P450 3A4 (CYP3A4) Isoenzyme

The CYP3A4 inhibition propensity of silibinin in comparison with that of recommended (non-3A4 substrates such as rosuvastatin) and non-recommended (3A4 substrates such as simvastatin) statins to clinically manage lorlatinib-associated dyslipidemia was initially predicted using the DL-CYP prediction server [39], a free web tool to evaluate the tendency of small molecules to inhibit five major CYP450 isoforms (1A2, 3C9, 2C19, 2D6, and 3A4). Using this deep autoencoder multitask neural network trained on more than 13,000 compounds, simvastatin showed the highest predicted value (0.93), which ranked very close to that obtained with the positive control ritonavir (0.97) (Table 3). The tendency of CYP3A4 inhibition by rosuvastatin was predicted to be as low as 0.2, whereas silibinin had no predicted inhibitory effect in silico (0.06) (Table 3).

Table 3. Prediction of human cytochrome P450 inhibition.

	Cytochrome P450 Isoforms				
Drug	**1A2**	**2C9**	**2C19**	**2D6**	**3A4**
Ritonavir	0.00	0.34	0.36	0.01	0.97
Simvastatin	0.00	0.02	0.04	0.00	0.93
Rosuvastatin	0.00	0.45	0.18	0.00	0.2
Silibinin	0.00	0.02	0.04	0.00	0.06

To facilitate the understanding of the predicted tendencies, we performed MD simulations for each of the CYP3A4-drug complexes. This approach considers the protein flexibility at the target-binding site during the molecular recognition process, allowing the user to confirm the kinetic stability and validate the binding poses obtained by docking. The CYP3A4 protein backbone root mean square deviation (RMSD) plots of the drugs' heavy

atoms, measured after superimposing CYP3A4 onto its reference structure during the MD simulation, were prepared in parallel. The approach is summarized in Figure 4 and shows as follows: the best poses of ritonavir, silibinin A, silibinin B, simvastatin, and rosuvastatin coupled to the catalytic cavity of CYP3A4 before (0 ns) and after (100 ns) the MD simulation, the time evolution of RMSD relative to the initial structure of CYP3A4 in the absence and presence of drugs, the binding free energy calculations under the MM/PBSA approximation from the entire MD simulation trajectory of 100 ns (or last 30 ns), and the identification of amino acid residues participating in the drug-CYP3A4 binding pocket. The MM/PBSA parameters, which estimate the free energy of the binding of small ligands to biological macromolecules, allows the correct ranking of drug candidates based on the fact that more positive energies indicate the occurrence of stronger binders (e.g., "strong" > 25 kcal/mol versus "weak" < 25 kcal/mol). Likewise, the results predicted a high affinity of ritonavir and simvastatin for the catalytic site of CYP3A4, reaching MM/PBSA values of ~70 and 40 kcal/mol, respectively (Figure 4). Silibinin A mimicked rosuvastatin as a predicted weak inhibitor of CYP3A4, showing MM/PBSA values of <20 kcal/mol. Silibinin B was predicted to encounter steric hindrance at the catalytic activity of CYP3A4 given its notable −60 kcal/mol MM/PBSA value (Figure 4).

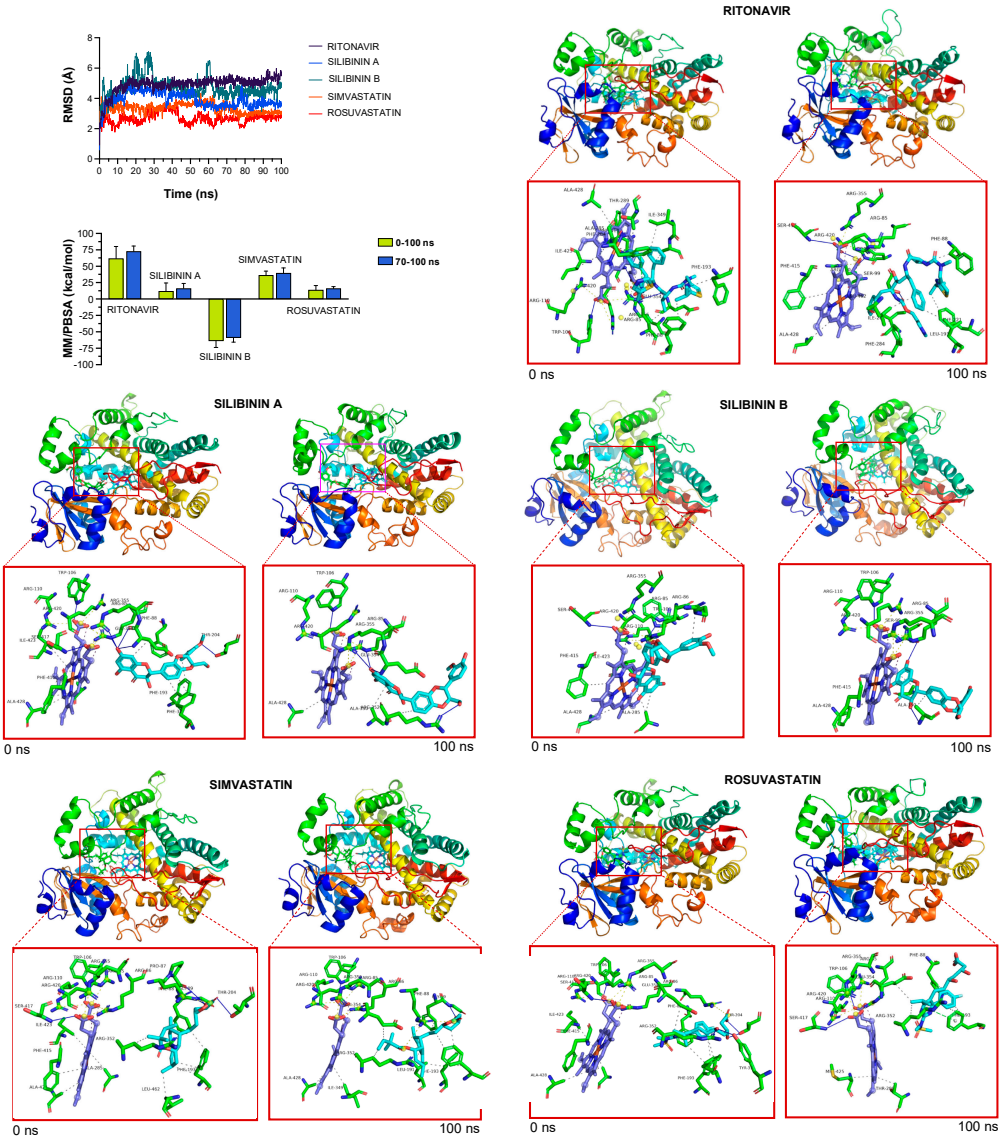

Figure 4. Incorporation models of CYP3A4-targeting drugs: ritonavir and statins *vs* silibinin. The root mean square deviation (RMSD, Å) of each drug's heavy atoms over the simulation time,

measured after superposing the protein onto its reference structure, and the molecular mechanics Poisson–Boltzmann surface area (MM/PBSA) binding energy analyses calculated from the entire trajectory of the 100 ns (or last 30 ns) MD simulation, are shown. The best poses of ritonavir, silibinin A, silibinin B, simvastatin, and rosuvastatin coupled to the catalytic site of CYP3A4 before (0 ns) and after (100 ns) the molecular dynamics (MD) simulation are shown. The protein is represented as a function of the hydrophobicity of its surface amino acids and the Na^+ and Cl^- ions have been eliminated to facilitate visualization. Each inset shows the detailed interactions of the participating amino acids involved and the type of interaction (hydrogen bonds, hydrophilic interactions, salt bridges, Π-stacking, etc.).

The inhibitory effects of graded concentrations of simvastatin, rosuvastatin, silibinin, and Eurosil 85®/Euromed –a standardized pharmaceutical preparation containing 60% silibinin with an enhanced bioavailability (>80%) that is commonly used in clinical research [40,41]—on CYP3A4 activity were finally evaluated using the Vivid® CYP450 Red screening assay, which employs microsomes prepared from insect cells (baculosomes) expressing a human CYP450 isoenzyme (CYP3A4 in this case) and human cytochrome P450 reductase, and utilizing the benzyloxy–methyl–resofurin (BOMR) red substrate. The Vivid® BOMR substrate is a blocked dye that yields a minimal fluorescence signal until metabolized by CYP3A4 into products that are highly fluorescent in aqueous solutions (Figure 5, *left panel*). Simvastatin strongly inhibited the enzymatic activity of CYP3A4, exhibiting an IC_{50} value as low as 1.8 ± 0.9 µmol/L. Up to 10-fold higher concentrations of silibinin (IC_{50} = 16.7 ± 8.9 µmol/L) and Eurosil 85®/Euromed (12.1 ± 1.2 µmol/L) were necessary to achieve the half-inhibitory concentration of CYP3A4 activity (Figure 5, *right panel*). Rosuvastatin likewise failed to show any significant inhibitory effect on CYP3A4 activity even when tested at very high concentrations (>300 µmol/L).

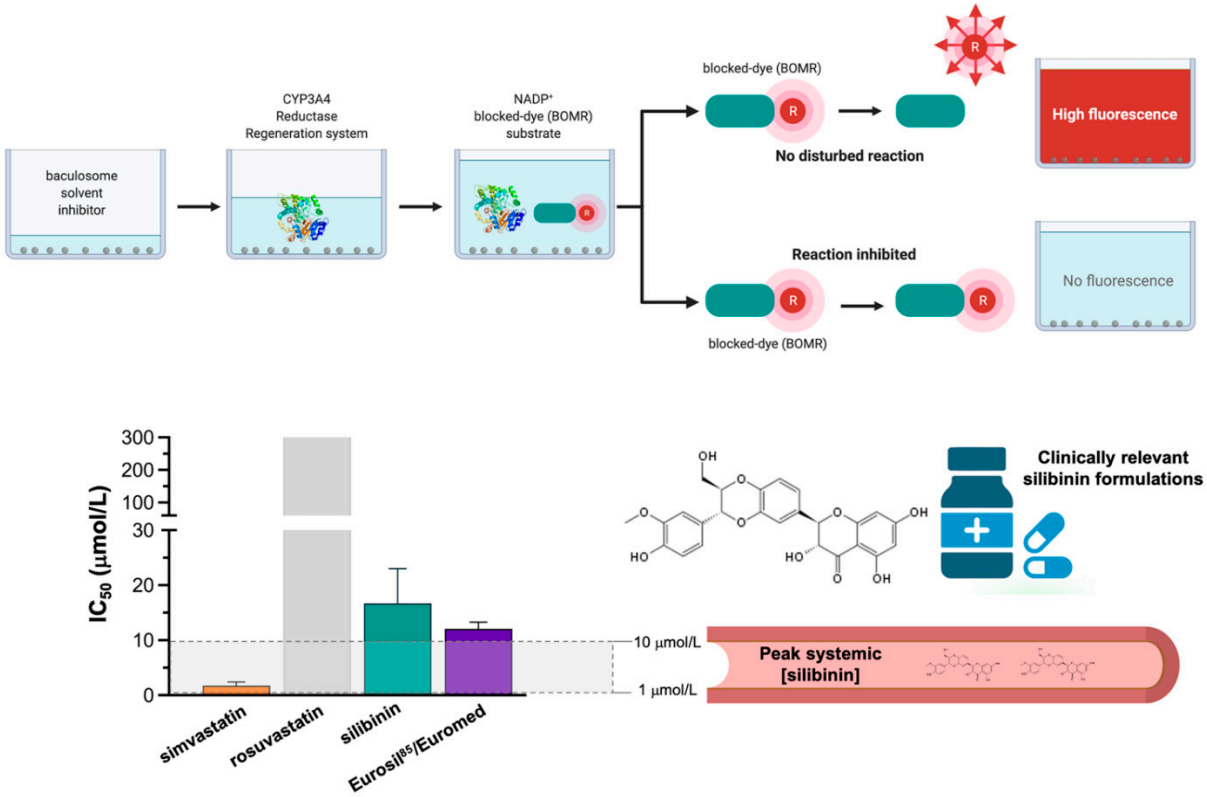

Figure 5. Potency of human CYP3A4 inhibition: statins *vs* silibinin. Percent inhibition and IC_{50} values of simvastatin, rosuvastatin, silibinin, and Eurosil 85® against recombinant human CYP3A4 expressed in baculosomes using the Vivid BOMR Red substrate. The results are presented as the means (*columns*) ± S.D. (*bars*) (n = 3 experimental curves in technical duplicates).

3. Discussion

Elevated plasma levels of cholesterol and triglycerides are a common adverse effect in the majority of patients with ALK-positive NSCLC treated with lorlatinib [14,15,17]. The molecular mechanisms of lorlatinib-related lipid disorders are likely multifactorial and are currently unclear. Because hyperlipidemia is a classic feature of nephrotic syndrome, the fact that lorlatinib is apparently the only ALK-TKI reported to induce acute kidney injury involving renal cyst formation or progression suggests that minimal change disease (nephrotic syndrome) should be viewed as a possible secondary cause of lorlatinib-induced hyperlipidemia [42–45]. Here, we provide pre-clinical evidence that the elevated plasma cholesterol and triglyceride levels in lorlatinib-treated lung cancer patients might be due, at least in part, to direct alterations in the hepatic accumulation of lipid intermediates. Moreover, we reveal that the flavonolignan silibinin has the capacity to protect hepatic cells against the lipid-modifying activity of lorlatinib (Figure 6).

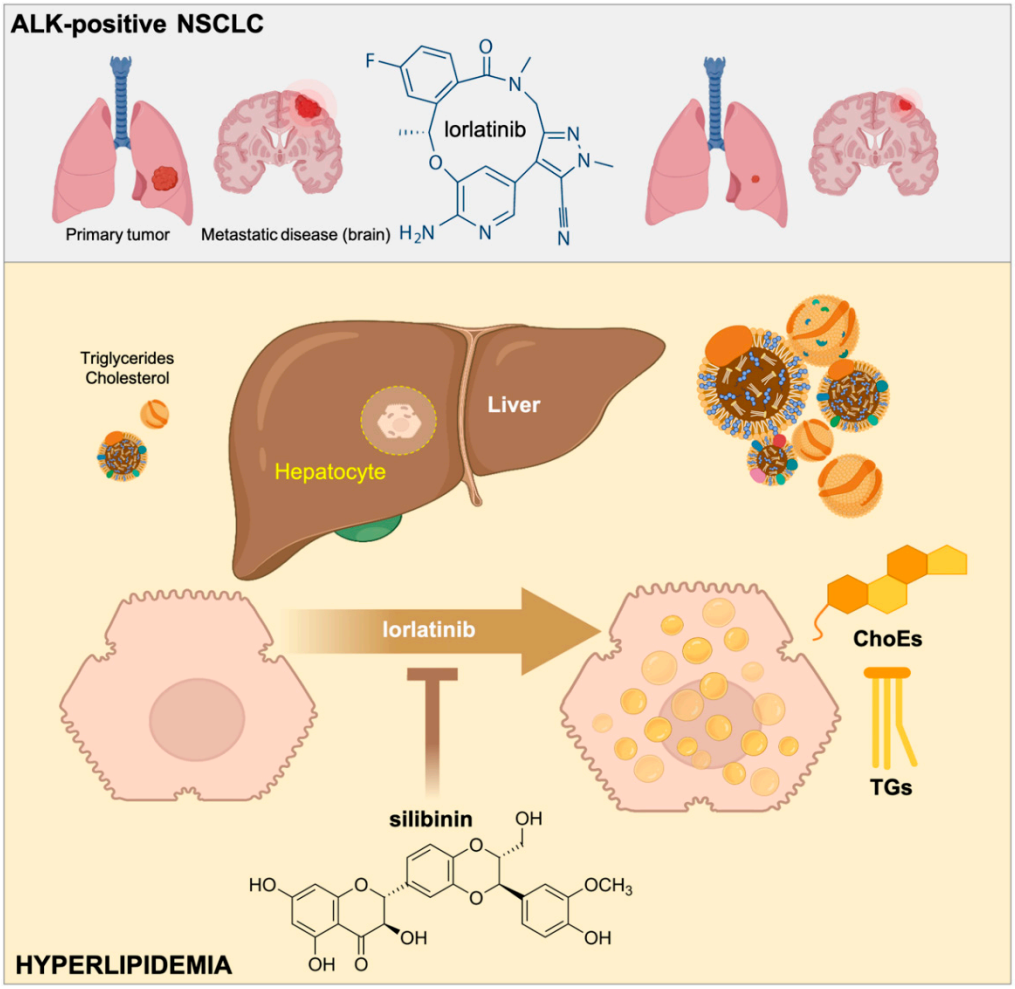

Figure 6. Silibinin suppresses the hyperlipidemic effects of lorlatinib in hepatic cells. The third generation ALK-TKI lorlatinib promotes the accumulation of cholesterol and triglycerides in human hepatic cells. The flavonolignan silibinin protects hepatic cells against the hypertriglyceridemic and hypercholesteremic effects of lorlatinib. Silibinin is a new candidate to clinically manage the undesirable hyperlipidemic activity of lorlatinib in patients with ALK-rearranged lung cancer.

Lorlatinib is rapidly absorbed to achieve peak plasma concentrations of >2 µmol/L 0.5–4 h after a single 100 mg oral dose and is widely distributed in different tissues [46,47], with the highest concentration found in the liver [48]. The hepatic accumulation of lorlatinib can be explained in terms of its low metabolism in this organ, with only 12% of lorlatinib

metabolized during first-pass hepatic metabolism or pre-systemic metabolism. We show that acute exposure to a clinically relevant concentration of lorlatinib (1 μmol/L) promotes a rapid and significant buildup of cholesteryl esters and tri-/di-glycerides in hepatic cells. We also found that longer exposure to lorlatinib drives the hallmarks of hepatic steatosis, such as the abnormal and excessive accumulation of neutral lipids in liver cells. While our study was not designed to investigate the precise molecular mechanisms involved in the hepatic alterations in cholesterol and triglycerides homeostasis in response to lorlatinib, it is reasonable to suggest that there is overlap in the targeted pathways for ALK-rearranged NSCLC growth and those that regulate hepatic function, leading to on-target or closely related off-target hepatic toxicity. It will be critical to understand the mechanistic pathways by which lorlatinib induces a dysregulation of lipid and cholesterol metabolism in hepatic cells. Because one of the major mechanisms of drug-induced liver injury (including TKIs such as lorlatinib) centrally involves mitochondrial perturbation and dysfunction [49,50], mitochondria might be viewed as a probable target through which lorlatinib alters lipid metabolism in human hepatocytes. Particularly, drugs inducing impairment of fatty acids oxidation are known to lead to lipid accumulation (steatosis) and steatohepatitis [50], thus suggesting that a plausible hypothesis for the hyperlipidemic mechanism of action of lorlatinib might involve a decrease in lipid catabolism in response to TKI-related mitochondrial dysfunction in hepatic cells, leading to a disbalance between fatty acid β-oxidation activity and cholesteryl esters/triglycerides synthesis [51]. Future studies will be needed to address this possibility. We acknowledge, however, that our pre-clinical findings in cell culture do not preclude the possibility that other mechanisms involving changes in peripheral tissues (e.g., adipose tissue, muscle), lipid uptake by the liver, or intestinal lipid absorption can contribute to the lorlatinib-induced lipid metabolic effects.

The flavonolignan silibinin has been shown to significantly temper the accumulation of hepatic and biliary triglycerides and cholesterol in cultured cells and animal models, and in patients with type 2 diabetes and chronic liver disease. We show here that silibinin suppresses the lipid-modifying activity of lorlatinib in human hepatic cells. Regardless of the mechanism through which silibinin protects the lipidome of hepatic cells against lorlatinib (e.g., by increasing the shift of fatty acids from triglycerides towards phospholipids and/or increasing the endogenous cholesterol conversion to bile acids), silibinin might represent an idoneous lipid-lowering agent in new treatment regimens for patients with NSCLC at the highest risk of developing brain metastases, such as those continuously exposed to ALK-TKIs [52]. As lorlatinib is effective against central nervous system metastasis even in patients pretreated with first- and second-generation ALK-TKIs [10], the known capacity of silibinin to provide better control of brain disease and allow a higher proportion of patients with NSCLC to receive additional lines of treatment [53,54] could be exploited by utilizing its ability to ameliorate lorlatinib-induced hyperlipidemia.

The low hepatic extraction ratio (<30%) of "low" clearance drugs such as lorlatinib can drive a change in the plasma counterpart when co-administered with another drug that is a metabolic inhibitor or inducer. Because lorlatinib is metabolized primarily by the CYP3A4 isoenzyme [55,56], lipid-lowering agents that do not interact with CYP3A4, such as rosuvastatin, should be co-administered in lorlatinib-treated patients. Our multi-faceted approach involving computational modeling, neural network-based prediction models to classify CYP inhibition, and in vitro validation using recombinant human CYP3A4, confirms and further extends the notion that exposure to standard doses of silibinin-containing milk thistle preparations leading to relatively low peak systemic concentrations (1–10 μmol/L) are expected to be accompanied by low-risk for an inhibitory interaction of the first-pass clearance of lorlatinib at the hepatic level [57]. Nonetheless, because notably higher intestinal concentrations of silibinin can be achieved when using gram doses of certain silibinin formulations that have been tested in patient populations [57,58], it cannot be excluded that clinically relevant inhibitory interactions with the lorlatinib-metabolizing CYP3A4 isoenzyme might occur at the intestinal level. Indeed, a limitation of our study is that the capacity of silibinin to protect hepatocytes from the hyperlipidemic activity of lorlatinib

was observed in two hepatoma-derived cell lines (Huh-7 and HepG2) that naturally express low expression of drug metabolizing enzymes such as CYP3A4 [59–61]. We therefore acknowledge that our cell-free evaluations of the in silico and in vitro metabolic interactions between lorlatinib and silibinin (versus statins) using computational descriptions (with crystal structures of CYP3A4) and biochemical assays (with recombinant CYP3A4) cannot be mechanistically extrapolated to the cell-based experiments showing the ability of silibinin to suppress the hypercholesterolemic and hypertriglyceridemic effects of lorlatinib in Huh-7 and HepG2 cells. We failed to observed significant toxic effects when combining lorlatinib with silibinin concentrations as high as 100 μmol/L to carry out lipidomic studies with Huh-7 cells growing confluent for more than 1 month, thereby ensuring an increased expression and catalytic activity of CYP3A4 [62,63]. However, the extrapolation of the in vitro results to accurately predict the toxicity as it would occur in vivo might require the usage of the newly developed human hepatoma cell lines such as HepaRG [64–66], which shows stable expression of liver-specific functions over a long period in culture, including high levels of CYP3A4.

4. Materials and Methods

4.1. Materials

Silibinin was purchased from Sigma-Aldrich (St. Louis, MO, USA; Cat. #S0417). Simvastatin (MK 733) and rosuvastatin (ZD4522) were obtained from Selleck Chemicals LLC (Houston, TX, USA; Cat. #S1792 and S2169, respectively). Eurosil^{85}/Euromed was kindly provided by Meda Pharma S.L. (Barcelona, Spain). All reagents were dissolved in sterile dimethylsulfoxide to prepare 10 mmol/L stock solutions, which were stored in aliquots at −20°C until use. Working concentrations were diluted in culture medium prior each experiment.

Grade MS methanol (MeOH) and 2-propanol, ammonium formate, formic acid, acetic acid, methyl *tert*-buthyl ether (MTBE) and standards for calibration curves were purchased from Sigma-Aldrich. Water (Milli-Q grade) was obtained from a Milli-Q integral water purification system (Millipore Corp., Burlington, MA, USA). For internal standards, SPLASH Lipidomix was purchased from Avanti Polar lipids (Alabaster, AL, USA; Cat. #330707).

4.2. Cell Lines

Huh-7 and HepG2 cells were kindly provided by Dr. Jose Manuel Fernández-Real in our institution (IDIBGI), and were cultured in complete Dulbecco's modified Eagle's medium (Gibco/Invitrogen, Carlsbad, CA, USA) supplemented with 10% fetal bovine serum, 2 mmol/L L-glutamine, and 100 IU/mL penicillin-streptomycin (all from Gibco/Invitrogen, Carlsbad, CA, USA).

4.3. Cell Viability Assays

Cell viability effects of lorlatinib were determined using the colorimetric MTT (3-4,5-dimethylthiazol-2-yl-2,5-diphenyl-tetrazolium bromide) reduction assay. Dose–response curves to graded concentrations of lorlatinib were plotted as a percentage of the control cell absorbance, which was obtained from control cells containing the vehicle (DMSO *v/v*) processed simultaneously. For each treatment, cell viability was evaluated using the following equation: (OD_{570} of the treated sample/OD_{570} of the untreated sample) × 100. Sensitivity to agents was expressed in terms of the concentrations required for a 50% (IC_{50}) reduction in cell viability. Since the percentage of control absorbance was considered to be the surviving fraction of cells, the IC_{50} values were defined as the concentration of drug that produced 50% reduction in control absorbance (by interpolation).

4.4. Non-Targeted Lipidomics

Lipid extraction, preparation of external calibration curves, and quality control approaches were carried out as described [18]. Samples (2 μL) were injected directly into a 1290 Infinity UHPLC system coupled with a dual Agilent jet stream ESI source to a

6550 QTOF-MS instrument (Agilent Technologies, Santa Clara, CA, USA). UHPLC-ESI-QTOF-MS conditions, data analysis and indirect quantification of selected lipid species using MassHunter Qualitative Analysis B.07.00 software (Agilent Technologies), and corroboration of the tentative characterization of compound match entities using the Lipid Maps database (www.lipidmaps.org, accessed on 1 July 2022) and targeted MS/MS acquisition on LC-QTOF-MS instrument, have been previously described in detail [18].

Differentially expressed lipid species from untargeted lipidomic data were analyzed by generating volcano plots indicating statistical significance versus magnitude of fold-change for each lipid species (cutoff of Benjamini–Hochberg corrected p-value < 0.05 and log2 fold-change > 1 or <1).

4.5. Triglyceride and Cholesterol Quantification

Quantification of cholesteryl esters and triglycerides in Huh-7 cells cultured in the absence/presence of lorlatinib and/or silibinin was performed using cholesterol (Cat. #MAK043) and triglyceride (Cat. #MAK266) quantification kits (Sigma-Aldrich).

4.6. Accumulation of Neutral Lipids

For assessment of neutral lipid formation, cells were washed in PBS, fixed with 4% paraformaldehyde for 30 min, washed in distilled water, and then briefly incubated in 60% isopropanol. Following equilibration, cells were stained with a working solution (60%) of Oil Red O for 20 min. An Oil Red O stock solution was prepared by dissolving 0.35% *w/v* Oil Red O in 100 mL 100% isopropanol. HCS LipidTOX™ Green Neutral Lipid Stain (Invitrogen; Cat. #H34475) was employed as a second staining cocktail for visualization of intracellular neutral lipids. Formaldehyde fixation and preparing/using the labeling solution was carried out as per the manufacturer's instructions.

4.7. Prediction of CYP450 Inhibition In Silico

The CYP450 inhibition propensity of silibinin, simvastatin, and rosuvastatin was predicted with the DL-CYP Prediction Server (http://www.pkumdl.cn:8000/deepcyp/home.php, accessed on 1 July 2022), a free web tool to evaluate the tendency of small molecules to inhibit five CYP450 major isoforms, namely 1A2, 2C9, 2C19, 2D6, and 3A4 [39]. All structure-data files (sdf) for tested compounds were downloaded from PubChem (National Center for Biotechnology Information) and used as the inputs to predict their level of inhibition against human CYP450 isoforms. The CYP3A4 inhibitor ritonavir was used as a positive control to predict the inhibition of CYP3A4 activity. The results were expressed as values between 0 and 1.

4.8. Docking Calculations, Molecular Dynamics Simulations, and Binding Free Energy Analysis

Docking calculations, molecular dynamics (MD) simulations, and molecular mechanics Poisson–Boltzmann surface area (MM/PBSA) calculations to determine the alchemical binding free energy of silibinin, simvastatin, and rosuvastatin against CYP3A4 7KVS were performed using procedures described in previous works from our group [67–73]. To perform the docking studies with AutoDockVina (v1.1.2, San Diego, CA, USA), the CYP3A4 7KVS crystal structure was transformed to the PDBQT format, including the atomic charges and atom-type definitions. These preparations were performed using the AutoDock/Vina plugin with scripts from the AutoDock Tools package [74]. YASARA dynamics v19.9.17 (Vienna, Austria) was employed for all MD simulations with the AMBER14 force field. All simulation steps were run using a pre-installed macro (md_run.mcr) within the YASARA suite. Data were collected every 100 ps during 100 ns. The MM/PBSA calculations of solvation binding energy were calculated using the YASARA macro md_analyzebindenergy.mcr, with more negative values indicating instability. MM/PBSA was implemented with the YASARA macro md_analyzebindenergy.mcr to calculate the binding free energy with solvation of the ligand, complex, and free protein, as previously described [67–73]. All

of the figures were prepared using PyMol 2.0 software and all interactions were detected using the protein-ligand interaction profiler (PLIP) algorithm [75].

4.9. CYP3A4 Inhibition

The characterization of the CYP3A4 inhibitory potency of silibinin, simvastatin, and rosuvastatin was outsourced to the SelectScreen P450 Profiling Service (ThermoFisher Scientific, Waltham, MA, USA) using CYP3A4-transfected baculosomes from the Vivid® CYP450 Red assay platform (Cat. No. P2856). The stringent validation process ensures the highest quality data possible for the 10-point titration, which was performed in duplicate (n = 3). An additional two control wells for each compound concentration tested are conducted to detect autofluorescent compound interference. Strict quality control protocols ensure that any assay results not meeting set specifications will be automatically repeated, this includes performing IC_{50} assays with a known inhibitor for each P450 on a per plate basis to ensure the validity of the data. To calculate percent inhibition due to presence of test compounds (i.e., silibinin, simvastatin, and rosuvastatin) or positive inhibition (i.e., ketoconazole for CYP3A4, which enables the subtraction of background during data analysis) we used the following equation:

$$\% \text{ inhibition} = (1 - \frac{X–B}{A–B}) \times 100\%$$

where X is the fluorescence intensity of test compound, A is the fluorescence intensity observed in the absence of inhibitor (DMSO-only control that accounts for possible inhibition caused by introduction of test compounds originally dissolved in organic solvents), and B is the fluorescence intensity observed in the presence of positive inhibition control.

4.10. Statistical Analysis

All cell-based observations were confirmed by at least three independent experiments performed in triplicate for each cell line and for each condition. Data are presented as mean ± SD. Two-group comparisons were performed using Student′s t-test for paired and unpaired values. Comparisons of means of ≥3 groups were performed by ANOVA, and the existence of individual differences, in case of significant F values with ANOVA, was tested by Scheffé′s multiple contrasts: p-values < 0.01 and <0.001 were considered to be statistically significant (denoted as * and **, respectively). All statistical tests were two-sided.

5. Conclusions

Hyperlipidemia, which encompasses hypercholesteremia and hypertriglyceridemia, is a unique adverse side effect of lorlatinib that is mainly controlled with dose interruptions/modification and lipid-lowering therapies. We report here that clinically relevant concentrations of lorlatinib directly modify the lipid profile of human hepatocytes. Silibinin, a flavonolignan with remarkable clinical efficacy against brain metastases in patients with ALK-rearranged NSCLC and capable of overcoming resistance to ALK-TKIs in vitro [76,77], protects the native lipidome of hepatic cells against the hyperlipidemic effects of lorlatinib and prevents lipid accumulation at therapeutically relevant concentrations. Although silibinin might become a new candidate to clinically manage the undesirable lorlatinib-induced hypercholesterolemic and hyperlipidemic effects in human hepatic cells, further studies will be required to fully define the inhibitory potential of silibinin against the lorlatinib-metabolizing CYP3A4 isoenzyme when used as specific orally bioavailable formulations (e.g., Eurosil 85®) before suggesting its therapeutic combination with lorlatinib in a clinical setting with ALK-rearranged lung cancer patients.

Supplementary Materials: The following supporting information can be downloaded at: https://www.mdpi.com/article/10.3390/ijms23179986/s1.

Author Contributions: Conceptualization, S.V., J.A.E., J.B-B., and J.A.M.; methodology, S.V., J.A.E., S.F.-A., J.J., E.C., and J.A.M.; formal analysis, S.V., J.A.E., S.F.-A., J.J., E.C., and J.A.M.; investigation, S.V., J.A.E., S.F.-A., J.J., E.C., and J.A.M.; validation, S.V., E.C., and J.A.M.; data curation, S.V., J.A.E., S.F.-A., J.J., E.C., J.B.-B., and J.A.M.; writing—original draft preparation, E.C., J.B.-B., and J.A.M..; writing—review and editing, J.A.M.; visualization, E.C. and J.A.M.; supervision, S.V., E.C., and J.A.M.; project administration, E.C.; funding acquisition, E.C., J.B.-B., and J.A.M. All authors have read and agreed to the published version of the manuscript.

Funding: Work in the Menendez laboratory is supported by the Spanish Ministry of Science and Innovation (Grant PID2019-10455GB-I00, Plan Nacional de l + D + I, founded by the European Regional Development Fund, Spain) and by an unrestricted research grant from the Fundació Oncolliga Girona (Lliga catalana d'ajuda al malalt de càncer, Girona). Work in the Jose A. Encinar laboratory is supported by the Spanish Ministry of Economy and Competitiveness (MINECO, Grant RTI2019-096724-B-C21) and the Generalitat Valenciana (PROMETEO/2021/059). Joaquim Bosch-Barrera is the recipient of Research Grants from Grupo Español de Cáncer de Pulmón (GECP), La Marató de TV3 foundation (201906), and the Health Research and Innovation Strategic Plan (SLT006/17/114; PERIS 2016–2020); Pla stratègic de recerca i innovació en salut; Departament de Salut, Generalitat de Catalunya. Elisabet Cuyàs holds a "Miguel Servet" research contract (CP20/00003) from the Instituto de Salud Carlos III (Spain) and is supported by the Spanish Ministry of Science and Innovation (Grant PI22/00297, Proyectos de I + D + I en Salud, Acción Estratégica en Salud 2021–2023, founded by the European Regional Development Fund, Spain).

Institutional Review Board Statement: Not applicable.

Informed Consent Statement: Not applicable.

Data Availability Statement: All data generated or analyzed during this study are included in this published article (and its supplementary information file).

Acknowledgments: The authors would like to heartily thank König (www.konig.cat) for their generous donation to fund our cancer research on silibinin in Girona. We are grateful to the Servicio de Supercomputación of the Granada University for letting us take advantage of the ALBAICIN computer cluster (https://supercomputacion.ugr.es/arquitecturas/albaicin/), which has provided ~80% of the calculation time necessary to prepare this manuscript. We wish to especially thank Santiago Melchor for his kind assistance and cooperation. We are also grateful to the Cluster of Scientific Computing (http://ccc.umh.es) of the Miguel Hernández University (UMH) for providing computer facilities. The authors would like to thank Kenneth McCreath for detailed editing of this manuscript.

Conflicts of Interest: J.B.-B. reports grants and personal fees from Roche-Genentech, grants from Pfizer and Pierre Fabre, and personal fees from MSD, BMS, AstraZeneca, Boehringer-Ingelheim, and Novartis, outside the submitted work. This study was partially supported by a research grant from Pfizer Global Research and Development to J.B.-B and J.A.M. The authors declare that the research was conducted in the absence of any commercial or financial relationships that could be construed as a potential conflict of interest.

References

1. Shaw, A.T.; Felip, E.; Bauer, T.M.; Besse, B.; Navarro, A.; Postel-Vinay, S.; Gainor, J.F.; Johnson, M.; Dietrich, J.; James, L.P.; et al. Lorlatinib in non-small-cell lung cancer with ALK or ROS1 rearrangement: An international, multicentre, open-label, single-arm first-in-man phase 1 trial. *Lancet Oncol.* **2017**, *18*, 1590–1599. [CrossRef]
2. Solomon, B.J.; Besse, B.; Bauer, T.M.; Felip, E.; Soo, R.A.; Camidge, D.R.; Chiari, R.; Bearz, A.; Lin, C.C.; Gadgeel, S.M.; et al. Lorlatinib in patients with ALK-positive non-small-cell lung cancer: Results from a global phase 2 study. *Lancet Oncol.* **2018**, *19*, 1654–1667. [CrossRef]
3. Shaw, A.T.; Bauer, T.M.; de Marinis, F.; Felip, E.; Goto, Y.; Liu, G.; Mazieres, J.; Kim, D.W.; Mok, T.; Polli, A.; et al. First-Line Lorlatinib or Crizotinib in Advanced *ALK*-Positive Lung Cancer. *N. Engl. J. Med.* **2020**, *383*, 2018–2029. [CrossRef] [PubMed]
4. Peng, L.; Zhu, L.; Sun, Y.; Stebbing, J.; Selvaggi, G.; Zhang, Y.; Yu, Z. Targeting ALK Rearrangements in NSCLC: Current State of the Art. *Front. Oncol.* **2022**, *12*, 863461. [CrossRef] [PubMed]

5. Yang, J.; Gong, W. Lorlatinib for the treatment of anaplastic lymphoma kinase-positive non-small cell lung cancer. *Expert Rev. Clin. Pharmacol.* **2019**, *12*, 173–178. [CrossRef]
6. Choo, J.R.; Soo, R.A. Lorlatinib for the treatment of *ALK*-positive metastatic non-small cell lung cancer. *Expert Rev. Anticancer Ther.* **2020**, *20*, 233–240. [CrossRef]
7. Johnson, T.W.; Richardson, P.F.; Bailey, S.; Brooun, A.; Burke, B.J.; Collins, M.R.; Cui, J.J.; Deal, J.G.; Deng, Y.L.; Dinh, D.; et al. Discovery of (10R)-7-amino-12-fluoro-2,10,16-trimethyl-15-oxo-10,15,16,17-tetrahydro-2H-8,4-(metheno)pyrazolo [4,3-h][2,5,11]-benzoxadiazacyclotetradecine-3-carbonitrile (PF-06463922), a macrocyclic inhibitor of anaplastic lymphoma kinase (ALK) and c-ros oncogene 1 (ROS1) with preclinical brain exposure and broad-spectrum potency against ALK-resistant mutations. *J. Med. Chem.* **2014**, *57*, 4720–4744.
8. Collier, T.L.; Normandin, M.D.; Stephenson, N.A.; Livni, E.; Liang, S.H.; Wooten, D.W.; Esfahani, S.A.; Stabin, M.G.; Mahmood, U.; Chen, J.; et al. Synthesis and preliminary PET imaging of ^{11}C and ^{18}F isotopologues of the ROS1/ALK inhibitor lorlatinib. *Nat. Commun.* **2017**, *8*, 15761. [CrossRef]
9. Costa, D.B.; Shaw, A.T.; Ou, S.H.; Solomon, B.J.; Riely, G.J.; Ahn, M.J.; Zhou, C.; Shreeve, S.M.; Selaru, P.; Polli, A.; et al. Clinical Experience with Crizotinib in Patients with Advanced ALK-Rearranged Non-Small-Cell Lung Cancer and Brain Metastases. *J. Clin. Oncol.* **2015**, *33*, 1881–1888. [CrossRef]
10. Bauer, T.M.; Shaw, A.T.; Johnson, M.L.; Navarro, A.; Gainor, J.F.; Thurm, H.; Pithavala, Y.K.; Abbattista, A.; Peltz, G.; Felip, E. Brain Penetration of Lorlatinib: Cumulative Incidences of CNS and Non-CNS Progression with Lorlatinib in Patients with Previously Treated ALK-Positive Non-Small-Cell Lung Cancer. *Target Oncol.* **2020**, *15*, 55–65. [CrossRef]
11. Felip, E.; Shaw, A.T.; Bearz, A.; Camidge, D.R.; Solomon, B.J.; Bauman, J.R.; Bauer, T.M.; Peters, S.; Toffalorio, F.; Abbattista, A.; et al. Intracranial and extracranial efficacy of lorlatinib in patients with ALK-positive non-small-cell lung cancer previously treated with second-generation ALK TKIs. *Ann. Oncol.* **2021**, *32*, 620–630. [CrossRef] [PubMed]
12. Yun, K.M.; Bazhenova, L.A. Update on Lorlatinib: Role in Reducing the Risk of Disease Progression in ALK-Positive NSCLC. *Cancer Manag. Res.* **2022**, *14*, 843–850. [CrossRef] [PubMed]
13. Syed, Y.Y. Lorlatinib: First Global Approval. *Drugs* **2019**, *79*, 93–98. [CrossRef]
14. Bauer, T.M.; Felip, E.; Solomon, B.J.; Thurm, H.; Peltz, G.; Chioda, M.D.; Shaw, A.T. Clinical Management of Adverse Events Associated with Lorlatinib. *Oncologist* **2019**, *24*, 1103–1110. [CrossRef] [PubMed]
15. Blais, N.; Adam, J.-P.; Nguyen, J.; Grégoire, J.C. Evaluation and Management of Dyslipidemia in Patients Treated with Lorlatinib. *Curr. Oncol.* **2021**, *28*, 265–272. [CrossRef]
16. Neuvonen, P.J.; Niemi, M.; Backman, J.T. Drug interactions with lipid-lowering drugs: Mechanisms and clinical relevance. *Clin. Pharmacol. Ther.* **2006**, *80*, 565–581. [CrossRef] [PubMed]
17. Reed, M.; Rosales, A.S.; Chioda, M.D.; Parker, L.; Devgan, G.; Kettle, J. Consensus Recommendations for Management and Counseling of Adverse Events Associated With Lorlatinib: A Guide for Healthcare Practitioners. *Adv. Ther.* **2020**, *37*, 3019–3030. [CrossRef]
18. Fernández-Arroyo, S.; Hernández-Aguilera, A.; de Vries, M.A.; Burggraaf, B.; van der Zwan, E.; Pouw, N.; Joven, J.; Cabezas, M.C. Effect of Vitamin D_3 on the Postprandial Lipid Profile in Obese Patients: A Non-Targeted Lipidomics Study. *Nutrients* **2019**, *11*, 1194. [CrossRef]
19. Nakabayashi, H.; Taketa, K.; Miyano, K.; Yamane, T.; Sato, J. Growth of human hepatoma cells lines with differentiated functions in chemically defined medium. *Cancer Res.* **1982**, *42*, 3858–3863.
20. Kawamoto, M.; Yamaji, T.; Saito, K.; Shirasago, Y.; Satomura, K.; Endo, T.; Fukasawa, M.; Hanada, K.; Osada, N. Identification of Characteristic Genomic Markers in Human Hepatoma HuH-7 and Huh7.5.1-8 Cell Lines. *Front. Genet.* **2020**, *11*, 546106. [CrossRef]
21. Ramboer, E.; Vanhaecke, T.; Rogiers, V.; Vinken, M. Immortalized Human Hepatic Cell Lines for In Vitro Testing and Research Purposes. *Methods Mol. Biol.* **2015**, *1250*, 53–76. [PubMed]
22. Berger, E.; Vega, N.; Weiss-Gayet, M.; Géloën, A. Gene Network Analysis of Glucose Linked Signaling Pathways and Their Role in Human Hepatocellular Carcinoma Cell Growth and Survival in HuH7 and HepG2 Cell Lines. *Biomed. Res. Int.* **2015**, *2015*, 821761. [CrossRef] [PubMed]
23. Bulutoglu, B.; Rey-Bedón, C.; Mert, S.; Tian, L.; Jang, Y.Y.; Yarmush, M.L.; Usta, O.B. A comparison of hepato-cellular in vitro platforms to study CYP3A4 induction. *PLoS ONE* **2020**, *15*, e0229106. [CrossRef] [PubMed]
24. Arzumanian, V.A.; Kiseleva, O.I.; Poverennaya, E.V. The Curious Case of the HepG2 Cell Line: 40 Years of Expertise. *Int. J. Mol. Sci.* **2021**, *22*, 13135. [CrossRef] [PubMed]
25. Bijak, M. Silybin, a Major Bioactive Component of Milk Thistle (Silybum marianum L. Gaernt.)-Chemistry, Bioavailability, and Metabolism. *Molecules* **2017**, *22*, 1942. [CrossRef]
26. Křen, V.; Valentová, K. Silybin and its congeners: From traditional medicine to molecular effects. *Nat. Prod. Rep.* **2022**, *39*, 1264–1281. [CrossRef]
27. Wang, X.; Zhang, Z.; Wu, S.C. Health Benefits of *Silybum marianum*: Phytochemistry, Pharmacology, and Applications. *J. Agric. Food Chem.* **2020**, *68*, 11644–11664. [CrossRef]
28. Federico, A.; Dallio, M.; Loguercio, C. Silymarin/Silybin and Chronic Liver Disease: A Marriage of Many Years. *Molecules* **2017**, *22*, 191. [CrossRef]

29. Hackett, E.S.; Twedt, D.C.; Gustafson, D.L. Milk thistle and its derivative compounds: A review of opportunities for treatment of liver disease. *J. Vet. Intern. Med.* **2013**, *27*, 10–16. [CrossRef]
30. Abenavoli, L.; Capasso, R.; Milic, N.; Capasso, F. Milk thistle in liver diseases: Past, present, future. *Phytother. Res.* **2010**, *24*, 1423–1432. [CrossRef]
31. Rikova, K.; Guo, A.; Zeng, Q.; Possemato, A.; Yu, J.; Haack, H.; Nardone, J.; Lee, K.; Reeves, C.; Li, Y.; et al. Global survey of phosphotyrosine signaling identifies oncogenic kinases in lung cancer. *Cell* **2007**, *131*, 1190–1203. [CrossRef] [PubMed]
32. Li, Y.; Ye, X.; Liu, J.; Zha, J.; Pei, L. Evaluation of EML4-ALK fusion proteins in non-small cell lung cancer using small molecule inhibitors. *Neoplasia* **2011**, *13*, 1–11. [CrossRef] [PubMed]
33. Samuels, E.R.; Sevrioukova, I.F. Rational Design of CYP3A4 Inhibitors: A One-Atom Linker Elongation in Ritonavir-Like Compounds Leads to a Marked Improvement in the Binding Strength. *Int. J. Mol. Sci.* **2021**, *22*, 852. [CrossRef] [PubMed]
34. Domanski, T.L.; He, Y.A.; Harlow, G.R.; Halpert, J.R. Dual role of human cytochrome P450 3A4 residue Phe-304 in substrate specificity and cooperativity. *J. Pharmacol. Exp. Ther.* **2000**, *293*, 585–591.
35. Hackett, J.C. Membrane-embedded substrate recognition by cytochrome P450 3A4. *J. Biol. Chem.* **2018**, *293*, 4037–4046. [CrossRef]
36. Sevrioukova, I.F.; Poulos, T.L. Understanding the mechanism of cytochrome P450 3A4: Recent advances and remaining problems. *Dalton Trans.* **2013**, *42*, 3116–3126. [CrossRef]
37. Sevrioukova, I.F.; Poulos, T.L. Structure and mechanism of the complex between cytochrome P4503A4 and ritonavir. *Proc. Natl. Acad. Sci. USA* **2010**, *107*, 18422–18427. [CrossRef]
38. Sevrioukova, I.F.; Poulos, T.L. Ritonavir analogues as a probe for deciphering the cytochrome P450 3A4 inhibitory mechanism. *Curr. Top. Med. Chem.* **2014**, *14*, 1348–1355. [CrossRef]
39. Li, X.; Xu, Y.; Lai, L.; Pei, J. Prediction of Human Cytochrome P450 Inhibition Using a Multitask Deep Autoencoder Neural Network. *Mol. Pharm.* **2018**, *15*, 4336–4345. [CrossRef]
40. Gillessen, A.; Schmidt, H.H. Silymarin as Supportive Treatment in Liver Diseases: A Narrative Review. *Adv. Ther.* **2020**, *37*, 1279–1301. [CrossRef]
41. Pérez-Sánchez, A.; Cuyàs, E.; Ruiz-Torres, V.; Agulló-Chazarra, L.; Verdura, S.; González-Álvarez, I.; Bermejo, M.; Joven, J.; Micol, V.; Bosch-Barrera, J.; et al. Intestinal Permeability Study of Clinically Relevant Formulations of Silibinin in Caco-2 Cell Monolayers. *Int. J. Mol. Sci.* **2019**, *20*, 1606. [CrossRef] [PubMed]
42. Schnell, P.; Bartlett, C.H.; Solomon, B.J.; Tassell, V.; Shaw, A.T.; de Pas, T.; Lee, S.H.; Lee, G.K.; Tanaka, K.; Tan, W.; et al. Complex renal cysts associated with crizotinib treatment. *Cancer Med.* **2015**, *4*, 887–896. [CrossRef] [PubMed]
43. Camidge, D.R.; Kim, E.E.; Usari, T.; Polli, A.; Lewis, I.; Wilner, K.D. Renal effects of crizotinib in patients with ALK-positive advanced NSCLC. *J. Thorac. Oncol.* **2019**, *14*, 1077–1085. [CrossRef] [PubMed]
44. Hong, M.H. Nephrotoxicity of cancer therapeutic drugs: Focusing on novel agents. *Kidney Res. Clin. Pract.* **2021**, *40*, 344–354. [CrossRef] [PubMed]
45. McGee, K.; Stone, N.J.; Wadhwani, S.; Kanwar, Y.S.; Villaflor, V.; Akhter, N. A possible mechanism of hyperlipidemia in a patient with metastatic non-small cell lung cancer on lorlatinib therapy. *J. Oncol. Pharm. Pract.* **2021**, *27*, 2010–2013. [CrossRef]
46. Hibma, J.E.; O'Gorman, M.; Nepal, S.; Pawlak, S.; Ginman, K.; Pithavala, Y.K. Evaluation of the absolute oral bioavailability of the anaplastic lymphoma kinase/c-ROS oncogene 1 kinase inhibitor lorlatinib in healthy participants. *Cancer Chemother. Pharmacol.* **2022**, *89*, 71–81. [CrossRef] [PubMed]
47. Chen, J.; Houk, B.; Pithavala, Y.K.; Ruiz-Garcia, A. Population pharmacokinetic model with time-varying clearance for lorlatinib using pooled data from patients with non-small cell lung cancer and healthy participants. *CPT Pharmacomet. Syst. Pharmacol.* **2021**, *10*, 148–160. [CrossRef]
48. Chen, W.; Shi, Y.; Qi, S.; Zhou, H.; Li, C.; Jin, D.; Li, G. Pharmacokinetic Study and Tissue Distribution of Lorlatinib in Mouse Serum and Tissue Samples by Liquid Chromatography-Mass Spectrometry. *J. Anal. Methods Chem.* **2019**, *2019*, 7574369. [CrossRef]
49. Rodríguez-Hernández, M.A.; de la Cruz-Ojeda, P.; López-Grueso, M.J.; Navarro-Villarán, E.; Requejo-Aguilar, R.; Castejón-Vega, B.; Negrete, M.; Gallego, P.; Vega-Ochoa, Á.; Victor, V.M.; et al. Integrated molecular signaling involving mitochondrial dysfunction and alteration of cell metabolism induced by tyrosine kinase inhibitors in cancer. *Redox Biol.* **2020**, *36*, 101510. [CrossRef]
50. Mihajlovic, M.; Vinken, M. Mitochondria as the Target of Hepatotoxicity and Drug-Induced Liver Injury: Molecular Mechanisms and Detection Methods. *Int. J. Mol. Sci.* **2022**, *23*, 3315. [CrossRef]
51. Yin, F.; Gupta, R.; Vergnes, L.; Driscoll, W.S.; Ricks, J.; Ramanathan, G.; Stewart, J.A.; Shih, D.M.; Faull, K.F.; Beaven, S.W.; et al. Diesel Exhaust Induces Mitochondrial Dysfunction, Hyperlipidemia, and Liver Steatosis. *Arterioscler. Thromb. Vasc. Biol.* **2019**, *39*, 1776–1786. [CrossRef]
52. Remon, J.; Besse, B. Brain Metastases in Oncogene-Addicted Non-Small Cell Lung Cancer Patients: Incidence and Treatment. *Front Oncol.* **2018**, *8*, 88. [CrossRef] [PubMed]
53. Bosch-Barrera, J.; Sais, E.; Cañete, N.; Marruecos, J.; Cuyàs, E.; Izquierdo, A.; Porta, R.; Haro, M.; Brunet, J.; Pedraza, S.; et al. Response of brain metastasis from lung cancer patients to an oral nutraceutical product containing silibinin. *Oncotarget* **2016**, *7*, 32006–32014. [CrossRef]
54. Priego, N.; Zhu, L.; Monteiro, C.; Mulders, M.; Wasilewski, D.; Bindeman, W.; Doglio, L.; Martínez, L.; Martínez-Saez, E.; Ramón, Y.; et al. STAT3 labels a subpopulation of reactive astrocytes required for brain metastasis. *Nat. Med.* **2018**, *24*, 1024–1035. [CrossRef] [PubMed]

55. Li, W.; Sparidans, R.W.; Wang, Y.; Lebre, M.C.; Wagenaar, E.; Beijnen, J.H.; Schinkel, A.H. P-glycoprotein (MDR1/ABCB1) restricts brain accumulation and cytochrome P450-3A (CYP3A) limits oral availability of the novel ALK/ROS1 inhibitor lorlatinib. *Int. J. Cancer* **2018**, *143*, 2029–2038. [CrossRef] [PubMed]
56. Hu, W.; Lettiere, D.; Tse, S.; Johnson, T.R.; Biddle, K.E.; Thibault, S.; Palazzi, X.; Chen, J.; Pithavala, Y.K.; Finkelstein, M. Liver Toxicity Observed With Lorlatinib When Combined With Strong CYP3A Inducers: Evaluation of Cynomolgus Monkey as a Nonclinical Model for Assessing the Mechanism of Combinational Toxicity. *Toxicol. Sci.* **2021**, *182*, 183–194. [CrossRef]
57. Brantley, S.J.; Graf, T.N.; Oberlies, N.H.; Paine, M.F. A systematic approach to evaluate herb-drug interaction mechanisms: Investigation of milk thistle extracts and eight isolated constituents as CYP3A inhibitors. *Drug Metab. Dispos.* **2013**, *41*, 1662–1670. [CrossRef] [PubMed]
58. Beckmann-Knopp, S.; Rietbrock, S.; Weyhenmeyer, R.; Böcker, R.H.; Beckurts, K.T.; Lang, W.; Hunz, M.; Fuhr, U. Inhibitory effects of silibinin on cytochrome P-450 enzymes in human liver microsomes. *Pharmacol. Toxicol.* **2000**, *86*, 250–256. [CrossRef]
59. Lin, J.; Schyschka, L.; Mühl-Benninghaus, R.; Neumann, J.; Hao, L.; Nussler, N.; Dooley, S.; Liu, L.; Stöckle, U.; Nussler, A.K.; et al. Comparative analysis of phase I and II enzyme activities in 5 hepatic cell lines identifies Huh-7 and HCC-T cells with the highest potential to study drug metabolism. *Arch. Toxicol.* **2012**, *86*, 87–95. [CrossRef]
60. Liu, Y.; Flynn, T.J.; Xia, M.; Wiesenfeld, P.L.; Ferguson, M.S. Evaluation of CYP3A4 inhibition and hepatotoxicity using DMSO-treated human hepatoma HuH-7 cells. *Cell. Biol. Toxicol.* **2015**, *31*, 221–230. [CrossRef]
61. Guo, L.; Dial, S.; Branham, W.; Liu, J.; Fang, J.L.; Green, B.; Deng, H.; Kaput, J.; Ning, B. Similarities and differences in the expression of drug-metabolizing enzymes between human hepatic cell lines and primary human hepatocytes. *Drug Metab. Dispos.* **2011**, *39*, 528–538. [CrossRef] [PubMed]
62. Sivertsson, L.; Ek, M.; Darnell, M.; Edebert, I.; Ingelman-Sundberg, M.; Neve, E.P. CYP3A4 catalytic activity is induced in confluent Huh7 hepatoma cells. *Drug Metab. Dispos.* **2010**, *38*, 995–1002. [CrossRef] [PubMed]
63. Sivertsson, L.; Edebert, I.; Palmertz, M.P.; Ingelman-Sundberg, M.; Neve, E.P. Induced CYP3A4 expression in confluent Huh7 hepatoma cells as a result of decreased cell proliferation and subsequent pregnane X receptor activation. *Mol. Pharmacol.* **2013**, *83*, 659–670. [CrossRef]
64. Kanebratt, K.P.; Andersson, T.B. HepaRG cells as an in vitro model for evaluation of cytochrome P450 induction in humans. *Drug Metab. Dispos.* **2008**, *36*, 137–145. [CrossRef] [PubMed]
65. Kanebratt, K.P.; Andersson, T.B. Evaluation of HepaRG cells as an in vitro model for human drug metabolism studies. *Drug Metab. Dispos.* **2008**, *36*, 1444–1452. [CrossRef] [PubMed]
66. Andersson, T.B.; Kanebratt, K.P.; Kenna, J.G. The HepaRG cell line: A unique in vitro tool for understanding drug metabolism and toxicology in human. *Expert Opin. Drug Metab. Toxicol.* **2012**, *8*, 909–920. [CrossRef] [PubMed]
67. Corominas-Faja, B.; Cuyàs, E.; Lozano-Sánchez, J.; Cufí, S.; Verdura, S.; Fernández-Arroyo, S.; Borrás-Linares, I.; Martin-Castillo, B.; Martin, Á.G.; Lupu, R.; et al. Extra-virgin olive oil contains a metabolo-epigenetic inhibitor of cancer stem cells. *Carcinogenesis* **2018**, *39*, 601–613. [CrossRef]
68. Verdura, S.; Cuyàs, E.; Lozano-Sánchez, J.; Bastidas-Velez, C.; Llorach-Parés, L.; Fernández-Arroyo, S.; Hernández-Aguilera, A.; Joven, J.; Nonell-Canals, A.; Bosch-Barrera, J.; et al. An olive oil phenolic is a new chemotype of mutant isocitrate dehydrogenase 1 (IDH1) inhibitors. *Carcinogenesis* **2019**, *40*, 27–40. [CrossRef]
69. Cuyàs, E.; Castillo, D.; Llorach-Parés, L.; Lozano-Sánchez, J.; Verdura, S.; Nonell-Canals, A.; Brunet, J.; Bosch-Barrera, J.; Joven, J.; Valdés, R.; et al. Computational de-orphanization of the olive oil biophenol oleacein: Discovery of new metabolic and epigenetic targets. *Food Chem. Toxicol.* **2019**, *131*, 110529. [CrossRef]
70. Encinar, J.A.; Menendez, J.A. Potential Drugs Targeting Early Innate Immune Evasion of SARS-Coronavirus 2 via 2′-O-Methylation of Viral RNA. *Viruses* **2020**, *12*, 525. [CrossRef]
71. Tramonti, A.; Cuyàs, E.; Encinar, J.A.; Pietzke, M.; Paone, A.; Verdura, S.; Arbusà, A.; Martin-Castillo, B.; Giardina, G.; Joven, J.; et al. Metformin Is a Pyridoxal-5′-phosphate (PLP)-Competitive Inhibitor of SHMT2. *Cancers* **2021**, *13*, 4009. [CrossRef] [PubMed]
72. Verdura, S.; Cuyàs, E.; Cortada, E.; Brunet, J.; Lopez-Bonet, E.; Martin-Castillo, B.; Bosch-Barrera, J.; Encinar, J.A.; Menendez, J.A. Resveratrol targets PD-L1 glycosylation and dimerization to enhance antitumor T-cell immunity. *Aging* **2020**, *12*, 8–34. [CrossRef] [PubMed]
73. Cuyàs, E.; Verdura, S.; Lozano-Sánchez, J.; Viciano, I.; Llorach-Parés, L.; Nonell-Canals, A.; Bosch-Barrera, J.; Brunet, J.; Segura-Carretero, A.; Sanchez-Martinez, M.; et al. The extra virgin olive oil phenolic oleacein is a dual substrate-inhibitor of catechol-O-methyltransferase. *Food Chem. Toxicol.* **2019**, *128*, 35–45. [CrossRef]
74. Seeliger, D.; de Groot, B.L. Ligand docking and binding site analysis with PyMOL and Autodock/Vina. *J. Comput. Aided Mol. Des.* **2010**, *24*, 417–422. [CrossRef]
75. Salentin, S.; Schreiber, S.; Haupt, V.J.; Adasme, M.F.; Schroeder, M. PLIP: Fully automated protein-ligand interaction profiler. *Nucleic Acids Res.* **2015**, *43*, W443–W447. [CrossRef] [PubMed]
76. Cuyàs, E.; Pérez-Sánchez, A.; Micol, V.; Menendez, J.A.; Bosch-Barrera, J. STAT3-targeted treatment with silibinin overcomes the acquired resistance to crizotinib in ALK-rearranged lung cancer. *Cell Cycle* **2016**, *15*, 3413–3418. [CrossRef] [PubMed]
77. Verdura, S.; Cuyàs, E.; Ruiz-Torres, V.; Micol, V.; Joven, J.; Bosch-Barrera, J.; Menendez, J.A. Lung Cancer Management with Silibinin: A Historical and Translational Perspective. *Pharmaceuticals* **2021**, *14*, 559. [CrossRef]

STUDY 5

Revisiting silibinin as a novobiocin-like Hsp90 C-terminal inhibitor: Computational modeling and experimental validation

Cuyàs E, Verdura S, Micol V, Joven J, Bosch-Barrera J, Encinar JA, Menendez JA.

Food Chem Toxicol. 2019 Oct;132:110645

doi: 10.1016/j.fct.2019.110645

Food and Chemical Toxicology 132 (2019) 110645

Contents lists available at ScienceDirect

Food and Chemical Toxicology

journal homepage: www.elsevier.com/locate/foodchemtox

Short communication

Revisiting silibinin as a novobiocin-like Hsp90 C-terminal inhibitor: Computational modeling and experimental validation

Elisabet Cuyàs[a,b,1], Sara Verdura[a,b,1], Vicente Micol[c], Jorge Joven[d], Joaquim Bosch-Barrera[b,e,f], José Antonio Encinar[c,**], Javier A. Menendez[a,b,*]

[a] ProCURE (Program Against Cancer Therapeutic Resistance), Metabolism and Cancer Group, Catalan Institute of Oncology, Girona, Spain
[b] Girona Biomedical Research Institute (IDIBGI), Girona, Spain
[c] Institute of Research, Development and Innovation in Biotechnology of Elche (IDiBE), and Molecular and Cell Biology Institute (IBMC), Miguel Hernández University (UMH), Elche, Spain
[d] Unitat de Recerca Biomèdica, Hospital Universitari Sant Joan, Institut d'Investigació Sanitària Pere Virgili, Universitat Rovira i Virgili, Reus, Spain
[e] Medical Oncology, Catalan Institute of Oncology (ICO), Girona, Spain
[f] Department of Medical Sciences, Medical School University of Girona, Girona, Spain

ARTICLE INFO

Keywords:
Silibinin
Hsp90
Cancer

ABSTRACT

The flavonolignan silibinin is the major component of the extract isolated from the seeds of the milk thistle (*Silybum marianum*). Herein, we performed an *in silico* analysis focusing on the molecular docking of the putative atomic interactions between silibinin and heat shock protein 90 (Hsp90), an adenosine triphosphate-dependent molecular chaperone differentially expressed in response to microenvironmental stress. Time-resolved fluorescence resonance energy transfer was employed to measure the capacity of silibinin to inhibit Hsp90 binding to other co-chaperones with enzymatic activity. Whereas silibinin is predicted to interact with several pockets in the C-terminal domain (CTD) of Hsp90α and β, its highest-ranking docked poses significantly overlap with those of novobiocin, a well-characterized Hsp90 CTD-targeting inhibitor. The net biochemical effect of silibinin was to inhibit the efficiency of Hsp90α/β CTD binding to its co-chaperone PPID/cyclophilin D in the low millimolar range, equivalent to that observed for novobiocin. The hepatotoxicant behavior of silibinin solely occurred at concentrations several thousand times higher than those of the Hsp90 N-terminal inhibitor geldanamycin. Silibinin might be viewed as a non-hepatotoxic, novobiocin-like Hsp90 inhibitor that binds the CTD to induce changes in Hsp90 conformation and alter Hsp90-co-chaperone-client interactions, thereby providing new paths to developing safe and efficacious Hsp90 inhibitors.

1. Introduction

Silibinin is the major bioactive component of silymarin, a flavonolignan extract obtained from the seeds of the milk thistle herb (*Silybum marianum*) (Abenavoli et al., 2018). Silibinin-containing silymarin and new formulations of silibinin have been employed over the last 40 years as anti-hepatotoxic agents and as components of nutritional supplements aimed at preventing hepatic steatosis and protecting liver from exposure to chemical and environmental toxins (Federico et al., 2017; Gazák et al., 2007 Abenavoli et al., 2018). Moreover, an ever-growing number of studies have demonstrated the capacity of silibinin to exhibit inhibitory activity against cultured cancer cells and tumor xenografts, to enhance the efficacy of other therapeutic agents, to reduce the toxicity of cancer treatments, and to prevent and overcome the emergence of cancer drug resistance (Bosch-Barrera and Menendez, 2015; 2017). More importantly, when used orally as part of more bioavailable formulations, silibinin has recently been shown to exhibit significant clinical activity in cancer patients with advanced systemic disease (Bosch-Barrera et al., 2014, 2016; Priego et al., 2018). Indeed, responses to silibinin-based therapy were notable in the central nervous system, where several complete responses were achieved in patients with non-small cell lung cancer (NSCLC) presenting brain metastases

* Corresponding author. Catalan Institute of Oncology (ICO), Girona Biomedical Research Institute (IDIBGI), Edifici M2, Parc Hospitalari Martí i Julià, E-17190, Salt, Girona, Spain.
** Corresponding author. Instituto de Investigación, Desarrollo e Innovación en, Biotecnología Sanitaria de Elche (IDiBE), Av. de la Universidad, Edif. Torregaitan, Despacho 2.08, E-03202, Elche, Alicante, Spain.
E-mail addresses: jant.encinar@umh.es (J.A. Encinar), jmenendez@iconcologia.net, jmenendez@idibgi.org (J.A. Menendez).
[1] These authors contributed equally.

https://doi.org/10.1016/j.fct.2019.110645
Received 26 February 2019; Received in revised form 27 May 2019; Accepted 23 June 2019
Available online 26 June 2019

(Priego et al., 2018).

Investigations into the molecular mechanisms involved in the aforementioned anti-cancer activities of silibinin have repeatedly confirmed its ability to function as a natural down-modulator of signal transducer and activator of transcription (STAT3) signaling (Agarwal et al., 2007; Bosch-Barrera and Menendez, 2015, 2017; Cuyàs et al., 2016). We recently combined computational and experimental approaches to confirm that silibinin can directly bind and inhibit STAT3 at both the Src homology-2 (SH2) dimerization domain and the DNA-binding transactivation domain (DBD) (Verdura et al., 2018). Accordingly, the suppressive effects of silibinin on brain metastases can be explained by its capacity to block STAT3 signaling in a sub-population of reactive astrocytes required for the maintenance of brain metastastic lesions, even at advanced stages of colonization (Priego et al., 2018). As a flavonoid, however, silibinin is expected to interact with a variety of molecular targets (Mateen et al., 2013; Tiwari and Mishra, 2015; Jahanafrooz et al., 2018), some of which might be highly relevant to those tumor lesions occurring in the brain. One such mechanism might involve heat shock protein 90 (Hsp90), an adenosine triphosphate (ATP)-dependent molecular chaperone that is critically required for the correct localization, folding, and stability of its client proteins, many of which are well-known driver oncoproteins such as STAT3.

Previous biochemical assays revealed that the inhibitory activity of silibinin against Hsp90 is likely the result of binding to the C-terminus of the protein (Zhao et al., 2011, 2012). Also, animal models confirmed the ability of silibinin to operate as an Hsp90 inhibitor targeting the pathogenesis of Cushing disease, which is caused by corticotroph adenomas of the pituitary that overexpress Hsp90 and hypersecrete adrenocorticotropin (Riebold et al., 2015a,b; Sbiera et al., 2015; Sugiyama et al., 2015). Because most of the Hsp90 client proteins belong to multiple signaling pathways, many of them linked specifically to metastatic processes, a single Hsp90 inhibitor is expected to provide the equivalent of “multitargeted” or combinatorial therapy, thereby overriding the danger of resistance phenomena. Although several Hsp90 inhibitors have demonstrated promising preclinical and clinical results in tumors that have become resistant to molecular-targeted agents, most of them are hindered by their low capacity to cross the blood-brain barrier (BBB), limited target inhibition and toxicities (Neckers and Workman, 2012; Travers et al., 2012; Blair et al., 2014; Chatterjee and Burns, 2017). Given the clinical benefit of a well-tolerated and safe oral treatment with a silibinin-containing nutraceutical for targeting secondary brain tumors (Bosch-Barrera et al., 2016; Priego et al., 2018) and the recently predicted BBB permeability of clinically relevant formulations of silibinin (Pérez-Sánchez et al., 2019), it might be relevant to reassess the proposed capacity of silibinin to target Hsp90. In this regard, liver toxicity, a leading systemic toxicity of drugs and chemicals, is demanding human-relevant *in vitro* solutions to overcome a major drawback for the therapeutic use of Hsp90 inhibition, namely the dose-limiting hepatotoxicity elicited by conventional geldanamycin-derivate Hsp90 inhibitors containing a benzoquinone moiety (Egorin et al., 1998; Dikalov et al., 2002; Cysyk et al., 2006; Lauber et al., 2015). Indeed, the clinical translation of Hsp90 blockade has largely been hampered by serious hepatotoxicity of first- and second-generation Hsp90 inhibitors. Given the well-known hepatoprotective effects of silymarin and its major active constituent silibinin and the accompanying lack of adverse effects even at high doses (Vargas-Mendoza et al., 2014; Soleimani et al., 2019), silibinin deserves to be studied as a clinically relevant non-hepatotoxic Hsp90 C-terminal inhibitor.

Herein, we present an *in silico* analysis focusing on the molecular docking of the putative atomic interactions between silibinin and Hsp90. Time-resolved fluorescence energy transfer (TR-FRET) technology was additionally employed to measure silibinin's capacity to inhibit Hsp90 binding to other co-chaperones with enzymatic activity. Comparative studies were conducted with the amino coumarin natural product novobiocin, a well-known inhibitor of the C-terminal domain (CTD) of Hsp90 (Marcu et al., 2000a,b; Matts et al., 2011). Finally, a comparative analysis of silibinin-versus geldanamycin-induced hepatotoxicity and superoxide production was conducted in HepG2 human hepatoma cells. We now provide computational and experimental evidence to propose silibinin as a novobiocin-like Hsp90 CTD inhibitor that induces changes in Hsp90 conformation and alter Hsp90-co-chaperone-client interactions without promoting unwanted biotransformation phenomena responsible for hepatotoxicity.

2. Materials and methods

2.1. Homology modeling

To date, 286 and 15 resolved structures have been deposited in the PDB for Hsp90α (UniProt code P07900, HS90A_HUMAN) and Hsp90β (UniProt code P08238, HS90B_HUMAN) proteins, respectively. For Hsp90β, the 5FWM structure represents a closed conformation. However, structures of Hsp90β in open conformations, or Hsp90α open or closed conformations have not yet been deposited in the PDB. Therefore, three-dimensional (3D) structural models of the full-length Hsp90β in open conformations were generated by homology modeling in automated mode (Biasini et al., 2014) using the 2IOQ structure as a template. Using the same methodology, 3D models were generated for the open and closed conformations of full-length Hsp90α using 2O1U and 5ULS, respectively, as templates. A description of this methodology has been previously reported (Bello-Pérez et al., 2018).

2.2. Molecular docking

The structures of silibinin (PubChem CID: 31553) and novobiocin (PubChem CID: 54675769) were obtained from the National Center for Biotechnology Information (NCBI) PubChem database (http://www.ncbi.nlm.nih.gov/pccompound).

Molecular docking experiments were carried out using YASARA v18.12.27 software (Krieger et al., 2004), as described (Encinar et al., 2015; Galiano et al., 2016). A total of 500 flexible docking runs were set and clustered (6 Å) around the putative binding sites, i.e., two complexed compounds belong to different clusters if the ligand Root-Mean-Square Deviation of their atomic positions is greater than a minimum of 6 Å around certain hot spot conformations. The YASARA pH command was set to 7.4. The YASARA software calculated the Gibbs free energy variation (ΔG, kcal/mol), with more positive energy values indicating stronger binding. To calculate this parameter, which is used to rank compounds, Autodock Vina uses a force field scoring function that considers the strength of electrostatic interactions, hydrogen bonding between all atoms of the two binding partners in the complex, intermolecular van der Waals forces, and also solvation and entropy contributions (Lionta et al., 2014). All the values are included in the corresponding tables with a negative sign. Only the ΔG value for the best compound docked in each cluster is shown. Dissociation constants were recalculated from the average binding energy of all compounds of each cluster. The key residues of each receptor monomer (chain 1 or 2) interacting with the best ligand in each cluster were detected using also YASARA v18.12.27 software (Krieger et al., 2004). All of the figures were prepared using PyMol 2.0 software and all the interactions were detected using the PLIP algorithm (Salentin et al., 2015).

2.3. TR-FRET-based Hsp90 CTD activity assays

To determine the effect of novobiocin and silibinin on the activity of Hsp90, we employed TR-FRET technology using either recombinant human Hsp90α (6 ng/reaction of HSP90α [535–732] Cat. #50316, protein lot #140103-G3) or Hsp90β (6 ng/reaction of HSP90β [535–724], Cat. #50313, protein lot #130607-G) CTDs and the PPID ligand (56 nmol/L, lot# 130703), all from BPS Bioscience (San Diego, CA). The TR-FRET signal from the assay correlates with the amount of PPID ligand binding to the HSP90 CTD.

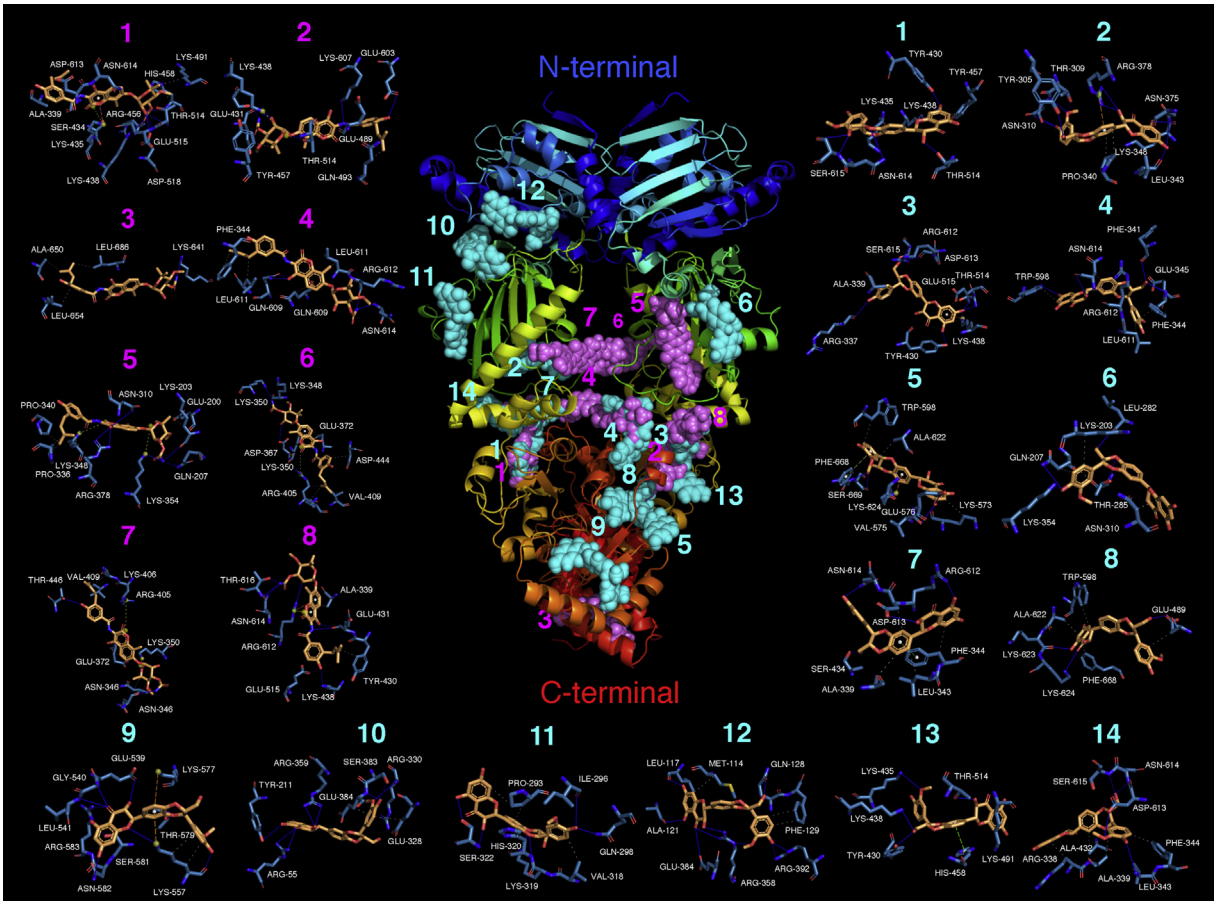

Fig. 1. Hsp90β in a closed conformation with docked novobiocin and silibinin. Figure depicts the backbone of the Hsp90β homodimer (PDB code 5FWM) with rainbow colors from the N-terminal (blue) to the C-terminal (red) domain. For each cluster of the docked compound (novobiocin and novobiocin cluster numbers are shown in violet while silibinin and silibinin cluster numbers are shown in cyan), only the molecule (spheres) with the best binding energy is shown. Each inset shows the detailed interactions of each compound docked to the protein, indicating the participating amino acids involved in the interaction and the type of interaction (hydrogen bonds, hydrophilic interactions, salt bridges, II-stacking, etc). (For interpretation of the references to color in this figure legend, the reader is referred to the Web version of this article.)

The compounds were diluted in 10% DMSO and 2 μL of the dilution was added to a 20 μL reaction so that the final concentration of DMSO was 1% in all of the reactions. All binding reactions were conducted at room temperature. The 20 μL reaction mixture in C-terminal assay buffer contained the Hsp90α/β CTD, the indicated amount of the inhibitor, PPID, and the reaction dyes. The reaction mixture was incubated for 120 min prior to reading the TR-FRET signal. For the negative control, buffer was added instead of PPID. Fluorescence signals for both the donor and acceptor dyes were measured using a Tecan Infinite M1000 plate reader (Männedorf, Switzerland). TR-FRET was recorded as the ratio of the fluorescence of the acceptor and the donor dyes (acceptor/donor).

Binding experiments were performed in duplicate at each concentration. The TR-FRET data were analyzed using Graphpad Prism computer software. In wells containing PPID and no compound, the TR-FRET signal (F_t) in each data set was defined as 100% activity. In wells without peptide ligand, the TR-FRET signal (F_b) in each data set was defined as 0% activity. The percentage activity in the presence of each compound was calculated according to the following equation: % activity = $[(F\text{-}F_b)/(F_t - F_b)] \times 100$, where F = the TR-FRET signal in the presence of the compound. The percentage inhibition was calculated according to the following equation: % inhibition = 100 - % activity. To calculate the IC_{50} values, the % activity versus a series of compound concentrations were plotted using non-linear regression analysis of sigmoidal dose-response generated with the equation Y = B + (T-B)/1 + 10∧((LogIC50-Z) × HillSlope), where Y = percent activity, B = minimum percent activity, T = maximum percent activity, Z = logarithm of compound concentration and Hill Slope = slope factor or Hill coefficient. The IC_{50} values were then determined as the concentration causing a half-maximal percent activity.

2.4. Reagents

Silibinin and novobiocin were purchased from Sigma-Aldrich (St. Louis, MO). Geldanamycin and ganetespib (STA-9090) were purchased from Selleckchem.com. All reagents were dissolved in dimethylsulfoxide (DMSO) to prepare 10 mmol/L stock solutions, which were stored at −80 °C until use.

2.5. Metabolic status assessment

Cell viability was determined using standard colorimetric MTT-based reduction assays.

2.6. Mitochondrial ROS measurements

To detect mitochondrial ROS, HepG2 liver cancer cells (a kind gift from Dr. Jose Manuel Fernández-Real, Girona, Spain) were treated with rotenone, geldanamycin, ganetespib (STA-909), novobiocin or silibinin for 18 h and then incubated at 37 °C with MitoSOX (5 μM; Invitrogen) for 20 min in PBS, washed three times with PBS and analyzed by flow cytometry.

2.7. Statistical analysis

All statistical analyses were performed using XLSTAT 2010 (Addinsoft™). Data are presented as mean ± S.D. Comparisons of means of ≥3 groups were performed by ANOVA, and the existence of individual differences, in case of significant *F* values at ANOVA, were tested by Scheffé's multiple contrasts. *P* values < 0.05 were considered to be statistically significant (denoted as *). All statistical tests were two-sided.

3. Results

Molecular docking assays of silibinin and novobiocin against Hsp90α and β isoforms, which are differently expressed in embryonic and adult tissues and exhibit significantly different behaviors with respect to substrate/client interactions under stress conditions (Taherian et al., 2008), were performed as previously described (Encinar et al., 2015; Galiano et al., 2016). The selected protein structures, either from the Protein Data Bank (PDB) or homology modeled, were subjected to geometry optimization using the repair function of the FoldX algorithm (Schymkowitz et al., 2005). To search for potential binding sites of silibinin and novobiocin, a global molecular docking procedure was performed with AutoDock Vina using YASARA software (Krieger and Vriend, 2014), where a total of 500 flexible docking runs were set and clustered around the putative binding sites.

3.1. Prediction of the Hsp90β-silibinin interactions

Docking simulations of novobiocin and silibinin in the closed conformation of Hsp90β (5FWM structure) produced eight and fourteen clusters of docking poses, respectively (Fig. 1). The docking results were ranked according to the ascent of the binding energies for novobiocin (up to −10.124 kcal/mol) and silibinin (up to −9.408 kcal/mol) (Table 1). A careful inspection of the different conformations showed that, in the #1 ranked cluster of both compounds, the Hsp90β-silibinin interaction shared approximately 80% of the twenty-four participating amino acid residues involved in the novobiocin binding mode to the chain 1 of closed Hsp90β (ALA339, PRO340, PHE341, LEU343, TYR430, GLU431, ALA432, SER434, LYS435, LYS438, ARG456, TYR457, HIS458, LYS491, TYR512, MET513, THR514, and GLY515; Table 1), and 100% of the three amino acid residues involved in the novobiocin binding mode to the chain 2 ASP613, ASN614, SER615; Table 1).

Upon generation of a computational homology model (Biasini et al., 2014) of Hsp90β in its open conformation (Dollins et al., 2007), docking simulations of novobiocin and silibinin similarly produced four clusters of docking poses for each compound (Fig. 2), with binding energies up to −9.41 kcal/mol for novobiocin and −8.789 kcal/mol for silibinin. The binding mode of silibinin in the #1 ranked cluster shared 50% of the twenty participating amino acid residues involved in the novobiocin binding mode to the chain 1 of closed Hsp90β (ASN30, TYR33, ILE38, ARG41, HIS205, GLU303, LYS306, TRP312, ASP314, and ARG337; Table 2).

3.2. Prediction of the Hsp90α-silibinin interactions

Docking simulations of novobiocin and silibinin in a homology model of the closed conformation of Hsp90α produced three and eight clusters of docking poses, respectively (Fig. 3). Binding energies were −9.043 kcal/mol for novobiocin and −9.703 kcal/mol for silibinin in the #1 ranked cluster; the binding mode of the docked silibinin was similar to the binding observed for novobiocin in the #2 ranked cluster, in which silibinin shared approximately 40% of the twenty-one participating amino acid residues involved in the novobiocin binding mode to the chain 1 of closed Hsp90α (ASN354, LYS356, LYS357, LYS358, GLU374, ASN383, LEU447, and GLU451), and 25% of the four amino acid residues involved in the novobiocin binding mode to the chain 2 (LEU619) (Table 3).

Upon generation of a computational homology model of Hsp90α in its open conformation, docking simulations of novobiocin and silibinin produced four and three clusters of docking poses, respectively (Fig. 4). Binding energies were −9.742 kcal/mol for novobiocin and −10.344 kcal/mol for silibinin in the #1 ranked cluster. The binding mode of silibinin in such cluster shared an approximately 52% of the twenty-seven amino acid residues involved in the novobiocin binding mode to the chain 1 of open Hsp90α (SER50, SER53, ASP54, ASP57, GLN212, PHE213, ILE214, GLY215, TRP297, PHE312, SER315, LEU316, LYS362, and TYR364; Table 4).

3.3. Silibinin inhibits Hsp90α/β activity

We investigated the inhibitory effect of silibinin and novobiocin on Hsp90 activity using time-resolved fluorescence resonance energy transfer (TR-FRET) assays, which were designed to measure the inhibition of the Hsp90α/β CTD binding to its protein target PPID/cyclophilin D. The assay samples contained terbium-labeled donor, dye-labeled acceptor, Hsp90α/β CTD, GST-tagged PPID and silibinin/novobiocin, and were incubated for 2 h. The Hsp90α/β CTD-PPID interaction was then assayed by measuring the TR-FRET signal using a fluorescence reader.

The addition of increasing concentrations of silibinin decreased the TR-FRET signal in a dose-dependent manner (Fig. 5A), suggesting that it inhibited the interaction between Hsp90α/β and PPID. The IC_{50} was 1 mmol/L when employing Hsp90α CTD and 2 mmol/L when using Hsp90β CTD. We also tested in parallel the effect of novobiocin in the TR-FRET competition assay. As expected, novobiocin dose-dependently decreased the TR-FRET signal with an IC_{50} of ~0.5 mmol/L (Fig. 5B).

3.4. Silibinin is less hepatotoxic than the Hsp90 N-terminal inhibitor geldanamycin

We next analyzed the hepatic tolerability of silibinin by the human liver cell line HepG2, which has been used to classify chemical entities for hepatotoxicity and proposed as a non-animal alternative for systemic toxicology (Van den Hof et al., 2014; Ramirez et al., 2018). When cellular viability was examined by MTT-based assays, HepG2 were markedly less susceptible toward silibinin and novobiocin as reflected by half-maximal cell viability inhibitory concentrations (IC_{50}) thousand of times beyond the IC_{50} values obtained with the Hsp90 N-terminal domain inhibitors geldanamycin and ganetespib (Wang et al., 2010; Shimamura et al., 2012) (Fig. 6A).

Mitochondrial O_2^- was then quantified with MitoSOX-Red staining in HepG2 cells (Fig. 6B). MitoSOX-reactive mitochondrial ROS levels were increased following exposure of HepG2 cells to rotenone, a mitochondrial respiratory complex I that has been shown to produce O_2^- (Shimura et al., 2017), in response to the Hsp90 inhibitor geldanamycin, which is known to promote superoxide formation by enzymatic and non-enzymatic redox cycling (Dikalov et al., 2002), but not in response to either the resorcionol-triazole Hsp90 inhibitor ganetespib, which lacks the benzoquinone moiety of geldanamycin (Jhaveri and Modi, 2015), or the Hsp90 CTD inhibitor novobiocin. Silibinin was the sole Hsp90 inhibitor tested capable of decreasing O_2^- levels in HepG2 cells compared with non-treated control cells (Fig. 6B).

4. Discussion

Hsp90 is important in maintaining the structural integrity of over 200 client proteins including many well-known signal transducers, some of which may have beneficial effects for metastasis-initiating cells. Indeed, Hsp90 is the most highly expressed cellular protein involved in the stabilization and degradation of other proteins under biophysical stress conditions such as those normally found in the harsh tumor

Table 1
Interactions between novobiocin/silibinin and the closed conformation of the Hsp90β dimer.

Cluster number	ΔG, [kcal/mol]	Dissoc. constant, [μM]	Participating amino acids interacting with novobiocin
1	−10.124	0.037932336	ARG337, ARG338, ALA339, PRO340, PHE341, LEU343, PHE344, TYR430, GLU431, ALA432, SER434, LYS435, LYS438, ARG456, TYR457, HIS458, MET466, SER490, LYS491, TYR512, MET513, THR514, GLU515, ASP518 (**chain 1**) and ASP613, ASN614, SER615 (**chain 2**)
2	−9.15	0.196318422	GLU603, LYS607, ASP613, TYR619, SER669, LEU670, GLU671, ASP672, PRO673 (**chain 1**) and TYR430, GLU431, SER434, LYS438, ARG456, TYR457, HIS458, MET466, GLU489, SER490, LYS491, GLN493, TYR512, MET513, THR514, GLU515, PRO516 (**chain 2**)
3	−8.977	0.262888594	LEU638, LYS641, ASP648, ALA650, VAL651, ASP653, LEU654, MET683, ILE684, LEU686, GLY687, LEU688 (**chain 1**) and ALA650, VAL651, ASP653, LEU654, LEU657, ARG682, MET683, ILE684, LEU686, GLY687, LEU688 (**chain 2**)
4	−8.918	0.290415188	PHE341, PHE344, GLU345, GLN609, ALA610, LEU611, ARG612, ASN614, MET617 (**chain, 1**) and PHE341, ASP342, PHE344, GLU345, GLN609, LEU611, ARG612, ASP613, THR616 (**chain 2**)
5	−8.875	0.312276094	GLU200 LYS203 LYS204 GLN207 TYR305 LEU308 THR309 ASN310 ASP311 PRO336 ARG338 ALA339 PRO340 PHE341 LYS348 LYS349 ASN351 LYS354 PHE361 ASP364 PHE376 ARG378 PHE433 (**chain 1**)
6	−8.832	0.335782594	ASN346 LYS347 LYS348 LYS349 LYS350 (**chain 1**) and ASN346 LYS350 ASP367 PRO371 GLU372 TYR373 ARG405 LYS406 VAL409 LYS410 GLU443 ASP444 SER445 THR446 ASN447 (**chain 2**)
7	−8.769	0.373454563	ASN346 LYS347 LYS350 ASP367 PRO371 GLU372 ARG405 LYS406 VAL409 LYS410 GLU443 ASP444 SER445 THR446 ASN447 (**chain 1**) and ASN346 LYS347 LYS348 LYS350 (**chain 2**)
8	−8.748	0.386928719	ARG612 ASP613 ASN614 SER615 THR616 MET617 (**chain 1**) and ARG338 ALA339 PHE341 TYR430 GLU431 ALA432 PHE433 SER434 LYS435 LYS438 ARG456 HIS458 MET466 THR514 GLU515 (**chain 2**)
Cluster number	ΔG, [kcal/mol]	Dissoc. constant, [μM]	Participating amino acids interacting with silibinin
1	−9.408	0.127011	ALA339, PRO340, PHE341, LEU343, PHE344, TYR430, GLU431, ALA432, PHE433, SER434, LYS435, LYS438, ARG456, TYR457, HIS458, LYS491, TYR512, MET513, THR514, GLU515 (**chain 1**) and ARG612, ASP613, ASN614, SER615 (**chain 2**)
2	−9.256	0.164158	TYR305, THR309, ASN310, ASP311, PRO336, ARG338, PRO340, ASP342, LEU343, PHE344, GLU345, ASN346, LYS348, LYS349, LYS350, ASN351, ASN352, ASN375, PHE376, ARG378 (**chain 1**)
3	−9.094	0.215779	ARG612, ASP613, ASN614, SER615, THR616 (**chain 1**) and ARG337, ARG338, ALA339, TYR430, GLU431, ALA432, SER434, LYS438, ARG456, TYR457, MET513, THR514, GLU515, ASP518 (**chain 2**)
4	−9.087	0.218343	TRP598, MET602, MET606, LYS607, ALA610, LEU611, ARG612, ASP613, ASN614, MET617, MET621 (**chain 1**) and PHE341, ASP342, LEU343, PHE344, GLU345, ASN346 (**chain 2**)
5	−8.873	0.313332	LYS573, LYS574, VAL575, GLU576, ILE591, VAL592, THR593, TRP598, THR599, ALA600, MET602, GLU603, ALA622, LYS623, LYS624, HIS625, PHE668, SER669 (**chain 1**)
6	−8.802	0.353222	VAL202, LYS203, GLN207, PHE208, GLU281, LEU282, ASN283, LYS284, THR285, PHE304, LYS306, SER307, LEU308, ASN310, ASP311, TRP312, LYS354, TYR356 (**chain 1**)
7	−8.632	0.470608	ALA339, PRO340, PHE341, ASP342, LEU343, PHE344, GLU345, GLU431, ALA432, PHE433, SER434, LYS435, GLU515 (**chain 1**) and LEU611, ARG612, ASP613, ASN614, SER615, THR616 (**chain 2**)
8	−8.596	0.500090	THR593, TRP598, THR599, MET602, GLU603, LYS607, GLY618, TYR619, ALA622, LYS623, LYS624, PHE668, SER669, LEU670, GLU671, ASP672, PRO673 (**chain 1**) and GLU489, SER490, GLN493 (**chain 2**)
9	−8.561	0.530522	GLU539, GLY540, LEU541, LEU543, GLU545, LYS550, MET553, LYS557, ALA558, GLU561, CYS564, LYS565, LYS577, THR579, ILE580, SER581, ASN582, ARG583, GLU627 (**chain 1**)
10	−8.452	0.637678	ASP52, ARG55, ASP122, SER124, GLY210, TYR211, TRP289, THR290, GLU328, PHE329, ARG330, ARG359, ASP382, SER383, GLU384, ASP385 (**chain 1**)
11	−8.425	0.667410	ILE288, ASN292, PRO293, ASP294, ILE296, GLN298, TYR301, VAL318, LYS319, HIS320, PHE321, SER322, GLU324, LEU332, GLU418 (**chain 1**)
12	−8.415	0.678770	PHE113, MET114, LEU117, GLN118, GLY120, ALA121, ASP122, ILE123, SER124, GLY127, GLN128, PHE129, VAL357, ARG358, GLU384, ASP385, LEU386, LEU388, ARG392 (**chain 1**)
13	−8.400	0.696174	ASP613 (**chain 1**) and TYR430, GLU431, SER434, LYS435, LYS438, ARG456, TYR457, HIS458, ASP464, SER490, LYS491, TYR512, MET513, THR514, GLU515 (**chain 2**)
14	−8.354	0.752379	GLU313, ARG337, ARG338, ALA339, PRO340, PHE341, LEU343, PHE344, LYS428, GLU431, ALA432, LYS435 (**chain 1**) and LEU611, ARG612, ASP613, ASN614, SER615 (**chain 2**)

microenvironment (Barrott and Haystead, 2013). Not surprisingly, Hsp90 inhibition has received special attention for therapeutic applications and, currently, more than twenty Hsp90-targeting drugs have entered clinical trials, with many more compounds in preclinical development (Neckers and Workman, 2012; Travers et al., 2012; Blair et al., 2014; Chatterjee and Burns, 2017). Here, we provide computational and experimental evidence confirming and extending previous studies suggesting that Hsp90 is a primary target of silibinin.

Although it should be acknowledged that Hsp90 inhibitors have shown limited efficacy as single agents in a majority of cancer patients, a particularly relevant exception to this is NSCLC harboring *ALK* gene rearrangements, a genotypically-defined NSCLC subtype in which the brain is frequently a site of disease progression (Gallegos Ruiz et al., 2008; Sequist et al., 2010; Socinski et al., 2013; Zhang et al., 2015). Inhibition of Hsp90 with drugs such as ganetespib, AUY922, retispamycin, and IPI-504 leads to degradation of the oncogenic ALK fusion protein and tumor regression, even in NSCLC with acquired resistance to ALK tyrosine kinase inhibitors. We show here that silibinin, whose administration in NSCLC patients with brain metastasis reduces lesions in the absence of adverse effects (Bosch-Barrera et al., 2016; Priego et al., 2018), is a novobiocin-like Hsp90 inhibitor that binds to a putative ATP site at the CTD of Hsp90. Of note, novobiocin used at high concentrations has been suggested to directly target the N-terminal ATP binding pocket of Hsp90 in addition to the more sensitive CTD binding site, which might be involved in the shared effects of novobiocin and silibinin. In this regard, structure activity relationship studies have identified some of the key structural features required for the scaffold cytotoxic activity of silibinin, in which Hsp90 inhibition could play a part (Zhao et al., 2011).

Refolding assays employing thermally denatured firefly luciferase, a sensitive model substrate to study folding and renaturation of denatured proteins after heat stress (Thulasiraman and Matts, 1996), revealed that silibinin could inhibit Hsp90-dependent refolding of luciferase in rabbit reticulocyte lysates by approximately 50%, at a concentration of 250 μmol/L (Zhao et al., 2011). Subsequent studies revealed the capacity of silibinin to induce a concentration-dependent

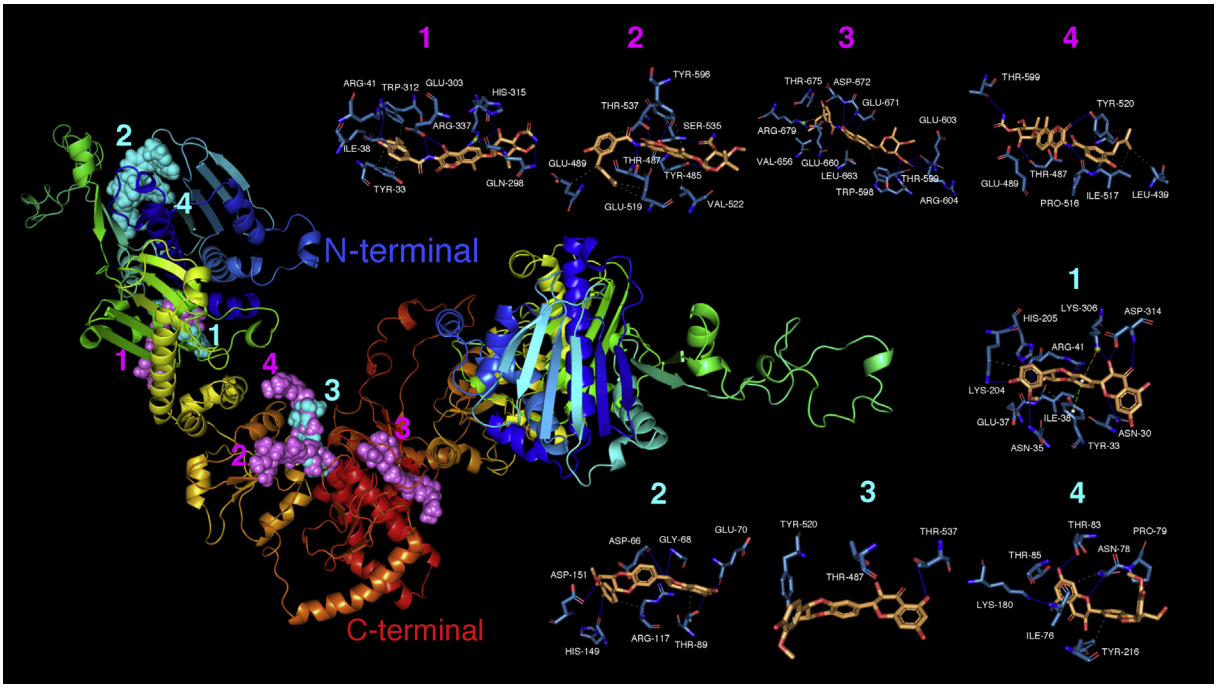

Fig. 2. Hsp90β in an open conformation with docked novobiocin and silibinin. Figure depicts the backbone of the Hsp90β homodimer generated by homology modeling with rainbow colors from the N-terminal (blue) to the C-terminal (red) domain. For each cluster of the docked compound (novobiocin and novobiocin cluster numbers are shown in violet while silibinin and silibinin cluster numbers are shown in cyan), only the molecule (spheres) with the best binding energy is shown. Each inset shows the detailed interactions of each compound docked to the protein, indicating the participating amino acids involved in the interaction and the type of interaction (hydrogen bonds, hydrophilic interactions, salt bridges, Π-stacking, etc). Note: For simplicity, the figure only displays the clusters in one of the subunits. (For interpretation of the references to color in this figure legend, the reader is referred to the Web version of this article.)

degradation of several Hsp90-dependent client proteins (e.g., HER2, Raf-1 and Akt) without affecting Hsp90 protein levels. Hsp90 plays an obligatory role for the heme-regulated eukaryotic initiation factor 2 alpha kinase (HRI) to acquire and maintain an activatable conformation (Uma et al., 1997). When assessing the ability of silibinin to inhibit Hsp90-dependent activation of HRI (Shao et al., 2001, 2003; Yun et al., 2004a,b), it was found to inhibit the Hsp90-dependent maturation and activation of newly synthesized HRI in a heme-deficient lysate in a dose-dependent manner (Zhao et al., 2011). Because it failed to disrupt the interactions between Hsp90 and the co-chaperone Cdc37 with HRI, silibinin was suggested to inhibit Hsp90 in a manner similar to that proposed for the prenylated isoflavone derrubone (Hadden et al., 2007; Hastings et al., 2008; Mays et al., 2010). Given their pharmacological similarity, subsequent studies suggested that silibinin should operate analogously to novobiocin, an amino coumarin that induces concentration-dependent degradation of Hsp90 client proteins by interacting with a previously unrecognized ATP-binding domain in the CTD of Hsp90 (Marcu et al., 2000a,b; Matts et al., 2011). When employing a refined binding assay in which silibinin was immobilized and recombinant Hsp90α CTD was allowed to bind (Young et al., 2003),

Table 2
Interactions between novobiocin/silibinin and the open conformation of the Hsp90β dimer.

Cluster number	ΔG, [kcal/mol]	Dissoc. constant, [μM]	Participating amino acids interacting with novobiocin
1	−9.41	0.126583	ASN30, TYR33, ILE38, ARG41, HIS205, GLN298, GLU299, GLY302, GLU303, LYS306, TRP312, ASP314, HIS315, LEU316, ALA317, VAL318, ARG337, LEU419, ASP422, ASN425 (**chain 1**)
2	−9.186	0.184745	TYR485, THR487, GLY488, GLU489, GLN493, PHE499, GLU519, VAL522, GLN523, LYS526, LEU533, VAL534, SER535, THR537, TYR596, ASN601, PHE668 (**chain 1**) and GLN674 (**chain 2**)
3	−8.739	0.392851	LYS574, GLY597, TRP598, THR599, ALA600, GLU603, ARG604, ILE605, ALA622, LYS652, VAL656, PHE659, GLU660, LEU663, GLY667, SER669, LEU670, GLU671, ASP672, THR675, ARG679 (**chain 1**) and GLU492, ASN496 (**chain 2**)
4	−8.505	0.583112	LEU439, THR487, GLY488, GLU489, PRO516, ILE517, GLU519, TYR520, THR537, TYR596, THR599, ALA600, ASN601, SER666 (**chain 1**)
Cluster number	ΔG, [kcal/mol]	Dissoc. constant, [μM]	Participating amino acids interacting with silibinin
1	−8.789	0.361058	ASN30, TYR33, ASN35, GLU37, ILE38, ARG41, LYS204, HIS205, GLU303, LYS306, TRP312, GLU313, ASP314, ARG337 (**chain 1**)
2	−8.459	0.630188	LEU65 ASP66 SER67 GLY68 GLU70 LEU71 LYS72 THR89 LYS148 HIS149 ASN150 ASP151 ILE175 GLY176 ARG177 (**chain 1**)
3	−8.178	0.101262	THR487, GLY488, GLU489, PHE499, THR514, GLU515, PRO516, GLU519, TYR520, THR537, TYR596, ALA600, ASN601, SER665, SER666, PHE668 (**chain 1**) and GLN674 (**chain 2**)
4	−7.819	0.1856081	ILE76 PRO77 ASN78 PRO79 GLU81 THR83 THR85 LYS180 ILE182 LEU193 GLU194 GLU195 TYR216 GLU218 LYS266 (**chain 1**)

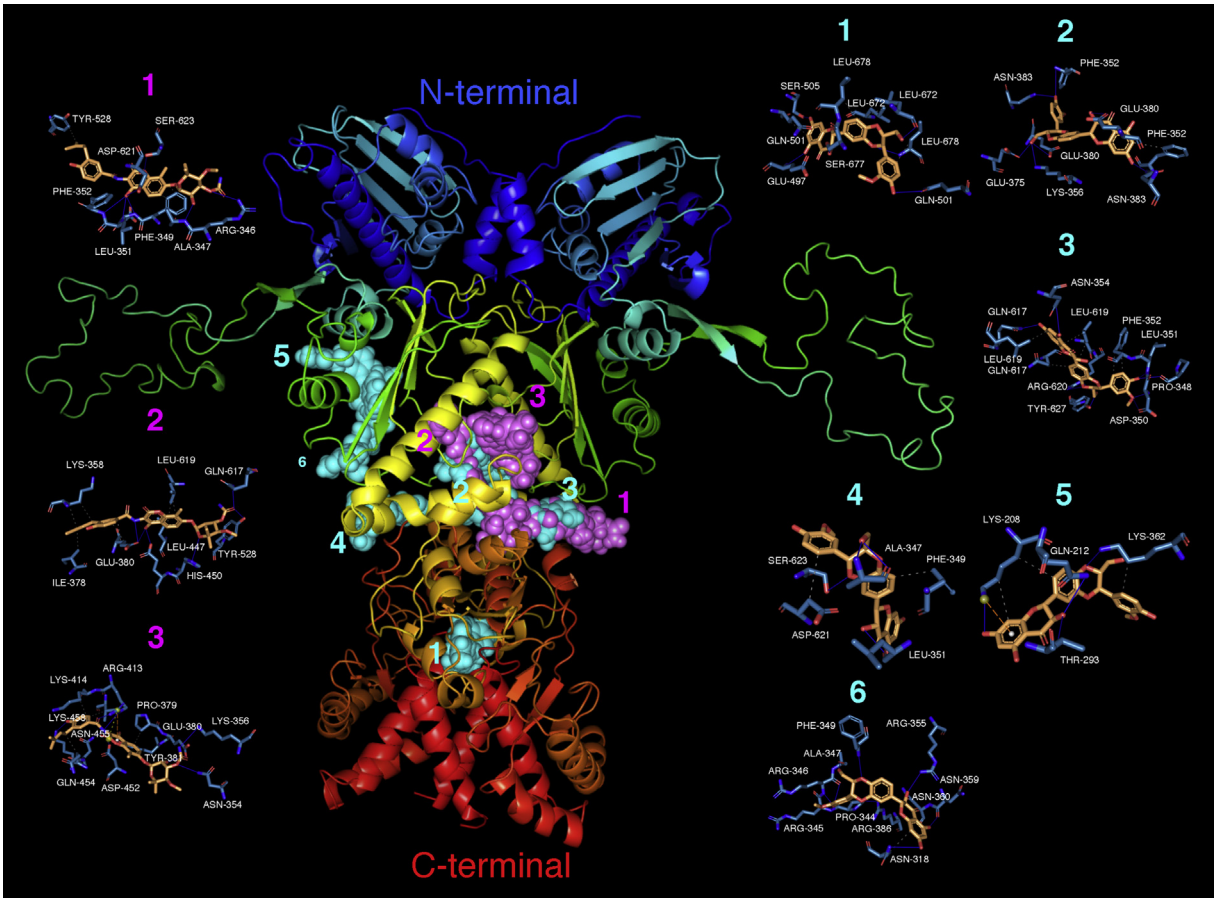

Fig. 3. Hsp90α in a closed conformation with docked novobiocin and silibinin. Figure depicts the backbone of the Hsp90α homodimer generated by homology modeling with rainbow colors from the N-terminal (blue) to the C-terminal (red) domain. For each cluster of the docked compound (novobiocin and novobiocin cluster numbers are shown in violet while silibinin and silibinin cluster numbers are shown in cyan), only the molecule (spheres) with the best binding energy is shown. Each inset shows the detailed interactions of each compound docked to the protein, indicating the participating amino acids involved in the interaction and the type of interaction (hydrogen bonds, hydrophilic interactions, salt bridges, Π-stacking, etc). (For interpretation of the references to color in this figure legend, the reader is referred to the Web version of this article.)

Table 3
Interactions between novobiocin/silibinin and the closed conformation of the Hsp90α dimer.

Cluster number	ΔG, [kcal/mol]	Dissoc. constant, [μM]	Participating amino acids interacting with novobiocin
1	−9.043	0.235176	TYR528, MET614, GLN617, LEU619, ARG620, ASP621, ASN622, SER623, TYR627 (**chain 1**) and ARG346, ALA347, PRO348, PHE349, ASP350, LEU351, PHE352, GLU353, GLU439, GLN440 (**chain 2**)
2	−8.826	0.339200	ASN354, LYS356, LYS357, LYS358, ASN360, ASP372, CYS374, GLU375, ILE378, PRO379, GLU380, LEU382, ASN383, LEU447, HIS450, GLU451, ILE525, TYR528, ILE613, MET614, GLN617 (**chain 1**) and LYS356, ALA616, ALA618, LEU619 (**chain 2**)
3	−8.624	0.477006	PRO379, GLU380, TYR381, ARG413, LYS414, VAL417, LYS418, HIS450, GLU451, ASP452, GLN454, ASN455, LYS458 (**chain 1**) and GLU353, ASN354, LYS356 (**chain 2**)

Cluster number	ΔG, [kcal/mol]	Dissoc. constant, [μM]	Participating amino acids interacting with silibinin
1	−9.703	0.077198	THR495, GLY496, GLU497, GLN501, VAL502, SER505, ASN609, ARG612, LEU672, SER673, SER674, GLY675, PHE676, SER677, LEU678, PRO681 (**chain 1**) and GLU497, GLN501, ARG612, LEU672, SER673, SER674, GLY675, PHE676, SER677, LEU678, PRO681 (**chain 2**)
2	−8.914	0.292382	PHE352, ASN354, ARG355, LYS356, LYS357, LYS358, GLU375, GLU380, TYR381, ASN383, LEU447, GLU451, LEU619 (**chain 1**) and LEU351, PHE352, ASN354, ARG355, LYS356, LYS358, GLU380, ASN383, LEU447, LEU619 (**chain 2**)
3	−8.557	0.534116	ASN354, GLN617, LEU619, ARG620, ASP621, SER623, TYR627 (**chain 1**) and PRO348, PHE349, ASP350, LEU351, PHE352, GLU353, GLN617, LEU619 (**chain 2**)
4	−8.246	0.902821	ARG346, ALA347, PHE349, LEU351, PHE352, GLU353, GLU439, GLN440 (**chain 1**) and LEU619, ARG620, ASP621, ASN622, SER623 (**chain 2**)
5	−8.187	0.997354	LYS208, LYS209, GLN212, LYS292, THR293, SER315, LEU316, THR317, ASN318, ASN359, ASN360, LYS362, ASP372, ARG386, GLY387 (**chain 1**)
6	−8.085	1.184721	TYR313, THR317, ASN318, ASP319, GLU321, PRO344, ARG345, ARG346, ALA347, PRO348, PHE349, ASP350, ARG355, ASN359, ASN360, LYS362, ARG386 (**chain 1**)

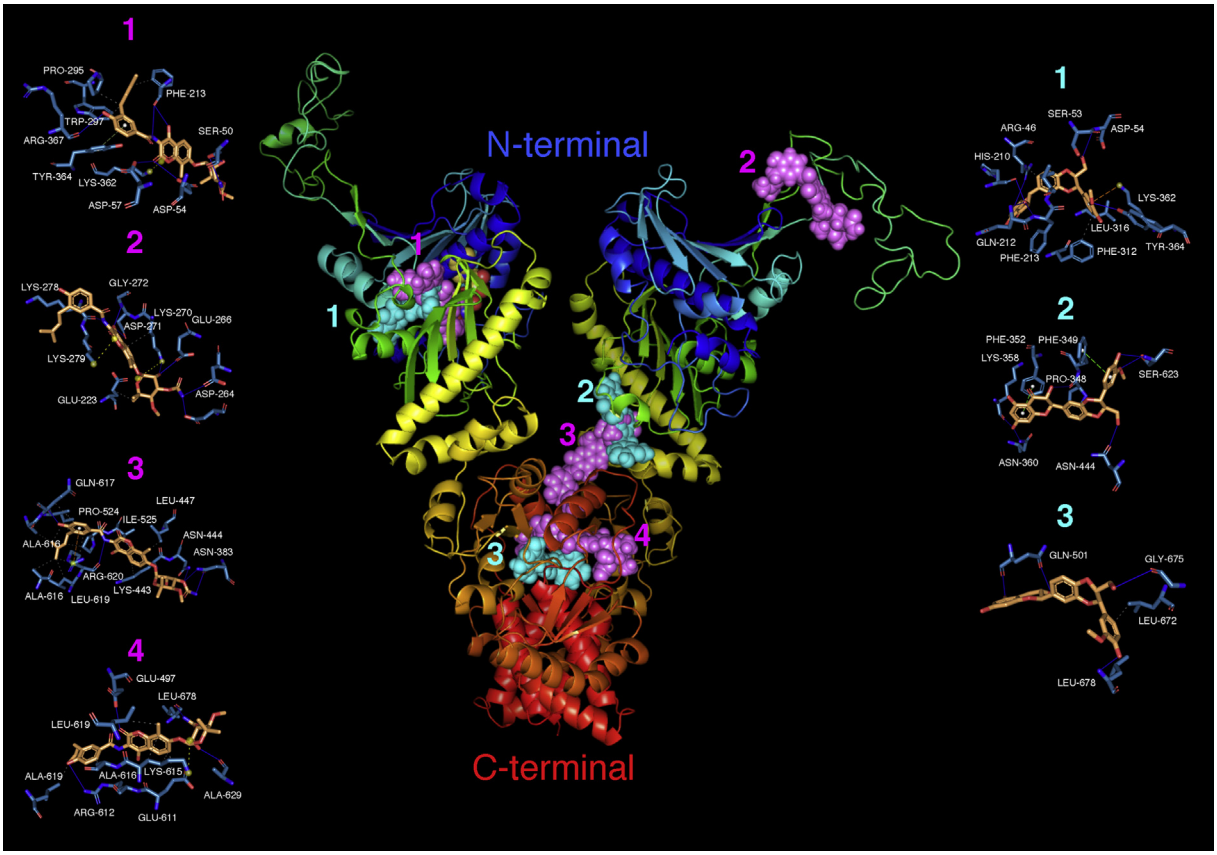

Fig. 4. Hsp90α in an open conformation with docked novobiocin and silibinin. Figure depicts the backbone of the Hsp90α homodimer generated by homology modeling with rainbow colors from the N-terminal (blue) to the C-terminal (red) domain. For each cluster of the docked compound (novobiocin and novobiocin cluster numbers are shown in violet while silibinin and silibinin cluster numbers are shown in cyan), only the molecule (spheres) with the best binding energy is shown. Each inset shows the detailed interactions of each compound docked to the protein, indicating the participating amino acids involved in the interaction and the type of interaction (hydrogen bonds, hydrophilic interactions, salt bridges, Π-stacking, etc). (For interpretation of the references to color in this figure legend, the reader is referred to the Web version of this article.)

Table 4
Interactions between novobiocin/silibinin and the open conformation of the Hsp90α dimer.

Cluster number	ΔG, [kcal/mol]	Dissoc. constant, [μM]	Participating amino acids interacting with novobiocin
1	−9.742	0.072280	SER50, ASN51, SER53, ASP54, ASP57, ARG60, VAL136, GLN212, PHE213, ILE214, GLY215, TYR216, ASN291, LYS292, THR293, LYS294, PRO295, ILE296, TRP297, PHE312, SER315, LEU316, ASN318, LYS362, TYR364, ARG367, PHE369 (**chain 1**)
2	−9.375	0.134286	ASN83, GLN85, ASP86, GLU200, GLU223, ASP240, LYS241, ASP264, GLU266, LYS270, ASP271, GLY272, LYS274, LYS275, LYS278, LYS279, ILE280, LYS283 (**chain 2**)
3	−9.311	0.149605	ALA347, PRO348, PHE349, PHE352, ASN383, PHE384, PHE441, LYS443, ASN444, LEU447, PRO524, ILE525, ARG612, ILE613, ALA616, GLN617 (**chain 1**) and ALA616, LEU619, ARG620 (**chain** 2)
4	−9.012	0.247808	GLU497, ARG612, LYS615, ALA616, LEU619, SER677 (**chain 1**) and GLU497, GLU611, ARG612, LYS615, ALA616, LEU619, MET625, ALA629, ALA630, PHE676, SER677, LEU678, GLU679 (**chain 2**)
Cluster number	ΔG, [kcal/mol]	Dissoc. constant, [μM]	Participating amino acids interacting with silibinin
1	−10.344	0.026166	ARG46, ILE49, SER50, SER53, ASP54, ASP57, LYS209, HIS210, SER211, GLN212, PHE213, ILE214, GLY215, TRP297, GLU311, PHE312, SER315, LEU316, TRP320, LYS362, TYR364, VAL388 (**chain 2**)
2	−9.03	0.240393	ALA347, PRO348, PHE349, PHE352, LYS356, LYS357, LYS358, ASN359, ASN360, GLU375, ASN383, PHE384, GLN440, PHE441, LYS443, ASN444 (**chain 1**) and ASP621, ASN622, SER623 (**chain 2**)
3	−8.902	0.298364	GLU497, ARG612, LEU672, GLY675, PHE676, SER677, LEU678, PRO681 (**chain 1**) and ILE494, THR495, GLY496, GLU497, GLN501, VAL502, SER505, ALA608, ASN609, ARG612, LEU672, GLY675, SER677, LEU678, PRO681 (**chain 2**)

excess silibinin and novobiocin were found to displace bound Hsp90α CTD in solution (Riebold et al., 2015a,b). Because both inhibitors induced chemical shift perturbations for a number of nuclear magnetic resonance (NMR) spectroscopy-detected amide signals, whereas only a few NMR signals were perturbed by either silibinin or novobiocin, it was proposed that both compounds should bind directly Hsp90α CTD in a similar region (Riebold et al., 2015a,b). Since then, however, no further understanding has been gained towards silibinin's mode of Hsp90 inhibition, either through interaction with the N-terminus, the C-terminus, or an alternative mode of action.

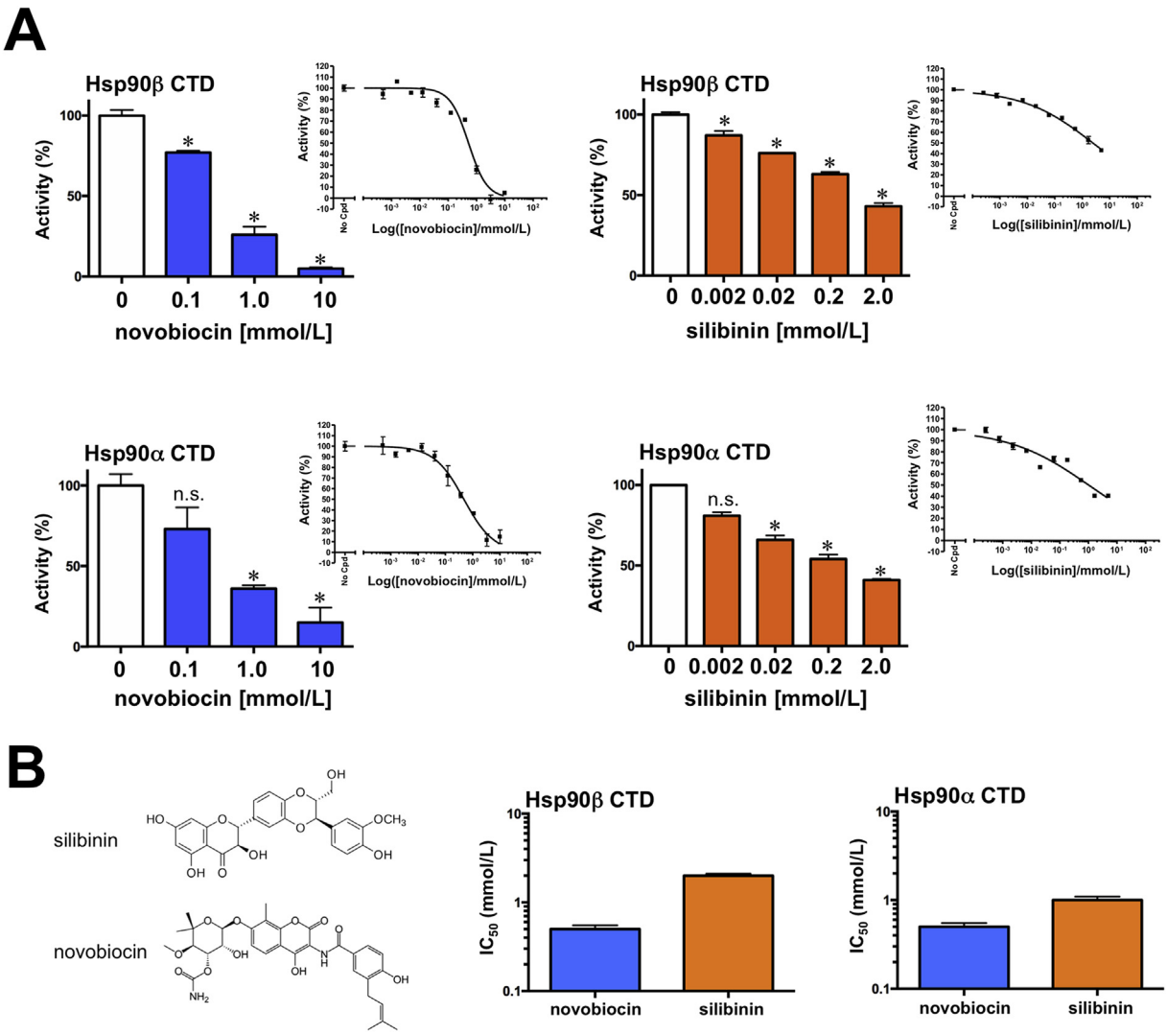

Fig. 5. Novobiocin and silibinin effects on Hsp90α/β CTD activity. **A.** The results of the effects of novobiocin and silibinin on Hsp90 CTD-PPID interaction are expressed as means (*columns*) ± SD (*bars*); two experimental replicates (*P < 0.05, statistically significant differences from the untreated (control) group; n.s. not statistically significant). **B**. The IC_{50} values were calculated from sigmoidal dose-response curves shown as inserts in **A**.

Here, we performed a first-in-class computational study aimed at disentangling the putative molecular interactions between silibinin and Hsp90α/β by exploiting existing structures such as the atomic cryoEM structure of the Hsp90-Cdc37-Cdk4 complex (5FWM, Verba et al., 2016) or, alternatively, by generating computational homology models. Hsp90 has two isoforms in the cytoplasm. Hsp90β is expressed constitutively to a high level in most tissues and is generally more abundant than Hsp90α. By contrast, Hsp90α is stress-inducible and overexpressed in many tumor cells (Csermely et al., 1998; Chen et al., 2005; Millson et al., 2007), suggesting that it may be more closely involved in disease processes. The two Hsp90 isoforms share some common functions, but they possess distinct characteristics: Hsp90α is primarily involved in signal transduction, growth, and development (Voss et al., 2000), whereas Hsp90β plays a role in the heat-shock response (Millson et al., 2007). Hsp90 is known to recognize structure elements of a protein, thereby allowing other co-chaperones with enzymatic activity such as protein phosphatases and cis/trans peptidyl-prolyl isomerases (PPIase activity) to fold and repair the Hsp90-bound client (Karagöz et al., 2014). One of the co-chaperones with PPIase activity is the tetratricopeptide domain-containing peptidyl-prolyl isomerase D (PPID)/cyclophilin 40 (Cyp40). Our approach reveals that, whereas silibinin is predicted to interact with several pockets in the C-terminus of Hsp90α and β, its highest-ranking docked poses significantly overlap with those of the well-characterized Hsp90 CTD-targeted inhibitor novobiocin. To date, however, only computational hypotheses have been proposed regarding the precise physical location and physiological role of the silibinin-binding site at the CTD of Hsp90 (Roy and Kapoor, 2016; Terracciano et al., 2018). Hsp90 is a very large protein with numerous conformation states, most of them lacking high-resolution structures. Moreover, while exerting its catalytic function, Hsp90 experiences great rearrangements in its secondary, tertiary, and quaternary structure. All of these features make it challenging to rationally explain the binding mode of silibinin, which has been described here solely for the open and closed states, but not for any of the multiple intermediate conformations of Hsp90α/β. Nonetheless, because the Hsp90-binding site of novobiocin involves a region of the CTD dimerization domain of the chaperone (Marcu et al., 2000a,b), it is tempting to speculate that silibinin may antagonize Hsp90 function by inducing a conformation favoring separation of the CTDs and release of substrate (Allan et al., 2006). Indeed, the currently predicted binding sites for both silibinin and novobiocin favorably locate in the broad C-terminal region of Hsp90, in many cases at the interface between the subunits making up the Hsp90 dimer. Given the high energies reported for the binding of silibinin to novobiocin-like locations at the CTD of Hsp90, it is reasonable to suggest that silibinin would impair the structural rearrangements necessary for Hsp90 functioning, perhaps involving

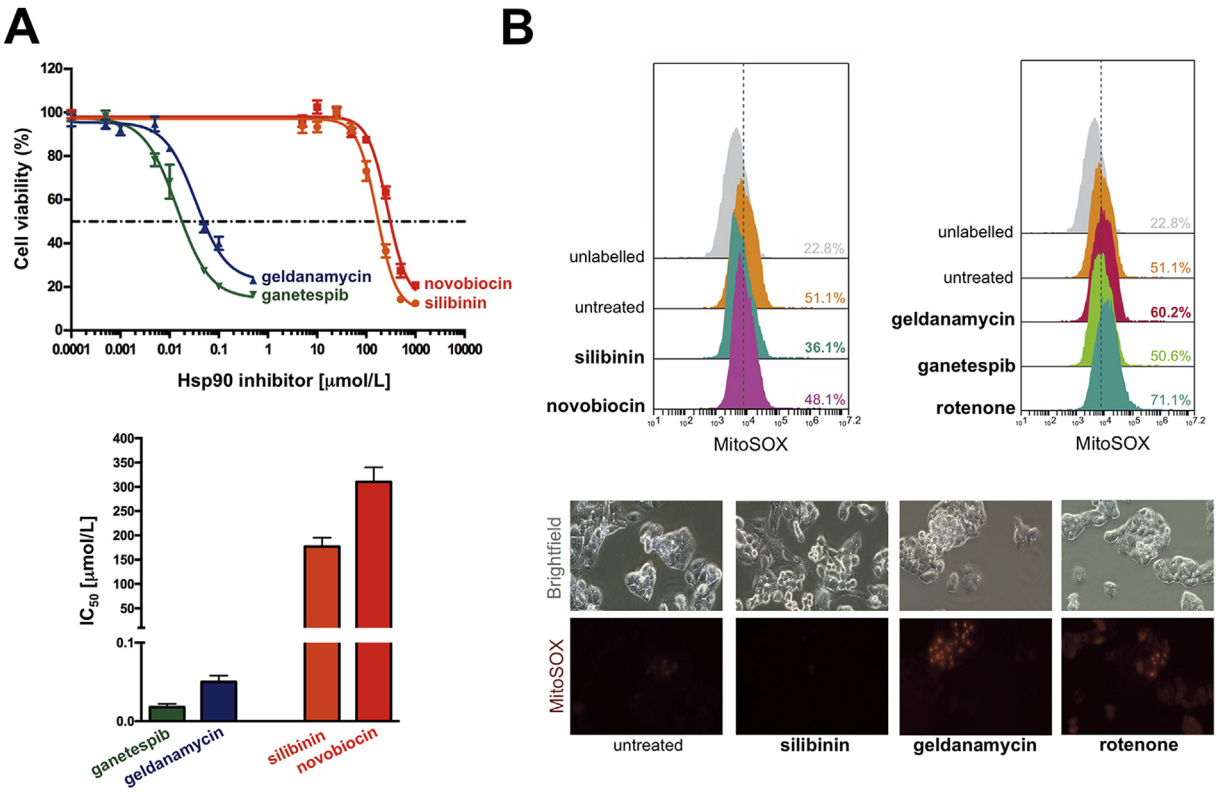

Fig. 6. Hepatotoxic and superoxide-producing effects of Hsp90 inhibitors. A. Dose-response curves obtained by MTT assays for HepG2 cells exposed to Hsp90 inhibitors. Plotted is the percentage of cell viability (y-axis) through exposure to geldanamycin, ganetespib (STA-909), novobiocin, and silibinin at increasing doses (x-axis). The results are expressed as means ± SD of three experimental replicates. The IC_{50} values were determined as the concentration causing a half-maximal percent cytotoxic activity. **B.** Histograms showing MitoSOX reactive ROS levels in HepG2 cells following 18 h treatment with 50 nmol/L geldanamycin, 50 nmol/L ganetespib (STA-909), 250 μmol/L novobiocin, 250 μmol/L silibinin, and 2 μmol/L rotenone. Inserts show fluorescence microphotographs demonstrating representative MitoSOX-reactive ROS (red) in HepG2 cells with the treatment conditions mentioned above. (For interpretation of the references to color in this figure legend, the reader is referred to the Web version of this article.)

competitive phenomena at the CTD ATP-binding site. The computational predictions of additional, numerous high-affinity binding sites in the middle domain of Hsp90 further suggest the ability of silibinin to disrupt the Hsp90-co-chaperone-client interactions. Accordingly, the net biochemical effect of silibinin was to inhibit the efficiency of the Hsp90α/β CTD binding to its co-chaperone PPID/cyclophilin D in a low millimolar range equivalent to that observed with novobiocin (Yun et al., 2004a,b).

The most clinically significant off-target, Hsp90-independent toxicity observed with the first-generation of geldanamycin-based inhibitors was dose-limiting hepatotoxicity (Nowakowski et al., 2006; Solit et al., 2007). Such impairment of liver function likely reflects the P450-associated redox active properties of the benzoquinone moiety of geldanamycin and the extent of geldanamycin-driven superoxide formation, which may stimulate hepatocytes oxidative injury (Samuni et al., 2010). Our findings support the notion that silibinin, which does not influence the activities of major P450 drug-metabolizing enzymes and is well tolerated *in vivo* (Kawaguchi-Suzuki et al., 2014; Soleimani et al., 2019), might provide an advantageous toxicological profile as a non-quinone Hsp90 inhibitor capable of decreasing hepatic ROS levels (Detaille et al., 2008; Serviddio et al., 2014). Moreover, next-generation Hsp90 inhibitors such ganetespib lacking the dose-limiting hepatotoxicity reported with the geldanamycin analogs (Wang et al., 2010; Shimamura et al., 2012; Jhaveri and Modi, 2015) are mostly aimed to block the binding of ATP to the N-terminus of Hsp90, a mechanism of action that activates a cytoprotective resistance response called heat shock response (HSR). Using HepG2 cells, a predictive model of hepatoxicants in which the Hsp90 inhibition-related endoplasmic reticulum stress and unfolded protein responses (Marcu et al., 2002; Davenport et al., 2007; Graner et al., 2017) are the main cellular effects underlying drug-induced liver injury (Van den Hof et al., 2014), we indirectly provide evidence that the client depletion activity of silibinin as a novobiocin-like C-terminal inhibitor of Hsp90 is not expected to trigger such undesirable HSR involving a large increase in several prosurvival proteins (Koay et al., 2016; Bhatia et al., 2018). Such triggering of less off-target effects by silibinin is supported by the notably lower difference between its inhibitory concentration required to block purified Hsp90 protein activity in biochemical assays (1–2 mmol/L) and its cytotoxic activity against cultured cancer cells (typically ranging from 50 to 150 μmol/L; Bosch-Barrera et al., 2017), a difference that might reach > 100-fold in the case of N-terminal-targeted Hsp90 inhibitors (Wang and McAlpine, 2015).

Our computational-experimental approach unequivocally confirms that silibinin might be viewed as a novobiocin-like Hsp90 inhibitor that binds the CTD of Hsp90 to induce changes in its conformation, and alter Hsp90-co-chaperone-client interactions (Zhao et al., 2011; Riebold et al., 2015a,b). Given the essential role of Hsp90 for the functional competence of STAT3 activity governing tumor microenvironment and metastatic progression (Bocchini et al., 2014; Cho et al., 2019), and the recently proposed model of stress-inducible expression of Hsp90β after the transition of quiescent astrocytes to the reactive phenotype (Sha et al., 2017), our current findings provide a new framework in which the non-mutually exclusive direct effects of silibinin on STAT3 and Hsp90 may explain its unexpected clinical activity in the molecular dialogue between metastatic cancer cells and the brain microenvironment.

5. Conclusions

Our computational findings coupled to experimental validation, together with the capacity of silibinin structure to avoid unwanted biotransformation phenomena responsible for hepatotoxicity and its lack of adverse effects even when employed at high doses, strongly suggest that the novobiocin-like behavior of silibinin as an Hsp90 CTD inhibitor might represent a new promising path to develop safe and efficacious Hsp90 inhibitors for cancer therapy.

Declaration of interests

The authors declare that they have no known competing financial interests or personal relationships that could have appeared to influence the work reported in this paper.

Acknowledgments

Work in the Menendez laboratory is supported by the Spanish Ministry of Science and Innovation (Grant SAF2016-80639-P, Plan Nacional de l + D + I, founded by the European Regional Development Fund, Spain) and by an unrestricted research grant from the Fundació Oncolliga Girona (Lliga catalana d'ajuda al malalt de càncer, Girona). Work in the Vicente Micol laboratory is supported by Grants AGL2015-67995-C3-1-R from the Spanish Ministry of Economy and Competitiveness (MINECO); PROMETEO/2016/006, ACOMP/2013/093, ACIF/2013/064, ACIF/2015/158, APOTIP/2017/003, and APOSTD/2018/097 (Generalitat Valenciana), and CIBER (CB12/03/30038, Fisiopatologia de la Obesidad y la Nutricion, CIBERobn, Instituto de Salud Carlos III. Spain). Joaquim Bosch-Barrera is the recipient of a Grant from the Health Research and Innovation Strategic Plan (SLT006/17/114; PERIS 2016–2020; Pla stratègic de recerca i innovació en salut; Departament de Salut, Generalitat de Catalunya). The Spanish Ministry of Economy and Competitiveness (MINECO, Project AGL2015-67995-C3-1-R) and the Generalitat Valenciana (PROMETEO/2016/006) supports work in the Encinar laboratory. The authors would like to thank Dr. Kenneth McCreath for editorial support.

Appendix A. Supplementary data

Supplementary data to this article can be found online at https://doi.org/10.1016/j.fct.2019.110645.

Transparency document

Transparency document related to this article can be found online at https://doi.org/10.1016/j.fct.2019.110645

References

Abenavoli, L., Izzo, A.A., Milić, N., Cicala, C., Santini, A., Capasso, R., 2018. Milk thistle (Silybum marianum): a concise overview on its chemistry, pharmacological, and nutraceutical uses in liver diseases. Phytother Res. 32, 2202–2213.

Agarwal, C., Tyagi, A., Kaur, M., Agarwal, R., 2007. Silibinin inhibits constitutive activation of Stat3, and causes caspase activation and apoptotic death of human prostate carcinoma DU145 cells. Carcinogenesis 28, 1463–1470.

Allan, R.K., Mok, D., Ward, B.K., Ratajczak, T., 2006. Modulation of chaperone function and cochaperone interaction by novobiocin in the C-terminal domain of Hsp90: evidence that coumarin antibiotics disrupt Hsp90 dimerization. J. Biol. Chem. 281, 7161–7171.

Barrott, J.J., Haystead, T.A., 2013. Hsp90, an unlikely ally in the war on cancer. FEBS J. 280, 1381–1396.

Bello-Pérez, M., Falcó, A., Galiano, V., Coll, J., Perez, L., Encinar, J.A., 2018. Discovery of nonnucleoside inhibitors of polymerase from infectious pancreatic necrosis virus (IPNV). Drug Des. Dev. Ther. 12, 2337–2359.

Bhatia, S., Diedrich, D., Frieg, B., Ahlert, H., Stein, S., Bopp, B., Lang, F., Zang, T., Kröger, T., Ernst, T., Kögler, G., Krieg, A., Lüdeke, S., Kunkel, H., Rodrigues Moita, A.J., Kassack, M.U., Marquardt, V., Opitz, F.V., Oldenburg, M., Remke, M., Babor, F., Grez, M., Hochhaus, A., Borkhardt, A., Groth, G., Nagel-Steger, L., Jose, J., Kurz, T., Gohlke, H., Hansen, F.K., Hauer, J., 2018. Targeting HSP90 dimerization via the C terminus is effective in imatinib-resistant CML and lacks the heat shock response. Blood 132, 307–320.

Biasini, M., Bienert, S., Waterhouse, A., Arnold, K., Studer, G., Schmidt, T., Kiefer, F., Gallo Cassarino, T., Bertoni, M., Bordoli, L., Schwede, T., 2014. SWISS-MODEL: modelling protein tertiary and quaternary structure using evolutionaryinformation. Nucleic Acids Res. 42 (Web Server issue), W252–W258.

Blair, L.J., Sabbagh, J.J., Dickey, C.A., 2014. Targeting Hsp90 and its co-chaperones to treat Alzheimer's disease. Expert Opin. Ther. Targets 18, 1219–1232.

Bocchini, C.E., Kasembeli, M.M., Roh, S.H., Tweardy, D.J., 2014. Contribution of chaperones to STAT pathway signaling. JAK-STAT 3, e970459.

Bosch-Barrera, J., Menendez, J.A., 2015. Silibinin and STAT3: a natural way of targeting transcription factors for cancer therapy. Cancer Treat Rev. 41, 540–546.

Bosch-Barrera, J., Corominas-Faja, B., Cuyàs, E., Martin-Castillo, B., Brunet, J., Menendez, J.A., 2014. Silibinin administration improves hepatic failure due to extensive liver infiltration in a breast cancer patient. Anticancer Res. 34, 4323–4327.

Bosch-Barrera, J., Sais, E., Cañete, N., Marruecos, J., Cuyàs, E., Izquierdo, A., Porta, R., Haro, M., Brunet, J., Pedraza, S., Menendez, J.A., 2016. Response of brain metastasis from lung cancer patients to an oral nutraceutical product containing silibinin. Oncotarget 7, 32006–32014.

Bosch-Barrera, J., Queralt, B., Menendez, J.A., 2017. Targeting STAT3 with silibinin to improve cancer therapeutics. Cancer Treat Rev. 58, 61–69.

Chatterjee, S., Burns, T.F., 2017. Targeting heat shock proteins in cancer: a promising therapeutic approach. Int. J. Mol. Sci. 18 (9) pii: E1978.

Chen, B., Piel, W.H., Gui, L., Bruford, E., Monteiro, A., 2005. The HSP90 family of genes in the human genome: insights into their divergence and evolution. Genomics 86, 627–637.

Cho T-M, Kim JY, Kim Y-J, Sung D, Oh E, Jang S, Farrand L, Hoang V-H, Nguyen C-T, Ann J, Lee J, Seo JH. C-terminal hsp90 inhibitor L80 elicits anti-metastatic effects in triple-negative breast cancer via STAT3 inhibiton. Cancer Lett., https://doi.org/10.1016/j.canlet.2019.01.029.

Csermely, P., Schnaider, T., Soti, C., Prohászka, Z., Nardai, G., 1998. The 90-kDa molecular chaperone family: structure, function, and clinical applications. A comprehensive review. Pharmacol. Ther. 79, 129–168.

Cuyàs, E., Pérez-Sánchez, A., Micol, V., Menendez, J.A., Bosch-Barrera, J., 2016. STAT3-targeted treatment with silibinin overcomes the acquired resistance to crizotinib in ALK-rearranged lung cancer. Cell Cycle 15, 3413–3418.

Cysyk, R.L., Parker, R.J., Barchi Jr., J.J., Steeg, P.S., Hartman, N.R., Strong, J.M., 2006. Reaction of geldanamycin and C17-substituted analogues with glutathione: product identifications and pharmacological implications. Chem. Res. Toxicol. 19, 376–381.

Davenport, E.L., Moore, H.E., Dunlop, A.S., Sharp, S.Y., Workman, P., Morgan, G.J., Davies, F.E., 2007. Heat shock protein inhibition is associated with activation of the unfolded protein responsepathway in myeloma plasma cells. Blood 110, 2641–2649.

Detaille, D., Sanchez, C., Sanz, N., Lopez-Novoa, J.M., Leverve, X., El-Mir, M.Y., 2008. Interrelation between the inhibition of glycolytic flux by silibinin and the lowering of mitochondrial ROS production in perifused rat hepatocytes. Life Sci. 82, 1070–1076.

Dikalov, S., Landmesser, U., Harrison, D.G., 2002. Geldanamycin leads to superoxide formation by enzymatic and non-enzymatic redox cycling. Implications for studies of Hsp90 and endothelial cell nitric-oxidase synthase. J. Biol. Chem. 277, 25480–25485.

Dollins, D.E., Warren, J.J., Immormino, R.M., Gewirth, D.T., 2007. Structures of GRP94-nucleotide complexes reveal mechanistic differences between the hsp90 chaperones. Mol. Cell 28, 41–56.

Egorin, M.J., Rosen, D.M., Wolff, J.H., Callery, P.S., Musser, S.M., Eiseman, J.L., 1998. Metabolism of 17-(allylamino)-17-demethoxygeldanamycin (NSC 330507) by murine and human hepatic preparations. Cancer Res. 58, 2385–2396.

Encinar, J.A., Fernández-Ballester, G., Galiano-Ibarra, V., Micol, V., 2015. In silico approach for the discovery of new PPARγ modulators among plant-derived polyphenols. Drug Des. Dev. Ther. 9, 5877–5895.

Federico, A., Dallio, M., Loguercio, C., 2017. Silymarin/Silybin and chronic liver disease: a marriage of many years. Molecules 22 (2) pii: E191.

Galiano, V., Garcia-Valtanen, P., Micol, V., Encinar, J.A., 2016. Looking for inhibitors of the dengue virus NS5 RNA-dependent RNA-polymerase using a molecular docking approach. Drug Des. Dev. Ther. 10, 3163–3181.

Gallegos Ruiz, M.I., Floor, K., Roepman, P., Rodriguez, J.A., Meijer, G.A., Mooi, W.J., Jassem, E., Niklinski, J., Muley, T., van Zandwijk, N., Smit, E.F., Beebe, K., Neckers, L., Ylstra, B., Giaccone, G., 2008. Integration of gene dosage and gene expression in non-small cell lung cancer, identification of HSP90 as potential target. PLoS One 3, e0001722.

Gazák, R., Walterová, D., Kren, V., 2007. Silybin and silymarin–new and emerging applications in medicine. Curr. Med. Chem. 14, 315–338.

Graner, A.N., Hellwinkel, J.E., Lencioni, A.M., Madsen, H.J., Harland, T.A., Marchando, P., Nguyen, G.J., Wang, M., Russell, L.M., Bemis, L.T., Anchordoquy, T.J., Graner, M.W., 2017. HSP90 inhibitors in the context of heat shock and the unfolded protein response: effects on a primary canine pulmonary adenocarcinoma cell line. Int. J. Hyperth. 33, 303–317.

Hadden, M.K., Galam, L., Gestwicki, J.E., Matts, R.L., Blagg, B.S., 2007. Derrubone, an inhibitor of the Hsp90 protein folding machinery. J Nat Prod 70, 2014–2018.

Hastings, J.M., Hadden, M.K., Blagg, B.S., 2008. Synthesis and evaluation of derrubone and select analogues. J. Org. Chem. 73, 369–373.

Jahanafrooz, Z., Motamed, N., Rinner, B., Mokhtarzadeh, A., Baradaran, B., 2018 Nov 15. Silibinin to improve cancer therapeutic, as an apoptotic inducer, autophagy modulator, cell cycle inhibitor, and microRNAs regulator. Life Sci. 213, 236–247.

Jhaveri, K., Modi, S., 2015. Ganetespib: research and clinical development. OncoTargets Ther. 8, 1849–1858.

Karagöz, G.E., Duarte, A.M., Akoury, E., Ippel, H., Biernat, J., Morán Luengo, T., Radli, M., Didenko, T., Nordhues, B.A., Veprintsev, D.B., Dickey, C.A., Mandelkow, E., Zweckstetter, M., Boelens, R., Madl, T., Rüdiger, S.G., 2014. Hsp90-Tau complex reveals molecular basis for specificity in chaperone action. Cell. 156, 963–974.

Kawaguchi-Suzuki, M., Frye, R.F., Zhu, H.J., Brinda, B.J., Chavin, K.D., Bernstein, H.J., Markowitz, J.S., 2014. The effects of milk thistle (Silybum marianum) on human cytochrome P450 activity. Drug Metab. Dispos. 42, 1611–1616.

Koay, Y.C., Wahyudi, H., McAlpine, S.R., 2016. Reinventing Hsp90 inhibitors: blocking C-

terminal binding events by Hsp90 using dimerized inhibitors. Chemistry 22, 18572–18582.
Krieger, E., Vriend, G., 2014. YASARA View - molecular graphics for all devices - from smartphones to workstations. Bioinformatics 30, 2981–2982.
Krieger, E., Darden, T., Nabuurs, S.B., Finkelstein, A., Vriend, G., 2004. Making optimal use of empirical energy functions: force-field parameterization in crystal space. Proteins 57, 678–683.
Lauber, K., Brix, N., Ernst, A., Hennel, R., Krombach, J., Anders, H., Belka, C., 2015. Targeting the heat shock response in combination with radiotherapy: sensitizing cancer cells to irradiation-induced cell death and heating up their immunogenicity. Cancer Lett. 368, 209–229.
Lionta, E., Spyrou, G., Vassilatis, D.K., Cournia, Z., 2014. Structure-based virtual screening for drug discovery: principles, applications and recent advances. Curr. Top. Med. Chem. 14, 1923–1938.
Marcu, M.G., Chadli, A., Bouhouche, I., Catelli, M., Neckers, L.M., 2000a. The heat shock protein 90 antagonist novobiocin interacts with a previously unrecognized ATP-binding domain in the carboxyl terminus of the chaperone. J. Biol. Chem. 275, 37181–37186.
Marcu, M.G., Schulte, T.W., Neckers, L., 2000b. Novobiocin and related coumarins and depletion of heat shock protein 90-dependent signaling proteins. J Natl Cancer Inst 92, 242–248.
Marcu, M.G., Doyle, M., Bertolotti, A., Ron, D., Hendershot, L., Neckers, L., 2002. Heat shock protein 90 modulates the unfolded protein response by stabilizing IRE1alpha. Mol. Cell. Biol. 22, 8506–8513.
Mateen, S., Raina, K., Agarwal, R., 2013. Chemopreventive and anti-cancer efficacy of silibinin against growth and progression of lung cancer. Nutr. Canc. 65 (Suppl. 1), 3–11.
Matts, R.L., Dixit, A., Peterson, L.B., Sun, L., Voruganti, S., Kalyanaraman, P., Hartson, S.D., Verkhivker, G.M., Blagg, B.S., 2011. Elucidation of the Hsp90 C-terminal inhibitor binding site. ACS Chem. Biol. 6, 800–807.
Mays, J.R., Hill, S.A., Moyers, J.T., Blagg, B.S., 2010. The synthesis and evaluation of flavone and isoflavone chimeras of novobiocin and derrubone. Bioorg. Med. Chem. 18, 249–266.
Millson, S.H., Truman, A.W., Rácz, A., Hu, B., Panaretou, B., Nuttall, J., Mollapour, M., Söti, C., Piper, P.W., 2007. Expressed as the sole Hsp90 of yeast, the alpha and beta isoforms of human Hsp90 differ with regard to their capacities for activation of certain client proteins, whereas only Hsp90betagenerates sensitivity to the Hsp90 inhibitor radicicol. FEBS J. 274, 4453–4463.
Neckers, L., Workman, P., 2012. Hsp90 molecular chaperone inhibitors: are we there yet? Clin. Cancer Res. 18, 64–76.
Nowakowski, G.S., McCollum, A.K., Ames, M.M., Mandrekar, S.J., Reid, J.M., Adjei, A.A., Toft, D.O., Safgren, S.L., Erlichman, C., 2006. A phase I trial of twice-weekly 17-allylamino-demethoxy-geldanamycin in patients with advanced cancer. Clin. Cancer Res. 12, 6087–6093.
Pérez-Sánchez, A., Cuyàs, E., Ruiz-Torres, V., Agulló-Chazarra, L., Verdura, S., González-Álvarez, I., Bermejo, M., Joven, J., Micol, V., Bosch-Barrera, J., Menendez, J.A., 2019. Intestinal permeability study of clinically relevant formulations of silibinin in caco-2 cell monolayers. Int. J. Mol. Sci. 20 pii: E1606.
Priego, N., Zhu, L., Monteiro, C., Mulders, M., Wasilewski, D., Bindeman, W., Doglio, L., Martínez, L., Martínez-Saez, E., Cajal, S.R.Y., Megías, D., Hernández-Encinas, E., Blanco-Aparicio, C., Martínez, L., Zarzuela, E., Muñoz, J., Fustero-Torre, C., Piñeiro-Yáñez, E., Hernández-Laín, A., Bertero, L., Poli, V., Sanchez-Martinez, M., Menendez, J.A., Soffietti, R., Bosch-Barrera, J., Valiente, M., 2018. STAT3 labels a subpopulation of reactive astrocytes required for brain metastasis. Nat. Med. 24, 1024–1035.
Ramirez, T., Strigun, A., Verlohner, A., Huener, H.A., Peter, E., Herold, M., Bordag, N., Mellert, W., Walk, T., Spitzer, M., Jiang, X., Sperber, S., Hofmann, T., Hartung, T., Kamp, H., van Ravenzwaay, B., 2018. Prediction of liver toxicity and mode of action using metabolomics in vitro in HepG2 cells. Arch. Toxicol. 92, 893–906.
Riebold, M., Kozany, C., Freiburger, L., Sattler, M., Buchfelder, M., Hausch, F., Stalla, G.K., Paez-Pereda, M., 2015a. A C-terminal HSP90 inhibitor restores glucocorticoid sensitivity and relieves a mouse allograft model of Cushing disease. Nat. Med. 21, 276–280.
Riebold, M., Kozany, C., Freiburger, L., Sattler, M., Buchfelder, M., Hausch, F., Stalla, G.K., Paez-Pereda, M., 2015b. A C-terminal HSP90 inhibitor restores glucocorticoid sensitivity and relieves a mouse allograft model of Cushing disease. Nat. Med. 21, 276–280.
Roy, S.S., Kapoor, M., 2016. In silico identification and computational analysis of the nucleotide binding site in the C-terminaldomain of Hsp90. J. Mol. Graph. Model. 70, 253–274.
Salentin, S., Schreiber, S., Haupt, V.J., Adasme, M.F., Schroeder, M., 2015. PLIP: fully automated protein-ligand interaction profiler. Nucleic Acids Res. 43, W443–W447.
Samuni, Y., Ishii, H., Hyodo, F., Samuni, U., Krishna, M.C., Goldstein, S., Mitchell, J.B., 2010. Reactive oxygen species mediate hepatotoxicity induced by the Hsp90 inhibitor geldanamycin and its analogs. Free Radic. Biol. Med. 48, 1559–1563.
Sbiera, S., Deutschbein, T., Weigand, I., Reincke, M., Fassnacht, M., Allolio, B., 2015. The new molecular landscape of cushing's disease. Trends Endocrinol Metab 26, 573–583.
Schymkowitz, J., Borg, J., Stricher, F., Nys, R., Rousseau, F., Serrano, L., 2005. The FoldX web server: an online force field. Nucleic Acids Res. 33, W382–W388 (Web Server issue).
Sequist, L.V., Gettinger, S., Senzer, N.N., Martins, R.G., Jänne, P.A., Lilenbaum, R., Gray, J.E., Iafrate, A.J., Katayama, R., Hafeez, N., Sweeney, J., Walker, J.R., Fritz, C., Ross, R.W., Grayzel, D., Engelman, J.A., Borger, D.R., Paez, G., Natale, R., 2010. Activity of IPI-504, a novel heat-shock protein 90 inhibitor, in patients with molecularly defined non-small-cell lung cancer. J. Clin. Oncol. 28, 4953–4960.
Serviddio, G., Bellanti, F., Stanca, E., Lunetti, P., Blonda, M., Tamborra, R., Siculella, L., Vendemiale, G., Capobianco, L., Giudetti, A.M., 2014. Silybin exerts antioxidant effects and induces mitochondrial biogenesis in liver of rat with secondary biliary cirrhosis. Free Radic. Biol. Med. 73, 117–126.
Sha, L., Wang, X., Li, J., Shi, X., Wu, L., Shen, Y., Xu, Q., 2017. Pharmacologic inhibition of Hsp90 to prevent GLT-1 degradation as an effective therapy for epilepsy. J. Exp. Med. 214, 547–563.
Shao, J., Grammatikakis, N., Scroggins, B.T., Uma, S., Huang, W., Chen, J.J., Hartson, S.D., Matts, R.L., 2001. Hsp90 regulates p50(cdc37) function during the biogenesis of the activeconformation of the heme-regulated eIF2 alpha kinase. J. Biol. Chem. 276, 206–214.
Shao, J., Irwin, A., Hartson, S.D., Matts, R.L., 2003. Functional dissection of cdc37: characterization of domain structure and amino acid residues critical for protein kinase binding. Biochemistry 42, 12577–12588.
Shimamura, T., Perera, S.A., Foley, K.P., Sang, J., Rodig, S.J., Inoue, T., Chen, L., Li, D., Carretero, J., Li, Y.C., Sinha, P., Carey, C.D., Borgman, C.L., Jimenez, J.P., Meyerson, M., Ying, W., Barsoum, J., Wong, K.K., Shapiro, G.I., 2012. Ganetespib (STA-9090), a nongeldanamycin HSP90 inhibitor, has potent antitumor activity in in vitro and in vivo models of non-small cell lung cancer. Clin. Cancer Res. 18, 4973–4985.
Shimura, T., Sasatani, M., Kawai, H., Kamiya, K., Kobayashi, J., Komatsu, K., Kunugita, N., 2017. ATM-mediated mitochondrial damage response triggered by nuclear DNA damage in normal human lung fibroblasts. Cell Cycle 16, 2345–2354.
Socinski, M.A., Goldman, J., El-Hariry, I., Koczywas, M., Vukovic, V., Horn, L., Paschold, E., Salgia, R., West, H., Sequist, L.V., Bonomi, P., Brahmer, J., Chen, L.C., Sandler, A., Belani, C.P., Webb, T., Harper, H., Huberman, M., Ramalingam, S., Wong, K.K., Teofilovici, F., Guo, W., Shapiro, G.I., 2013. A multicenter phase II study of ganetespib monotherapy in patients with genotypically defined advanced non-small cell lung cancer. Clin. Cancer Res. 19, 3068–3077.
Soleimani, V., Delghandi, P.S., Moallem, S.A., Karimi, G., 2019. Safety and toxicity of silymarin, the major constituent of milk thistle extract: an updated review. Phytother Res. https://doi.org/10.1002/ptr.6361. ([Epub ahead of print]).
Solit, D.B., Ivy, S.P., Kopil, C., Sikorski, R., Morris, M.J., Slovin, S.F., Kelly, W.K., DeLaCruz, A., Curley, T., Heller, G., Larson, S., Schwartz, L., Egorin, M.J., Rosen, N., Scher, H.I., 2007. Phase I trial of 17-allylamino-17-demethoxygeldanamycin in patients with advanced cancer. Clin. Cancer Res. 13, 1775–1782.
Sugiyama, A., Kageyama, K., Murasawa, S., Ishigame, N., Niioka, K., Daimon, M., 2015. Inhibition of heat shock protein 90 decreases ACTH production and cell proliferation in AtT-20 cells. Pituitary 18, 542–553.
Taherian, A., Krone, P.H., Ovsenek, N., 2008. A comparison of Hsp90alpha and Hsp90beta interactions with cochaperones and substrates. Biochem. Cell Biol. 86, 37–45.
Terracciano, S., Russo, A., Chini, M.G., Vaccaro, M.C., Potenza, M., Vassallo, A., Riccio, R., Bifulco, G., Bruno, I., 2018. Discovery of new molecular entities able to strongly interfere with Hsp90 C-terminal domain. Sci. Rep. 8, 1709.
Thulasiraman, V., Matts, R.L., 1996. Effect of geldanamycin on the kinetics of chaperone-mediated renaturation of firefly luciferase in rabbit reticulocyte lysate. Biochemistry 35, 13443–13450.
Tiwari, P., Mishra, K.P., 2015. Silibinin in cancer therapy: a promising prospect. Cancer Res Front 1, 303–318.
Travers, J., Sharp, S., Workman, P., 2012. HSP90 inhibition: two-pronged exploitation of cancer dependencies. Drug Discov. Today 17, 242–252.
Uma, S., Hartson, S.D., Chen, J.J., Matts, R.L., 1997. Hsp90 is obligatory for the heme-regulated eIF-2alpha kinase to acquire and maintain an activable conformation. J. Biol. Chem. 272, 11648–11656.
Van den Hof, W.F., Coonen, M.L., van Herwijnen, M., Brauers, K., Wodzig, W.K., van Delft, J.H., Kleinjans, J.C., 2014. Classification of hepatotoxicants using HepG2 cells: a proof of principle study. Chem. Res. Toxicol. 27, 433–442.
Vargas-Mendoza, N., Madrigal-Santillán, E., Morales-González, A., Esquivel-Soto, J., Esquivel-Chirino, C., García-Luna Y González-Rubio, M., Gayosso-de-Lucio, J.A., Morales-González, J.A., 2014. Hepatoprotective effect of silymarin. World J. Hepatol. 6, 144–149.
Verba, K.A., Wang, R.Y., Arakawa, A., Liu, Y., Shirouzu, M., Yokoyama, S., Agard, D.A., 2016. Atomic structure of Hsp90-Cdc37-Cdk4 reveals that Hsp90 traps and stabilizes an unfolded kinase. Science 352, 1542–1547.
Verdura, S., Cuyàs, E., Llorach-Parés, L., Pérez-Sánchez, A., Micol, V., Nonell-Canals, A., Joven, J., Valiente, M., Sánchez-Martínez, M., Bosch-Barrera, J., Menendez, J.A., 2018. Silibinin is a direct inhibitor of STAT3. Food Chem. Toxicol. 116, 161–172.
Voss, A.K., Thomas, T., Gruss, P., 2000. Mice lacking HSP90beta fail to develop a placental labyrinth. Development 127, 1–11.
Wang, Y., McAlpine, S.R., 2015. N-terminal and C-terminal modulation of Hsp90 produce dissimilar phenotypes. Chem Commun (Camb) 51, 1410–1413.
Wang, Y., Trepel, J.B., Neckers, L.M., Giaccone, G., 2010. STA-9090, a small-molecule Hsp90 inhibitor for the potential treatment of cancer. Curr. Opin. Investig. Drugs 11, 1466–1476.
Young, J.C., Hoogenraad, N.J., Hartl, F.U., 2003. Molecular chaperones Hsp90 and Hsp70 deliver preproteins to the mitochondrial import receptor Tom70. Cell 112, 41–50.
Yun, B.G., Huang, W., Leach, N., Hartson, S.D., Matts, R.L., 2004a. Novobiocin induces a distinct conformation of Hsp90 and alters Hsp90-cochaperone-client interactions. Biochemistry 43, 8217–8229.
Yun, B.G., Huang, W., Leach, N., Hartson, S.D., Matts, R.L., 2004b. Novobiocin induces a distinct conformation of Hsp90 and alters Hsp90-cochaperone-client interactions. Biochemistry 43, 8217–8229.
Zhang, I., Zaorsky, N.G., Palmer, J.D., Mehra, R., Lu, B., 2015. Targeting brain metastases in ALK-rearranged non-small-cell lung cancer. Lancet Oncol. 16, e510–e521.
Zhao, H., Brandt, G.E., Galam, L., Matts, R.L., Blagg, B.S., 2011. Identification and initial SAR of silybin: an Hsp90 inhibitor. Bioorg. Med. Chem. Lett 21, 2659–2664.
Zhao, H., Yan, B., Peterson, L.B., Blagg, B.S., 2012. 3-Arylcoumarin derivatives manifest anti-proliferative activity through Hsp90 inhibition. ACS Med. Chem. Lett. 3, 327–331 Epub 2012 Feb 26.

STUDY 6

Silibinin is a direct inhibitor of STAT3

Verdura S, Cuyàs E, Llorach-Parés L, Pérez-Sánchez A, Micol V, Nonell-Canals A, Joven J, Valiente M, Sánchez-Martínez M, Bosch-Barrera J, Menendez JA.

Food Chem Toxicol. 2018 Jun;116(Pt B):161-172

doi: 10.1016/j.fct.2018.04.028

Food and Chemical Toxicology 116 (2018) 161–172

Contents lists available at ScienceDirect

Food and Chemical Toxicology

journal homepage: www.elsevier.com/locate/foodchemtox

Silibinin is a direct inhibitor of STAT3

Sara Verdura[a,b,1], Elisabet Cuyàs[a,b,1], Laura Llorach-Parés[c], Almudena Pérez-Sánchez[d], Vicente Micol[d,e], Alfons Nonell-Canals[c], Jorge Joven[f], Manuel Valiente[g], Melchor Sánchez-Martínez[c], Joaquim Bosch-Barrera[h,i,**], Javier A. Menendez[a,b,*]

[a] Program Against Cancer Therapeutic Resistance (ProCURE), Metabolism and Cancer Group, Catalan Institute of Oncology, Girona, Spain
[b] Molecular Oncology Group, Girona Biomedical Research Institute (IDIBGI), Girona, Spain
[c] Mind the Byte, Barcelona, Spain
[d] Instituto de Biología Molecular y Celular (IBMC), Miguel Hernández University (UMH), Elche, Alicante, Spain
[e] CIBER, Fisiopatología de la Obesidad y la Nutrición, CIBERobn, Instituto de Salud Carlos III (CB12/03/30038), Spain
[f] Unitat de Recerca Biomèdica, Hospital Universitari de Sant Joan, IISPV, Rovira i Virgili University, Reus, Spain
[g] Brain Metastasis Group, Molecular Oncology Program, Spanish National Cancer Research Centre (CNIO), Madrid, Spain
[h] Department of Medical Oncology, Catalan Institute of Oncology, Girona, Spain
[i] Department of Medical Sciences, Medical School, University of Girona, Girona, Spain

ARTICLE INFO

Keywords:
Silibinin
STAT3
Cancer
Metastasis

ABSTRACT

We herein combined experimental and computational efforts to delineate the mechanism of action through which the flavonolignan silibinin targets STAT3. Silibinin reduced IL-6 inducible, constitutive, and acquired feedback activation of STAT3 at tyrosine 705 (Y705). Silibinin attenuated the inducible phospho-activation of Y705 in GFP-STAT3 genetic fusions without drastically altering the kinase activity of the STAT3 upstream kinases JAK1 and JAK2. A comparative computational study based on docking and molecular dynamics simulation over 14 different STAT3 inhibitors (STAT3i) predicted that silibinin could directly bind with high affinity to both the Src homology-2 (SH2) domain and the DNA-binding domain (DBD) of STAT3. Silibinin partially overlapped with the cavity occupied by other STAT3i in the SH2 domain to indirectly prevent Y705 phosphorylation, yet showing a unique binding mode. Moreover, silibinin was the only STAT3i predicted to establish direct interactions with DNA in its targeting to the STAT3 DBD. The prevention of STAT3 nuclear translocation, the blockade of the binding of activated STAT3 to its consensus DNA sequence, and the suppression of STAT3-directed transcriptional activity confirmed silibinin as a direct STAT3i. The unique characteristics of silibinin as a bimodal SH2- and DBD-targeting STAT3i make silibinin a promising lead for designing new, more effective STAT3i.

1. Introduction

The aberrant activation of signal transducer and activator of transcription 3 (STAT3) contributes to cancer initiation and progression in a multi-faceted manner via promotion of cell proliferation/survival, invasion/migration, angiogenesis, and immune-evasion (Chang et al., 2013; Sansone and Bromberg, 2012; Yu et al., 2009, 2014). Feedback activation of STAT3 additionally mediates tumor resistance to a broad spectrum of cancer therapies, including radiotherapy, conventional chemotherapy, and modern targeted therapies (Lee et al., 2014; Poli and Camporeale, 2015; Tan et al., 2014; Zhao et al., 2016). STAT3 activation associates also with the generation and maintenance of cancer stem cells (CSC), a particularly aggressive type of malignant cell defined in terms of functional traits including tumor/metastasis-initiating capacity and therapy resistance (Kroon et al., 2013; Misra et al., 2018; Schroeder et al., 2014; Wang et al., 2018). Not surprisingly, the activation status of STAT3 is a strong predictor of poor prognosis and is an independent risk factor for tumor recurrence and post-therapy progression (Chen et al., 2013; Liu et al., 2012; Tong et al., 2017; Wu et al., 2016). These observations have motivated great efforts over the last decade to clinically exploit the beneficial effects of inhibiting STAT3 in human malignancies. Accordingly, a large number of STAT3 inhibitors (STAT3i) have been developed as potential cancer therapeutics (Fagard et al., 2013; Furtek et al., 2016a; b; Jin et al., 2016; Miklossy et al.,

* Corresponding author. Catalan Institute of Oncology (ICO), Girona Biomedical Research Institute (IDIBGI), Edifici M2, Parc Hospitalari Martí i Julià, E-17190 Salt, Girona, Spain.
** Corresponding author. Catalan Institute of Oncology (ICO), Hospital Dr. Josep Trueta de Girona, Avda. de França s/n, 17007, Girona, Spain
E-mail addresses: jbosch@iconcologia.net (J. Bosch-Barrera), jmenendez@iconcologia.net, jmenendez@idibgi.org (J.A. Menendez).
[1] These authors contributed equally.

https://doi.org/10.1016/j.fct.2018.04.028
Received 8 March 2018; Received in revised form 3 April 2018; Accepted 13 April 2018
Available online 14 April 2018
0278-6915/

2013; Siveen et al., 2014; Yue and Turkson, 2009).

STAT3i can be classified as indirect or direct according to their mode of action. Indirect STAT3i interfere with cytokine- and growth factor receptor-activated upstream kinases such as the Janus kinases (JAK) that phosphorylate STAT3. Direct STAT3i bind to STAT3 protein domains critically involved in STAT3 activation/dimerization (Src homology 2 domain, SH2) or DNA binding (DNA-binding domain, DBD). The usage of broad-spectrum indirect STAT3i (e.g., JAK inhibitors), however, often results in undesirable off-target effects. Research into direct STAT3i has focused mainly on targeting the SH2 domain, the protein-protein interface responsible for the formation of STAT3 dimers by reciprocal phosphotyrosine-SH2 interactions following activation of the tyrosine 705 (Y705) residue. Unfortunately, only a limited number of direct, SH2-targeted STAT3i have reached preclinical and clinical trials. This is due mostly to the intrinsic difficulty in developing small molecules capable of efficaciously disrupting protein-protein interactions over a large surface such as those involving SH2-mediated STAT3 dimerization, while maintaining drug-like properties *in vivo*. Moreover, the sole blockade of active STAT3 dimers might not be sufficient to fully abrogate STAT3 signaling (Nkansah et al., 2013; Timofeeva et al., 2012). Although targeting of the STAT3 DBD and disruption of its DNA binding activity has the potential to circumvent the transcriptional activation of STAT3 irrespective of its activation/dimerization status (Huang et al., 2016), very few small molecules have been reported to date as STAT3 DBD inhibitors. This is mainly due to the previously thought undruggable nature of the DBD and potentially limited selectivity (Huang et al., 2016), and also the lack of adequate assay systems (Furtek et al., 2016a; b). Furthermore, there are only three crystal structures available [PDB ID: 4E68 (Nkansah et al., 2013), 3CWG (Ren et al., 2008), and 1BG1 (Becker et al., 1998)] of the mouse but not human core STAT3 fragment containing the SH2 and DBD domains in the Protein Data Bank (http://www.rcsb.org), and co-crystal structures of STAT3i bound to STAT3 are lacking.

There is ever-growing evidence that the flavonolignan silibinin, the major bioactive constituent of the seed extract of the plant Milk thistle (*Silybum marianum*) (Agarwal et al., 2006; Cufí et al., 2013a,b; Gažák et al., 2007), possesses drug-like properties with proven clinical activity via inhibition of STAT3 signaling (Chittezhath et al., 2008; Cuyàs et al., 2016; Shukla et al., 2015; Singh et al., 2009). Although initial clinical experiences with silibinin supplementation in cancer patients have been disappointing (Flaig et al., 2010; Hoh et al., 2006; Siegel et al., 2014), new silibinin formulations with improved water solubility, absorption, and bioavailability appear to translate into proven therapeutic benefits (Bosch-Barrera et al., 2014, 2016). Unfortunately, whereas the possibility of providing oncologists with new silibinin formulations or silibinin derivatives capable of functioning as STAT3i in a clinical setting may broaden their therapeutic armamentarium (Bosch-Barrera and Menendez, 2015; Bosch-Barrera et al., 2017), the precise mechanism through which silibinin targets STAT3 remains unknown. Here, we aimed to combine experimental and *in silico* efforts to clearly delineate the molecular bases of the silibinin-STAT3 interaction.

2. Materials and methods

2.1. Reagents

Recombinant IL-6 (Cat. No. 7270-IL-25) was obtained from R&D. ONE-Glo™ Luciferase Assay System (Cat. No E6110) and the pGL4.47 (luc2P/STAT-3 inducible element [SIE]/Hygro) vector (Cat. No E4041) were purchased from Promega (Madison, WI, USA). TransAM® Transcription Factor ELISA (Cat. No 45196) was obtained from Active Motif (Carlsbad, CA, USA). Antibodies against total STAT3 (124H6, Cat. No 9139) and phospho-STAT3 Tyr705 (D3A7, Cat. No 9145S) were purchased from Cell Signaling Technology (Beverly, MA, USA). H2228 and H2228/CR cells were generously provided by Daniel B. Costa (Division of Hematology/Oncology, Beth Israel Deaconess Medical Center, Boston, USA).

2.2. LanthaScreen STAT3 GripTite inhibitor screen

To characterize the STAT3 inhibitory potency of silibinin, IC_{50} determinations for phospho-$STAT3^{Y705}$ were outsourced to Invitrogen (Life Technologies) using the LanthaScreen STAT3 GripTite inhibitor screen service. Briefly, cells were thawed and resuspended in Assay Medium (OPTI-MEM, 1% csFBS, 0.1 mmoL/L NEAA, 1 mmoL/L sodium pyruvate, 100 U/mL/100 µg/mL Pen/Strep) to a concentration of 625,000 cells/mL. Thirty-two microliters of the cell suspension were added to each well of a white tissue culture-treated assay plate (20,000 cells/well) and incubated for 16–26 h at 37 °C/5% CO_2 in a humidified incubator. Then, 4 µL of the control inhibitor JAK Inhibitor I or silibinin was added to the appropriate assay wells followed by the addition of 4 µL of Assay Medium. The assay plate was incubated for 30–60 min at 37 °C/5% CO_2 in a humidified incubator. Then 4 µL of a 10 × control activator, IFN-α or IL-6 at the pre-determined EC_{80} concentration, was added to wells containing the control inhibitor or silibinin. The assay plate was then incubated as before for 30 min. Next, the assay medium was aspirated from the wells and 20 µL of LanthaScreen Cellular Assay Lysis Buffer containing 5 nmoL/L of LanthaScreen Tb-anti-$STAT3^{Y705}$ antibody was added. The assay plate was incubated for 60 min at room temperature and then read with a fluorescent plate reader.

2.3. Z′-LYTE JAK kinase activity assay

To characterize the JAK1/JAK2 kinase inhibitory potency of silibinin, IC_{50} determinations for JAK1/JAK2 kinase activity were outsourced to Invitrogen (Life Technologies) using the FRET-based Z-LYTE™ SelectScreen Kinase Profiling Service. The 2 × JAK1/Tyr 06 or JAK2/Tyr 06 mixture was prepared in 50 mmoL/L HEPES pH 6.5, 0.01% BRIJ-35, 10 mmoL/L MgCl2, 1 mmoL/L EGTA, and 0.02% NaN_3. The final 10 µL Kinase Reaction consisted of 21.2–91.5 ng JAK1 (or JAK2) and 2 µmoL/L Tyr 06 in 50 mmoL/L HEPES pH 7.0, 0.01% BRIJ-35, 10 mmoL/L $MgCl_2$, 1 mmoL/L EGTA, and 0.01% NaN_3. After incubation for 1 h, 5 µL of a 1:128 dilution of Development Reagent A was added.

SelectScreen Kinase Profiling Service uses XLfit software from ID Business Solutions (UK). The dose response curve is fitted to model number 205 (sigmoidal dose-response model). If the bottom of the curve does not fit between −20% and 20% inhibition, it is set to 0% inhibition. If the top of the curve does not fit between 70% and 130% inhibition, it is set to 100% inhibition.

2.4. Computational modeling of human STAT3

The homology-modeling software tools SWISS-MODEL and I-TASSER were employed to generate a computational homology model of human STAT3. The human amino acidic sequence [UniprotID P40763] was extracted from Uniprotkb and, in both cases, the three-dimensional crystal structure of the mouse STAT3 homodimer bound to DNA [PDB ID 1BG1 (Becker et al., 1998)] was employed as template. Whereas SWISS-MODEL generated a homology model that failed to cover a few residues on the SH2 domain, I-TASSER employed 1BG1 and other templates including 4E68 (unphosphorylated mouse STAT3 core protein binding to double-stranded DNA (Nkansah et al., 2013)), 3CWG (unphosphorylated mouse STAT3 core fragment (Ren et al., 2008)), and 1YVL (unphosphorylated mouse STAT1 (Mao et al., 2005)) to cover a larger extent of the protein. All the PDB entries used to generate structures were constructed as monomers and then assembled as dimers using 1BG1 as template.

2.5. Docking calculations

All docking calculations were performed using Itzamna and Kin (www.mindthebyte.com), classical docking, and blind-docking software tools. Protein structures from RSCB PDB as well as the above-mentioned human homology models were directly employed for docking calculations using the SH2 and DBD cavities defined in the literature as STAT3 binding regions. Two runs were carried out for each calculation to avoid false positives.

2.6. Molecular dynamics (MD) simulations

Docking post-processing allowing conformational selections/induced fit events to optimize the interactions were performed via short (1 ns) MD simulations using NAMD version 2.10 over the best-docked complexes, which were selected based on the interaction energy. The Ambers99SB-ILDN and the GAFF forcefield set of parameters were employed for STAT3 and STAT3i including silibinin, respectively. The GAFF parameters were obtained using Acpype software, whereas the STAT3 structures were modeled using the leap module of Amber Tools. Simulations were carried out in explicit solvent using the TIP3P water model with the imposition of periodic boundary conditions *via* a cubic box. Electrostatic interactions were calculated by the particle-mesh Ewald method using constant pressure and temperature conditions. Each complex was solvated with a minimum distance of 10 Å from the surface of the complex to the edge of the simulation box. Na^+ or Cl^- ions were also added to the simulation to neutralize the overall charge of the systems. The temperature was maintained at 300 K using a Langevin thermostat, and the pressure was maintained at 1 atm using a Langevin Piston barostat. The time step employed was 2 fs. Bond lengths to hydrogens were constrained with the SHAKE algorithm. Before production runs, the structure was energy minimized followed by a slow heating-up phase using harmonic position restraints on the heavy atoms of the protein. Subsequently, the system was energy minimized until volume equilibration, followed by the production run without any position restraints.

2.7. Binding free energy analysis

Molecular Mechanics/Generalized Borne Surface Area (MM/GBSA) calculations were performed to calculate the alchemical binding free energy (ΔG_{bind}) of silibinin and direct STAT3i against STAT3. MM/GBSA rescoring was performed using the MMPBSA.py algorithm within AmberTools. The snapshots generated in the 1 ns MD simulation were imputed into the post-simulation MM/GBSA calculations of binding free energy. Graphical representations were prepared using PyMOL program and PLIP version 1.3.0.

2.8. Interaction analysis

The predicted binding site residues of silibinin to the SH2 and DBD domains of STAT3 were defined using evidence-based interaction analyses of known STAT3 inhibitors with well-defined binding residues in the SH2 and DBS sites.

2.9. Indirect immunofluorescence microscopy

Cells seeded on a glass plate were fixed with methanol and incubated with the respective antibodies against STAT3 and phospho-STAT3 Tyr705. Antibody binding was localized with either a goat anti-rabbit IgG (H + L) secondary antibody, Alexa Fluor® 594 conjugate or a goat anti-mouse IgG (H + L) secondary antibody, Alexa Fluor® 488 conjugate (both from Invitrogen). Nuclei were counterstained with Hoechst 33342. Images were obtained with a Nikon Eclipse 50i fluorescence microscope including NIS-Elements imaging software.

2.10. STAT3 luciferase reporter assay

Luciferase activities of HEK293T cells transfected with the pGL4.47 reporter, in which five copies of the STAT3 DNA binding site-containing the SIE drives transcription of the luciferase-reporter gene luc2P (Photinus pyralis, 2), were measured using a Dual-Luciferase Reporter Assay System (ONE-Glo™, Promega).

2.11. STAT3 TransAM™ enzyme-linked immunosorbent assay

The STAT3 DNA-binding assay was performed using the TransAM™ Transcription Factor ELISA. Briefly, nuclear extracts from IL-6-stimulated cells containing activated STAT3 were directly added with graded concentrations of silibinin and complete binding buffer to microtiter wells coated with the STAT3 consensus sequence (5′-TTCCCGGAA-3′) for 3 h at room temperature. The wells were washed three times with 1 × wash buffer, and incubated with STAT3 antibody for 1 h. The wells were then washed as before and incubated with a horseradish peroxide-conjugated secondary antibody at room temperature for 1 h. After washing again, 100 µL of developing solution was added to the wells, which was quenched with 100 µL of stop solution, and the absorbance was measured at 450 nm.

2.12. Statistical analysis

All statistical analyses were performed using XLSTAT 2010 (Addinsoft™). For all experiments, at least three independent biological replicates were performed with $n \geq 3$ technical replicates per experiment. No statistical method was used to predetermine sample size. Investigators were not blinded to data allocation. Experiments were not randomized. Data are presented as mean ± S.D. Two-group comparisons were performed using Student's *t*-test for paired and unpaired values. Comparisons of means of ≥3 groups were performed by ANOVA, and the existence of individual differences, in case of significant *F* values at ANOVA, were tested by Scheffé's multiple contrasts. *P* values < 0.05 were considered to be statistically significant (denoted as *). All statistical tests were two-sided.

3. Results

3.1. Silibinin inhibits Y705 STAT3 phosphorylation in cell-based assays

We initially assessed the ability of silibinin to interfere with the three known activating modes of Y705 STAT3 phosphorylation, namely IL-6-inducible, constitutive, and acquired (feedback hyperactivation), in a panel of non-small cell lung carcinoma (NSCLC) cell lines (Fig. 1A). H460 and PC9 cell lines, which do not express persistently hyperphosphorylated STAT3, were used to determine whether silibinin could inhibit Y705 STAT3 phosphorylation induced by the pro-inflammatory cytokine IL-6. Immunoblotting procedures revealed that silibinin treatment completely prevented the capacity of IL-6 to induce the phosphorylation of Y705 STAT3 in H460 cells (Fig. 1B). Moreover, the ability of IL-6 to augment by 4.0-fold the phosphorylation of Y705 STAT3 in PC9 cells was reduced to 2.1-fold in the presence of silibinin (Fig. 1B). This prevention of IL-6-inducible Y705 STAT3 phosphorylation was accompanied by a rapid and noteworthy reduction in the protein level of the key STAT3 target gene c-MYC in H460 and PC9 cells (Fig. 1B).

Treatment with graded concentrations of silibinin dose-dependently abrogated Y705 STAT3 phosphorylation in the H2228 cell line, which exhibits constitutive hyperphosphorylation of STAT3 (Fig. 1C). Silibinin also suppressed, in a dose-dependent manner, the acquired feedback hyperactivation of Y705 STAT3 in H3122CR cells, which has been shown to occur as a non-genetic mechanism of acquired resistance to the ALK-tyrosine kinase inhibitor crizotinib in ALK-rearranged H3122 parental cells (Cuyàs et al., 2016) (Fig. 1D).

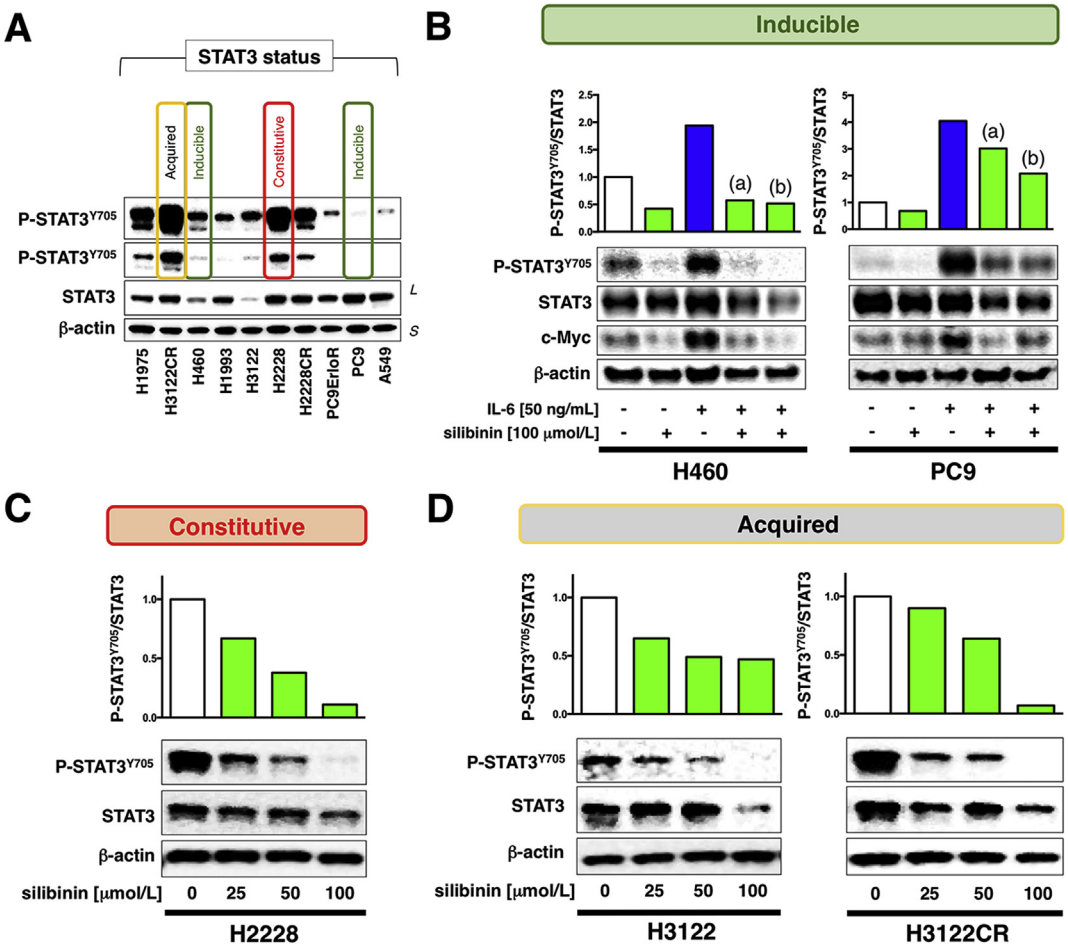

Fig. 1. Silibinin inhibits phosphorylation of STAT3 Y705. A. Baseline levels of STAT3 and P-STAT3^{Tyr705} in various NSCLC cell lines were detected by immunoblotting using specific antibodies (S: short exposure; L: long exposure) **B.** Silibinin inhibits STAT3 Y705 phosphorylation induced by IL-6. H460 and PC-9 cells were serum-starved overnight, and then left untreated or treated with 100 μmoL/L silibinin. After 3 h, the untreated and silibinin-treated cells were stimulated with IL-6 for 1 h to induce phosphorylated Y705 STAT3 (a). Alternatively, overnight serum-starved cells were left untreated or stimulated with IL-6. After 1 h, the untreated and IL-6-stimulated cells were treated with silibinin for 3 h (b). **C.** Silibinin inhibits constitutively active STAT3 Y705 phosphorylation. H2228 cells were serum-starved overnight and treated with graded concentrations of silibinin (0, 25, 50, and 100 μmoL/L) for 48 h. **D.** Silibinin inhibits acquired phospho-activation of STAT3 at Y705. Crizotinib-responsible H2228 cells (low phospho-STAT3^{Y705} at baseline) and crizotinib-resistant H2228/CR derivatives (high, acquired phospho-STAT^{Y705}) were serum-starved overnight and treated with graded concentrations of silibinin (0, 25, 50, and 100 μmoL/L) for 48 h. Figures show representative immunoblots and densitometric analyses of multiple ($n = 3$) independent experiments.

3.2. Silibinin inhibits Y705 STAT3 phosphorylation in a JAK1/JAK2-independent manner

We used the LanthaScreen® STAT3 GripTite™ HEK293 human cell line that constitutively expresses a GFP-STAT3 fusion protein to confirm the STAT3 inhibitory activity of silibinin. Because the activation state of the tyrosine kinases JAK1 and JAK2 is considered to be the main effector mechanism for Y705 STAT3 phosphorylation (Chang et al., 2013; Sansone and Bromberg, 2012; Yu et al., 2009), and given that the JAK/STAT3 signaling pathway is functionally intact in the STAT3 GripTite™ cell line, the GFP-STAT3 fusion protein serves as a direct substrate for assessing IL-6- and IFN-α-inducible STAT3 phosphorylation. We pre-incubated serum-starved STAT3 GripTite™ HEK293 cells with graded concentrations of silibinin for 1 h prior to stimulation with IL-6 or IFN-α (for 30 min) at the pre-determined EC_{80} effective concentration for optimized JAK-mediated GFP-STAT3 phosphorylation. A lytic immunoassay was then developed in which the phosphorylation state of GFP-STAT3 was detected in cell lysates using a terbium-labeled anti-pY705-STAT3 antibody in a time-resolved FRET (TR-FRET) readout (Supplementary Fig. S1A). The IL-6 stimulation/silibinin inhibitor screen provided a Z′ factor of 0.74, which indicated good signal separation and plate uniformity, whereas the IFN-α stimulation/silibinin inhibitor screen provided a Z' factor of 0.57, which was acceptable by high-throughput screening standards. Both assays showed a dose-dependent decrease in the TR-FRET signals with IC_{50} values of 320 μmoL/L for IL-6-stimulated phosphorylation of Y705 STAT3 and 182 μmoL/L for IFN-α-stimulated phosphorylation of Y705 STAT3 (Fig. 2A). We then used the FRET-based Z-LYTE™Kinase Assay to detect and characterize the ability of silibinin to directly operate as a JAK1/JAK2 kinase inhibitor (Supplementary Fig. S1B). When ten concentrations of silibinin over five logarithmic decades were selected, we failed to detect any significant inhibitory activity of silibinin towards the kinase activity of JAK1 and JAK2 (Fig. 2B).

3.3. Generation of a computational homology model of the human STAT3 protein: A comparative study of silibinin and multiple STAT3i

To test whether the inhibitory mode of action of silibinin against STAT3 might involve its direct binding to the STAT3 protein, we generated a computational homology model of human STAT3 protein (see the *Material and methods* section for details).

Fig. 3A depicts all the STAT3i included in our comparative *in silico* analysis of the binding of silibinin to STAT3, including Stattic (Schust et al., 2006), S31-M2011 (Furqan et al., 2013), TPCA-1 (Nan et al.,

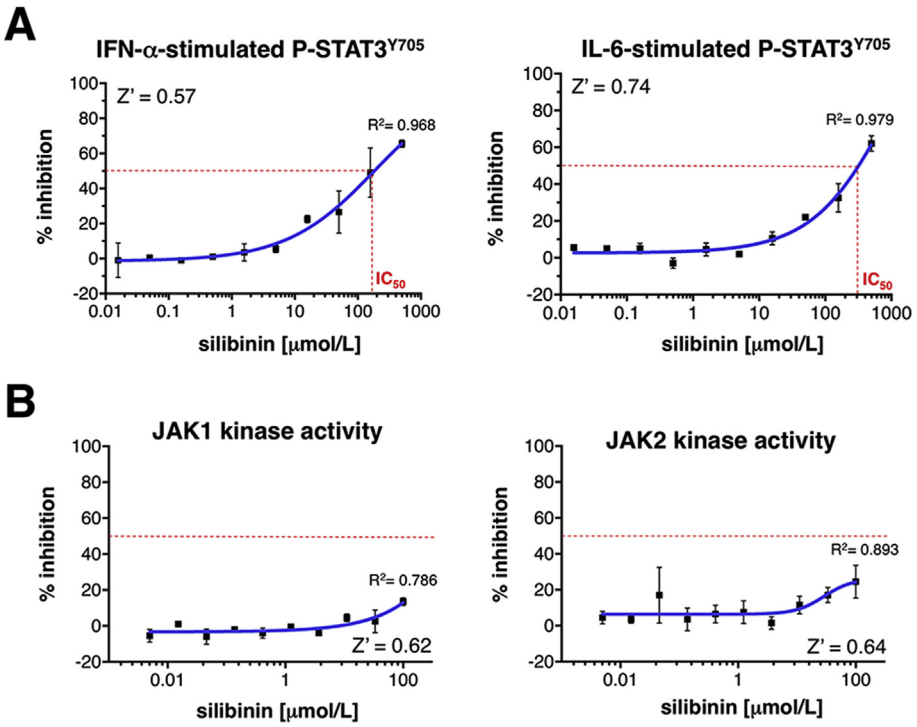

Fig. 2. Silibinin inhibits phospho-activation of STAT3 without targeting the STAT3 kinase JAK1/JAK2. A. Graphs shows the 520/490 nm emission ratios of silibinin-treated LanthaScreen® STAT3 GripTite™ cells (one representative experiment carried out in triplicate). **B.** Figure shows dose-response curves of ATP-dependent JAK1/JAK2 kinase activities for one representative experiment carried out in triplicate, created by plotting FRET signal of the Z′-LYTE Kinase assay as the function of silibinin concentration. See Supplementary Figs. S1A and B for schematic description of details concerning LanthaScreen® and Z′-LYTE assays.

2014), OPB-31121 (Brambilla et al., 2015), LLL-12 (Lin et al., 2010), lnS3-54A18 (Zhao et al., 2016), HO-3687 (Rath et al., 2014), BP5-087 (Eiring et al., 2015), STX-0119 (Matsuno et al., 2010), ISS610 (Shahani et al., 2011), SH-4-054 (Ali et al., 2016), S31-1757 (Zhang et al., 2013), Compound 50 (Lai et al., 2015), and Compound 24 (Lai et al., 2015). When classical docking calculations were performed against cavities of both the SH2 domain and the DBD (Fig. 3B–D), we observed that all the STAT3i as well as silibinin were placed in the middle of the corresponding regions of each domain by sharing residues between both chains. Although this behavior reproduced a plausible binding mode capable of disrupting the STAT3 dimer, as previously reported for some STAT3i, it is acknowledged that the majority of STAT3i have been

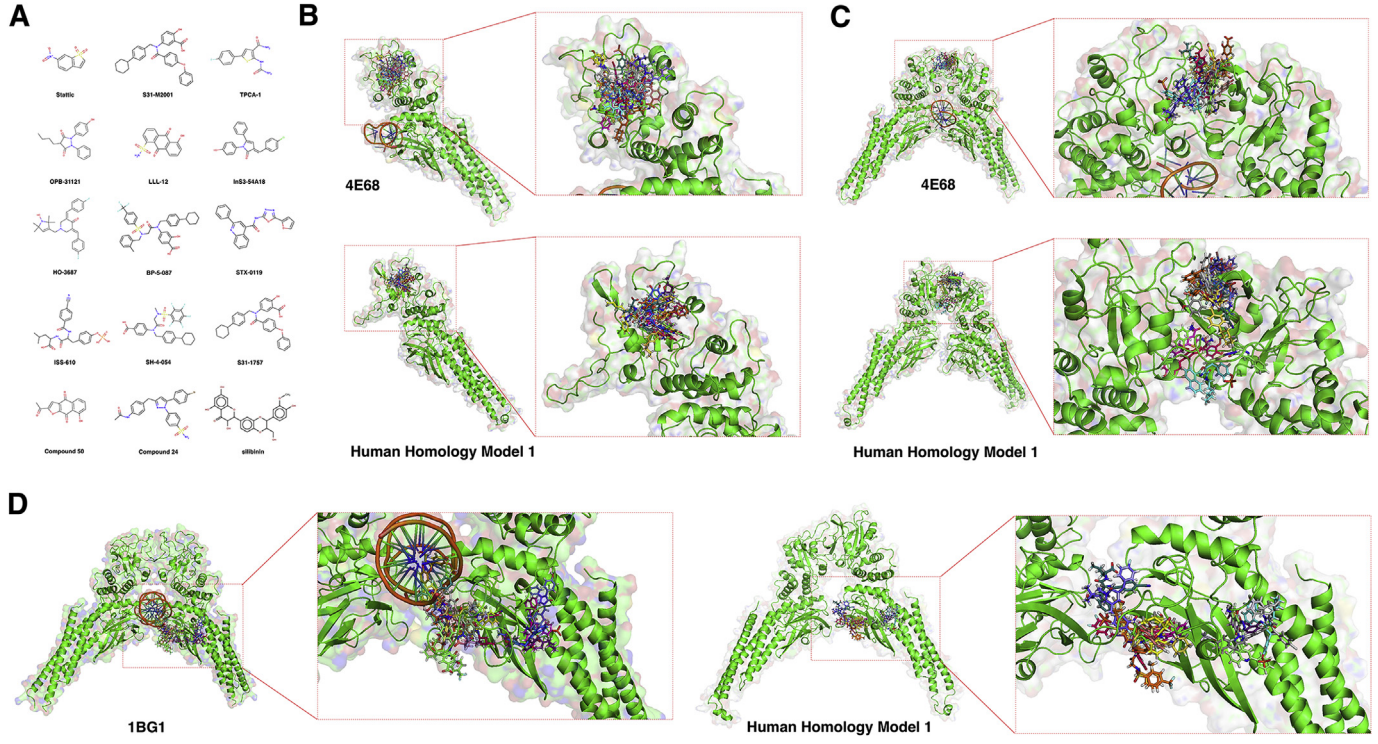

Fig. 3. Silibinin is computationally predicted to behave as a direct STAT3i. A. Chemical structures of the direct STAT3i included in a comparative computational study of silibinin as a direct STAT3i. **B**, **C**, and **D**. Overall structures and views of the interactions between direct STAT3i with the monomeric SH2 binding region (**A**), the binding region between SH2 dimers (**B**), and the DBD domain at STAT3 DBD domain-DNA complex (**C**) assembled from PDBIDs 4E68 and 1BG1, or human homology model 1, as specified.

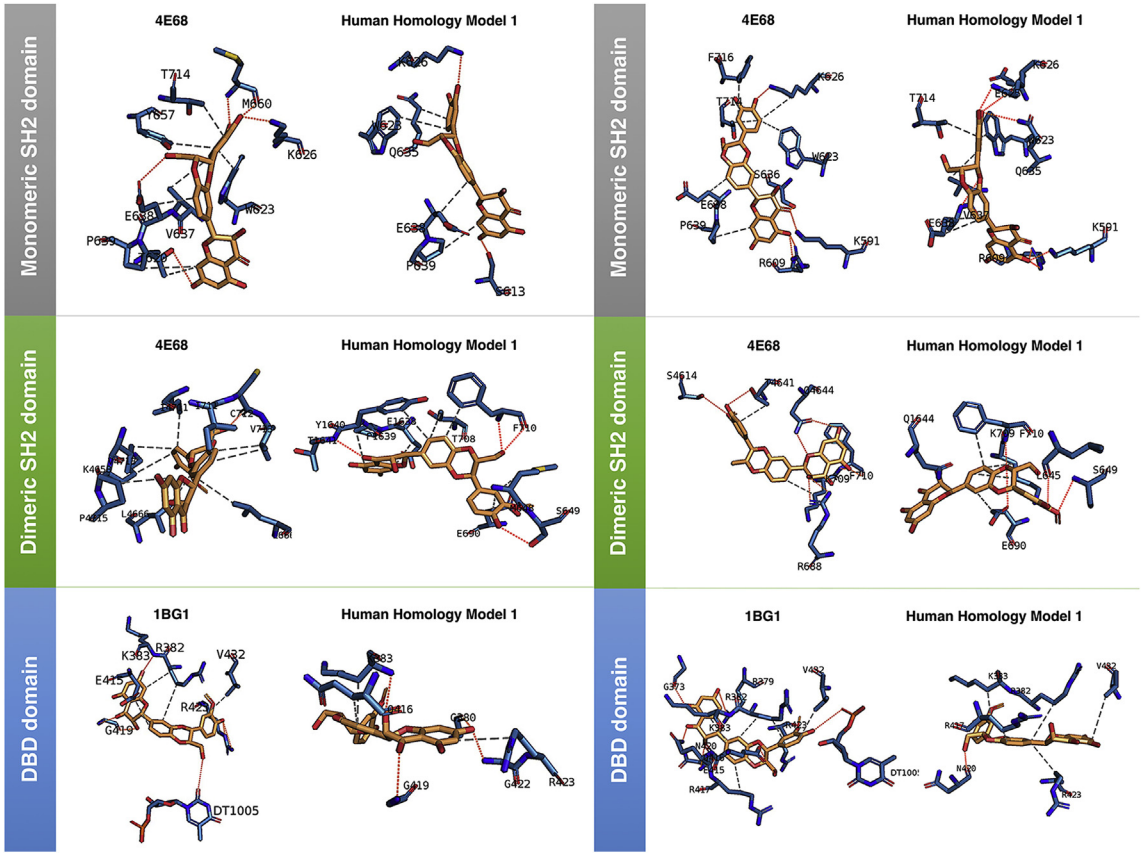

Fig. 4. Mode of binding of silibinin to SH2 activation/dimerization and DNA binding (DBD) domains of STAT3. Figure shows in sticks all the pharmacophoric interaction residues involved in the *in silico* binding of silibinin to the SH2 and DBD domains of STAT3, using PLIP. Orange dashed lines represent hydrogen bond interactions; grey dashed lines represent hydrophobic interactions. The main residues involved in silibinin interaction with the protein backbone are shown in black; the residue numbers shown correspond to the original PDB file numbering. *Left panels* correspond to binding poses resulting from simple, rigid docking studies; *right panels* correspond to self-docking poses under molecular dynamics (MD) simulations modeling the backbone and ligand (silibinin) flexibility. (For interpretation of the references to colour in this figure legend, the reader is referred to the Web version of this article.)

suggested to bind the corresponding SH2 or DBD domain solely in one of the monomers, without sharing residues with the other one. To explore in more detail the latter behavior, we performed docking simulations to the monomeric structures, to mimic the desired binding of known STAT3i. The binding energies obtained from *in silico* binding experiments using rigid docking calculations, which were run twice to avoid false positives, are summarized in Table S1 (SH2 domain of monomeric structures), Table S2 (SH2 domain of dimeric structures), and Table S3 (DBD of dimeric structures). This approach predicted the ability of silibinin to directly bind the mouse and human STAT3 structures, with energy values ranging from −5.9 kcaL/mol to −8.5 kcaL/mol when using the mouse crystal structures 1BG1, 3CWG, 4E68, and from −5.6 kcaL/mol to −9.0 kcaL/mol when using the human homology models 1 and 2.

To add protein flexibility to the analysis and to better test the stability of the silibinin-STAT3 complexes, we carried out short MD simulations of 1 ns and applied MM/GBSA calculations to estimate more reliable binding energies, which are summarized in Table S4, S5, and S6. For MD simulations and MM/GBSA calculations, we selected mouse 4E68 and human homology model 1 to investigate the interactions with the SH2 domain, whereas mouse 1BG1 and human homology model 1 were selected to investigate the interactions with the DBD. Such approaches predicted the capacity of silibinin to bind mouse and human STAT3 structures with energy values ranging from −24.5797 kcaL/mol to −40.5752 kcaL/mol when using the mouse crystal structures 1BG1 and 4E68, and from −20.0086 kcaL/mol to −36.4145 kcaL/mol when using the human homology model 1.

3.4. Silibinin is predicted to bind to the SH2 and the DBD domains of STAT3

The binding modes of well-characterized direct STAT3i were significantly shared between the mouse PDB crystal structures and the human homology models, highlighting a high degree of conservation of the SH2 and DBD domains between mouse and human STAT3 proteins. The evaluation of the binding mode of silibinin to the monomeric form of the SH2 domain revealed a common group of predicted interacting residues shared with other direct STAT3i (Table S7); namely, M660, E638, K626, 7620, P639, V637, Y657, W623, and T714 in the mouse crystal structure 4E68, and S613, K626, P639, Q635, W623, and E638 in the human homology model 1. Silibinin was predicted not to share any interacting residue with S31-757 in the human homology model 1 of the monomeric form of the SH2 domain.

When evaluating the binding of silibinin to the dimeric form of the SH2 domain, we observed that silibinin was predicted to place differently to the remainder of the direct STAT3i (Table S8). Accordingly, silibinin was predicted to share with other direct STAT3 inhibitors a significant number of interacting residues in the human homology model 1 (K1658, M655, I1711, P1715, K709, V713, E652, V1713, L1666, I711, L666), but only a few interacting residues in the mouse crystal structure 4E68 (Q4644, E4638, and M648). Silibinin was predicted not to share any interacting residues with S31-M2001 and STX-0119 in the human homology model 1 of the dimeric form of the SH2 domain.

The evaluation of the binding mode of silibinin to the DBD revealed a common group of putative interacting residues shared with other

direct STAT3i (Table S9); namely, R423, K383, G419, R382, V432, and E415 in the mouse crystal structure 1BG1, and G419, G422, K383, G390, Q416, and R423 in the human homology model 1. Silibinin was predicted not to share any interacting residues with Stattic, S31-M2001, ln53–5418, S31-1757, and Compound 24 in the mouse crystal structure 1BG1, or S31-M2011, ln53-54A18, STX-0119, Compound 50, and Compound 24, in the human homology model 1.

3.5. The predicted binding mode of silibinin to STAT3 domains is different to other STAT3i

Silibinin was predicted to establish hydrogen bond interactions with S613, K626, E638, and M660 within the binding pocket of the monomeric SH2 domain of STAT3 (Fig. 4). Silibinin was predicted to additionally establish hydrophobic interactions with T620, W623, Q635, V637, E638, P639, Y657, and T714 (Fig. 4). The binding and putative inhibitory capacity of silibinin against the SH2 domain of STAT3 is underscored by the fact that it was predicted to share a significant number of interacting residues (W623, K626, Q635, V637, E638, Y657, and T714), or interact with those placed nearby or adjacent to those that were identified upon an extensive bibliographic search for key interacting residues employed by existing SH2-targeted STAT3i (F588, I589, S590, K591, E594, R595, R609, S611, E612, W623, K626, Q635, S636, V637, E638, Y657, I659, C687, Y705, T714, P715, T716, T717, and S727) (Fig. 4).

Silibinin was predicted to establish hydrogen bond interactions with S649, F710, and C722 (α chain), and T641 (β chain) within the binding pocket of the dimeric SH2 domains of STAT3 (Fig. 4). Silibinin was predicted to additionally establish hydrophobic interactions with M648, S649, L666, T708, F710, I711, and V713 (α chain) and with E638, P639, Y640, K658, I711, and V713 (β chain) (Fig. 4). Although most of these residues were placed nearby or adjacent to the above-mentioned key interacting residues employed by existing SH2-targeted STAT3 inhibitors (Supplementary Fig. S2), E638 was identified as the sole key interacting residue shared with silibinin, thus supporting the notion that direct STAT3i including silibinin might employ the binding pocket within the monomeric, but not the dimeric, SH2 domain of STAT3.

Silibinin was predicted to establish hydrogen bond interactions with R382, K383, G419, G422, R423, and G380 within the DBD of dimeric STAT3 (Fig. 4). Silibinin was predicted to additionally establish hydrophobic interactions with R382, K383, E415, R423, and V432. It should be noted that all these residues were included in the list of key interacting DBD residues that were identified upon an extensive bibliographic search of direct STAT3i; namely, Q326, P327, P330, M331, H332, K340, T341, V343, F345, T412, E415, N420, R423, I431, V432, S465, N466, I467, Q469, M470, W474, and N485. Moreover, despite the fact that DNA was complexed in the 1BG1 crystal structure for all the docking and MD simulations, silibinin was the sole STAT3i that was predicted to establish a hydrogen bond interaction with DT1005 (Fig. 4).

3.6. Silibinin prevents nuclear accumulation of activated STAT3

Since Y705 phosphorylation and dimerization of STAT3 is a prerequisite for its cytokine-induced nuclear translocation, we would expect a direct STAT3 SH2 domain inhibitor such as silibinin to inhibit IL-6-induced nuclear translocation of phospho-active STAT3. To test this, PC9 cells were seeded on coverslips and stimulated for 24 h with IL-6 in the absence or presence of silibinin. In untreated conditions, immunofluorescence microscopy showed that STAT3 was uniformly distributed between the cytoplasm and nucleus in PC9 cells; conversely, a greater number of STAT3 molecules appeared to be more prominently nuclear following IL-6 stimulation (Fig. 5A). The presence of silibinin failed to significantly alter the distribution pattern of total STAT3 in the absence of IL-6 stimulation; however, silibinin co-treatment suppressed IL-6-induced nuclear accumulation of STAT3. Moreover, when cells were stained for phosphorylated Y705 STAT3, we confirmed that IL-6-mediated nuclear accumulation of STAT3 is a molecular event largely dependent on the Y705 phosphorylation, which permits STAT3 to form dimers and enter the nuclei. Such IL-6-induced conspicuous STAT3 Y705 phosphorylation and translocation into the nucleus was completely prevented in the presence of silibinin (Fig. 5A).

3.7. Silibinin blocks transcriptional activity of STAT3

We then examined whether silibinin suppresses the transcriptional activity of STAT3 after IL-6 stimulation using a dual-luciferase assay system. HEK293 cells were transiently transfected with a reporter plasmid containing the STAT3-binding response element driving the expression of the luciferase gene. The STAT3-luciferase reporter construct responded exquisitely, in a dose-dependent manner, to graded concentrations of IL-6 (Fig. 5B). A concentration of silibinin as low as 100 μmoL/L completely prevented the transcriptional activity of STAT3 after stimulation with graded concentrations of IL-6. Moreover, when cells transiently transfected with the STAT3-luciferase reporter construct were stimulated with an optimal STAT3 activating concentration of IL-6 (50 ng/mL) in the presence of graded concentrations of silibinin, we confirmed the ability of silibinin to dramatically inhibit STAT3-dependent luciferase activity in a dose-dependent manner, with IC_{50} values lower than 25 μmoL/L (Fig. 5B).

3.8. Silibinin reduces the DNA binding activity of STAT3

Such a potent inhibitory effect of silibinin on the transcriptional activity of STAT3 might reflect not only its ability to influence tyrosine phosphorylation and nuclear accumulation of STAT3, but also the *in silico* predicted capability of silibinin to establish direct interactions with DNA in its inhibitory targeting to the DBD of STAT3. To evaluate the hypothesis that silibinin might also alter STAT3 retention via DNA binding, we employed the ELISA-based TransAM™ method to quantitatively evaluate the ability of the STAT3 residing in cellular nuclear extracts to bind its corresponding DNA consensus sequence (immobilized on the 96-well plate) when exposed to silibinin (Supplementary Fig. S1C). Nuclear extracts from IL-6-stimulated H460 and PC9 cells containing Y705-phosphorylated STAT3 were incubated with increasing concentrations of silibinin to directly determine the potency of silibinin to inhibit the DNA-binding activity of STAT3. A dose-dependent reduction in the DNA-binding activity of STAT3 was observed in the presence of silibinin (up to 60% at 200 μmoL/L silibinin; Fig. 6). When nuclear extracts obtained from H2228 cells, which exhibit constitutive activation of STAT3, were incubated in the presence of graded concentrations of silibinin, their STAT3 DNA binding activity was similarly reduced by up to 60% at 200 μmoL/L silibinin compared with vehicle-treated controls (Fig. 6).

4. Discussion

Although silibinin is known to be an inhibitor of STAT3 signaling, it remained to be clarified whether silibinin should be classified as an indirect STAT3i via kinase inhibition of the JAK/STAT pathway or as a direct STAT3i capable of binding and interfering with specific domains of the STAT3 protein. As with many other plant-derived secondary metabolites including cucurbitacin, curcumin, indirubin, cryptotanshinone, resveratrol, flavopiridol, and galiellalactone (Schust et al., 2006), silibinin has repeatedly been shown to inhibit STAT3 signaling in cancer cells (Jin et al., 2016; Bosch-Barrera and Menendez, 2015). While some of these natural products might operate as STAT3i through unknown targets, or have been shown to inhibit kinases upstream of STAT3 (JAK1/2, Src), others have been suggested to directly bind to STAT3 functional domains; for example, the SH2 domain, blocking STAT3 dimerization, or the STAT3 DBD, preventing sequence-specific

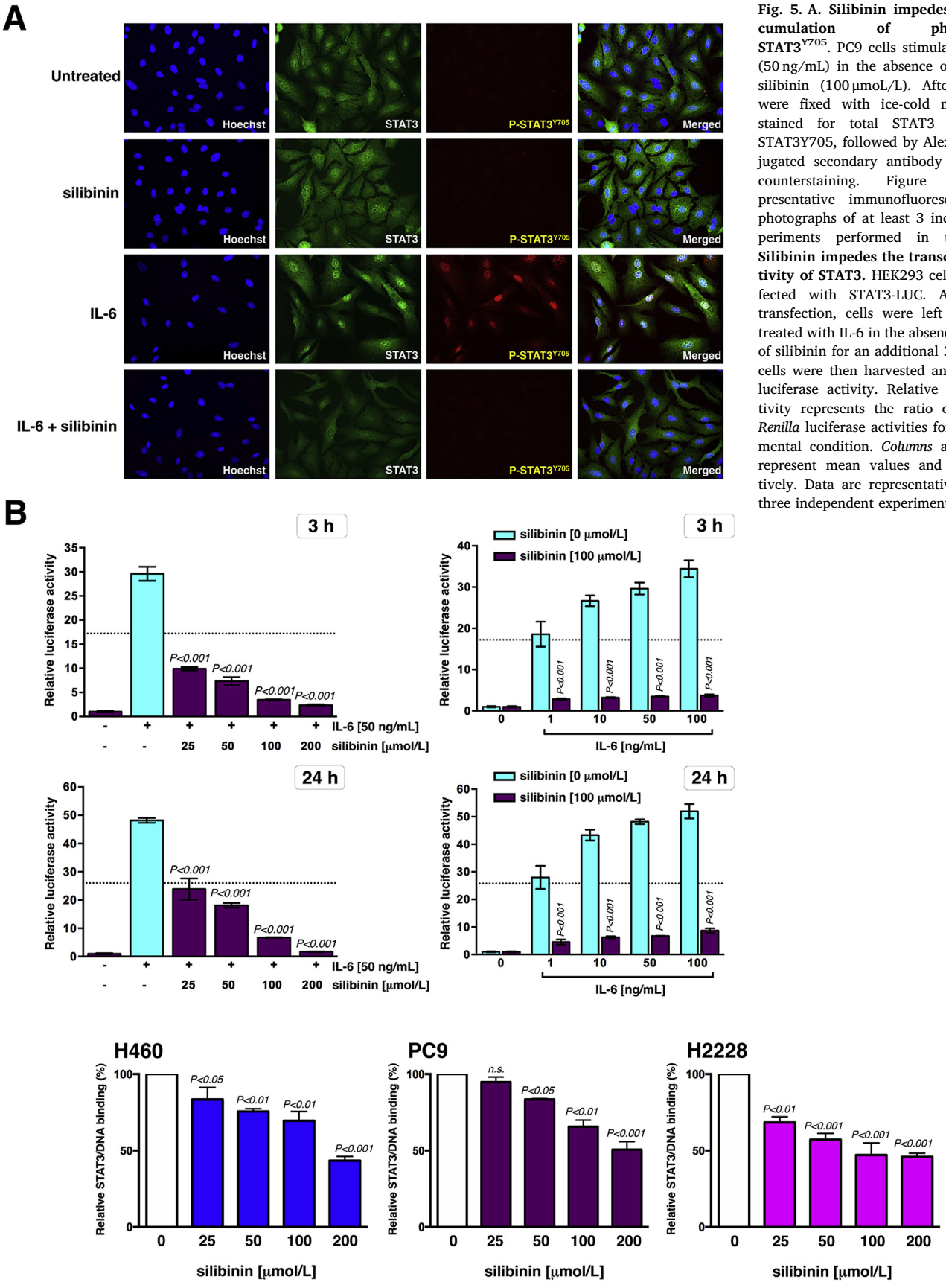

Fig. 5. A. Silibinin impedes nuclear accumulation of phospho-active STAT3^{Y705}. PC9 cells stimulated with IL-6 (50 ng/mL) in the absence or presence of silibinin (100 μmoL/L). After 24 h, cells were fixed with ice-cold methanol and stained for total STAT3 or phospho-STAT3Y705, followed by Alexa Fluor®-conjugated secondary antibody and Hoechst counterstaining. Figure shows representative immunofluorescence microphotographs of at least 3 independent experiments performed in triplicate. **B. Silibinin impedes the transcriptional activity of STAT3.** HEK293 cells were transfected with STAT3-LUC. At 24 h after transfection, cells were left untreated or treated with IL-6 in the absence or presence of silibinin for an additional 3 or 24 h. The cells were then harvested and assayed for luciferase activity. Relative luciferase activity represents the ratio of *Firefly* and *Renilla* luciferase activities for each experimental condition. *Columns* and *error bars* represent mean values and S.D., respectively. Data are representative of at least three independent experiments.

Fig. 6. Silibinin inhibits the DNA-binding activity of STAT3. The nuclear extracts from cells stimulated with IL-6 for 3 h were subjected to TransAM™ assays in microtitre wells coated with the STAT3 consensus sequence in the absence or presence of graded concentrations of silibinin for 3 h (see Supplementary Fig. S1C for schematic description of details concerning TransAM™ assays). *Columns* and *error bars* represent mean values and S.D., respectively. Data are representative of at least three independent experiments.

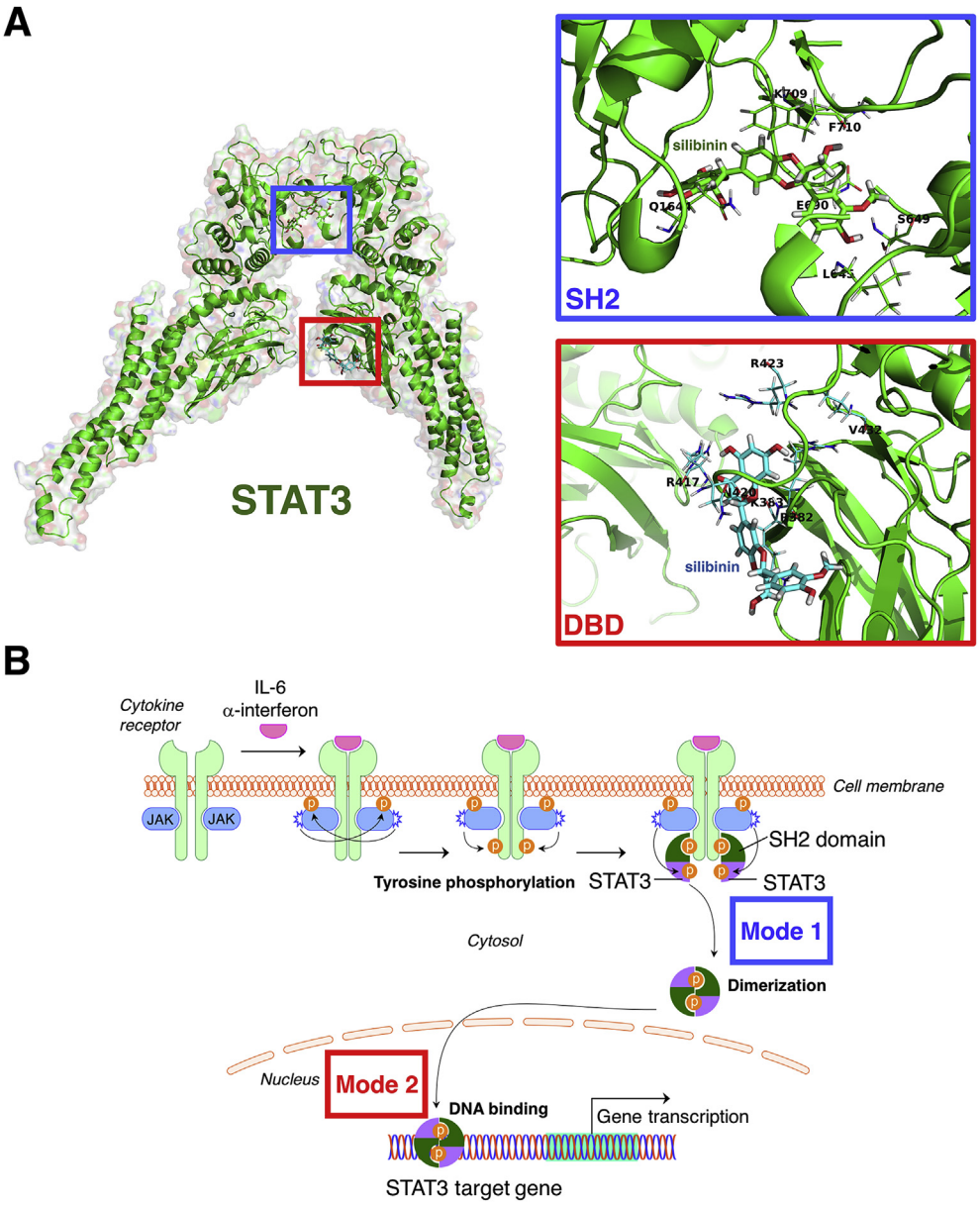

Fig. 7. Silibinin is a bimodal SH2- and DBD-targeted STAT3i. A. Global view of the STAT3 homodimer structure containing DNA (human homology model 2) and location of silibinin at the SH2 activation/dimerization and DNA-binding domains. **B.** Silibinin targeting of the SH2 domain of STAT3 monomers might prevent binding of STAT3 to activated cell surface receptors but also block dimerization (and subsequent trans-phosphorylation) of STAT3 molecules in the cytosol, thereby impeding nuclear accumulation of phospho-active STAT3. Silibinin additionally establishes direct interactions with DNA in its direct targeting of the DBD of STAT3, resulting in a significant inhibitory effect on STAT3-DNA binding. The bimodal SH2- and DBD-targeted behavior of silibinin might explain the proven therapeutic activity of silibinin in areas of unmet clinical need such as STAT3-dependent lung cancer and melanoma brain metastasis.

DNA binding ability and STAT3 transactivation activity. We now report that silibinin appears to work synergistically on STAT3 function through a bimodal mechanism of action involving blockade of the function of the STAT3 SH2 domain, which is crucial for both STAT3 activation and nuclear translocation, and of STAT3 transcriptional activity, which might involve not only disruption of STAT3 dimerization, but also a direct inhibition of the ability of STAT3 to bind DNA (Fig. 7A).

The STAT3 inhibitory activity of silibinin was not influenced by the pre-existing phosphorylation status of STAT3, as significant inhibitory effects were observed in cells with inducible, constitutive, and acquired phosphorylation at the Y705 site. LanthaScreen™-based cellular profiling assays revealed that silibinin attenuates the induced phospho-activation of Y705 in GFP-STAT3 genetic fusions without drastically altering the *in vitro* kinase activity of the STAT3 upstream kinases JAK1 and JAK2. Although these findings are consistent with the notion that silibinin exerts its pY705 STAT3 inhibitory effects by directly preventing the activating kinases from binding to the STAT3 SH2 domain, we acknowledge that further experimentation testing the direct effects of silibinin against other up-stream STAT3 kinases (e.g., SRC, ABL) and non-canonical STAT3 activators is needed before unambiguously concluding that silibinin exclusively operates as a direct STAT3i.

When we modeled the atomic details for the silibinin-driven inhibition of the activating phosphorylation Y705 on the SH2 domain, our first-in-class computational homology model of the human STAT3 protein allowing comparative docking and molecular dynamics simulation studies over fourteen different STAT3i, predicted that silibinin should molecularly behave as a direct STAT3i capable of establishing high-affinity interactions with the SH2 domain of STAT3. Using the binding site of the direct STAT3i OPB-31121, for which we dispose of detailed structural information explaining its inhibitory activity on the STAT3 SH2 domain (Brambilla et al., 2015), one could visualize the predicted ability of silibinin to interact with up to 60% of all the residues involved in the binding mode of a wide variety of structurally diverse STAT3i (Fig. 7A). The predicted ability of silibinin to bind the SH2 activation/dimerization domain therefore appears to rely on its capacity to overlap with the same cavity occupied by the majority of direct STAT3i to indirectly prevent Y705 phosphorylation in the monomeric SH2 domain of STAT3, but showing a unique binding mode.

Silibinin treatment is known to diminish nuclear DNA binding of

constitutively active STAT3 homodimers (Agarwal et al., 2007). Because Y705 phosphorylation is required for STAT3 to bind to specific DNA target sites but nuclear import of STAT3 takes place constitutively and independently of tyrosine phosphorylation (Liu et al., 2005; Reich and Liu, 2006), we employed immunofluorescence microscopy to visualize whether the *in silico* predicted ability of silibinin to operate as a direct STAT3i of the SH2 activation/dimerization domain translated into an altered intracellular localization of STAT3/phospho-active STAT3 *in cellulo*. The ability of silibinin to prevent the nuclear concentration of unphosphorylated STAT3 and Y705-phosphorylated STAT3 in response to IL-6 stimulation occurred without apparent accumulation of STAT3 in the cytoplasmic compartment. Although further work is needed to unambiguously exclude any indirect effect of silibinin in the importins-driven STAT3 trafficking to the nucleus (Liu et al., 2005; Cimica et al., 2011), our findings are compatible with a mechanism of action involving direct targeting of silibinin to the SH2 domain of STAT3 monomers, capable of preventing not only binding of STAT3 to activated cell surface receptors, but also to block dimerization (and subsequent trans-phosphorylation) of STAT3 molecules in the cytosol, thereby impeding nuclear accumulation of phospho-active STAT3.

To further evaluate the physiological role of silibinin on STAT3-mediated transactivation, we examined whether silibinin-driven changes in the sub-cellular accumulation of STAT3 correlated with changes in its transcriptional regulatory activity. Silibinin treatment was found to elicit the complete suppression of the IL-6-stimulated STAT3 transcriptional activity in living cells and, remarkably, such strong capability of silibinin to block STAT3-driven luciferase expression was evident even at concentrations that failed to completely shutdown the activating phosphorylation Y705 at the SH2 dimerization domain. Moreover, although *in vitro* experiments based on the detection of an STAT3 epitope that is accessible only when STAT3 is activated and bound to its DNA consensus binding site confirmed the *in silico* prediction of the capacity of silibinin to establish direct interactions with DNA in its targeting to the DBD of STAT3, once again the STAT3 DNA-binding inhibitory activity of silibinin took place at significantly higher concentrations than those needed to inhibit STAT3-driven transcriptional activity. Because parallel immunoblotting experiments with IL-6-stimulated nuclear extracts showed that silibinin can block the binding of activated STAT3 to its consensus DNA sequence in isolated nuclear extracts without altering the phosphorylation status of Y705 (data not shown), these findings altogether suggest that the ability of silibinin to inhibit STAT3-directed transcription in living cells does not rely exclusively on the SH2 domain-related inhibition of STAT3 dimerization in the cytosol, but also involves direct inhibition of STAT3 via binding to the DBD regardless of the STAT3 dimerization status. Nevertheless, the unique behavior of silibinin as a bimodal SH2- and DBD-STAT3i that strongly disrupts STAT3 transcriptional activity is definitively supported by the fact that cells engineered to overexpress a constitutively active form of STAT3 (Bromberg et al., 1999), which dimerizes spontaneously, binds to DNA and activates transcription, remain largely unresponsive to the inhibitory effects of silibinin in key transcriptional targets of STAT3 (Shukla et al., 2015; Priego et al., 2018). The so-called STAT3C mutant, in which the SH2 domain A661 and N663 residues are substituted with cysteine residues allowing a disulfide bond to form between two unphosphorylated STAT3 monomers, still requires Y705 phosphorylation for functional activation via promotion of maximal DNA binding affinity, slower off-rate, and protection from inactivation from phosphatases, resulting in the accumulation of transcriptionally active STAT3 dimer complexes (Liddle et al., 2006). We recently reported that the decreased ability of silibinin to bind the STAT3C mutant translates into refractoriness of STAT3C-expressing cells to silibinin (Priego et al., 2018), demonstrating the STAT3-dependency on the phenotypic effects of silibinin.

Beyond common issues in the development of other anti-cancer drug families such as rapid degradation, lack of cell penetrance or lack of binding specificity, the observation that inhibition of active STAT3 dimers alone via targeting to the SH2 domain may not be sufficient in efficaciously preventing STAT3 activity (Huang et al., 2016) together with the preliminary support to the notion that targeting the DBD may prove more efficient in abrogating STAT3 activity than targeting the SH2 domain in cellular systems (Furtek et al., 2016b), can largely explain why the majority of direct STAT3i have yet to enter clinical evaluation. We have recently reported that silibinin-driven STAT3 blocking translates into proven therapeutic activity in areas of unmet clinical need such as lung cancer and melanoma brain metastasis, which portend a poor prognosis and have few therapeutic options (Bosch-Barrera et al., 2016; Priego et al., 2018). We now report the unique characteristics of silibinin as a promising lead of a new generation of bimodal SH2- and DBD-targeting STAT3i (Fig. 7B) that may transform the clinical management of secondary brain tumors.

5. Conclusion

To the best of our knowledge, this is the first report establishing that the flavonolignan silibinin is a novel direct STAT3i. Our systematic approach performed at multiple levels of integration including *in vitro*, *in silico* computational modeling, and *in cellulo* experimentation, demonstrates that: a.) silibinin could directly bind the SH2 domain of STAT3 to prevent Y705 phosphorylation-related STAT3 activation and dimerization; b.) silibinin could establish direct interactions with DNA in its targeting to the STAT3 DNA-binding domain (DBD); and c.) silibinin impedes the activation, dimerization, nuclear translocation, DNA-binding, and transcriptional activity of STAT3. Our findings showing the unique features and putative direct modes of action of silibinin against STAT3 will be highly relevant for further development and design of new, more effective silibinin-based STAT3i.

Conflicts of interest

L.L-P, A. N-C, and M. S-M are employees of Mind the Byte S.L. All other authors have no competing interests to declare.

Acknowledgments

This work was supported by grants from the Ministerio de Ciencia e Innovación (Grant SAF2016-80639-P to J. A. Menendez), Plan Nacional de I + D + I, Spain, and the Agència de Gestió d'Ajuts Universitaris i de Recerca (AGAUR) (Grant 2014 SGR229 to J. A. Menendez). This study was supported also by unrestricted research grants from Roche Pharma (Spain) and Astellas Pharma (Spain) to the Program Against Cancer Therapeutic Resistance (ProCURE, Catalan Institute of Oncology). Joaquim Bosch-Barrera is supported by SEOM, Pfizer (Grant WI190764), Boehringer Ingelheim, Meda Pharma, and Pla strategic de recerca i innovació en salut 2016–2020 de la Generalitat de Catalunya (SLT006/17/114). Elisabet Cuyàs is supported by a Sara Borrell post-doctoral contract (CD15/00033) from the Ministerio de Sanidad y Consumo, Fondo de Investigación Sanitaria (FIS), Spain. The authors would like to thank Dr. Kenneth McCreath for editorial support.

Appendix A. Supplementary data

Supplementary data related to this article can be found at http://dx.doi.org/10.1016/j.fct.2018.04.028.

Transparency document

Transparency document related to this article can be found online at http://dx.doi.org/10.1016/j.fct.2018.04.028.

References

Agarwal, C., Tyagi, A., Kaur, M., Agarwal, R., 2007. Silibinin inhibits constitutive activation of Stat3, and causes caspase activation and apoptotic death of human prostate carcinoma DU145 cells. Carcinogenesis 28, 1463–1470. https://doi.org/10.1093/carcin/bgm042.

Agarwal, R., Agarwal, C., Ichikawa, H., Singh, R.P., Aggarwal, B.B., 2006. Anticancer potential of silymarin: from bench to bed side. Anticancer Res. 26, 4457–4498.

Ali, A.M., Gómez-Biagi, R.F., Rosa, D.A., Lai, P.-S., Heaton, W.L., Park, J.S., Eiring, A.M., Vellore, N.A., de Araujo, E.D., Ball, D.P., Shouksmith, A.E., Patel, A.B., Deininger, M.W., O'Hare, T., Gunning, P.T., 2016. Disarming an electrophilic warhead: retaining potency in tyrosine kinase inhibitor (TKI)-Resistant CML lines while circumventing pharmacokinetic liabilities. ChemMedChem 11, 850–861. https://doi.org/10.1002/cmdc.201600021.

Becker, S., Groner, B., Muller, C.W., 1998. Three-dimensional structure of the Stat3beta homodimer bound to DNA. Nature 394, 145–151. https://doi.org/10.1038/28101.

Bosch-Barrera, J., Corominas-Faja, B., Cuyàs, E., Martin-Castillo, B., Brunet, J., Menendez, J.A., 2014. Silibinin administration improves hepatic failure due to extensive liver infiltration in a breast cancer patient. Anticancer Res. 34, 4323–4328.

Bosch-Barrera, J., Menendez, J.A., 2015. Silibinin and STAT3: a natural way of targeting transcription factors for cancer therapy. Canc. Treat Rev. 41, 540–546. https://doi.org/10.1016/j.ctrv.2015.04.008.

Bosch-Barrera, J., Queralt, B., Menendez, J.A., 2017. Targeting STAT3 with silibinin to improve cancer therapeutics. Canc. Treat Rev. 58, 61–69. https://doi.org/10.1016/j.ctrv.2017.06.003.

Bosch-Barrera, J., Sais, E., Cañete, N., Marruecos, J., Cuyàs, E., Izquierdo, A., Porta, R., Haro, M., Brunet, J., Pedraza, S., Menendez, J.A., 2016. Response of brain metastasis from lung cancer patients to an oral nutraceutical product containing silibinin. Oncotarget 7, 32006–32014. https://doi.org/10.18632/oncotarget.7900.

Brambilla, L., Genini, D., Laurini, E., Merulla, J., Perez, L., Fermeglia, M., Carbone, G.M., Pricl, S., Catapano, C.V., 2015. Hitting the right spot: mechanism of action of OPB-31121, a novel and potent inhibitor of the Signal Transducer and Activator of Transcription 3 (STAT3). Mol. Oncol 9, 1194–1206. https://doi.org/10.1016/j.molonc.2015.02.012.

Bromberg, J.F., Wrzeszczynska, M.H., Devgan, G., Zhao, Y., Pestell, R.G., Albanese, C., Darnell, J.E., 1999. Stat3 as an oncogene. Cell 98, 295–303. https://doi.org/10.1016/S0092-8674(00)81959-5.

Chang, Q., Bournazou, E., Sansone, P., Berishaj, M., Gao, S.P., Daly, L., Wels, J., Theilen, T., Granitto, S., Zhang, X., Cotari, J., Alpaugh, M.L., de Stanchina, E., Manova, K., Li, M., Bonafe, M., Ceccarelli, C., Taffurelli, M., Santini, D., Altan-Bonnet, G., Kaplan, R., Norton, L., Nishimoto, N., Huszar, D., Lyden, D., Bromberg, J., 2013. The IL-6/JAK/Stat3 feed-forward loop drives tumorigenesis and metastasis. Neoplasia 15, 848–862.

Chen, Y., Wang, J., Wang, X., Liu, X., Li, H., Lv, Q., Zhu, J., Wei, B., Tang, Y., 2013. STAT3, a poor survival predicator, Is associated with lymph node metastasis from breast cancer. J. Breast Cancer 16, 40–49. https://doi.org/10.4048/jbc.2013.16.1.40.

Chittezhath, M., Deep, G., Singh, R.P., Agarwal, C., Agarwal, R., 2008. Silibinin inhibits cytokine-induced signaling cascades and down-regulates inducible nitric oxide synthase in human lung carcinoma A549 cells. Mol. Canc. Therapeut. 7, 1817–1826. https://doi.org/10.1158/1535-7163.MCT-08-0256.

Cimica, V., Chen, H.-C., Iyer, J.K., Reich, N.C., 2011. Dynamics of the STAT3 transcription factor: nuclear import dependent on Ran and importin-β1. PLoS One 6, e20188. https://doi.org/10.1371/journal.pone.0020188.

Cufí, S., Bonavia, R., Vazquez-Martin, A., Corominas-Faja, B., Oliveras-Ferraros, C., Cuyàs, E., Martin-Castillo, B., Barrajón-Catalán, E., Visa, J., Segura-Carretero, A., Bosch-Barrera, J., Joven, J., Micol, V., Menendez, J.A., 2013a. Silibinin meglumine, a water-soluble form of milk thistle silymarin, is an orally active anti-cancer agent that impedes the epithelial-to-mesenchymal transition (EMT) in EGFR-mutant non-small-cell lung carcinoma cells. Food Chem. Toxicol. 60, 360–368. https://doi.org/10.1016/j.fct.2013.07.063.

Cufí, S., Bonavia, R., Vazquez-Martin, A., Oliveras-Ferraros, C., Corominas-Faja, B., Cuyàs, E., Martin-Castillo, B., Barrajón-Catalán, E., Visa, J., Segura-Carretero, A., Joven, J., Bosch-Barrera, J., Micol, V., Menendez, J.A., 2013b. Silibinin suppresses EMT-driven erlotinib resistance by reversing the high miR-21/low miR-200c signature in vivo. Sci. Rep. 3, 2459. https://doi.org/10.1038/srep02459.

Cuyàs, E., Pérez-Sánchez, A., Micol, V., Menendez, J.A., Bosch-Barrera, J., 2016. STAT3-targeted treatment with silibinin overcomes the acquired resistance to crizotinib in ALK-rearranged lung cancer. Cell Cycle 1–6. https://doi.org/10.1080/15384101.2016.1245249.

Eiring, A.M., Page, B.D.G., Kraft, I.L., Mason, C.C., Vellore, N.A., Resetca, D., Zabriskie, M.S., Zhang, T.Y., Khorashad, J.S., Engar, A.J., Reynolds, K.R., Anderson, D.J., Senina, A., Pomicter, A.D., Arpin, C.C., Ahmad, S., Heaton, W.L., Tantravahi, S.K., Todic, A., Colaguori, R., Moriggl, R., Wilson, D.J., Baron, R., O'Hare, T., Gunning, P.T., Deininger, M.W., 2015. Combined STAT3 and BCR-ABL1 inhibition induces synthetic lethality in therapy-resistant chronic myeloid leukemia. Leukemia 29, 586–597. https://doi.org/10.1038/leu.2014.245.

Fagard, R., Metelev, V., Souissi, I., Baran-Marszak, F., 2013. STAT3 inhibitors for cancer therapy: have all roads been explored? JAK-STAT 2, e22882. https://doi.org/10.4161/jkst.22882.

Flaig, T.W., Glodé, M., Gustafson, D., Van Bokhoven, A., Tao, Y., Wilson, S., Su, L.J., Li, Y., Harrison, G., Agarwal, R., Crawford, E.D., Lucia, M.S., Pollak, M., 2010. A study of high-dose oral silybin-phytosome followed by prostatectomy in patients with localized prostate cancer. Prostate 70, 848–855. https://doi.org/10.1002/pros.21118.

Furqan, M., Akinleye, A., Mukhi, N., Mittal, V., Chen, Y., Liu, D., 2013. STAT inhibitors for cancer therapy. J. Hematol. Oncol. 6, 90. https://doi.org/10.1186/1756-8722-6-90.

Furtek, S.L., Backos, D.S., Matheson, C.J., Reigan, P., 2016a. Strategies and approaches of targeting STAT3 for cancer treatment. ACS Chem. Biol. 11, 308–318. https://doi.org/10.1021/acschembio.5b00945.

Furtek, S.L., Matheson, C.J., Backos, D.S., Reigan, P., 2016b. Evaluation of quantitative assays for the identification of direct signal transducer and activator of transcription 3 (STAT3) inhibitors. Oncotarget 7, 77998–78008. https://doi.org/10.18632/oncotarget.12868.

Gažák, R., Walterová, D., Křen, V., 2007. Silybin and silymarin–new and emerging applications in medicine. Curr. Med. Chem. 14, 315–338. https://doi.org/10.2174/092986707779941159.

Hoh, C., Boocock, D., Marczylo, T., Singh, R., Berry, D.P., Dennison, A.R., Hemingway, D., Miller, A., West, K., Euden, S., Garcea, G., Farmer, P.B., Steward, W.P., Gescher, A.J., 2006. Pilot study of oral silibinin, a putative chemopreventive agent, in colorectal cancer patients: silibinin levels in plasma, colorectum, and liver and their pharmacodynamic consequences. Clin. Canc. Res. 12, 2944–2950. https://doi.org/10.1158/1078-0432.CCR-05-2724.

Huang, W., Dong, Z., Chen, Y., Wang, F., Wang, C.J., Peng, H., He, Y., Hangoc, G., Pollok, K., Sandusky, G., Fu, X.-Y., Broxmeyer, H.E., Zhang, Z.-Y., Liu, J.-Y., Zhang, J.-T., 2016. Small-molecule inhibitors targeting the DNA-binding domain of STAT3 suppress tumor growth, metastasis and STAT3 target gene expression in vivo. Oncogene 35, 783–792. https://doi.org/10.1038/onc.2015.215.

Jin, Y., Kim, Y., Lee, Y.-J., Han, D.C., K.B, M., 2016. Natural products targeting STAT3 signaling pathways in cancer cells. Biodesign 4, 1–17.

Kroon, P., Berry, P.A., Stower, M.J., Rodrigues, G., Mann, V.M., Simms, M., Bhasin, D., Chettiar, S., Li, C., Li, P.K., Maitland, N.J., Collins, A.T., 2013. JAK-STAT blockade inhibits tumor initiation and clonogenic recovery of prostate cancer stem-like cells. Canc. Res. 73, 5288–5298. https://doi.org/10.1158/0008-5472.CAN-13-0874.

Lai, P.-S., Rosa, D.A., Magdy Ali, A., Gómez-Biagi, R.F., Ball, D.P., Shouksmith, A.E., Gunning, P.T., 2015. A STAT inhibitor patent review: progress since 2011. Expert Opin. Ther. Pat. 25, 1397–1421. https://doi.org/10.1517/13543776.2015.1086749.

Lee, H.-J., Zhuang, G., Cao, Y., Du, P., Kim, H.-J., Settleman, J., 2014. Drug resistance via feedback activation of Stat3 in oncogene-addicted cancer cells. Canc. Cell 26, 207–221. https://doi.org/10.1016/j.ccr.2014.05.019.

Liddle, F.J., Alvarez, J.V., Poli, V., Frank, D.A., 2006. Tyrosine phosphorylation is required for functional activation of disulfide-containing constitutively active STAT mutants. Biochemistry 45, 5599–5605. https://doi.org/10.1021/bi0525674.

Lin, L., Hutzen, B., Li, P.-K., Ball, S., Zuo, M., DeAngelis, S., Foust, E., Sobo, M., Friedman, L., Bhasin, D., Cen, L., Li, C., Lin, J., 2010. A novel small molecule, LLL12, inhibits STAT3 phosphorylation and activities and exhibits potent growth-suppressive activity in human cancer cells. Neoplasia 12, 39–50.

Liu, L., McBride, K.M., Reich, N.C., 2005. STAT3 nuclear import is independent of tyrosine phosphorylation and mediated by importin- 3. Proc. Natl. Acad. Sci. Unit. States Am. 102, 8150–8155. https://doi.org/10.1073/pnas.0501643102.

Liu, X., He, Z., Li, C.-H., Huang, G., Ding, C., Liu, H., 2012. Correlation analysis of JAK-STAT pathway components on prognosis of patients with prostate cancer. Pathol. Oncol. Res. 18, 17–23. https://doi.org/10.1007/s12253-011-9410-y.

Mao, X., Ren, Z., Parker, G.N., Sondermann, H., Pastorello, M.A., Wang, W., McMurray, J.S., Demeler, B., Darnell, J.E., Chen, X., 2005. Structural bases of unphosphorylated STAT1 association and receptor binding. Mol. Cell 17, 761–771. https://doi.org/10.1016/j.molcel.2005.02.021.

Matsuno, K., Masuda, Y., Uehara, Y., Sato, H., Muroya, A., Takahashi, O., Yokotagawa, T., Furuya, T., Okawara, T., Otsuka, M., Ogo, N., Ashizawa, T., Oshita, C., Tai, S., Ishii, H., Akiyama, Y., Asai, A., 2010. Identification of a new series of STAT3 inhibitors by virtual screening. ACS Med. Chem. Lett. 1, 371–375. https://doi.org/10.1021/ml1000273.

Miklossy, G., Hilliard, T.S., Turkson, J., 2013. Therapeutic modulators of STAT signalling for human diseases. Nat. Rev. Drug Discov. 12, 611–629. https://doi.org/10.1038/nrd4088.

Misra, S.K., De, A., Pan, D., 2018. Targeted delivery of STAT-3 modulator to breast cancer stem-like cells downregulates a series of stemness genes. Mol. Canc. Therapeut. 17, 119–129. https://doi.org/10.1158/1535-7163.MCT-17-0070.

Nan, J., Du, Y., Chen, X., Bai, Q., Wang, Y., Zhang, X., Zhu, N., Zhang, J., Hou, J., Wang, Q., Yang, J., 2014. TPCA-1 is a direct dual inhibitor of STAT3 and NF-κb and regresses mutant EGFR-associated human non-small cell lung cancers. Mol. Canc. Therapeut. 13, 617–629. https://doi.org/10.1158/1535-7163.MCT-13-0464.

Nkansah, E., Shah, R., Collie, G.W., Parkinson, G.N., Palmer, J., Rahman, K.M., Bui, T.T., Drake, A.F., Husby, J., Neidle, S., Zinzalla, G., Thurston, D.E., Wilderspin, A.F., 2013. Observation of unphosphorylated STAT3 core protein binding to target dsDNA by PEMSA and X-ray crystallography. FEBS Lett. 587, 833–839. https://doi.org/10.1016/j.febslet.2013.01.065.

Poli, V., Camporeale, A., 2015. STAT3-Mediated metabolic reprograming in cellular transformation and implications for drug resistance. Front. Oncol 5 (121). https://doi.org/10.3389/fonc.2015.00121.

Priego, N., Zhu, L., Monteiro, C., Mulders, M., Wasilewski, D., Bindeman, W., Doglio, L., Martínez, L., Martínez-Saez, E., Ramón y Cajal, S., Megías, D., Hernández-Encinas, E., Blanco-Aparicio, C., Martínez, L., Zarzuela, E., Muñoz, J., Fustero-Torres, C., Pineiro, E., Hernández-Laín, A., Bertero, L., Poli, V., Sánchez-Martínez, M., Menendez, J.A., Soffietti, R., Bosch-Barrera, J., Valiente, V., 2018. STAT3 labels a subpopulation of reactive astrocytes required for brain metastasis. Nat. Med (in press).

Rath, K.S., Naidu, S.K., Lata, P., Bid, H.K., Rivera, B.K., McCann, G.A., Tierney, B.J., ElNaggar, A.C., Bravo, V., Leone, G., Houghton, P., Hideg, K., Kuppusamy, P., Cohn, D.E., Selvendiran, K., 2014. HO-3867, a safe STAT3 inhibitor, is selectively cytotoxic to ovarian cancer. Canc. Res. 74, 2316–2327. https://doi.org/10.1158/0008-5472.CAN-13-2433.

Reich, N.C., Liu, L., 2006. Tracking STAT nuclear traffic. Nat. Rev. Immunol. 6, 602–612.

https://doi.org/10.1038/nri1885.
Ren, Z., Mao, X., Mertens, C., Krishnaraj, R., Qin, J., Mandal, P.K., Romanowski, M.J., McMurray, J.S., Chen, X., 2008. Crystal structure of unphosphorylated STAT3 core fragment. Biochem. Biophys. Res. Commun. 374, 1–5. https://doi.org/10.1016/j.bbrc.2008.04.049.
Sansone, P., Bromberg, J., 2012. Targeting the interleukin-6/jak/stat pathway in human malignancies. J. Clin. Oncol. 30, 1005–1014. https://doi.org/10.1200/JCO.2010.31.8907.
Schroeder, A., Herrmann, A., Cherryholmes, G., Kowolik, C., Buettner, R., Pal, S., Yu, H., Müller-Newen, G., Jove, R., 2014. Loss of androgen receptor expression promotes a stem-like cell phenotype in prostate cancer through STAT3 signaling. Canc. Res. 74, 1227–1237. https://doi.org/10.1158/0008-5472.CAN-13-0594.
Schust, J., Sperl, B., Hollis, A., Mayer, T.U., Berg, T., 2006. Stattic: a small-molecule inhibitor of STAT3 activation and dimerization. Chem. Biol. 13, 1235–1242. https://doi.org/10.1016/j.chembiol.2006.09.018.
Shahani, V.M., Yue, P., Fletcher, S., Sharmeen, S., Sukhai, M.A., Luu, D.P., Zhang, X., Sun, H., Zhao, W., Schimmer, A.D., Turkson, J., Gunning, P.T., 2011. Design, synthesis, and in vitro characterization of novel hybrid peptidomimetic inhibitors of STAT3 protein. Bioorg. Med. Chem. 19, 1823–1838. https://doi.org/10.1016/j.bmc.2010.12.010.
Shukla, S.K., Dasgupta, A., Mehla, K., Gunda, V., Vernucci, E., Souchek, J., Goode, G., King, R., Mishra, A., Rai, I., Nagarajan, S., Chaika, N.V., Yu, F., Singh, P.K., 2015. Silibinin-mediated metabolic reprogramming attenuates pancreatic cancer-induced cachexia and tumor growth. Oncotarget 6, 41146–41161. https://doi.org/10.18632/oncotarget.5843.
Siegel, A.B., Narayan, R., Rodriguez, R., Goyal, A., Jacobson, J.S., Kelly, K., Ladas, E., Lunghofer, P.J., Hansen, R.J., Gustafson, D.L., Flaig, T.W., Yann Tsai, W., Wu, D.P.H., Lee, V., Greenlee, H., 2014. A phase I dose-finding study of silybin phosphatidylcholine (milk thistle) in patients with advanced hepatocellular carcinoma. Integr. Canc. Ther. 13, 46–53. https://doi.org/10.1177/1534735413490798.
Singh, R.P., Raina, K., Deep, G., Chan, D., Agarwal, R., 2009. Silibinin suppresses growth of human prostate carcinoma PC-3 orthotopic xenograft via activation of extracellular signal-regulated kinase 1/2 and inhibition of signal transducers and activators of transcription signaling. Clin. Canc. Res. 15, 613–621. https://doi.org/10.1158/1078-0432.CCR-08-1846.
Siveen, K.S., Sikka, S., Surana, R., Dai, X., Zhang, J., Kumar, A.P., Tan, B.K.H., Sethi, G., Bishayee, A., 2014. Targeting the STAT3 signaling pathway in cancer: role of synthetic and natural inhibitors. Biochim. Biophys. Acta Rev. Canc 1845, 136–154. https://doi.org/10.1016/j.bbcan.2013.12.005.
Tan, F.H., Putoczki, T.L., Stylli, S.S., Luwor, R.B., 2014. The role of STAT3 signaling in mediating tumor resistance to cancer therapy. Curr. Drug Targets 15, 1341–1353. https://doi.org/10.2174/1389450115666141120104146.
Timofeeva, O.A., Chasovskikh, S., Lonskaya, I., Tarasova, N.I., Khavrutskii, L., Tarasov, S.G., Zhang, X., Korostyshevskiy, V.R., Cheema, A., Zhang, L., Dakshanamurthy, S., Brown, M.L., Dritschilo, A., 2012. Mechanisms of unphosphorylated STAT3 transcription factor binding to DNA. J. Biol. Chem. 287, 14192–14200. https://doi.org/10.1074/jbc.M111.323899.
Tong, M., Wang, J., Jiang, N., Pan, H., Li, D., 2017. Correlation between p-STAT3 overexpression and prognosis in lung cancer: a systematic review and meta-analysis. PLoS One 12. https://doi.org/10.1371/journal.pone.0182282.
Wang, T., Fahrmann, J.F., Lee, H., Li, Y.-J., Tripathi, S.C., Yue, C., Zhang, C., Lifshitz, V., Song, J., Yuan, Y., Somlo, G., Jandial, R., Ann, D., Hanash, S., Jove, R., Yu, H., 2018. JAK/STAT3-Regulated fatty acid β-oxidation is critical for breast cancer stem cell self-renewal and chemoresistance. Cell Metabol. 27, 136–150. e5. https://doi.org/10.1016/j.cmet.2017.11.001.
Wu, P., Wu, D., Zhao, L., Huang, L., Shen, G., Huang, J., Chai, Y., 2016. Prognostic role of STAT3 in solid tumors: a systematic review and meta-analysis. Oncotarget 7, 19863–19883. https://doi.org/ https://doi.org/10.18632/oncotarget.7887.
Yu, H., Lee, H., Herrmann, A., Buettner, R., Jove, R., 2014. Revisiting STAT3 signalling in cancer: new and unexpected biological functions. Nat. Rev. Canc. 14, 736–746. https://doi.org/10.1038/nrc3818.
Yu, H., Pardoll, D., Jove, R., 2009. STATs in cancer inflammation and immunity: a leading role for STAT3. Nat. Rev. Canc. 9, 798–809. https://doi.org/10.1038/nrc2734.
Yue, P., Turkson, J., 2009. Targeting STAT3 in cancer: how successful are we? Expert Opin. Investig. Drugs 18, 45–56. https://doi.org/10.1517/13543780802565791.
Zhang, X., Sun, Y., Pireddu, R., Yang, H., Urlam, M.K., Lawrence, H.R., Guida, W.C., Lawrence, N.J., Sebti, S.M., 2013. A novel inhibitor of STAT3 homodimerization selectively suppresses STAT3 activity and malignant transformation. Canc. Res. 73, 1922–1933. https://doi.org/10.1158/0008-5472.CAN-12-3175.
Zhao, C., Li, H., Lin, H.J., Yang, S., Lin, J., Liang, G., 2016. Feedback activation of STAT3 as a cancer drug-resistance mechanism. Trends Pharmacol. Sci. 37, 47–61. https://doi.org/10.1016/j.tips.2015.10.001.

V. DISCUSSION

Chapter 1. Silibinin and molecular drivers of brain metastasis-initiating cells: Inhibitor of DNA-binding/differentiation 3 (ID3)

Pathogenic roles of ID transcription factors in cancer. The Inhibitors of DNA Binding / Differentiation (ID) proteins, specifically ID1 to ID4, are key transcriptional regulators in controlling cell differentiation. These proteins inhibit the DNA binding capacity of basic helix-loop-helix (bHLH) transcription factors, which are essential for cell fate determination. Their action maintains the self-renewal and multipotency of stem and progenitor cells during development by aligning cell fate determination with extracellular interactions within the cellular microenvironment. ID protein expression is typically low in most adult tissues. However, it can be reactivated in a variety of diseases, including cancer (Norton, 2000; Sikder et al., 2003).

ID proteins are expressed at high levels in nearly all human tumors. Their presence is associated with an aggressive cancer phenotype and poor clinical outcome (Lasorella et al., 2014; Perk et al., 2005). They have been implicated in conferring tumor-initiating properties and resistance to chemotherapy and radiotherapy, particularly in cancer stem cell-like populations during the early stages of tumor growth and metastasis (Cells et al., 2012; Huang, 2007). In addition, ID proteins can modulate the tumor microenvironment by promoting the activation and recruitment of endothelial cells to support tumor angiogenesis at both primary and metastatic sites. This effect is also associated with an increase in endothelial cell "stemness", which may facilitate transmigration of cancer cells across the BBB and reorganization of the brain vasculature, facilitating brain metastasis (Das & Felty, 2014; Jayanta K Das, 2022).

ID3: An untargeted transcription factor for the prevention or treatment of metastasis initiation. Disrupting the regulatory roles of ID proteins in cancer cells could have potential anti-metastatic benefits. However, direct targeting of ID proteins with small molecule inhibitors is notoriously difficult. Challenges include the paucity of mutations or genomic rearrangements in *ID* genes in most cancers, the complex nature of ID protein-containing transcription complexes, and the convergence of multiple signaling pathways on *ID* gene promoters. Some progress has been made with systemic targeting using siRNA/anti-sense

oligonucleotides and peptides that promote ID protein degradation. In particular, a pan-ID antagonist, AGX51, has mimicked the effects of *ID1* and *ID3* gene loss in preclinical models, reducing resistant tumor growth and metastasis. The bone morphogenic protein (BMP) signaling pathway, a key regulator of ID expression, has emerged as a potential therapeutic option to target ID1/3 expression, as BMP signaling is involved in cancer cell fate decisions through the regulation of ID1/3. Accordingly, inhibition of BMP signaling has been shown to reduce cancer cell growth and stemness by downregulating ID proteins, particularly ID1. This leaves *ID3* as a largely undruggable gene that cannot be targeted for the prevention or treatment of cancer metastasis (Roschger & Cabrele, 2017).

Silibinin is a novel inhibitor of ID3 in brain endothelial cells and therapy-resistant NSCLC cells. In the context of NSCLC, the expression of ID proteins serves as a prognostic marker for clinical outcomes, especially after chemoradiotherapy. While ID1 and ID3 expressions are positively correlated, it should be emphasized that ID1 levels are more predominant in NSCLC (Castañon et al., 2013; Gil-Bazo et al., 2014). Nevertheless, the influence of ID3 on the regulation of cell proliferation through its interaction with the function of CDKis makes ID3 a critical target for therapeutic intervention (Roschger & Cabrele, 2017).

We provide evidence that silibinin antagonizes the expression of the metastasis-promoting transcription factor ID3 in endothelial and tumor cells. First, we show that a correlation between ID3 expression and poor prognosis in NSCLC may be mediated by the BMP pathway, which is known to influence stem-like phenotypes not only in tumor cells but also in the endothelial compartment, suggesting a multi-faceted impact on tumor growth and metastasis when ID3 activation is prevented. Silibinin appears to block *ID3* gene transcription by interfering with the BMP/SMAD/ID3 axis. Silibinin could potentially serve as an effective blocker of the ALK1 receptor signaling, which is involved in several biological processes beyond angiogenesis, including ALK1-driven regulation of the immune response in the tumor microenvironment (Bocci et al., 2019). This finding opens avenues for combination therapies that exploit the immunomodulatory effects of silibinin. In addition, our study highlights the redox-sensitive nature of ID3, which contributes to the formation of mesenchymal-like vascular lesions. The therapeutic potential of silibinin may therefore be significant in preventing microvascular complications associated with NSCLC, particularly in the brain

where ID3 contributes to neovascularization and abnormal vascular formation. Our research also suggests that high levels of ID3 in NSCLC cell lines may be associated with increased cell plasticity, immunosuppression, therapy resistance, and poor prognosis due to the reactivation of embryonic processes such as EMT. The suppression of ID3 overexpression by silibinin in treatment-resistant NSCLC cells suggests that silibinin may have the potential to overcome drug resistance by modulating the dynamics of EMT in NSCLC.

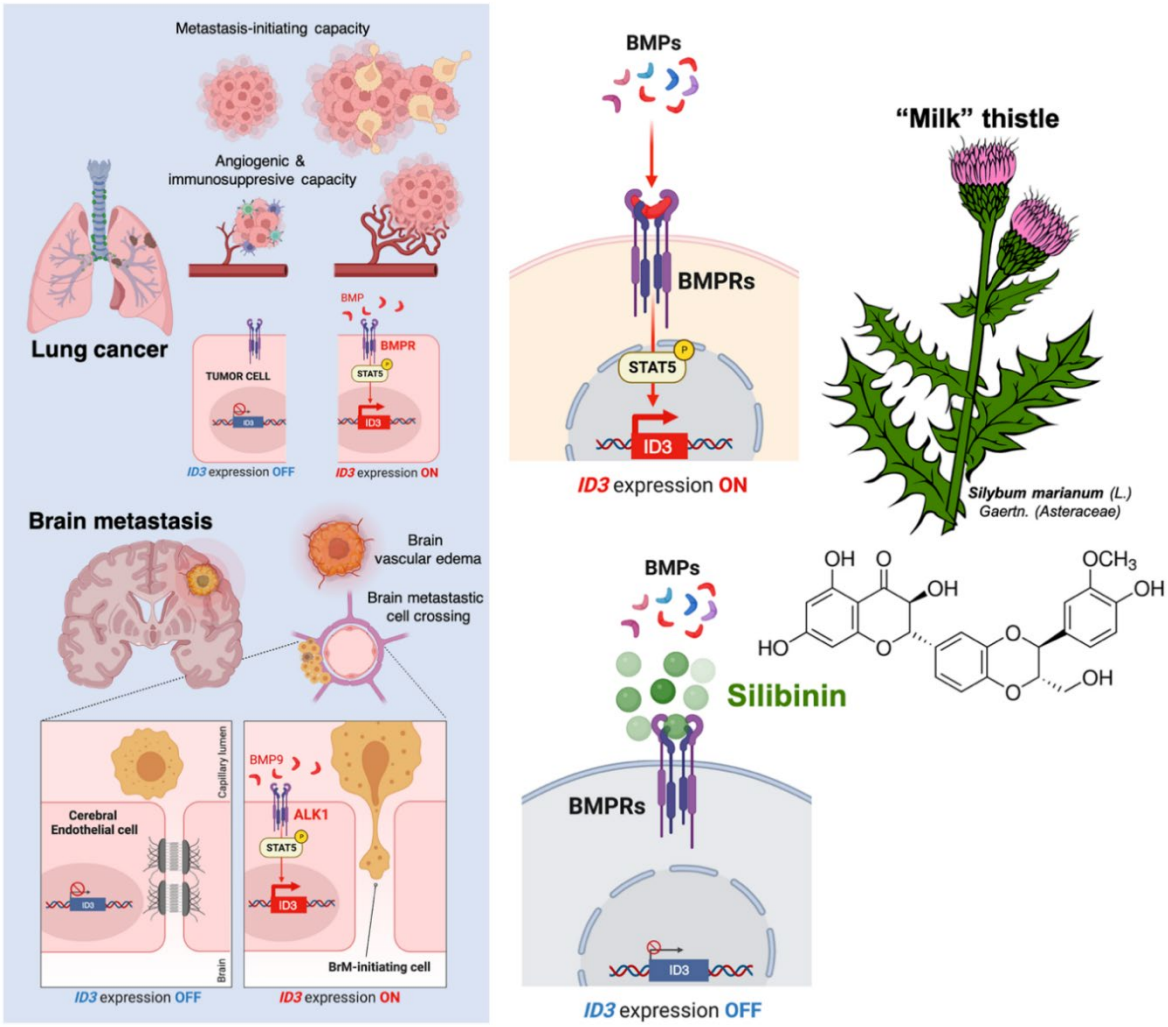

Figure 15. Silibinin is a novel suppressor of the metastasis-promoting transcription factor ID3. Created with Biorender. Aberrant activation of *ID3* gene expression confers metastatic ability and chemo-/radioresistance to certain subpopulations of CSC-like cells in primary tumorigenesis and during the early stages of metastatic colonization. ID3 can extrinsically promote metastatic dissemination by remodeling the tumor microenvironment and promoting the activation and recruitment of ECs to support tumor immune escape and angiogenesis at the primary and metastatic sites. Activation of ID3 also contributes to the stemness of ECs, a phenomenon that may facilitate not only the passage of brain metastatic cells across the BBB, but also the reorganization of the cerebral

microvasculature in reactive niches of primary and secondary brain tumors. Interfering with the intrinsic and extrinsic regulatory actions of ID3 may provide additive or even synergistic anti-metastatic effects. Our research combined bioinformatic analyses, immunoblotting, qRT-PCR, luciferase reporter assays, computational modeling, and kinase assays to elucidate how silibinin might modulate ID3 expression in endothelial and NSCLC cells. Results from NSCLC patient datasets indicate a strong correlation between ID3 expression and BMP9/ACVRL1/ALK1 and BMP6 levels, with silibinin effectively inhibiting the ALK1-phospho-SMAD1/5-ID3 axis in brain endothelial cells. Notably, silibinin disrupts ID3 expression by targeting BMP-responsive elements within the *ID3* gene enhancers, which are critical in BMP signaling pathways. Silibinin also demonstrates direct inhibition of BMPR kinase activity *in vitro*, with particular potency against ACVRL1/ALK1 and BMPR2. *In vivo*, oral silibinin was found to significantly reduce ID3 overexpression in NSCLC xenograft models. These findings suggest that silibinin may serve as a novel therapeutic to reduce the metastatic spread of NSCLC by suppressing ID3 in endothelial and tumor cells.

Synopsis chapter 1

- ***Silibinin blocks the inducible activation of ID3 in brain endothelial cells and prevents the constitutive, acquired, and adaptive expression of ID3 in NSCLC cells.***
- ***Silibinin inhibits the transcription of the ID3 gene through BMP-responsive elements and directly inhibits the kinase activity of the BMP receptors ACVRL1/ALK1 and BMPR2.***
- ***A water-soluble form of silibinin suppresses ID3 overexpression in vivo at clinically relevant concentrations***.

Chapter 2. Silibinin and NSCLC resistance to targeted therapies: EMT-driven escape to ALK-TKIs

Overcoming resistance to ALK-TKIs: An unmet clinical need for NSCLC patients. The identification of molecular subtypes of NSCLC based on specific oncogenic drivers, in particular the ALK fusion oncogene, has significantly altered the natural history of the disease (Seidel et al., 2013; Thai et al., 2021). The use of the first-generation ALK-TKI crizotinib has led to remarkable improvements in clinical outcomes for the subset of patients with ALK-rearranged NSCLC. However, most patients eventually relapse due to acquired resistance, primarily through *on target* ALK-dependent mechanisms characterized by secondary

mutations in the *ALK* gene, which is observed in up to 30-35% of patients treated with crizotinib and increases to approximately 50% in patients treated with second-generation ALK-TKIs such as ceritinib, alectinib and brigatinib (Toyokawa & Seto, 2015). The emergence of more selective and potent third-generation ALK TKIs, such as lorlatinib, has improved the treatment of patients with resistant mutant forms of ALK, which are common causes of resistance to first- and second-generation ALK TKIs. Despite these advances, ALK-independent *off-target* mechanisms of acquired resistance that do not involve the *ALK* gene are increasingly being recognized (Lin & Shaw, 2016).

EMT: A central node of resistance to ALK-TKIs. A key process in understanding primary and secondary resistance to ALK-TKIs is EMT, a phenomenon in which epithelial cells acquire mesenchymal characteristics (Gower et al., 2014, 2016). EMT is now understood to be a common downstream node where multiple resistance mechanisms converge (Haider et al., 2020). First, different ALK rearrangements themselves are known to induce an EMT signature in NSCLC, albeit with a remarkable degree of heterogeneity (Gower et al., 2014, 2016). ALK-positive NSCLC cells that exhibit an EMT-like signature are inherently less sensitive to ALK TKIs than those that retain an epithelial-like signature (Kim et al., 2013). Second, ALK-rearranged NSCLC tumors may lose their dependence on ALK and instead rely on alternative activation of pathways such as EGFR, KRAS/MAPK, cKIT, MET, HER2/HER3, AXL, and IGF-1/IGF-1R, all of which are capable of generating an EMT phenotype (Dagogo-Jack & Shaw, 2016; Gouji et al., 2014; Toyokawa & Seto, 2015). Third, the EMT phenotype associated with resistance to ALK-TKIs may arise secondary to activation of TGFβ signaling, possibly triggered by hypoxic conditions or other mechanisms yet to be identified (Kogita et al., 2014). Fourth, ALK resistance mutations and an EMT component may coexist in different tumor cell subpopulations in patients resistant to crizotinib. However, the distribution of these mutations and phenotypes is not uniform; ALK resistance mutations occur predominantly in epithelial-type tumor cells, while the mesenchymal phenotype is more likely to exhibit cross-resistance to both crizotinib and newer generation ALK-TKIs, including alectinib, ceritinib and lorlatinib, further suggesting that EMT is a central node of resistance to multi-generation ALK-TKIs (Fukuda et al., 2019; Gainor & Shaw, 2013).

Silibinin directly and indirectly targets TGFβ-related acquisition of mesenchymal phenotypes in ALK-rearranged NSCLC cells. Our study investigated whether the EMT phenomenon that drives resistance to first-generation ALK-TKIs also promotes cross-resistance to newer ALK-TKIs. We also investigated the potential of silibinin, which was previously reported to exert anti-EMT and anti-TGFβ signaling activities in non-cancer and cancer cell models, to re-sensitize drug-resistant mesenchymal NSCLC cells to ALK-TKIs. Our research in *in vitro* ALK-rearranged NSCLC models has confirmed the important role of EMT in the development of resistance to ALK-TKIs. The mesenchymal phenotype induced by EMT has been identified as an independent mechanism of resistance to the first-generation ALK-TKI, crizotinib. This resistance extends beyond crizotinib and affects the efficacy of second- and third-generation ALK TKIs designed to target crizotinib-resistant ALK mutations. Taken together, our findings suggest that ALK-rearranged NSCLC cells exposed to prolonged crizotinib or TGFβ stimulation evolve to an ALK-TKI-refractory mesenchymal phenotype. This evolution increases their resistance to second-generation ALK TKIs such as brigatinib and leads to complete non-responsiveness to third-generation ALK TKIs such as lorlatinib. Our study sheds light on an important molecular scenario: plasticity along the EMT spectrum significantly influences the likelihood that ALK-rearranged NSCLC cells will develop cross-resistance to multigenerational ALK TKIs. This finding underscores the potential utility of EMT scores –developed from pan-cancer EMT signatures derived from preclinical and clinical data– in predicting resistance to ALK-TKIs in both primary and metastatic tumors.

Previous studies from our laboratory have shown that the anti-tumor activity of silibinin is, at least in part, due to its influence on EMT-related molecular features in cancer cells. It effectively modulates key transcriptional regulators of EMT, including transcription factors such as SNAIL, SLUG, ZEB, and microRNAs such as miR-21/miR-200c (Cufí, Bonavia, Vazquez-Martin, Corominas-Faja, et al., 2013; Cufí, Bonavia, Vazquez-Martin, Oliveras-Ferraros, et al., 2013). In addition, silibinin has demonstrated the ability to inhibit fibrotic responses in various tissues by suppressing the TGFβ1/SMAD2/3 signaling pathway (Ko et al., 2017; R. Liu et al., 2020). Our study confirmed the ability of silibinin to control TGFβ/SMAD signaling. The mechanism involves deactivation of SMAD2, prevention of SBE-driven transcriptional responses, and transcriptional downregulation of TGFβ-associated genes. Our study further investigated the direct inhibitory effect of silibinin on TGFβR1/2 kinase

activities. The molecular interaction of silibinin with TGFβ receptors was significant, particularly its binding to the ATP-binding domain of TGFβR kinases. This binding inhibits their ATP kinase activity, effectively blocking downstream signaling cascades. The *in silico* models predict the interaction of silibinin with the catalytic site of TGFβR1/ALK5 and TGFβR2, with differences in binding contacts compared to pan- and selective TGFβR inhibitors. Our research has also addressed the stereochemical aspects of silibinin, in particular the different biological activities of its diastereomers A and B. While *in silico* data suggest a significant interaction with TGFβR kinases, experimental assays such as the LanthaScreen™ Eu Kinase Binding Assay reveal a less straightforward correlation. This discrepancy highlights the need to use optically pure components of silibinin for a thorough molecular understanding and therapeutic development of its anti-TGFβR inhibitory activity. However, we acknowledge that while silibinin acts as a direct inhibitor, its effect occurs at micromolar concentration ranges, which may imply a more complex mechanism than direct kinase inhibition in its sensitizing activity against ALK TKIs. Secretome profiling further confirmed the ability of silibinin to normalize the elevated release of TGFβ in the extracellular milieu of ALK-TKI-resistant NSCLC cells and to significantly reduce SMAD2/3 phosphorylation.

Our extensive studies underscore the importance of EMT in the development of resistance to ALK-TKIs in ALK-rearranged NSCLC. Silibinin, with its direct inhibition of TGFβR kinase activity and blockade of the SMAD signaling cascade, represents a promising therapeutic approach to overcome this resistance. As EMT is increasingly recognized as a driver of innate and acquired resistance to various cytotoxic and targeted drugs, the potential of clinically relevant, bioavailable formulations of silibinin in the treatment of ALK-TKI-resistant NSCLC is a promising avenue for future research and clinical application.

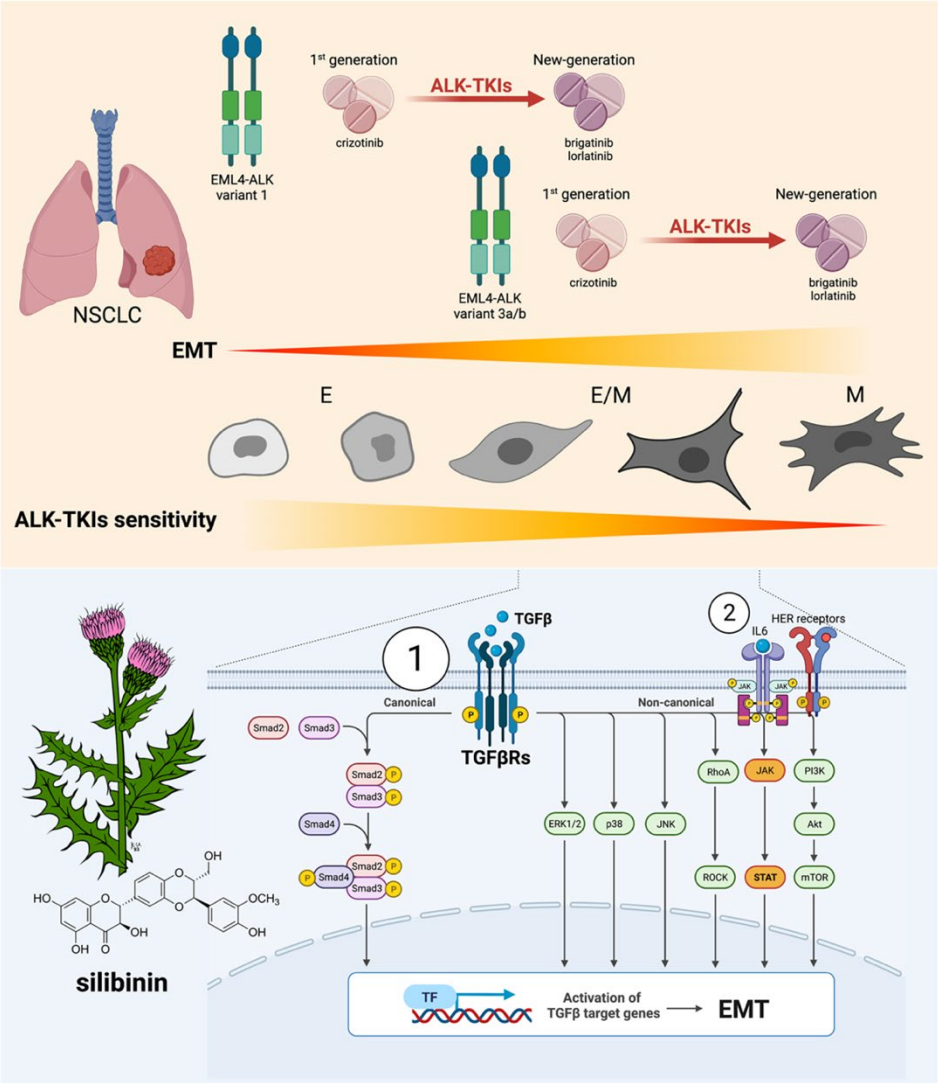

Figure 16. Exploring silibinin as a treatment for EMT-induced resistance to multiple-generation ALK-TKIs in ALK-rearranged NSCLC. Created with Biorender. The flexibility within the EMT spectrum may be key to understanding the varying degrees of resistance to multigeneration ALK-TKIs in ALK-rearranged NSCLC cells. In particular, epithelial cell populations, such as those harboring EML4-ALK variant 1, have a reduced tendency to develop mesenchymal characteristics that are resistant to new generation ALK-TKIs. In contrast, more mesenchymal ALK-rearranged NSCLC cells, such as those harboring EML4-ALK variant 3a/b, are more likely to develop this resistant mesenchymal phenotype. Upon chronic exposure to crizotinib, ALK-rearranged NSCLC cells that undergo a complete, late-stage EMT develop marked resistance to second-generation ALK TKIs such as brigatinib and a complete non-responsiveness to third-generation ALK TKIs such as lorlatinib. This is in contrast to cells that undergo only a partial or hybrid E/M transition. Silibinin counteracts EMT-driven cross-resistance to multi-generation ALK-TKIs. Our results highlight the ability to do this by reducing the overactivity of the TGFβ/SMAD pathway (**mechanism 1**). In addition, silibinin could potentially increase sensitivity to ALK-TKIs through direct inhibition of $STAT_3$ and EGFR. Thus, silibinin may prevent a functional landscape of resistance to ALK inhibition in NSCLC, which is often

associated with the activation of the IL6/JAK1/STAT3 and HER pathways (**mechanism 2**). In addition, our study also recognizes the potential role of silibinin as a novobiocin-like inhibitor of HSP90 (see below), which may also contribute to its efficacy against ALK-TKI resistance. This potential is based on silibinin's ability to promote the degradation of client proteins, including mutant ALK and TGFβ receptors, in mesenchymal ALK-rearranged cells with acquired resistance to ALK-TKIs.

Synopsis chapter 2

- ***The propensity of ALK-rearranged NSCLC cells to undergo EMT is a determinant of de novo (primary) and acquired (secondary) resistance to multi-generation ALK-TKIs.***
- ***Silibinin overcomes EMT-induced resistance to multi-generation ALK-TKIs and restores their efficacy by directly targeting of the transforming growth factor-beta (TGFβ)/SMAD signaling pathway.***

Chapter 3. Silibinin and NSCLC resistance to targeted therapies: STAT3- and lysosome trapping-driven escape to the multi-TKI nintedanib

Nintedanib: An anti-angiogenic multi-TKI with limited activity in NSCLC. Nintedanib, also known as BIBF 1120, is an oral angiokinase inhibitor agent that targets multiple growth factor receptors, including VEGFR1-3, PDGFRα/β, and FGFR 1-4, as well as the non-receptor tyrosine kinases FLT-3 and SRC (Hilberg et al., 2008, 2018). This broad inhibitory profile suggests that nintedanib could potentially provide therapeutic benefit in cases where other anti-angiogenic agents have proven ineffective. In the pivotal Phase III LUME-Lung 1 clinical trial, nintedanib in combination with docetaxel demonstrated a significant improvement in progression-free survival compared to docetaxel alone in patients with advanced NSCLC who had previously received one line of platinum-based therapy (Reck et al., 2014). The introduction of immunotherapy as a second- and third-line treatment option for NSCLC, coupled with the lack of new efficacy data on the nintedanib/docetaxel combination in real-world clinical practice, has discouraged lung oncologists from using this combination outside of clinical trials (Corral et al., 2019; Grohé et al., 2019).

Cancer cell-intrinsic effects of nintedanib: A need for sensitizing strategies. The therapeutic effects of nintedanib extend beyond the tumor angiogenic cell compartment to the proliferation and survival of cancer cells themselves, providing an autonomous pathway for tumor cells to counteract nintedanib-induced adaptive responses in the tumor microenvironment (Hilberg et al., 2008, 2018). However, a number of mechanisms appear to largely preclude the cytotoxic activity of nintedanib against tumor cells (Awasthi et al., 2015; Hilberg et al., 2008). First, the anti-proliferative and apoptotic activity of nintedanib on tumor cells appears to be mediated, at least in part, by direct or indirect inhibition of STAT3 (C.-Y. Y. Liu et al., 2017; Tai et al., 2014). Overexpression and constitutive hyperactivation of STAT3 are sufficient to suppress the anti-proliferative and apoptotic effects of nintedanib on cancer cells, highlighting the critical role of STAT3 activation status in determining the non-angiogenic cancer cell-targeting activity of nintedanib (Tai et al., 2014). Despite decades of research, very few FDA-approved STAT3 inhibitors (STAT3is) have emerged, making it a challenging target for therapeutic intervention aimed at sensitizing cancer cells to nintedanib (Furtek et al., 2016; Masciocchi et al., 2011; M. Zhao & Gao, 2011). Second, nintedanib has a weakly basic nature (pK = 7.9), which allows it to be fully protonated in low pH environments such as lysosomes. This phenomenon is referred to as "lysosomal trapping" and has been identified as a mechanism of therapeutic resistance in FGFR-driven NSCLC cells (Englinger et al., 2017). Lysosomal trapping may prevent nintedanib from accessing the receptor TKs located in the cytoplasm of cancer cells, ultimately reducing its efficacy. Therapeutic prevention of the lysosomal accumulation of nintedanib may re-sensitize nintedanib-resistant lung cancer cells to the cytotoxic effects of nintedanib.

Silibinin suppresses STAT3 activation-driven resistance to nintedanib. Our study uncovered intracellular pathways in NSCLC cells that may be critical for the evasion and adaptation of NSCLC cells to nintedanib. NSCLC cells with poor response to nintedanib exhibited increased levels of phospho-STAT3^{Tyr705} activation, which remained unresponsive to nintedanib treatment. These findings suggest that the resistance of NSCLC cells to nintedanib may depend, at least in part, on redundant or compensatory STAT3 signaling within the tumor cells themselves. Conversely, the suppression of this nintedanib-refractory STAT3 hyperactivation by co-treatment with silibinin resulted in synergistic anticancer effects. In FGFR-overexpressing cancer cells, STAT3 phosphorylation is driven by the

concomitant FGFR-dependent activation of SRC and JAK2 kinase (Bohrer et al., 2014; Li et al., 2019). Since PDGFRβ has been reported to induce the JAK2/STAT3 pathway by activating SRC (Vignais et al., 1996), nintedanib may inhibit JAK2 through its direct inhibition of PDGFRβ and SRC. Thus, the combined inhibition of multiple events contributing to STAT3 activation by nintedanib and silibinin appears to effectively prevent NSCLC cells from evading STAT3 inhibition. These findings highlight the potential of direct STAT3 inhibition with silibinin (*see below*) as a promising clinical strategy to overcome intrinsic NSCLC resistance to nintedanib.

Silibinin reduces lysosomal trapping of nintedanib. An intriguing aspect of the pharmacology of nintedanib is its ability to accumulate in lysosomes, reducing its effective concentration in the cytosol and compromising its therapeutic potential. To counteract this sequestration and restore sensitivity to nintedanib, researchers have explored the use of chemicals that neutralize lysosomal acidification, such as chloroquine and bafilomycin A1 (Englinger et al., 2017). These compounds effectively suppress the lysosomal sequestration of nintedanib. We demonstrated that extensive lysosomal sequestration occurs in nintedanib-refractory NSCLC cells. Furthermore, silibinin was found to partially but significantly reduce the lysosomal sequestration of nintedanib in these refractory NSCLC cells. The exact mechanism by which silibinin reverses the lysosomal sequestration of nintedanib remains unclear, although it is known to act as an iron chelator even under acidic pH conditions. Whether silibinin acts as a metal-binding substrate for P-glycoprotein, facilitating its transport into lysosomes and triggering lysosomal membrane destabilization, remains a topic for future investigation. Given that STAT3 plays a role in the regulation of cytosolic and lysosomal pH and that it enhances the lysosomal system (B. Liu et al., 2018), the STAT3 inhibitory activity of silibinin may also affect lysosomal acidification, thereby exerting synergistic growth inhibitory effects in combination with nintedanib. Nevertheless, the significant reduction in subcellular lysosomal trapping represents an unexpected mechanism by which silibinin may enhance the availability of nintedanib at the target site in NSCLC cells.

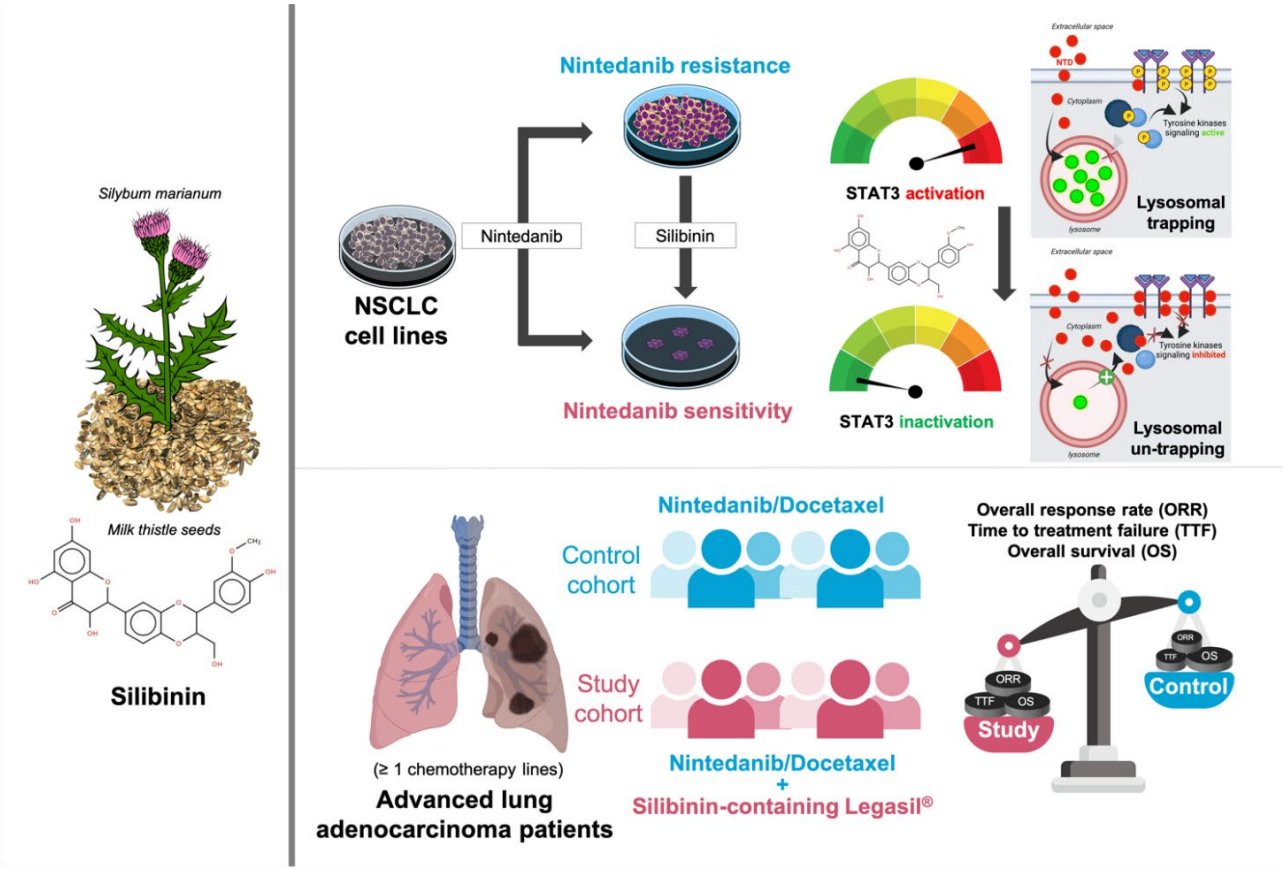

Figure 17. Silibinin overcomes tumor cell-intrinsic resistance to nintedanib in NSCLC. Created with Biorender. We investigated the molecular basis and clinical benefit of adding silibinin to the nintedanib/docetaxel treatment regimen for NSCLC. Our investigation involved assessing the nature of the tumoricidal interaction between nintedanib and silibinin, examining their impact on $STAT_3$ activity in a panel of human NSCLC cell lines, investigating how silibinin may affect lysosomal drug sequestration, and conducting a retrospective observational multicenter study to evaluate the efficacy of silibinin-based nutraceutical interventions in second- and third-line NSCLC patients receiving the nintedanib/docetaxel combination.**1**. NSCLC cells with poorer cytotoxic responses to nintedanib exhibited a persistent, nintedanib-unresponsive activated $STAT_3$ state. $STAT_3$ deactivation by co-treatment with silibinin promoted synergistic cytotoxicity. **2**. Silibinin partially, but significantly, reduced the massive lysosomal entrapment of nintedanib that occurs in nintedanib-refractory NSCLC cells, thereby enhancing the ability of nintedanib to reach its intracellular targets. **3**. Supplementation with the silibinin-based nutraceutical Legasil® in NSCLC patients receiving nintedanib/docetaxel was associated with increased clinical responses and a significantly longer time to treatment failure.

In conclusion, our study represents a comprehensive exploration of the combination of silibinin with nintedanib/docetaxel therapy in advanced NSCLC. Silibinin demonstrates the

potential to enhance the therapeutic efficacy of nintedanib by addressing resistance mechanisms related to STAT3 activation and lysosomal sequestration. While the clinical results of our study are promising, further research and clinical trials are warranted to validate the clinical significance of these findings and to determine the optimal treatment strategies for patients with advanced NSCLC.

Synopsis chapter 3

- ***Two molecular mechanisms that drive NSCLC tumor cell-intrinsic resistance to nintedanib, namely STAT3 hyperactivation and lysosomal trapping, are amenable to pharmacological intervention with silibinin.***
- ***Legasil®, a commercially available formulation of silibinin, is an effective anticancer adjunct to nintedanib/docetaxel combination in NSCLC patients.***

Chapter 4. Silibinin and avoiding side-effects using targeted therapy in NSCLC: The hyperlipidemic effects of lorlatinib

Hyperlipidemic effects of the third-generation ALK-TKI lorlatinib. Lorlatinib, known by its trade name PF-06463922, is a third-generation ALK-TKI specifically designed to overcome resistance observed to first- and second-generation ALK TKIs (Choo & Soo, 2020; Peng et al., 2022; J. Yang & Gong, 2019). Despite its efficacy for the treatment of ALK-positive metastatic NSCLC in patients whose disease has progressed after treatment with a first- or second-line ALK-TKIs such as crizotinib, alectinib or ceritinib, lorlatinib is associated with a unique adverse event profile that is significantly different from other ALK-TKIs. The most common adverse events associated with lorlatinib treatment are hypercholesterolemia and hypertriglyceridemia, which affect a significant proportion of patients (61% and 82%, respectively) and typically occur within the first few weeks of lorlatinib treatment. This condition often leads to temporary discontinuation or dose reduction of lorlatinib in clinical settings and requires prompt initiation of lipid-lowering medications (Bauer et al., 2019; Blais et al., 2021).

The management of lorlatinib-induced hyperlipidemia is an important clinical issue. The majority of patients (more than 80%) are started on at least one lipid-lowering agent within three weeks of the first dose of lorlatinib, and approximately 25% of these patients eventually require a second agent to adequately control their lipid levels. Statins are the most commonly prescribed lipid-lowering agents; however, the selection and dosing of statins must be carefully considered due to the differential metabolism of the CYP450 pathway (Neuvonen et al., 2006). Lorlatinib is primarily metabolized by CYP3A4; therefore, 3A4 statin substrates such as atorvastatin, lovastatin, and simvastatin should be avoided in lorlatinib-treated patients. Non-3A4 statin substrates such as rosuvastatin, pravastatin, and pitavastatin, which are not significantly metabolized by CYP3A4 enzymes, have a reduced risk of adverse interactions with lorlatinib (Neuvonen et al., 2006; Reed et al., 2020). Currently, rosuvastatin is the only lipid-lowering agent specifically recommended for the treatment of lorlatinib-associated hyperlipidemia due to its low involvement with CYP450 enzymes that may interact with lorlatinib (Neuvonen et al., 2006; Reed et al., 2020).

The need for new lipid-lowering agents that can synergistically interact with the anti-tumor effects of lorlatinib. Understanding the primary causes of lorlatinib-induced hypercholesterolemia/hypertriglyceridemia is critical to improving the prognosis and survival of NSCLC patients with ALK translocations. Our study has focused on whether lorlatinib could directly promote hypercholesterolemic and hypertriglyceridemic effects in human hepatocytes. Our investigation involved the use of non-targeted lipidomics, including ultra-high pressure liquid chromatography accurate mass quadrupole time-of-flight mass spectrometry with electrospray ionization (UHPLC-ESI-QTOF-MS/MS), and imaging of neutral lipids in hepatoma tissue-derived Huh-7 and HepG2 cells, which were used as surrogates for primary hepatocytes. In addition, our study investigated whether silibinin, which is known for its hepatoprotective properties in patients with acute and chronic liver injury and has been shown to interact synergistically with multi-generation ALK-TKIs (*see above*), could prevent the lipid-modifying activity of lorlatinib in hepatocytes. Our research also included an evaluation of the potential drug-drug interactions of silibinin, in particular its interaction with and inhibition of CYP3A4 activity, compared to commonly used statins.

Lorlatinib-promoted modification of the hepatic cell lipidome: An unforeseen mechanism of lorlatinib-induced hyperlipidemia. The elevated plasma levels of cholesterol and triglycerides commonly observed in patients with ALK-positive NSCLC treated with lorlatinib are thought to be multifactorial and not fully understood. One hypothesis links these lipid abnormalities to nephrotic syndrome, as lorlatinib is the only ALK-TKI reported to cause acute kidney injury with formation or progression of renal cysts (McGee et al., 2021). This suggests a secondary cause of lorlatinib-induced hyperlipidemia. Preclinical evidence supports the alternative hypothesis that elevated plasma cholesterol and triglyceride levels in lorlatinib-treated NSCLC patients may be due to direct changes in hepatic lipid accumulation.

Lorlatinib is rapidly absorbed and reaches high plasma concentrations, particularly in the liver. The accumulation of lorlatinib in the liver is due to its poor metabolism in this organ (Chen et al., 2019; Hibma et al., 2022). In a detailed lipidomic analysis using semi-targeted UHPLC-ESI-QTOF-MS/MS, it was observed that short-term administration of lorlatinib to hepatic cells leads to an increased accumulation of different molecular species of cholesteryl esters and triglycerides. This lipidomic change is indicative of a shift toward a hyperlipidemic state.

Our findings suggest that the elevated plasma cholesterol and triglyceride levels observed in lorlatinib-treated NSCLC patients may be due to primary alterations in hepatic lipid metabolism, specifically the accumulation of lipid intermediates. However, the exact molecular mechanisms explaining why lorlatinib exposure leads to the accumulation of cholesteryl esters and tri-/di-glycerides in hepatic cells, which may induce hepatic steatosis upon prolonged lorlatinib exposure, remain unclear. There may be an overlap between the pathways that are targeted for growth in ALK-rearranged NSCLC and those that regulate liver function. This may result in hepatic toxicity. Mitochondrial dysfunction, a common mechanism in drug-induced liver injury, may play a role in the effects of lorlatinib on lipid metabolism, possibly through impaired fatty acid oxidation.

Silibinin prevents lorlatinib-induced hyperlipidemia. Lorlatinib-induced hyperlipidemia, which includes hypercholesterolemia and hypertriglyceridemia, is primarily treated with dose

adjustments and lipid-lowering therapies such as statins (Reed et al., 2020). Our study evaluated the lipidomic interactions of lorlatinib with silibinin. Silibinin treatment maintained lipidomic homeostasis in hepatocytes and counteracted the lipid accumulation induced by lorlatinib. This was confirmed by lipid staining techniques, which showed that the ability of lorlatinib to induce neutral lipid overload in hepatocytes upon prolonged exposure was largely attenuated when silibinin was co-administered.

Since lorlatinib is primarily metabolized by the CYP3A4 isoenzyme, it is important to co-administer it with lipid-lowering agents that do not interact with CYP3A4, such as rosuvastatin. Using computational modeling and cell-free biochemical assays were used to evaluate the interaction of silibinin with CYP3A4, we confirmed that standard doses of silibinin-containing milk thistle preparations have a low risk of inhibitory interaction with the hepatic clearance of lorlatinib. However, higher intestinal concentrations of certain silibinin formulations may still interact with the lorlatinib-metabolizing CYP3A4 isoenzyme at the intestinal level. This is in contrast to the effects observed with statins such as rosuvastatin (recommended) and simvastatin (not recommended) in the setting of lorlatinib-associated dyslipidemia.

Silibinin is known to reduce hepatic and biliary triglycerides and cholesterol in various models and patient populations. Our results provide preclinical evidence that silibinin may also suppress the lipid-modifying effects of lorlatinib in human liver cells. Silibinin shows potential to protect liver cells from the hyperlipidemic effects of lorlatinib and to prevent lipid accumulation. Silibinin, which was found to be highly effective in bypassing resistance to ALK-TKIs in our pre-clinical approach (*see above*)s, could therefore be an idoneous lipid-lowering agent in treatment regimens for NSCLC patients at high risk of brain metastases, especially those exposed to ALK TKIs.

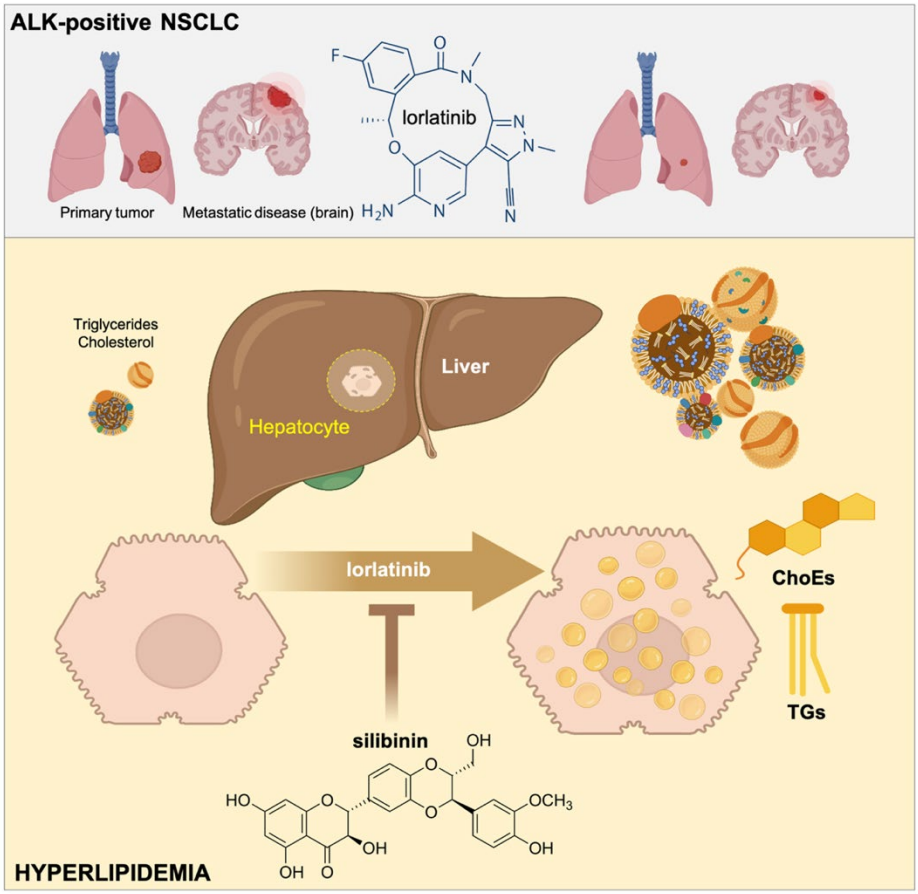

Figure 18. Silibinin suppresses the hyperlipidemic effects of lorlatinib in hepatic cells. Created with Biorender.The results of our studies provide the first evidence that the hyperlipidemic effects of the third-generation ALK-TKI lorlatinib may involve, at least in part, the induction of increased cholesterol and triglyceride content in liver cells. Furthermore, these effects can be prevented or reversed by silibinin, suggesting a novel therapeutic strategy to manage the undesirable lipid-modifying effects of lorlatinib in patients with ALK-positive NSCLC.

Our study has limitations including the use of hepatoma-derived cell lines with low expression of drug-metabolizing enzymes such as CYP3A4. Results from *in silico* and *in vitro* metabolic interactions between lorlatinib and silibinin may not be fully extrapolated to the *in vivo* setting. The study also notes that the combination of lorlatinib with high concentrations of silibinin did not show significant toxic effects in lipidomic studies with hepatoma cells. However, accurate prediction of *in vivo* toxicity may require the use of advanced human hepatoma cell lines with stable expression of liver-specific functions, including CYP3A4. Thus, despite its potential, further studies are needed to fully understand the inhibitory potential of silibinin against the lorlatinib-metabolizing CYP3A4 isoenzyme before its therapeutic

combination with lorlatinib can be recommended in clinical settings for ALK-rearranged lung cancer patients.

Synopsis chapter 4

- ***The ALK-TKI lorlatinib directly alters the lipid profile of human hepatocytes at clinically relevant concentrations.***
- ***Silibinin protects hepatocytes from the hyperlipidemic effects of lorlatinib and prevents lipid accumulation.***
- ***Silibinin could be a potential lipid-lowering agent in treatment regimens for NSCLC patients at high risk of brain metastases, especially those exposed to ALK TKIs.***

Chapter 5. Silibinin and cancer cell-intrinsic targets in brain metastases: HSP90

HSP90 and brain metastasis. The so-called METPlatform (medium-throughput drug-screening platform) is an *ex vivo* organotypic culture-based drug screening system that has been developed to overcome the limited efficacy of existing therapies in improving the survival of cancer patients with brain metastases. This platform takes advantage of organotypic brain cultures to evaluate therapeutic agents directly on brain metastases, providing a cost-effective and rapid identification of biologically relevant drug candidates. Using organotypic brain cultures for medium throughput screening of a broad library of anti-cancer compounds, the METPlatform identified HSP90 as a promising target to exploit the vulnerabilities of brain metastasis (Zhu et al., 2022). HSP90 is a molecular chaperone involved in protein folding and cellular proteostasis that cancer cells rely on for survival, oncogenic transformation and immune evasion. HSP90 plays a critical role in maintaining the conformational stability of over 200 client proteins under the stressful conditions of the tumor microenvironment, many of which are signal transducers that contribute to the metastatic potential of cancer cells (Barrott & Haystead, 2013). The METPlatform's validation of HSP90 as a viable target led to the demonstration of potent anti-metastatic activity of

DEBIO-0932, a second-generation HSP90 inhibitor with the ability to penetrate the BBB, which is being evaluated in a Phase I/II trial in patients with advanced NSCLC (NCT01714037), in both experimental and human metastases. This work provided the rationale and proof-of-principle to include patients with brain metastases in ongoing clinical trials of BBB-permeable HSP90 inhibitors and/or to develop a specific BBB-permeable HSP90 inhibitor for this patient population in the adjuvant setting following neurosurgery, taking into account the potential toxic effects prior to further clinical consideration (Zhu et al., 2022). Indeed, most HSP90 inhibitors face challenges such as poor BBB permeability, limited target inhibition, and toxicity.

Silibinin and HSP90 in primary brain tumors. HSP90 plays a key pathogenic role in Cushing's disease, a condition characterized by excessive ACTH secretion due to glucocorticoid-resistant corticotropic adenoma. Normally, the glucocorticoid receptor (GR) represses the transcription of ACTH precursor genes, but mutations causing glucocorticoid resistance are rare. Corticotropic adenomas overexpress HSP90, which impairs GR function. Accordingly, the use of N-terminal and C-terminal HSP90 inhibitors, acting at different stages of the HSP90 catalytic cycle and affecting corticotroph cell proliferation and GR transcriptional activity, could be considered as treatment strategies for the clinical management of Cushing's disease. Silibinin was found to release mature GR from HSP90, allowing it to exit the chaperone cycle and enhance its transcriptional activity, thereby demonstrating anti-tumorigenic effects and alleviating symptoms of Cushing's disease in a mouse model. This suggested that the pathogenesis of the disease, which is associated with HSP90 overexpression and misregulated GR sensitivity, could be addressed pharmacologically with the HSP90 inhibitory activity of silibinin. The study proposed that silibinin counteracts the pathogenic mechanism of HSP90 overexpression leading to glucocorticoid resistance. Unlike N-terminal inhibitors, which prevent folding of client proteins by blocking ATP hydrolysis, silibinin was predicted to act as an HSP90 C-terminal domain (CTD) inhibitor capable of increasing the number of stable, high ligand affinity GRs by releasing them after final folding (Riebold et al., 2015). The research findings were consistent with previous studies on the action of novobiocin, another HSP90 inhibitor, and

highlighted the potential of silibinin to restore glucocorticoid sensitivity in Cushing's disease by acting as a non-toxic HSP90 inhibitor (Sbiera et al., 2015; Sugiyama et al., 2015).

Silibinin is a non-hepatotoxic inhibitor of HSP90. We hypothesized that silibinin, which is predicted to bind the C-terminal domain of HSP90, may provide a therapeutic approach to brain metastasis that could potentially circumvent resistance seen with other treatments. Previous studies have shown that silibinin can inhibit the refolding of denatured proteins such as firefly luciferase—an HSP90-dependent process—by approximately 50% at certain concentrations, demonstrating its ability to disrupt the chaperone function of HSP90 (Thulasiraman & Matts, 1996; H. Zhao et al., 2011). In addition, silibinin was found to induce the degradation of several HSP90 client proteins without altering HSP90 levels, suggesting a selective inhibitory effect on HSP90's activity rather than its expression (H. Zhao et al., 2011). Molecular studies have shown that silibinin does not disrupt the interaction of HSP90 with its co-chaperones, suggesting a unique mechanism of inhibition. The features of silibinin necessary for its HSP90-related cytotoxic activity were further elucidated by structural-activity relationship (SAR) studies. Advanced computational methods, including the cryo-EM structure of the Hsp90-Cdc37-Cdk4 complex, have been used to understand the interaction between silibinin and HSP90 isoforms.

In our study, we performed *in silico* molecular docking analyses and *in vitro* time-resolved fluorescence energy transfer (TR-FRET) assays to investigate the interaction of silibinin with HSP90 and its efficacy in inhibiting Hsp90's association with co-chaperones. Our *in silico* studies have predicted that silibinin binds to multiple pockets in the C-terminus of HSP90 α and β isoforms, with the highest ranked docking positions overlapping with those of novobiocin, supporting the theory that silibinin acts as a novobiocin-like HSP90 inhibitor. The effects of silibinin were compared with those of novobiocin, a known HSP90 C-terminal domain (CTD) inhibitor, and geldanamycin, a traditional Hsp90 inhibitor known for its hepatotoxicity. Our study concluded that silibinin functions similarly to novobiocin, altering the conformation of HSP90 and its interaction with co-chaperones, while not inducing hepatotoxicity, thus supporting silibinin as a viable non-toxic HSP90 inhibitor. Despite the structural complexity of HSP90 and its multiple conformational states, our computational

modeling suggests that silibinin may interfere with structural rearrangements that are essential for the function of HSP90. This could involve competitive interaction at the CTD ATP-binding site and potentially interfere with HSP90 co-chaperone-client interactions, leading to a general inhibition of HSP90 chaperoning activity.

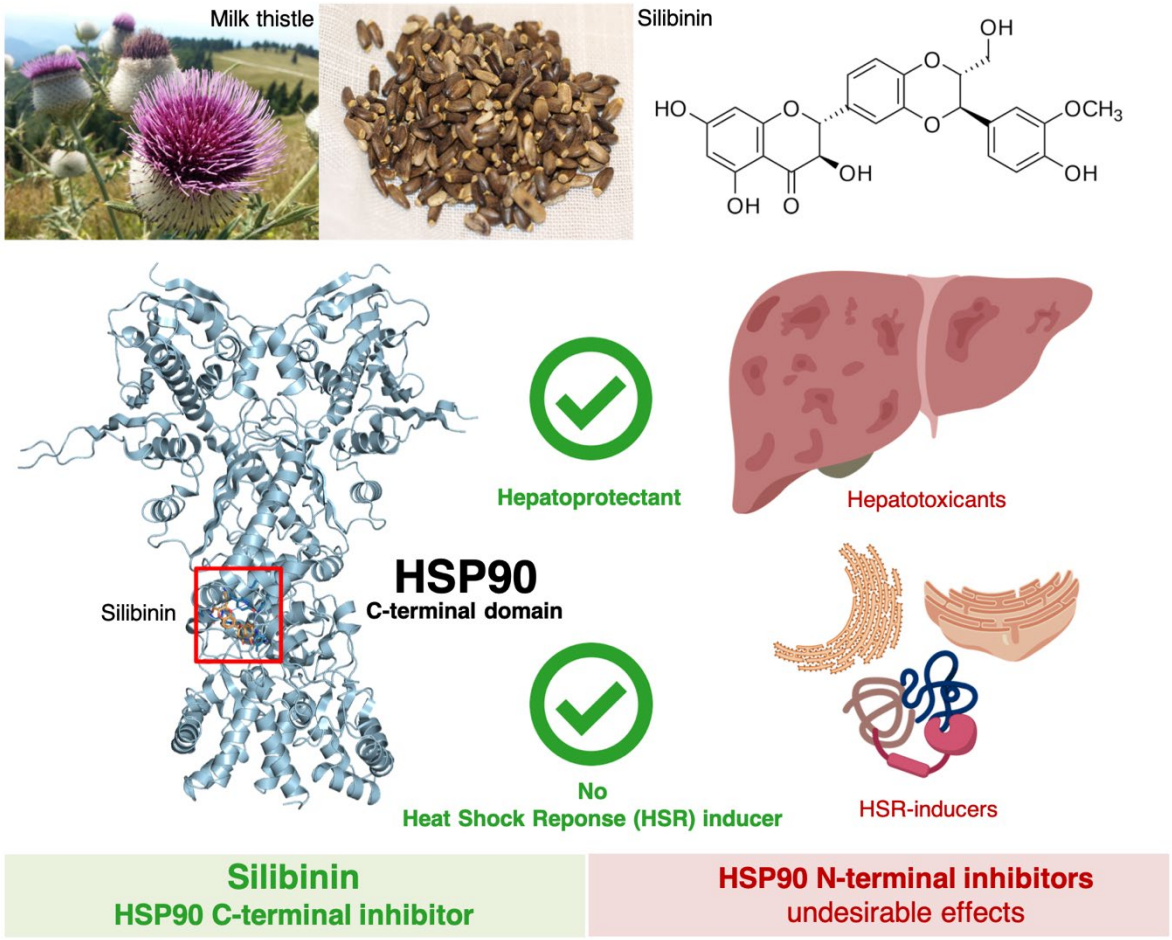

Figure 19. Silibinin is a C-terminal inhibitor of HSP90. Created with Biorender. Our computational and experimental data support the potential of silibinin as a non-toxic, potent HSP90 inhibitor was therefore supported by both. Its ability to disrupt the interaction of HSP90 with client proteins, combined with its expected lack of unmanageable side effects, positions silibinin as a promising candidate for the treatment of NSCLC brain metastasis. The toxicity profile of silibinin differs significantly from that of first-generation HSP90 inhibitors. Unlike geldanamycin-based inhibitors, which are known to cause hepatotoxicity, silibinin does not affect P450 drug-metabolizing enzymes and appears to reduce hepatic reactive oxygen species levels, suggesting a more favorable toxicological profile. In our hands, the hepatotoxic behavior of silibinin occurred only at concentrations several thousand times higher than those of the HSP90 N-terminal inhibitor geldanamycin. Silibinin may provide a new avenue for the incorporation of HSP90 inhibitors for treatment of brain metastases due to its predicted ability to cross the BBB and its established safety and hepatoprotective properties, which may overcome the hepatotoxicity associated with other HSP90 inhibitors.

Synopsis chapter 5

- ***Silibinin is computationally predicted to overlap with the novobiocin binding mode to the HSP90 CTD.***
- ***Silibinin reduces the efficiency of the binding of the HSP90 CTD to its co-chaperone-client interactions in the low millimolar range without significant hepatotoxicity.***
- ***Silibinin targeted inhibition of HSP90 may represent a first-in-class strategy against a tumor cell-intrinsic mechanism promoting brain metastasis colonization in NSCLC patients.***

Chapter 6. Silibinin and microenvironmental targets in brain metastases: $STAT_3$

Brain metastases: A major unmet clinical need in NSCLC. The development of brain metastases is a devastating diagnosis that affects the quality of life and survival of patients with NSCLC. Symptoms that may be irreversible even after successful treatment of intracranial disease include headache, nausea, vomiting, seizures, neurocognitive decline, and focal neurological deficit. Conventional treatments such as surgery, chemotherapy and radiation are mainly palliative and largely ineffective, making brain metastases a fatal disease for 90% of NSCLC patients within two years of initial diagnosis (with a median survival of 7-10 months) (Ernani & Stinchcombe, 2019; Owen & Souhami, 2014).

The incidence of NSCLC-associated brain metastases is expected to increase not only because of the improved diagnostic accuracy of brain imaging, but also because of the growing number of systemic therapies that are successful extracranially but fail to provide therapeutic benefit in the brain. Because radiotherapy offers superior access the brain compared to poorly efficacious chemotherapy, whole-brain radiotherapy (WBRT) and stereotactic radiosurgery (SRS) remain the mainstay of treatment for both established brain metastases and prophylactic prevention or early elimination of brain micrometastases.

Cranial irradiation improves overall brain control, but there is no corresponding improvement in overall survival, and it may worsen quality of life due to neurotoxicity. Not surprisingly, the clinical management of NSCLC brain metastases over the past two decades has aimed to move away from radiotherapy to integrate targeted therapy and immunotherapy. EGFR- and ALK-TKIs able to optimally penetrate the BBB show remarkable preventive effects against brain metastases. However, patients with EGFR-mutant and ALK-rearranged NSCLC tumors –which naturally have a greater central nervous system (CNS) tropism– inevitably relapse on EGFR- and ALK-TKI-based therapy (Ernani & Stinchcombe, 2019; Owen & Souhami, 2014). CNS progression rates would be closely linked to an enhanced ability of drug-tolerant, brain metastasis-initiating cells to escape immune surveillance. Accordingly, one of the most active areas of investigation is how best to incorporate immune checkpoint inhibitors (ICIs) into new treatment regimens for NSCLC patients at highest risk of developing brain metastases, such as those continuously exposed to EGFR and ALK TKIs (Rosell & Karachaliou, 2016). However, in the emerging era of immunotherapy, there is a lack of robust clinical evidence regarding the benefit of ICIs, such as anti-PD1/PD-L1 monoclonal antibodies, in controlling brain versus extracranial NSCLC metastases (Enright et al., 2021; Y. Yang et al., 2022).

STAT3-positive reactive astrocytes in the brain tumor microenvironment: A therapeutic opportunity against brain metastasis. Disabling the orchestration of the crosstalk between the brain tumor microenvironment and brain-resident cancer cells may provide help in addressing the unmet clinical need of treating brain metastases in NSCLC patients. Astrocytes, which are critical for the homeostasis of the brain microenvironment homeostasis by actively participating in the repair and scarring of brain injury, have emerged as the major host brain cell-type contributing to the pathogenesis and pathophysiology of brain metastasis (Wasilewski et al., 2017). Astrocytes become reactive and reprogram their microenvironment when responding to their encounter with NSCLC cancer cells metastasizing to the brain.

The identification of molecular drivers of the biological outcomes of brain metastatic cells in different types of reactive astrocytes (RA) may provide a proof-of-concept to consider the pharmacological targeting of the brain microenvironment in the treatment of NSCLC patients with brain metastases. Activation of STAT3 in a specific subpopulation of RA

surrounding brain metastatic lesions, a phenomenon that correlates with significantly reduced survival from diagnosis of intracranial metastases, fulfils such a mechanistic requirement. A distinct population of RA exhibit increased tyrosine (Y705) nuclear phosphorylation (i.e., transcriptional activation) of $STAT_3$ in response to cytokines secreted by tumor cells that initiate a brain macro-metastasis. Phospho-$STAT_3^+$ RA are functionally distinct from other RA commonly found in all brain metastases because they acquire stem-like properties and secrete phenotype-associated cytokines that drive an immunosuppressive microenvironment by preventing both adaptive ($CD8^+$ T-cells) and innate (macrophages/microglia) immune responses (McFarland & Benveniste, 2019; Priego et al., 2018).

Silibinin: A naturally occurring direct inhibitor of $STAT_3$. We provide a comprehensive and in-depth evaluation of the intricate and multifaceted mechanisms by which silibinin acts as a potent inhibitor of the $STAT_3$ signaling pathway. The primary objective of this comprehensive study was to elucidate whether silibinin acts as an indirect $STAT_3$ inhibitor ($STAT_3$i) by modulating the JAK/STAT pathway or as a direct $STAT_3$i by targeting specific domains within the $STAT_3$ protein. In addition, this investigation aimed to provide comprehensive comparisons between silibinin and other compounds known for their $STAT_3$ inhibitory properties, thus contributing to a better understanding of the molecular interactions and modes of action underlying the $STAT_3$ inhibitory effects of silibinin. Our study demonstrates for the first time that silibinin is a naturally occurring direct inhibitor of $STAT_3$, inhibiting $STAT_3$ phospho-activation, dimerization, nuclear translocation, DNA-binding, and transcriptional activity.

Our computational approaches predicted a multifaceted nature of silibinin's mechanism of action, which appears to affect two key facets of $STAT_3$ functionality, namely inhibition of the phospho-activating SH2 domain and direct disruption of DNA-binding domain (DBD)-driven transcriptional activity. Our study harnesses the power of computational homology modeling techniques to unravel the intricate molecular interactions that govern silibinin's inhibition of $STAT_3$. This approach facilitates a deeper understanding through comparative docking and molecular dynamics simulations, yielding predictions that silibinin is capable of forming high-affinity interactions with the $STAT_3$ SH2 domain that mirror the actions of

known direct STAT3 inhibitors. In particular, the unique binding mode of silibinin allows it to occupy the same cavity as other direct STAT3 inhibitors, thereby effectively preventing the phosphorylation of Y705 within the monomeric SH2 domain of STAT3.

Our experimental evidence strongly supports the computationally predicted role of silibinin as a direct inhibitor of STAT3. Importantly, its inhibitory effect on STAT3 remains consistent across a spectrum of cellular contexts, regardless of the pre-existing phosphorylation status of STAT3 at the critical Y705 site. A key revelation emerged from cellular profiling assays using advanced LanthaScreen™ technology, confirming that silibinin effectively limits phosphorylation of Y705 without causing substantial changes in the kinase activity of upstream STAT3 kinases such as JAK1 and JAK2.

Direct inhibition of the phospho-activating/dimerizing SH2 domain: Silibinin is predicted to effectively inhibit the function of the STAT3 SH2 domain, a critical component for STAT3 activation and subsequent translocation of STAT3 to the nucleus. This inhibition strategically disrupts the ability of STAT3 to bind to cell surface receptors upon activation and interrupts the dimerization process. As a result, silibinin prevents the nuclear accumulation of phosphorylated STAT3 and effectively attenuates its transcriptional activity.

Direct disruption of the DBD-dependent transcriptional activity: A notable feature of the predicted action of silibinin is that it directly targets the DBD of STAT3. This inhibits the ability of STAT3 to bind to DNA and initiate transcription of target genes. Notably, this inhibition is observed at much higher concentrations than those required for inhibition of the SH2 domain, underscoring the importance of the SH2 domain inhibition in the ability of silibinin to suppress STAT3-mediated transcriptional activity.

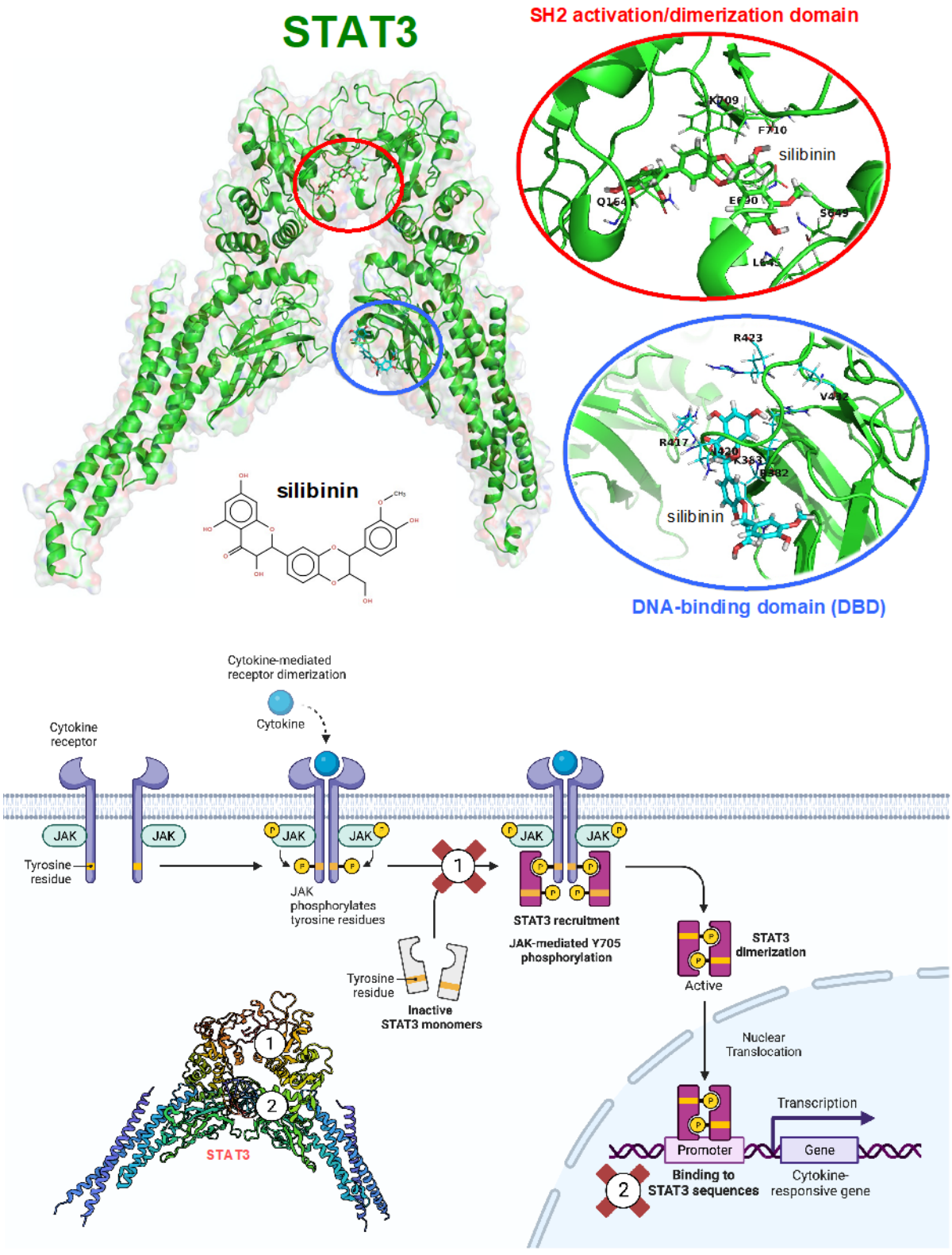

Figure 20. Silibinin: A bimodal SH2- and DBD-targeted inhibitor of STAT3. Created with Biorender. The anti-STAT3 activity of silibinin appears to involve a dual inhibitory mechanism by targeting the phospho-activatable Src homology 2 (SH2) domain responsible for STAT3 dimerization and the DNA-binding domain (DBD). Our biochemical analyses showed that silibinin reduced Y705 phospho-activation in GFP-STAT3 constructs without affecting the kinase activities of the upstream STAT3

kinases JAK1/2. To rule out the notion of silibinin as a JAK inhibitor, we undertook on a computational investigation using docking and molecular dynamics simulations in comparison to various STAT3 inhibitors with known mechanisms of action. This approach first predicted a high-affinity binding of silibinin to the SH2 domain, which partially but differently overlaps with the binding site of other SH2-targeted STAT3is, thereby preventing Y705 phosphorylation (**mechanism 1**). Experiments with NSCLC cells confirmed the ability of silibinin to prevent IL-6 inducible, constitutive, and feedback (acquired) activation of STAT3. Silibinin-induced disruption of the STAT3 phospho-Y705 interaction with the SH2 domain, a critical event for DNA binding and transcriptional activity, was demonstrated by its blocking of STAT3 nuclear translocation. Computational predictions also suggested a high-affinity interaction of silibinin with the STAT3 DBD, affecting the ability of STAT3 to interact with STAT3-binding DNA sequences (**mechanism 2**). Experiments with NSCLC cells confirmed the ability of silibinin to directly block the binding of activated STAT3 to its consensus DNA sequence, thereby suppressing STAT3-directed transcriptional activity.

Silibinin as a STAT3 inhibitor: An efficient suppressor of phospho-STAT3+ reactive astrocytes in brain metastases. The behavior of silibinin as a bimodal STAT3 inhibitor with a pronounced effect on the transcriptional activity of STAT3, as predicted by our studies, has been supported by compelling evidence in follow-up studies. Importantly, the ability of silibinin to prevent the brain metastasis-promoting phenotype of phospho-STAT3+ RA was found to be strictly STAT3-dependent. The so-called STAT3C mutant—a genetic variant in which residues A661 and N663 of the SH2 domain are replaced by cysteine residues, facilitating the formation of a disulfide bond between two unphosphorylated STAT3 monomers, was found to confer a conformation of STAT3 that mimics the active resulting from Y705 phosphorylation but prevents the direct binding of silibinin. The STAT3C mutant still requires Y705 phosphorylation for its functional activation, resulting in promotion of maximal DNA binding affinity, a slower dissociation rate, and protection from inactivation by phosphatases. Astrocytes engineered to overexpress a constitutively active form of STAT3, characterized by spontaneous dimerization, DNA binding, and transcriptional activation, show remarkable resilience to the inhibitory effects of silibinin on key STAT3-dependent transcriptional targets. Collectively, these findings clearly underscore the central role of STAT3 in mediating the phenotypic responses induced by silibinin (Priego et al., 2018).

Experimental therapeutic suppression of phospho-STAT3^{+} RA with silibinin was found to phenocopy the consequences of STAT3 functional ablation in RA to also impair experimental brain metastasis of NSCLC. The ability of silibinin to strongly reduce experimental brain metastasis, regardless of the primary tumor source (i.e., lung cancer, breast cancer, and

melanoma), even at advanced stages of brain metastasis colonization, was demonstrated in *ex vivo* studies using brain tissue slice cultures and in vivo studies using brain-tropic cancer cells stereotactically injected into the cerebral cortex of mice (Priego et al., 2018).

Silibinin to treat brain metastases in NSCLC patients: A pilot study. In a single-center, comparative retrospective cohort study of survival outcomes in patients with NSCLC and brain metastases (n=18), our group evaluated 18 patients who received Legasil™ and compared them with a control group of 38 patients treated with WBRT and other systemic treatments at the same institution (Catalan Institute of Oncology, Girona) in 2015-2016. Both groups had similar in their clinical profiles, but the Legasil™ group started with a lower average performance status and a slightly higher rate of certain EGFR and ALK alterations in their tumors. Both groups received the same radiation and chemotherapy regimens. However, the Legasil™ group showed better control of their brain metastases, which allowed them to receive more lines of treatment. This seemed to help because their median survival time after brain metastases were diagnosed was much longer –over 15 months compared to just 4 months in the control group, which was a statistically significant difference (P<0.0001). Even when we excluded patients with *EGFR* and *ALK* gene mutations, the Legasil™ group still showed a survival advantage. And when we measured survival using an expected survival model for lung cancer brain metastases, the Legasil™ group performed better than predicted, while the control group had a median survival of approximately 7 months (P=0.0010) (Priego et al., 2018). We have therefore provided evidence that the use of Legasil™ –an oral nutraceutical product containing a clinically relevant bioavailable formulation of silibinin with predicted ability to cross the BBB (Pérez-Sánchez et al., 2019)– had significant intracranial activity and resulted in a greater than 4-fold survival benefit compared to standard-of-care in a small cohort of NSCLC patients with established brain metastases (Priego et al., 2018).

Silibinin: An opportunity to develop next-generation derivatives for the prevention and treatment of NSCLC brain metastasis. Brain-penetrating versions of silibinin capable of blocking STAT3-driven astrocyte reactivity could significantly improve survival outcomes in NSCLC patients with brain metastases. In the aforementioned *ex vivo*, *in vivo* and clinical studies, silibinin was administered as part of the commercially available nutraceutical named

Legasil™, which uses the so-called Eurosil^{85}/Euromed formulation. Eurosil^{85}/Euromed is a patented extraction process that enhances the oral absorption and bioavailability of silibinin, has the highest intestinal permeability rate and potential to cross the BBB compared to other clinically relevant formulations of silibinin such as silibinin-meglumine –a water-soluble form of silibinin complexed with the amino-sugar meglumine– and silibinin-phosphatidylcholine – the phytolipid delivery system Siliphos™ (Pérez-Sánchez et al., 2019).

Synopsis chapter 6

- ***Silibinin is predicted to bind directly the SH2 domain of STAT3 to prevent Y705 phosphorylation-related STAT3 activation and dimerization and to establish direct interactions with DNA in its targeting to the STAT3 DNA-binding domain (DBD).***
- ***Silibinin inhibits STAT3 activation, dimerization, nuclear translocation, DNA binding, and transcriptional activity.***
- ***Silibinin may act as a bimodal SH2- and DBD-targeting STAT3 inhibitor with demonstrated therapeutic activity in brain metastasis.***
- ***Silibinin-targeted inhibition of phospho-STAT3^{+} reactive astrocytes may represent a first-in-class microenvironmental therapy against brain metastasis in NSCLC patients.***

GENERAL DISCUSSION

This dissertation project provides an in-depth, comprehensive exploration of the flavonolignan silibinin, grounded in molecular pharmacology and cancer biology, as a multifaceted therapeutic agent for the treatment of NSCLC, particularly in the context of highly unmet clinical needs such as resistance to targeted therapies and preventing or treating brain metastases.

First, we elucidated an interaction between silibinin and molecular drivers of brain metastasis-initiating cells, focusing on inhibitor of DNA-binding/differentiation 3 (ID_3). This unexpected anti-ID_3 behavior suggests a therapeutically relevant effect of silibinin in regulating the metastatic colonization capacity of NSCLC (**mechanism 1** in **Fig. 15**). Silibinin appears to achieve this ID_3 suppressive effect through transcriptional repression mediated by bone morphogenetic protein (BMP)-responsive elements and by inhibiting the kinase activity of the BMP receptors ACVRL1/ALK1 and BMPR2. The clinical relevance of these findings is supported by the in vivo efficacy of a water-soluble silibinin formulation that suppresses ID_3 overexpression at concentrations achievable in a clinical setting. Second, we addressed the challenge of NSCLC resistance to targeted therapies, in particular the EMT-driven escape of ALK-TKIs. On the one hand, we confirmed that the EMT phenomenon is a critical driver of such resistance, providing NSCLC cells with the ability to evade drug-mediated inhibition. On the other hand, we discovered the ability of silibinin to reverse EMT-induced therapeutic resistance (**mechanism 2** in **Fig. 16**), thereby restoring the efficacy of ALK TKIs. This is based on its direct modulation of the TGFβ/SMAD signaling axis. This mechanism appears to be critical as it implies a downstream effect on a large number of EMT-related genes and pathways, potentially reversing the mesenchymal phenotype and restoring the cellular sensitivity to ALK inhibition. Third, we investigated the effect of silibinin on cancer cell intrinsic mechanisms of NSCLC resistance to multi-targeted kinase inhibitors used as anti-angiogenics, such as nintedanib. In this scenario, silibinin was found to interfere with $STAT_3$ hyperactivation and nintedanib sequestration in lysosomal "drug safe houses" (**mechanism 3** in **Fig. 17**). These are two key mechanisms that causally contribute to nintedanib resistance in NSCLC cells. Accordingly, we report that the inclusion of the silibinin-containing nutraceutical Legasil® as an adjuvant has enhanced the anticancer potential of the

nintedanib/docetaxel regimen in the clinical management of patients with NSCLC. Fourth, in the context of mitigating the adverse effects of targeted therapies in NSCLC, we have extended the well-established hepatoprotective role of silibinin to combat the undesirable hyperlipidemic effects of the third-generation ALK-TKI lorlatinib (**mechanism 4** in **Fig. 18**). By protecting hepatocytes from lorlatinib-induced dysregulation of lipid metabolism and the consequent accumulation of triglycerides/cholesterol, silibinin emerges as a potential lipid-lowering adjunct in the treatment of NSCLC, particularly in ALK-positive patients predisposed to brain metastasis receiving ALK-TKI therapy. Fifth, we presented a novel approach to investigate the inhibitory interaction of silibinin with a key tumor cell intrinsic target in brain metastasis, namely HSP90. Computational predictions suggested that silibinin can mimic the binding of novobiocin to the CTD of HSP90, thereby disrupting co-chaperone-client interactions. In the absence of significant hepatotoxicity at the HSP90-inhibitory concentrations of silibinin, this mechanism holds promise as a strategy for directly targeting tumor cell intrinsic factors that promote and maintain brain metastasis colonization (**mechanism 5** in **Fig. 19**). Sixth and finally, we have described the bimodal inhibition of $STAT_3$ by silibinin through its targeting of the phospho-activating/dimerizing SH_2 and DBD domains. By preventing the activation, dimerization, nuclear translocation, and DNA-binding capacity of $STAT_3$, silibinin ultimately interferes with the $STAT_3$-driven transcriptional activity associated with the pro-metastatic activity of RA surrounding metastatic lesions in the brain (**mechanism 6** in **Fig. 20**). The therapeutic implications of this bimodal inhibition strategy are profound and offer a potentially groundbreaking approach to brain microenvironment therapy for brain-metastatic NSCLC patients.

Collectively, our findings highlight the flavonolignan silibinin as a multifaceted molecule capable of acting on multiple molecular pathways to circumvent therapeutic resistance and thwart brain metastasis in NSCLC (**Fig. 21**). Our findings underscore the potential of silibinin (or silibinin derivatives) to synergize with existing therapies, to overcome mechanisms of therapeutic resistance, and to prevent and/or treat brain metastases that are currently untreatable. The complexity of silibinin's pharmacodynamics, ranging from direct molecular interactions to broader systemic effects, may provide a compelling rationale for its incorporation into future treatment paradigms, heralding a new chapter in NSCLC therapeutics. Given that the prevention and treatment of metastatic disease remains a highly

unmet clinical need in advanced NSCLC, it may be tempting to suggest that silibinin and/or next-generation silibinin derivatives would be incorporated into the scarce armamentarium currently available for the prevention and treatment of biologically aggressive NSCLC subtypes prone to brain metastasis. Critical drivers for silibinin sensitivity versus resistance in specific NSCLC molecular subtypes can be identified using CRISPR-based functional genomics. In this regard, we have recently used CRISPR-based chemosensitivity screenings to unravel the selective vulnerability of silibinin-treated cancer cells to the glutamine fructose-6-phosphate aminotransferase 2 (GFPT2) inhibitor azaserine, thereby illustrating how the therapeutic use of silibinin could be capitalized in specific NSCLC subtypes (e.g., *KRAS/STK11* co-mutant tumors) with exquisite dependence on the (azaserine-targeted) hexosamine biosynthetic pathway (see **Appendix I**). Nevertheless, we recognize the need for prospective, powered clinical trials to confirm the clinical relevance of silibinin-based therapeutic interventions in patients with advanced NSCLC.

Silibinin treatment has been considered exceptionally safe after acute or long-term chronic administration in both animals and humans. Thus, using silibinin as a lead structure, one could speculate on the generation of a battery of derivatives with improved selectivity towards brain metastatic cancer cells and enhanced brain targeting. One could envision a medicinal chemistry approach involving physical (e.g., incorporation of permeability enhancers, carriers as protective and delivery systems, application of benign biodegradable polymers) or chemical (e.g., non-targeted or cell compartment-targeted approaches to improve lipophilicity/membrane permeability, product penetration into the gastrointestinal tract, protection against degradation, and enhanced stability to promote gastrointestinal absorption) approaches to the design and synthesis of a battery of silibinin derivatives with improved medicinal properties over the parent molecule will ensure sufficient novelty and utility to allow their patent registration.

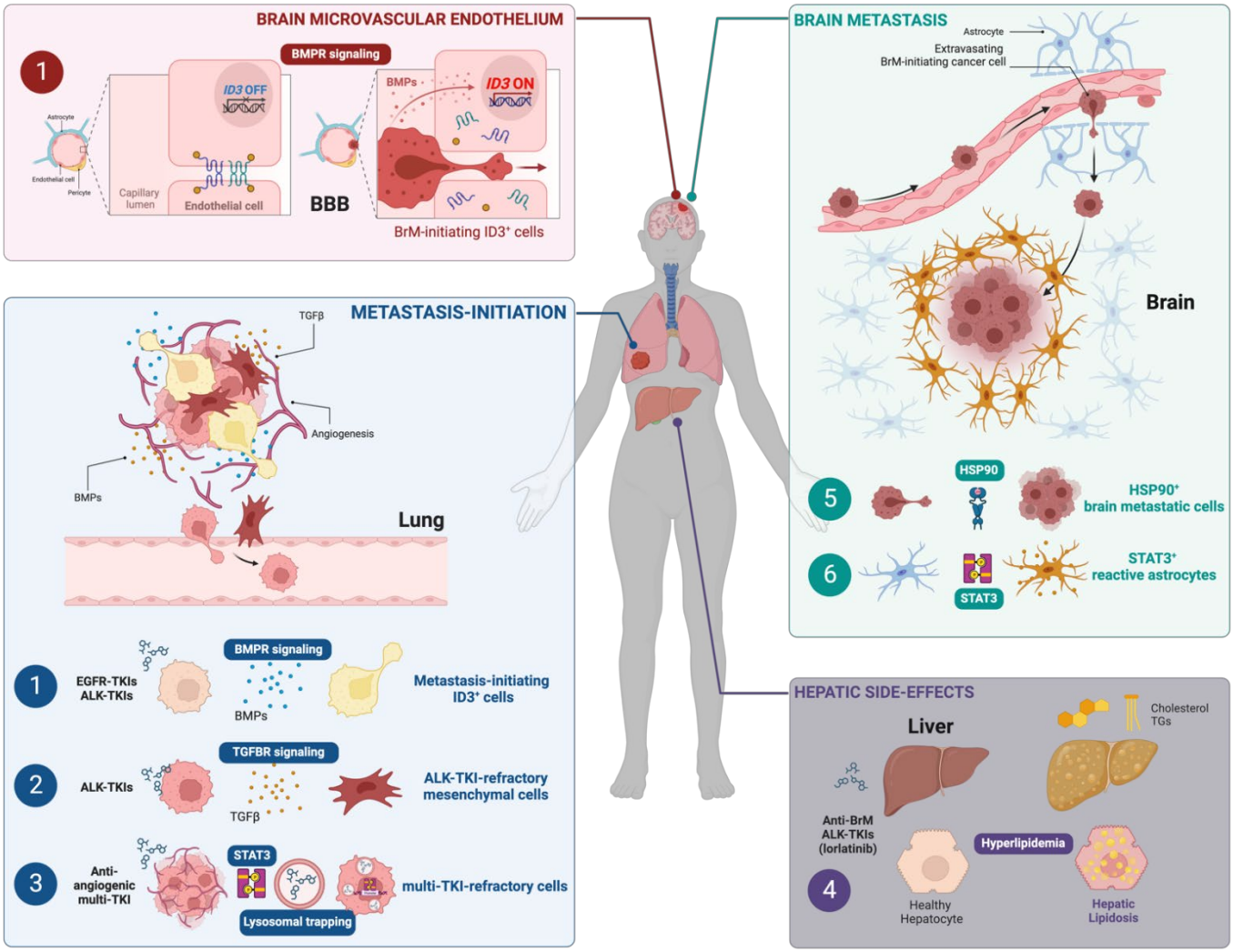

Figure 21. The flavonolignan silibinin in NSCLC: Molecular mechanisms and therapeutic implications. Created with Biorender. Our studies have shown that silibinin exhibits a variety of molecular mechanisms that could be exploited therapeutically to target the metastatic progression of NSCLC. It has been shown that silibinin suppresses several pathways directly or indirectly associated with the metastatic capacity of NSCLC, including the expression of the pro-metastatic ID3 transcription factor in tumor cells and brain endothelial cells, which enhances metastasis-initiation and immune-escape properties at the primary tumor site as well as at the BBB extravasation sites (**mechanism 1**), the acquisition of an EMT-driven, multi-resistant motile phenotype (**mechanism 2**), and the cancer cell-intrinsic resistance mechanisms (i.e., STAT3 hyperactivation and lysosomal trapping) to anti-angiogenic drugs (i.e., the multi-TKI nintedanib) (**mechanism 3**). Silibinin was found to prevent hepatic lipidosis, an undesirable side-effect that impairs the therapeutic efficacy of ALK-TKIs with anti-brain metastatic activity (i.e., lorlatinib; **mechanism 4**). Silibinin was predicted to directly interact with key molecular targets (cancer cell-intrinsic and microenvironmental) that

maintain and promote the survival and growth of NSCLC metastatic cells in the brain environment. One such intrinsic mechanism involves HSP90, an ATP-dependent molecular chaperone that is critical for the proper localization, folding, and stability of its client proteins in the stressful brain environment (**mechanism 5**). A microenvironmental mechanism involves activation of $STAT_3$ in a subpopulation of reactive astrocytes, which is required to enable colonization and adaptation of disseminated NSCLC cells to the brain microenvironment (**mechanism 6**). The dual role of silibinin in inhibiting both cancer cell intrinsic and microenvironmental drivers of brain metastasis (HSP90 and $STAT_3$, respectively), its non-toxic nature, and its ability to cross the BBB provide a compelling rationale for its use as a therapeutic scaffold for the development of safer and more effective anti-brain metastasis therapies in NSCLC patients. Clinical use of the BBB-permeable, silibinin-containing nutraceutical (Legasil™) has demonstrated significant effects against brain metastases in NSCLC patients, with improved survival times and a reduction in brain tumor-associated swelling. BBB: Blood Brain Barrier; BrM: Brain Metastasis.

VI. CONCLUSIONS

In conclusion, our phenotypic drug discovery approach has confirmed that:

The molecular promiscuity of silibinin to target multi-factorial mechanisms underlying the biological aggressiveness of NSCLC tumors, including those that drive therapeutic resistance and the ability to metastasize and colonize the brain, can be exploited to develop novel prevention and treatment strategies for NSCLC. This conclusion is based on the following discoveries:

1. **Silibinin is a suppressor of the metastasis-promoting transcription factor ID3 in NSCLC tumor cells and brain endothelial cells.**

2. **Silibinin overcomes the EMT-driven NSCLC resistance to next-generation ALK-TKIs.**

3. **Silibinin suppresses NSCLC-intrinsic resistance to the anti-angiogenic multi-TKI nintedanib.**

4. **Silibinin suppresses the hyperlipidemic effects of the third-generation ALK-TKI lorlatinib in hepatic cells.**

5. **Silibinin is a novobiocin-like C-terminal domain inhibitor of HSP90, a tumor cell-intrinsic target in NSCLC brain metastatic cells.**

6. **Silibinin is a direct, dual-mode inhibitor of STAT3, a microenvironment target in the reactive astrocytes that maintain NSCLC brain metastasis.**

The polypharmacology of the phytochemical silibinin, a flavonolignan derived from the milk thistle plant, may be a valuable strategy in the nutraceutical treatment of NSCLC using clinically relevant formulations of silibinin.

Lessons learned from the natural chemistry of silibinin could be a guide for the development of next-generation silibinin derivatives with improved therapeutic activities against NSCLC.

VII. BIBLIOGRAPHY

Abenavoli, L., Capasso, R., Milic, N., & Capasso, F. (2010). Milk thistle in liver diseases: Past, present, future. In *Phytotherapy Research* (Vol. 24, Issue 10, pp. 1423–1432). https://doi.org/10.1002/ptr.3207

Abenavoli, L., Izzo, A. A., Milić, N., Cicala, C., Santini, A., & Capasso, R. (2018). Milk thistle (Silybum marianum): A concise overview on its chemistry, pharmacological, and nutraceutical uses in liver diseases. In *Phytotherapy Research* (Vol. 32, Issue 11, pp. 2202–2213). John Wiley and Sons Ltd. https://doi.org/10.1002/ptr.6171

Akhtar, M., Haider, A., Rashid, S., & Al-Nabet, A. D. M. H. (2019). Paget's "seed and Soil" Theory of Cancer Metastasis: An Idea Whose Time has Come. *Advances in Anatomic Pathology*, *26*(1), 69–74. https://doi.org/10.1097/PAP.0000000000000219

Aktas, B., Tewes, M., Fehm, T., Hauch, S., Kimmig, R., & Kasimir-Bauer, S. (2009). Stem cell and epithelial-mesenchymal transition markers are frequently overexpressed in circulating tumor cells of metastatic breast cancer patients. *Breast Cancer Research*, *11*(4), 1–9. https://doi.org/10.1186/bcr2333

Alberg, A. J., Brock, M. V., Ford, J. G., Samet, J. M., & Spivack, S. D. (2013). Epidemiology of Lung Cancer. *CHEST*, *Diagnosis and Management of Lung Cancer*. https://doi.org/10.1378/chest.1435S1

Alberg, A. J., & Samet, J. M. (2003). Epidemiology of lung cancer. In *Chest* (Vol. 123, Issue 1 SUPPL., pp. 21S-49S). American College of Chest Physicians. https://doi.org/10.1378/chest.123.1_suppl.21S

Aldea, M., Andre, F., Marabelle, A., Dogan, S., Barlesi, F., & Soria, J. C. (2021). Overcoming resistance to tumor-targeted and immune-targeted therapies. In *Cancer Discovery* (Vol. 11, Issue 4, pp. 874–899). American Association for Cancer Research Inc. https://doi.org/10.1158/2159-8290.CD-20-1638

Alexandrov, L. B., Nik-Zainal, S., Wedge, D. C., Aparicio, S. A. J. R., Behjati, S., Biankin, A. V., Bignell, G. R., Bolli, N., Borg, A., Børresen-Dale, A. L., Boyault, S., Burkhardt, B., Butler, A. P., Caldas, C., Davies, H. R., Desmedt, C., Eils, R., Eyfjörd, J. E., Foekens, J. A., … Stratton, M. R. (2013). Signatures of mutational processes in human cancer. *Nature*, *500*(7463), 415–421. https://doi.org/10.1038/nature12477

Altorki, N. K., Markowitz, G. J., Gao, D., Port, J. L., Saxena, A., Stiles, B., McGraw, T., & Mittal, V. (2019). The lung microenvironment: an important regulator of tumour growth

and metastasis. In *Nature Reviews Cancer* (Vol. 19, Issue 1, pp. 9–31). Nature Publishing Group. https://doi.org/10.1038/s41568-018-0081-9

Anton Gillessen, & Hartmut H-J Schmidt. (2020). Silymarin as Supportive Treatment in Liver Diseases: A Narrative Review. *Adv Ther*, *37*, 1279–1301. https://doi.org/10.6084/m9.figshare.11778396

Ashrafi, A., Akter, Z., Modareszadeh, P., Modareszadeh, P., Berisha, E., Alemi, P. S., Chacon Castro, M. del C., Deese, A. R., & Zhang, L. (2022). Current Landscape of Therapeutic Resistance in Lung Cancer and Promising Strategies to Overcome Resistance. In *Cancers* (Vol. 14, Issue 19). MDPI. https://doi.org/10.3390/cancers14194562

Awasthi, N., Hinz, S., Brekken, R. A., Schwarz, M. A., & Schwarz, R. E. (2015). Nintedanib, a triple angiokinase inhibitor, enhances cytotoxic therapy response in pancreatic cancer. *Cancer Letters*, *358*(1), 59–66. https://doi.org/10.1016/j.canlet.2014.12.027

Bade, B. C., & Dela Cruz, C. S. (2020). Lung Cancer 2020: Epidemiology, Etiology, and Prevention. In *Clinics in Chest Medicine* (Vol. 41, Issue 1, pp. 1–24). W.B. Saunders. https://doi.org/10.1016/j.ccm.2019.10.001

Barrott, J. J., & Haystead, T. A. J. (2013). Hsp90, an unlikely ally in the war on cancer. In *FEBS Journal* (Vol. 280, Issue 6, pp. 1381–1396). https://doi.org/10.1111/febs.12147

Bauer, T. M., Felip, E., Solomon, B. J., Thurm, H., Peltz, G., Chioda, M. D., & Shaw, A. T. (2019). Clinical Management of Adverse Events Associated with Lorlatinib. *The Oncologist*, *24*(8), 1103–1110. https://doi.org/10.1634/theoncologist.2018-0380

Baxevanos, P., & Mountzios, G. (2018). Novel chemotherapy regimens for advanced lung cancer: have we reached a plateau? *Annals of Translational Medicine*, *6*(8), 139–139. https://doi.org/10.21037/atm.2018.04.04

Bijak, M. (2017). Silybin, a Major Bioactive Component of Milk Thistle (Silybum marianum L. Gaernt.)—Chemistry, Bioavailability, and Metabolism. In *Molecules* (Vol. 22, Issue 11). MDPI AG. https://doi.org/10.3390/molecules22111942

Blais, N., Adam, J. P., Nguyen, J., & Grégoire, J. C. (2021). Evaluation and management of dyslipidemia in patients treated with lorlatinib. *Current Oncology*, *28*(1), 265–272. https://doi.org/10.3390/curroncol28010029

Bocci, M., Sjölund, J., Kurzejamska, E., Lindgren, D., Marzouka, N. A. D., Bartoschek, M., Höglund, M., & Pietras, K. (2019). Activin receptor-like kinase 1 is associated with

immune cell infiltration and regulates CLEC14A transcription in cancer. *Angiogenesis*, *22*(1), 117–131. https://doi.org/10.1007/s10456-018-9642-5

Boffa, D. J. (2018). The eighth edition lung cancer stage classification. In *Lung Cancer: A Practical Approach to Evidence-Based Clinical Evaluation and Management* (pp. 57–66). Elsevier. https://doi.org/10.1016/B978-0-323-48565-4.00003-5

Bohrer, L. R., Chuntova, P., Bade, L. K., Beadnell, T. C., Leon, R. P., Brady, N. J., Ryu, Y., Goldberg, J. E., Schmechel, S. C., Koopmeiners, J. S., McCarthy, J. B., & Schwertfeger, K. L. (2014). Activation of the FGFR-STAT3 pathway in breast cancer cells induces a hyaluronan-rich microenvironment that licenses tumor formation. *Cancer Research*, *74*(1), 374–386. https://doi.org/10.1158/0008-5472.CAN-13-2469

Bosch, M. E., Díez, R. A., Agudo, S. G., & Estela, A. C. (2016). Nintedanib in combination with docetaxel for second-line treatment of advanced non-small-cell lung cancer; GENESIS-SEFH drug evaluation report. *Farmacia Hospitalaria*, *40*(4), 316–327. https://doi.org/10.7399/fh.2016.40.4.10455

Bosch-Barrera, J., & Menendez, J. A. (2015). Silibinin and STAT3: A natural way of targeting transcription factors for cancer therapy. In *Cancer Treatment Reviews* (Vol. 41, Issue 6). https://doi.org/10.1016/j.ctrv.2015.04.008

Bosch-Barrera, J., Sais, E., Cañete, N., Marruecos, J., Cuyàs, E., Izquierdo, A., Porta, R., Haro, M., Brunet, J., Pedraza, S., & Menendez, J. A. (2016). Response of brain metastasis from lung cancer patients to an oral nutraceutical product containing silibinin. *Oncotarget*, *7*(22), 32006–32014. https://doi.org/10.18632/oncotarget.7900

Boyero, L., Sánchez-Gastaldo, A., Alonso, M., Noguera-Uclés, J. F., Molina-Pinelo, S., & Bernabé-Caro, R. (2020). Primary and acquired resistance to immunotherapy in lung cancer: Unveiling the mechanisms underlying of immune checkpoint blockade therapy. In *Cancers* (Vol. 12, Issue 12, pp. 1–36). MDPI AG. https://doi.org/10.3390/cancers12123729

Brabletz, T., Jung, A., Reu, S., Porzner, M., Hlubek, F., Kunz-Schughart, L. A., Knuechel, R., & Kirchner, T. (2001). Variable β-catenin expression in colorectal cancers indicates tumor progression driven by the tumor environment. *Proceedings of the National Academy of Sciences of the United States of America*, *98*(18), 10356–10361. https://doi.org/10.1073/pnas.171610498

Byun, H. J., Darvin, P., Kang, D. Y., Sp, N., Joung, Y. H., Park, J. H., Kim, S. J., & Yang, Y. M. (2017). Silibinin downregulates MMP2 expression via Jak2/STAT3 pathway and inhibits the migration and invasive potential in MDA-MB-231 cells. *Oncology Reports*, *37*(6), 3270–3278. https://doi.org/10.3892/or.2017.5588

Castañon, E., Bosch-Barrera, J., López, I., Collado, V., Moreno, M., López-Picazo, J. M., Arbea, L., Lozano, M. D., Calvo, A., & Gil-Bazo, I. (2013). Id1 and Id3 co-expression correlates with clinical outcome in stage III-N2 non-small cell lung cancer patients treated with definitive chemoradiotherapy. *Journal of Translational Medicine*, *11*(1). https://doi.org/10.1186/1479-5876-11-13

Cells, C. C., Brien, C. A. O., Kreso, A., Ryan, P., Hermans, K. G., Gibson, L., Wang, Y., Tsatsanis, A., Gallinger, S., & Dick, J. E. (2012). Article ID1 and ID3 Regulate the Self-Renewal Capacity. *Cancer Cell*, *21*(6), 777–792. https://doi.org/10.1016/j.ccr.2012.04.036

Cha, Y. J., Cho, B. C., Kim, H. R., Lee, H. J., & Shim, H. S. (2016). A case of ALK-rearranged adenocarcinoma with small cell carcinoma-like transformation and resistance to crizotinib. *Journal of Thoracic Oncology*, *11*(5), e55–e58. https://doi.org/10.1016/j.jtho.2015.12.097

Chaffer, C. L., & Weinberg, R. A. (2011). A perspective on cancer cell metastasis. *Science*, *331*(6024), 1559–1564. https://doi.org/10.1126/science.1203543

Chan, B. A., & Hughes, B. G. M. (2015). Targeted therapy for non-small cell lung cancer: Current standards and the promise of the future. In *Translational Lung Cancer Research* (Vol. 4, Issue 1, pp. 36–54). https://doi.org/10.3978/j.issn.2218-6751.2014.05.01

Charles S. Dela Cruz, Lynn T. Tanoue, & Richard A. Matthay. (2011). Lung Cancer: Epidemiology, Etiology, and Prevention. *Clin Chest Med*, *32*(4), 11. https://doi.org/10.1016/j.ccm.2011.09.001.Lung

Chatterjee, S., Bhattacharya, S., Socinski, M. A., & Burns, T. F. (2016). HSP90 Inhibitors in Lung Cancer: Promise Still Unfulfilled. In *Clinical Advances in Hematology & Oncology* (Vol. 14, Issue 5).

Chen, P. N., Hsieh, Y. S., Chiou, H. L., & Chu, S. C. (2005). Silibinin inhibits cell invasion through inactivation of both PI3K-Akt and MAPK signaling pathways. *Chemico-Biological Interactions*, *156*(2–3), 141–150. https://doi.org/10.1016/j.cbi.2005.08.005

Chen, W., Shi, Y., Qi, S., Zhou, H., Li, C., Jin, D., & Li, G. (2019). Pharmacokinetic study and tissue distribution of lorlatinib in mouse serum and tissue samples by liquid

chromatography-mass spectrometry. *Journal of Analytical Methods in Chemistry*, *2019*. https://doi.org/10.1155/2019/7574369

Chen, X., Chen, S., & Yu, D. (2020). Metabolic reprogramming of chemoresistant cancer cells and the potential significance of metabolic regulation in the reversal of cancer chemoresistance. In *Metabolites* (Vol. 10, Issue 7, pp. 1–15). MDPI AG. https://doi.org/10.3390/metabo10070289

Chittezhath, M., Deep, G., Singh, R. P., Agarwal, C., & Agarwal, R. (2008). Silibinin inhibits cytokine-induced signaling cascades and down-regulates inducible nitric oxide synthase in human lung carcinoma A549 cells. *Molecular Cancer Therapeutics*, *7*(7), 1817–1826. https://doi.org/10.1158/1535-7163.MCT-08-0256

Choi, Y. L., Yamashita, Y., Ueno, T., Takashima, J., Nakajima, T., Yatabe, Y., Takeuchi, K., Hamada, T., Haruta, H., Ishikawa, Y., Kimura, H., Mitsudomi, T., Tanio, Y., & Mano, H. (2010). EML4-ALK Mutations in Lung Cancer That Confer Resistance to ALK Inhibitors. In *n engl j med* (Vol. 18).

Choo, J. R. E., & Soo, R. A. (2020). Lorlatinib for the treatment of ALK-positive metastatic non-small cell lung cancer. *Expert Review of Anticancer Therapy*, *20*(4), 233–240. https://doi.org/10.1080/14737140.2020.1744438

Chu, S. C., Chiou, H. L., Chen, P. H., Yang, S. F., & Hsieh, Y. S. (2004). Silibinin inhibits the invasion of human lung cancer cells via decreased productions of urokinase-plasminogen activator and matrix metalloproteinase-2. *Molecular Carcinogenesis*, *40*(3), 143–149. https://doi.org/10.1002/mc.20018

Coakley, M., & Popat, S. (2020). Management of lung cancer. In *Medicine (United Kingdom)* (Vol. 48, Issue 4, pp. 273–278). Elsevier Ltd. https://doi.org/10.1016/j.mpmed.2020.01.003

Collins, L. G., Haines, C., Perkel, R., & Enck, R. E. (2007). *Lung Cancer: Diagnosis and Management*. http://familydoctor.org/161.xml.

Collisson, E. A., Campbell, J. D., Brooks, A. N., Berger, A. H., Lee, W., Chmielecki, J., Beer, D. G., Cope, L., Creighton, C. J., Danilova, L., Ding, L., Getz, G., Hammerman, P. S., Hayes, D. N., Hernandez, B., Herman, J. G., Heymach, J. V., Jurisica, I., Kucherlapati, R., … Cheney, R. (2014). Comprehensive molecular profiling of lung adenocarcinoma: The cancer genome atlas research network. *Nature*, *511*(7511), 543–550. https://doi.org/10.1038/nature13385

Corominas-Faja, B., Oliveras-Ferraros, C., Cuyàs, E., Segura-Carretero, A., Joven, J., Martin-Castillo, B., Barrajón-Catalán, E., Micol, V., Bosch-Barrera, J., & Menendez, J. A. (2013). Stem cell-like ALDHbright cellular states in EGFR-mutant non-small cell lung cancer a novel mechanism of acquired resistance to erlotinib targetable with the natural polyphenol silibinin. *Cell Cycle*, *12*(21). https://doi.org/10.4161/cc.26417

Corral, J., Majem, M., Rodríguez-Abreu, D., Carcereny, E., Cortes, A., Llorente, M., López Picazo, J. M., García, Y., Domine, M., & López Criado, M. P. (2019). Efficacy of nintedanib and docetaxel in patients with advanced lung adenocarcinoma treated with first-line chemotherapy and second-line immunotherapy in the nintedanib NPU program. *Clinical and Translational Oncology*, *21*(9), 1270–1279. https://doi.org/10.1007/s12094-019-02053-7

Craene, B. De, & Berx, G. (2013). Regulatory networks defining EMT during cancer initiation and progression. *Nature Reviews Cancer*, *13*(2), 97–110. https://doi.org/10.1038/nrc3447

Cree, I. A., & Charlton, P. (2017). Molecular chess? Hallmarks of anti-cancer drug resistance. In *BMC Cancer* (Vol. 17, Issue 1). BioMed Central Ltd. https://doi.org/10.1186/s12885-016-2999-1

Cufí, S., Bonavia, R., Vazquez-Martin, A., Corominas-Faja, B., Oliveras-Ferraros, C., Cuyàs, E., Martin-Castillo, B., Barrajón-Catalán, E., Visa, J., Segura-Carretero, A., Bosch-Barrera, J., Joven, J., Micol, V., & Menendez, J. A. (2013). Silibinin meglumine, a water-soluble form of milk thistle silymarin, is an orally active anti-cancer agent that impedes the epithelial-to-mesenchymal transition (EMT) in EGFR-mutant non-small-cell lung carcinoma cells. *Food and Chemical Toxicology*, *60*. https://doi.org/10.1016/j.fct.2013.07.063

Cufí, S., Bonavia, R., Vazquez-Martin, A., Oliveras-Ferraros, C., Corominas-Faja, B., Cuyàs, E., Martin-Castillo, B., Barrajón-Catalán, E., Visa, J., Segura-Carretero, A., Joven, J., Bosch-Barrera, J., Micol, V., & Menendez, J. A. (2013). Silibinin suppresses EMT-driven erlotinib resistance by reversing the high miR-21/low miR-200c signature in vivo. *Scientific Reports*. https://doi.org/10.1038/srep02459

Cuyàs, E., Pérez-Sánchez, A., Micol, V., Menendez, J. A., & Bosch-Barrera, J. (2016). STAT3-targeted treatment with silibinin overcomes the acquired resistance to crizotinib in ALK-rearranged lung cancer. *Cell Cycle*, *15*(24), 3413–3418. https://doi.org/10.1080/15384101.2016.1245249

Dagogo-Jack, I., & Shaw, A. T. (2016). Crizotinib resistance: Implications for therapeutic strategies. In *Annals of Oncology* (Vol. 27, pp. iii42–iii50). Oxford University Press. https://doi.org/10.1093/annonc/mdw305

Dardaei, L., Wang, H. Q., Singh, M., Fordjour, P., Shaw, K. X., Yoda, S., Kerr, G., Yu, K., Liang, J., Cao, Y., Chen, Y., Lawrence, M. S., Langenbucher, A., Gainor, J. F., Friboulet, L., Dagogo-Jack, I., Myers, D. T., Labrot, E., Ruddy, D., … Engelman, J. A. (2018). SHP2 inhibition restores sensitivity in ALK-rearranged non-small-cell lung cancer resistant to ALK inhibitors. *Nature Medicine*, *24*(4), 512–517. https://doi.org/10.1038/nm.4497

Das, J. K., & Felty, Q. (2014). PCB153-induced overexpression of ID3 contributes to the development of microvascular lesions. *PLoS ONE*, *9*(8). https://doi.org/10.1371/journal.pone.0104159

de Jong, D., Das, J. P., Ma, H., Pailey Valiplackal, J., Prendergast, C., Roa, T., Braumuller, B., Deng, A., Dercle, L., Yeh, R., Salvatore, M. M., & Capaccione, K. M. (2023). Novel Targets, Novel Treatments: The Changing Landscape of Non-Small Cell Lung Cancer. In *Cancers* (Vol. 15, Issue 10). MDPI. https://doi.org/10.3390/cancers15102855

Dingcheng Gao, D. J. N. A. S. M. K. B. K. M. V. M. (2008). Endothelial Progenitor Cells Controlthe Angiogenic Switch in MouseLung Metastasis. *Science*, *319*(195), 195–198.

Dinic, J., Podolski-Renic, A., Stankovic, T., Bankovic, J., & Pesic, M. (2015). New Approaches With Natural Product Drugs for Overcoming Multidrug Resistance in Cancer. *Current Pharmaceutical Design*, *21*(38), 5589–5604. https://doi.org/10.2174/1381612821666151002113546

Dobiasová, S., Řehořová, K., Kučerová, D., Biedermann, D., Káňová, K., Petrásková, L., Koucká, K., Václavíková, R., Valentová, K., Ruml, T., Macek, T., Křen, V., & Viktorová, J. (2020). Multidrug resistance modulation activity of silybin derivatives and their anti-inflammatory potential. *Antioxidants*, *9*(5). https://doi.org/10.3390/antiox9050455

Dong, J., Li, B., Lin, D., Zhou, Q., & Huang, D. (2019). Advances in Targeted Therapy and Immunotherapy for Non-small Cell Lung Cancer Based on Accurate Molecular Typing. In *Frontiers in Pharmacology* (Vol. 10). Frontiers Media S.A. https://doi.org/10.3389/fphar.2019.00230

Dongre, A., & Weinberg, R. A. (2019). New insights into the mechanisms of epithelial–mesenchymal transition and implications for cancer. *Nature Reviews Molecular Cell Biology*, *20*(2), 69–84. https://doi.org/10.1038/s41580-018-0080-4

Du, B., & Shim, J. S. (2016). Targeting epithelial-mesenchymal transition (EMT) to overcome drug resistance in cancer. In *Molecules* (Vol. 21, Issue 7). MDPI AG. https://doi.org/10.3390/molecules21070965

Du, X., Shao, Y., Qin, H. F., Tai, Y. H., & Gao, H. J. (2018). ALK-rearrangement in non-small-cell lung cancer (NSCLC). *Thoracic Cancer*, *9*(4), 423–430. https://doi.org/10.1111/1759-7714.12613

Eberhardt, W. E. E., De Ruysscher, D., Weder, W., Le Péchoux, C., De Leyn, P., Hoffmann, H., Westeel, V., Stahel, R., Felip, E., Peters, S., Kerr, K., Besse, B., Vansteenkiste, J., Edelman, M., Mok, T., O'Byrne, K., Novello, S., Bubendorf, L., Marchetti, A., … Dooms, C. (2015). 2nd ESMO Consensus Conference in Lung Cancer: Locally advanced stage III non-small-cell lung cancer. *Annals of Oncology*, *26*(8), 1573–1588. https://doi.org/10.1093/annonc/mdv187

Engelman, J., Zejnullahu, K., Mitsudomi T, & et al. (2007). MET Amplification Leads to Gefitinib Resistance in Lung Cancer by Activating ERBB3 Signaling. *Science*, *316*, 1039–1043.

Englinger, B., Kallus, S., Senkiv, J., Heilos, D., Gabler, L., Van Schoonhoven, S., Terenzi, A., Moser, P., Pirker, C., Timelthaler, G., Jäger, W., Kowol, C. R., Heffeter, P., Grusch, M., & Berger, W. (2017). Intrinsic fluorescence of the clinically approved multikinase inhibitor nintedanib reveals lysosomal sequestration as resistance mechanism in FGFR-driven lung cancer. *Journal of Experimental and Clinical Cancer Research*, *36*(1). https://doi.org/10.1186/s13046-017-0592-3

Enright, T. L., Witt, J. S., Burr, A. R., Yadav, P., Leal, T., & Baschnagel, A. M. (2021). Combined Immunotherapy and Stereotactic Radiotherapy Improves Neurologic Outcomes in Patients with Non–small-cell Lung Cancer Brain Metastases. *Clinical Lung Cancer*, *22*(2), 110–119. https://doi.org/10.1016/j.cllc.2020.10.014

Ernani, V., & Stinchcombe, T. E. (2019). Management of Brain Metastases in Non-Small-Cell Lung Cancer. In *J Oncol Pract* (Vol. 15). https://doi.org/10.

Eslami-S, Z., Cortés-Hernández, L. E., & Alix-Panabières, C. (2020). The Metastatic Cascade as the Basis for Liquid Biopsy Development. In *Frontiers in Oncology* (Vol. 10). Frontiers Media S.A. https://doi.org/10.3389/fonc.2020.01055

Ettinger, D. S., Wood, D. E., Aisner, D. L., Akerley, W., Bauman, J. R., Bharat, A., Bruno, D. S., Chang, J. Y., Chirieac, L. R., D'Amico, T. A., DeCamp, M., Dilling, T. J., Dowell, J.,

Gettinger, S., Grotz, T. E., Gubens, M. A., Hegde, A., Lackner, R. P., Lanuti, M., … Hughes, M. (2022). Non-Small Cell Lung Cancer, Version 3.2022. *JNCCN Journal of the National Comprehensive Cancer Network*, *20*(5), 497–530. https://doi.org/10.6004/jnccn.2022.0025

Ettinger, D. S., Wood, D. E., Aisner, D. L., Akerley, W., Bauman, J. R., Bharat, A., Bruno, D. S., Chang, J. Y., Chirieac, L. R., D'Amico, T. A., Dilling, T. J., Dowell, J., Gettinger, S., Gubens, M. A., Hegde, A., Hennon, M., Lackner, R. P., Lanuti, M., Leal, T. A., … Hughes, M. (2021). NCCN Guidelines Insights: Non–Small Cell Lung Cancer, Version 2.2021. *Journal of the National Comprehensive Cancer Network*, *19*(3), 254–266. https://doi.org/10.6004/jnccn.2021.0013

Federico, A., Dallio, M., & Loguercio, C. (2017). Silymarin/Silybin and chronic liver disease: A marriage of many years. In *Molecules* (Vol. 22, Issue 2). MDPI AG. https://doi.org/10.3390/molecules22020191

Frampton, G. M., Ali, S. M., Rosenzweig, M., Chmielecki, J., Lu, X., Bauer, T. M., Akimov, M., Bufill, J. A., Lee, C., Jentz, D., Hoover, R., Ignatius Ou, S. H., Salgia, R., Brennan, T., Chalmers, Z. R., Jaeger, S., Huang, A., Elvin, J. A., Erlich, R., … Miller, V. A. (2015). Activation of MET via diverse exon 14 splicing alterations occurs in multiple tumor types and confers clinical sensitivity to MET inhibitors. *Cancer Discovery*, *5*(8), 850–860. https://doi.org/10.1158/2159-8290.CD-15-0285

Fukuda, K., Takeuchi, S., Arai, S., Katayama, R., Nanjo, S., Tanimoto, A., Nishiyama, A., Nakagawa, T., Taniguchi, H., Suzuki, T., Yamada, T., Nishihara, H., Ninomiya, H., Ishikawa, Y., Baba, S., Takeuchi, K., Horiike, A., Yanagitani, N., Nishio, M., & Yano, S. (2019). Epithelial-to-mesenchymal transition is a mechanism of ALK inhibitor resistance in lung cancer independent of ALK mutation status. *Cancer Research*, *79*(7), 1658–1670. https://doi.org/10.1158/0008-5472.CAN-18-2052

Furtek, S. L., Backos, D. S., Matheson, C. J., & Reigan, P. (2016). Strategies and Approaches of Targeting STAT3 for Cancer Treatment. In *ACS Chemical Biology* (Vol. 11, Issue 2, pp. 308–318). American Chemical Society. https://doi.org/10.1021/acschembio.5b00945

Gainor, J. F., & Shaw, A. T. (2013). Emerging paradigms in the development of resistance to tyrosine kinase inhibitors in lung cancer. In *Journal of Clinical Oncology* (Vol. 31, Issue 31, pp. 3987–3996). American Society of Clinical Oncology. https://doi.org/10.1200/JCO.2012.45.2029

Ganesh, K., & Massagué, J. (2021). Targeting metastatic cancer. In *Nature Medicine* (Vol. 27, Issue 1, pp. 34–44). Nature Research. https://doi.org/10.1038/s41591-020-01195-4

Gazdar, A. F., Bunn, P. A., & Minna, J. D. (2017). Small-cell lung cancer: What we know, what we need to know and the path forward. *Nature Reviews Cancer*, *17*(12), 725–737. https://doi.org/10.1038/nrc.2017.87

Genova, C., Rijavec, E., Truini, A., Coco, S., Sini, C., Barletta, G., Dal Bello, M. G., Alama, A., Savarino, G., Pronzato, P., Boccardo, F., & Grossi, F. (2013). Pemetrexed for the treatment of non-small cell lung cancer. *Expert Opinion on Pharmacotherapy*, *14*(11), 1545–1558. https://doi.org/10.1517/14656566.2013.802774

George, J., Lim, J. S., Jang, S. J., Cun, Y., Ozretić, L., Kong, G., Leenders, F., Lu, X., Fernández-Cuesta, L., Bosco, G., Müller, C., Dahmen, I., Jahchan, N. S., Park, K.-S., Yang, D., Karnezis, A. N., Vaka, D., Torres, A., Wang, M. S., … Thomas, R. K. (2015). Comprehensive genomic profiles of small cell lung cancer. *Nature*, *524*(7563), 47–53. https://doi.org/10.1038/nature14664

Gil-Bazo, I., Castanon Alvarez, E., Lopez, I., Ponz-Sarvisé, M., Rolfo, C. D., Santisteban, M., Lopez-Picazo, J. M., Fusco, J. P., Ceniceros, L., Legaspi, J., & Soltermann, A. (2014). Inhibitor of Differentiation-1 (Id1) and Id3 Expression Correlates with Epithelial-Mesenchymal Transition (Emt)-Related Proteins (Emtrp) in Non-Small Cell Lung Carcinoma (Nsclc). *Annals of Oncology*, *25*, iv565. https://doi.org/10.1093/annonc/mdu359.6

Gouji, T., Takashi, S., Mitsuhiro, T., & Yukito, I. (2014). Crizotinib can overcome acquired resistance to CH5424802: Is amplification of the MET gene a key factor? In *Journal of Thoracic Oncology* (Vol. 9, Issue 3). https://doi.org/10.1097/JTO.0000000000000113

Gouvinhas, C., De Mello, R. A., Oliveira, D., Castro-Lopes, J. M., Castelo-Branco, P., Dos Santos, R. S., Hespanhol, V., & Pozza, D. H. (2018). Lung cancer: A brief review of epidemiology and screening. In *Future Oncology* (Vol. 14, Issue 6, pp. 567–575). Future Medicine Ltd. https://doi.org/10.2217/fon-2017-0486

Gower, A., Hsu, W. H., Hsu, S. T., Wang, Y., & Giaccone, G. (2016). EMT is associated with, but does not drive resistance to ALK inhibitors among EML4-ALK non-small cell lung cancer. *Molecular Oncology*, *10*(4), 601–609. https://doi.org/10.1016/j.molonc.2015.11.007

Gower, A., Wang, Y., & Giaccone, G. (2014). Oncogenic drivers, targeted therapies, and acquired resistance in non-small-cell lung cancer. In *Journal of Molecular Medicine* (Vol. 92, Issue 7, pp. 697–707). Springer Verlag. https://doi.org/10.1007/s00109-014-1165-y

Grohé, C., Gleiber, W., Haas, S., Losem, C., Mueller-Huesmann, H., Schulze, M., Franke, C., Basara, N., Atz, J., & Kaiser, R. (2019). Nintedanib plus docetaxel after progression on immune checkpoint inhibitor therapy: Insights from VARGADO, a prospective study in patients with lung adenocarcinoma. *Future Oncology*, *15*(23), 2699–2706. https://doi.org/10.2217/fon-2019-0262

Haider, T., Pandey, V., Banjare, N., Gupta, P. N., & Soni, V. (2020). Drug resistance in cancer: mechanisms and tackling strategies. In *Pharmacological Reports* (Vol. 72, Issue 5, pp. 1125–1151). Springer Science and Business Media Deutschland GmbH. https://doi.org/10.1007/s43440-020-00138-7

Halaby, R. (2019). Influence of lysosomal sequestration on multidrug resistance in cancer cells. In *Cancer Drug Resistance* (Vol. 2, Issue 1, pp. 31–42). OAE Publishing Inc. https://doi.org/10.20517/cdr.2018.23

Halliday, P. R., Blakely, C. M., & Bivona, T. G. (2019). Emerging Targeted Therapies for the Treatment of Non-small Cell Lung Cancer. In *Current Oncology Reports* (Vol. 21, Issue 3). Current Medicine Group LLC 1. https://doi.org/10.1007/s11912-019-0770-x

Hammerman, P. S., Voet, D., Lawrence, M. S., Voet, D., Jing, R., Cibulskis, K., Sivachenko, A., Stojanov, P., McKenna, A., Lander, E. S., Gabriel, S., Getz, G., Imielinski, M., Helman, E., Hernandez, B., Pho, N. H., Meyerson, M., Chu, A., Hye-Chun, J. E., … Shen, R. (2012). Comprehensive genomic characterization of squamous cell lung cancers. *Nature*, *489*(7417), 519–525. https://doi.org/10.1038/nature11404

Hanahan, D., & Weinberg, R. A. (2000). The Hallmarks of Cancer. *Cell*, *100*(1), 57–70. https://doi.org/10.1016/S0092-8674(00)81683-9

Hanahan, D., & Weinberg, R. A. (2011). Review Hallmarks of Cancer : The Next Generation. *Cell*, *144*(5), 646–674. https://doi.org/10.1016/j.cell.2011.02.013

Herbst, R. S., Morgensztern, D., & Boshoff, C. (2018). The biology and management of non-small cell lung cancer. In *Nature* (Vol. 553, Issue 7689, pp. 446–454). Nature Publishing Group. https://doi.org/10.1038/nature25183

Hibma, J. E., O'Gorman, M., Nepal, S., Pawlak, S., Ginman, K., & Pithavala, Y. K. (2022). Evaluation of the absolute oral bioavailability of the anaplastic lymphoma kinase/c-

ROS oncogene 1 kinase inhibitor lorlatinib in healthy participants. *Cancer Chemotherapy and Pharmacology*, *89*(1), 71–81. https://doi.org/10.1007/s00280-021-04368-1

Hilberg, F., Roth, G. J., Krssak, M., Kautschitsch, S., Sommergruber, W., Tontsch-Grunt, U., Garin-Chesa, P., Bader, G., Zoephel, A., Quant, J., Heckel, A., & Rettig, W. J. (2008). BIBF 1120: Triple angiokinase inhibitor with sustained receptor blockade and good antitumor efficacy. *Cancer Research*, *68*(12), 4774–4782. https://doi.org/10.1158/0008-5472.CAN-07-6307

Hilberg, F., Tontsch-Grunt, U., Baum, A., Le, A. T., Doebele, R. C., Lieb, S., Gianni, D., Voss, T., Garin-Chesa, P., Haslinger, C., & Kraut, N. (2018). Triple angiokinase inhibitor nintedanib directly inhibits tumor cell growth and induces tumor shrinkage via blocking oncogenic receptor tyrosine kinases. *Journal of Pharmacology and Experimental Therapeutics*, *364*(3), 494–503. https://doi.org/10.1124/jpet.117.244129

Hou, X., Du, H., Quan, X., Shi, L., Zhang, Q., Wu, Y., Liu, Y., Xiao, J., Li, Y., Lu, L., Ai, X., Zhan, M., Yuan, S., & Sun, L. (2018). Silibinin inhibits NSCLC metastasis by targeting the EGFR/LOX pathway. *Frontiers in Pharmacology*, *9*(FEB). https://doi.org/10.3389/fphar.2018.00021

Hraběta, J., Belhajová, M., Šubrtová, H., Rodrigo, M. A. M., Heger, Z., & Eckschlager, T. (2020). Drug sequestration in lysosomes as one of the mechanisms of chemoresistance of cancer cells and the possibilities of its inhibition. In *International Journal of Molecular Sciences* (Vol. 21, Issue 12, pp. 1–18). MDPI AG. https://doi.org/10.3390/ijms21124392

Hu, Y., Yagüe, E., Zhao, J., Wang, L., Bai, J., Yang, Q., Pan, T., Zhao, H., Liu, J., & Zhang, J. (2018). Sabutoclax, pan-active BCL-2 protein family antagonist, overcomes drug resistance and eliminates cancer stem cells in breast cancer. *Cancer Letters*, *423*, 47–59. https://doi.org/10.1016/j.canlet.2018.02.036

Huang, L., Cai, J., Guo, H., Gu, J., Tong, Y., Qiu, B., Wang, C., Li, M., Xia, L., Zhang, J., Wu, H., Kong, X., Xia, Q., Hospital, R., Jiao, S., Science, H., Hospital, F. A., & Medical, N. (2019). *ID3 Promotes Stem Cell Features and Predicts Chemotherapeutic Response of Intrahepatic Cholangiocarcinoma* (Vol. 65). https://doi.org/10.1002/hep.30404

Huang, S. (2007). Regulation of metastases by signal transducer and activator of transcription 3 signaling pathway: Clinical implications. In *Clinical Cancer Research*. https://doi.org/10.1158/1078-0432.CCR-06-2313

Iglesias, V. S., Giuranno, L., Dubois, L. J., Theys, J., & Vooijs, M. (2018). Drug resistance in non-small cell lung cancer: A potential for NOTCH targeting? In *Frontiers in Oncology* (Vol. 8, Issue JUL). Frontiers Media S.A. https://doi.org/10.3389/fonc.2018.00267

Jang-Ming Su, Ya-Ying Hsu, Pinpin Lin, & Han Chang. (2016). Nuclear Accumulation of Heat-shock Protein 90 Is Associated with Poor Survival and Metastasis in Patients with Non-small Cell Lung Cancer. *ANTICANCER RESEARCH*, *36*, 2197–2204.

Jayanta K Das, A. D. D. R. Q. F. (2022). Brain infiltration of breast cancer stem cells is facilitated by paracrine signaling by inhibitor of differentiation 3 to nuclear respiratory factor 1. *J Cancer Res Clin Oncol*, *148*(10), 2881–2891.

Jonckheere, S., Adams, J., De Groote, D., Campbell, K., Berx, G., & Goossens, S. (2022). Epithelial-Mesenchymal Transition (EMT) as a Therapeutic Target. In *Cells Tissues Organs* (Vol. 211, Issue 2, pp. 157–182). S. Karger AG. https://doi.org/10.1159/000512218

Kahlert, C., Lahes, S., Radhakrishnan, P., Dutta, S., Mogler, C., Herpel, E., Brand, K., Steinert, G., Schneider, M., Mollenhauer, M., Reissfelder, C., Klupp, F., Fritzmann, J., Wunder, C., Benner, A., Kloor, M., Huth, C., Contin, P., Ulrich, A., … Weitz, J. (2011). Overexpression of ZEB2 at the invasion front of colorectal cancer is an independent prognostic marker and regulates tumor invasion in Vitro. *Clinical Cancer Research*, *17*(24), 7654–7663. https://doi.org/10.1158/1078-0432.CCR-10-2816

Kaipa, J. M., Starkuviene, V., Erfle, H., Eils, R., & Gladilin, E. (2020). Transcriptome profiling reveals Silibinin dose-dependent response network in non-small lung cancer cells. *PeerJ*, *8*. https://doi.org/10.7717/peerj.10373

Kalluri, R., & Weinberg, R. A. (2009). The basics of epithelial-mesenchymal transition. *Journal of Clinical Investigation*, *119*(6), 1420–1428. https://doi.org/10.1172/JCI39104

Karachaliou, N., Mayo, C., Costa, C., Magrí, I., Gimenez-Capitan, A., Molina-Vila, M. A., & Rosell, R. (2013). KRAS mutations in lung cancer. In *Clinical Lung Cancer* (Vol. 14, Issue 3, pp. 205–214). https://doi.org/10.1016/j.cllc.2012.09.007

Kawada, I., & Soejima, K. (2008). Screening of epidermal growth factor receptor mutation in lung cancer. In *Respiration and Circulation* (Vol. 56, Issue 6, pp. 617–622). https://doi.org/10.1056/nejmoa0904554

Kim, H. R., Kim, W. S., Choi, Y. J., Choi, C. M., Rho, J. K., & Lee, J. C. (2013). Epithelial-mesenchymal transition leads to crizotinib resistance in H2228 lung cancer cells with

EML4-ALK translocation. *Molecular Oncology*, *7*(6), 1093–1102. https://doi.org/10.1016/j.molonc.2013.08.001

Kim, S., Jeon, M., Lee, J., Han, J., Oh, S. J., Jung, T., Nam, S. J., Kil, W. H., & Lee, J. E. (2014). Induction of fibronectin in response to epidermal growth factor is suppressed by silibinin through the inhibition of STAT3 in triple negative breast cancer cells. *Oncology Reports*. https://doi.org/10.3892/or.2014.3450

Ko, J. W., Shin, N. R., Park, S. H., Lee, I. C., Ryu, J. M., Kim, H. J., Cho, Y. K., Kim, J. C., & Shin, I. S. (2017). Silibinin inhibits the fibrotic responses induced by cigarette smoke via suppression of TGF-β1/Smad 2/3 signaling. *Food and Chemical Toxicology*, *106*, 424–429. https://doi.org/10.1016/j.fct.2017.06.016

Kogita, A., Togashi, Y., Hayashi, H., Sogabe, S., Terashima, M., De Velasco, M. A., Sakai, K., Fujita, Y., Tomida, S., Takeyama, Y., Okuno, K., Nakagawa, K., & Nishio, K. (2014). Hypoxia induces resistance to ALK inhibitors in the H3122 non-small cell lung cancer cell line with an ALK rearrangement via epithelial-mesenchymal transition. *International Journal of Oncology*, *45*(4), 1430–1436. https://doi.org/10.3892/ijo.2014.2574

Křen, V. (2021). Chirality matters: Biological activity of optically pure silybin and its congeners. In *International Journal of Molecular Sciences* (Vol. 22, Issue 15). MDPI. https://doi.org/10.3390/ijms22157885

Kunita, A., Baeriswyl, V., Meda, C., Cabuy, E., Takeshita, K., Giraudo, E., Wicki, A., Fukayama, M., & Christofori, G. (2018). Inflammatory Cytokines Induce Podoplanin Expression at the Tumor Invasive Front. *American Journal of Pathology*, *188*(5), 1276–1288. https://doi.org/10.1016/j.ajpath.2018.01.016

Lambert, A. W., Pattabiraman, D. R., & Weinberg, R. A. (2017). Emerging Biological Principles of Metastasis. *Cell*, *168*(4), 670–691. https://doi.org/10.1016/j.cell.2016.11.037

Lasorella, A., Benezra, R., & Iavarone, A. (2014). The ID proteins : master regulators of cancer stem cells and tumour aggressiveness. *Nature Publishing Group*, *21*(January). https://doi.org/10.1038/nrc3638

Lauro, S., Onesti, C. E., Righini, R., & Marchetti, P. (2014). The Use of Bevacizumab in Non-Small Cell Lung Cancer: An Update. *Anticancer Research*, *34*, 1534–1546.

Le, T., & Gerber, D. E. (2019). Newer-generation EGFR inhibitors in lung cancer: How are they best used? In *Cancers* (Vol. 11, Issue 3). MDPI AG. https://doi.org/10.3390/cancers11030366

Leiter, A., Veluswamy, R. R., & Wisnivesky, J. P. (2023). The global burden of lung cancer: current status and future trends. *Nature Reviews Clinical Oncology*, *20*, 624–639.

Li, P., Huang, T., Zou, Q., Liu, D., Wang, Y., Tan, X., Wei, Y., & Qiu, H. (2019). FGFR2 Promotes Expression of PD-L1 in Colorectal Cancer via the JAK/STAT3 Signaling Pathway. *The Journal of Immunology*, *202*(10), 3065–3075. https://doi.org/10.4049/jimmunol.1801199

Lim, Z. F., & Ma, P. C. (2019). Emerging insights of tumor heterogeneity and drug resistance mechanisms in lung cancer targeted therapy. In *Journal of Hematology and Oncology* (Vol. 12, Issue 1). BioMed Central Ltd. https://doi.org/10.1186/s13045-019-0818-2

Lin, J. J., & Shaw, A. T. (2016). Resisting Resistance: Targeted Therapies in Lung Cancer. In *Trends in Cancer* (Vol. 2, Issue 7, pp. 350–364). Cell Press. https://doi.org/10.1016/j.trecan.2016.05.010

Lindeman, N. I., Cagle, P. T., Aisner, D. L., Arcila, M. E., Beasley, M. B., Bernicker, E. H., Colasacco, C., Dacic, S., Hirsch, F. R., Kerr, K., Kwiatkowski, D. J., Ladanyi, M., Nowak, J. A., Sholl, L., Temple-Smolkin, R., Solomon, B., Souter, L. H., Thunnissen, E., Tsao, M. S., … Yatabe, Y. (2018). Updated molecular testing guideline for the selection of lung cancer patients for treatment with targeted tyrosine kinase inhibitors guideline from the college of American pathologists, the international association for the study of lung cancer, and the association for molecular pathology. *Archives of Pathology and Laboratory Medicine*, *142*(3), 321–346. https://doi.org/10.5858/arpa.2017-0388-CP

Liu, B., Palmfeldt, J., Lin, L., Colaço, A., Clemmensen, K. K. B., Huang, J., Xu, F., Liu, X., Maeda, K., Luo, Y., & Jäättelä, M. (2018). STAT3 associates with vacuolar H+-ATPase and regulates cytosolic and lysosomal pH. *Cell Research*, *28*(10), 996–1012. https://doi.org/10.1038/s41422-018-0080-0

Liu, C.-Y. Y., Huang, T.-T. T., Chu, P.-Y. Y., Huang, C.-T. T., Lee, C.-H. H., Wang, W.-L. L., Lau, K.-Y. Y., Tsai, W.-C. C., Chao, T.-I. I., Su, J.-C. C., Chen, M.-H. H., Shiau, C.-W. W., Tseng, L.-M. M., & Chen, K.-F. F. (2017). The tyrosine kinase inhibitor nintedanib activates SHP-1 and induces apoptosis in triple-negative breast cancer cells. *Experimental & Molecular Medicine*. https://doi.org/10.1038/emm.2017.114

Liu, R., Chen, Y., Liu, G., Li, C., Song, Y., Cao, Z., Li, W., Hu, J., Lu, C., & Liu, Y. (2020). PI3K/AKT pathway as a key link modulates the multidrug resistance of cancers. In *Cell Death and Disease* (Vol. 11, Issue 9). Springer Nature. https://doi.org/10.1038/s41419-020-02998-6

Liu, R., Wang, Q., Ding, Z., Zhang, X., Li, Y., Zang, Y., & Zhang, G. (2020). Silibinin augments the antifibrotic effect of valsartan through inactivation of TGF-β1 signaling in kidney. *Drug Design, Development and Therapy*, *14*, 603–611. https://doi.org/10.2147/DDDT.S224308

Lockwood, W. W., Wilson, I. M., Coe, B. P., Chari, R., Pikor, L. A., Thu, K. L., Solis, L. M., Nunez, M. I., Behrens, C., Yee, J., English, J., Murray, N., Tsao, M. S., Minna, J. D., Gazdar, A. F., Wistuba, I. I., MacAulay, C. E., Lam, S., & Lam, W. L. (2012). Divergent genomic and epigenomic landscapes of lung cancer subtypes underscore the selection of different oncogenic pathways during tumor development. *PLoS ONE*, *7*(5). https://doi.org/10.1371/journal.pone.0037775

Lu, T., Yang, X., Huang, Y., Zhao, M., Li, M., Ma, K., Yin, J., Zhan, C., & Wang, Q. (2019). Trends in the incidence, treatment, and survival of patients with lung cancer in the last four decades. *Cancer Management and Research*, *11*, 943–953. https://doi.org/10.2147/CMAR.S187317

Lu, W., & Kang, Y. (2019). Epithelial-Mesenchymal Plasticity in Cancer Progression and Metastasis. *Developmental Cell*, *49*(3), 361–374. https://doi.org/10.1016/j.devcel.2019.04.010

Maitrejean, M., Comte, G., Barron, D., El Kirat, K., lle Conseil, G., & Di Pietro, A. (1999). The Flavanolignan Silybin and its Hemisynthetic Derivatives, a Novel Series of Potential Modulators of P-Glycoprotein. *Bioorganic and Medicinal Chemistry Letters*, 157–160.

Marcucci, F., Stassi, G., & De Maria, R. (2016). Epithelial-mesenchymal transition: A new target in anticancer drug discovery. *Nature Reviews Drug Discovery*, *15*(5), 311–325. https://doi.org/10.1038/nrd.2015.13

Marine, J. C., Dawson, S. J., & Dawson, M. A. (2020). Non-genetic mechanisms of therapeutic resistance in cancer. In *Nature Reviews Cancer* (Vol. 20, Issue 12, pp. 743–756). Nature Research. https://doi.org/10.1038/s41568-020-00302-4

Martin, L. P., Hamilton, T. C., & Schilder, R. J. (2008). Platinum resistance: The role of DNA repair pathways. In *Clinical Cancer Research* (Vol. 14, Issue 5, pp. 1291–1295). https://doi.org/10.1158/1078-0432.CCR-07-2238

Masciocchi, D., Gelain, A., Villa, S., Meneghetti, F., & Barlocco, D. (2011). Signal transducer and activator of transcription 3 (STAT3): A promising target for anticancer therapy. In *Future Medicinal Chemistry* (Vol. 3, Issue 5, pp. 567–597). https://doi.org/10.4155/fmc.11.22

Masters, G. A., Temin, S., Azzoli, C. G., Giaccone, G., Baker, S., Brahmer, J. R., Ellis, P. M., Gajra, A., Rackear, N., Schiller, J. H., Smith, T. J., Strawn, J. R., Trent, D., & Johnson, D. H. (2015). Systemic therapy for stage IV non-small-cell lung cancer: American society of clinical oncology clinical practice guideline update. In *Journal of Clinical Oncology* (Vol. 33, Issue 30, pp. 3488–3515). American Society of Clinical Oncology. https://doi.org/10.1200/JCO.2015.62.1342

Mateen, S., Raina, K., Agarwal, C., Chan, D., & Agarwal, R. (2013). Silibinin synergizes with histone deacetylase and DNA methyltransferase inhibitors in upregulating e-cadherin expression together with inhibition of migration and invasion of human non-small cell lung cancer cells. *Journal of Pharmacology and Experimental Therapeutics*, *345*(2), 206–214. https://doi.org/10.1124/jpet.113.203471

Mateen, S., Raina, K., & Agarwal, R. (2013). Chemopreventive and anti-cancer efficacy of silibinin against growth and progression of lung cancer. *Nutrition and Cancer*, *65*(SUPPL.1), 3–11. https://doi.org/10.1080/01635581.2013.785004

Mateen, S., Tyagi, A., Agarwal, C., Singh, R. P., & Agarwal, R. (2010). Silibinin inhibits human nonsmall cell lung cancer cell growth through cell-cycle arrest by modulating expression and function of key cell-cycle regulators. *Molecular Carcinogenesis*. https://doi.org/10.1002/mc.20595

McDonald, F., De Waele, M., Hendriks, L. E. L., Faivre-Finn, C., Dingemans, A. M. C., & Van Schil, P. E. (2017). Management of stage I and II nonsmall cell lung cancer. In *European Respiratory Journal* (Vol. 49, Issue 1). European Respiratory Society. https://doi.org/10.1183/13993003.00764-2016

McFarland, B. C., & Benveniste, E. N. (2019). Reactive astrocytes foster brain metastases via STAT3 signaling. *Annals of Translational Medicine*, *7*(S3), S83–S83. https://doi.org/10.21037/atm.2019.04.17

McGee, K., Stone, N. J., Wadhwani, S., Kanwar, Y. S., Villaflor, V., & Akhter, N. (2021). A possible mechanism of hyperlipidemia in a patient with metastatic non-small cell lung cancer on lorlatinib therapy. *Journal of Oncology Pharmacy Practice*, *27*(8), 2010–2013. https://doi.org/10.1177/1078155221004698

Meza, R., Meernik, C., Jeon, J., & Cote, M. L. (2015). Lung cancer incidence trends by gender, race and histology in the United States, 1973-2010. *PLoS ONE*, *10*(3). https://doi.org/10.1371/journal.pone.0121323

Min, H. Y., & Lee, H. Y. (2021). Mechanisms of resistance to chemotherapy in non-small cell lung cancer. In *Archives of Pharmacal Research* (Vol. 44, Issue 2, pp. 146–164). Pharmaceutical Society of Korea. https://doi.org/10.1007/s12272-021-01312-y

Mithoowani, H., & Febbraro, M. (2022). Non-Small-Cell Lung Cancer in 2022: A Review for General Practitioners in Oncology. In *Current Oncology* (Vol. 29, Issue 3, pp. 1828–1839). MDPI. https://doi.org/10.3390/curroncol29030150

Mitsudomi, T., & Yatabe, Y. (2010). Epidermal growth factor receptor in relation to tumor development: EGFR gene and cancer. In *FEBS Journal* (Vol. 277, Issue 2, pp. 301–308). https://doi.org/10.1111/j.1742-4658.2009.07448.x

Molavi, O., Narimani, F., Asiaee, F., Sharifi, S., Tarhriz, V., Shayanfar, A., Hejazi, M., & Lai, R. (2017). Silibinin sensitizes chemo-resistant breast cancer cells to chemotherapy. *Pharmaceutical Biology*. https://doi.org/10.1080/13880209.2016.1270972

Moustakas, A., & de Herreros, A. G. (2017). Epithelial–mesenchymal transition in cancer. *Molecular Oncology*, *11*(7), 715–717. https://doi.org/10.1002/1878-0261.12094

Myall, N. J., Yu, H., Soltys, S. G., Wakelee, H. A., & Pollom, E. (2021). Management of brain metastases in lung cancer: evolving roles for radiation and systemic treatment in the era of targeted and immune therapies. *Neuro-Oncology Advances*, *3*(Supplement_5), v52–v62. https://doi.org/10.1093/noajnl/vdab106

Neuvonen, P. J., Niemi, M., & Backman, J. T. (2006). Drug interactions with lipid-lowering drugs: Mechanisms and clinical relevance. *Clinical Pharmacology and Therapeutics*, *80*(6), 565–581. https://doi.org/10.1016/j.clpt.2006.09.003

Nieto, M. A., Huang, R. Y. Y. J., Jackson, R. A. A., & Thiery, J. P. P. (2016). Emt: 2016. *Cell*, *166*(1), 21–45. https://doi.org/10.1016/j.cell.2016.06.028

Norton, J. D. (2000). ID helix-loop-helix proteins in cell growth, differentiation and tumorigenesis. *Journal of Cell Science*, *113*, 3897–3905.

Ocaña, O. H., Córcoles, R., Fabra, Á., Moreno-Bueno, G., Acloque, H., Vega, S., Barrallo-Gimeno, A., Cano, A., & Nieto, M. A. (2012). Metastatic Colonization Requires the Repression of the Epithelial-Mesenchymal Transition Inducer Prrx1. *Cancer Cell*, *22*(6), 709–724. https://doi.org/10.1016/j.ccr.2012.10.012

Ohyashiki, J. (2018). Seed and soil hypothesis revisited. *Journal of Tokyo Medical University*, *76*(2), 181–184.

Owen, S., & Souhami, L. (2014). The management of brain metastases in non-small cell lung cancer. In *Frontiers in Oncology* (Vol. 4, Issue SEP). Frontiers Research Foundation. https://doi.org/10.3389/fonc.2014.00248

Peng, L., Zhu, L., Sun, Y., Stebbing, J., Selvaggi, G., Zhang, Y., & Yu, Z. (2022). Targeting ALK Rearrangements in NSCLC: Current State of the Art. In *Frontiers in Oncology* (Vol. 12). Frontiers Media S.A. https://doi.org/10.3389/fonc.2022.863461

Pérez-Sánchez, A., Cuyàs, E., Ruiz-Torres, V., Agulló-Chazarra, L., Verdura, S., González-álvarez, I., Bermejo, M., Joven, J., Micol, V., Bosch-Barrera, J., & Menendez, J. A. (2019). Intestinal permeability study of clinically relevant formulations of silibinin in caco-2 cell monolayers. *International Journal of Molecular Sciences*, *20*(7). https://doi.org/10.3390/ijms20071606

Perk, J., Iavarone, A., & Benezra, R. (2005). ID FAMILY OF HELIX - LOOP - HELIX PROTEINS IN CANCER. *NATURE REVIEWS*, *5*(July), 603–614. https://doi.org/10.1038/nrc1673

Pignon, J. P., Tribodet, H., Scagliotti, G. V., Douillard, J. Y., Shepherd, F. A., Stephens, R. J., Dunant, A., Torri, V., Rosell, R., Seymour, L., Spiro, S. G., Rolland, E., Fossati, R., Aubert, D., Ding, K., Waller, D., & Le Chevalier, T. (2008). Lung adjuvant cisplatin evaluation: A pooled analysis by the LACE collaborative group. *Journal of Clinical Oncology*, *26*(21), 3552–3559. https://doi.org/10.1200/JCO.2007.13.9030

Planchard, D., Popat, S., Kerr, K., Novello, S., Smit, E. F., Faivre-Finn, C., Mok, T. S., Reck, M., Van Schil, P. E., Hellmann, M. D., & Peters, S. (2018). Metastatic non-small cell lung cancer: ESMO Clinical Practice Guidelines for diagnosis, treatment and follow-up. *Annals of Oncology*, *29*, iv192–iv237. https://doi.org/10.1093/annonc/mdy275

Polyak, K., & Weinberg, R. A. (2009). Transitions between epithelial and mesenchymal states: Acquisition of malignant and stem cell traits. *Nature Reviews Cancer*, *9*(4), 265–273. https://doi.org/10.1038/nrc2620

Pontis, F., Roz, L., Fortunato, O., & Bertolini, G. (2023). The metastatic niche formation: focus on extracellular vesicle-mediated dialogue between lung cancer cells and the microenvironment. In *Frontiers in Oncology* (Vol. 13). Frontiers Media S.A. https://doi.org/10.3389/fonc.2023.1116783

Popper, H. (2020). Primary tumor and metastasis-sectioning the different steps of the metastatic cascade. *Translational Lung Cancer Research*, *9*(5), 2277–2300. https://doi.org/10.21037/tlcr-20-175

Popper, H. H. (2016). Progression and metastasis of lung cancer. *Cancer and Metastasis Reviews*, *35*(1), 75–91. https://doi.org/10.1007/s10555-016-9618-0

Priego, N., Zhu, L., Monteiro, C., Mulders, M., Wasilewski, D., Bindeman, W., Doglio, L., Martínez, L., Martínez-Saez, E., Cajal, S. R. Y., Megías, D., Hernández-Encinas, E., Blanco-Aparicio, C., Martínez, L., Zarzuela, E., Muñoz, J., Fustero-Torre, C., Piñeiro-Yáñez, E., Hernández-Laín, A., … Valiente, M. (2018). STAT3 labels a subpopulation of reactive astrocytes required for brain metastasis article. *Nature Medicine*, *24*(7), 1024–1035. https://doi.org/10.1038/s41591-018-0044-4

Psaila, B., & Lyden, D. (2009). The metastatic niche: adapting the foreign soil. *Nature Reviews Cancer*, *9*(4), 285–293. https://doi.org/10.1038/nrc2621

Quail, D. F., & Joyce, J. A. (2013). Microenvironmental regulation of tumor progression and metastasis. *Nature Medicine*, *19*(11), 1423–1437. https://doi.org/10.1038/nm.3394

Ramasamy, K., & Agarwal, R. (2008). Multitargeted therapy of cancer by silymarin. In *Cancer Letters*. https://doi.org/10.1016/j.canlet.2008.03.053

Rami-Porta, R., Giroux, D. J., & Goldstraw, P. (2011). The new TNM classification of lung cancer in practice educational aims. *Breathe*, *7*(4), 348–360. https://doi.org/10.1183/20734735.000111

Reck, M., Kaiser, R., Mellemgaard, A., Douillard, J. Y., Orlov, S., Krzakowski, M., von Pawel, J., Gottfried, M., Bondarenko, I., Liao, M., Gann, C. N., Barrueco, J., Gaschler-Markefski, B., & Novello, S. (2014). Docetaxel plus nintedanib versus docetaxel plus placebo in patients with previously treated non-small-cell lung cancer (LUME-Lung 1): A phase 3, double-blind, randomised controlled trial. *The Lancet Oncology*, *15*(2), 143–155. https://doi.org/10.1016/S1470-2045(13)70586-2

Reck, M., Popat, S., Reinmuth, N., De Ruysscher, D., Kerr, K. M., & Peters, S. (2014). Metastatic non-small-cell lung cancer (NSCLC): ESMO Clinical Practice Guidelines for

diagnosis, treatment and follow-up. *Annals of Oncology*, *25*, iii27–iii39. https://doi.org/10.1093/annonc/mdu199

Reed, M., Rosales, A.-L. S., Chioda, M. D., Parker, L., Devgan, G., & Kettle, J. (2020). Consensus Recommendations for Management and Counseling of Adverse Events Associated With Lorlatinib: A Guide for Healthcare Practitioners. *Advances in Therapy*, *37*, 3019–3030. https://doi.org/10.6084/m9.figshare.12011814

Remon, J., Reguart, N., García-Campelo, R., Conde, E., Lucena, C. M., Persiva, O., Navarro-Martin, A., & Rami-Porta, R. (2021). Lung Cancer in Spain. In *Journal of Thoracic Oncology* (Vol. 16, Issue 2, pp. 197–204). Elsevier Inc. https://doi.org/10.1016/j.jtho.2020.09.026

Rho, J. K., Choi, Y. J., Jeon, B. S., Choi, S. J., Cheon, G. J., Woo, S. K., Kim, H. R., Kim, C. H., Choi, C. M., & Lee, J. C. (2010). Combined treatment with silibinin and epidermal growth factor receptor tyrosine kinase inhibitors overcomes drug resistance caused by T790M mutation. *Molecular Cancer Therapeutics*, *9*(12), 3233–3243. https://doi.org/10.1158/1535-7163.MCT-10-0625

Riebold, M., Kozany, C., Freiburger, L., Sattler, M., Buchfelder, M., Hausch, F., Stalla, G. K., & Paez-Pereda, M. (2015). A C-terminal HSP90 inhibitor restores glucocorticoid sensitivity and relieves a mouse allograft model of Cushing disease. *Nature Medicine*, *21*(3), 276–280. https://doi.org/10.1038/nm.3776

Robert Benezra. (2001). Role of Id Proteins in Embryonic and Tumor Angiogenesis. *Trends Cardiovascular Medicine*, *11*, 237–241.

Robey, R. W., Shukla, S., Finley, E. M., Oldham, R. K., Barnett, D., Ambudkar, S. V, Fojo, T., & Bates, S. E. (2008). Inhibition of P-glycoprotein (ABCB1)-and multidrug resistance-associated protein 1 (ABCC1)-mediated transport by the orally administered inhibitor, CBT-1®. *Biochem Pharmacol*, *75*(6), 1302–1312.

Roche, J. (2018). The epithelial-to-mesenchymal transition in cancer. *Cancers*, *10*(2), 10–13. https://doi.org/10.3390/cancers10020052

Roschger, C., & Cabrele, C. (2017). The Id-protein family in developmental and cancer-associated pathways. In *Cell Communication and Signaling*. https://doi.org/10.1186/s12964-016-0161-y

Rosell, R., & Karachaliou, N. (2016). Trends in immunotherapy for brain metastases. In *The Lancet Oncology* (Vol. 17, Issue 7, pp. 859–860). Lancet Publishing Group. https://doi.org/10.1016/S1470-2045(16)30091-2

Rotow, J., & Bivona, T. G. (2017). Understanding and targeting resistance mechanisms in NSCLC. In *Nature Reviews Cancer* (Vol. 17, Issue 11, pp. 637–658). Nature Publishing Group. https://doi.org/10.1038/nrc.2017.84

Sadava, D., & Kane, S. E. (2013). Silibinin reverses drug resistance in human small-cell lung carcinoma cells. *Cancer Letters*, *339*(1), 102–106. https://doi.org/10.1016/j.canlet.2013.07.017

Saller, R., Meier, R., & Brignoli, R. (2001). The Use of Silymarin in the Treatment of Liver Diseases. *Drugs*, *61*(14), 2035–2063.

Saller, R., Melzer, J., Reichling, J., Brignoli, R., & Meier, R. (2007). An updated systematic review of the pharmacology of silymarin. In *Forschende Komplementarmedizin* (Vol. 14, Issue 2, pp. 70–80). https://doi.org/10.1159/000100581

Sbiera, S., Deutschbein, T., Weigand, I., Reincke, M., Fassnacht, M., & Allolio, B. (2015). The New Molecular Landscape of Cushing's Disease. In *Trends in Endocrinology and Metabolism* (Vol. 26, Issue 10, pp. 573–583). Elsevier Inc. https://doi.org/10.1016/j.tem.2015.08.003

Schroeder, T., Bittrich, P., Kuhne, J. F., Noebel, C., Leischner, H., Fiehler, J., Schroeder, J., Schoen, G., & Gellißen, S. (2020). Mapping distribution of brain metastases: does the primary tumor matter? *Journal of Neuro-Oncology*, *147*(1), 229–235. https://doi.org/10.1007/s11060-020-03419-6

Seidel, D., Zander, T., Heukamp, L. C., Peifer, M., Bos, M., Fernández-Cuesta, L., Leenders, F., Lu, X., Ansén, S., Gardizi, M., Nguyen, C., Berg, J., Russell, P., Wainer, Z., Schildhaus, H. U., Rogers, T. M., Solomon, B., Pao, W., Carter, S. L., … Lang, U. (2013a). A genomics-based classification of human lung tumors. *Science Translational Medicine*, *5*(209). https://doi.org/10.1126/scitranslmed.3006802

Seidel, D., Zander, T., Heukamp, L. C., Peifer, M., Bos, M., Fernández-Cuesta, L., Leenders, F., Lu, X., Ansén, S., Gardizi, M., Nguyen, C., Berg, J., Russell, P., Wainer, Z., Schildhaus, H. U., Rogers, T. M., Solomon, B., Pao, W., Carter, S. L., … Lang, U. (2013b). A genomics-based classification of human lung tumors. *Science Translational Medicine*, *5*(209). https://doi.org/10.1126/scitranslmed.3006802

Sequist, L. V., Waltman, B. A., Dias-Santagata, D., Digumarthy, S., Turke, A. B., Fidias, P., Bergethon, K., Shaw, A. T., Gettinger, S., Cosper, A. K., Akhavanfard, S., Heist, R. S., Temel, J., Christensen, J. G., Wain, J. C., Lynch, T. J., Vernovsky, K., Mark, E. J., Lanuti, M., … Engelman, J. A. (2011). Genotypic and histological evolution of lung cancers acquiring resistance to EGFR inhibitors. *Science Translational Medicine*, *3*(75). https://doi.org/10.1126/scitranslmed.3002003

Sharma, G., Singh, R. P., Chan, D. C., & Agarwal, R. (2003). Silibinin induces growth inhibition and apoptotic cell death in human lung carcinoma cells. *Anticancer Research*, *23*(3B), 2649–2655.

Sharma, P., Hu-Lieskovan, S., Wargo, J. A., & Ribas, A. (2017). Primary, Adaptive, and Acquired Resistance to Cancer Immunotherapy. In *Cell* (Vol. 168, Issue 4, pp. 707–723). Cell Press. https://doi.org/10.1016/j.cell.2017.01.017

Shi, J., Hua, X., Zhu, B., Ravichandran, S., Wang, M., Nguyen, C., Brodie, S. A., Palleschi, A., Alloisio, M., Pariscenti, G., Jones, K., Zhou, W., Bouk, A. J., Boland, J., Hicks, B., Risch, A., Bennett, H., Luke, B. T., Song, L., … Landi, M. T. (2016). Somatic Genomics and Clinical Features of Lung Adenocarcinoma: A Retrospective Study. *PLoS Medicine*, *13*(12), 1–24. https://doi.org/10.1371/journal.pmed.1002162

Siddiqui, F., Vaqar, S., & Siddiqui, A. H. (2023). Lung Cancer. *Cambridge Handbook of Psychology, Health and Medicine, Second Edition*, 605–606. https://doi.org/10.1017/CBO9780511543579.138

Siegel, R. L., Miller, K. D., Wagle, N. S., & Jemal, A. (2023). Cancer statistics, 2023. *CA: A Cancer Journal for Clinicians*, *73*(1), 17–48. https://doi.org/10.3322/caac.21763

Sikder, H. A., Meghann K.Devlin. Meghann K, Dunlap, S., Ryu, B., & Alani, R. M. (2003). Id proteins in cell growth and tumorigenesis. *Cancer Cell*, *3*, 525–530.

Singh, R. P., Mallikarjuna, G. U., Sharma, G., Dhanalakshmi, S., Tyagi, A. K., Chan, D. C. F., Agarwal, C., & Agarwal, R. (2004). Oral silibinin inhibits lung tumor growth in athymic nude mice and forms a novel chemocombination with doxorubicin targeting nuclear factor κB-mediated inducible chemoresistance. *Clinical Cancer Research*. https://doi.org/10.1158/1078-0432.CCR-04-1435

Soto, M. S., Larkin, J. R., Martin, C., Khrapitchev, A. A., MacZka, M., Economopoulos, V., Scott, H., Escartin, C., Bonvento, G., Serres, S., & Sibson, N. R. (2020). STAT3-mediated astrocyte reactivity associated with brain metastasis contributes to neurovascular

dysfunction. *Cancer Research*, *80*(24), 5642–5655. https://doi.org/10.1158/0008-5472.CAN-20-2251

Stewart, D. J. (2007). Mechanisms of resistance to cisplatin and carboplatin. In *Critical Reviews in Oncology/Hematology* (Vol. 63, Issue 1, pp. 12–31). https://doi.org/10.1016/j.critrevonc.2007.02.001

Sugiyama, A., Kageyama, K., Murasawa, S., Ishigame, N., Niioka, K., & Daimon, M. (2015). Inhibition of heat shock protein 90 decreases ACTH production and cell proliferation in AtT-20 cells. *Pituitary*, *18*(4), 542–553. https://doi.org/10.1007/s11102-014-0607-4

Sun, C. Y., Nie, J., Huang, J. P., Zheng, G. J., & Feng, B. (2019). Targeting STAT3 inhibition to reverse cisplatin resistance. In *Biomedicine and Pharmacotherapy* (Vol. 117). Elsevier Masson SAS. https://doi.org/10.1016/j.biopha.2019.109135

Sung, H., Ferlay, J., Siegel, R. L., Laversanne, M., Soerjomataram, I., Jemal, A., & Bray, F. (2021). Global Cancer Statistics 2020: GLOBOCAN Estimates of Incidence and Mortality Worldwide for 36 Cancers in 185 Countries. *CA: A Cancer Journal for Clinicians*, *71*(3), 209–249. https://doi.org/10.3322/caac.21660

Tai, W. T., Shiau, C. W., Li, Y. S., Chang, C. W., Huang, J. W., Hsueh, T. T., Yu, H. C., & Chen, K. F. (2014). Nintedanib (BIBF-1120) inhibits hepatocellular carcinoma growth independent of angiokinase activity. *Journal of Hepatology*, *61*(1), 89–97. https://doi.org/10.1016/j.jhep.2014.03.017

Takeuchi, K., Soda, M., Togashi, Y., Suzuki, R., Sakata, S., Hatano, S., Asaka, R., Hamanaka, W., Ninomiya, H., Uehara, H., Lim Choi, Y., Satoh, Y., Okumura, S., Nakagawa, K., Mano, H., & Ishikawa, Y. (2012). RET, ROS1 and ALK fusions in lung cancer. *Nature Medicine*, *18*(3), 378–381. https://doi.org/10.1038/nm.2658

Tew, K. D. (2016). Glutathione-associated enzymes in anticancer drug resistance. In *Cancer Research* (Vol. 76, Issue 1, pp. 7–9). American Association for Cancer Research Inc. https://doi.org/10.1158/0008-5472.CAN-15-3143

Thai, A. A., Solomon, B. J., Sequist, L. V., Gainor, J. F., & Heist, R. S. (2021a). Lung cancer. In *The Lancet* (Vol. 398, Issue 10299, pp. 535–554). Elsevier B.V. https://doi.org/10.1016/S0140-6736(21)00312-3

Thai, A. A., Solomon, B. J., Sequist, L. V., Gainor, J. F., & Heist, R. S. (2021b). Lung cancer. In *The Lancet* (Vol. 398, Issue 10299, pp. 535–554). Elsevier B.V. https://doi.org/10.1016/S0140-6736(21)00312-3

Thakur, C. (2019). An Overview, Current Challenges of Drug Resistance, and Targeting Metastasis Associated With Lung Cancer. In *Nanotechnology-Based Targeted Drug Delivery Systems for Lung Cancer* (pp. 21–38). Elsevier. https://doi.org/10.1016/b978-0-12-815720-6.00002-2

Thandra, K. C., Barsouk, A., Saginala, K., Aluru, J. S., & Barsouk, A. (2021). Epidemiology of lung cancer. In *Wspolczesna Onkologia* (Vol. 25, Issue 1, pp. 45–52). Termedia Publishing House Ltd. https://doi.org/10.5114/wo.2021.103829

Thomas, A., Rajan, A., & Giaccone, G. (2012). Tyrosine Kinase Inhibitors in Lung Cancer. In *Hematology/Oncology Clinics of North America* (Vol. 26, Issue 3, pp. 589–605). https://doi.org/10.1016/j.hoc.2012.02.001

Thulasiraman, V., & Matts, R. L. (1996). *Effect of Geldanamycin on the Kinetics of Chaperone-Mediated Renaturation of Firefly Luciferase in Rabbit Reticulocyte Lysate †*.

Tissot, C., Couraud, S., Tanguy, R., Bringuier, P. P., Girard, N., & Souquet, P. J. (2016). Clinical characteristics and outcome of patients with lung cancer harboring BRAF mutations. *Lung Cancer*, *91*, 23–28. https://doi.org/10.1016/j.lungcan.2015.11.006

Toyokawa, G., & Seto, T. (2015). Updated evidence on the mechanisms of resistance to ALK inhibitors and strategies to overcome such resistance: Clinical and preclinical data. In *Oncology Research and Treatment* (Vol. 38, Issue 6, pp. 291–298). S. Karger AG. https://doi.org/10.1159/000430852

Tulpule, A., & Bivona, T. G. (2020). Acquired Resistance in Lung Cancer. *Annual Review of Cancer Biology Annu. Rev. Cancer Biol*, *5*, 279–297. https://doi.org/10.1146/annurev-cancerbio-030419

Tyagi, A., Agarwal, C., Dwyer-Nield, L. D., Singh, R. P., Malkinson, A. M., & Agarwal, R. (2012). Silibinin modulates TNF-α and IFN-γ mediated signaling to regulate COX2 and iNOS expression in tumorigenic mouse lung epithelial LM2 cells. *Molecular Carcinogenesis*, *51*(10), 832–842. https://doi.org/10.1002/mc.20851

Tyagi, A., Singh, R. P., Ramasamy, K., Raina, K., Redente, E. F., Dwyer-Nield, L. D., Radcliffe, R. A., Malkinson, A. M., & Agarwal, R. (2009). Growth inhibition and regression of lung tumors by silibinin: Modulation of angiogenesis by macrophage-associated cytokines and nuclear factor-κB and signal transducers and activators of transcription 3. *Cancer Prevention Research*, *2*(1), 74–83. https://doi.org/10.1158/1940-6207.CAPR-08-0095

Verdura, S., Cuyàs, E., Ruiz-Torres, V., Micol, V., Joven, J., Bosch-Barrera, J., & Menendez, J. A. (2021). Lung cancer management with silibinin: A historical and translational perspective. *Pharmaceuticals*, *14*(6). https://doi.org/10.3390/ph14060559

Vignais, M.-L., Sadowski, H. B., Watling, † Diane, Rogers, N. C., & Gilman, M. (1996). Platelet-Derived Growth Factor Induces Phosphorylation of Multiple JAK Family Kinases and STAT Proteins. In *MOLECULAR AND CELLULAR BIOLOGY* (Vol. 16, Issue 4).

Vinod, S. K., & Hau, E. (2020). Radiotherapy treatment for lung cancer: Current status and future directions. In *Respirology* (Vol. 25, Issue S2, pp. 61–71). Blackwell Publishing. https://doi.org/10.1111/resp.13870

Volm, M., Mattern, J., & Samsel, B. (1991). Overexpression of P-glycoprotein and glutathione S-transferase-t in resistant non-small cell lung carcinomas of smokers. In *Br. J. Cancer* (Vol. 64).

Wang, Y. X., Cai, H., Jiang, G., Zhou, T. B., & Wu, H. (2014). Silibinin inhibits proliferation, induces apoptosis and causes cell cycle arrest in human gastric cancer MGC803 cells via STAT3 pathway inhibition. *Asian Pacific Journal of Cancer Prevention*, *15*(16), 6791–6798. https://doi.org/10.7314/APJCP.2014.15.16.6791

Wang, Z., Xing, Y., Li, B., Li, X., Liu, B., & Wang, Y. (2022). Molecular pathways, resistance mechanisms and targeted interventions in non-small-cell lung cancer. In *Molecular Biomedicine* (Vol. 3, Issue 1). Springer. https://doi.org/10.1186/s43556-022-00107-x

Wasilewski, D., Priego, N., Fustero-Torre, C., & Valiente, M. (2017). Reactive astrocytes in brain metastasis. In *Frontiers in Oncology* (Vol. 7, Issue DEC). Frontiers Media S.A. https://doi.org/10.3389/fonc.2017.00298

Wellington, K., Jarvis, B., & Agarwal, R. (2001). Silymarin: A Review of its Clinical Properties in the Management of Hepatic Disorders. *BioDrugs*, *15*(7), 465–489.

Wilson, C., Nicholes, K., Bustos, D., Lin, E., Song, Q., Stephan, J.-P., Kirkpatrick, D. S., & Settleman, J. (2014). Overcoming EMT-associated resistance to anti-cancer drugs via Src/FAK pathway inhibition. *Oncotarget*, *5*(17). www.impactjournals.com/oncotarget/

Witta, S. E., Gemmill, R. M., Hirsch, F. R., Coldren, C. D., Hedman, K., Ravdel, L., Helfrich, B., Dziadziuszko, R., Chan, D. C., Sugita, M., Chan, Z., Baron, A., Franklin, W., Drabkin, H. A., Girard, L., Gazdar, A. F., Minna, J. D., & Bunn, P. A. (2006). Restoring E-cadherin expression increases sensitivity to epidermal growth factor receptor inhibitors in lung

cancer cell lines. *Cancer Research*, *66*(2), 944–950. https://doi.org/10.1158/0008-5472.CAN-05-1988

Woodard, G. A., Jones, K. D., & Jablons, D. M. (2016). Lung cancer staging and prognosis. In *Cancer Treatment and Research* (Vol. 170, pp. 47–75). Kluwer Academic Publishers. https://doi.org/10.1007/978-3-319-40389-2_3

Xie, X., Li, X., Tang, W., Xie, P., & Tan, X. (2022). Primary tumor location in lung cancer: The evaluation and administration. In *Chinese Medical Journal* (Vol. 135, Issue 2, pp. 127–136). Lippincott Williams and Wilkins. https://doi.org/10.1097/CM9.0000000000001802

Xu, S., Zhang, H., Wang, A., Ma, Y., Gan, Y., & Li, G. (2020). Silibinin suppresses epithelial-mesenchymal transition in human non-small cell lung cancer cells by restraining RHBDD1. *Cellular and Molecular Biology Letters*, *25*(1). https://doi.org/10.1186/s11658-020-00229-6

Yang, J., & Gong, W. (2019). Lorlatinib for the treatment of anaplastic lymphoma kinase-positive non-small cell lung cancer. *Expert Review of Clinical Pharmacology*, *12*(3), 173–178. https://doi.org/10.1080/17512433.2019.1570846

Yang, Y., Deng, L., Yang, Y., Zhang, T., Wu, Y., Wang, L., & Bi, N. (2022). Efficacy and Safety of Combined Brain Radiotherapy and Immunotherapy in Non-Small-Cell Lung Cancer With Brain Metastases: A Systematic Review and Meta-Analysis. In *Clinical Lung Cancer* (Vol. 23, Issue 2, pp. 95–107). Elsevier Inc. https://doi.org/10.1016/j.cllc.2021.06.009

Yasuda, H., Park, E., Yun, C. H., Sng, N. J., Lucena-Araujo, A. R., Yeo, W. L., Huberman, M. S., Cohen, D. W., Nakayama, S., Ishioka, K., Yamaguchi, N., Hanna, M., Oxnard, G. R., Lathan, C. S., Moran, T., Sequist, L. V., Chaft, J. E., Riely, G. J., Arcila, M. E., … Costa, D. B. (2013). Structural, biochemical, and clinical characterization of epidermal growth factor receptor (EGFR) exon 20 insertion mutations in lung cancer. *Science Translational Medicine*, *5*(216). https://doi.org/10.1126/scitranslmed.3007205

Zhang, F., Shen, M., Yang, L., Yang, X., Tsai, Y., Keng, P. C., Chen, Y., Lee, S. O., & Chen, Y. (2017). Simultaneous targeting of ATM and Mcl-1 increases cisplatin sensitivity of cisplatin-resistant non-small cell lung cancer. *Cancer Biology and Therapy*, *18*(8), 606–615. https://doi.org/10.1080/15384047.2017.1345391

Zhang, J., Yang, P. L., & Gray, N. S. (2009). Targeting cancer with small molecule kinase inhibitors. In *Nature Reviews Cancer* (Vol. 9, Issue 1, pp. 28–39). https://doi.org/10.1038/nrc2559

Zhao, H., Brandt, G. E., Galam, L., Matts, R. L., & Blagg, B. S. J. (2011). Identification and initial SAR of silybin: An Hsp90 inhibitor. *Bioorganic and Medicinal Chemistry Letters*, *21*(9), 2659–2664. https://doi.org/10.1016/j.bmcl.2010.12.088

Zhao, J., & Agarwal, R. (1999). Tissue distribution of silibinin, the major active constituent of silymarin, in mice and its association with enhancement of phase II enzymes: implications in cancer chemoprevention. In *Carcinogenesis* (Vol. 20, Issue 11).

Zhao, M., & Gao, F.-H. (2011). Small Molecule Inhibitors of STAT3 for Cancer Therapy. In *Current Medicinal Chemistry* (Vol. 18).

Zhu, L., Retana, D., García-Gómez, P., Álvaro-Espinosa, L., Priego, N., Masmudi-Martín, M., Yebra, N., Miarka, L., Hernández-Encinas, E., Blanco-Aparicio, C., Martínez, S., Sobrino, C., Ajenjo, N., Artiga, M., Ortega-Paino, E., Torres-Ruiz, R., Rodríguez-Perales, S., Soffietti, R., Bertero, L., … Nicolás, P. (2022). A clinically compatible drug-screening platform based on organotypic cultures identifies vulnerabilities to prevent and treat brain metastasis. *EMBO Molecular Medicine*, *14*(3). https://doi.org/10.15252/emmm.202114552

VIII. APPENDIX I

pharmaceuticals

MDPI

Review

Lung Cancer Management with Silibinin: A Historical and Translational Perspective

Sara Verdura [1,2,†], Elisabet Cuyàs [1,2,†], Verónica Ruiz-Torres [3], Vicente Micol [3], Jorge Joven [4], Joaquim Bosch-Barrera [2,5,6,*] and Javier A. Menendez [1,2,*]

1 Girona Biomedical Research Institute (IDIBGI), 17190 Girona, Spain; sverdura@idibgi.org (S.V.); ecuyas@idibgi.org (E.C.)
2 Metabolism and Cancer Group, Program against Cancer Therapeutic Resistance (ProCURE), Catalan Institute of Oncology, 17007 Girona, Spain
3 Instituto de Investigación, Desarrollo e Innovación en Biotecnología Sanitaria de Elche (IDiBE) and Instituto de Biología Molecular y Celular (IBMC), Universidad Miguel Hernández (UMH), 03202 Elche, Spain; vruiz@umh.es (V.R.-T.); vmicol@umh.es (V.M.)
4 Unitat de Recerca Biomèdica (URB-CRB), Hospital Universitari de Sant Joan, Institut d'Investigació Sanitària Pere Virgili, Universitat Rovira i Virgili, 43201 Reus, Spain; jjoven@grupsagessa.com
5 Medical Oncology, Catalan Institute of Oncology, Dr. Josep Trueta Hospital of Girona, 17007 Girona, Spain
6 Department of Medical Sciences, Faculty of Medicine, University of Girona (UdG), 17003 Girona, Spain
* Correspondence: jbosch@iconcologia.net (J.B.-B.); jmenendez@idibgi.org (J.A.M.)
† Both authors contributed equally to this work.

Abstract: The flavonolignan silibinin, the major bioactive component of the silymarin extract of *Silybum marianum* (milk thistle) seeds, is gaining traction as a novel anti-cancer therapeutic. Here, we review the historical developments that have laid the groundwork for the evaluation of silibinin as a chemopreventive and therapeutic agent in human lung cancer, including translational insights into its mechanism of action to control the aggressive behavior of lung carcinoma subtypes prone to metastasis. First, we summarize the evidence from chemically induced primary lung tumors supporting a role for silibinin in lung cancer prevention. Second, we reassess the preclinical and clinical evidence on the effectiveness of silibinin against drug resistance and brain metastasis traits of lung carcinomas. Third, we revisit the transcription factor STAT3 as a central tumor-cell intrinsic and microenvironmental target of silibinin in primary lung tumors and brain metastasis. Finally, by unraveling the selective vulnerability of silibinin-treated tumor cells to drugs using CRISPR-based chemosensitivity screenings (e.g., the hexosamine biosynthesis pathway inhibitor azaserine), we illustrate how the therapeutic use of silibinin against targetable weaknesses might be capitalized in specific lung cancer subtypes (e.g., *KRAS/STK11* co-mutant tumors). Forthcoming studies should take up the challenge of developing silibinin and/or next-generation silibinin derivatives as novel lung cancer-preventive and therapeutic biomolecules.

Keywords: silibinin; silymarin; non-small cell lung cancer; EMT; metastasis; STAT3

Citation: Verdura, S.; Cuyàs, E.; Ruiz-Torres, V.; Micol, V.; Joven, J.; Bosch-Barrera, J.; Menendez, J.A. Lung Cancer Management with Silibinin: A Historical and Translational Perspective. *Pharmaceuticals* **2021**, *14*, 559. https://doi.org/10.3390/ph14060559

Academic Editor: Thomas Efferth

Received: 12 May 2021
Accepted: 9 June 2021
Published: 11 June 2021

1. Introduction

Phytochemicals are biologically active compounds synthesized by plants (*Phyto* means "plant" in Greek). The term, however, is generally employed for those influencing human health. Flavonoids are a subclass of polyphenol phytochemicals that are commonly present in fruits, vegetables, nuts, seeds, herbs, spices, stems, flowers, teas, and red wine [1,2]. As they have existed in nature for millions of years, flavonoids have a long historical association with animal species throughout evolution, which likely explains their myriad biochemical and pharmacological properties [3]. Although not without limitations, the mutualistic relationship between plant flavonoids and animals, which is embraced in the concept of xenohormesis [4,5], can be applied to human pathophysiology; in particular, the

various bioactivities of flavonoids (e.g., anti-inflammatory, antioxidant, antiallergic, hepatoprotective, antithrombotic, antiviral, and anticarcinogenic) in numerous biological systems.

Flavonolignans are a minor subclass of flavonoids comprising a flavonoid moiety and a lignan (phenylpropanoid) part. They were first isolated from the seeds of milk thistle (*Silybum marianum* (L.) Gaertn.), an annual/biannual plant of the *Asteraceae* family flowering in July–August with characteristic reddish-purple flowers. The milk thistle is indigenous to South Europe, South Russia, Asia Minor, and North Africa, but has also been naturalized in North and South America and in South Australia. The so-called silymarin extract of milk thistle, which was classified by the World Health Organization as an official medicine with health-promoting properties in the 1970s, is obtained through organic solvent extraction and represents 1.5–3% of the dry weight of the fruit. Silymarin contains a mixture of flavonolignans of mainly four isomers: silibinin (or silybin), isosilybin, silychristin, and silydianin. There is also a minor fraction of polymeric and oxidized polyphenolic components [6–12], including two pairs of diastereomers—-silibinin A/B and isosilybin A/B. Silibinin is composed of a 1:1 mixture of silibinin A and B and comprises 50–70% of the extract and 20–40% of the commonly used pharmaceutical preparations [11,13,14]. Whereas the chemical composition of milk thistle fruits includes other flavonoids (e.g., taxifolin, quercetin, kaempferol, apigenin), the highest concentration of silymarin corresponds to silibinin, which is considered the major bioactive component [15–18].

Originally described as a cure for the venom of poisonous snakes, silibinin is the most extensively studied flavonolignan and is currently clinically employed to treat amatoxin/*Amanita* mushroom poisoning or lipotoxic injury in fatty liver diseases. Here, we review the historical context of the development of silibinin research in lung cancer (Figure 1). A literature search (silibinin AND lung cancer) was initially conducted in the electronic database PubMed with no date-range restriction. No quality-assessment scale systems were used to evaluate the collected studies. Manuscripts were screened by checking the title and abstract or reading the full text to determine their inclusion. In addition, we provide some experimental results to illustrate how we might capitalize on the therapeutic use of silibinin against targetable weaknesses in specific subgroups of patients with lung cancer.

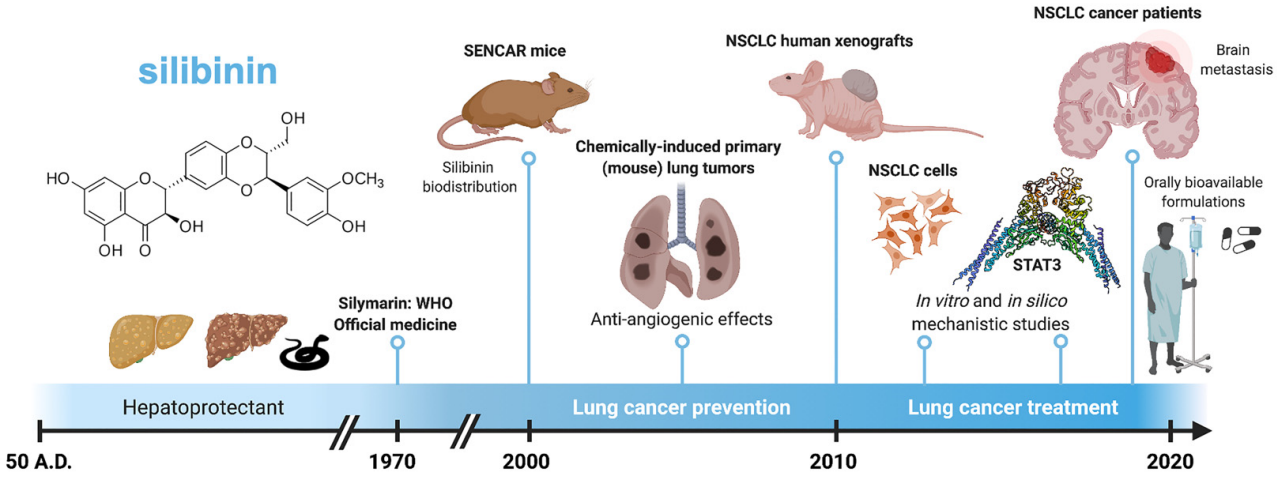

Figure 1. Key milestones in the timeline of silibinin research in lung cancer. Originally employed as a hepatoprotectant and a remedy for the bites of poisonous snakes hundreds of years ago, silibinin has recently demonstrated significant clinical activity in patients with non-small cell lung cancer and brain metastases when used in new orally bioavailable formulations. Created with BioRender.

2. Silibinin-Containing Milk Thistle Fruits and Human Health: A Brief Historical Overview

The name milk thistle originates from a legend that Mary, when leaving for Egypt with the infant Jesus, found shelter in a bower formed from the thorny leaves of *S. marianum*. While nursing Jesus, she spilled some breast milk onto the plant, and this resulted in the characteristic milky-white veins of the plant's leaves.

Milk thistle fruits have been used for over 2000 years in the treatment of liver- and biliary-related diseases. While the first record of *S. marianum* can be found in the Old Testament (Genesis 3:18), it had already been used in ancient Greece and in millenarian Indian and Chinese medicines to resolve liver and gallbladder problems. Theophrastus of Eresos (fourth century B.C.), Pedanios Dioscorides (50 A.D.), and Plinius the Elder (first century A.D.) were the first to report the medicinal benefits of milk thistle fruits. In his work "*De Materia Medica*", Dioscorides described *S. marianum* as a remedy for the bites of poisonous snakes and for melancholic depression, which was believed to be a "liver complaint" at that time.

Used in the Middle Ages as an antidote for liver toxins, renaissance and humanistic naturalists and physicians included milk thistle in their herbal medicine armamentarium. Native American Indians, 19th century physicians, and herbalists also employed preparations of milk thistle fruits to treat a variety of diseases, particularly liver pathologies. In the last 40–50 years, the use of silibinin-dependent, bioactive silymarin extracts for treatment of liver disorders such as alcoholic liver disease, nonalcoholic liver disease, drug-induced liver injury, cirrhosis, viral hepatitis, and mushroom poisoning has been well documented [12,18,19]. Patients with liver disorders treated with silymarin show a more rapid improvement in liver function than those receiving placebo. Likewise, in patients with alcoholic liver cirrhosis, administration of silymarin for several years resulted in a significantly reduced mortality rate [15,20]. Not surprisingly, silymarin is one of the most frequently sold dietary supplements for hepatitis and cirrhosis in the USA and Europe [21].

3. Silibinin to Therapeutically Manage Lung Cancer: Pioneering Studies

Dr. Agarwal and colleagues at the University of Colorado Health Sciences Center (Denver, USA) pioneered the investigation of silibinin to prevent and treat human malignancies in different experimental models of skin [22,23], prostate [24,25], and lung [26,27] cancer. Based on the strong antioxidant activity of silymarin and the fact that it was already in clinical use for a range of liver, gall bladder, and even dermatological conditions [28], they conducted a series of cancer-centered studies with silymarin in both short-term cell culture and long-term animal models. Using SENCAR mice, which are highly sensitive to tumor initiation and promotion in response to carcinogens and promoters [29,30], they initially assessed the tissue biodistribution and conjugate formation of systematically administered silibinin in different mouse tissues and its effect on phase II detoxification enzymes [26]. They found that silibinin could rapidly distribute as both free and conjugated forms and significantly induced phase II enzymes in the tissues examined. These findings strongly suggested that silibinin might reach target organs to exert anti-cancer effects, providing the first basis to evaluate the cancer preventive and interventive effects of silibinin in experimental models of carcinogenesis [26]. Using established cell models of small cell (SCLC) and non-small cell (NSCLC) lung carcinoma, the Agarwal group was the first to report that micromolar concentrations of silibinin could significantly increase growth inhibition, cell cycle arrest, and apoptotic cell death [31], warranting further studies to establish the efficacy and mechanism(s) of action of silibinin as a non-toxic therapeutic agent in additional lung tumor models.

4. Silibinin and Lung Cancer Prevention: Evidence from Chemically Induced Primary Lung Tumors

The Agarwal group demonstrated that oral silibinin (200 mg/kg, 5 d/wk for 33 days) inhibited NSCLC A549 xenograft tumor growth and suppressed the systemic toxicity of

co-administered doxorubicin in athymic BALB/c *nu/nu* mice through a mechanism likely dependent on the regulation of nuclear factor kappaB (NFκB), a key player in the chemoresistance and dose-related (acute and cumulative) toxicity of anthracyclines [32]. In contrast to these findings, Yan and colleagues reported the failure of 0.05% and 0.1% silibinin in the diet (*wt/wt*) to significantly reduce tumor multiplicity and load in a mouse model of tobacco-driven lung carcinogenesis [33]. In another study by the Agarwal group, the lack of efficacy of silibinin in preventing benzo(a)pyrene-induced pulmonary adenoma formation and growth reported in the aforementioned Yan study was not observed when the effects of dietary silibinin (0–1% *wt/wt*) on the growth, progression, and angiogenesis of lung tumors induced by urethane (a carcinogenic contaminant of alcoholic beverages and other fermentation products) were tested in A/J mice [34]. Chronic oral consumption of silibinin significantly lowered lung tumor multiplicity, prevented lung tumors from growing beyond a small size (in a dose-dependent fashion), and blunted tumor angiogenesis, a plausible mechanism contributing to the efficacy of silibinin in this model [34].

Mechanistically, the cancer-preventive activity of silibinin was initially attributed to the reduced lung tumor expression of the angiogenic factor vascular endothelial growth factor (VEGF), mediated by the suppression of VEGF regulators such as cyclooxygenase-2 (COX2) and inducible nitric oxide synthase (iNOS) [34]. Silibinin appeared to target multiple cytokine (IFNγ, IL-1β, and TNF-α)-induced signaling pathways such as the signal transducer and activator of transcription 3 (STAT3) to ultimately lower COX2 and iNOS expression in lung cancer cells [35,36]. When the chemotherapeutic effects of oral silibinin on the growth and progression of established, urethane-induced, lung adenocarcinomas in A/J mice were studied, its strong ability to suppress both tumor number and size correlated with a reduced antiangiogenic activity mediated by decreased cytokine production in tumor-associated macrophages and suppression of NFκB and STAT3 activation in lung cancer cells [36]. Importantly, the capacity of silibinin to prevent urethane-induced lung tumorigenesis in mice was completely lost upon genetic ablation of *Nos2* (iNOS) [37], strongly suggesting that silibinin exerts its chemopreventive and angiopreventive effects through blockade of iNOS expression in lung tumors. Careful examination of the mechanism of action of silibinin on cell signaling elicited by a cytokine mixture (IFNγ + TNF-α) in tumor-derived LM2 mouse lung epithelial cells revealed that its ability to regulate the expression of metalloproteinases and the angiogenesis drivers COX2 and iNOS was causally mediated through impairment of STAT3 activation and nuclear localization [38]. As no 50% lethal dose (LD_{50}) has been reported in laboratory animals, and silibinin treatment has been considered exceptionally safe after acute or long-term chronic administration in both animals and humans, these findings strongly supported the investigation of silibinin as a chemopreventive agent for suppressing lung tumor growth and progression in humans [27].

5. Silibinin and Lung Cancer Treatment: Evidence from Laboratory In Vitro and Animal Models

An ever-growing number of studies have tested the capacity of silibinin to exert inhibitory activities against cultured cancer cells and tumor xenografts, to enhance the efficacy of other therapeutic agents (reviewed in [39,40]), and to block the emergence of cancer drug resistance in pre-clinical models of lung cancer, including those involving NSCLC-targeted therapies such as epidermal growth factor receptor (EGFR)- and anaplastic lymphoma kinase (ALK)-tyrosine kinase inhibitors (TKIs).

5.1. Silibinin and Lung Cancer Drug Resistance

Early studies evaluating silibinin against established cell lines representative of different NSCLC subtypes revealed that micromolar concentrations significantly inhibited cell proliferation by inducing cell cycle arrest and modulating multiple cell cycle regulators, including cyclin-dependent kinases and their corresponding cyclins [41,42]. In later studies, we and others described the capacity of silibinin to exert cytostatic, cytotoxic, and apoptotic effects in various

NSCLC cell models [43–45]. Importantly, silibinin could restore drug sensitivity to NSCLC cells with acquired resistance to EGFR- and ALK-TKIs in vitro and in vivo.

Rho and colleagues investigated whether the addition of silibinin to EGFR-targeted therapy using first-generation EGFR-TKIs (gefitinib or erlotinib) could overcome primary and acquired resistance due to the presence of the *EGFR T790M* mutation [46]. They found that silibinin enhanced the ability of EGFR-TKIs to downregulate EGFR signals by inhibiting receptor dimerization of EGFR family members (EGFR, HER2, and HER3) in vitro. Moreover, the combination silibinin and erlotinib suppressed tumor growth in erlotinib-resistant (*EGFR T790M*) PC-9 NSCLC xenografts [46]. The ability of silibinin to resensitize NSCLC cells to EGFR- and ALK-TKIs occurs even in the absence of secondary *EGFR* mutations. Using gefitinib- and erlotinib-refractory NSCLC cell models in which EGFR-TKI resistance occurs via the activation of bypass survival signals with other receptor tyrosine kinases (e.g., hyperactive insulin-like growth factor-1 receptor [IGF-1R]) [47] and/or epithelial-to-mesenchymal transition (EMT) [48,49], a water-soluble form of silibinin complexed with the amino-sugar meglumine could efficiently restore EGFR-TKI sensitivity in NSCLC mouse xenografts [48,49]. Mechanistically, silibinin could differentially eliminate cancer stem cell (CSC)-like cells within EGFR-TKI-refractory heterogeneous NSCLC populations with aldehyde dehydrogenase isoform 1 (ALDHA1) overexpression and self-renewal capacity [43,50]. Using a model of ALK-translocated NSCLC in which acquired refractoriness to the ALK-TKI crizotinib was driven by activation of TGFβ-induced EMT in the absence of secondary mutations in the kinase domain of ALK, silibinin-induced inhibition of STAT3 was found to synergistically interact with crizotinib to reverse acquired resistance and restore sensitivity in crizotinib-resistant cells [46].

Although scarce, new studies are beginning to shed light on the ability of silibinin to reverse the multidrug resistance (MDR) phenotype of lung cancer cells. Silibinin has been shown to act synergistically with some chemotherapeutics (e.g., doxorubicin, etoposide) in multidrug-resistant SCLC cells through a mechanism that might involve the direct inhibition of adenosine triphosphate binding cassette (ABC)-transporters such as human P-glycoprotein and multidrug resistance-associated protein-1, as well as the downregulation of the expression of the respective *ABCB1* and *ABCC1* genes [51–56]. Because most patients with advanced EGFR- or ALK-positive NSCLC will receive chemotherapy at some point during their treatment course, it would seem desirable to evaluate whether silibinin specifically impacts EGFR mutation- and ALK translocation-driven chemosensitivity profiles. Using the CRISPR/Cas9-edited *EML4-ALK* fusion isogenic model in A549 NSCLC cells, which naturally harbor other genomic aberrations inherent in NSCLC (e.g., *KRAS/STK11* co-mutation), we recently performed a chemical sensitivity screen to evaluate how silibinin modulates the sensitivity of these cells to a variety of chemotherapeutics (Figure 2; Figure S1). The *EML-ALK* fusion CCL-185IG derivative acquired a notably enhanced responsiveness to silibinin when co-treated with the dihydrofolate reductase inhibitor aminopterin—-the original clinical anti-folate—-and azaserine, a glutamine-fructose-6-phosphate transaminase (GFPT) inhibitor that blocks N-linked glycosylation and the hexosamine biosynthesis pathway. Silibinin co-treatment also prevented EML-ALK fusion-driven resistance to the platinum agents cisplatin and carboplatin. Further studies are warranted to evaluate whether EGFR- and ALK-positive tumors acquire sensitivity to certain silibinin-containing chemotherapeutic combinations once they are resistant to EGFR- and ALK-TKIs and available TKI options are exhausted.

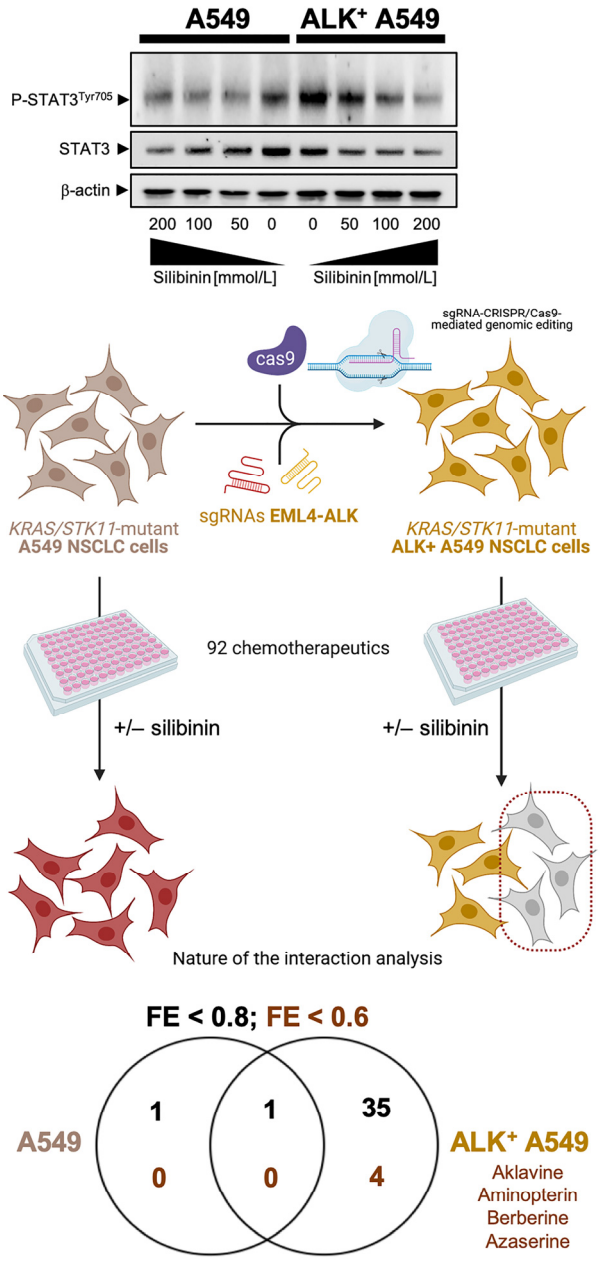

Figure 2. EML4-ALK-dependent chemosensitizing effects of silibinin in non-small cell lung cancer cells. We utilized the Phenotypic Microarray system, marketed and sold by Biolog (www.biolog.com, access date: 30 May 2021) to measure the sensitivity of an A549 non-small cell lung cancer (NSCLC) cell line with an *EML4-ALK* fusion isogenic oncogene (https://www.nature.com/articles/d42473-019-00011-z, access date: 30 May 2021) to a variety of growth inhibitors (in total, 92) in microplates (PM-M11 to PM-M14). This approach enables the simultaneous testing of tens of phenotypes and the identification of shared versus selective sensitivities to a wide variety of mechanistically distinct drugs. We chose a silibinin concentration of 100 µmol/L, which was notably lower than the IC_{50} value against A549 cells and consistently reduced cell viability by less than 5% in multiple experiments using the colorimetric redox-sensitive dye employed in the Biolog technology. A set of "negative" control plates cultured in the presence of the silibinin vehicle DMSO were used to assess the inherent response of A549/ALK⁺ A549 cells to growth inhibitors. A set of "positive" plates cultured in the presence of 100 µmol/L silibinin served to assess the nature of the interaction between silibinin and the 92 drugs pre-loaded in the 96-well plates (4 graded concentrations/each). We assessed the nature of the cytotoxic responses based on synergistic, additive, or antagonistic categories using an arbitrarily defined ratio of observed effect/theoretical effect, the so-called fractional effect (FE)

method (Figure S1). Briefly, the theoretical effect of the combination was calculated by adding the effects of each drug used alone at the concentration tested in the combination to that obtained when silibinin was tested alone (i.e., "negative" control plates + effect of silibinin as single agent). This theoretical effect was compared with the actual effect obtained during the combinatorial experiment ("positive" plates, i.e., drugs in combination with silibinin) carried out strictly in parallel. The different interactions were then defined as follows: "additivity" was an observed effect equal to the theoretical effect, and the ratio between them ranged between 0.8 and 1.2; "synergy" was an observed effect higher than the theoretical effect, and the ratio between them was less than 0.8; and "antagonism" was an observed effect lower than the theoretical effect, and the ratio between them was more than 1.2. The interaction between silibinin and a given drug was initially scored as "synergistic" when at least two FEs were <0.8. A truly synergistic interaction was scored when data sets were re-assessed using a stricter threshold criterion (i.e., at least two FEs were <0.6). The representative immunoblots presented in the upper part of the figure show Western blot analyses of cell lysates from A549 parental cells and ALK + A549 derivatives cultured in the absence or presence of graded concentrations of silibinin (24 h) immunoblotted with anti-phospho-STAT3^{Tyr705}, anti-total STAT3, and anti-β-actin. Created with BioRender. (+/−, plus/minus).

5.2. Silibinin and Lung Cancer Metastatic Traits

5.2.1. Inhibition of Cell Invasion

Early studies observed that, in the absence of cytotoxic effects, silibinin could exert dose- and time-dependent inhibitory effects on the invasion and motility (but not on the adhesion) of highly metastatic NSCLC cell models [57]. Mechanistic studies revealed that silibinin decreased the expression of metalloproteinase-2 (MMP-2) and urokinase plasminogen activator, and enhanced the expression of tissue inhibitor of metalloproteinase (TIMP-2) [57]. The negative effect of silibinin on NSCLC invasiveness and metastasis, by changing the balance between MMPs and TIMPs in favor of the inhibitors, appeared to occur downstream of its ability to inactivate PI3K-AKT and MAPK signaling pathways [58,59]. More recent mechanistic studies have established, however, that the mechanism of action of silibinin against MMPs might causally involve silibinin-driven inhibition of STAT3 activation and nuclear translocation [60].

5.2.2. Inhibition of Epithelial-to-Mesenchymal Transition

Beyond MMPs and TIMPs, which have key roles in tumor cell invasion and metastasis by digesting the basement membrane and extracellular matrix components, silibinin can target lung cancer metastastic traits by inhibiting EMT per se. EMT is a highly complex molecular reprogramming process whereby cells lose their epithelial features and acquire a mesenchymal phenotype, allowing them to detach from the primary tumor, invade adjacent stroma, enter systemic circulation, and form distant metastasis. EMT also contributes to tumor aggressiveness by enhancing the resistance of cancer cells to chemotherapy, radiation therapy and targeted therapy, which is a key feature of tumor- and metastasis-initiating CSCs (reviewed in [61–63]).

Various mechanisms of resistance to EGFR- and ALK-TKIs in NSCLC are linked to the activation of EMT-like phenomena, irrespective of the EGFR and ALK mutation status [64–72]. Silibinin has been reported to restore drug sensitivity to EGFR-mutant NSCLC xenografts with EMT-driven resistance to gefitinib and erlotinib. Silibinin treatment also impedes the regrowth of gefitinib-unresponsive xenograft NSCLC tumors, resulting in drastic tumor growth prevention in vivo [48]. Similarly, silibinin was found to fully activate a reciprocal mesenchymal-to-epithelial transition in erlotinib-refractory cells and prevent the highly migratogenic phenotype of erlotinib-resistant NSCLC cells [49].

The ability of silibinin to block EMT and to impede the acquisition of transcriptional and morphological behavior of transitioning cells appears to occur in a multi-faceted manner. Silibinin can fine-tune the epigenetic dynamics of key EMT-driven events. For

instance, silibinin was found to fully reverse the EMT-related high miR-21/low miR-200c microRNA signature and repress the expession of the mesenchymal markers SNAIL, ZEB1, and N-cadherin in erlotinib-refractory NSCLC human xenografts [49]. Because epigenetic modulation of the miR-21 oncogene and the miR-200c tumor suppressor is causally associated with transition to a CSC-like state [73–77], these findings indicated that silibinin might regulate the epigenetic plasticity of microRNAs, contributing to the evolving and adapting phenotypes of lung carcinomas. Indeed, combinatorial treatment with silibinin and histone deacetylase and DNA methyltransferase inhibitors modulated EMT events in NSCLC cell lines, including reversion of the inverse expression pattern of ZEB1 and E-cadherin, tempering their migratory and invasive potential [78]. In the same line, silibinin was recently shown to suppress migration, invasion, and EMT expression by repressing the expression of Rhomboid domain containing 1, a well-known promoter of cell migration, invasion, EMT, and stem cell-like phenotypes in multiple cancer types including lung cancer [79]. The initially reported capacity of silibinin to target EGFR signaling [46] has been shown to involve the suppression of the downstream matrix remodeling enzyme lysyl oxidase, a key contributor to the early steps of metastastic colonization by enhancing tumor invasion, migration, and the formation of pre-metastatic niche [80–83]. Silibinin in combination with EGFR blockade prevented NSCLC cell migration in vitro and tumor metastasis in an orthotopic implantation metastasis model by targeting the EGFR/LOX pathway [84]. In contrast to other EMT-targeting compounds, a recent transcriptomic profiling study revealed that de novo responsiveness of NSCLC cells to silibinin does not correlate with their intrinsic EMT stage [85]. Rather, silibinin responsiveness appears to be linked to a subnetwork of tightly interconnected genes of cell cycle, survival, and stress response (e.g., *BIRC5*, *FOXM1*, and *BRCA1*) whose transcriptomic pattern is under control of STAT3 [85].

5.2.3. Inhibition of Brain Metastasis

Our resent findings have positioned silibinin as a successful therapy to treat established brain metastasis in patients with NSCLC. In 2016, we presented the first evidence for oral silibinin as part of a bioavailable formulation with predicted capacity to cross the blood–brain barrier (BBB) [86], which resulted in significant clinical and radiological improvement of brain metastasis in two patients with poor performance status that progressed after whole brain radiotherapy and chemotherapy [87]. The suppressive effects of silibinin on progressive brain metastasis, which included a marked reduction in peritumoral brain edema, occurred in the absence of changes to the primary lung tumor outgrowth [87]. We then compared our clinical series of patients with NSCLC treated with the silibinin-containing nutraceutical Legasil® (n = 18; single-agent silibinin n = 3 and silibinin plus additional therapy n = 15) with patients treated at the same institution who completed whole-brain radiation therapy for NSCLC brain metastasis and who received systemic therapy but not silibinin (n = 38). In such a small cohort, silibinin demonstrated highly significant clinical activity with a 75% overall response rate in the brain including three complete responses and ten partial responses [88]. Indeed, the patients receiving silibinin as palliative care (n = 3) benefited from additional treatment lines as a result of their general status improvement and magnetic resonance imaging-based brain responses. The overall survival from the diagnosis of brain metastasis was significantly superior in the cohort of patients treated with the silibinin-containing nutraceutical (15.5 months) than in the control cohort (4.0 months), a trend that was maintained when patients with EGFR and ALK oncogenic driver mutations were excluded from the analysis [88].

A subpopulation of reactive astrocytes surrounding brain metastases has been identified that is driven by STAT3 activation and is characterized by nuclear accumulation of phospho-active STAT3 [88,89]. NSCLC metastatic tumor cells that have initiated a brain macro-metastasis secrete various factors that trigger astrocytes in the surrounding area to become reactive with enhanced STAT3 activation. In turn, phospho-STAT3+ reactive astrocytes produce cytokines and other factors to escape innate and adaptive anti-tumor

immune responses [88]. Investigations into the molecular mechanisms involved in the aforementioned clinico-molecular activities of silibinin revealed that silibinin efficiently suppresses the ability of brain metastastic NSCLC cells to co-opt a pro-metastatic program driven by STAT3 in a subpopulation of reactive astrocytes surrounding metastatic lesions [88]. Blocking STAT3 signaling in reactive astrocytes in the brain microenvironment with silibinin reduced brain metastasis growth and disease burden.

6. STAT3: A primary Tumor-Cell Intrinsic and Microenvironmental Target of Silibinin in Lung Cancer

Central to the tumor cell-intrinsic and microenvironmental effects of silibinin in lung cancer is the transcriptional factor STAT3 (Figure 3).

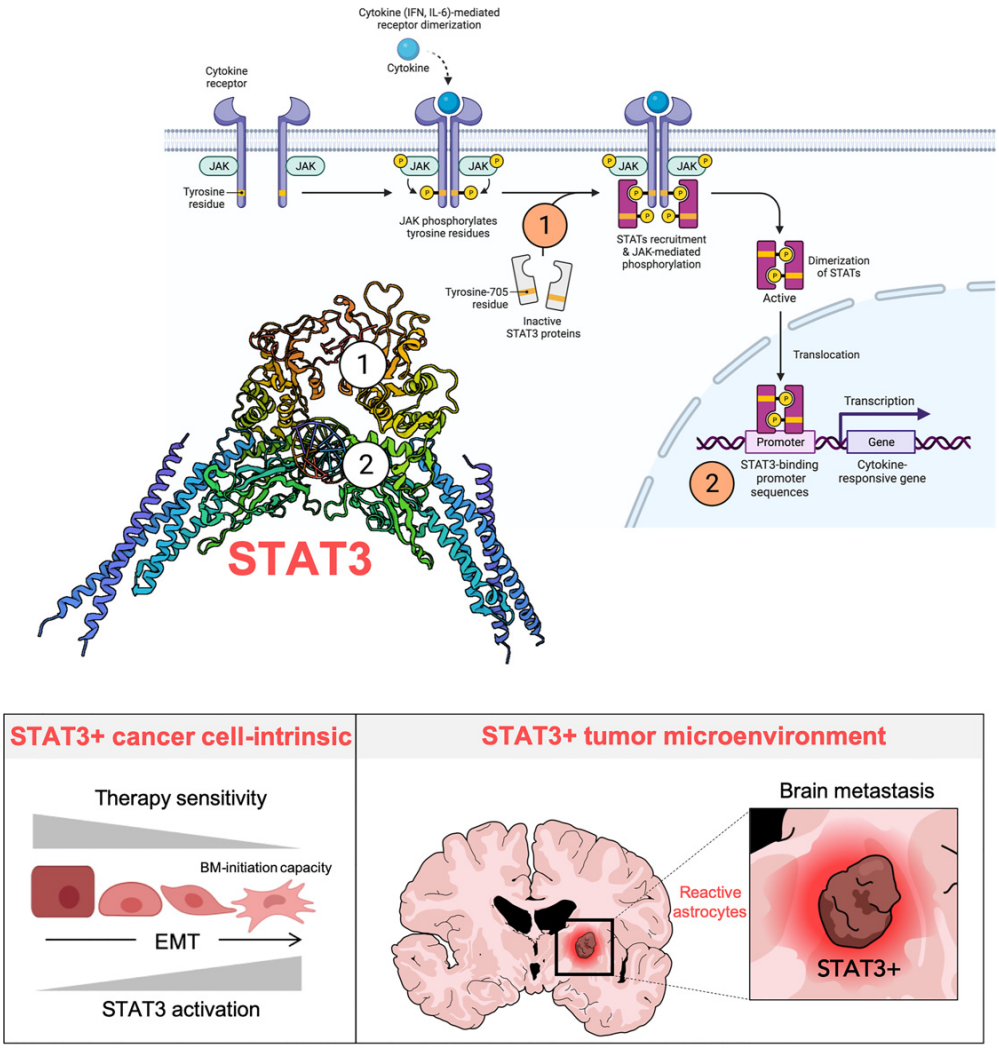

Figure 3. Silibinin mechanism of action in lung cancer: A STAT3-centric view. Aberrant activation of JAK/STAT3 signaling, in particular STAT3, participates in the initiation, development, and therapeutic resistance of lung cancer via promotion of proliferation, survival, inflammation, angiogenesis, and metastasis. Silibinin is a unique blocker of the JAK/STAT3 signal transduction cascade that operates as a bimodal SH2- and DBD-targeting direct STAT3 inhibitor (STAT3i) while sparing JAK activity. STAT3 participates in multiple layers of the EMT regulatory network, and feedback activation of STAT3 is a common cause of resistance to many chemotherapies and targeted cancer therapies. At the lung cancer cell-intrinsic level, silibinin-containing combinatorial treatments can overcome drug resistance and reduce the brain metastasis-initiating capacity of lung cancer cells. Brain metastasis cells promote the co-option of a pro-metastatic program driven by STAT3 activation in a subpopulation of reactive astrocytes surrounding metastatic lesions. Blocking microenvironmental STAT3 signaling in reactive astrocytes with silibinin reduces the growth of brain metastases from primary NSCLC tumors, even at advanced stages of colonization. Created with BioRender.

6.1. Identification of Silibinin as a Direct STAT3 Inhibitor

We recently combined experimental, computational, and clinical efforts to investigate how silibinin imparts therapeutic benefits to patients with lung cancer by targeting STAT3. We found that the primary mechanism of action of silibinin involves a unique, bimodal Src Homology-2 domain (SH2; STAT3 dimerization) and DBD (STAT3 DNA-binding domain)-targeted inhibitory effect against STAT3 [89]. Biochemical approaches demonstrated that silibinin attenuates the tyrosine (Y705) phospho-activation in GFP-STAT3 genetic fusions without significantly altering the kinase activity of the STAT3 upstream kinases JAK1 and JAK2. Once we discarded the possibility that silibinin was a direct JAK inhibitor, we performed a comparative computational study based on docking and molecular dynamics simulations over structurally diverse STAT3 inhibitors. Silibinin was predicted to show a unique mode of high-affinity binding to the SH2 domain, partially overlapping with the cavity occupied by other direct STAT3 inhibitors to indirectly prevent Y705 phosphorylation. Silibinin treatment of cultured NSCLC cells prevented IL-6 inducible, constitutive, and acquired feedback activation of STAT3 [89]. In silico approaches also predicted that silibinin could directly bind with high affinity to the STAT3 DBD, uniquely involving the establishment of direct interactions with DNA. Because STAT3 dimerization is mediated by the interaction between a phospho-Y705-containing peptide and the SH2 domain, which is essential for its DNA binding and subsequent transcriptional activity, the demonstration that silibinin prevented STAT3 nuclear translocation, blocked the binding of activated STAT3 to its consensus DNA sequence, and suppressed STAT3-directed transcriptional activity further confirmed the molecular behavior of silibinin as a bona fide direct STAT3 inhibitor [89].

6.2. STAT3-Targeted Cancer Cell-Intrinsic and Microenvironmental Effects of Silibinin

The so-called STAT3C mutant, a constitutively active form of STAT3, has been employed to confirm STAT3 as a primary tumor-cell intrinsic and microenvironmental target of silibinin [90,91]. This mutant has substitutions of the A661 and N663 residues of the SH2 domain with cysteines, allowing a disulfide bond to form between two unphosphorylated STAT3 monomers; yet, it still requires Y705 phosphorylation for functional activation via promotion of maximal DNA binding affinity and protection from inactivation by phosphatases (slower off-rate), resulting in the accumulation of transcriptionally active STAT3 dimer complexes. In silico modeling of the conformation of silibinin in the binding pocket within the SH2 domain of native and A662C/N664C-mutant structures predicted a reduced ability of silibinin to bind with high affinity to the SH2 domain of the STAT3C mutant [88]. Accordingly, cancer cells engineered to overexpress STAT3C remain largely unresponsive to the inhibitory effects of silibinin on key transcriptional and phenotypic targets of STAT3 (e.g., c-myc expression and metabolic reprogramming) [88,92]. Moreover, overexpression of constitutively active STAT3C in astrocytes suffices to prevent the regulatory effects of silibinin, thus demonstrating the STAT3-dependency on the phenotypic effects of silibinin towards the microenvironment of NSCLC brain metastasis [88].

We should acknowledge that STAT3 might also represent a potential therapeutic target in the early prevention/treatment of lung-to-brain metastases. Using patient-derived stem cell lines from lung-to-brain metastases, Singh and colleagues identified STAT3 and miR-21 as cooperative regulators of stemness, migration, and brain-metastasis initiation capacity of lung cancer cells [93]. The dual STAT3/miR-21 inhibitory activity of silibinin [49,89] might therefore be revisited in terms of its ability to target not only the growth of established brain metastasis, but also the early machinery activated by brain-metastasis initiating cells to escape the primary lung tumor, migrate, and invade the neural niche.

Taking advantage of the CRISPR/Cas9-edited homozygous Y705F mutant STAT3 protein in DLD-1$^{STAT3Y705F/Y705F}$ cells, we recently performed a chemical sensitivity screen to evaluate how STAT3 phosphorylation at Tyr705 might be required for silibinin-induced chemosensitization events (Figure 4; Figure S2). The ability of silibinin to synergistically cooperate with aminopterin was lost in DLD-1$^{STAT3Y705F/Y705F}$ cells, thereby suggesting

that the nature of the interaction more likely relied on the capacity of aminopterin to operate as a JAK/STAT inhibitor independently of its primary dihydrofolate reductase target [94]. The synergistic interaction between silibinin and the GFPT inhibitor azaserine was, however, only partially prevented when the ability of silibinin to block IL6-induced Y705 phosphorylation was abolished, suggesting that silibinin may directly operate on the N-linked glycosylation/hexosamine biosynthesis pathway.

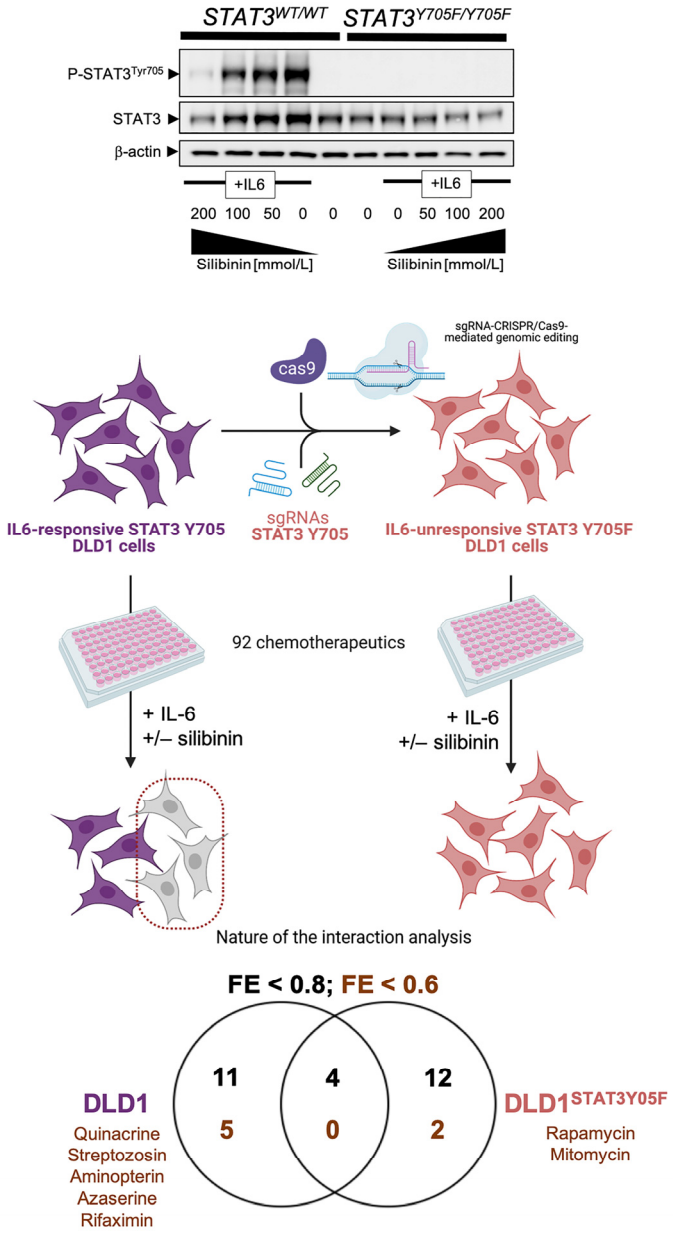

Figure 4. STAT3 Tyr705-dependent chemosensitizing effects of silibinin. We utilized the Phenotypic Microarray system, marketed and sold by Biolog (www.biolog.com, access date: 30 May 2021), to measure the sensitivity of DLD1 ($STAT3^{WT/WT}$) cancer cells and a homozygous $STAT3^{Y705F/Y705F}$ knock-in isogenic derivative (Horizon Discovery, Cat.# HD 115-016) to a wide variety of 92 growth inhibitors in microplates (PM-M11 to PM-M14) following an identical procedure to that described in Figure 2. The representative immunoblots presented in the upper part of the figure show western blot analyses of cell lysates from DLD1 $STAT3^{WT/WT}$ parental cells and DLD1 $STAT3^{Y705F/Y705F}$ derivatives cultured in the absence or presence of graded concentrations of silibinin (24 h) immunoblotted with anti-phospho-$STAT3^{Tyr705}$, anti-total STAT3, and anti-β-actin. Created with BioRender. (+/−, plus/minus).

6.3. Silibinin versus Other Natural Products Exhibiting STAT3 Inhibitory Activity

Natural products have historically been an important resource of chemical scaffolds and bioactive substructures in the discovery of STAT3 inhibitors. A large list of natural products have been reported in the literature to exhibit STAT3 inhibitory activity, including curcumin, berbamine, resveratrol, caffeic acid, capsaicin, cryptotanshinone, celastrol, avicin D, withaferin A, betulinic acid, ursolic acid, oleanolic acid, cucurbitacin, diosgenin, emodin, honokiol, flavopiridol, evodiamine, carbazole, sanguarine, and guggulsterone (reviewed in [95]). Despite the fact some of these natural products have reached clinical development, the precise STAT3-targeting mechanism(s) of action of the majority has yet to be fully elucidated, as they might inhibit STAT3 indirectly and are expected to block several targets. Resveratrol (3,5,4′-trihydroxystilbene), a widely studied polyphenolic compound found in red grapes and several other plants, was originally reported to inhibit constitutive and IL-6-induced STAT3 activity in multiple tumor cell types [96,97]. Although thought to be primarily a STAT3 inhibitor, resveratrol has also been found to modulate STAT1 activity, thus highlighting that selectivity for STAT3 over STAT1 should be carefully considered for the development of natural product-like STAT3 inhibitors [98]. Comparative in silico docking studies aimed to study the binding specificity of STAT inhibitors established that those compounds exclusively targeting the highly conserved phosphotyrosine binding pocket of the SH2 domain should be expected to lack selectivity towards STAT3, given that STAT1 and STAT3 have identical active residues at this site [99,100]. The predicted ability of silibinin to bind the SH2 activation/dimerization domain relies on its capacity to overlap with up to 60% of all the residues involved in the binding mode of a wide variety of structurally diverse STAT3is, but showing a unique binding mode [89]. By targeting the SH2 domain of STAT3 monomers, silibinin can prevent not only binding of STAT3 to activated cell surface receptors, but also to block cytosolic STAT3 dimerization, thereby preventing nuclear accumulation of phospho-active STAT3 [89]. Importantly, the ability of silibinin to inhibit the transcriptional activity of STAT3 in cells does not rely exclusively on its ability to antagonize STAT3 dimerization in the cytosol and STAT3 tyrosine phosphorylation, but also involves an additional direct inhibition of STAT3 via binding to the DBD irrespective of the STAT3 dimerization status [89]. Accordingly, silibinin is the best-positioned natural lead for a new generation of bimodal SH2- and DBD-targeting STAT3is that might become incorporated into the clinical management of lung tumors. While the clinical value of silibinin as a bona fide anti-lung cancer therapy remains uncertain with respect to its bioavailability and BBB permeability, we are rapidly accumulating information to help identify the best silibinin formulation that would reach cancer tissues and have clinical activity, including a meaningful formulation against lung brain metastases [86].

7. Silibinin and Lung Cancer: The Past, Present, and Future (a Corollary)

The milk thistle, whose main bioactive component is the flavonolignan silibinin, was originally described as a remedy for the bites of poisonous snakes in "*De Materia Medica*" by Dioscorides (50 A.D.). Almost 2000 years later, new formulations of silibinin are being clinically developed to protect liver against injury from mushroom poisoning or lipotoxic injury in fatty liver diseases. An ever-expanding number of studies are exploring the capacity of silibinin to exert inhibitory activity against cultured cancer cells and tumor xenografts, to enhance the efficacy of other therapeutic agents, and to overcome the emergence of cancer drug resistance in pre-clinical lung cancer models [101]. Although silibinin has shown chemopreventive and chemosensitizing activity against various human malignancies through multiple molecular pathways [102,103], lung cancer is becoming the paradigm for how the deconstruction of a central mechanism of action of silibinin (i.e., STAT3) has enabled this natural compound to reach clinical development. Perhaps more importantly, silibinin-driven STAT3 blockade holds immense promise in areas of highly unmet clinical need such as lung cancer brain metastasis, which portend a poor prognosis and have very few therapeutic options [87,88]. Here, we have reviewed the historical context and provided new translational insights into how an old hepatoprotective remedy

could be viewed as a novel lung cancer-preventive and therapeutic biomolecule, which might serve as a guiding example for other tumor types in the future.

Forthcoming studies should accept the challenge of developing silibinin and/or next-generation silibinin derivatives with improved lung cancer-preventing and treatment traits. We need to disentangle how silibinin prevents the generation of metastasis-initiating subpopulations within chemoresistant and/or TKI-tolerant lung tumors. In this regard, it would be important to elucidate the molecular mechanisms through which silibinin prevents brain tropism of metastatic lung cancer cells by targeting their capacities to self-renew and/or remodel the tumor microenvironment. We also need to molecularly deconstruct and functionally monitor the ability of silibinin to regulate the immune-escape mechanisms of lung cancer cells (and/or brain metastasis-initiating lung cancer cells), to influence the response to T-cells, and to interact with immune checkpoint inhibitors (e.g., anti-CTLA-4 and anti-PD-1/PD-L1 antibodies) in therapy-resistant lung carcinomas. Finally, we need to evaluate how silibinin interacts with the BBB to impede transmigration of brain metastasis-initiating cells and/or to regulate the metabolism and brain accumulation of targeted therapies. The unraveling of an unforeseen, selective vulnerability of silibinin-treated tumor cells to the hexosamine biosynthesis pathway inhibitor azaserine using genomically edited isogenic models might exemplify how to exploit the therapeutic usage of silibinin in combination with certain targetable weaknesses in specific subtypes of lung cancer (e.g., *KRAS/STK11* co-mutant tumors with dependence on the hexosamine biosynthesis pathway through GFPT2 [104]). Using silibinin as a lead structure to guide development, it would be possible to use synthetic chemistry approaches to generate a battery of silibinin derivatives with enhanced radiosensitizing capacity and augmented brain targeting. These approaches, together with the utilization of clinically relevant models of lung cancer to test the efficacy and toxicity of silibinin and/or silibinin derivatives, should allow for the incorporation of this flavonolignan as a modern therapeutic approach for medical management of human lung cancer.

8. Conclusions

- The deconstruction and validation of a central mechanism of action of silibinin (i.e., STAT3) has enabled this natural compound to reach clinical development in lung cancer;
- Silibinin is capable of reaching target cancer tissues and groundbreakingly provides survival advantages to lung cancer patients with brain metastasis when used as part of formulations with an optimized oral bioavailability;
- Critical drivers for silibinin responsiveness versus resistance in specific lung cancer molecular subtypes can be identified using CRISPR-based functional genomics;
- Lessons from natural chemistry of silibinin can offer novel approaches for synthetic chemistry in lung cancer drug discovery.

Supplementary Materials: The following are available online at https://www.mdpi.com/article/10.3390/ph14060559/s1, Figure S1. (a) Original uncropped immunoblots for Figure 2. (b) Original raw data of the phenotypic microarray system analyzed in Figure 2. Figure S2. (a) Original uncropped immunoblots for Figure 4. (b) Original raw data of the phenotypic microarray system analyzed in Figure 4.

Author Contributions: S.V., J.B.-B. and J.A.M. conceived the scope of the manuscript. S.V., E.C., J.B.-B. and J.A.M. drafted and edited the final version of the manuscript. S.V., E.C., V.R.-T., V.M., J.J., and J.B.-B. helped with formatting of the manuscript, schematics and literature search and selection. All authors have read and agreed to the published version of the manuscript.

Funding: Work in the Menendez laboratory is supported by the Spanish Ministry of Science and Innovation (grants SAF2016-80639-P and PID2019-10455GB-I00, Plan Nacional de l+D+I, founded by the European Regional Development Fund, Spain) and by an unrestricted research grant from the Fundació Oncolliga Girona (Lliga catalana d'ajuda al malalt de càncer, Girona). Elisabet Cuyàs is a recipient of a research contract "Miguel Servet" (CP20/00003) from the Instituto de Salud Carlos III, Spanish Ministry of Science and Innovation (Spain). Joaquim Bosch-Barrera is the recipient of Research Grants from Grupo Español de Cáncer de Pulmón (GECP), La Marató de TV3 foundation (201906), and the Health Research and Innovation Strategic Plan (SLT006/17/114; PERIS 2016-2020;

Pla stratègic de recerca i innovació en salut; Departament de Salut, Generalitat de Catalunya). The authors would like to heartily thank König (www.konig.cat, access date: 30 May 2021) for their generous donation to fund our cancer research on silibinin in Girona.

Institutional Review Board Statement: Not applicable.

Informed Consent Statement: Not applicable.

Data Availability Statement: The data that support the findings of this study are available from the corresponding authors, upon reasonable request.

Acknowledgments: The authors would like to thank Kenneth McCreath for editorial support.

Conflicts of Interest: Joaquim Bosch-Barrera reports grants and personal fees from Roche-Genentech, grants from Pfizer and Pierre Fabre, and personal fees from MSD, BMS, AstraZeneca, Boehringer-Ingelheim, and Novartis, outside the submitted work. The authors declare that the research was conducted in the absence of any commercial or financial relationships that could be construed as a potential conflict of interest.

References

1. Middleton, E., Jr.; Kandaswami, C.; Theoharides, T.C. The effects of plant flavonoids on mammalian cells: Implications for inflammation, heart disease, and cancer. *Pharmacol. Rev.* **2000**, *52*, 673–751. [PubMed]
2. Romano, B.; Pagano, E.; Montanaro, V.; Fortunato, A.L.; Milic, N.; Borrelli, F. Novel insights into the pharmacology of flavonoids. *Phytother. Res.* **2013**, *27*, 1588–1596. [CrossRef] [PubMed]
3. Barrajón-Catalán, E.; Herranz-López, M.; Joven, J.; Segura-Carretero, A.; Alonso-Villaverde, C.; Menéndez, J.A.; Micol, V. Molecular promiscuity of plant polyphenols in the management of age-related diseases: Far beyond their antioxidant properties. *Adv. Exp. Med. Biol.* **2014**, *824*, 141–159.
4. Howitz, K.T.; Sinclair, D.A. Xenohormesis: Sensing the chemical cues of other species. *Cell* **2008**, *133*, 387–391. [CrossRef]
5. Menendez, J.A.; Joven, J.; Aragonès, G.; Barrajón-Catalán, E.; Beltrán-Debón, R.; Borrás-Linares, I.; Camps, J.; Corominas-Faja, B.; Cufí, S.; Fernández-Arroyo, S.; et al. Xenohormetic and anti-aging activity of secoiridoid polyphenols present in extra virgin olive oil: A new family of gerosuppressant agents. *Cell Cycle* **2013**, *12*, 555–578. [CrossRef]
6. Kim, N.C.; Graf, T.N.; Sparacino, C.M.; Wani, M.C.; Wall, M.E. Complete isolation and characterization of silybins and isosilybins from milk thistle (*Silybum marianum*). *Org. Biomol. Chem.* **2003**, *1*, 1684–1689. [CrossRef]
7. Gazák, R.; Walterová, D.; Kren, V. Silybin and silymarin—New and emerging applications in medicine. *Curr. Med. Chem.* **2007**, *14*, 315–338. [CrossRef] [PubMed]
8. Lee, J.I.; Narayan, M.; Barrett, J.S. Analysis and comparison of active constituents in commercial standardized silymarin extracts by liquid chromatography-electrospray ionization mass spectrometry. *J. Chromatogr. B Analyt. Technol. Biomed. Life Sci.* **2007**, *845*, 95–103. [CrossRef]
9. Abenavoli, L.; Capasso, R.; Milic, N.; Capasso, F. Milk thistle in liver diseases: Past, present, future. *Phytother. Res.* **2010**, *24*, 1423–1432. [CrossRef]
10. Hackett, E.S.; Twedt, D.C.; Gustafson, D.L. Milk thistle and its derivative compounds: A review of opportunities for treatment of liver disease. *J. Vet. Intern. Med.* **2013**, *27*, 10–16. [CrossRef] [PubMed]
11. Bijak, M. Silybin, a Major Bioactive Component of Milk Thistle (*Silybum marianum* L. Gaernt.)—Chemistry, Bioavailability, and Metabolism. *Molecules* **2017**, *22*, 1942.
12. Abenavoli, L.; Izzo, A.A.; Milić, N.; Cicala, C.; Santini, A.; Capasso, R. Milk thistle (*Silybum marianum*): A concise overview on its chemistry, pharmacological, and nutraceutical uses in liver diseases. *Phytother. Res.* **2018**, *32*, 2202–2213. [CrossRef] [PubMed]
13. Biedermann, D.; Vavříková, E.; Cvak, L.; Křen, V. Chemistry of silybin. *Nat. Prod. Rep.* **2014**, *31*, 1138–1157. [CrossRef]
14. Vargas-Mendoza, N.; Madrigal-Santillán, E.; Morales-González, A.; Esquivel-Soto, J.; Esquivel-Chirino, C.; García-Luna, Y.; González-Rubio, M.; Gayosso-de-Lucio, J.A.; Morales-González, J.A. Hepatoprotective effect of silymarin. *World J. Hepatol.* **2014**, *6*, 144–149. [CrossRef]
15. Saller, R.; Meier, R.; Brignoli, R. The use of silymarin in the treatment of liver diseases. *Drugs* **2001**, *61*, 2035–2063. [CrossRef] [PubMed]
16. Saller, R.; Melzer, J.; Reichling, J.; Brignoli, R.; Meier, R. An updated systematic review of the pharmacology of silymarin. *Forsch. Komplementmed.* **2007**, *14*, 70–80. [CrossRef]
17. Loguercio, C.; Festi, D. Silybin and the liver: From basic research to clinical practice. *World J. Gastroenterol.* **2011**, *17*, 2288–2301. [CrossRef]
18. Federico, A.; Dallio, M.; Loguercio, C. Silymarin/Silybin and Chronic Liver Disease: A Marriage of Many Years. *Molecules* **2017**, *22*, 191. [CrossRef]
19. Tajmohammadi, A.; Razavi, B.M.; Hosseinzadeh, H. *Silybum marianum* (milk thistle) and its main constituent, silymarin, as a potential therapeutic plant in metabolic syndrome: A review. *Phytother. Res.* **2018**, *32*, 1933–1949. [CrossRef]

20. Gillessen, A.; Schmidt, H.H. Silymarin as Supportive Treatment in Liver Diseases: A Narrative Review. *Adv. Ther.* **2020**, *37*, 1279–1301. [CrossRef]
21. Wellington, K.; Jarvis, B. Silymarin: A review of its clinical properties in the management of hepatic disorders. *BioDrugs* **2001**, *15*, 465–489. [CrossRef] [PubMed]
22. Singh, R.P.; Agarwal, R. Mechanisms and preclinical efficacy of silibinin in preventing skin cancer. *Eur. J. Cancer* **2005**, *41*, 1969–1979. [CrossRef]
23. Prasad, R.R.; Paudel, S.; Raina, K.; Agarwal, R. Silibinin and non-melanoma skin cancers. *J. Tradit. Complement. Med.* **2020**, *10*, 236–244. [CrossRef] [PubMed]
24. Singh, R.P.; Agarwal, R. Prostate cancer prevention by silibinin. *Curr. Cancer Drug Targets* **2004**, *4*, 1–11. [CrossRef] [PubMed]
25. Singh, R.P.; Agarwal, R. Prostate cancer chemoprevention by silibinin: Bench to bedside. *Mol. Carcinog.* **2006**, *45*, 436–442. [CrossRef]
26. Zhao, J.; Agarwal, R. Tissue distribution of silibinin, the major active constituent of silymarin, in mice and its association with enhancement of phase II enzymes: Implications in cancer chemoprevention. *Carcinogenesis* **1999**, *20*, 2101–2108. [CrossRef]
27. Mateen, S.; Raina, K.; Agarwal, R. Chemopreventive and anti-cancer efficacy of silibinin against growth and progression of lung cancer. *Nutr. Cancer* **2013**, *65* (Suppl. 1), 3–11. [CrossRef] [PubMed]
28. Singh, R.P.; Agarwal, R. Cosmeceuticals and silibinin. *Clin. Dermatol.* **2009**, *27*, 479–484. [CrossRef]
29. Slaga, T.J. SENCAR mouse skin tumorigenesis model versus other strains and stocks of mice. *Environ. Health Perspect.* **1986**, *68*, 27–32. [CrossRef] [PubMed]
30. Ewing, M.W.; Conti, C.J.; Kruszewski, F.H.; Slaga, T.J.; DiGiovanni, J. Tumor progression in Sencar mouse skin as a function of initiator dose and promoter dose, duration, and type. *Cancer Res.* **1988**, *48*, 7048–7054.
31. Sharma, G.; Singh, R.P.; Chan, D.C.; Agarwal, R. Silibinin induces growth inhibition and apoptotic cell death in human lungcarcinoma cells. *Anticancer Res.* **2003**, *23*, 2649–2655.
32. Singh, R.P.; Mallikarjuna, G.U.; Sharma, G.; Dhanalakshmi, S.; Tyagi, A.K.; Chan, D.C.; Agarwal, C.; Agarwal, R. Oral silibinin inhibits lung tumor growth in athymic nude mice and forms a novel chemocombination with doxorubicin targeting nuclear factor kappaB-mediated inducible chemoresistance. *Clin. Cancer Res.* **2004**, *10*, 8641–8647. [CrossRef]
33. Yan, Y.; Wang, Y.; Tan, Q.; Lubet, R.A.; You, M. Efficacy of deguelin and silibinin on benzo(a)pyrene-induced lung tumorigenesis in A/J mice. *Neoplasia* **2005**, *7*, 1053–1057. [CrossRef]
34. Singh, R.P.; Deep, G.; Chittezhath, M.; Kaur, M.; Dwyer-Nield, L.D.; Malkinson, A.M.; Agarwal, R. Effect of silibinin on the growth and progression of primary lung tumors in mice. *J. Natl. Cancer Inst.* **2006**, *98*, 846–855. [CrossRef] [PubMed]
35. Chittezhath, M.; Deep, G.; Singh, R.P.; Agarwal, C.; Agarwal, R. Silibinin inhibits cytokine-induced signaling cascades and down-regulates inducible nitric oxide synthase in human lung carcinoma A549 cells. *Mol. Cancer Ther.* **2008**, *7*, 1817–1826. [CrossRef]
36. Tyagi, A.; Singh, R.P.; Ramasamy, K.; Raina, K.; Redente, E.F.; Dwyer-Nield, L.D.; Radcliffe, R.A.; Malkinson, A.M.; Agarwal, R. Growth inhibition and regression of lung tumors by silibinin: Modulation of angiogenesis by macrophage-associated cytokines and nuclear factor-kappaB and signal transducers and activators of transcription 3. *Cancer Prev. Res. (Phila)* **2009**, *2*, 74–83. [CrossRef]
37. Ramasamy, K.; Dwyer-Nield, L.D.; Serkova, N.J.; Hasebroock, K.M.; Tyagi, A.; Raina, K.; Singh, R.P.; Malkinson, A.M.; Agarwal, R. Silibinin prevents lung tumorigenesis in wild-type but not in iNOS−/− mice: Potential of real-time micro-CT in lung cancer chemoprevention studies. *Clin. Cancer Res.* **2011**, *17*, 753–761. [CrossRef]
38. Tyagi, A.; Agarwal, C.; Dwyer-Nield, L.D.; Singh, R.P.; Malkinson, A.M.; Agarwal, R. Silibinin modulates TNF-alpha and IFN-gamma mediated signaling to regulate COX2 and iNOS expression in tumorigenic mouse lung epithelial LM2 cells. *Mol. Carcinog.* **2012**, *51*, 832–842. [CrossRef] [PubMed]
39. Bosch-Barrera, J.; Menendez, J.A. Silibinin and STAT3: A natural way of targeting transcription factors for cancer therapy. *Cancer Treat. Rev.* **2015**, *41*, 540–546. [CrossRef] [PubMed]
40. Bosch-Barrera, J.; Queralt, B.; Menendez, J.A. Targeting STAT3 with silibinin to improve cancer therapeutics. *Cancer Treat. Rev.* **2017**, *58*, 61–69. [CrossRef] [PubMed]
41. Mateen, S.; Tyagi, A.; Agarwal, C.; Singh, R.P.; Agarwal, R. Silibinin inhibits human nonsmall cell lung cancer cell growth through cell-cycle arrest by modulating expression and function of key cell-cycle regulators. *Mol. Carcinog.* **2010**, *49*, 247–258. [CrossRef]
42. Mateen, S.; Raina, K.; Jain, A.K.; Agarwal, C.; Chan, D.; Agarwal, R. Epigenetic modifications and p21-cyclin B1 nexus in anticancer effect of histone deacetylase inhibitors in combination with silibinin on non-small cell lung cancer cells. *Epigenetics* **2012**, *7*, 1161–1172. [CrossRef]
43. Corominas-Faja, B.; Oliveras-Ferraros, C.; Cuyàs, E.; Segura-Carretero, A.; Joven, J.; Martin-Castillo, B.; Barrajón-Catalán, E.; Micol, V.; Bosch-Barrera, J.; Menendez, J.A. Stem cell-like ALDH(bright) cellular states in EGFR-mutant non-small cell lung cancer: A novel mechanism of acquired resistance to erlotinib targetable with the natural polyphenol silibinin. *Cell Cycle* **2013**, *12*, 3390–3404. [CrossRef] [PubMed]
44. Cuyàs, E.; Pérez-Sánchez, A.; Micol, V.; Menendez, J.A.; Bosch-Barrera, J. STAT3-targeted treatment with silibinin overcomes the acquired resistance to crizotinib in ALK-rearranged lung cancer. *Cell Cycle* **2016**, *15*, 3413–3418. [CrossRef]

45. Liang, Z.; Yang, Y.; Wang, H.; Yi, W.; Yan, X.; Yan, J.; Li, Y.; Feng, Y.; Yu, S.; Yang, J.; et al. Inhibition of SIRT1 signaling sensitizes the antitumor activity of silybin against human lung adenocarcinoma cells in vitro and in vivo. *Mol. Cancer Ther.* **2014**, *13*, 1860–1872. [CrossRef]
46. Rho, J.K.; Choi, Y.J.; Jeon, B.S.; Choi, S.J.; Cheon, G.J.; Woo, S.K.; Kim, H.R.; Kim, C.H.; Choi, C.M.; Lee, J.C. Combined treatment with silibinin and epidermal growth factor receptor tyrosine kinase inhibitors overcomes drug resistance caused by T790M mutation. *Mol. Cancer Ther.* **2010**, *9*, 3233–3243. [CrossRef] [PubMed]
47. Vazquez-Martin, A.; Cufí, S.; Oliveras-Ferraros, C.; Torres-Garcia, V.Z.; Corominas-Faja, B.; Cuyàs, E.; Bonavia, R.; Visa, J.; Martin-Castillo, B.; Barrajón-Catalán, E.; et al. IGF-1R/epithelial-to-mesenchymal transition (EMT) crosstalk suppresses the erlotinib-sensitizing effect of EGFR exon 19 deletion mutations. *Sci. Rep.* **2013**, *3*, 2560. [CrossRef] [PubMed]
48. Cufí, S.; Bonavia, R.; Vazquez-Martin, A.; Corominas-Faja, B.; Oliveras-Ferraros, C.; Cuyàs, E.; Martin-Castillo, B.; Barrajón-Catalán, E.; Visa, J.; Segura-Carretero, A.; et al. Silibinin meglumine, a water-soluble form of milk thistle silymarin, is an orally active anti-cancer agent that impedes the epithelial-to-mesenchymal transition (EMT) in EGFR-mutant non-small-cell lung carcinoma cells. *Food Chem. Toxicol.* **2013**, *60*, 360–368.
49. Cufí, S.; Bonavia, R.; Vazquez-Martin, A.; Oliveras-Ferraros, C.; Corominas-Faja, B.; Cuyàs, E.; Martin-Castillo, B.; Barrajón-Catalán, E.; Visa, J.; Segura-Carretero, A.; et al. Silibinin suppresses EMT-driven erlotinib resistance by reversing the high miR-21/low miR-200c signature in vivo. *Sci. Rep.* **2013**, *3*, 2459. [CrossRef]
50. Shien, K.; Toyooka, S.; Yamamoto, H.; Soh, J.; Jida, M.; Thu, K.L.; Hashida, S.; Maki, Y.; Ichihara, E.; Asano, H.; et al. Acquired resistance to EGFR inhibitors is associated with a manifestation of stem cell-like properties in cancer cells. *Cancer Res.* **2013**, *73*, 3051–3061. [CrossRef]
51. Maitrejean, M.; Comte, G.; Barron, D.; El Kirat, K.; Conseil, G.; Di Pietro, A. The flavanolignan silybin and its hemisynthetic derivatives, a novel series of potential modulators of P-glycoprotein. *Bioorg. Med. Chem. Lett.* **2000**, *10*, 157–160. [CrossRef]
52. Dzubák, P.; Hajdúch, M.; Gazák, R.; Svobodová, A.; Psotová, J.; Walterová, D.; Sedmera, P.; Kren, V. New derivatives of silybin and 2,3-dehydrosilybin and their cytotoxic and P-glycoprotein modulatory activity. *Bioorg. Med. Chem.* **2006**, *14*, 3793–3810. [CrossRef] [PubMed]
53. Sadava, D.; Kane, S.E. Silibinin reverses drug resistance in human small-cell lung carcinoma cells. *Cancer Lett.* **2013**, *339*, 102–106. [CrossRef]
54. Dinic, J.; Podolski-Renic, A.; Stankovic, T.; Bankovic, J.; Pesic, M. New Approaches With Natural Product Drugs for Overcoming Multidrug Resistance in Cancer. *Curr. Pharm. Des.* **2015**, *21*, 5589–5604. [CrossRef] [PubMed]
55. Dobiasová, S.; Řehořová, K.; Kučerová, D.; Biedermann, D.; Káňová, K.; Petrásková, L.; Koucká, K.; Václavíková, R.; Valentová, K.; Ruml, T.; et al. Multidrug Resistance Modulation Activity of Silybin Derivatives and Their Anti-inflammatory Potential. *Antioxidants* **2020**, *9*, 455. [CrossRef]
56. Lee, C.K.; Choi, J.S. Effects of silibinin, inhibitor of CYP3A4 and P-glycoprotein in vitro, on the pharmacokinetics of paclitaxel after oral and intravenous administration in rats. *Pharmacology* **2010**, *85*, 350–356. [CrossRef] [PubMed]
57. Chu, S.C.; Chiou, H.L.; Chen, P.N.; Yang, S.F.; Hsieh, Y.S. Silibinin inhibits the invasion of human lung cancer cells via decreased productions of urokinase-plasminogen activator and matrix metalloproteinase-2. *Mol. Carcinog.* **2004**, *40*, 143–149. [CrossRef]
58. Chen, P.N.; Hsieh, Y.S.; Chiou, H.L.; Chu, S.C. Silibinin inhibits cell invasion through inactivation of both PI3K-Akt and MAPK signaling pathways. *Chem. Biol. Interact.* **2005**, *156*, 141–150. [CrossRef]
59. Chen, P.-N.; Hsieh, Y.-S.; Chiang, C.-L.; Chiou, H.-L.; Yang, S.-F.; Chu, S.-C. Silibinin inhibits invasion of oral cancer cells by suppressing the MAPK pathway. *J. Dent. Res.* **2006**, *85*, 220–225. [CrossRef]
60. Byun, H.J.; Darvin, P.; Kang, D.Y.; Sp, N.; Joung, Y.H.; Park, J.H.; Kim, S.J.; Yang, Y.M. Silibinin downregulates MMP2 expression via Jak2/STAT3 pathway and inhibits the migration and invasive potential in MDA-MB-231 cells. *Oncol. Rep.* **2017**, *37*, 3270–3278. [CrossRef]
61. Davis, F.M.; Stewart, T.A.; Thompson, E.W.; Monteith, G.R. Targeting EMT in cancer: Opportunities for pharmacological intervention. *Trends Pharmacol. Sci.* **2014**, *35*, 479–488. [CrossRef]
62. Marcucci, F.; Stassi, G.; De Maria, R. Epithelial-mesenchymal transition: A new target in anticancer drug discovery. *Nat. Rev. Drug Discov.* **2016**, *15*, 311–325. [CrossRef]
63. Shibue, T.; Weinberg, R.A. EMT, CSCs, and drug resistance: The mechanistic link and clinical implications. *Nat. Rev. Clin. Oncol.* **2017**, *14*, 611–629. [CrossRef]
64. Frederick, B.A.; Helfrich, B.A.; Coldren, C.D.; Zheng, D.; Chan, D.; Bunn, P.A., Jr.; Raben, D. Epithelial to mesenchymal transition predicts gefitinib resistance in cell lines of head and neck squamous cell carcinoma and non-small cell lung carcinoma. *Mol. Cancer Ther.* **2007**, *6*, 1683–1691. [CrossRef] [PubMed]
65. Byers, L.A.; Diao, L.; Wang, J.; Saintigny, P.; Girard, L.; Peyton, M.; Shen, L.; Fan, Y.; Giri, U.; Tumula, P.K.; et al. An epithelial-mesenchymal transition gene signature predicts resistance to EGFR and PI3K inhibitors and identifies Axl as a therapeutic target for overcoming EGFR inhibitor resistance. *Clin. Cancer Res.* **2013**, *19*, 279–290. [CrossRef]
66. Guo, F.; Liu, X.; Qing, Q.; Sang, Y.; Feng, C.; Li, X.; Jiang, L.; Su, P.; Wang, Y. EML4-ALK induces epithelial-mesenchymal transition consistent with cancer stem cell properties in H1299 non-small cell lung cancer cells. *Biochem. Biophys. Res. Commun.* **2015**, *459*, 398–404. [CrossRef] [PubMed]
67. Kim, H.R.; Kim, W.S.; Choi, Y.J.; Choi, C.M.; Rho, J.K.; Lee, J.C. Epithelial-mesenchymal transition leads to crizotinib resistance in H2228 lung cancer cells with EML4-ALK translocation. *Mol. Oncol.* **2013**, *7*, 1093–1102. [CrossRef] [PubMed]

68. Gower, A.; Hsu, W.H.; Hsu, S.T.; Wang, Y.; Giaccone, G. EMT is associated with, but does not drive resistance to ALK inhibitors among EML4-ALK non-small cell lung cancer. *Mol. Oncol.* **2016**, *10*, 601–609. [CrossRef]
69. Kogita, A.; Togashi, Y.; Hayashi, H.; Sogabe, S.; Terashima, M.; De Velasco, M.A.; Sakai, K.; Fujita, Y.; Tomida, S.; Takeyama, Y.; et al. Hypoxia induces resistance to ALK inhibitors in the H3122 non-small cell lung cancer cell line with an ALK rearrangement via epithelial-mesenchymal transition. *Int. J. Oncol.* **2014**, *45*, 1430–1436. [CrossRef]
70. Nakamichi, S.; Seike, M.; Miyanaga, A.; Chiba, M.; Zou, F.; Takahashi, A.; Ishikawa, A.; Kunugi, S.; Noro, R.; Kubota, K.; et al. Overcoming drug-tolerant cancer cell subpopulations showing AXL activation and epithelial-mesenchymal transition is critical in conquering ALK-positive lung cancer. *Oncotarget* **2018**, *9*, 27242–27255. [CrossRef]
71. Debruyne, D.N.; Bhatnagar, N.; Sharma, B.; Luther, W.; Moore, N.F.; Cheung, N.K.; Gray, N.S.; George, R.E. ALK inhibitor resistance in ALK(F1174L)-driven neuroblastoma is associated with AXL activation and induction of EMT. *Oncogene* **2016**, *35*, 3681–3689. [CrossRef] [PubMed]
72. Wei, J.; van der Wekken, A.J.; Saber, A.; Terpstra, M.M.; Schuuring, E.; Timens, W.; Hiltermann, T.J.N.; Groen, H.J.M.; van den Berg, A.; Kok, K. Mutations in EMT-Related Genes in ALK Positive Crizotinib Resistant Non-Small Cell Lung Cancers. *Cancers* **2018**, *10*, 10. [CrossRef] [PubMed]
73. Sekar, D.; Krishnan, R.; Panagal, M.; Sivakumar, P.; Gopinath, V.; Basam, V. Deciphering the role of microRNA 21 in cancer stem cells (CSCs). *Genes Dis.* **2016**, *3*, 277–281. [CrossRef] [PubMed]
74. Khan, A.Q.; Ahmed, E.I.; Elareer, N.R.; Junejo, K.; Steinhoff, M.; Uddin, S. Role of miRNA-Regulated Cancer Stem Cells in the Pathogenesis of Human Malignancies. *Cells* **2019**, *8*, 840. [CrossRef] [PubMed]
75. Lim, Y.Y.; Wright, J.A.; Attema, J.L.; Gregory, P.A.; Bert, A.G.; Smith, E.; Thomas, D.; Lopez, A.F.; Drew, P.A.; Khew-Goodall, Y.; et al. Epigenetic modulation of the miR-200 family is associated with transition to a breast cancer stem-cell-like state. *J. Cell Sci.* **2013**, *126*, 2256–2266. [CrossRef]
76. Burk, U.; Schubert, J.; Wellner, U.; Schmalhofer, O.; Vincan, E.; Spaderna, S.; Brabletz, T. A reciprocal repression between ZEB1 and members of the miR-200 family promotes EMT and invasion in cancer cells. *EMBO Rep.* **2008**, *9*, 582–589. [CrossRef]
77. Wellner, U.; Schubert, J.; Burk, U.C.; Schmalhofer, O.; Zhu, F.; Sonntag, A.; Waldvogel, B.; Vannier, C.; Darling, D.; zur Hausen, A.; et al. The EMT-activator ZEB1 promotes tumorigenicity by repressing stemness-inhibiting microRNAs. *Nat. Cell Biol.* **2009**, *11*, 1487–1495. [CrossRef] [PubMed]
78. Mateen, S.; Raina, K.; Agarwal, C.; Chan, D.; Agarwal, R. Silibinin synergizes with histone deacetylase and DNA methyltransferase inhibitors in upregulating E-cadherin expression together with inhibition of migration and invasion of human non-small cell lung cancer cells. *J. Pharmacol. Exp. Ther.* **2013**, *345*, 206–214. [CrossRef]
79. Xu, S.; Zhang, H.; Wang, A.; Ma, Y.; Gan, Y.; Li, G. Silibinin suppresses epithelial-mesenchymal transition in human non-small cell lung cancer cells by restraining RHBDD1. *Cell Mol. Biol. Lett.* **2020**, *25*, 36. [CrossRef]
80. Erler, J.T.; Bennewith, K.L.; Nicolau, M.; Dornhöfer, N.; Kong, C.; Le, Q.T.; Chi, J.T.; Jeffrey, S.S.; Giaccia, A.J. Lysyl oxidase is essential for hypoxia-induced metastasis. *Nature* **2006**, *440*, 1222–1226. [CrossRef] [PubMed]
81. Barker, H.E.; Cox, T.R.; Erler, J.T. The rationale for targeting the LOX family in cancer. *Nat. Rev. Cancer* **2012**, *12*, 540–552. [CrossRef] [PubMed]
82. Cox, T.R.; Gartland, A.; Erler, J.T. Lysyl Oxidase, a Targetable Secreted Molecule Involved in Cancer Metastasis. *Cancer Res.* **2016**, *76*, 188–192. [CrossRef] [PubMed]
83. Johnston, K.A.; Lopez, K.M. Lysyl oxidase in cancer inhibition and metastasis. *Cancer Lett.* **2018**, *417*, 174–181. [CrossRef]
84. Hou, X.; Du, H.; Quan, X.; Shi, L.; Zhang, Q.; Wu, Y.; Liu, Y.; Xiao, J.; Li, Y.; Lu, L.; et al. Silibinin Inhibits NSCLC Metastasis by Targeting the EGFR/LOX Pathway. *Front. Pharmacol.* **2018**, *9*, 21. [CrossRef]
85. Kaipa, J.M.; Starkuviene, V.; Erfle, H.; Eils, R.; Gladilin, E. Transcriptome profiling reveals Silibinin dose-dependent response network in non-small lung cancer cells. *PeerJ* **2020**, *8*, e10373. [CrossRef]
86. Pérez-Sánchez, A.; Cuyàs, E.; Ruiz-Torres, V.; Agulló-Chazarra, L.; Verdura, S.; González-Álvarez, I.; Bermejo, M.; Joven, J.; Micol, V.; Bosch-Barrera, J.; et al. Intestinal Permeability Study of Clinically Relevant Formulations of Silibinin in Caco-2 Cell Monolayers. *Int. J. Mol. Sci.* **2019**, *20*, 1606. [CrossRef]
87. Bosch-Barrera, J.; Sais, E.; Cañete, N.; Marruecos, J.; Cuyàs, E.; Izquierdo, A.; Porta, R.; Haro, M.; Brunet, J.; Pedraza, S.; et al. Response of brain metastasis from lung cancer patients to an oral nutraceutical product containing silibinin. *Oncotarget* **2016**, *7*, 32006–32014. [CrossRef]
88. Priego, N.; Zhu, L.; Monteiro, C.; Mulders, M.; Wasilewski, D.; Bindeman, W.; Doglio, L.; Martínez, L.; Martínez-Saez, E.; Ramón, Y.; et al. STAT3 labels a subpopulation of reactive astrocytes required for brain metastasis. *Nat. Med.* **2018**, *24*, 1024–1035. [CrossRef]
89. Sarmiento Soto, M.; Larkin, J.R.; Martin, C.; Khrapitchev, A.A.; Maczka, M.; Economopoulos, V.; Scott, H.; Escartin, C.; Bonvento, G.; Serres, S.; et al. STAT3-Mediated Astrocyte Reactivity Associated with Brain Metastasis Contributes to Neurovascular Dysfunction. *Cancer Res.* **2020**, *80*, 5642–5655. [CrossRef] [PubMed]
90. Verdura, S.; Cuyàs, E.; Llorach-Parés, L.; Pérez-Sánchez, A.; Micol, V.; Nonell-Canals, A.; Joven, J.; Valiente, M.; Sánchez-Martínez, M.; Bosch-Barrera, J.; et al. Silibinin is a direct inhibitor of STAT3. *Food Chem. Toxicol.* **2018**, *116*, 161–172. [CrossRef] [PubMed]
91. Bromberg, J.F.; Wrzeszczynska, M.H.; Devgan, G.; Zhao, Y.; Pestell, R.G.; Albanese, C.; Darnell, J.E., Jr. Stat3 as an oncogene. *Cell* **1999**, *98*, 295–303. [CrossRef]

92. Liddle, F.J.; Alvarez, J.V.; Poli, V.; Frank, D.A. Tyrosine phosphorylation is required for functional activation of disulfide-containing constitutively active STAT mutants. *Biochemistry* **2006**, *45*, 5599–5605. [CrossRef] [PubMed]
93. Shukla, S.K.; Dasgupta, A.; Mehla, K.; Gunda, V.; Vernucci, E.; Souchek, J.; Goode, G.; King, R.; Mishra, A.; Rai, I.; et al. Silibinin-mediated metabolic reprogramming attenuates pancreatic cancer-induced cachexia and tumor growth. *Oncotarget* **2015**, *6*, 41146–41161. [CrossRef]
94. Singh, M.; Garg, N.; Venugopal, C.; Hallett, R.; Tokar, T.; McFarlane, N.; Mahendram, S.; Bakhshinyan, D.; Manoranjan, B.; Vora, P.; et al. STAT3 pathway regulates lung-derived brain metastasis initiating cell capacity through miR-21 activation. *Oncotarget* **2015**, *6*, 27461–27477. [CrossRef] [PubMed]
95. Thomas, S.; Fisher, K.H.; Snowden, J.A.; Danson, S.J.; Brown, S.; Zeidler, M.P. Methotrexate Is a JAK/STAT Pathway Inhibitor. *PLoS ONE* **2015**, *10*, e0130078. [CrossRef]
96. Miklossy, G.; Hilliard, T.S.; Turkson, J. Therapeutic modulators of STAT signalling for human diseases. *Nat. Rev. Drug Discov.* **2013**, *12*, 611–629. [CrossRef] [PubMed]
97. Shakibaei, M.; Harikumar, K.B.; Aggarwal, B.B. Resveratrol addiction: To die or not to die. *Mol. Nutr. Food Res.* **2009**, *53*, 115–128. [CrossRef]
98. Li, T.; Wang, W.; Chen, H.; Li, T.; Ye, L. Evaluation of anti-leukemia effect of resveratrol by modulating STAT3 signaling. *Int. Immunopharmacol.* **2010**, *10*, 18–25. [CrossRef]
99. Liu, L.J.; Leung, K.H.; Chan, D.S.; Wang, Y.T.; Ma, D.L.; Leung, C.H. Identification of a natural product-like STAT3 dimerization inhibitor by structure-based virtual screening. *Cell Death Dis.* **2014**, *5*, e1293. [CrossRef]
100. Szelag, M.; Sikorski, K.; Czerwoniec, A.; Szatkowska, K.; Wesoly, J.; Bluyssen, H.A. In silico simulations of STAT1 and STAT3 inhibitors predict SH2 domain cross-binding specificity. *Eur. J. Pharmacol.* **2013**, *720*, 38–48. [CrossRef]
101. Tuli, H.S.; Mittal, S.; Aggarwal, D.; Parashar, G.; Parashar, N.C.; Upadhyay, S.K.; Barwal, T.S.; Jain, A.; Kaur, G.; Savla, R.; et al. Path of Silibinin from diet to medicine: A dietary polyphenolic flavonoid having potential anti-cancer therapeutic significance. In *Seminars in Cancer Biology*; Academic Press: Cambridge, MA, USA, 2020.
102. Liakopoulou, C.; Kazazis, C.; Vallianou, N.G. Silimarin and Cancer. *Anticancer Agents Med. Chem.* **2018**, *18*, 1970–1974. [CrossRef] [PubMed]
103. Delmas, D.; Xiao, J.; Vejux, A.; Aires, V. Silymarin and Cancer: A Dual Strategy in Both in Chemoprevention and Chemosensitivity. *Molecules* **2020**, *25*, 2009. [CrossRef] [PubMed]
104. Kim, J.; Lee, H.M.; Cai, F.; Ko, B.; Yang, C.; Lieu, E.L.; Muhammad, N.; Rhyne, S.; Li, K.; Haloul, M.; et al. The hexosamine biosynthesis pathway is a targetable liability in KRAS/LKB1 mutant lung cancer. *Nat. Metab.* **2020**, *2*, 1401–1412. [CrossRef] [PubMed]